PENNARAPTORAN THEROPOD DINOSAURS
PAST PROGRESS AND NEW FRONTIERS

EDITED BY

MICHAEL PITTMAN AND XING XU

BULLETIN OF THE AMERICAN MUSEUM OF NATURAL HISTORY

SHOUT
SHARE
IT

PENNARAPTORAN THEROPOD DINOSAURS
PAST PROGRESS AND NEW FRONTIERS

Edited by

MICHAEL PITTMAN
Vertebrate Palaeontology Laboratory
Division of Earth and Planetary Science
The University of Hong Kong, Hong Kong

XING XU
Key Laboratory of Vertebrate Evolution and Human Origins
Institute of Vertebrate Paleontology & Paleoanthropology and
CAS Center for Excellence in Life and Paleoenvironment, Beijing

BULLETIN OF THE AMERICAN MUSEUM OF NATURAL HISTORY
Number 440, 353 pp., 58 figures, 46 tables
Issued August 21, 2020

Copyright © American Museum of Natural History 2020

ISSN 0003-0090

CONTENTS

Introduction 4
MICHAEL PITTMAN AND XING XU

SECTION 1. SYSTEMATICS, FOSSIL RECORD, AND BIOGEOGRAPHY............................7

Chapter 1. Pennaraptoran systematics 7
MICHAEL PITTMAN, JINGMAI O'CONNOR, DANIEL J. FIELD, ALAN H. TURNER, WAISUM MA, PETER MAKOVICKY, AND XING XU

Chapter 2. The fossil record of Mesozoic and Paleocene pennaraptorans 37
MICHAEL PITTMAN, JINGMAI O'CONNOR, EDISON TSE, PETER MAKOVICKY, DANIEL J. FIELD, WAISUM MA, ALAN H. TURNER, MARK A. NORELL, RUI PEI, AND XING XU

Chapter 3. The impact of unstable taxa in coelurosaurian phylogeny and resampling support measures for parsimony analyses 97
DIEGO POL AND PABLO A. GOLOBOFF

Chapter 4. The biogeography of coelurosaurian theropods and its impact on their evolutionary history 117
ANYANG DING, MICHAEL PITTMAN, PAUL UPCHURCH, JINGMAI O'CONNOR, DANIEL J. FIELD, AND XING XU

Chapter 5. Timing the extant avian radiation: the rise of modern birds, and the importance of modeling molecular rate variation 159
DANIEL J. FIELD, JACOB S. BERV, ALLISON Y. HSIANG, ROBERT LANFEAR, MICHAEL J. LANDIS, AND ALEX DORNBURG

SECTION 2. ANATOMICAL FRONTIERS 183

Chapter 6. Disparity and macroevolutionary transformation of the maniraptoran manus 183
SERGIO M. NEBREDA, GUILLERMO NAVALÓN, IRIS MENÉNDEZ, TROND SIGURDSEN, LUIS M. CHIAPPE, AND JESÚS MARUGÁN-LOBÓN

Chapter 7. Tooth vs. beak: the evolutionary developmental control of the avian feeding apparatus 205
SHUO WANG, JOSEF STIEGLER, PING WU, AND CHENG-MING CHUONG

Chapter 8. Functional morphology of the oviraptorosaurian and scansoriopterygid skull 229
WAISUM MA, MICHAEL PITTMAN, STEPHAN LAUTENSCHLAGER, LUKE E. MEADE, AND XING XU

Chapter 9. Fossil microbodies are melanosomes: evaluating and rejecting the 'fossilised decay-associated microbes' hypothesis 251
ARINDAM ROY, CHRISTOPHER S. ROGERS, THOMAS CLEMENTS, MICHAEL PITTMAN, OLIVIER HABIMANA, PETER MARTIN, AND JAKOB VINTHER

Section 3. Early-Flight Study: Methods, Status, and Frontiers 277
Chapter 10. Methods of studying early theropod flight 277
Michael Pittman, Ashley M. Heers, Francisco J. Serrano, Daniel J. Field, Michael B. Habib, T. Alexander Dececchi, Thomas G. Kaye, and Hans C.E. Larsson

Chapter 11. High flyer or high fashion? A comparison of flight potential among small-bodied paravians 295
T. Alexander Dececchi, Hans C.E. Larsson, Michael Pittman, and Michael B. Habib

Chapter 12. Navigating functional landscapes: a bird's eye view of the evolution of avialan flight 321
Hans C.E. Larsson, Michael B. Habib, and T. Alexander Dececchi

Chapter 13. Laser-stimulated fluorescence refines flight modeling of the Early Cretaceous bird *Sapeornis* 333
Francisco J. Serrano, Michael Pittman, Thomas G. Kaye, Xiaoli Wang, Xiaoting Zheng, and Luis M. Chiappe

Chapter 14. Pectoral girdle morphology in early-diverging paravians and living ratites: implications for the origin of flight 345
Fernando E. Novas, Federico L. Agnolín, Federico Brisson Egli, and Gastón E. Lo Coco

PREFACE

The origin of birds and flight was a major event in the history of life. A wealth of spectacular fossils of early birds and their closest relatives has demonstrated that birds are maniraptoran theropod dinosaurs, with Pennaraptora being the most relevant theropod group to the "dinosaur-bird" transition. Pennaraptora comprises birds themselves as well as the pennaceous feathered dromaeosaurids, troodontids, scansoriopterygids, and oviraptorosaurians. Fossils and neontological insights show that many salient avian traits originated deep within theropod evolutionary history, accumulating over a significant temporal and phylogenetic interval and often appearing in a complex mosaic across phylogeny. This includes endothermic physiology, unique reproductive strategies, as well as flight itself. Hallmark features necessary for flight appeared among pennaraptoran dinosaurs including a laterally oriented, long, and robust forelimb; a refined "flight ready" brain; and large, vaned flight feathers. Proxies for modern flight capability, modelling work and functional morphology support flight and near-flight capabilities among paravian pennaraptorans, with powered flight probably evolving independently multiple times. However, in order to deepen our understanding of avian and flight origins as well as other important pennaraptoran evolutionary events, more progress is needed in achieving better systematic consensus both within and between clades.

In this context, the inaugural discussion-focused International Pennaraptoran Dinosaur Symposium (IPDS) was held at the University of Hong Kong between March 29 and April 1, 2018, with the goal of making substantial advances in our understanding of pennaraptoran palaeobiology and evolution. The conference documented past progress, worked toward consensus on key unresolved issues, and broke new ground in the field. This volume curates the main outcomes of the IPDS symposium including priority areas identified for future research. The volume involved 49 experts from more than 10 countries whose views cover much of the current discussion on this topic. The volume is made up of 14 chapters organized in three sections:

SECTION ONE: SYSTEMATICS, FOSSIL RECORD, AND BIOGEOGRAPHY: This section surveys the pennaraptoran fossil record and underscores parts where further attention is likely to make headway in answering pressing questions in the field. The current state of pennaraptoran systematics is presented, providing the context needed to understand the group's evolution. Areas of uncertainty and controversy are highlighted and suggested improvements proposed. This section includes a chapter dedicated to improving how rogue taxa/wildcards are identified in phylogenetic analyses, which is of interest to the broader palaeontological community. Section one also uses an updated coelurosaurian phylogeny to present the first quantitative palaeobiogeographic analysis of the Coelurosauria. This allowed identification of key tectonic drivers of evolution, providing a stronger basis for investigating evolutionary drivers among pennaraptorans as well as non-pennaraptoran theropods, other dinosaur groups, and Mesozoic vertebrates more generally.

SECTION TWO: ANATOMICAL FRONTIERS: This section focuses on recent discoveries in pennaraptoran anatomy, particularly of the hand and head. It explores the implications this knowledge has and will have on our understanding of pennaraptoran palaeobiology and evolution. These discoveries involve a wide range of adopted approaches including geometric morphometrics, mechanical advantage calculations, and evo-devo approaches as well as the phylogenetic context provided in section one. The world of fossil pennaraptorans has become technicolored in recent years thanks to the advent of melanosome-based paleocolor reconstruction. As an important reappraisal of this work, an actuo-paleontological experiment is presented that quantitatively tests the premise of this method for the first time.

SECTION THREE: EARLY FLIGHT STUDY: METHODS, STATUS, AND FRONTIERS: This section begins by detailing the methods currently available for studying early theropod flight and discusses the priorities to address in future methodological development work. As an example, a methodological frontier is explored by marrying recent advances in soft-tissue imaging with quantitative methods of early flight study to create a new framework on which to build. Section three also covers recent efforts to identify the small pennaraptorans that first took to the skies, what their flight capabilities were and how their flight might have been acquired. A new broader context is proposed for flight behavior in a conceptual chapter about its functional landscape. Wing-assisted incline running (WAIR), a behavior seen in modern birds, is part of this functional landscape and a proposed stage of early flight development. To stimulate further exploration of this functional landscape, chapter 14 argues that this behavior is a later innovation instead on the basis of experimental data collected from modern ostriches.

We would like to thank our contributing authors for realizing this ambitious project, which was made possible through the support of Kenneth H.C. Fung, Trustee of Sir Kenneth Fung Ping Fan Foundation and First Initiative Foundation. The Faculty of Science of the University of Hong Kong and the Division of Paleontology at the American Museum of Natural History (especially Mark A. Norell) are also thanked for their support. We would like to thank our reviewers James Clark and Fernando Novas as well as Robert Dudley for his comments on section three of the volume. Their feedback greatly improved the quality of the volume. Journal staff especially Robert Voss and Mary Knight are thanked for their great help and patience throughout the project. Marianne E. Phillips is thanked for proofreading multiple drafts of the text. We hope you enjoy the volume and that it stimulates our science to even greater heights.

Michael Pittman and Xing Xu
March 9, 2020

SECTION 1. SYSTEMATICS, FOSSIL RECORD, AND BIOGEOGRAPHY

Chapter 1

Pennaraptoran Systematics

MICHAEL PITTMAN,[1] JINGMAI O'CONNOR,[2] DANIEL J. FIELD,[3] ALAN H. TURNER,[4] WAISUM MA,[5] PETER MAKOVICKY,[6] AND XING XU[2]

ABSTRACT

New and important pennaraptoran specimens continue to be discovered on a regular basis. Yet, with these discoveries the number of viable phylogenetic hypotheses has increased, including ones that challenge the traditional grouping of dromaeosaurids and troodontids within a monophyletic Deinonychosauria. This chapter will cover recent efforts to address prevailing phylogenetic uncertainties and controversies, both between and within key clades, including deinonychosaurian monophyly, the phylogenetic position of anchiornithines and scansoriopterygids, and the interrelationships of enantiornithines. While recent discoveries mainly from Asia have created much of the latest uncertainty and controversy, new material, particularly from Asia, promises to rather fittingly address these issues. Further curatorship of long-standing phylogenetic datasets and more prevalent use of extended analytical protocols will be essential to meeting this challenge, especially for groups whose boundaries have been blurred. As it becomes increasingly difficult to study all fossil materials, owing to their growing numbers and ever disparate locations, broader use of digital fossils and online character databases for character coding is acutely needed to ensure that errors arising from remote, rather than firsthand, scoring are reduced as far as possible, particularly at this time of rapid data accumulation.

---

[1] Vertebrate Palaeontology Laboratory, Division of Earth and Planetary Science, the University of Hong Kong, Hong Kong.

[2] Key Laboratory of Vertebrate Evolution and Human Origins, Institute of Vertebrate Paleontology & Paleoanthropology, Beijing; CAS Center for Excellence in Life and Paleoenvironment, Beijing.

[3] Department of Earth Sciences, University of Cambridge, Cambridge.

[4] Department of Anatomical Sciences, Stony Brook University, Stony Brook, NY.

[5] School of Geography, Earth and Environmental Sciences, University of Birmingham, Birmingham, U.K.

[6] Department of Earth and Environmental Sciences, University of Minnesota, Minneapolis, MN.

PENNARAPTORAN SYSTEMATICS TODAY

This chapter will cover clade definitions, the relationships within clades as well as the occasional controversial relationships between different clades. Phylogenies arising from a recent iteration of the Theropod Working Group (TWiG) matrix by Pei et al. (2020) and the recent Mesozoic avialan matrix of Wang et al. (2018a) are used as the main comparative backbones in this section (see Methods), with every effort made to incorporate key findings from all previous work. We opt to consider a range of crown bird phylogenies here given substantial disagreements between them (see Crown Birds section below).

PENNARAPTORA FOTH ET AL., 2014: A node-based clade defined as the last common ancestor of *Oviraptor philoceratops* Osborn, 1924, *Deinonychus antirrhopus* Ostrom, 1969, and *Passer domesticus* Linnaeus, 1758, and all its descendants (Foth et al., 2014). Pennaraptora was proposed by Foth et al. (2014) on the basis of a phylogenetic analysis using a modified TWiG data matrix with the Latin *penna* meaning "bird feather" in reference to the pennaceous feathering shared by these animals. While it is possible that such feathers may yet have a wider distribution among theropods (Foth et al., 2014), as hinted by evidence from earlier-diverging coelurosaurians such as ornithomimosaurians (Zelenitsky et al., 2012; but see Xu, 2020), a close phylogenetic relationship between Paraves and Oviraptorosauria has been recovered by a range of studies including with both clades as sister taxa (Senter et al., 2012; Turner et al., 2012; Xu et al., 2015; Lefèvre et al., 2017), with Paraves in a sister relationship with a (Therizinosauria + Oviraptorosauria) clade (Makovicky et al., 2005), and with Paraves, Therizinosauria, Oviraptorosauria and Alvarezsauroidea in a polytomy (Choiniere et al., 2010). Agnolín and Novas (2013) recovered Alvarezsauroidea as the most closely related clade to Paraves with Oviraptorosauria sister to this grouping. Therizinosaurians and alvarezsauroids have been consistently recovered as the closest relatives of pennaraptorans. Each clade has been recovered as the most closely related to Pennaraptora (Therizinosauria: Senter et al., 2012; Turner et al., 2012; Xu et al., 2015; Alvarezsauroidea: Senter, 2007; Zanno, 2010) as well as in a trichotomy with Pennaraptora (Brusatte et al., 2014).

OVIRAPTOROSAURIA BARSBOLD, 1976: A stem-based taxon containing all maniraptorans closer to *Oviraptor philoceratops* Osborn, 1924, than to *Passer domesticus* Linnaeus, 1758 (sensu Sereno, 1998; Maryańska et al., 2002). Oviraptorosaurian fossils had been referred to ornithomimosaurians (e.g., Gauthier, 1986) and birds (e.g., Maryańska et al., 2002) largely due to their edentulous jaws, even though Oviraptorosauria had already been proposed as a new taxon (Barsbold, 1976). Despite being known from more than 40 reported genera, fully resolved interrelationships remain out of reach for a large portion of known oviraptorosaurian taxa, partly because some of them are missing significant amounts of data owing to their preservation as flattened and/or highly fragmentary specimens (Ji et al., 1998; Lü and Zhang, 2005; Zanno and Sampson, 2005; Sullivan et al., 2011; Longrich et al., 2013). Another obstacle to reconstructing fully resolved interrelationships is the lack of overlap between the elements preserved in specimens of different species. For example, several North American caenagnathid species are based solely on lower jaw remains whereas others are based on postcranial holotypes (Longrich et al., 2013), complicating the testing of taxonomic assignments and reconstruction of quantitative phylogenetic hypotheses (but see Funston and Currie, 2016, for an alternative view). *Incisivosaurus* has been recovered as the earliest-diverging oviraptorosaurian by a number of analyses that excluded oviraptorosaurian taxa known from poorly preserved specimens, e.g., *Protarchaeopteryx*, *Ningyuansaurus*, and *Luoyanggia* (Longrich et al., 2013; Brusatte et al., 2014; Lamanna et al., 2014; Lü et al., 2016, 2017; Pei et al., 2020) (figs. 1, 2A, C). However, if these poorly known taxa are included, early-diverging oviraptorosaurians collapse into a polytomy (Funston and Currie, 2016; Yu et al., 2018; fig. 2B, D). Oviraptorosauria has two main lineages, the Caenagnathidae and the Oviraptoridae, that are consistently recovered as monophyletic sister taxa (Longrich et al., 2013; Lamanna et al., 2014; Lü et al., 2015; Funston and Currie, 2016; Lü et al., 2016; Lü et al., 2017; Yu et al., 2018; fig. 2A–D). These two lineages together form the Caenagnathoidea, which is sister to *Avimimus* (Lamanna et al., 2014; Pei et al., 2020) (fig. 1). Within Caenagnathidae, *Microvenator* and the giant *Gigantoraptor* are consistently recovered as early-diverging members, whereas the interrelationships between later-diverging members remain unresolved largely due to the issue of nonoverlapping elements between specimens of different species (Lamanna et al., 2014; Lü et al., 2015; Lü et al., 2016; Lü et al., 2017; fig. 2C). Taxonomic revision of problematic taxa like *Caenagnathus sternbergi*, *Macrophalangia canadensis*, and "Alberta dentary morph 3" (fig. 2A) and the exclusion of poorly known taxa from the matrix like *Leptorhynchos gaddisi* and *Ojoraptorsaurus* has improved topological resolution among later-diverging caenagnathids (Funston and Currie, 2016; Yu et al., 2018; fig. 2B, D). *Elmisaurus*, *Apatoraptor*, and *Leptorhynchos elegans* are consistently recovered as the three latest-diverging caenagnathids, although the position of *Apatoraptor* and *Leptorhynchos gaddisi* interchanged in two recent analyses (Funston and Currie, 2016; Yu et al., 2018; fig. 2B, D). Previously, two sister clades have been recovered within Oviraptoridae, the Oviraptorinae and Ingeniinae (Longrich et al., 2010). Over the past decade, successive discoveries of new Chinese oviraptorids preserving interesting character combinations have unsurprisingly collapsed many parts of the phylogeny into different polytomies (Longrich et al., 2013; Lamanna et al., 2014; Lü et al., 2015, 2016, 2017). Funston and Currie (2016) and Yu et al. (2018) provide the most highly resolved interrelationships among oviraptorids to date: *Nankangia* is recovered as the earliest-diverging oviraptorid and all polytomies are resolved (fig. 2B, D). The oviraptorid interrelationships of these two phylogenies are largely consistent with those of other recent analyses (Lamanna et al., 2014; Lü et al., 2015, 2016, 2017), except the placement of *Ganzhousaurus* at an earlier-diverging position (fig. 2B–D). However, this topological resolution may be short-lived as many newly reported Chinese specimens have yet to be included, e.g., *Huanansaurus*, *Tongtianlong*, *Beibeilong*, and *Corythoraptor* (Lü et al., 2015, 2016, 2017; Pu et al., 2017). Thus, while a phenomenal amount of oviraptorosaurian material is known, including specimens subject to detailed monographic work, future work combining and updating existing phylogenetic datasets is a much-needed priority (Funston and Currie, 2016; Lü et al., 2017).

Oviraptorosauria is generally seen as the sister clade of Paraves, together forming the more inclusive clade Pennaraptora (Brusatte et al., 2014; Foth et al., 2014; Xu et al., 2017; Pei et al., 2020) (see Pennaraptora and Paraves sections below). However, the phylogenetic placement of Scansoriopterygidae within Pennaraptora has been contentious. Scansoriopterygids have been placed within Avialae (Xu et al., 2011; Senter et al., 2012; O'Connor and Sullivan, 2014), as an early-diverging lineage within Oviraptorosauria (Agnolín and Novas, 2013; Brusatte et al., 2014; Agnolín et al. 2019; Pei et al., 2020), as an early-diverging paravian clade outside the traditional (Deinonychosauria + Avialae) clade (Turner et al., 2012; Xu et al., 2015; Lefèvre et al., 2017), and in a polytomy with Deinonychosauria and Avialae (Xu et al., 2017). Herein we consider Scansoriopterygidae to be early-branching oviraptorosaurians (fig. 1). More exhaustive descriptions of scansoriopterygid specimens as well as application of developmental insights to the study of nonadult scansoriopterygids may help to give this group a more stable phylogenetic position. This is sorely needed to deepen our understanding of oviraptorosaurians and early-diverging pennaraptorans more broadly.

Paraves Sereno 1997: A stem-based taxon containing *Passer domesticus* Linnaeus, 1758, and all coelurosaurians closer to it than to *Ovi-*

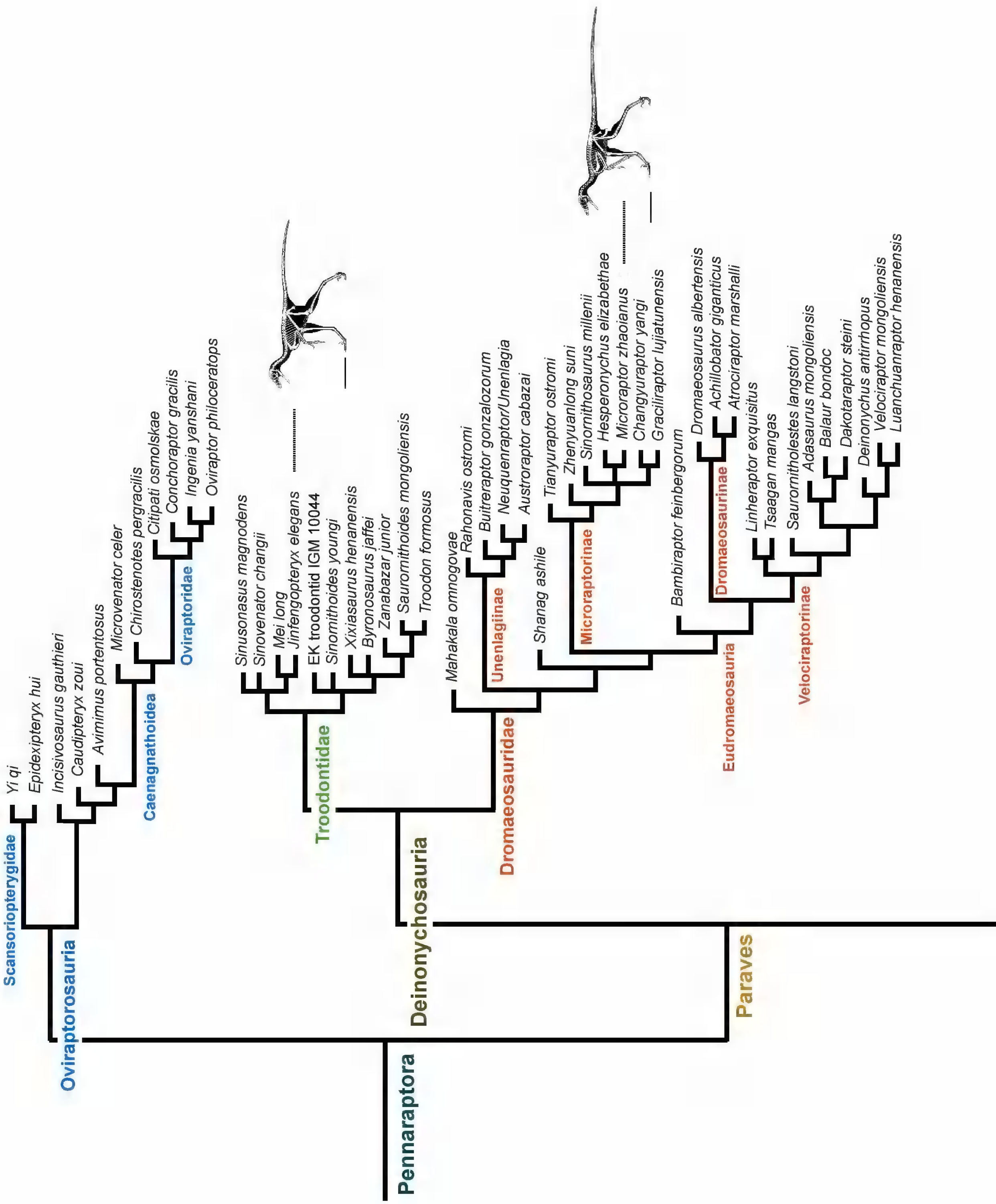
Pennaraptora
Oviraptorosauria
Scansoriopterygidae
Yi qi
Epidexipteryx hui
Incisivosaurus gauthieri
Caudipteryx zoui
Avimimus portentosus
Caenagnathoidea
Microvenator celer
Chirostenotes pergracilis
Oviraptoridae
Citipati osmolskae
Conchoraptor gracilis
Ingenia yanshani
Oviraptor philoceratops
Paraves
Deinonychosauria
Troodontidae
Sinusonasus magnodens
Sinovenator changii
Mei long
Jinfengopteryx elegans
EK troodontid IGM 10044
Sinornithoides youngi
Xixiasaurus henanensis
Byronosaurus jaffei
Zanabazar junior
Saurornithoides mongoliensis
Troodon formosus
Dromaeosauridae
Mahakala omnogovae
Unenlagiinae
Rahonavis ostromi
Buitreraptor gonzalozorum
Neuquenraptor/Unenlagia
Austroraptor cabazai
Shanag ashile
Microraptorinae
Tianyuraptor ostromi
Zhenyuanlong suni
Sinornithosaurus millenii
Hesperonychus elizabethae
Microraptor zhaoianus
Changyuraptor yangi
Graciliraptor lujiatunensis
Eudromaeosauria
Bambiraptor feinbergorum
Dromaeosaurinae
Dromaeosaurus albertensis
Achillobator giganticus
Atrociraptor marshalli
Velociraptorinae
Linheraptor exquisitus
Tsaagan mangas
Saurornitholestes langstoni
Adasaurus mongoliensis
Balaur bondoc
Dakotaraptor steini
Deinonychus antirrhopus
Velociraptor mongoliensis
Luanchuanraptor henanensis

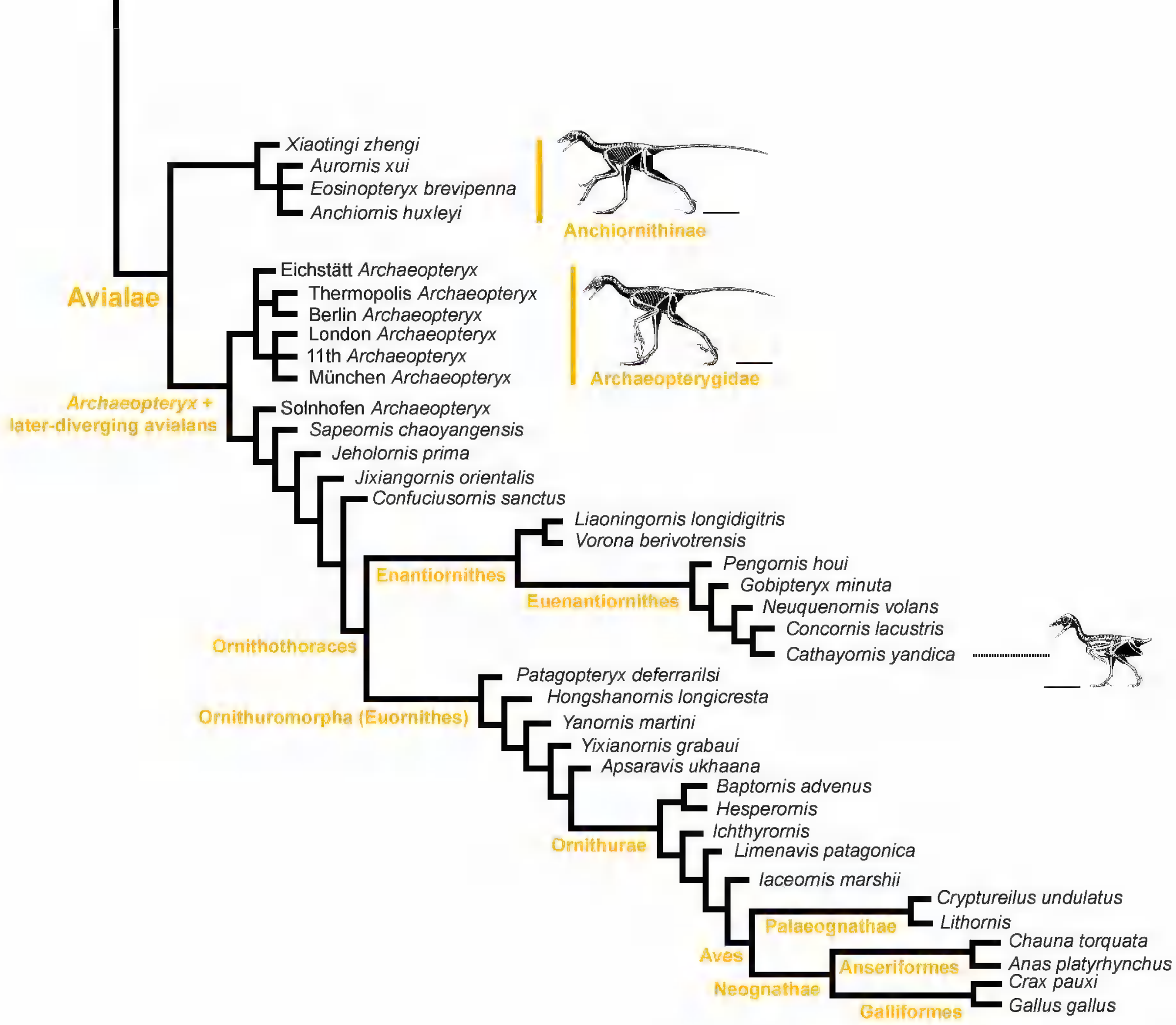
Xiaotingi zhengi
Aurornis xui
Eosinopteryx brevipenna
Anchiornis huxleyi
Anchiornithinae
Avialae
Eichstätt Archaeopteryx
Thermopolis Archaeopteryx
Berlin Archaeopteryx
London Archaeopteryx
11th Archaeopteryx
München Archaeopteryx
Archaeopterygidae
Archaeopteryx + later-diverging avialans
Solnhofen Archaeopteryx
Sapeornis chaoyangensis
Jeholornis prima
Jixiangornis orientalis
Confuciusornis sanctus
Liaoningornis longidigitris
Vorona berivotrensis
Enantiornithes
Euenantiornithes
Pengornis houi
Gobipteryx minuta
Neuquenornis volans
Concornis lacustris
Cathayornis yandica
Ornithothoraces
Patagopteryx deferrarilsi
Hongshanornis longicresta
Ornithuromorpha (Euornithes)
Yanornis martini
Yixianornis grabaui
Apsaravis ukhaana
Baptornis advenus
Hesperornis
Ichthyrornis
Ornithurae
Limenavis patagonica
Iaceornis marshii
Crypturellus undulatus
Lithornis
Palaeognathae
Aves
Chauna torquata
Anseriformes
Anas platyrhynchus
Neognathae
Crax pauxi
Gallus gallus
Galliformes

FIG. 1. Pennaraptoran reduced strict consensus tree using extended implied character weighting in analysis of updated TWiG dataset (modified from Pei et al., 2020). Skeletal reconstructions used with the permission of Scott A. Hartman. Scale bars = 10 cm.

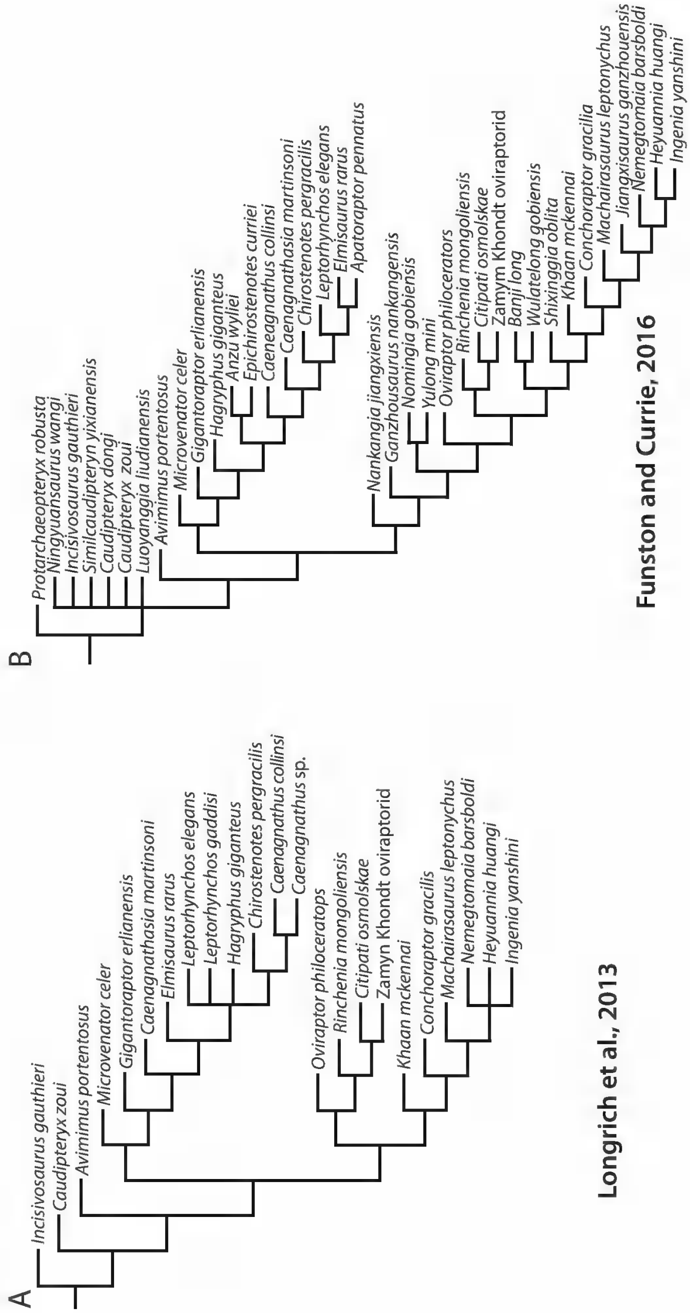
A
Incisivosaurus gauthieri
Caudipteryx zoui
Avimimus portentosus
Microvenator celer
Gigantoraptor erlianensis
Caenagnathasia martinsoni
Elmisaurus rarus
Leptorhynchos elegans
Leptorhynchos gaddisi
Hagryphus giganteus
Chirostenotes pergracilis
Caenagnathus collinsi
Caenagnathus sp.
Oviraptor philoceratops
Rinchenia mongoliensis
Citipati osmolskae
Zamyn Khondt oviraptorid
Khaan mckennai
Conchoraptor gracilis
Machairasaurus leptonychus
Nemegtomaia barsboldi
Heyuannia huangi
Ingenia yanshini
Longrich et al., 2013
B
Protarchaeopteryx robusta
Ningyuansaurus wangi
Incisivosaurus gauthieri
Similcaudipteryn yixianensis
Caudipteryx dongi
Caudipteryx zoui
Luoyanggia liudianensis
Avimimus portentosus
Microvenator celer
Gigantoraptor erlianensis
Hagryphus giganteus
Anzu wyliei
Epichirostenotes curriei
Caeneagnathus collinsi
Caenagnathasia martinsoni
Chirostenotes pergracilis
Leptorhynchos elegans
Elmisaurus rarus
Apatoraptor pennatus
Nankangia jiangxiensis
Ganzhousaurus nankangensis
Nomingia gobiensis
Yulong mini
Oviraptor philoceratops
Rinchenia mongoliensis
Citipati osmolskae
Zamym Khondt oviraptorid
Banji long
Wulatelong gobiensis
Shixinggia oblita
Khaan mckennai
Conchoraptor gracilia
Machairasaurus leptonychus
Jiangxisaurus ganzhouensis
Nemegtomaia barsboldi
Heyuannia huangi
Ingenia yanshini
Funston and Currie, 2016

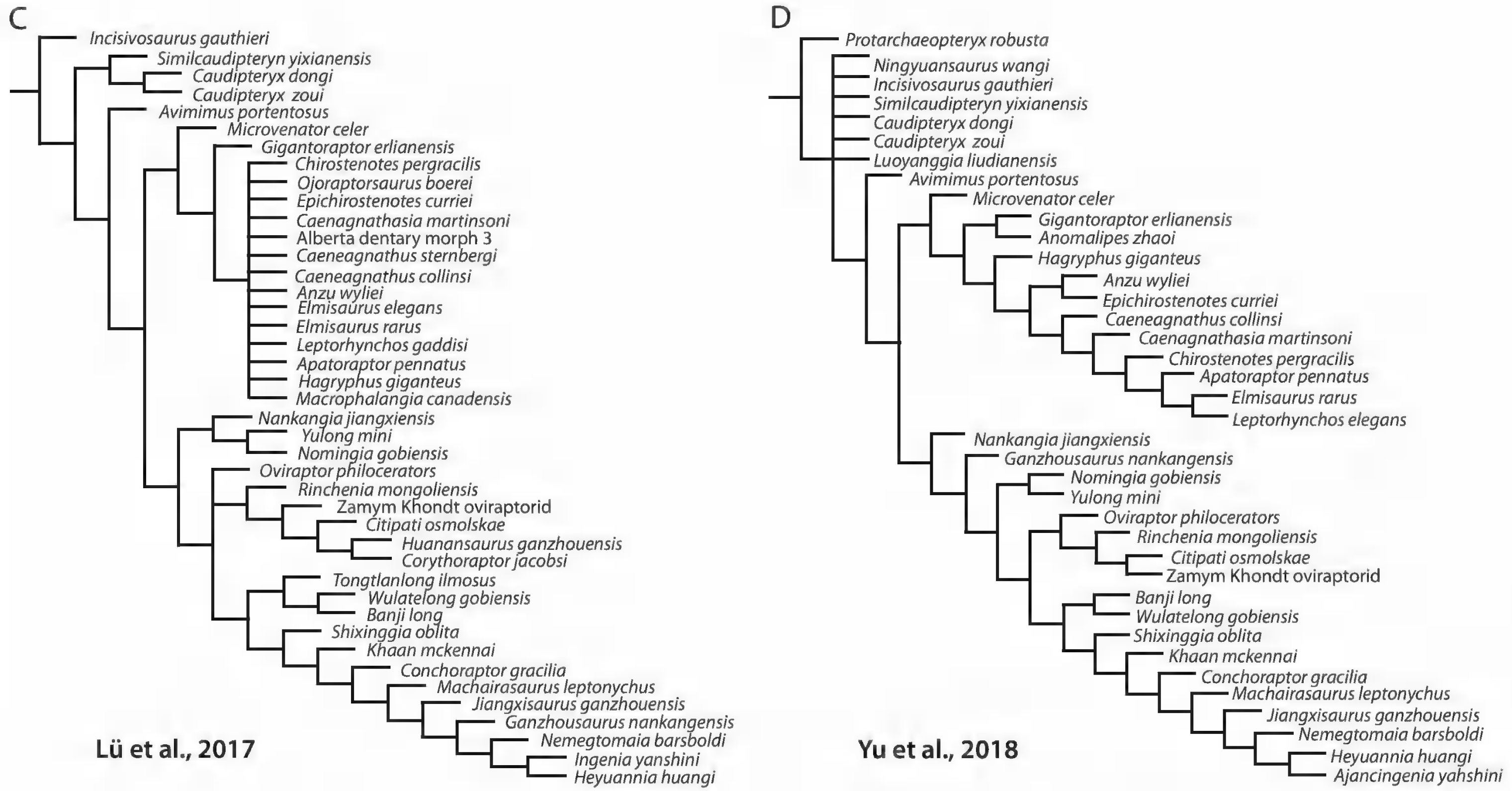
C
Incisivosaurus gauthieri
Similcaudipteryn yixianensis
Caudipteryx dongi
Caudipteryx zoui
Avimimus portentosus
Microvenator celer
Gigantoraptor erlianensis
Chirostenotes pergracilis
Ojoraptorsaurus boerei
Epichirostenotes curriei
Caenagnathasia martinsoni
Alberta dentary morph 3
Caeneagnathus sternbergi
Caeneagnathus collinsi
Anzu wyliei
Elmisaurus elegans
Elmisaurus rarus
Leptorhynchos gaddisi
Apatoraptor pennatus
Hagryphus giganteus
Macrophalangia canadensis
Nankangia jiangxiensis
Yulong mini
Nomingia gobiensis
Oviraptor philocerators
Rinchenia mongoliensis
Zamym Khondt oviraptorid
Citipati osmolskae
Huanansaurus ganzhouensis
Corythoraptor jacobsi
Tongtlanlong ilmosus
Wulatelong gobiensis
Banji long
Shixinggia oblita
Khaan mckennai
Conchoraptor gracilia
Machairasaurus leptonychus
Jiangxisaurus ganzhouensis
Ganzhousaurus nankangensis
Nemegtomaia barsboldi
Ingenia yanshini
Heyuannia huangi
Lü et al., 2017
D
Protarchaeopteryx robusta
Ningyuansaurus wangi
Incisivosaurus gauthieri
Similcaudipteryn yixianensis
Caudipteryx dongi
Caudipteryx zoui
Luoyanggia liudianensis
Avimimus portentosus
Microvenator celer
Gigantoraptor erlianensis
Anomalipes zhaoi
Hagryphus giganteus
Anzu wyliei
Epichirostenotes curriei
Caeneagnathus collinsi
Caenagnathasia martinsoni
Chirostenotes pergracilis
Apatoraptor pennatus
Elmisaurus rarus
Leptorhynchos elegans
Nankangia jiangxiensis
Ganzhousaurus nankangensis
Nomingia gobiensis
Yulong mini
Oviraptor philocerators
Rinchenia mongoliensis
Citipati osmolskae
Zamym Khondt oviraptorid
Banji long
Wulatelong gobiensis
Shixinggia oblita
Khaan mckennai
Conchoraptor gracilia
Machairasaurus leptonychus
Jiangxisaurus ganzhouensis
Nemegtomaia barsboldi
Heyuannia huangi
Ajancingenia yahshini
Yu et al., 2018

FIG. 2. Existing oviraptorosaurian phylogenies. **A.** Adams consensus tree of Longrich et al. (2013). **B.** Strict consensus tree of Funston and Currie (2016). **C.** Strict consensus tree of Lü et al. (2017). **D.** Strict consensus of Yu et al. (2018).

raptor philoceratops Osborn, 1924 (sensu Holtz and Osmólska, 2004; after Turner et al., 2012). The last main iteration of the TWiG matrix (Pei et al., 2020) produced a pruned, reduced consensus tree that reaffirmed that Paraves comprises exclusively of Deinonychosauria and Avialae (Gauthier, 1986; Sereno, 1997; Norell et al., 2001; Senter et al., 2004, 2012; Turner et al., 2007a, 2012), bringing recent uncertainty associated with the Brusatte et al. (2014) matrix iteration to a close. Disregarding the most unstable taxa, reasonable group supports (frequency differences between 76 and 100) were calculated by means of no-zero-weight symmetric resampling (Goloboff et al., 2003) for Paraves and the key internal nodes Troodontidae, Dromaeosauridae, Unenlagiinae, and Eudromaeosauria in a recent TWiG study (Pei et al., 2020). The no-zero-weight resampling increases or decreases character weights, but never eliminates characters. With no-zero-weight resampling, support is lowered only because of conflict among characters and not just because of absence of information; it is thus an appropriate resampling scheme for palaeontological datasets. The identification of rogue taxa was carried out in two steps, first identifying a list of possible rogues with a heuristic procedure (the *chkmoves* command of TNT), then selecting taxon subsets from that list with an optimality-based method (the *prupdn* command of TNT). This combined routine was implemented in a script called *bothprunes* (see Pei et al., 2020, for additional details). Other datasets generally have low nodal supports for paravian nodes (Senter et al., 2012; Turner et al., 2012; Brusatte et al., 2014; Foth et al., 2014; Xu et al., 2015), with Bremer supports typically between 1 and 2 for most of them (but see Xu et al., 2015). Despite the differences in pennaraptoran interrelationships recovered in previous studies (Zheng et al., 2009; Xu et al., 2010, 2011, 2015; Senter et al., 2012; Turner et al., 2012; Evans et al., 2013; Godefroit et al., 2013a, 2013b; Brusatte et al., 2014; Foth et al., 2014; Cau et al., 2015; DePalma et al., 2015) there are some seemingly robust paravian synapomorphies: a laterally facing glenoid fossa was recovered by Pei et al. (2020) and at the equivalent node by Turner et al. (2012) and Brusatte et al. (2014) and is related to the extension of the glenoid floor onto the external surface of the scapula, a paravian synapomorphy of Agnolín and Novas (2013), Senter et al. (2012), and Xu et al. (2015), and a synapomorphy of Foth et al. (2014) for the node (*Jinfengopteryx* + Paraves). Agnolín and Novas (2013), Brusatte et al. (2014), and Pei et al. (2020) recover paravians as sharing a proximal surface of ulna that is divided into two distinct fossae. At the paravian node in Pei et al. (2020) and at the node (Deinonychosauria + Avialae) in Turner et al. (2012) and Brusatte et al. (2014), an acromion margin of the scapula with a laterally everted anterior edge is also shared. Three equivalent paravian synapomorphies were recovered by Pei et al. (2020), Brusatte et al. (2014), and Senter et al. (2012), one of which was also recovered by Xu et al. (2015) and Agnolín and Novas (2013): basipterygoid process absent or very subtle; carotid process present on posterior cervical vertebrae; posterior trochanter is developed as a slightly projected tubercle or flange. Additionally, short and stout proximal chevrons were recovered as a common synapomorphy in this study and in Brusatte et al. (2014) and Xu et al. (2015). Some paravian synapomorphies have been shown to have a more inclusive distribution. For example, large maxillary and dentary teeth and an astragalus fused to the calcaneum but not to the tibia were paravian synapomorphies in the analysis of Turner et al. (2012), but Pei et al. (2020) found these to be avialan and deinonychosaurian synapomorphies respectively. However, some reconstructed tree topologies have been so seemingly different that their synapomorphies have no overlap with other studies. For example, Foth et al. (2014) found that avialans share closer affinities to troodontids than to dromaeosaurids and recovered anchiornithines as early-diverging birds.

DEINONYCHOSAURIA COLBERT AND RUSSELL, 1969: A node-based taxon containing the last common ancestor of *Troodon formosus* Leidy, 1856, and *Velociraptor mongoliensis* Osborn, 1924, and all its descendants (sensu Sereno, 1998; after Turner et al., 2012). Dromaeosaurids and troodontids have been traditionally united as the Deinonychosauria by the "sickle claw" on their second toe among other characteristics and considered the sister group of birds (Gauthier, 1986; Sereno, 1997; Norell et al., 2001, 2009; Makovicky et al., 2005; Novas and Pol, 2005; Senter, 2007; Senter et al., 2012; Turner et al., 2012). A deluge of discoveries over the last decade has called this status quo into question (Lü et al., 2007; Senter et al., 2012; Evans et al., 2013; Godefroit et al., 2013a; Godefroit et al., 2013b; Foth et al., 2014; DePalma et al., 2015; Lü and Brusatte, 2015; Pittman et al., 2015), seemingly supporting every combination of taxa and demonstrating that historically diagnostic features of the clade have more inclusive distributions than once thought or have parallel origins (Zheng et al., 2009; Xu et al., 2010, 2015; Xu et al., 2011; Senter et al., 2012; Turner et al., 2012; Evans et al., 2013; Godefroit et al., 2013a, 2013b; Brusatte et al., 2014; Foth et al., 2014; Cau et al., 2015; DePalma et al., 2015). Deinonychosaurian monophyly was reaffirmed in a recent TWiG study under both extended implied-weighting and equal-weighting searches and in the strict consensus trees (Pei et al., 2020; fig. 1), as well as independently (Lefèvre et al., 2017). Seemingly robust synapomorphies of this clade include: a splenial exposed as a broad triangle in the lateral surface of the dentary between the dentary and angular (Senter et al., 2012; Turner et al., 2012; Pei et al., 2020); dorsal vertebrae with interspinous ligament scars that terminate below the apex of the neural spine (Turner et al., 2012; Pei et al., 2020); an astragalus fused to the calcaneum but not to the tibia (Turner et al., 2012; Brusatte et al., 2014; Pei et al., 2020); penultimate phalanx of digit II highly modified for extreme hyperextension, and its ungual is larger and more curved than that of digit III (Turner et al., 2012; Pei et al., 2020), but a dromaeosaurid synapomorphy in Brusatte et al. (2014) and equivalent to synapomorphies of Senter et al. (2012) and Xu et al. (2015); slightly raised bicipital scar of the ulna (Turner et al., 2012; Pei et al., 2020).

DROMAEOSAURIDAE MATTHEW AND BROWN, 1922: A stem-based taxon containing *Dromaeosaurus albertensis* Matthew and Brown, 1922, and all deinonychosaurians closer to it than to *Troodon formosus* Leidy, 1856, or *Passer domesticus* Linnaeus, 1758 (sensu Sereno, 1998; after Turner et al., 2012). This clade is consistently supported by robust synapomorphies, particularly in relation to the paroccipital process of the skull. The dromaeosaurid paroccipital process is: elongate and slender with nearly parallel dorsal and ventral edges (Turner et al., 2012; Brusatte et al., 2014; Foth et al., 2014; Pei et al., 2020); has a dorsal edge twisted anterolaterally at its distal end (Turner et al., 2012; Brusatte et al., 2014; Foth et al., 2014; Pei et al., 2020); possesses a ventral flange at its distal end (Brusatte et al., 2014; Pei et al., 2020); and has a ventral edge at its base that is situated at the midheight of the occipital condyle or further ventrally (Brusatte et al., 2014; Pei et al., 2020). Other cranium-based synapomorphies include dentary and maxillary teeth with confluent tooth crowns and roots (Turner et al., 2012; Brusatte et al., 2014; Foth et al., 2014; Pei et al., 2020) as well as an anterior location of the anterior tympanic recess and anterior tympanic crista, with little or no development of the recess posterior to the basipterygoid processes (Turner et al., 2012; Brusatte et al., 2014; Foth et al., 2014; Pei et al., 2020). Past studies are contradictory on the absence/presence of the accessory tympanic recess dorsal to the crista interfenestralis: absent according to Turner et al. (2012) and Pei et al. (2020) but present according to Brusatte et al. (2014) and Foth et al. (2014). Two of the few robust postcranial synapomorphies are: posterior trunk vertebrae with parapophyses projected distinctly on pedicels (Turner et al., 2012; Brusatte et al., 2014; Foth et al., 2014; Pei et al., 2020) and a well-developed ginglymus on the distal end of metatarsal II (Turner et al., 2012; Agnolín and Novas, 2013; Brusatte et al., 2014; Foth et al., 2014; Pei et al., 2020). Rogue taxa can significantly impact support for previously recovered dromaeosaurid synapomorphies, e.g., many synapomorphies are shared with the analysis of Foth et al. (2014) only if *Pyroraptor* is pruned. The basic dromaeosaurid topology places unenlagiines at an earlier-diverging position and microraptorines and Eudromaeosauria at later-diverging positions (Senter, 2007; Senter et al., 2012; Turner et al., 2012; Evans et al., 2013; Brusatte et al., 2014; Foth et al., 2014; Han et al., 2014; DePalma et al., 2015; Lü and Brusatte, 2015; Pei et al., 2020; fig. 1). However, some analyses have suggested that unenlagiines and microraptorines are early-branching members of Averaptora, a paravian clade that includes avialans and is most closely related to dromaeosaurids (Agnolín and Novas, 2011; Agnolín and Novas, 2013). *Mahakala* is typically recovered as the earliest-diverging dromaeosaurid (Turner et al., 2007a, 2012; Brusatte et al., 2014; Pei et al., 2020) potentially forming a clade with an additional dromaeosaurid from the Djadokhta Formation, *Halszkaraptor escuilliei* (Cau et al., 2017). This early-diverging clade is then followed by the Unenlagiinae. Unenlagiinae Bonaparte, 1999, is a stem-based taxon containing *Unenlagia comahuensis* Novas and Puerta, 1997, and all coelurosaurs closer to it than to *Velociraptor mongoliensis* Osborn, 1924, *Dromaeosaurus albertensis* Matthew and Brown, 1922, *Microraptor zhaoianus* Xu et al., 2000, and *Passer domesticus* Linnaeus, 1758 (sensu Sereno et al., 2005; after Turner et al., 2012). Within the group, *Austroraptor* is typically recovered as a sister taxon of *Unenlagia*, which are both in turn sister to *Buitreraptor* (Turner et al., 2012; Agnolín and Novas, 2013; Pei et al., 2020). *Rahonavis*, originally described as a long, bony-tailed bird (Forster et al., 1996), has been identified as a member of the Unenlagiinae (Makovicky et al., 2005) with additional referred material and anatomical work continuing to support that relationship (Forster et al., 2020), but some authors still find it to be an early-diverging avialan (Agnolín and Novas, 2013; Agnolín et al. 2019). Unenlagiine synapomorphies shared by some recent studies include a pubic shaft that is vertically oriented when articulated and an ilium with a reduced supraacetabular crest that is still separate from the antitrochanter (Foth et al., 2014; Pei et al., 2020) and has a postacetabular process with a concave dorsal edge (Agnolín and Novas, 2013; Pei et al., 2020). (Microraptorinae + Eudromaeosauria) is usually recovered as the latest-diverging dromaeosaurid clade (Senter et al., 2012; Turner et al., 2012; Brusatte et al., 2014; Xu et al., 2015; Pei et al., 2020; fig. 1). Pei et al. (2020) found this clade to lack a deep and sharp groove on the lateral side of the dentary and to have a relatively reduced maxillary fenestra.

Microraptorinae Senter et al., 2004, is a stem-based taxon containing *Microraptor zhaoianus* Xu et al., 2000, and all coelurosaurians closer to it than to *Dromaeosaurus albertensis* Matthew and Brown, 1922, *Velociraptor mongoliensis* Osborn, 1924, *Unenlagia comahuensis* Novas and Puerta, 1997, and *Passer domesticus* Linnaeus, 1758 (sensu Sereno et al., 2005; after Turner et al., 2012). Microraptorine interrelationships have been elusive in main TWiG dataset studies (Turner et al., 2012; Brusatte et al., 2014) as well as related ones (Lü and Brusatte, 2015), but some datasets relying on TWiG data as its backbone have recovered resolved microraptorine topologies (Senter et al., 2012; Xu et al., 2015). Both Pei et al. (2020) and Gianechini et al. (2018) extended this improved resolution to a main TWiG study by recovering the two largest microraptorines, *Tianyuraptor* and *Zhenyuanlong*, as the earliest-diverging microraptorines (fig. 1), as suggested by Senter et al. (2012) for *Tianyuraptor*, but contrary to the eudromaeosaurian affinity recovered by DePalma et al. (2015). This is supported by the lack of prominent median posterior process along the posterior edge of the ischium in *Tianyuraptor* and *Zhenyuanlong*, unlike other microraptorines and some early-diverging paravians (Pei et al., 2020). Clarifying the character state distributions of several potentially important features will help to test this phylogenetic hypothesis. For example, a posteriorly curved pubis and a radial shaft less than half of the ulnar width were recovered as synapomorphies of smaller-bodied microraptorines excluding *Tianyuraptor* (Pei et al., 2020), but as microraptorine synapomorphies by Xu et al. (2015) and Agnolín and Novas (2013). Pei et al. (2020) found a proximally pinched metatarsal III was shared by a more inclusive group of microraptorines excluding *Tianyuraptor* and *Zhenyuanlong*, whereas Senter et al. (2012) recovered this as a microraptorine synapomorphy. Small-bodied microraptorines have a subarctometatarsalian foot that is absent in *Zhenyuanlong* and has an uncertain condition in *Tianyuraptor*. The plesiomorphic unspecialized pedal phalanx II-2 appears to be present in small-bodied microraptorines whereas the specialized condition exists in *Zhenyuanlong* but is unknown in *Tianyuraptor*. Pruning incomplete specimens like IVPP V22530 substantially improves the resolution of later-diverging microraptorine interrelationships (Pei et al., 2020). Using automated phylogenetic analysis pipelines (Pei et al., 2020) to further explore the impact of rogue taxa on microraptorine phylogeny would therefore be worthwhile. It is important to bear in mind that some studies have recovered microraptorines as the closest avialan relatives as part of a paravian clade called Averaptora, rather than as dromaeosaurids (Agnolín and Novas, 2011, 2013). Thus, more work is clearly needed to bridge this large discrepancy.

Eudromaeosauria Longrich and Currie, 2009, includes the vast majority of dromaeosaurids. It is a node-based taxon containing the last common ancestor of *Saurornitholestes langstoni* Sues, 1978, *Deinonychus antirrhopus* Ostrom, 1969, *Dromaeosaurus albertensis* Matthew and Brown, 1922, and *Velociraptor mongoliensis* Osborn, 1924, and all its descendants (Longrich and Currie, 2009; sensu Turner et al., 2012). Long-standing eudromaeosaurian synapomorphies include: a sharp demarcation between the postorbital process and the frontal orbital margin in dorsal view (Turner et al., 2012; Pei et al., 2020); a pedal phalanx II-2 with a long and lobate flexor heel with the midline ridge extending onto its dorsal surface (Turner et al., 2012; Pei et al., 2020); thoracic centra approximately equal in anteroposterior length and midpoint mediolateral width (Foth et al., 2014, after *Pyroraptor* is pruned; Pei et al., 2020); lateral surfaces of dorsal vertebrae possess pneumatic foramina (Pei et al., 2020; equivalent node in Xu et al., 2015; clade with equivalent taxa in Agnolín and Novas, 2013).

A relatively early-diverging position was recovered for the diminutive *Bambiraptor* within Eudromaeosauria (Senter et al., 2012; Agnolín and Novas, 2013; DePalma et al., 2015; Pei et al., 2020; fig. 1), but *Bambiraptor* and *Saurornitholestes* were nested within Velociraptorinae in recent main TWiG dataset studies (Turner et al., 2012; Brusatte et al., 2014), and indeed their taxonomic distinction is based on a few traits that are known to change ontogenetically. The long-standing monophyletic subclades Dromaeosaurinae and Velociraptorinae are still maintained, but not without pruning several species known from fragmentary remains (*Yurgovuchia*, *Acheroraptor*, *V. osmolskae*, and *Utahraptor*) (Pei et al., 2020; fig. 1). Dromaeosaurinae Matthew and Brown, 1922, is a stem-based taxon containing *Dromaeosaurus albertensis* Matthew and Brown, 1922, and all coelurosaurians closer to it than to *Velociraptor mongoliensis* Osborn, 1924, *Microraptor zhaoianus* Xu, 2000, *Unenlagia comahuensis* Novas and Puerta, 1997, and *Passer domesticus* Linnaeus, 1758 (sensu Sereno et al., 2005; after Turner et al., 2012). Dromaeosaurines appear to share serrations on all premaxillary and maxillary teeth and have premaxillary teeth that all have a D-shaped cross section (Turner et al., 2012; Pei et al., 2020). However, Pei et al. (2020) recovered these synapomorphies despite pruning *Utahraptor*. That study found *Dromaeosaurus* in a sister relationship with (*Achillobator* + *Atrociraptor*) as in Turner et al. (2012), but unlike Xu et al. (2015), where *Dromaeosaurus* is later diverging than *Achillobator* and *Atrociraptor* and also unlike Brusatte et al. (2014) where these taxa are paraphyletic. Velociraptorinae Barsbold, 1983, is a stem-based taxon containing *Velocirap-*

tor mongoliensis Osborn, 1924, and all coelurosaurians closer to it than to *Dromaeosaurus albertensis* Matthew and Brown, 1922, *Microraptor zhaoianus* Xu, 2000, *Unenlagia comahuensis* Novas and Puerta, 1997, and *Passer domesticus* Linnaeus, 1758 (sensu Sereno et al., 2005; after Turner et al., 2012). Pei et al. (2020) recovered (*Linheraptor* + *Tsaagan*) as the earliest-diverging velociraptorine clade, but remaining velociraptorine interrelationships were controversial as they differed between the two weighting schemes adopted. Later-diverging velociraptorine interrelationships were better resolved at the expense of *Luanchuanraptor* and *V. osmolskae*: *Deinonychus* was recovered as a later-diverging velociraptorine than (*Linheraptor* + *Tsaagan*), which has a sister relationship with *Adasaurus* and the clade (*Balaur* + *Dakotaraptor*). *Balaur*, a strange double-sickle-clawed velociraptorine (Csiki et al., 2010; Turner et al., 2012; Brusatte et al., 2013; Lü and Brusatte, 2015), has also been recovered as an avialan (Cau et al., 2015). *Dakotaraptor* is a eudromaeosaurian that has been recovered as both a velociraptorine (Pei et al., 2020) and as a dromaeosaurine (DePalma et al., 2015). Recent analyses have not converged on the same velociraptorine synapomorphies (Turner et al., 2012; Brusatte et al., 2014; Pei et al., 2020), but some potential ones are worth bearing in mind: cranial nerve X–XII openings located in a shallow bowl-like depression; basal tubera dorsoventrally deeper than the occipital condyle. Pei et al. (2020) recovered *Yurgovuchia*, *Acheroraptor*, *V. osmolskae*, and *Utahraptor* as rogue taxa in their analysis. This is not unexpected as they are all based on fragmentary material that is missing the anatomy relating to dromaeosaurine and velociraptorine synapomorphies. *Utahraptor* is the best preserved among these four taxa but still has a poorly resolved phylogenetic position despite possessing at least one dromaeosaurine synapomorphy (Pei et al., 2020). Ongoing descriptive work on a range of different-sized *Utahraptor* individuals (Jim Kirkland, personal commun.) has particular promise in further elucidating eudromaeosaurian phylogeny. Dromaeosaurids are known for their "rodlike" tails that deviate from the typical coelurosaurian tail condition (Senter et al., 2012; Pittman et al., 2013), but unlike Senter et al. (2012), Pei et al. (2020) did not recover tail-based synapomorphies at any internal dromaeosaurid nodes except as a trait of *Luanchuanraptor*. This hints that their tail evolution may be more complex than previously appreciated or that a more sequential evolutionary pattern may yet emerge as more anatomical data becomes available in the future.

TROODONTIDAE GILMORE, 1924: This group is defined as a stem-based taxon containing *Troodon formosus* Leidy, 1856, and all coelurosaurians closer to it than to *Velociraptor mongoliensis* Osborn, 1924, or *Passer domesticus* Linnaeus, 1758 (sensu Sereno, 1998; after Turner et al., 2012). Troodontid phylogeny is probably the least resolved of the paravian groups and does not have subclades established to the same degree as in dromaeosaurid and avialan phylogeny. Seemingly persistent troodontid synapomorphies include a laterally expanded supraorbital crest of the lacrimal anterior and dorsal to the orbit (Turner et al., 2012; Foth et al., 2014; Pei et al., 2020) (excluding anchiornithines); an asymmetrical foot with a slender metatarsal II and a very robust metatarsal IV (Turner et al., 2012; Foth et al., 2014; Pei et al., 2020) (excluding anchiornithines); metatarsal IV wider than either II or III (Turner et al., 2012; Pei et al., 2020) (excluding anchiornithines); smaller, more numerous and more closely appressed anterior dentary teeth compared to those in the middle of the tooth row (Senter et al., 2012; Brusatte et al., 2014; Pei et al., 2020) (in Brusatte et al., 2014, the anchiornithines are included); metatarsal II shorter than IV, but reaching distally further than the base of the metatarsal IV trochlea (Foth et al., 2014; Pei et al., 2020); absence of the basisphenoid recess between the basisphenoid and basioccipital (Xu et al., 2015; Pei et al., 2020); oval foramen magnum taller than wide (Xu et al., 2015; Pei et al., 2020); dentary teeth set in an open groove (Xu et al., 2015; Pei et al., 2020); postorbital process of the laterosphenoid with pneumatic depression on ventral surface (Xu et al., 2015; Pei et al., 2020); and conjoined basal tubera narrower than the occipital condyle (Xu et al., 2015; Pei et al., 2020). In Brusatte et al. (2014) the concave step in the anterior margin of the maxilla is a troodontid synapomorphy, but this same anatomical feature was recovered as a paravian synapomorphy by Pei et al. (2020). In general, some Jehol troodontids such as *Sinovenator* and *Jingfengopteryx* are often recovered as the earliest-diverging members of the group, sometimes including a pair of small-bodied Mongolian troodontids as well in a Jingfengopterygid clade (Turner et al., 2012). Other taxa like *Sinusonasus* and *Jianianhualong*, which have transitional features, are later diverging in their systematic positions, and most Late Cretaceous troodontids are the latest-diverging within the group. In some analyses the transitional taxa collapse nodes into polytomies and produce a single nested troodontid clade with no distinction between Jehol or Mongolian groups (Xu et al., 2017). Main TWiG datasets recover at least two troodontid clades of varying composition (reduced strict consensus tree: Brusatte et al., 2014; Pei et al., 2020; fig. 1; strict consensus tree: Turner et al., 2012) near the base of the troodontid phylogeny, but have yet to include *Jianianhualong* and other new taxa that seem to be blurring traditional clade lines. Anchiornithines have been recovered as the earliest-diverging troodontids in some analyses of past TWiG dataset iterations (e.g., Turner et al., 2012; Brusatte et al., 2014; Gianechini et al., 2018) as well as modified versions of them (Agnolín et al. 2019) whilst other studies have resolved them with early-diverging avialans (e.g., Agnolín and Novas, 2013; Pei et al., 2020; fig. 1) or as early-diverging paravians (e.g., Lefèvre et al., 2017). *Anchiornis* is known from hundreds of fossils preserved in different postures (Hu et al., 2009; Pei et al., 2017; Wang et al., 2017a), offering the most complete picture of anchiornithine anatomy currently available. This taxon has a key role to play in further investigating the taxonomic status of anchiornithines. In this study *Xiaotingia* maintains its close affinities with *Anchiornis* as part of the Anchiornithinae (fig. 1). Its phylogenetic position has also been contentious, since it was originally recovered as part of a deinonychosaurian subclade with *Anchiornis* and *Archaeopteryx* (Xu et al., 2011) and later recovered as a troodontid (Turner et al., 2012).

MESOZOIC AVIALAE: Avialae Gauthier, 1986, is a stem-based taxon containing *Passer domesticus* Linnaeus, 1758, and all coelurosaurians closer to it than to *Dromaeosaurus albertensis* Matthew and Brown, 1922, or *Troodon formosus* Leidy, 1856 (sensu Maryańska et al., 2002; after Turner et al., 2012). Although our understanding of the phylogenetic relationships of Mesozoic birds has improved enormously over the past three decades, there remain major challenges as systematists scramble to keep up with the rapidly expanding species diversity primarily coming out of the Jehol deposits in northeastern China. Current analyses targeted at Mesozoic bird relationships have experienced a decline in overall support as new taxa with unusual character combinations blur the distinction between major clades (Zhou et al., 2012). This is primarily because character matrices have failed to keep abreast of new morphological diversity through revision and expansion of the character set. This is not to say that character matrices have not been expanded, but with new species and even clades identified every year, it is unsurprising that most analyses fail even to keep up with new operational taxonomic units (OTUs).

Most, but not all, 21st-century descriptions of new taxa have included a phylogenetic analysis to support taxonomic inferences based on morphological observations. All major analyses stem from either the Norell and Clarke (2001) data set, which consists of 201 characters, or the Chiappe (2002) data set, consisting of 169 characters. Generally, Norell and Clarke's (2001) matrix includes more characters targeted at resolving later-diverging avialans derived from their work on *Apsaravis* (Clarke and Norell, 2002) and Clarke's (2004) revision of *Ichthyornis*, whereas the Chiappe (2002) character list focuses more

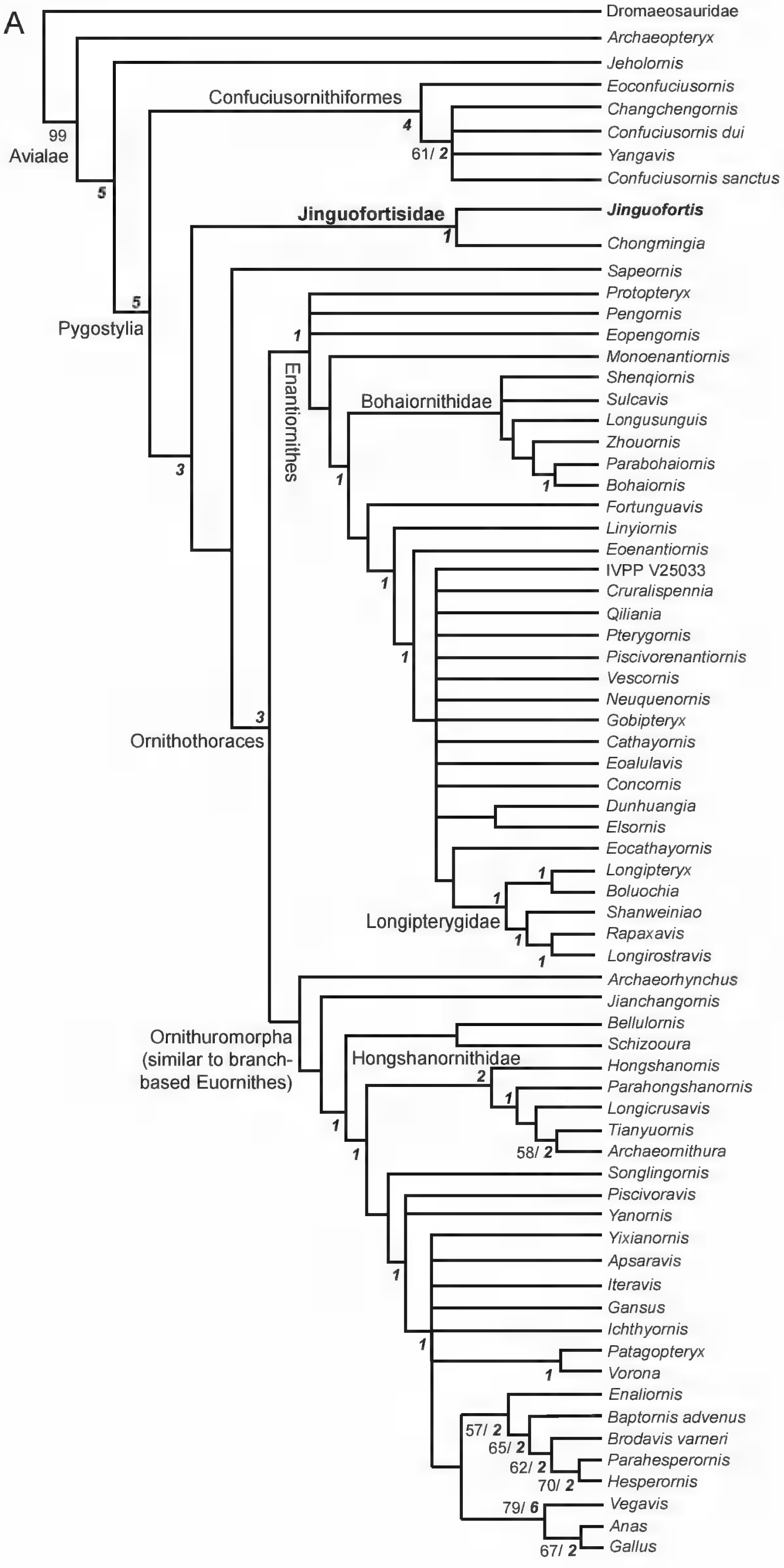
A
Dromaeosauridae
Archaeopteryx
Jeholornis
Confuciusornithiformes
Eoconfuciusornis
Changchengornis
Confuciusornis dui
Yangavis
Confuciusornis sanctus
4
61/ 2
99
Avialae
5
Jinguofortisidae
Jinguofortis
Chongmingia
1
Sapeornis
5
Pygostylia
Protopteryx
Pengornis
Eopengornis
1
Monoenantiornis
Enantiornithes
Bohaiornithidae
Shenqiornis
Sulcavis
Longusunguis
Zhouornis
Parabohaiornis
Bohaiornis
1
1
3
Fortunguavis
Linyiornis
Eoenantiornis
IVPP V25033
Cruralispennia
Qiliania
Pterygornis
Piscivorenantiornis
Vescornis
Neuquenornis
Gobipteryx
Cathayornis
Eoalulavis
Concornis
Dunhuangia
Elsornis
Eocathayornis
Longipteryx
Boluochia
Shanweiniao
Rapaxavis
Longirostravis
1
1
1
1
1
1
Longipterygidae
3
Ornithothoraces
Archaeorhynchus
Jianchangornis
Bellulornis
Schizooura
Hongshanornithidae
Hongshanornis
Parahongshanornis
Longicrusavis
Tianyuornis
Archaeornithura
2
1
58/ 2
Ornithuromorpha
(similar to branch-
based Euornithes)
1
1
Songlingornis
Piscivoravis
Yanornis
Yixianornis
Apsaravis
Iteravis
Gansus
Ichthyornis
Patagopteryx
Vorona
1
1
1
Enaliornis
Baptornis advenus
Brodavis varneri
Parahesperornis
Hesperornis
57/ 2
65/ 2
62/ 2
70/ 2
Vegavis
Anas
Gallus
79/ 6
67/ 2

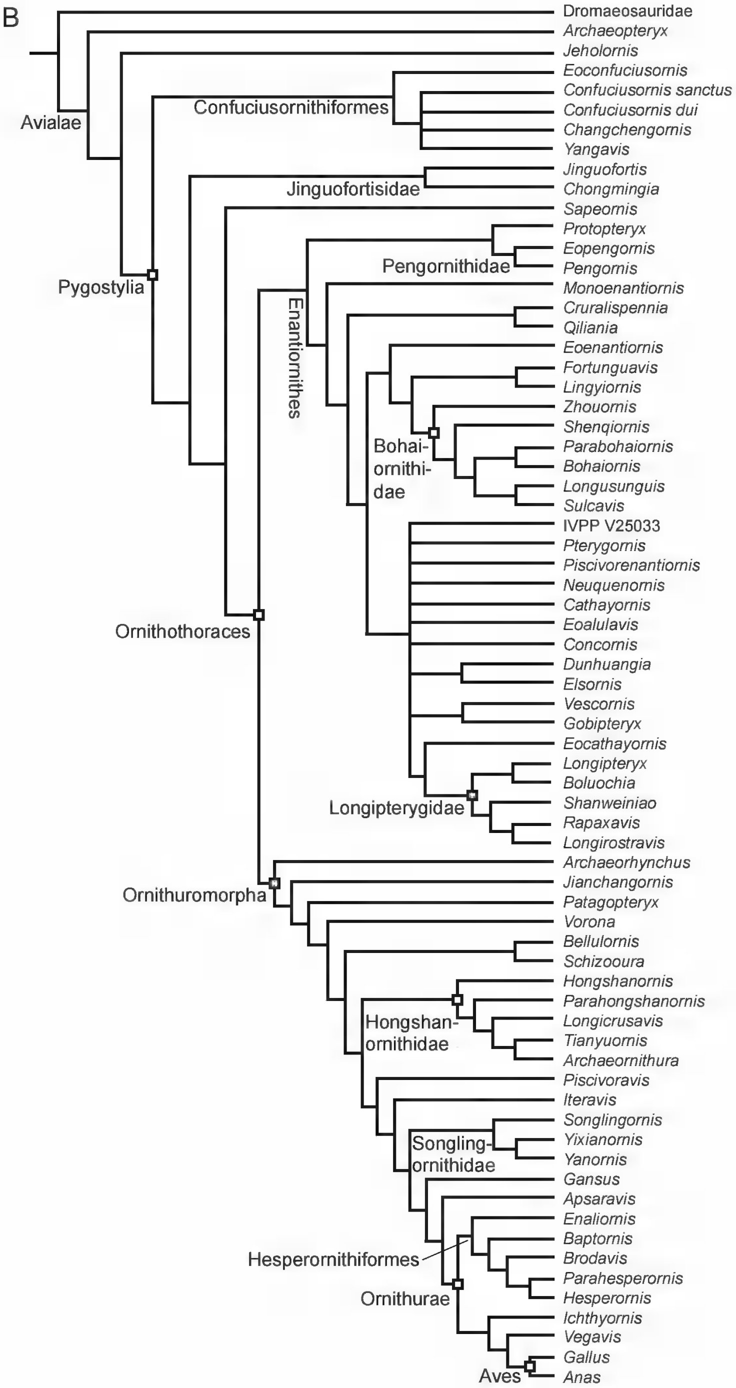
B
Dromaeosauridae
Archaeopteryx
Jeholornis
Eoconfuciusornis
Confuciusornis sanctus
Confuciusornis dui
Changchengornis
Yangavis
Avialae
Confuciusornithiformes
Jinguofortis
Chongmingia
Jinguofortisidae
Sapeornis
Protopteryx
Eopengornis
Pengornis
Pengornithidae
Pygostylia
Monoenantiornis
Cruralispennia
Qiliania
Enantiornithes
Eoenantiornis
Fortunguavis
Lingyiornis
Zhouornis
Shenqiornis
Parabohaiornis
Bohaiornis
Longusunguis
Sulcavis
Bohai-ornithi-dae
IVPP V25033
Pterygornis
Piscivorenantiornis
Neuquenornis
Cathayornis
Eoalulavis
Concornis
Dunhuangia
Elsornis
Vescornis
Gobipteryx
Eocathayornis
Longipteryx
Boluochia
Shanweiniao
Rapaxavis
Longirostravis
Ornithothoraces
Longipterygidae
Archaeorhynchus
Jianchangornis
Patagopteryx
Vorona
Ornithuromorpha
Bellulornis
Schizooura
Hongshanornis
Parahongshanornis
Longicrusavis
Tianyuornis
Archaeornithura
Hongshan-ornithidae
Piscivoravis
Iteravis
Songlingornis
Yixianornis
Yanornis
Songling-ornithidae
Gansus
Apsaravis
Enaliornis
Baptornis
Brodavis
Parahesperornis
Hesperornis
Hesperornithiformes
Ornithurae
Ichthyornis
Vegavis
Gallus
Anas
Aves

FIG. 3. Wang et al. (2018a) analysis of 70 taxa scored across 280 morphological characters. Published results using **A.** new technologies; **B.** traditional search using implied weighting, k = 16.

heavily on early-diverging birds based on his work on the El Brete enantiornithines and the early-diverging ornithuromorph *Patagopteryx* (Chiappe, 1995). Chiappe (2002) included Allosauroidea, Velociraptorinae, and the Troodontidae as outgroups but did not illustrate their relative relationships. The Alvarezsauroidea, at one time considered to be a clade of flightless birds (Suzuki et al., 2002), were also initially included (Chiappe, 2002). In contrast, Norell and Clarke (2001) used the OTU Dromaeosauridae to root their analysis. Following their usage, all subsequent analyses born from the Chiappe (2002) list have also used the Dromaeosauridae as the outgroup (O'Connor et al., 2011; Zhou et al., 2014; Wang et al., 2018a) (fig. 3).

The Chiappe (2002) character list was expanded by Gao et al. (2008), whose new matrix included 15 new taxa and 73 additional characters (total 242 characters), some of which were new and others taken from Norell and Clarke (2001). This list was further expanded to include three new characters and a large number of additional taxa (O'Connor et al., 2009, 2011). The O'Connor et al. (2011) character list has since been expanded independently by Wang et al. (2014, 2018a) and Atterholt et al. (2018). Wang et al. (2014) added 17 new characters (262 characters) and Atterholt et al. (2018) added seven (252 characters). In both cases the added characters were targeted towards increasing resolution in the Enantiornithes. The Wang et al. (2014) matrix was modified by Chiappe et al. (2019), in which some characters were added while others were deleted and some scorings were modified (212 characters). Wang and colleagues expanded their matrix again in 2018, and it has 70 taxa scored over 280 (18 new) characters (Wang et al., 2018a; fig. 3). In 2014, Li's group added 19 characters to the Norell and Clarke (2001) matrix but included only 36 taxa (Li et al., 2014).

All these aforementioned analyses stem from careful firsthand observation of almost all the analyzed OTUs. However, they all fail at one critical level: in only using the OTU Dromaeosauridae as the outgroup, these analyses included only one potential avialan ancestor. This made it impossible to test hypotheses regarding the closest dinosaurian relatives of Avialae. A notable recent difference between the analyses of these various workers is the parameters utilized for the analysis. For example, although Wang et al. (2017b) and O'Connor et al. (2016) both use the TNT software (Goloboff et al., 2008a), Wang et al. (2018a) have recently shifted to using "new technology" search algorithms (fig. 3A). O'Connor et al. (2014; Atterholt et al., 2018) continue to use traditional search terms and have more recently started applying implied weighting (Goloboff et al., 2008b) to account for the extreme homoplasy observed during early avialan evolution because this method more strongly weights characters that have more homology (less homoplasy) (Wang and O'Connor, 2017; Xu, 2018). Here, the Wang et al. (2018a) analysis is rerun with a traditional search using implied weighting (Goloboff et al., 2008b) with a gentle concavity (Goloboff et al., 2018), k = 16 (fig. 3B) (see Methods). The results are presented together with the results published by Wang et al. (2018a) based on "new technology" search algorithms in TNT (fig. 3A).

There are a few other matrices that have been utilized in attempts to resolve the phylogeny of Mesozoic birds (Cau and Arduini, 2008; Lefèvre et al., 2014). However, these appear to rely heavily on published information, which is often incomplete if taxa are not monographed and can at times be inaccurate (e.g., "*Dalingheornis*": Zhang et al., 2006; Lockley et al., 2007). Controversial taxa that have received only preliminary study can produce erroneous results in analyses when their purported morphologies are taken at face value (e.g., *Jixiangornis* (Ji et al., 2002; Lefèvre et al., 2014)).

There are several relationships in Mesozoic avialan phylogeny that have stabilized in recent analyses, and other regions of the tree where recent analyses still fail to find consensus. *Archaeopteryx* is the earliest-diverging avialan according to the definition above followed by most Mesozoic ornithologists (possible troodontids such as

Anchiornis are not included in these analyses) and *Jeholornis*, another long bony-tailed bird, is typically resolved as later diverging than *Archaeopteryx* but earlier diverging than the Pygostylia, all birds whose abbreviated tail ends in a fused, compound element, the pygostyle (Li et al., 2014; Atterholt et al., 2018; Wang et al., 2018a). The Enantiornithes and the Ornithuromorpha (node-based definition that we follow in this volume because of the preference of our authors; Euornithes Sereno et al., 1998, is the stem-based definition) are consistently resolved as sister taxa, forming the Ornithothoraces (Chiappe, 2002; Clarke, 2004; Gao et al., 2008; Wang et al., 2018a). The relative placement of the two major recognized early-diverging pygostylian clades, the Sapeornithiformes and Confuciusornithiformes, is unstable; the two groups have both been resolved as the sister taxon to the Ornithothoraces (Li et al., 2014; Wang et al., 2014). The "mosaic" distribution of derived avialan features within Paraves obscures attempts at resolving aspects of early avialan phylogeny. For example, while the absence of an ossified sternum suggests *Sapeornis* is earlier diverging, it has a more reduced (and thus derived) manus with only two manual unguals, whereas in *Confuciusornis* the manus retains the plesiomorphic condition of three manual unguals, and these are hypertrophied relative to most other paravians (Chiappe et al., 1999; Zhou and Zhang, 2002; Zheng et al., 2014) (fig. 4). The Wang et al. (2018a) analysis suggests that the Confuciusornithiformes are the earliest-diverging pygostylians known, even more primitive than the recently identified Jinguofortisidae (fig. 3).

Enantiornithine phylogeny is poorly resolved (O'Connor et al., 2011; Wang et al., 2018a), but several groups have become apparent in recent analyses. *Protopteryx*, *Iberomesornis*, and the Pengornithidae are fairly consistently resolved as very early-diverging taxa (Wang et al., 2017b; Atterholt et al., 2018; Wang et al., 2018a). Jehol "longirostrine" taxa are commonly resolved into two clades, one formed by *Longirostravis*, *Shanweiniao*, and *Rapaxavis*, and the other by *Longipteryx* and *Boluochia* (O'Connor et al., 2009, 2016; Wang et al., 2014; Zhou et al., 2014). These two clades are often but not always resolved forming a larger clade (the Longipterygidae; fig. 3) (Wang et al., 2014, 2018a). The most diverse and reasonably resolved clade of enantiornithines is the Bohaiornithidae, although its recognition through cladistic analysis required additional characters to be added and scored in relevant phylogenetic data matrices (Wang et al., 2014, 2018a) and a recent analysis included in the description of a new bohaiornithid-like species failed to resolve this clade (Chiappe et al., 2019). The only recognized Late Cretaceous family is the Avisauridae (Chiappe, 1992). Through the support of seven additional characters targeted at avisaurid relationships, this clade has recently been demonstrated to consist of North American and South American subclades, each consisting of three taxa (Atterholt et al., 2018).

The Ornithuromorpha is slightly more resolved than the Enantiornithes, probably due to its lesser diversity (fig. 3). *Archaeorhynchus* and *Patagopteryx* are consistently resolved as among the earliest-diverging taxa (You et al., 2006; Li et al., 2014; O'Connor et al., 2016; Wang et al., 2017b), although in the enlarged analysis of Wang et al. (2018a) *Patagopteryx* has a later-diverging position. The secondary loss of flight in the Late Cretaceous *Patagopteryx* may be creating a false signal interpreted by some analyses as indicative of an earlier-diverging position (fig. 1B). *Vorona*, *Chaoyangia*, *Jianchangornis*, and *Zhongjianornis* are also consistently resolved as early-diverging taxa (Wang et al., 2014; Zhou et al., 2014; O'Connor et al., 2016). The most diverse family is the Hongshanornithidae (Wang et al., 2015; 2017b; 2018a). *Yanornis*, *Yixianornis*, and *Songlingornis* are often grouped together based on sternal morphology forming a clade referred to as the Songlingornithidae (Clarke et al., 2006; Li et al., 2014; Wang et al., 2018a). *Gansus* from the slightly younger Xiagou Formation is typically resolved as later diverging than Jehol ornithuromorphs (Zhou et al., 2014; Wang et al., 2018b).

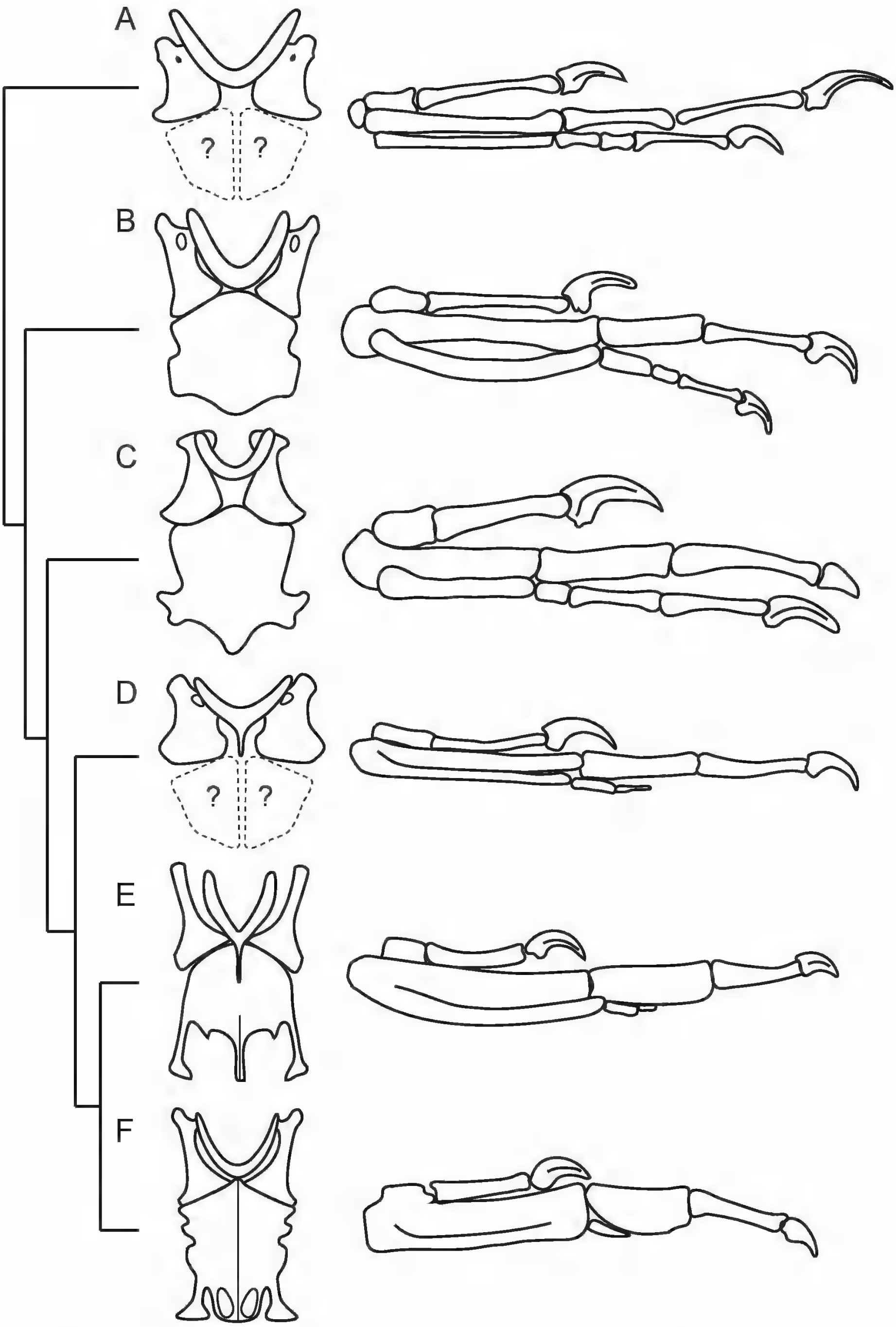

FIG. 4. Major evolutionary transformations in the avian furcula, coracoid and sternum, and manus in context of a simplified phylogeny, as documented in **A.** *Archaeopteryx*, **B.** *Jeholornis*, **C.** *Confuciusornis*, **D.** *Sapeornis*, **E.** Early Cretaceous Enantiornithes (*Parabohaiornis*), and **F.** Early Cretaceous Ornithuromorpha (*Yanornis*). Generally during early avian evolution, the furcula, coracoid, and sternum become more craniocaudally elongate, while the manual digits become reduced and fusion between the metacarpals increases. Illustrations not to scale.

The Ornithurae generally consists of *Ichthyornis, Hesperornis*, and Aves, although whether the *Ichthyornis* lineage or the Hesperornithiformes is more closely related to modern birds is unresolved (Clarke, 2004; O'Connor et al., 2011; Li et al., 2014; Wang et al., 2018a). Since the most common definition of Ornithurae is node based with *Hesperornis* and living birds as reference taxa (Gauthier and de Queiroz, 2001), this means that *Ichthyornis* may or may not be a member of this clade. It is for this reason that stem-based definitions may better serve until early avialan relationships are better understood. Although *Ichthyornis* was traditionally resolved as later diverging (Chiappe, 2002; Clarke, 2004; You et al., 2006), increased character sampling in the Hesperornithiformes resulted in this clade moving crownward (O'Connor et al., 2011). New cranial information on *Ichthyornis* supports the earlier-diverging position of this taxon (Atterholt et al., 2018; Field et al., 2018). However, the position resolved for this taxon using the Wang et al. (2018a) matrix is quite different depending on how the data is analyzed, further highlighting the uncertainty that surrounds the relative placement of these later-diverging lineages (fig. 3).

In recent analyses, Bremer support is typically very low (O'Connor et al., 2017; Wang et al., 2018a). This likely reflects similarities between early-diverging ornithuromorphs and enantiornithines that have blurred the distinction between these two major clades and not missing data (O'Connor and Zhou, 2013). Take, for example, the taxon *Schizooura lii*: although clearly a member of the Ornithuromorpha, this species possesses a Y-shaped enantiornithine-like furcula; the coracoid lacks a lateral process (at one time a synapomorphy of the Ornithuromorpha); and the cranial surface of the humerus is flat (Zhou et al., 2012). *Chaoyangia* preserves two features observed clearly only in ornithuromorphs, but sometimes is resolved in the Enantiornithes, and thus a well-resolved tree can be found only if it is excluded (O'Connor et al., 2014). In many recent analyses, Ornithothoraces forms a single clade in trees only one or two steps longer than the most parsimonious solution (O'Connor and Zhou, 2013; Wang et al., 2018a). This mosaic distribution of morphologies among taxa and the dwindling number of clear morphological differences between the Enantiornithes and the Ornithuromorpha as early-diverging taxa are uncovered has diminished the number of synapomorphies in support of each node, resulting in weak support for most traditional clades (O'Connor et al., 2014; Zelenkov, 2017). The only way to increase support is to identify new synapomorphies for each clade and increase the amount of morphological data incorporated into the character matrix, no easy task given the varying preservational limitations set by the known diversity and the rapid rate of discovery principally in China (O'Connor and Zhou, 2013), but also elsewhere (de Souza Carvalho et al., 2015; Atterholt et al., 2018). Currently, all synapomorphies in support of Ornithothoraces, Enantiornithes, and Ornithuromorpha are ambiguous because of the large number of taxa and substantial amount of preservational variability between specimens. Although the rate of discovery has outpaced the rate at which character sets have been expanded, the Wang et al. (2018a) dataset exemplifies the continual efforts that are being made to encapsulate greater morphological variation. This dataset has roughly 100 more characters than datasets from 15 years ago and double the number of OTUs.

It is often difficult to compare results of various analyses due to differences in the included taxa. Nearly half of all Mesozoic avialans are not even included in phylogenetic analyses because of their highly fragmentary nature (O'Connor, 2009; O'Connor et al., 2014). With the exception of specimens from a few key deposits, most of the Mesozoic fossil record consists of incomplete taxa based on a small number of incomplete elements (e.g., *Flexomornis, Limenavis*), a single bone (e.g., *Avisaurus, Yungavolucris*), or sometimes less (e.g., *Lectavis, Almatiornis*). Such incomplete OTUs in already weakly supported phylogenies can result in the collapse of the Ornithothoraces (e.g., *Chaoyangia*), and some (e.g., *Mystiornis, Flexomornis*) even cause the Pygostylia to collapse (O'Connor and Zhou, 2013; O'Connor et al., 2014; Atterholt et al., 2018).

Zhongornis is known only from a single young juvenile specimen and, given the extreme ontogenetic changes likely experienced by most paravians, its phylogenetic affinities cannot be determined with any certainty at this time. Originally considered a member of a distinct lineage of birds characterized by a tail morphology intermediate between that of *Archaeopteryx* and that of pygostylians (Gao et al., 2008), the specimen was later suggested to be a juvenile scansoriopterygid (O'Connor and Sullivan, 2014). New data on pygostyle formation suggests that *Zhongornis* may in fact be a juvenile pygostylian (Rashid et al., 2018).

Anchiornithine taxa—*Anchiornis*, *Aurornis*, *Eosinopteryx*, and *Xiaotingia*—have been gathered into a distinct clade of early branching avialans (Anchiornithinae: we use this stem-based taxon containing *Anchiornis* instead of Anchiornithidae because the former was proposed earlier [Xu et al. 2016]) either all together (Agnolín and Novas, 2011; Agnolín and Novas, 2013; Foth et al., 2014; Pei et al., 2017, 2020; Rashid et al., 2018) or as a subset of the four taxa (Xu et al., 2011). This contrasted with past analyses involving the main TWiG data matrix or modified versions, which recovered anchiornithines or a subset of them as part of the Troodontidae (Turner et al., 2012; Brusatte et al., 2014; Agnolín et al., 2019), as well as previous studies that found them to be early-diverging deinonychosaurians (Senter et al., 2012; Xu et al., 2015) or early-diverging paravians (Lefèvre et al., 2017). Despite such major differences in the phylogenetic position of this clade these avialan synapomorphies stand out (Turner et al., 2012; Brusatte et al., 2014; Foth et al., 2014): transition point proximal to caudal 7; in lateral view, the dorsal border of the antorbital fossa is formed by the lacrimal and nasal.

Eight individual *Archaeopteryx* specimens (of 11 published) were recently recovered in a polytomous clade that is sister to the nonanchiornithine avialans (Pei et al., 2020; fig. 1). With the Haarlem specimen pruned (recently proposed as an anchiornithine: Foth and Rauhut, 2017), six *Archaeopteryx* specimens (the London, Berlin, Munich, Thermopolis, Eichstätt, and 11th specimens) form a group sister to a large avialan clade comprising of the Solnhofen specimen and remaining later-diverging avialans. However, the former group was supported by synapomorphies that cannot be scored in the Solnhofen specimen, so additional data may yet show a monophyletic *Archaeopteryx* group (although some fragmentary specimens are probably only referable to more inclusive Mesozoic avialan clades: Rauhut et al., 2018).

Rahonavis was originally described as an early-diverging avialan (Forster et al., 1996) and has been found in a later-diverging position than *Archaeopteryx* (Cau, 2018; Novas et al., 2018). However, it has also been recovered as a dromaeosaurid by a range of other studies (Makovicky et al., 2005; Turner et al., 2012), which is the position favored in this volume.

CROWN BIRDS (AVES): The last decade has seen a great deal of progress with regard to resolving the interrelationships of the major groups of living birds. A series of large-scale "phylogenomic" studies has iteratively brought us closer than ever to a complete picture of crown bird interordinal relationships (e.g., Ericson et al., 2006; Hackett et al., 2008; McCormack et al., 2013; Jarvis et al., 2014; Claramunt and Cracraft, 2015; Prum et al., 2015; Kimball et al., 2019). Ongoing work seeks to continue progress on resolving recalcitrant portions of the bird tree of life, as well as achieving the goal of sequencing and analyzing the whole genomes of all known extant avialan species.

Crown birds (Aves) comprise nearly 11,000 described extant species, and are divided into two major subclades: Palaeognathae and Neognathae (Gill and Donsker, 2017). Palaeognathae comprises the paraphyletic, flightless ratites (i.e., the extant ostriches, rheas, kiwis, emus, and cassowaries), and the volant tinamous of the New World. Over the last decade, the surprising hypothesis that ratites are paraphyletic with respect to tinamous has received accumulating support from molecular phylogenetic data sets (Hackett et al., 2008; Harshman et al., 2008; Phillips et al., 2010; Haddrath and Baker, 2012; Smith et al., 2013; Baker et al., 2014; Jarvis et al., 2014; Mitchell et al., 2014; Prum et al., 2015; Yonezawa et al., 2016; Grealy et al., 2017; Reddy et al., 2017) and is corroborated by embryological data (Faux and Field, 2017), suggesting that flightlessness and large body size have arisen repeatedly throughout palaeognath evolutionary history. Neognathae are divided into Galloanserae (chickenlike and ducklike birds) and the major clade Neoaves, which represents over 95% of living bird diversity. The earliest fossil crown bird yet identified, *Asteriornis* from the Maastrichtian of Belgium, appears to represent an early galloanseran (Field et al., 2020). This implies that at least the stem lineages of Palaeognathae, Galloanserae, and Neoaves were present in the Late Cretaceous.

The phylogenetic interrelationships of the major subclades of Neoaves are hotly contested, and according to one recent high-profile phylogenomic study, represent "the greatest unresolved challenge in dinosaur systematics" (Prum et al., 2015). While several recent studies have sought to clarify the deep branching pattern among the major neoavian clades (e.g., Hackett et al., 2008; Jarvis et al., 2014; Prum et al., 2015; Reddy et al., 2017; Kimball et al., 2019), these studies have recovered incompatible neoavian topologies, raising questions about the influence of data type, taxon sampling, and analytical approach in driving topological results. Indeed, recent work (Suh, 2016) hypothesises that a consistent, bifurcating branching pattern along much of the backbone of Neoaves may never be obtained, since the early evolutionary history of Neoaves may have been characterized by extremely rapid cladogenesis and high rates of incomplete lineage sorting. Although the subject is still controversial (see Field et al., chapter 5, on molecular rate variation), the hypothesis of a rapid radiation of Neoaves in the aftermath of the end-Cretaceous mass extinction has gained mounting support in recent years (Feduccia, 1995; Ericson et al., 2006; Longrich et al., 2011; Feduccia, 2014; Jarvis et al., 2014; Prum et al., 2015; Berv and Field, 2018). Importantly, uncertainty regarding the precise origination times of the deepest clades of crown birds, as well as Aves itself, has clouded understanding of the influence of the end-Cretaceous mass extinction on avialan evolution. However, the known neoavian fossil record is entirely post-Cretaceous at present (Longrich et al., 2011; Field, 2017; Ksepka et al., 2017), consistent with the idea that lingering topological uncertainty at the base of Neoaves may indeed be related to rapid early Cenozoic cladogenesis (see Field et al., chapter 5, on molecular rate variation).

Despite ongoing controversy related to the branching pattern at the base of Neoaves, recent phylogenetic studies are consistent in recognizing about 10 major constituent neoavian subclades (Reddy et al., 2017; Field et al., chapter 5). Figure 5 depicts competing topological hypotheses presented by two recent avialan phylogenomic studies (Jarvis et al., 2014; Prum et al., 2015), illustrating that despite some topological uncertainty, the composition of most major clades is consistent across studies. Major outstanding topological controversies influencing our understanding of avialan macroevolution include:

1. Which clade is the sister taxon to the rest of Neoaves? Some recent studies (e.g., Jarvis et al., 2014) recovered a monophyletic "Columbea" comprising Mirandornithes (Podicipediformes and Phoenicopteriformes) and Columbimorphae (Columbiformes, Pterocliformes, and Mesitornithiformes) in this position, although Prum et al. (2015) recovered Strisores (which comprises a paraphyletic "Caprimulgiformes" and Apodiformes) as sister to all other Neoaves. In turn, the monophyly of Columbea was not recovered by Prum et al. (2015), and the interrelationships of Strisores are still hotly contested (Chen et al., 2019).

2. Are most aquatic avialan lineages part of a monophyletic aquatic radiation? Prum et al. (2015) recovered a topology in which most aquatic birds (with the exception of Anseri-

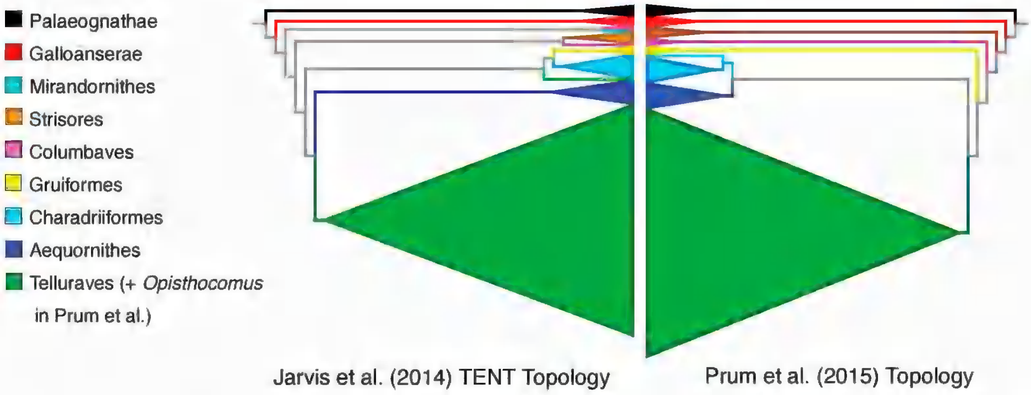
Palaeognathae
Galloanserae
Mirandornithes
Strisores
Columbaves
Gruiformes
Charadriiformes
Aequornithes
Telluraves (+ *Opisthocomus* in Prum et al.)
Jarvis et al. (2014) TENT Topology
Prum et al. (2015) Topology

FIG. 5. Competing phylogenetic topologies for crown birds from recent phylogenomic studies of Jarvis et al. (2014) and Prum et al. (2015). Both topologies support Palaeognathae (black) and Galloanserae (red) as successive sister taxa to the rest of extant birds (Neoaves). Interrelationships within Neoaves differ, but the same major constituent clades are largely supported (see legend). The monotypic hoatzin (*Opisthocomus hoazin*) is inferred to be the sister taxon of Telluraves in Prum et al. (2015), and sister to a Charadriiformes + Gruiformes clade in Jarvis et al. (2014). Prum et al. (2015) supports a monophyletic Columbaves (fuschia), uniting Otidimorphae (bustards, cuckoos, turacos) and Columbimorphae (doves, mesites, sandgrouse), whereas Jarvis et al. (2014) find Columbimorphae as the sister taxon to Mirandornithes, and Otidimorphae as sister to Strisores.

formes, kingfishers, and aquatic gruiforms and passerines like dippers) formed a large monophyletic clade. This clade, dubbed Aequorlitornithes, united Aequornithes, Charadriiformes, and Mirandornithes, suggesting that adaptation to aquatic habits may have taken place fewer times throughout avialan evolutionary history than previously thought. However, the monophyly of this clade has not been obtained by other large-scale phylogenomic studies (Jarvis et al., 2014; Reddy et al., 2017; Kimball et al., 2019).

While ongoing large-scale phylogenetic studies are likely to shed light on these and other questions related to neoavian phylogeny in the relatively short-term, targeted phylogenomic studies of major avialan subclades are continuously illuminating finer-scale phylogenetic relationships across the bird tree of life. For example, a recent phylogenomic study of passerines (a massive avian subclade comprising over 6000 living species) represents the first effort to sequence representatives of all extant passerine families, revealing important insight into this charismatic superradiation (Oliveros et al., 2019).

DISCUSSION

Pennaraptoran systematics has dramatically improved over the past few decades through immense efforts from all corners of the globe, but there remain areas to improve in all clades, particularly the enigmatic Scansoriopterygidae and Anchiornithinae.

Contentious Groups and Groups with ‘Blurry’ Boundaries: For groups with contentious phylogenetic positions like the Anchiornithinae and Scansoriopterygidae and for groups with “blurry” boundaries, an automated pipeline of phylogenetic analysis, like the one described in Methods, will be helpful in further exploring phylogenetic placement through easier and more efficient running of analyses using alternative character codings and considering all phylogenetically informative but highly fragmentary specimens.

Powered-flight Origins: The topology in figure 1 provided the context to determine that only paravians meet the minimum thresholds of modern powered flight (in terms of wing loading and specific lift estimates seen in today’s flying birds: see Pei et al. (2020) for details). This is despite the reduced body size, pennaceous feathers, and capable respiratory system among nonparavian pennaraptorans (Turner et al., 2007a; Dececchi and Larsson, 2013; Benson et al., 2014; Foth et al., 2014; Lee et al., 2014; Xu et al., 2014; Brusatte et al., 2015). Powered flight potential among microraptorines and unenlagiines underscores the need for more intensive systematic study of these groups, particularly the more enigmatic unenlagiines (Pei et al., 2020). Recovered early-diverging positions of the larger microraptorines *Tianyuraptor* and *Zhenyuanlong* imply a decrease in body size and an increase in relative forelimb length across Microraptorinae (Pei et al., 2020). Discovering microraptorines that cover temporal and geographical ranges outside the currently known Early Cretaceous Asian forms and Late Cretaceous North American ones may yet reveal the drivers and development of this flight potential.

METHODS

MAIN NONAVIALAN PENNARAPTORAN ANALYSIS DISCUSSED

(Pei et al., 2020)

The study of Pei et al. (2020) was based on the Theropod Working Group dataset [TWiG dataset] of Brusatte et al. (2014), which was significantly expanded with data pertinent to paravian phylogeny, including nine dromaeosaurid terminals (Late Cretaceous microraptorine IVPP V22530, *Changyuraptor*, *Zhenyuanlong*, *Luanchuanraptor*, *Acheroraptor*, *Linheraptor*, *Yurgovuchia*, *Dakotaraptor*, and *Velociraptor osmolskae*), revised codings and data obtained from laser-stimulated fluorescence (LSF) imaging (Kaye et al., 2015; Wang et al., 2017a). The phylogenetic analysis was automated using a master script executed in TNT version 1.5 (Goloboff et al., 2008a; Goloboff and Catalano, 2016), which helped identify and correctly score errors/problems more quickly and easily. This script automated thorough searches, as well as the subsequent diagnosis and characterization of results. All the scripts and batch files for initial analysis, diagnosis, and other tasks, are available (with full descriptions) in Pei et al. (2020). Tree searches used the extended search algorithms of TNT ("new technologies"), initially using 5 random addition sequence Wagner trees followed by TBR, sectorial searches [CSS, RSS, and XSS], and 5 cycles of tree-drifting, followed by tree-fusing (see Goloboff, 1999, for details). The search calculated the consensus as trees of optimal score were repeatedly found (eliminating branches of minimum length zero (Coddington and Scharff, 1994); subsequent consensus calculation after pruning rogue taxa more conservatively collapsed trees with TBR branch-swapping (Goloboff and Farris, 2001)), stopping the search only when the consensus becomes stable to new hits, thereby validating the accuracy of the consensus for the corresponding dataset and optimality criterion. The optimal score was therefore independently found as many times as needed to obtain a stable consensus; this validation procedure was performed three times for greater reliability. All our analyses included implied weighting (XIW) (Goloboff, 1993), with modifications proposed by Goloboff (2014) that prevent improper inflation of weights due to missing entries (characters with missing entries have their weights downweighted faster). Missing entries were assumed to have 0.8 of the homoplasy in observed entries, but not extrapolating beyond 5 times the observed homoplasy. The analyses used a concavity of 10, which mildy weights against characters with homoplasy. For the complete methodological details see Pei et al. (2020).

MAIN EARLY-DIVERGING AVIALAN ANALYSIS DISCUSSED

(after Wang et al., 2018a)

The Mesozoic avialan analysis of Wang et al. (2018a) was rerun using a traditional search (heuristic search using tree-bisection reconnection retaining the single shortest tree from every 1000 replications, followed by a second round of tree-bisection reconnection) using implied weighting with the k value of 16 (fig. 3B). The results of this analysis are presented together with those of Wang et al. (2018a), which used extended search algorithms ("new technologies") in TNT (fig. 3A).

ACKNOWLEDGMENTS

This study benefitted from discussions at the International Pennaraptoran Symposium, held at the University of Hong Kong and supported by Kenneth H.C. Fung and First Initiative Foundation. This study was supported by the Research Grant Council of Hong Kong's General Research Fund (17103315 to M.P., X.X., and P.A.G.). It was also supported by the University of Hong Kong's Faculty of Science and University Research Committee Post-doctoral Fellow Scheme, Conference Grant, and Seed Fund for Basic Research (all to M.P.), and the National Science Foundation of China (41688103, 41120124002, and 91514302, to X.X.), a Proyecto de Unidad Ejecutora from CONICET (PUE0070 to P.A.G) and a UK Research and Innovation Future Leaders Fellowship (MR/S032177/1 to D.J.F.). Scott A. Hartman is thanked for the use of his skeletal reconstructions.

REFERENCES

Agnolín, F.L., and F.E. Novas. 2011. Unenlagiid theropods: are they members of the Dromaeosauridae (Theropoda, Maniraptora)? Anais da Academia Brasileira de Ciências 83 (1): 117–162.

Agnolín, F.L., and F.E. Novas. 2013. Avian ancestors: a review of the phylogenetic relationships of the theropods Unenlagiidae, Microraptoria, *Anchiornis* and Scansoriopterygidae, Dordrecht: Springer.

Agnolín, F.L., M.J. Motta, F. Brissón Egli, G. Lo Coco, and F.E. Novas. 2019. Paravian phylogeny and the dinosaur-bird transition: an overview. Frontiers in Earth Science 6 (252). [doi: 10.3389/feart.2018.002520]

Atterholt, J.A., J.H. Hutchison, and J. O'Connor. 2018. The most complete enantiornithine from North America and a phylogenetic analysis of the Avisauridae. PeerJ 6: e.5910.

Baker, A.J., O. Haddrath, J.D. McPherson, and A. Cloutier. 2014. Genomic support for a moa-tinamou clade and adaptive morphological convergence in flightless ratites. Molecular Biology and Evolution 31 (7): 1686–1696.

Barsbold, R. 1976. On the evolution and systematics of the late Mesozoic dinosaurs. Sovmestnaâ Sovetsko-Mongolskaâ Paleontologičeskaâ Ekspediciâ, Trudy 3: 68–75. [in Russian]

Barsbold, R. 1983. Carnivorous dinosaurs from the Cretaceous of Mongolia. Sovmestnaâ Sovetsko-Mongolskaâ Paleontologičeskaâ Ekspediciâ, Trudy 19: 1–119.

Benson, R.B.J., et al. 2014. Rates of dinosaur body mass evolution indicate 170 million years of sustained ecological innovation on the avian stem lineage. PLOS Biology 12 (5): e1001853.

Berv, J.S., and D.J. Field. 2018. Genomic signature of an avian Lilliput effect across the K-Pg extinction. Systematic Biology 67 (1): 1–13.

Bonaparte, J.F. 1999. Tetrapod faunas from South America and India: a paleobiogeographic interpretation. Proceedings of the Indian National Science Academy 65: 427–437.

Brusatte, S.L., et al. 2013. The osteology of *Balaur bondoc*, an island-dwelling dromaeosaurid (Dinosauria: Theropoda) from the Late Cretaceous of Romania. Bulletin of the American Museum of Natural History 374: 1–100.

Brusatte, S.L., G.T. Lloyd, S.C. Wang, and M.A. Norell. 2014. Gradual assembly of avian body plan culminated in rapid rates of evolution across the dinosaur-bird transition. Current Biology 24: 2386–2392.

Brusatte, S.L., J.M.K. O'Connor, and E.D. Jarvis. 2015. The origin and diversification of birds. Current Biology 25: R888-R898.

Cau, A. 2018. The assembly of the avian body plan: a 160-million-year long process. Bollettino della Società Paleontologica Italiana 57: 1–25.

Cau, A., and P. Arduini. 2008. *Enantiophoenix electrophyla* gen. et sp. nov. (Aves, Enantiornithes) from the Upper Cretaceous (Cenomanian) of Lebanon and its phylogenetic relationships. Atti della Società Italiana di Scienze Naturali e del Museo Civico di Storia Naturale di Milano 149: 293–324.

Cau, A., T. Brougham, and D. Naish. 2015. The phylogenetic affinities of the bizarre Late Cretaceous Romanian theropod *Balaur bondoc* (Dinosauria, Maniraptora): dromaeosaurid or flightless bird? PeerJ 3: e1032.

Cau, A., et al. 2017. Synchrotron scanning reveals amphibious ecomorphology in a new clade of bird-like dinosaurs. Nature 552: 395–399.

Chen, A., N.D. White, R.B.J. Benson, M.J. Braun, and D.J. Field. 2019. Total-evidence framework reveals complex morphological evolution in nightbirds (Strisores). Diversity 11 (9): 143.

Chiappe, L.M. 1992. Enantiornithine (Aves) tarsometatarsi and the avian affinities of the Late Cretaceous Avisauridae. Journal of Vertebrate Paleontology 12: 344–350.

Chiappe, L.M. 1995. The phylogenetic position of the Cretaceous birds of Argentina: Enantiornithes and *Patagopteryx deferrariisi*. *In* D.S. Peters (editor) Acta Palaeornithologica: 55–63. Senckenberg: Forschungsinstitut Senckenberg.

Chiappe, L.M. 2002. Basal bird phylogeny: problems and solutions. *In* L.M. Chiappe and L.M. Witmer (editors), Mesozoic birds: above the heads of dinosaurs: 448–472. Berkeley: University of California Press.

Chiappe, L.M., S. Ji, Q. Ji, and M.A. Norell. 1999. Anatomy and systematics of the Confuciusornithidae (Theropoda: Aves) from the Late Mesozoic of northeastern China. Bulletin of the American Museum of Natural History 242: 1–89.

Chiappe, L.M., et al. 2019. New *Bohaiornis*-like bird from the Cretaceous of China: enantiornithine interrelationships and flight performance. PeerJ 7 (e7846): 1–50.

Choiniere, J.N., et al. 2010. A basal alvarezsauroid theropod from the early Late Jurassic of Xinjiang, China. Science 327: 571–574.

Claramunt, S., and J. Cracraft. 2015. A new time tree reveals Earth history's imprint on the evolution of modern birds. Science Advances 1: e1501005.

Clarke, J.A. 2004. Morphology, phylogenetic taxonomy, and systematics of *Ichthyornis* and *Apatornis* (Avialae: Ornithurae). Bulletin of the American Museum of Natural History 286: 1–179.

Clarke, J.A., and M.A. Norell. 2002. The morphology and phylogenetic position of *Apsaravis ukhaana* from the Late Cretaceous of Mongolia. American Museum Novitates 3387: 1–46.

Clarke, J.A., Z. Zhou, and F. Zhang. 2006. Insight into the evolution of avian flight from a new clade of Early Cretaceous ornithurines from China and the morphology of *Yixianornis grabaui*. Journal of Anatomy 208: 287–308.

Coddington, J.A., and N. Scharff. 1994. Problems with zero-length branches. Cladistics 10: 415–423.

Colbert, E.H., and D.A. Russell. 1969. The small Cretaceous dinosaur *Dromaeosaurus*. American Museum Novitates 2380: 1–49.

Csiki, Z., V. Mátyás, S.L. Brusatte, and M.A. Norell. 2010. An aberrant island-dwelling theropod dinosaur from the Late Cretaceous of Romania. Proceedings of the National Academy of Sciences of the United States of America 107: 15357–15361.

Dececchi, T.A., and H.C.E. Larsson. 2013. Body and limb size dissociation at the origin of birds: uncoupling allometric constraints across a macroevolutionary transition. Evolution 67: 2741–2752.

DePalma, R.A., D.A. Burnham, L.D. Martin, P.L. Larson, and R.T. Bakker. 2015. The first giant raptor (Theropoda: Dromaeosauridae) from the Hell Creek Formation. Paleontological Contributions 14: 1–16.

de Souza Carvalho, I., et al. 2015. A Mesozoic bird from Gondwana preserving feathers. Nature Communications 6: 1–5.

Ericson, P.G.P., et al. 2006. Diversification of Neoaves: integration of molecular sequence data and fossils. Biology Letters 2: 543–547.

Evans, D.C., D.W. Larson, and P.J. Currie. 2013. A new dromaeosaurid (Dinosauria: Theropoda) with Asian affinities from the latest Cretaceous of North America. Naturwissenschaften 100: 1041–1049.

Evans, D.C., T.M. Cullen, D.W. Larson, and A. Rego. 2017. A new species of troodontid theropod (Dinosauria: Maniraptora) from the Horseshoe Canyon Formation (Maastrichtian) of Alberta, Canada. Canadian Journal of Earth Sciences 54: 813–826.

Faux, C., and D.J. Field. 2017. Distinct developmental pathways underlie independent losses of flight in ratites. Biology Letters 13 (7): 20170234.

Feduccia, A. 1995. Explosive evolution in Tertiary birds and mammals. Science 267: 637–638.

Feduccia, A. 2014. Avian extinction at the end of the Cretaceous: assessing the magnitude and subsequent explosive radiation. Cretaceous Research 50: 1–15.

Field, D.J. 2017. Big-time insights from a tiny bird fossil. Proceedings of the National Academy of Sciences of the United States of America 114: 7750–7752.

Field, D.J., et al. 2018. Complete *Ichthyornis* skull illuminates mosaic assembly of the avian head. Nature 557: 96–100.

Field, D.J., et al. 2020. Late Cretaceous neornithine from Europe illuminates the origins of crown birds. Nature 579: 397–401.

Forster, C.A., L.M. Chiappe, D.W. Krause, and S.D. Sampson. 1996. The first Cretaceous bird from Madagascar. Nature 382: 532–534.

Forster, C.A., Chiappe, L.M., O'Connor P.M., and A.H. Turner. 2020. The osteology of the Late Cretaceous paravian *Rahonavis ostromi*. Palaeontologica Electronica 23 (2): a29.

Foth, C., and O.W.M. Rauhut. 2017. Re-evaluation of the Haarlem *Archaeopteryx* and the radiation of maniraptoran theropod dinosaurs. BMC Evolutionary Biology 17: 236.

Foth, C., H. Tischlinger, and O.W.M. Rauhut. 2014. New specimen of *Archaeopteryx* provides insights into the evolution of pennaceous feathers. Nature 511: 79–82.

Funston, G.F., and P.J. Currie. 2016. A new caenagnathid (Dinosauria: Oviraptorosauria) from the Horseshoe Canyon Formation of Alberta, Canada, and a reevaluation of the relationships of Caenagnathidae. Journal of Vertebrate Paleontology 36: e1160910.

Gao, C., et al. 2008. A new basal lineage of Early Cretaceous birds from China and its implications on the evolution of the avian tail. Palaeontology 51 (4): 775–791.

Gauthier, J.A. 1986. Saurischian monophyly and the origin of birds. *In* K. Padian (editor) The origin of birds and the evolution of flight: 1–55. San Francisco: California Academy of Science.

Gauthier, J., and K. de Queiroz. 2001. Feathered dinosaurs, flying dinosaurs, crown dinosaurs, and the name "Aves." *In* J. Gauthier and L.F. Gall (editors), New perspectives on the origin and early evolution of birds: 7–41. New Haven, CT: Peabody Museum of Natural History.

Gianechini, F.A., P.J. Makovicky, S. Apesteguía, and I. Cerda. 2018. Postcranial skeletal anatomy of the holotype and referred specimens of *Buitreraptor gonzalezorum* Makovicky, Apesteguía and Agnolín 2005 (Theropoda, Dromaeosauridae), from the Late Cretaceous of Patagonia. PeerJ 6: e4558.

Gill, F., and D. Donsker (editors). 2017. IOC World Bird List (v 7.3). Online resource (https://www.worldbirdnames.org/).

Gilmore, C.W. 1924. On *Troodon validus*, an ornithopodous dinosaur from the Belly River Cretaceous of Alberta, Canada. Edmonton: University of Alberta Press, 43 pp.

Godefroit, P., et al. 2013a. A Jurassic avialan dinosaur from China resolves the early phylogenetic history of birds. Nature 498: 359–362.

Godefroit, P., et al. 2013b. Reduced plumage and flight ability of a new Jurassic paravian theropod from China. Nature Communications 4: 1394.

Goloboff, P. 1993. Estimating character weights during tree search. Cladistics 9: 83–91.

Goloboff, P.A. 1999. Analyzing large data sets in reasonable times: solutions for composite optima. Cladistics 15: 415–428.

Goloboff, P.A. 2014. Extended implied weighting. Cladistics 30: 260–272.

Goloboff, P.A., and J.S. Farris. 2001. Methods for quick consensus estimation. Cladistics 17: S26–S34.

Goloboff, P.A., et al. 2003. Improvements to resampling measures of group support. Cladistics 19: 324–332.

Goloboff, P.A., J. Farris, and K. Nixon. 2008a. TNT: a free program for phylogenetic analysis. Cladistics 24: 774–786.

Goloboff, P.A., J.M. Carpenter, J.S. Arias, and D.R.M. Esquivel. 2008b. Weighting against homoplasy improves phylogenetic analysis of morphological data sets. Cladistics 24 (5): 758–773.

Goloboff, P.A., and S.A. Catalano. 2016. TNT version 1.5, including a full implementation of phylogenetic morphometrics. Cladistics 32: 221–238.

Goloboff, P.A., A. Torres, and J.S. Arias. 2018. Weighted parsimony outperforms other methods of phylogenetic inference under models appropriate for morphology. Cladistics 34: 407–437.

Grealy, A., et al. 2017. Eggshell palaeogenomics: Palaeognath evolutionary history revealed through ancient nuclear and mitochondrial DNA from Madagascan elephant bird (*Aepyornis* sp.) eggshell. Molecular Phylogenetics and Evolution 109: 151–163.

Hackett, S.J., et al. 2008. A phylogenomic study of birds reveals their evolutionary history. Science 320: 1763–1768.

Haddrath, O., and A.J. Baker. 2012. Multiple nuclear genes and retroposons support vicariance and dispersal of the palaeognaths, and an Early Cretaceous origin of modern birds. Proceedings of the Royal Society of London B: Biological Sciences 279: 4617–4625.

Han, G., et al. 2014. A new raptorial dinosaur with exceptionally long feathering provides insights into dromaeosaurid flight performance. Nature Communications 5: 4382.

Harshman, J., et al. 2008. Phylogenomic evidence for multiple losses of flight in ratite birds. Proceedings of the National Academy of Sciences of the United States of America 105: 13462.

Holtz, T.R., and H. Osmólska. 2004. Saurischia. *In* D.B. Weishampel, P. Dodson, and H. Osmólska (editors), The Dinosauria: 21–24. Berkeley: University of California Press.

Hu, D., L. Hou, L. Zhang, and X. Xu. 2009. A pre-*Archaeopteryx* troodontid theropod from China with long feathers on the metatarsus. Nature 461: 640.

Jarvis, E.D., et al. 2014. Whole-genome analyses resolve early branches in the tree of life of modern birds. Science 346: 1320–1331.

Ji, Q., P.J. Currie, M.A. Norell, and S.-A. Ji. 1998. Two feathered dinosaurs from northeastern China. Nature 393: 753–761.

Ji, Q., et al. 2002. A new avialian bird – *Jixiangornis orientalis* gen. et sp. nov. – from the Lower Cretaceous of Western Liaoning, NE China. Journal of Nanjing University (Natural Sciences) 38: 723–736.

Kaye, T.G., et al. 2015. Laser-stimulated fluorescence in paleontology. PLoS One 10: e0125923.

Kimball, R.T., et al. 2019. A phylogenomic supertree of birds. Diversity 11: 109.

Ksepka, D.T., T. Stidham, and T. Williamson. 2017. Early Paleocene landbird supports rapid phylogenetic and morphological diversification of crown birds after the K-Pg mass extinction. Proceedings of the National Academy of Sciences of the United States of America 114 (30): 8047–8052.

Lamanna, M.C., H.D. Sues, E.R. Schachner, and T.R. Lyson. 2014. A new large-bodied oviraptorosaurian theropod dinosaur from the latest Cretaceous of western North America. PLoS One 9: e92022.

Lee, M.S.Y., A. Cau, D. Naish, and G.J. Dyke. 2014. Sustained miniaturization and anatomical innovation in the dinosaurian ancestors of birds. Science 345: 562–566.

Lefèvre, U., D.Y. Hu, F. Escuillié, G.D. Dyke, and P. Godefroit. 2014. A new long-tailed basal bird from the Lower Cretaceous of north-eastern China. Biological Journal of the Linnean Society 113: 790–804.

Lefèvre, U., et al. 2017. A new Jurassic theropod from China documents a transitional step in the macrostructure of feathers. Science of Nature 104: 74.

Leidy, J. 1856. Notices of the remains of extinct reptiles and fishes discovered by Dr. F.V. Hayden in the badlands of the Judith river, Nebraska Territory. Proceedings of the Academy of Natural Sciences of Philadelphia 8: 72–73.

Li, Z.H., Z.H. Zhou, M. Wang, and J.A. Clarke. 2014. A new specimen of large-bodied basal enantiornithine *Bohaiornis* from the Early Cretaceous of China and the inference of feeding ecology in Mesozoic birds. Journal of Paleontology 88: 99–108.

Linnaeus, C. 1758. Systema naturae per regna tria naturae, secundum classes, ordines, genera, species, cum characteribus, differentiis, synonymis, locis, 10th ed. Holmiae [Stockholm]: Laurentii Salvii.

Lockley, M.G., R.H. Li, J.D. Harris, M. Matsukawa, and M.W. Liu. 2007. Earliest zygodactyl bird feet: evidence from Early Cretaceous roadrunner-like tracks. Naturwissenschaften 94: 657–665.

Longrich, N.R., and P.J. Currie. 2009. A microraptorine (Dinosauria-Dromaeosauridae) from the Late Cretaceous of North America. Proceedings of the National Academy of Sciences of the United States of America 106: 5002–5007.

Longrich, N.R., P.J. Currie, and Z. Dong. 2010. A new oviraptorid (Dinosauria: Theropoda) from the Upper Cretaceous of Bayan Mandahu, Inner Mongolia. Palaeontology 53: 945–960.

Longrich, N.R., T. Tokaryk, and D.J. Field. 2011. Mass extinction of birds at the Cretaceous–Paleogene (K–Pg) boundary. Proceedings of the National Academy of Sciences of the United States of America 108: 15253–15257.

Longrich, N.R., K. Barnes, S. Clark, and L. Millar. 2013. Caenagnathidae from the Upper Campanian Aguja Formation of West Texas, and a Revision of the Caenagnathinae. Bulletin of the Peabody Museum of Natural History 54: 23–49.

Lü, J.C., and S.L. Brusatte. 2015. A large, short-armed, winged dromaeosaurid (Dinosauria: Theropoda) from the Early Cretaceous of China and its implications for feather evolution. Scientific Reports 5: 11775.

Lü, J.C., and B.K. Zhang. 2005. A new oviraptorid (Theropod: Oviraptorosauria) from the Upper Cretaceous of the Nanxiong Basin, Guangdong Province of southern China. Acta Palaeontologica Sinica 44: 412–422.

Lü, J.C., et al. 2007. New dromaeosaurid dinosaur from the Late Cretaceous Qiupa Formation of Luanchuan area, western Henan, China. Geological Bulletin of China 26: 777–786.

Lü, J.C., et al. 2015. A new oviraptorid dinosaur (Dinosauria: Oviraptorosauria) from the Late Cretaceous of Southern China and its paleobiogeographical implications. Scientific Reports 5: 11490.

Lü, J.C., R.J. Chen, S.L. Brusatte, Y.X. Zhu, and C.Z. Shen. 2016. A Late Cretaceous diversification of Asian oviraptorid dinosaurs: evidence from a new species preserved in an unusual posture. Scientific Reports 6: 35780.

Lü, J.C., et al. 2017. High diversity of the Ganzhou Oviraptorid Fauna increased by a new "cassowary-like" crested species. Scientific Reports 7 (1): 6393.

Makovicky, P.J., S. Apesteguía, F.L. Agnolín. 2005. The earliest dromaeosaurid theropod from South America. Nature 437: 1007–1011.

Maryańska, T., H. Osmólska, and M. Wolsan. 2002. Avialan status for Oviraptorosauria. Acta Palaeontologica Polonica 47: 97–116.

Matthew, W.D., and B. Brown. 1922. The family Deinodontidae, with notice of a new genus from the Cretaceous of Alberta. Bulletin of the American Museum of Natural History 46: 367–385.

McCormack, J.E., et al. 2013. A phylogeny of birds based on over 1,500 loci collected by target enrichment and high-throughput sequencing. PLoS One 8: e54848.

Mitchell, K.J., et al. 2014. Ancient DNA reveals elephant birds and kiwi are sister taxa and clarifies ratite bird evolution. Science 344: 898–900.

Norell, M.A., and J.A. Clarke. 2001. Fossil that fills a critical gap in avian evolution. Nature 409: 181–184.

Norell, M.A., J.M. Clark, and P.J. Makovicky. 2001. Phylogenetic relationships among coelurosaurian theropods. *In* Gauthier, J., and L.F. Gall (editors), New perspectives on the origin and early evolution of birds: 49–68. New Haven, CT: Peabody Museum of Natural History, Yale University.

Novas, F.E., and D. Pol. 2005. New evidence on deinonychosaurian dinosaurs from the Late Cretaceous of Patagonia. Nature 433: 858–861.

Novas, F.E., and P.F. Puerta. 1997. New evidence concerning avian origins from the Late Cretaceous of Patagonia. Nature 387: 390–392.

Novas, F.E., D. Pol, J.I. Canale, J.D. Porfiri, and J.O. Calvo. 2009. A bizarre Cretaceous theropod dinosaur from Patagonia and the evolution of Gondwanan dromaeosaurids. Proceedings of the Royal Society B Biological Sciences 276: 1101–1007.

Novas, F.E., F. Brissón Egliae, F.L. Agnolín, F.A. Gianechini, and I. Cerda. 2018. Postcranial osteology of a new specimen of *Buitreraptor gonzalezorum* (Theropoda, Unenlagiidae). Cretaceous Research 83: 127–167.

O'Connor, J.K. 2009. A systematic review of Enantiornithes (Aves: Ornithothoraces). Ph.D. dissertation, Department of Earth Sciences, University of Southern California, Los Angeles.

O'Connor, J.K., and C. Sullivan. 2014. Reinterpretation of the Early Cretaceous maniraptoran (Dinosauria: Theropoda) *Zhongornis haoae* as a scansoriopterygid-like non-avian, and morphological resemblances between scansoriopterygids and basal oviraptorosaurs. Vertebrata Palasiatica 52: 3–30.

O'Connor, J.K., and Z.H. Zhou. 2013. A redescription of *Chaoyangia beishanensis* (Aves) and a comprehensive phylogeny of Mesozoic birds. Journal of Systematic Palaeontology 11: 889–906.

O'Connor, J.K., et al. 2009. Phylogenetic support for a specialized clade of Cretaceous enantiornithine birds with information from a new species. Journal of Vertebrate Paleontology 29: 188–204.

O'Connor, J.K., L.M. Chiappe, and A. Bell. 2011. Premodern birds: avian divergences in the Mesozoic. *In* G.D. Dyke and G. Kaiser (editors), Living dinosaurs: the evolutionary history of birds: 39–114. Hoboken, NJ: J. Wiley and Sons.

O'Connor, J.K., A. Averianov, and N.Z. Zelenkov. 2014. A confuciusornithiform (Aves: Pygostylia) -like tarsometatarsus from the Early Cretaceous of Siberia and a discussion of the evolution of avian hindlimb musculature. Journal of Vertebrate Paleontology 34: 647–656.

O'Connor, J.K., M. Wang, and H. Hu. 2016. A new ornithuromorph (Aves) with an elongate rostrum from the Jehol Biota and the early evolution of rostralization in birds. Journal of Systematic Palaeontology 14: 939–948.

O'Connor, J.K., X.T. Zheng, H. Hu, X.L. Wang, and Z.H. Zhou. 2017. The morphology of *Chiappeavis magnapremaxillo* (Pengornithidae: Enantiornithes) and a comparison of aerodynamic function in Early Cretaceous avian tail fans. Vertebrata Palasiatica 55: 1–18.

Oliveros, C.H., et al. 2019. Earth history and the passerine superradiation. Proceedings of the National Academy of Sciences of the United States of America 116: 7916–7925.

Osborn, H.F. 1924. Three new Theropoda, *Protoceratops* zone, central Mongolia. American Museum Novitates 144: 1–12.

Ostrom, J.H. 1969. Osteology of *Deinonychus antirrhopus*, an unusual theropod dinosaur from the Lower Cretaceous of Montana. Bulletin of the Peabody Museum of Natural History 30: 1–165.

Pei, R., Q.G. Li, Q.J. Meng, M.A. Norell, and K.Q. Gao. 2017. New specimens of *Anchiornis huxleyi* (Theropoda: Paraves) from the Middle-Late Jurassic of northeastern China. Bulletin of the American Museum of Natural History 411: 1–67.

Pei, R., et al. In press. Potential for powered flight neared by most close avialan relatives but few crossed its thresholds. Current Biology.

Phillips, M.J., G.C. Gibb, E.A. Crimp, and D. Penny. 2010. Tinamous and moa Flock together: mitochondrial genome aequence analysis reveals independent losses of flight among ratites. Systematic Biology 59: 90–107.

Pittman, M., S.M. Gatesy, P. Upchurch, A. Goswami, and J.R. Hutchinson. 2013. Shake a tail feather: the evolution of the theropod tail into a stiff aerodynamic surface. PLoS One 8: e63115.

Pittman, M., R. Pei, Q.W. Tan, and X. Xu. 2015. The first dromaeosaurid (Dinosauria: Theropoda) from the Lower Cretaceous Bayan Gobi Formation of Nei Mongol, China. PeerJ 3: e1480.

Prum, R.O., et al. 2015. A comprehensive phylogeny of birds (Aves) using targeted next-generation DNA sequencing. Nature 526: 569–573.

Pu, H.Y., et al. 2017. Perinate and eggs of a giant caenagnathid dinosaur from the Late Cretaceous of central China. Nature Communications 8: 14952.

Rashid, D.J., et al. 2018. Avian tail ontogeny, pygostyle formation, and interpretation of juvenile Mesozoic specimens. Scientific Reports 8: 9014.

Rauhut, O.W.M., C. Foth, and H. Tischlinger. 2018. The oldest *Archaeopteryx* (Theropoda: Avialiae): a new specimen from the Kimmeridgian/Tithonian boundary of Schamhaupten, Bavaria. PeerJ 6: e4191.

Reddy, S., et al. 2017. Why do phylogenomic data sets yield conflicting trees? Data type influences the avian tree of life more than taxon sampling. Systematic Biology 66: 857–879.

Senter, P. 2007. A new look at the phylogeny of Coelurosauria (Dinosauria: Theropoda). Journal of Systematic Palaeontology 5: 429–463.

Senter, P., R. Barsbold, B. Britt, and D.A. Burnham. 2004. Systematics and evolution of Dromaeosauridae (Dinosauria, Theropoda). Bulletin of the Gunma Museum of Natural History 8: 1–20.

Senter, P., J.I. Kirkland, D.D. DeBlieux, S. Madsen, and N. Toth. 2012. New dromaeosaurids (Dinosauria: Theropoda) from the Lower Cretaceous of Utah, and the evolution of the dromaeosaurid tail. PLoS One 7: e36790.

Sereno, P.C. 1997. The origin and evolution of dinosaurs. Annual Review of Earth and Planetary Sciences 25: 435–489.

Sereno, P.C. 1998. A rationale for phylogenetic definitions, with application to the higher-level taxonomy of Dinosauria. Neues Jahrbuch für Geologie und Palaeontologie Abhandlungen 210: 41–83.

Sereno, P.C., S. McAllister, and S.L. Brusatte. 2005. TaxonSearch: a relational database for suprageneric taxa and phylogenetic definitions. PhyloInformatics 8: 1–21.

Smith, J.V., E.L. Braun, and R.T. Kimball. 2013. Ratite nonmonophyly: independent evidence from 40 novel loci. Systematic Biology 62: 35–49.

Sues, H.D. 1978. A new small theropod dinosaur from the Judith River Formation (Campanian) of Alberta Canada. Zoological Journal of the Linnean Society 62: 381–400.

Suh, A. 2016. The phylogenomic forest of bird trees contains a hard polytomy at the root of Neoaves. Zoologica Scripta 45 (S1): 50–62.

Sullivan, R.M., S.E. Jasinski, and M.P.A. van Tomme. 2011. A new caenagnathid *Ojoraptorsaurus boerei*, n. gen., n. sp. (Dinosauria, Oviraptorosauria), from the Upper Cretaceous Ojo Alamo Formation (Naashoibito member), San Juan basin, New Mexico. Bulletin of the New Mexico Museum of Natural History and Science 53: 418–428.

Suzuki, S., et al. 2002. A new specimen of *Shuvuuia deserti* Chiappe et al., 1998 from the Mongolian Late Cretaceous with a discussion of the relationships of alvarezsaurids to other theropod dinosaurs. Contributions in Science of the Natural History Museum of Los Angeles County 494: 1–18.

Turner, A.H., D. Pol, J.A. Clarke, G.M. Erickson, and M.A. Norell. 2007a. A basal dromaeosaurid and size evolution preceding avian flight. Science 317: 1378–1381.

Turner, A.H., S.H. Hwang, and M.A. Norell. 2007b. A small derived theropod from Öösh, Early Cretaceous, Baykhangor Mongolia. American Museum Novitates 3557: 1–27.

Turner, A.H., P.J. Makovicky, and M.A. Norell. 2012. A review of dromaeosaurid systematics and paravian phylogeny. Bulletin of the American Museum of Natural History 371: 1–206.

van der Reest, A.J., and P.J. Currie. 2017. Troodontids (Theropoda) from the Dinosaur Park Formation, Alberta, with a description of a unique new taxon: implications for deinonychosaur diversity in North America. Canadian Journal of Earth Sciences 54: 919–935.

Wang, M., J.K. O'Connor, N.Z. Zelenkov, and Z.H. Zhou. 2014. A new diverse enantiornithine family (Bohaiornithidae fam. nov.) from the Lower Cretaceous of China with information from two new species. Vertebrata Palasiatica 52: 31–76.

Wang, M., et al. 2015. The oldest record of Ornithuromorpha reveals heterogeneous rates of morphological evolution among Early Cretaceous birds. Nature Communications 6: 6987.

Wang, M., J.K. O'Connor, Y.H. Pan, and Z.H. Zhou. 2017b. A bizarre Early Cretaceous enantiornithine bird with unique crural feathers and an ornithuromorph plough-shaped pygostyle. Nature Communications 8: 1–12.

Wang, M., T.A. Stidham, and Z.H. Zhou. 2018a. A new clade of basal Early Cretaceous pygostylian birds and developmental plasticity of the avian shoulder girdle. Proceedings of the National Academy of Sciences of the United States of America 115: 10708–10713.

Wang, W., and J.K. O'Connor. 2017. Morphological coevolution of the pygostyle and tail feathers in Early Cretaceous birds. Vertebrata Palasiatica 55: 289–314.

Wang, X.L., et al. 2017a. Basal paravian functional anatomy illuminated by high-detail body outline. Nature Communications 8: 14576.

Wang, X., et al. 2018b. The earliest evidence for a supraorbital salt gland in dinosaurs in new Early Cretaceous ornithurines. Scientific Reports 8: 1–12.

Xu, X. 2018. Mosaic evolution in birds: brain vs. feeding apparatus. Science Bulletin 63: 812–813.

Xu, X. 2020. Filamentous integuments in nonavialan theropods and their kin: advances and future perspectives for understanding the evolution of feathers. In C. Foth, C. and O.W.M. Rauhut (editors), The evolution of feathers: 67–78. Cham, Switzerland: Springer.

Xu, X., Z.H. Zhou, and X.L. Wang. 2000. The smallest known non-avian theropod dinosaur. Nature 408: 705–708.

Xu, X., et al. 2010. A new dromaeosaurid (Dinosauria: Theropoda) from the Upper Cretaceous Wulansuhai Formation of Inner Mongolia, China. Zootaxa 2403: 1–9.

Xu, X., H.L. You, K. Du, and F.L. Han. 2011. An *Archaeopteryx*-like theropod from China and the origin of Avialae. Nature 475: 465–470.

Xu, X., et al. 2014. An integrative approach to understanding bird origins. Science 346: 12532931–12532939.

Xu, X., et al. 2015. A bizarre Jurassic maniraptoran theropod with preserved evidence of membranous wings. Nature 521: 70–73.

Xu, X., et al. 2016. An updated review of the Middle-Late Jurassic Yanliao Biota: chronology, taphonomy, paleontology, and paleoecology. Acta Geologica Sinica (English Edition) 90: 2229-2243.

Xu, X., et al. 2017. Mosaic evolution in an asymmetrically feathered troodontid dinosaur with transitional features. Nature Communications 8: 14972.

Yonezawa, T., et al. 2016. Phylogenomics and morphology of extinct paleognaths reveal the origin and evolution of the ratites. Current Biology 27: 68–77.

You, H.L., et al. 2006. A nearly modern amphibious bird from the Early Cretaceous of northwestern China. Science 312: 1640–1643.

Yu, Y., et al. 2018. A new caenagnathid dinosaur from the Upper Cretaceous Wangshi Group of Shandong, China, with comments on size variation among oviraptorosaurs. Scientific Reports 8: 5030.

Zanno, L.E. 2010. A taxonomic and phylogenetic re-evaluation of Therizinosauria (Dinosauria: Maniraptora). Journal of Systematic Palaeontology 8: 503–543.

Zanno, L.E., and S.D. Sampson. 2005. A new oviraptorosaur (Theropoda, Maniraptora) from the Late Cretaceous (Campanian) of Utah. Journal of Vertebrate Paleontology 25: 897–904.

Zelenitsky, D., et al. 2012. Feathered non-avian dinosaurs from North American provide insight into wing origins. Science 338: 510–514.

Zelenkov, N.Z. 2017. Early Cretaceous enantiornithine birds (Aves, Ornithothoraces) and establishment of the Ornithuromorpha morphological type. Paleontological Journal 51: 628–642.

Zhang, Z., et al. 2006. The first Mesozoic heterodactyl bird from China. Acta Geologica Sinica 80: 631–635.

Zheng, X.T., H.L. You, X. Xu, and Z.M. Dong. 2009. An Early Cretaceous heterodontosaurid dinosaur with filamentous integumentary structures. Nature 458: 334–336.

Zheng, X.T., et al. 2014. On the absence of sternal elements in *Anchiornis* (Paraves) and *Sapeornis* (Aves) and the complex early evolution of the avian sternum. Proceedings of the National Academy of Sciences of the United States of America 111: 13900–13905.

Zhou, S., Z.H. Zhou, and J.K. O'Connor. 2012. A new toothless ornithurine bird (*Schizooura lii* gen. et sp. nov.) from the Lower Cretaceous of China. Vertebrata PalAsiatica 50: 9–24.

Zhou, S., J.K. O'Connor, and M. Wang. 2014. A new species from an ornithuromorph dominated locality of the Jehol Group. Chinese Science Bulletin 59: 5366–5378.

Zhou, Z., and F. Zhang. 2002. Largest bird from the Early Cretaceous and its implications for the earliest avian ecological diversification Naturwissenschaften 89: 34–38.

Chapter 2

The Fossil Record of Mesozoic and Paleocene Pennaraptorans

MICHAEL PITTMAN,[1] JINGMAI O'CONNOR,[2] EDISON TSE,[1]
PETER MAKOVICKY,[3] DANIEL J. FIELD,[4] WAISUM MA,[5] ALAN H. TURNER,[6]
MARK A. NORELL,[7] RUI PEI,[2] AND XING XU[2]

ABSTRACT

An unabated surge of new and important discoveries continues to transform knowledge of pennaraptoran biology and evolution amassed over the last 150+ years. This chapter summarizes progress made thus far in sampling the pennaraptoran fossil record of the Mesozoic and Paleocene and proposes priority areas of attention moving forward.

Oviraptorosaurians are bizarre, nonparavian pennaraptorans first discovered in North America and Mongolia within Late Cretaceous rocks in the early 20th century. We now know that oviraptorosaurians also occupied the Early Cretaceous and their unquestionable fossil record is currently limited to Laurasia. Early Cretaceous material from China preserves feathers and other soft tissues and ingested remains including gastroliths and other stomach contents, while brooding specimens and age-structured, single-species accumulations from China and Mongolia provide spectacular behavioral insights. Less specialized early oviraptorosaurians like *Incisivosaurus* and *Microvenator* remain rare, and ancestral forms expected in the Late Jurassic are yet to be discovered, although some authors have suggested *Epidexipteryx* and possibly other scansoriopterygids may represent early-diverging oviraptorosaurians.

Long-armed scansoriopterygids from the Middle-Late Jurassic of Laurasia are either early-diverging oviraptorosaurians or paravians, and some have considered them to be early-diverging avialans. Known from five (or possibly six) feathered specimens from China, only two mature individuals exist, representing these taxa. These taxa, *Yi* and *Ambopteryx*, preserve stylopod-supported wing membranes that are the only known alternative to the feathered, muscular wings that had been exclusively associated with dinosaurian flight. Thus, scansoriopterygid specimens—particularly those preserving soft tissue—remain a key priority for future specimen collection.

Dromaeosaurids and troodontids were first discovered in North America and Mongolia in Late Cretaceous rocks. More recent discoveries show that these animals originated in the Late Jurassic, were strikingly feathered, lived across diverse climes and environments, and at least in the case of dromaeosaurids, attained a global distribution and the potential for aerial locomotion at small size.

---

[1] Vertebrate Palaeontology Laboratory, Division of Earth and Planetary Science, the University of Hong Kong, Hong Kong.

[2] Key Laboratory of Vertebrate Evolution and Human Origins, Institute of Vertebrate Paleontology & Paleoanthropology, Beijing; and CAS Center for Excellence in Life and Paleoenvironment, Beijing.

[3] Department of Earth and Environmental Sciences, University of Minnesota, Minneapolis, MN.

[4] Department of Earth Sciences, University of Cambridge, Cambridge.

[5] School of Geography, Earth and Environmental Sciences, University of Birmingham, Birmingham, U.K.

[6] Department of Anatomical Sciences, Stony Brook University, Stony Brook, NY.

[7] Division of Paleontology, American Museum of Natural History, New York.

China and Mongolia have yielded the most dromaeosaurid and troodontid specimens and taxa, but Gondwanan troodontids are almost unknown compared to southern dromaeosaurids, so the fidelity of this biogeographical signal is worth further exploration. Discovery of well-preserved Middle-Late Jurassic material will be crucial for understanding the origin of key dromaeosaurid and troodontid traits, with the controversial anchiornithines potentially already offering this if their troodontid status can be solidified.

In line with the preferences of most theropod palaeontologists, birds are defined herein as members of Avialae, including stem and crown taxa, whilst Aves herein refers to crown-group birds (see Pittman et al., chapter 1, for the precise definition of Avialae adopted; elsewhere, typically among ornithologists, Aves refers to stem and crown taxa whilst Neornithes refers to crown-group birds). Despite taphonomic bias against avialans in the fossil record, their Early Cretaceous record is fairly robust largely due to the high taxonomic and ecological diversity preserved within the rich Jehol deposits of northeastern China. *Archaeopteryx* (and possibly the controversial Middle-Late Jurassic anchiornithines) show what some of the earliest birds were like, but better-preserved soft tissues hold the key to understanding their substantially different anatomy and flight capabilities to crown-group birds (Aves).

The Late Cretaceous–early Paleocene fossil record of crown birds is especially poor, and improved sampling will be necessary to clarify our understanding of avialan survivorship, ecological selectivity, and recovery across the end-Cretaceous mass extinction. Deposits of Eocene age, such as Messel and Green River, have been especially useful for documenting the early evolutionary history of crown birds. However, the discovery of new Cretaceous and/or Palaeogene bird-bearing lagerstätten from Gondwana will be important for accurately determining ancestral biogeographic patterns.

BACKGROUND

Pennaraptorans are a clade of vaned feathered coelurosaurian dinosaurs that are comprised of the Oviraptorosauria, Scansoriopterygidae, Dromaeosauridae, Troodontidae, and Avialae (see Pittman et al., in the previous chapter for additional information). They include the only dinosaurs to have evolved flight and the only ones to have persisted to the present day.

OVIRAPTOROSAURIA

Oviraptorosaurian fossils were first discovered in the 1920s and are now represented by more than 40 genera spanning a size range across three orders of magnitude (table 1). The 1920s to 1940s, the 1970s, 1980s, 1990s, and the past 20 years have been key periods in our documentation of the oviraptorosaurian fossil record, which is limited to Laurasian continents and dominated by discoveries from Asia and North America (fig. 1). The last 30 years have seen the discovery of most known oviraptorosaurian taxa, particularly from the Cretaceous of China and the Late Cretaceous of North America and Mongolia. These discoveries have greatly broadened our understanding of this group, including in regard to the evolution of their beaked and strangely pneumatized skulls, as well as the origin of brooding in theropod dinosaurs.

ASIA: This continent is the home of the first described oviraptorosaurian species (Osborn, 1924), the eponymous species *Oviraptor*. Asia is also home to more than 75% of valid oviraptorosaurian genera. The most important sources of Asian oviraptorosaurians are the Early Cretaceous (Hauterivian-Aptian) Jehol Lagerstätte of northeastern China, the Campanian-Maastrichtian Ganzhou oviraptorid fauna of southern

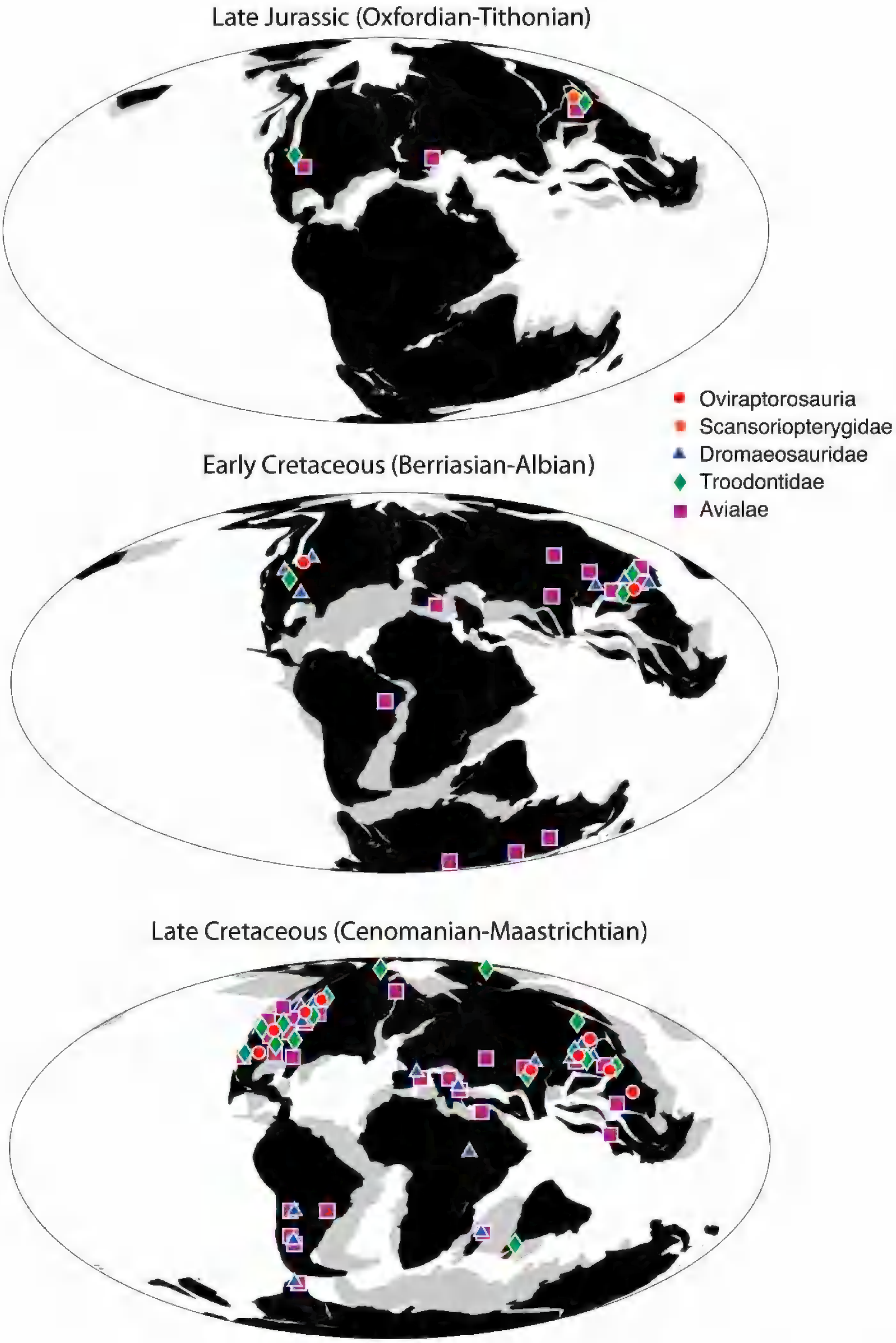
Late Jurassic (Oxfordian-Tithonian)
Early Cretaceous (Berriasian-Albian)
Late Cretaceous (Cenomanian-Maastrichtian)
● Oviraptorosauria
● Scansoriopterygidae
▲ Dromaeosauridae
◆ Troodontidae
■ Avialae

FIG. 1. Geographic distribution of pennaraptoran theropods illustrated on palaeogeographic globes of the Late Jurassic (Oxfordian-Tithonian), Early Cretaceous (Berriasian-Albian), and Late Cretaceous (Cenomanian-Maastrichtian). Palaeomaps modified from GPlates (www.gplates.org) (Müller et al., 2018).

TABLE 1

Oviraptorosaurian fossil record

Continent	Geological Unit	Country	Period	Age	Age Reference	Taxa	Reference
Asia	Jehol Group (Yixian Formation; Jiufotang Formation)	China	Early Cretaceous	Barremian-Aptian	Chang et al., 2009, 2017; Pan et al., 2013	*Incisivosaurus*, *Caudipteryx*, *Ningyuansaurus*, *Protarchaeopteryx*, *Similicaudipteryx* (possibly *Incisivosaurus*), *Xingtianosaurus*; *Similicaudipteryx*	Ji and Ji, 1997; Ji et al., 1998; 2012; Zhou et al., 2000; Xu et al., 2002a, 2010a; He et al., 2008; Balanoff et al., 2009; Qiu et al., 2019
	Nanxiong Formation	China	Late Cretaceous	Campanian-Maastrichtian	Bureau of Geology and Mineral Resources of Jiangxi Province, 1984	*Banji*, *Corythoraptor*, *Ganzhousaurus*, *Huanansaurus*, *Jiangxisaurus*, *Nankangia*, *Tongtianlong*	Xu and Han, 2010; Lü et al., 2013a; Wang et al., 2013a; Wei et al., 2013; Lü et al., 2015, 2016, 2017
	Haoling Formation	China	Early Cretaceous	Aptian/Albian	Xu et al., 2012a	*Luoyanggia*	Lü et al., 2009
	Dalangshan Formation	China	Late Cretaceous	Maastrichtian	Bureau of Geology and Mineral Resources of Guangdong Province, 1988	*Heyuannia*	Lü, 2003
	Pingling Formation	China	Late Cretaceous	Maastrichtian	Zhao et al., 1991	*Shixinggia*	Lü and Zhang, 2005
	Qiupa Formation	China	Late Cretaceous	Campanian-Maastrichtian	Jiang et al., 2011	*Yulong*	Lü et al., 2013b
	Gaogou Formation	China	Late Cretaceous	Cenomanian-Turonian	Liang et al., 2009	*Beibeilong*	Pu et al., 2017
	Erlian (Iren Dabasu) Formation	China	Late Cretaceous	Campanian-Maastrichtian	van Itterbeeck et al., 2005; Bonnetti et al., 2014	*Avimimus*, *Caenagnathasia*, *Gigantoraptor*	Kurzanov, 1981; Xu et al., 2007; Yao et al., 2015; Ma et al., 2017
	Wulansuhai (Bayan Mandahu) Formation	China	Late Cretaceous	Campanian	Godefroit et al., 2008	*Machairasaurus*, *Wulatelong*	Longrich et al., 2010; Xu et al., 2013b
	Wangshi Group	China	Late Cretaceous	Campanian	An et al., 2016	*Anomalipes*	Yu et al., 2018
	Djadokhta Formation	Mongolia	Late Cretaceous	Campanian	van Itterbeeck et al., 2005; Dingus et al., 2008; Hasegawa et al., 2009	*Avimimus*, *Citipati*, *Khaan*, *Oviraptor*	Osborn, 1924; Kurzanov, 1981; Clark et al., 2001; Clark et al., 2002; Balanoff and Norell, 2012

TABLE 1 *continued*

Continent	Geological Unit	Country	Period	Age	Age Reference	Taxa	Reference
Asia	Barun Goyot Formation	Mongolia	Late Cretaceous	Campanian-Maastrichtian	Gradziński and Jerzykiewicz, 1974a, b; Fanti et al., 2012	*Ajancingenia/'Ingenia'/Heyuannia yanshini*, *Avimimus*, *Conchoraptor*, *Nemegtomaia*	Barsbold, 1981; 1986; Longrich et al., 2010; Fanti et al., 2012; Funston et al., 2017
	Nemegt Formation	Mongolia	Late Cretaceous	Maastrichtian	Jerzykiewicz and Russell, 1991; Shuvalov, 2000; van Itterbeeck et al., 2005	*Avimimus*, *Elmisaurus*, *Gobiraptor*; *Nemegtomaia*, *Nomingia*, *Rinchenia*	Barsbold, 1981, 1986, 2000; Lü et al., 2004, 2005; Longrich et al., 2010; Osmólska, 1981; Fanti et al., 2012; Currie et al., 2015; Funston et al., 2017; Lee et al., 2019
	Bissekty Formation	Uzbekistan	Late Cretaceous	Turonian	Sues and Averianov, 2014, 2015	*Caenagnathasia*	Currie et al., 1993; Sues and Averianov, 2015
North America	Cloverly Formation	U.S.	Early Cretaceous	pre-Aptian-Albian	Oreska et al., 2013; Farke et al., 2014	*Microvenator*	Makovicky, 1998
	Aguja Formation	U.S.	Late Cretaceous	Campanian-Maastrichtian	Lehman, 1985; Sankey, 2001	*Leptorhynchos*	Longrich et al., 2013
	Two Medicine Formation	U.S.	Late Cretaceous	Campanian	Rogers et al., 1993; Foreman et al., 2008	*Chirostenotes*?	Osmólska et al., 2004
	Hell Creek Formation	U.S.	Late Cretaceous	Maastrichtian	Hoganson and Edward, 2002; Fastovsky and Bercovici, 2016	*Anzu*, *Chirostenotes*?	Osmólska et al., 2004; Lamanna et al., 2014
	Kaiparowits Formation	U.S.	Late Cretaceous	Campanian	Roberts et al., 2005; Jinnah et al., 2009; Zanno et al., 2011	*Hagryphus*	Zanno and Sampson, 2005
	Ojo Alamo Formation	U.S.	Late Cretaceous	Maastrichtian	Sullivan and Lucas, 2006; Sullivan et al., 2001	*Ojoraptorsaurus*	Sullivan et al., 2011
	Belly River Formation	Canada	Late Cretaceous	Campanian	Eberth, 2005	*Chirostenotes*	Gilmore, 1924
	Dinosaur Park Formation	Canada	Late Cretaceous	Campanian	Eberth, 2005; Brown et al., 2013	*Caenagnathus*, *Chirostenotes*, *Leptorhynchos*	Osmólska et al., 2004; Longrich et al., 2013; Funston and Currie, 2014; Funston et al., 2015
	Horseshoe Canyon Formation	Canada	Late Cretaceous	Campanian-Maastrichtian	Eberth and Braman, 2012; Quinney et al., 2013	*Epichirostenotes*, *Apatoraptor*	Sullivan et al., 2011; Funston and Currie, 2016

China (Nanxiong Formation) as well as the southern Mongolian Campanian Djadokhta Formation (and the similar Wulansuhai (Bayan Mandahu) Formation in China), Campanian-Maastrichtian Barun Goyot Formation, and the Maastrichtian Nemegt Formation.

Jehol oviraptorosaurians represent the oldest unequivocal oviraptorosaurian records, and the six described taxa include some articulated specimens preserving feathers, gastroliths, and stomach contents. The early-diverging oviraptorosaurians *Incisivosaurus*, *Protarchaeopteryx*, *Similicaudipteryx*, *Caudipteryx*, *Xingtianosaurus*, and *Ningyuansaurus* are the only known toothed forms and have less specialized skulls compared to later oviraptorosaurians (Ji et al., 1998; Zhou et al., 2000; Xu et al., 2002a; Balanoff et al., 2009; Qiu et al., 2019). *Caudipteryx* is known for its pennaceous feathered arms, gastroliths, and a tail plume probably used for display purposes (Ji et al., 1998; Zhou et al., 2000; Pittman et al., 2013; Persons et al., 2014). It is known from two species (Ji et al., 1998; Zhou et al., 2000), although this is contested. Both specimens were recovered from the ~125 Ma Yixian Formation in Liaoning province, with both 2-D and 3-D preservations. Two specimens of *Similicaudipteryx*, another Yixian Formation genus, show radical changes to feather morphology during ontogeny (Xu et al., 2010a). However, these two specimens might be specimens of *Incisivosaurus* (Xu, 2020). *Ningyuansaurus* possibly preserves seeds within its body cavity (Ji et al., 2012). *Xingtianosaurus* is the most recently named Jehol genus, which is known from an articulated postcranial skeleton (Qiu et al., 2019). *Luoyanggia* is an Aptian- to Albian-aged oviraptorid from the Haoling Formation of Henan, central China, which was previously thought to be Late Cretaceous in age (Lü et al., 2009; Xu et al., 2012a).

The Late Cretaceous Ganzhou fauna of Jiangxi, southern China, has the greatest known diversity of oviraptorid oviraptorosaurians with seven reported genera in the Campanian-Maastrichtian Nanxiong Formation: *Banji*, *Huanansaurus*, *Jiangxisaurus*, *Tongtianlong*, *Ganzhousaurus*, *Nankangia*, and *Corythoraptor* (Xu and Han, 2010; Lü et al., 2013a, 2015, 2016, 2017; Wang et al., 2013a; Wei et al., 2013). Embryos of an oviraptorid have also been recovered from this formation (Wang et al., 2016a). *Heyuannia* is an oviraptorid genus described from a partial skeleton from the Maastrichtian Dalangshan Formation of Guangdong, southern China (Lü, 2003). "*Ingenia*," or *Ajancingenia yanshini*, from the Campanian-Maastrichtian Barun Goyot Formation of southern Mongolia (Barsbold, 1981; Easter, 2013) has been referred to this genus as a second species, *H. yanshini*, but this involves a very large geographical and temporal separation between species (Funston et al., 2017). *Shixinggia* is another described Guangdong oviraptorid from the Maastrichtian Pingling Formation (Lü and Zhang, 2005). *Yulong* is a chicken-sized oviraptorid represented by excellent fossil material from the Upper Cretaceous Qiupa Formation of Henan, central China (Lü et al., 2013b), while *Beibeilong* is a caenagnathid known from a perinate skeleton and some eggs from the Cenomanian-Turonian Gaogou Formation of the same province (Pu et al., 2017). *Anomalipes* is a recently reported caenagnathid from the Campanian Wangshi Group of Shandong Province, known only from hind-limb elements (Yu et al., 2018). The largest known oviraptorosaurian—the caenagnathid *Gigantoraptor*—was recovered in the northernmost frontier of China from the Campanian-Maastrichtian Erlian (Iren Dabasu) Formation of Nei Mongol (Inner Mongolia) (Xu et al., 2007). This is also the locality for one of the smallest oviraptorosaurians, *Avimimus*, which was first reported from similarly aged rocks in Mongolia (Kurzanov, 1981), although these assignments would benefit from review, as they may represent different taxa. The Campanian Wulansuhai (Bayan Mandahu) Formation, also in the Gobi Desert region, is the home to the oviraptorids *Machairasaurus* and *Wulatelong* and some other indeterminate oviraptorid material (Longrich et al., 2010; Xu et al., 2013b).

Mongolian oviraptorosaurians are dominated by oviraptorids, with three genera from the Campanian Djadokhta Formation (*Oviraptor*, *Citipati*, and *Khaan*) (Osborn, 1924; Clark et al., 2001, 2002; Balanoff and Norell, 2012), four genera from the Maastrichtian Nemegt Formation (*Gobiraptor*, *Nomingia*, *Rinchenia*, and *Nemegtomaia*) (Barsbold, 1986; Barsbold et al., 2000; Lü et al., 2004, 2005; Fanti et al., 2012; Funston et al., 2017; Lee et al., 2019) and three from the Campanian-Maastrichtian Barun Goyot Formation ("*Ingenia*"/*Ajancingenia*/*Heyuannia yanshini*, *Conchoraptor*, and *Nemegtomaia* [also from the Nemegt]; see Fanti et al., 2012, for details of Maastrichtian portion) (Barsbold, 1981; 1986; Longrich et al., 2010; Funston et al., 2017). Several skeletons are known for *Khaan* and *Citipati* from the rich fossil beds of Ukhaa Tolgod, including brooding specimens, single species group associations and embryos (Norell et al., 1995, 2001; Clark et al., 2001).

Avimimus is a small, early-diverging oviraptorosaurian closer to Caenagnathidae and Oviraptoridae that is known from multiple formations in Mongolia, including the Djadokhta, Nemegt, and Barun Goyot (Kurzanov, 1981; Longrich et al., 2010). *Elmisaurus* is a caenagnathid from the Nemegt Formation (Osmólska, 1981; Currie et al., 2016). The holotype of the caenagnathid *Caenagnathasia* is a pair of dentaries from a single individual recovered from the Turonian Bissekty Formation of Uzbekistan (Currie et al., 1993). A partial dentary referred to *Caenagnathasia* is known from the Erlian (Iren Dabasu) Formation of Nei Mongol, China (Yao et al., 2015). Few caenagnathid skull elements have been reported in Asia; these are from the perinate *Beibeilong* and the mandible of *Gigantoraptor* and a similarly sized specimen from the Gobi Desert (Xu et al., 2007; Tsuihiji et al., 2015; Ma et al., 2017; Pu et al., 2017).

North America: The early-diverging caenagnathid *Microvenator* was recovered from the Aptian-Albian Cloverly Formation and is a historically important specimen and likely that of a juvenile. It is the continent's oldest oviraptorosaurian (Makovicky and Sues, 1998). Late Cretaceous caenagnathids dominate the North American oviraptorosaurian fossil record. *Chirostenotes*, currently known from the species *C. pergracilis*, was the first discovered caenagnathid as well as the first described North American oviraptorosaur (Gilmore, 1924). The Campanian Dinosaur Park Formation of Canada is the most important source of North American caenagnathids including *Chirostenotes* (also referred to possible material in the Campanian Two Medicine and Maastrichtian Hell Creek formations of the northern United States [Osmólska et al., 2004]), *Leptorhynchos* (Longrich et al., 2013) (also the Campanian-Maastrichtian Aguja Formation of the southern United States) as well as *Caenagnathus*, the caenagnathid that lends its name to the clade (Currie et al., 1993). *Hagryphus* is a caenagnathid from the Campanian Kaiparowits Formation of Utah, known from forelimb material (Zanno and Sampson, 2005). Moving into the latest Cretaceous, *Epichirostenotes* and *Apatoraptor* are caenagnathids from the Campanian-Maastrichtian Horseshoe Canyon Formation of Canada. Both have preserved skull elements, and the holotype of *Apatoraptor* is a largely articulated partial skeleton. *Ojoraptorsaurus* is a caenagnathid known from pubic bones recovered from the Maastrichtian Ojo Alamo Formation of the southwestern United States (Sullivan et al., 2011; Funston and Currie, 2016). *Anzu* is the largest described caenagnathid from North America and is one of the best-preserved North American oviraptorosaurians (Lamanna et al., 2014). It is known from the Maastrichtian Hell Creek Formation of North and South Dakota (Lamanna et al., 2014). Fossil eggshell material and undescribed skeletal material from the top of the Cedar Mountain Formation (Cenomanian-Turonian) of Utah represents an even larger taxon that was similarly sized to *Gigantoraptor* (Makovicky et al., 2015; Tucker et al., 2020).

Europe: Oviraptorosaurians are poorly known from Europe with representation from only isolated postcranial material (Naish et al., 2001; Csiki and Grigorescu, 2005) whose referrals have been subsequently challenged (Csiki et al., 2010; Allain et al., 2014).

Isolated elements from Cretaceous strata of Gondwana have been interpreted as deriving from oviraptorosaurians, but these records have not withstood subsequent reevaluation. An isolated cervical from the Maastrichtian El Brete Formation of Argentina was described as an oviraptorosaurian (Frankfurt and Chiappe, 1999), but has since been reinterpreted as a noasaurid theropod (Agnolín and Martinelli, 2007). Elements from the Lower Cretaceous Otway Group of Australia described as an oviraptorosaurian lower jaw fragment and dorsal vertebra (Currie et al., 1996), have since been attributed to Unenlagiinae or other theropod clades (Agnolín et al., 2010). To date, no unambiguous records of oviraptorosaurians from Gondwanan continents exist.

SCANSORIOPTERYGIDAE

Scansoriopterygids are a bizarre group of early-diverging Laurasian oviraptorosaurians or paravians, known only from the Middle and Late Jurassic Haifanggou Formation and Late Jurassic Tiaojishan Formation of north China so far (~168–155 Ma) (Czerkas and Yuan, 2002; Zhang et al., 2002; Zhang et al., 2008a; Turner et al., 2012; Brusatte et al., 2014; Xu et al., 2015a; Wang et al. 2019a; Pei et al., in press) (fig. 1; table 2). Known from five (or six: O'Connor and Sullivan, 2014) feathered Chinese specimens, only one definitive and possibly two somatically mature individuals exist. Two of these specimens (*Yi qi* and *Ambopteryx longibrachium*) possess feathered, membranous wings (Xu et al., 2015a; Wang et al., 2019a) and one possesses a pygostyle (Wang et al., 2019a). *Epidendrosaurus* and *Epidexipteryx* are two well-accepted genera, but *Scansoriopteryx* may be the same genus as *Epidendrosaurus*. The Early Cretaceous *Zhongornis*, originally described as a bird (Gao et al., 2008), may be a scansoriopterygid instead (O'Connor and Sullivan, 2014), but this has been contested (Rashid et al., 2018). The notion that scansoriopterygids are early-branching avialans (Xu et al., 2011a; Czerkas and Feduccia, 2014) has been replaced by anatomical evidence grouping some or all scansoriopterygids with oviraptorosaurians (Turner et al., 2012; Agnolín and Novas, 2013; Brusatte et al., 2014; Pei

TABLE 2

Scansoriopterygid fossil record

Continent	Geological Unit	Country	Period	Age	Age Reference	Taxa	Reference
Asia	Haifanggou and Tiaojishan formations	China	Middle–Late Jurassic	Kimmeridgian-Bathonian	Liu et al., 2012; Wang et al., 2013c; Sullivan et al., 2014; Tian et al., 2015	*Ambopteryx*, *Epidendrosaurus*, *Epidexipteryx*, *Scansoriopteryx* (possibly a synonym of *Epidendrosaurus*), *Yi*, possibly *Zhongornis*	Czerkas and Yuan, 2002; Zhang et al., 2002; Gao et al., 2008; Zhang et al., 2008a; O'Connor and Sullivan, 2014; Xu et al., 2015b; Rashid et al., 2018; Wang et al., 2019a

TABLE 3
Dromaeosaurid fossil record

Continent	Geological Unit	Country	Period	Age	Age Reference	Taxa	Reference
Asia	Bayan Gobi Formation	China	Early Cretaceous	Aptian-Albian	Pittman et al., 2015	IVPP V22530	Pittman et al., 2015
	Jehol Group (Yixian Formation; Jiufotang Formation)	China	Early Cretaceous	Barremian-Aptian	He et al., 2004; Chang et al., 2009, 2017; Pan et al., 2013	*Changyuraptor Graciliraptor, Sinornithosaurus, Tianyuraptor, Zhenyuanlong, Zhongjianosaurus; Microraptor, Wulong*	Xu et al., 1999, 2000, 2003; Xu and Wang, 2004a; Hwang et al., 2002; Longrich and Currie, 2009; Zheng et al., 2009; Gong et al., 2012; Han et al., 2014; Lü and Brusatte, 2015; Xu and Qin, 2017; Pei et al., 2014; Poust et al., 2020
	Wulansuhai/Bayan Mandahu Formation	China	Late Cretaceous	Campanian	Godefroit et al., 2008	*Linheraptor, Velociraptor osmolskae*	Godefroit et al., 2008; Xu et al., 2010b, 2015a
	Qiupa Formation	China	Late Cretaceous	Campanian-Maastrichtian	Jiang et al., 2011	*Luanchuanraptor*	Lü et al., 2007
	Bayan Shireh Formation	Mongolia	Late Cretaceous	Cenomanian-Santonian	Shuvalov, 2000; van Itterbeeck et al., 2005; Kurumada et al., 2020	*Achillobator*	Perle et al., 1999
	Djadokhta Formation	Mongolia	Late Cretaceous	Campanian	van Itterbeeck et al., 2005; Dingus et al., 2008; Hasegawa et al., 2009	*Halszkaraptor, Mahakala, Tsaagan, Velociraptor mongoliensis*	Osborn, 1924; Norell et al., 2006; Turner et al., 2007b, 2011; Cau et al., 2017
	Barun Goyot Formation	Mongolia	Late Cretaceou	Campanian-Maastrichtian	Gradzinski and Jerzykiewicz, 1974a, 1947b; Fanti et al., 2012	*Hulsanpes* (possibly not a dromaeosaurid)	Osmólska, 1982; Turner et al., 2012; Cau and Madzia, 2018
	Nemegt Formation	Mongolia	Late Cretaceous	Maastrichtian	Jerzykiewicz and Russell, 1991; Shuvalov, 2000; van Itterbeeck et al., 2005	*Adasaurus*	Barsbold, 1983
	Öösh Formation	Mongolia	Early Cretaceous	Berriasian-Barremian	Turner et al., 2007c	*Shanag*	Turner et al., 2007c
	Jinju Formation	South Korea	Early Cretaceous	Aptian	Kim et al., 2018	suspected microraptorine tracks	Kim et al., 2018
	Bissekty Formation	Uzbekistan	Late Cretaceous	Turonian	Sues and Averianov, 2014, 2015	*Itemirus*	Kurzanov, 1976; Sues and Averianov, 2014

TABLE 3 *continued*

Continent	Geological Unit	Country	Period	Age	Age Reference	Taxa	Reference
Europe	Jydegaard Formation	Denmark	Early Cretaceous	Berriasian-Valanginian	Bonde and Christiansen, 2003	*Dromaeosauroides*	Bonde and Christiansen 2003; Christiansen and Bonde, 2003
	Lulworth Formation	U.K.	Early Cretaceous	Berriasian	Milner, 2002	*Nuthetes*	Owen, 1854; Milner, 2002; Sweetman 2004; Rauhut et al., 2010
	Wessex Formation	U.K.	Early Cretaceous	Barremian	Howse and Milner 1993	*Ornithodesmus*	Seeley, 1887; Howse and Milner, 1993; Norell and Makovicky, 1997
	Grés à Reptiles Formation	France	Late Cretaceous	Campanian-Maastrichtian	Walker et al., 2007	*Pyroraptor*	Allain and Taquet, 2000; Turner et al., 2012
	Sebeş Formation	Romania	Late Cretaceous	Maastrichtian	Brusatte et al., 2013	*Balaur*	Csiki et al., 2010; Brusatte et al., 2013
South America	Allen Formation	Argentina	Late Cretaceous	Campanian-Maastrichtian	Armas and Sánchez, 2015	*Austroraptor*	Novas et al., 2009; Currie and Paulina-Carabajal, 2012
	Candeleros Formation	Argentina	Late Cretaceous	Cenomanian-Turonian	Leanza et al., 2004	*Buitreraptor*	Makovicky et al., 2005; Novas et al., 2018; Gianechini et al., 2018
	Portezuelo Formation	Argentina	Late Cretaceous	Turonian-Coniacian	Calvo et al., 2007	*Neuquenraptor*, *Unenlagia*, *Pamparaptor*	Novas and Puerta, 1997; Calvo et al., 2004; Makovicky et al., 2005; Novas and Pol, 2005; Porfiri et al., 2011; Brissón Egli et al., 2017; Novas et al., 2018
	Huincul Formation	Argentina	Late Cretaceous	Cenomanian-Turonian	Garrido, 2010; Motta et al., 2020	*Overoraptor* (nonavialan paravian, possibly unenlagiine dromaeosaurid)	Motta et al., 2020
	Los Blanquitos Formation	Argentina	Late Cretaceous	Maastrichtian	Martínez and Novas, 2006	*Unquillosaurus*	Powell, 1979; Novas and Agnolín, 2004; Martínez and Novas, 2006
North America	Dinosaur Park Formation	Canada	Late Cretaceous	Campanian	Eberth, 2005; Brown et al., 2013	*Dromaeosaurus*, *Hesperonychus*, *Saurornitholestes*	Matthew and Brown, 1922; Sues, 1978; Currie, 1995; Longrich and Currie, 2009; Turner et al., 2012; Currie and Evans, 2020

TABLE 3 *continued*

Continent	Geological Unit	Country	Period	Age	Age Reference	Taxa	Reference
North America	Horseshoe Canyon Formation	Canada	Late Cretaceous	Campanian-Maastrichtian	Eberth and Braman, 2012; Quinney et al., 2013	*Atrociraptor*	Currie and Varricchio, 2004
	Wapiti Formation	Canada	Late Cretaceous	Campanian	Bell and Currie, 2015	*Boreonykus*	Bell and Currie, 2015
	Antlers Formation	U.S.	Early Cretaceous	Aptian-Albian	Brinkman et al., 1998	*Deinonychus*	Brinkman et al., 1998
	Cedar Mountain Formation	U.S.	Early Cretaceous	Barremian?-Aptian	Senter et al., 2012	*Utahraptor, Yurgovuchia*	Kirkland et al., 1993; Senter et al., 2012
	Cloverly Formation	U.S.	Early Cretaceous	pre-Aptian–Albian	Oreska et al., 2013; Farke et al., 2014	*Deinonychus*	Ostrom, 1969
	Hell Creek Formation	U.S.	Late Cretaceous	Maastrichtian	Hoganson and Edward, 2002; Fastovsky and Bercovici, 2016	*Acheroraptor, Dakotaraptor*	Evans et al., 2013; DePalma et al., 2015
	Morrison Formation	U.S.	Late Jurassic	Kimmeridgian-Tithonian	Trujillo and Kowallis, 2015	teeth of dromaeosaurids?	Foster and Heckert, 2011
	Ojo Alamo Formation	U.S.	Late Cretaceous	Maastrichtian	Sullivan and Lucas, 2006; Sullivan et al., 2001; Jasinski et al., 2020	*Dineobellator*	Jasinski et al., 2020
	Two Medicine Formation	U.S.	Late Cretaceous	Campanian	Rogers et al., 1993; Foreman et al., 2008	*Bambiraptor*	Burnham et al., 2000
Africa	Maevarano Formation	Madagascar	Late Cretaceous	Maastrichtian	Rogers et al., 2013	*Rahonavis*	Forster et al., 1998; Makovicky et al., 2005
	Wadi Milk Formation	Sudan	Early to Late Cretaceous	Albian-Cenomanian	Turner et al., 2012	Wadi Milk dromaeosaurid	Rauhut and Werner, 1995
Antarctica	Snow Hill Island Formation	–	Late Cretaceous	Maastrichtian	Case et al., 2007	*Imperobator* (indeterminate deinonychosaurian material or nondromaeosaurid paravian)	Case et al., 2007; Turner et al., 2012; Ely and Case, 2019

et al., in press) or as early-branching paravians (Turner et al., 2012; Godefroit et al., 2013a, 2013b; Xu et al., 2015a; Wang et al., 2019a).

DROMAEOSAURIDAE

Dromaeosaurid fossils have been found on almost all modern continental landmasses including members that appear to have had volant capabilities (Turner et al., 2012; Pei et al., in press; fig. 1; table 3).

NORTH AMERICA: In 1922, *Dromaeosaurus*, from the Campanian Dinosaur Park Formation of Alberta, Canada, was the first dromaeosaurid to be described. It lends its name to the clade and is known from partial cranial and very fragmentary postcranial material (Matthew and Brown, 1922; Currie, 1995). The Dinosaur Park Formation has also yielded *Saurornitholestes*, a relatively completely known taxon thought to be from only one species, *Saurornitholestes langstoni* (Sues, 1978; Turner et al., 2012). This taxon lacked a proper diagnosis until recently and is likely represented by multiple partial skeletons. Recently, an exquisite skull and skeleton from Dinosaur Provincial Park were recovered allowing for a revised diagnosis (Currie and Evans, 2020). Evidence of tooth-marked bones and a broken tip of a tooth still embedded in a bone suggest that this taxon ate azhdarchid pterosaurs on occasion (Currie and Jacobsen, 1995). *Hesperonychus elizabethae* is known from a single incomplete pelvis and referred pedal bones recovered from the Dinosaur Park Formation (Longrich and Currie, 2009. This taxon is North America's only named microraptorine and the youngest one worldwide by almost 45 million years (Longrich and Currie, 2009). *Atrociraptor marshalli* is a fragmentary taxon recovered from the similarly aged Horseshoe Canyon Formation from the same part of Canada (Currie and Varricchio, 2004). It consists of a partial rostrum, including both premaxillae, a right maxilla, and both dentaries. The snout of this dromaeosaurid appears to be quite short and deep, given the abbreviated nature of the facial process of the maxilla. Across the border in neighboring Montana, the Campanian Two Medicine Formation is home to the relatively well-preserved dromaeosaurid *Bambiraptor* (Burnham et al., 2000). The holotype of *Bambiraptor feinbergi* is quite small and typically considered a juvenile to subadult (Currie and Varricchio, 2004; Norell and Makovicky, 2004). However, attempts at histologically sampling the single known skeleton of this taxon have been unsuccessful. It is possible that *Bambiraptor* is a juvenile specimen of *Saurornitholestes* (Burnham et al., 2000; Norell and Makovicky, 2004): both taxa lack detailed and adequate diagnoses and differ only in the length of the suborbital process of the frontal, a feature that is undoubtedly influenced by ontogeny. Furthermore, the *Bambiraptor feinbergi* type specimen is known to be a chimera, as there are elements of three different similarly sized lower legs included in the holotype. The youngest North American dromaeosaurids are from the Maastrichtian Hell Creek and Ojo Alamo formations of the United States. From the Hell Creek Formation: the velociraptorine *Acheroraptor temertyorum*, which is known from a complete right maxilla and a referred right dentary (Evans et al., 2013) as well as the significantly larger *Dakotaraptor steini*, which was originally described as a dromaeosaurine (DePalma et al., 2015), but recently recovered as a velociraptorine (Pei et al., in press). From the Ojo Alamo Formation: the velociraptorine *Dineobellator notohesperus*, which is known from fragmentary cranial and postcranial material (Jasinski et al., 2020). *Deinonychus*, *Utahraptor*, and *Yurgovuchia* are the oldest widely accepted dromaeosaurids from North America with an Aptian/Albian age for the former (Ostrom, 1969) and a Barremian age for the latter two taxa (Kirkland et al., 1993; Senter et al., 2012). *Deinonychus* and *Utahraptor* are known from a large amount of material, much of it undescribed (personal commun., J. Kirkland), and *Utahraptor ostrommaysorum* remains the largest dromaeosaurid known. *Yurgovuchia doellingi* is represented by associated postcranial remains. The oldest record of Dromaeosauridae in North America relates to controversial fragmentary material from the Late Jurassic Morrison Formation (Heckert and Foster, 2011). *Deinonychus antirrhopus* remains the best-represented dromaeosaurid from North America. It is known from at least eight partially articulated and disarticulated skeletons from the Cloverly and Antlers formations. A partial egg associated with an adult has also been recovered (Grellet-Tinner and Makovicky, 2006). The osteology of this taxon was described in detail in Ostrom's monograph (Ostrom, 1969) and has been revisited by subsequent studies (Norell and Makovicky, 1997, 1999; Norell et al., 2006).

ASIA: *Velociraptor*, arguably the most famous dromaeosaurid, was the second dromaeosaurid to be described, in 1924 (Osborn, 1924). It is one of the best-known genera, with several complete or near-complete skeletons, and lends its name to the subfamily Velociraptorinae. *Velociraptor* was recovered from the Campanian Djadokhta Formation of southern Mongolia, which is among the most productive strata for dromaeosaurids anywhere on Earth. Several specimens of *Velociraptor* tell us much about its palaeobiology. The famous "fighting dinosaurs" appears to preserve *Velociraptor* attacking a large *Protoceratops* (Kielan-Jaworowska and Barsbold, 1972). Another specimen shows the presence of quill knobs on the ulna (Turner et al., 2007a), and yet another preserves stomach contents that include the remains of a pterosaur (Currie and Jacobsen, 1995). A second species, *V. osmolskae*, is known from paired maxillae and a left lacrimal described from similar rocks across the border in Nei Mongol, China (Wulansuhai (Bayan Mandahu) Formation) (Godefroit et al., 2008). This appears to be a valid taxon despite the paucity of its preserved fossil material (Turner et al., 2012). Djadokhta Formation outcrops at Ukhaa Tolgod have yielded *Tsaagan mangas*, a velociraptorine larger than *Velociraptor* (Norell et al., 2006) that is closely related to *Linheraptor exquisitus*, with a nearly complete holotype skeleton from the Wulansuhai Formation (Xu et al., 2010b, 2015b). The Djadokhta Formation has also yielded the earliest diverging noneudromaeosaurian dromaeosaurid *Mahakala omnogovae*, which is known from a partial skeleton including the back of the skull (Turner et al., 2007b; Turner et al., 2011). It was recovered from the Tögrögiin Shiree locality in Mongolia. Recent work described an additional dromaeosaurid from the Djadokhta Formation, *Halszkaraptor escuilliei*, and recovered it as the sister taxon to *Mahakala*, although parts of the sole specimen have been forged (Cau et al., 2017). *Hulsanpes* is another enigmatic specimen purported to be a dromaeosaurid (Osmólska, 1982). It is from the Campanian -Maastrichtian Barun Goyot Formation at the Khulsan locality in Mongolia. It consists only of a partial right metatarsus and pes (and possibly an associated braincase). Although considered a dromaeosaurid by recent analyses (Cau et al., 2017; Cau and Madzia, 2018), because of the extremely fragmentary nature of the material this identification has been repeatedly challenged (Turner et al., 2012).

The Gobi Desert has yielded a number of taxa occupying other parts of the Late Cretaceous: *Achillobator* from the Cenomanian-Santonian Bayan Shireh Formation (Perle et al., 1999) and *Adasaurus* from the Maastrichtian Nemegt Formation (Bayankhongor) of southwestern Mongolia (Barsbold, 1983). *Adasaurus* was only recently well figured and described (Turner et al., 2012). IGM 100/20 is the only specimen considered to be *Adasaurus* and is known from a partial skull and postcranial skeleton. Additional cranial and postcranial remains (IGM 100/22 and 100/23) likely pertain to a different taxon from the older Baynshiree Formation. *Shanag* is the only Early Cretaceous Mongolian dromaeosaurid, belonging to the Berriasian-Barremian Öösh Formation (Turner et al., 2007c).

In contrast, China has a large number of Early Cretaceous forms, but fewer Late Cretaceous ones. The Barremian-Aptian Yixian Formation and Aptian Jiufotang Formation of northeastern China, which yield part of the Jehol Biota, are home to many microraptorines, a non-eudromaeosaurian subclade that is known only from one fragmentary specimen outside Asia (Longrich and Currie, 2009). Despite their name, microraptorines were not all small and appear to be reasonably large ancestrally (Pei et al., in press). Their well-known arm and leg feathers are exemplified in the group's namesake *Microraptor*, where they are extremely long and are thought to have enabled volant capabilities, although this remains an area of intense study

(Dyke et al., 2013; Dececchi et al., 2016; Pei et al., in press). *Microraptor* is from the Aptian Jiufotang Formation and is known from three species *M. zhaoianus*, *M. gui*, and *M. hanqingi* (Xu et al., 2000, 2003; Gong et al., 2012); however, the status of *M. gui* (Senter et al. 2004) and *M. hanqingi* have been questioned (Turner et al., 2012; Pei et al., 2014). The other known Jiufotang microraptorine is *Wulong* (Poust et al., 2020). The Yixian Formation has the microraptorines *Changyuraptor* (Han et al., 2014), *Graciliraptor* (Xu and Wang, 2004a), *Sinornithosaurus* (Xu et al., 1999), *Zhongjianosaurus* (Xu and Qin, 2017) and the larger seemingly early-diverging forms *Tianyuraptor* and *Zhenyuanlong* (Zheng et al., 2009; Lü and Brusatte, 2015; Pei et al., in press). Microraptorines are otherwise rare in Asia: IVPP V22530 is from the younger Aptian-Albian Bayan Gobi Formation of Nei Mongol, northern China (Pittman et al., 2015) and suspected microraptorine tracks have been discovered in the Aptian Jinju Formation of Gyeongsangnamdo, South Korea (Kim et al., 2018). *Shanag* is possibly a microraptorine as well, as found in some phylogenetic analyses (Gianechini et al., 2018). *Luanchuanraptor*, known from a partial skeleton, was discovered from the Campanian-Maastrichtian Qiupa Formation of Henan, central China (Lü et al., 2007), and a recent analysis found it closely related to its Late Cretaceous Mongolian relative *Velociraptor* (Pei et al., in press). Tracks of two differently sized coeval deinonychosaurs have been found in the Barremian-Aptian Tianjialoue Formation of Shandong, eastern China, but the identity of their makers remains elusive (Li et al., 2008a).

A small partial braincase forms the type of *Itemirus medullaris* from the Turonian Bissekty Formation of Uzbekistan, which was originally described as an earlier-diverging theropod (Kurzanov, 1976). More recently, two phylogenetic analyses have recovered it as a velociraptorine (Longrich and Currie, 2009) and dromaeosaurine (Sues and Averianov, 2014).

EUROPE: *Variraptor* was named as a dromaeosaurid from the Late Campanian–Early Maastrichtian Grès à Reptiles Formation of France (LeLoeuff and Buffetaut, 1998). However, it was shown to lack dromaeosaurid synapomorphies and was superseded by *Pyroraptor* (Late Campanian–Early Maastrichtian of La Boucharde, France) as the only known Late Cretaceous European dromaeosaurid taxon (Allain and Taquet, 2000; Turner et al., 2012). Prior to the discovery of *Pyroraptor*, only indeterminate Late Cretaceous dromaeosaurid material had been known in Europe (Allain and Taquet, 2000) from elsewhere in France (Buffetaut et al., 1986; LeLoeuff et al., 1992; LeLoeuff and Buffetaut, 1998) and from Portugal (Antunes and Sigogneau, 1992) and Romania (Weishampel and Jianu, 1996). Despite being represented by only extremely fragmentary remains, the unique biogeography of *Pyroraptor* and its near contemporaneousness with Late Cretaceous taxa from neighboring continents (Campanian and Maastrichtian of Provence, France) made it an important taxon (Allain and Taquet, 2000). Understanding of Late Cretaceous European dromaeosaurids dramatically increased with the discovery of *Balaur*, a more complete partial skeleton of an island-dwelling velociraptorine from the Maastrichtian Sebeş Formation of Alba county, Romania (Csiki et al., 2010; Brusatte et al., 2013). The animal is perhaps most distinctive for its double sickle claw on the foot, due to the unusual hypertrophy of the first pedal ungual in addition to the typically enlarged and trenchant second pedal ungual of dromaeosaurids and other deinonychosaurs. Although recently argued to be an avialan (Cau et al., 2015), its status as a velociraptorine was recently reaffirmed (Pei et al., in press).

Knowledge of Early Cretaceous European dromaeosaurids is sparse and superficial. Reexamination of historic reptilian tooth and fragmentary jaw material from the Berriasian Lulworth Formation of the U.K. led to *Nuthetes* being reassigned as a dromaeosaurid taxon (Milner, 2002), and then being narrowed to the subfamily Velociraptorinae (Sweetman, 2004). However, this assignment was later contested by one of the original authors as possible tyrannosaurid material instead (Rauhut et al., 2010). Six fused sacral vertebrae from the Berriasian-Barremian Wessex Formation of the U.K.

TABLE 4
Troodontid fossil record

Continent	Geological Unit	Country	Period	Age	Age Reference	Taxa	Reference
Asia	Ejinhoro Formation	China	Early Cretaceous	Aptian-Albian	Sereno, 2010	*Sinornithoides*	Russell and Dong, 1993
	Huajiying Formation	China	Early Cretaceous	Hauterivian-Barremian	Pan et al., 2013	*Jinfengopteryx*	Ji et al., 2005
	Majiacun Formation	China	Late Cretaceous	Coniacian-Santonian	Tan et al., 2015	*Xixiasaurus*	Lü et al., 2010
	Wulansuhai/ Bayan Mandahu Formation	China	Late Cretaceous	Campanian	Godefroit et al., 2008	*Linhevenator*, *Philovenator*	Xu et al., 2011b, 2012b
	Jehol Group (Yixian Formation)	China	Early Cretaceous	Barremian-Aptian	Chang et al., 2009, 2017; Pan et al., 2013	*Daliansaurus*, *Jianianhualong*, *Liaoningvenator*, *Mei*, *Sinovenator*, *Sinusonasus*, *Yixianosaurus* (possibly an avialan)	Xu et al., 2002b, 2017; Xu and Wang, 2003, 2004b; Xu and Norell, 2004; Chang et al., 2017; Shen et al., 2017a, 2017b; Yin et al., 2018
	Kallamedu Formation	India	Late Cretaceous	Maastrichtian	Goswami et al., 2013	troodontid tooth	Goswami et al., 2013
	Khamareen Us locality	Mongolia	Early Cretaceous	Cenomanian	Makovicky and Norell, 2004	MPC-D 100/44	Barsbold et al., 1987; Makovicky and Norell, 2004
	Khamaryn Ar locality	Mongolia	Early Cretaceous	Barremian-Albian	Tsuihiji et al., 2016; Lucas, 2006	MPC-D 100/140	Tsuihiji, et al., 2016
	Djadokhta Formation	Mongolia	Late Cretaceous	Campanian	van Itterbeeck et al., 2005; Dingus et al., 2008; Hasegawa et al., 2009	*Almas*, *Byronosaurus*, *Gobivenator*, *Saurornithoides*	Osborn, 1924; Norell et al., 2000; Makovicky et al., 2003; Bever and Norell, 2009; Tsuihiji et al., 2014; Pei et al., 2017a
	Nemegt Formation	Mongolia	Late Cretaceous	Maastrichtian	Jerzykiewicz and Russell, 1991; Shuvalov, 2000; van Itterbeeck et al., 2005	*Borogovia*, *Tochisaurus*, *Zanabazar*	Barsbold, 1974; Osmólska, 1987; Kurzanov and Osmólska, 1991; Norell et al., 2009

TABLE 4 *continued*

Continent	Geological Unit	Country	Period	Age	Age Reference	Taxa	Reference
Asia	Kakanaut Formation	Russia	Late Cretaceous	Maastrichtian	Herman et al., 2016	*Troodon* ?	Godefroit et al., 2009
	Udurchukan Formation	Russia	Late Cretaceous	Maastrichtian	Averianov and Sues, 2007	*Troodon* ?	Averianov and Sues, 2007
	Dzharakuduk Formation	Uzbekistan	Late Cretaceous	Cenomanian	Averianov and Sues, 2007	*Urbacodon*	Averianov and Sues, 2007
North America	Dinosaur Park Formation	Canada	Late Cretaceous	Campanian	Eberth, 2005; Brown et al., 2013	*Latenivenatrix*, *Polyodontosaurus*/ *Stenonychosaurus*/ *Troodon* ?	Gilmore, 1932; Sternberg, 1932; Brown et al., 2013; Evans et al., 2017; van der Reest and Currie, 2017
	Horseshoe Canyon Formation	Canada	Late Cretaceous	Campanian-Maastrichtian	Eberth and Braman, 2012; Quinney et al., 2013	*Albertavenator*, *Troodon*	Ryan et al., 1998; Evans et al., 2017
	Old Man Formation	Canada	Late Cretaceous	Campanian	Eberth, 2005	*Troodon*	Ryan and Russell, 2001
	Scollard Formation	Canada	Late Cretaceous-Palaeogene	Maastrichtian-Palaeocene	Khidir and Catuneanu, 2010	*Troodon*	Weishampel et al., 2004
	St. Mary River Formation	Canada	Late Cretaceous	Maastrichtian	Jackson and Varricchio, 2017	*Troodon*	Weishampel et al., 2004
	Wapiti Formation	Canada	Late Cretaceous	Campanian-Maastrichtian	Fanti et al., 2013	*Troodon*	Ryan and Russell, 2001
	El Gallo Formation	Mexico	Late Cretaceous	Campanian	López-Conde et al., 2018	*Troodon*	Weishampel et al., 2004
	Cedar Mountain Formation	U.S.	Early Cretaceous	Berremian?-Aptian	Senter et al., 2012	*Geminiraptor*	Senter et al., 2010
	Dakota Formation	U.S.	Early to Late Cretaceous	Albian-Cenomanian	Barclay et al., 2015	*Troodon*	Eaton et al., 1999
	Ferris Formation	U.S.	Late Cretaceous–Palaeogene	Maastrichtian-Palaeocene	Lillegraven and Eberle, 1999	*Troodon*	Lillegraven and Eberle, 1999

TABLE 4 *continued*

Continent	Geological Unit	Country	Period	Age	Age Reference	Taxa	Reference
North America	Hell Creek Formation	U.S.	Late Cretaceous	Maastrichtian	Hoganson and Edward, 2002; Fastovsky and Bercovici, 2016	*Troodon*	Fastovsky and Bercovici, 2016
	Judith River Formation	U.S.	Late Cretaceous	Campanian	Lawver and Jackson, 2017	*Troodon*	Leidy, 1856; Varricchio and Jackson, 2004
	Kaiparowits Formation	U.S.	Late Cretaceous	Campanian	Roberts et al., 2005; Jinnah et al., 2009; Zanno et al., 2011	*Talos*, *Troodon*	Eaton et al., 1999; Zanno et al., 2011
	Kirtland Formation	U.S.	Late Cretaceous	Campanian	Sullivan and Lucas, 2006	'*Saurornitholestes*'	Sullivan, 2006; Evans et al., 2014
	Lance Formation	U.S.	Late Cretaceous	Maastrichtian	Elżanowski et al., 2000	*Pectinodon*/*Troodon* ?	Carpenter, 1982
	Morrison Formation	U.S.	Late Jurassic	Kimmeridgian-Tithonian	Trujillo and Kowallis, 2015	*Hesperornithoides*, *Koparion*	Chure, 1994; Hartman et al., 2019
	Prince Creek Formation	U.S.	Late Cretaceous	Maastrichtian	Fiorillo et al., 2016	*Troodon*	Fiorillo et al., 2016
	Wahweap Formation	U.S.	Late Cretaceous	Campanian	Moran et al., 2010	*Troodon*	Eaton et al., 1999
	Two Medicine Formation	U.S./ Canada	Late Cretaceous	Campanian	Rogers et al., 1993; Foreman et al., 2008	*Troodon* ?	Foreman et al., 2008
Europe	Painten Formation	Germany	Late Jurassic	Tithonian	Foth and Rauhut, 2017	*Ostromia* (anchiornithine; possibly an early-diverging avialan)	Foth and Rauhut, 2017
Antarctica	Snow Hill Island Formation	–	Late Cretaceous	Maastrichtian	Case et al., 2007	*Imperobator* (indeterminate deinonychosaurian material or nondromaeosaurid paravian)	Case et al., 2007; Turner et al., 2012; Ely and Case, 2019

form the type of *Ornithodesmus cluniculus* (Seeley, 1887), which probably belongs to a dromaeosaurid (Norell and Makovicky, 1997; Naish and Martill, 2007). However, this specimen has a complex taxonomic history including past identifications as a bird, pterosaur, troodontid, and earlier-diverging theropod (Anonymous, 1887; Seeley, 1887; Howse and Milner, 1993; Naish et al., 2001). *Dromaeosauroides bornholmensis* is a taxon known from a tooth from the Early Cretaceous of Denmark (Bonde and Christiansen, 2003).

AFRICA: *Rahonavis ostromi* of the Maastrichtian Maevarano Formation (Rogers et al., 2013) of Madagascar's Mahajanga Basin was first described as an avialan (Forster et al., 1998) as supported by others (Agnolín and Novas, 2013; Cau, 2018; Novas et al., 2018). However, it has also been recognized as one of the first discovered Gondwanan dromaeosaurids (Makovicky et al., 2005; Turner et al., 2012; Pei et al., in press), which we follow in this volume. A dromaeosaurid from the Albian-Cenomanian Wadi Milk Formation of Sudan (Dromaeosauridae incertae sedis (Turner et al., 2012)) is the first and only African record reaching into the Early Cretaceous (Rauhut and Werner, 1995).

SOUTH AMERICA: The discovery of *Unenlagia* from the Turonian-Coniacian Portezuelo Formation of Patagonia, Argentina (Calvo et al., 2007) provides strong support that dromaeosaurids were not exclusively Laurasian, but occupied Gondwana as well (Novas and Puerta, 1997). This landmark discovery was followed by recognition of a second species, *U. paynemili*, in addition to the original *U. comahuensis* from the same formation (Calvo et al., 2004) as well as the new genus *Neuquenraptor* (Novas and Pol, 2005). However, the latter might be a junior synonym of *Unenlagia* (Makovicky et al., 2005), but this remains unclear (Brissón Egli et al., 2017). *Buitreraptor* from the Cenomanian-Turonian Candeleros Formation of Patagonia extended the South American record of dromaeosaurids into the earliest Late Cretaceous (Makovicky et al., 2005) and also provided evidence for a monophyletic Unenlagiinae in Gondwana, while *Austroraptor* demonstrated that their record extended to the end of the Cretaceous (Campanian-Maastrichtian Allen Formation) (Novas et al., 2009) and solidified Patagonia, Argentina, as a hotspot for dromaeosaurid fossils. *Pamparaptor* is based on a deinonychosaurian foot from the Portezuelo Formation that is distinct from specimens of *Unenlagia* (Porfiri et al., 2011). This material has possible unenlagiine affinities, but does not nest exclusively with that clade in phylogenetic analyses (Gianechini et al., 2018). *Overoraptor* of the Cenomanian-Turonian Hiuncul Formation of Patagonia is known from fragmentary postcranial material (Motta et al., 2020). Described as a paravian, it was recovered as a stem avialan in a phylogenetic analysis (Motta et al., 2020). However, the closeness of its phylogenetic position to contemporaneous Patagonian unenlagiine dromaeosaurids as well as its highly modified deinonychosaurian digit II-2, suggests that *Overoraptor* might instead be an unenlagiine. *Unquillosaurus* is based on a left pubis from the Maastrichtian Los Blanquitos Formation of Patagonia (Powell, 1979). It may be a dromaeosaurid (Martínez and Novas, 2006) and was previously proposed as an indeterminate maniraptoran theropod (Novas and Agnolín, 2004) and as an earlier-diverging theropod (Powell, 1979). South American records outside Argentina are rare, but possible unenlagiine elements have been reported from the Late Cretaceous Bauru group of Brazil (Candeiro et al., 2012; Delcourt and Grillo, 2017).

ANTARCTICA: Two isolated teeth associated with a partial left foot and fragments from the right foot from the Maastrichtian Snow Hill Island Formation of James Ross Island, Antarctica were referred to Dromaeosauridae (Case et al., 2007). These were subsequently reinterpreted as indeterminate deinonychosaurian material (Turner et al., 2012). Ely and Case (2019) have recently described this specimen as *Imperobator antarcticus*, and recovered it as a nondromaeosaurid paravian.

TROODONTIDAE

Troodontids were first recognized in the late 19th century in North America and it is on that continent and in Asia where most fossils have been found (fig. 1; table 4). Troodontids are otherwise scarce and have been traditionally thought of as a Laurasian group, but a single tooth now suggests that troodontids were possibly present in Gondwana (fig. 1; table 4).

NORTH AMERICA: The first troodontid genus *Troodon* was given to a tooth discovered in the Campanian Judith River Formation of Montana in the mid-19th century (Leidy, 1856). Originally thought to belong to a fossil lizard and then a pachycephalosaur, this is one of three historic North American troodontid genera, alongside *Polyodontosaurus* (Gilmore, 1932) and *Stenonychosaurus* (Sternberg, 1932). North American Campanian- and Maastrichtian-aged troodontids have experienced a prolonged period of taxonomic instability, including the role of *Troodon* as a wastebasket taxon (see Zanno et al., 2011, for further details) once it was recognized as a theropod (Sternberg, 1945). Campanian material referred to this genus comes from the Judith River Formation (Lawver and Jackson, 2017) as well as the Dinosaur Park (Brown et al., 2013) and Oldman formations of Alberta, Canada (Ryan and Russell, 2001), the Two Medicine Formation of Alberta, Canada, and Montana (Foreman et al., 2008), the Kaiparowits and Wahweap formations of Utah (Eaton et al., 1999), the El Gallo Formation of Baja California, Mexico (Weishampel et al., 2004) and the Campanian-Maastrichtian Wapiti, Horseshoe Canyon and St. Mary River formations of Alberta, Canada (Ryan et al., 1998; Ryan and Russell, 2001). The Two Medicine material includes eggs, some with embryos, and nests (Varricchio and Jackson, 2016) as well as skeletons. *Troodon* has been reported from Maastrichtian strata including the Ferris Formation of Wyoming (Lillegraven and Eberle, 1999), the Hell Creek Formation of Montana, Wyoming, North Dakota, and South Dakota (Fastovsky and Bercovici, 2016), the Prince Creek Formation of Alaska (Fiorillo et al., 2016), the Lance Formation of Wyoming (Carpenter, 1982), and the Scollard Formation of Alberta, Canada (Weishampel et al., 2004). *Troodon* has even been assigned to material from the Lower Cretaceous Dakota Formation of Utah (Eaton et al., 1999), although this rock unit, now known as the Naturita Formation, has been reassigned to the early Late Cretaceous (Tucker et al., 2020). Material from the Dinosaur Park Formation has been assigned a different species name, *T. inequalis*, from the original *T. formosus* (Currie, 2005). The discovery of *Talos*, a partial postcranial skeleton from the Campanian Kaiparowits Formation of Utah, provided a chance to reappraise North American troodontid material, which led to the suggestion that *Troodon* is a nomen dubium and support for the genus *Pectinodon* (Longrich, 2008; Zanno et al., 2011). The latter, known from teeth and juvenile skeletal material from the Maastrichtian Lance Formation of Wyoming, was originally described as an additional species of *Troodon*, *T. bakkeri* (Carpenter, 1982). Continued efforts to address the taxonomic confusion arising from North America's problematic, highly fragmentary historic holotypes led to the resurrection of the genus *Stenonychosaurus* for some troodontid skeletal material from the Dinosaur Park Formation (Evans et al., 2017). This analysis was supported by subsequent work that assigned some of this *Stenonychosaurus* material to the new genus *Latenivenatrix* (van der Reest and Currie, 2017). *Albertavenator* was named from a distinctive partial left frontal recovered from the Maastrichtian Horseshoe Canyon Formation of Alberta, Canada (Evans et al., 2017). "*Saurornitholestes*" *robustus* from the Campanian Kirtland Formation of San Juan Basin, New Mexico, is an indeterminate troodontid frontal (Evans et al., 2014), originally referred to a new species of the dromaeosaurid *Saurornitholestes* (Sullivan, 2006). *Geminiraptor*, an incomplete maxilla from the Cedar Mountain Formation of Utah is arguably one of the most important North American troodontid specimens because, as the only Early Cretaceous record, it provides a crucial point of comparison with better-known Chinese contemporaries (Senter et al., 2010). A tooth that is the holotype of *Koparion* (Chure, 1994), and the partial articulated skeleton that forms the type of *Hesperornithoides miessleri* (Hartman et al., 2019) are possible Jurassic troodontid records, both from the Morrison Formation of the western United States.

ASIA: The Gobi Desert of Mongolia provided the first Asian record of troodontids: *Saurornithoides* from the Campanian Djadokhta Formation of southern Mongolia (Osborn, 1924). Its reasonably complete skull and partial postcranium was particularly important in the early days of troodontid research. This animal was known from one species, *S. mongoliensis*, that was later joined by a second species, *S. junior*, from the younger Maastrichtian Nemegt Formation (Barsbold, 1974), although *S. junior* is now ascribed to *Zanabazar* (Norell et al., 2009). Other Djadokhta taxa include *Byronosaurus*, which is known from a large amount of cranial material and some postcranial material (Norell et al., 2000; Makovicky et al., 2003) including, perhaps, two perinates (Bever and Norell, 2009; but see Pei et al., 2017a). *Gobivenator* and *Almas* are well-preserved, recently described specimens from this formation, with *Gobivenator* one of the best three-dimensionally preserved troodontids in existence (Tsuihiji et al., 2014; Pei et al., 2017a). *Linhevenator tani*, known from a partial, eroded skeleton, was discovered from the similar Campanian Wulansuhai (Bayan Mandahu) Formation across the border in Nei Mongol, northern China (Xu et al., 2011b, 2012b). A single leg from the same formation was originally identified as a juvenile *Saurornithoides* specimen (Currie and Peng, 1993) and was later assigned to the new taxon *Philovenator* (Xu et al., 2012b). Mongolia and Russia provide the latest Cretaceous records. *Borogovia* and *Tochisaurus* are known from fragmentary hind-limb elements (Osmólska, 1987; Kurzanov and Osmólska, 1991), and like *Zanabazar*, were recovered from the Maastrichtian Nemegt Formation of southern Mongolia. "*Troodon*" records from the Maastrichtian Kakanaut and Udurchukan formations of Russia are expected to belong to one or more new genera given the recent revisions to *Troodon* taxonomy in North America (Averianov and Sues, 2007; Zanno et al., 2011; Evans et al., 2017; van der Reest and Currie, 2017). A single tooth from the Maastrichtian Kallamedu Formation of India potentially represents the only troodontid record from Gondwana (Goswami et al., 2013), despite the group being known for over 150 years. Occurrences from China and Uzbekistan extend the Asian troodontid record back into the earliest Late Cretaceous as well as the Early Cretaceous, providing the only described taxa from these time intervals worldwide. *Xixiasaurus* is from the Coniacian-Santonian Majiacun Formation (Lü et al., 2010) of Henan, China, and *Urbacodon* is from the Cenomanian Dzharakuduk Formation of Navoi Viloyat, Uzbekistan (Averianov and Sues, 2007). The Early Cretaceous troodontid record of Asia is well represented in China by at least eight named genera. The oldest record is *Jinfengopteryx* from the Hauterivian-Barremian Huajiying (Qiaotou) Formation of Hebei, China, that was originally described as an avialan and whose stomach may contain preserved seeds (Ji et al., 2005; Pan et al., 2013). *Sinovenator, Mei, Sinusonasus, Daliansaurus, Liaoningvenator*, and *Jianianhualong* were all discovered from the Barremian-Aptian Yixian Formation of northern China (Xu et al., 2002b, 2017; Xu and Norell, 2004; Xu and Wang, 2004b; Pan et al., 2013; Chang et al., 2017; Shen et al., 2017a, 2017b). This formation and the Djadokhta Formation represent the most important sources of troodontid material globally. *Sinovenator* was the first troodontid reported from the Yixian Formation (Xu et al., 2002b). Initially represented by a partial skull and a few incomplete postcranial skeletons (Xu et al., 2002b), later material included a partial skull with a well-preserved braincase (Yin et al., 2018). *Mei* was first described on the basis of an exquisitely-preserved skeleton with a bird-like sleeping posture, which is arguably the most complete Early Cretaceous troodontid specimen known (Xu and Norell, 2004; Pan et al., 2013). *Sinusonasus, Daliansaurus*, and *Liaoningvenator* all have a similar size as *Sinovenator*, and each of them were reported from a single, near com-

TABLE 5
Mesozoic avialan fossil record

Continent	Geological Unit	Country	Period	Age	Age Reference	Taxa	Reference
Asia	Haifanggou and Tiaojishan formations	China	Middle-Late Jurassic	Bathonian-Oxfordian	Gao and Shubin, 2012; Liu et al., 2012; Wang et al., 2013c; Sullivan et al., 2014; Tian et al., 2015	*Anchiornis*, *Aurornis* (possibly a synonym of *Anchiornis*), *Caihong*, *Eosinopteryx*, *Pedopenna*, *Serikornis*, *Xiaotingia* (possibly all troodontids)	Xu and Zhang, 2005; Xu et al., 2009, 2011a; Hu et al., 2009, 2018; Godefroit et al., 2013a, 2013b; Lefèvre et al., 2017; Pei et al., 2017b
	Dabeigou Formation	China	Early Cretaceous	Hauterivian-Barremian	Zhang et al., 2008b	*Jinguofortis*, *Eoconfuciusornis*	Zhang et al., 2008b; Wang et al., 2018
	Huajiying Formation	China	Early Cretaceous	Hauterivian-Barremian	Pan et al., 2013	*Archaeornithura*, *Cruralispennia*, *Eoconfuciusornis*, *Eopengornis*, *Hebeiornis* (*Vescornis*), *Jibeinia*, *Orienantius*, *Protopteryx*	Hou, 1997a; Zhang and Zhou, 2000; Zhang et al., 2004; Jin et al., 2008; Wang et al., 2014a,,, 2015a, 2017; Pan et al., 2016; Zheng et al., 2017; Navalón et al., 2018, Chiappe et al., 2019a; Liu et al., 2019
	Qiaotou Formation	China	Early Cretaceous	Barremian	Wang et al., 2010	*Shenqiornis*	Wang et al., 2010
	Jehol Group (Yixian Formation; Jiufotang Formation)	China	Early Cretaceous	Barremian-Aptian	Chang et al., 2009, 2017; Pan et al., 2013	*Archaeorhynchus*, *Changchengornis*, *Confuciusornis*, *Dalingheornis*, *Dingavis*, *Eoenantiornis*, *Eogranivora*, *Grabauornis*, *Gretcheniao*, *Hongshanornis*, *Iteravis*, *Jeholornis*, *Jixiangornis* (likely a synonym of *Jeholornis*), *Junornis*, *Liaoningornis*, *Longicrusavis*, *Longirostravis*, *Mirusavis*, *Monoenantiornis*, *Paraprotopteryx*, *Sapeornis*, *Shanweiniao*, *Sulcavis*, *Tianyuornis*, *Xinghaiornis*, *Yangavis*, *Yanornis*, *Zhongornis* (possibly a scansoriopterygian)	Hou et al., 1995, 1996, 1997b, 1999a, 1999b, 2002, 2004; Hou, 1996, 1997b; Chiappe et al., 1999, 2007, 2014, 2019b; Ji et al., 1999, 2002a, 2002b; Xu et al., 1999; Zhang et al., 2006, 2009; Zhou and Zhang, 2005, 2006a, 2006b; Gao et al., 2008, 2012; O'Connor et al., 2009, 2010, 2011a, 2013, 2016c; Li et al., 2010; Wang et al., 2013d, 2013e, 2019c; ; Zheng et al., 2007, 2013, 2014, 2018; Dalsätt et al., 2014; Lefèvre et al., 2014; Zhou et al., 2014a; Hu and O'Connor, 2017; Liu et al., 2017; Wang and Zhou, 2018

TABLE 5 *continued*

Continent	Geological Unit	Country	Period	Age	Age Reference	Taxa	Reference
Asia						*Alethoalaornis, Archaeorhynchus, Bellulornis, Bohaiornis, Boluochia, Cathayornis* (*Largirostrornis, Longchengornis*), *Chaoyangia, Chiappeavis, Chongmingia, Confuciusornis, Dalianraptor* (might be a chimera), *Dapingfangornis, Eocathayornis, Fortunguavis, Gracilornis, Hournis, Huoshanornis, Jeholornis* (*Shenzhouraptor*), *Jianchangornis, Linyiornis, Longipteryx, Longusunguis, Mengciusornis, Parabohaiornis, Parahongshanornis, Parapengornis, Pengornis, Piscivoravis, Piscivorenantiornis, Pterygornis, Rapaxavis, Sapeornis, Schizooura, Shangyang, Shengjingornis, Sinornis, Songlingornis, Xiangornis, Yanornis, Yixianornis, Yuanjiawaornis, Zhongjianornis, Zhouornis*	Sereno and Rao, 1992; Zhou et al., 1992, 2004, 2008, 2009, 2010, 2012, 2013, 2014; Hou and Zhang, 1993; Zhou, 1995, 2002; Hou, 1997a; Hou et al., 2002; Czerkas and Ji, 2002; Ji et al., 2002a; Zhou and Hou, 2002; Zhou and Zhang, 2001, 2002a, 2002b, 2003a, 2003b,, 2006a; Gong et al., 2004; Dalsätt et al., 2006;; Li et al., 2006, 2007, 2008, 2010a, 2010b, 2011, 2012, 2014b; Morschhauser et al., 2009; Yuan, 2010; Hu et al., 2010, 2011, 2015a, 2015b; Li and Hou, 2011O'Connor et al., 2011a, 2012, 2016a; Pu et al., 2013; Wang et al., 2010b, 2014b, 2014d, 2014e, 2016b, 2016c, 2016d, 2019d; Zhang et al., 2001, 2013; Wang and Zhou, 2018, 2019
	Jingchuan Formation	China	Early Cretaceous	Barremian-Aptian?	Lockley et al., 2012	*Otogornis* (originally assigned to the Yijinhuoluo Formation), enantiornithines	Hou, 1994; Li et al., 2008b; Zhang et al., 2010; Wang and Liu, 2015
	Xiagou Formation	China	Early Cretaceous	Aptian	O'Connor et al., 2016b	*Avimaia, Changmaornis, Dunhuangia, Feitianius, Gansus, Jiuquanornis, Qiliania, Yumenornis*	Hou and Liu, 1984; You et al., 2006, 2010; Ji et al., 2011; Wang et al., 2013b, 2013f, 2015b; O'Connor et al., 2016b; Bailleul et al., 2019
	Jiangdihe Formation	China	Late Cretaceous	Turonian-Santonian	Wang et al., 2014c	*Parvavis*	Wang et al., 2014c
	Qiupa Formation	China	Late Cretaceous	Campanian-Maastrichtian	Jiang et al., 2011	enantiornithines	Xu et al., 2011c
	Kuwajima Formation	Japan	Early Cretaceous	Barremian	Sano and Yabe, 2017	enantiornithines	Matsuoka et al., 2002

TABLE 5 *continued*

Continent	Geological Unit	Country	Period	Age	Age Reference	Taxa	Reference
Asia	Kitadani Formation	Japan	Early Cretaceous	Aptian	Sano and Yabe, 2017	*Fukuipteryx*	Imai et al., 2019
	Sinuiju series	North Korea	Early Cretaceous	-	Gao et al., 2009	confuciusornithiforms, enantiornithines	Gao et al., 2009
	"Burmese Amber"	Myanmar	Late Cretaceous	Cenomanian	Xing et al., 2017	enantiornithines; *Elektorornis*	Xing et al., 2016, 2017, 2019a,b,c
	Khodzhakul Svita	Uzbekistan	Early Cretaceous	Albian	Kurochkin, 2000	*Horezmavis*	Kurochkin, 2000
	Bissetky Formation	Uzbekistan	Late Cretaceous	Coniacian	Panteleev, 2018	enantiornithines, ornithuromorphs (*Zhyraornis*)	Nessov, 1984; Kurochkin, 2000; Panteleev, 2018
	"Kushmurun"	Kazakhstan	Late Cretaceous	Maastrichtian	Dyke et al., 2006	*Asiahesperornis*	Nessov and Prizemlin, 1991; Dyke et al., 2006
	Ilek Formation	Russia	Early Cretaceous	Barremian-Aptian	O'Connor et al., 2014	*Evgenavis*, *Mystiornis*	Kurochkin et al, 2011; O'Connor et al., 2014
	Rybuskha Formation	Russia	Late Cretaceous	Campanian	Kurochkin, 2000	*Hesperornis*	Marsh, 1872; Kurochkin, 2000
	"Ouadi al Gabour"	Lebanon	Late Cretaceous	Cenomanian	Cau and Arduini, 2008	*Enantiophoenix*	Cau and Arduini, 2008
	Andaikhudag Formation	Mongolia	Early Cretaceous	Hauterivian-Barremian	Zelenkov and Averianov, 2016	*Ambiortus*, *Holbotia*	Kurochkin, 1982; O'Connor and Zelenkov, 2013; Zelenkov and Averianov, 2016
	Barun Goyot Formation	Mongolia	Late Cretaceous	Campanian-Maastrichtian	Gradziński and Jerzykiewicz, 1974a, 1974b	*Gobipteryx*, *Hollanda*, nests of enantiornithines?	Elżanowski, 1974; Elżanowski, 1977; Bell et al., 2010; Varricchio and Barta, 2015
	Djadokhta Formation	Mongolia	Late Cretaceous	Campanian?	van Itterbeeck et al., 2005; Dingus et al., 2008; Hasegawa et al., 2009	*Apsaravis*, *Gobipteryx*, nests of enantiornithines?	Chiappe et al., 2001; Norell and Clarke, 2001; Varricchio and Barta, 2015
	Nemegt Formation	Mongolia	Late Cretaceous	Maastrichtian?	Jerzykiewicz and Russell, 1991; Shuvalov, 2000; van Itterbeeck et al., 2005	*Brodavis*, *Gurilynia*, *Judinornis*	Nessov and Borkin, 1983; Kurochkin, 1999; Martin et al., 2012
Australia	Wonthaggi Formation	Australia	Early Cretaceous	Barremian-Aptian	Close et al., 2009	enantiornithines	Rich et al., 1999; Close et al., 2009

TABLE 5 *continued*

Continent	Geological Unit	Country	Period	Age	Age Reference	Taxa	Reference
Australia	Toolebuc Formation	Australia	Early Cretaceous	Albian	Close et al., 2009	enantiornithines	Molnar, 1986
	Griman Creek Formation	Australia	Early Cretaceous	Albian	Close et al., 2009	enantiornithines	Molnar, 1999
Europe	Solnhofen Limestone (Altmühltal Formation)	Germany	Late Jurassic	Tithonian	Rauhut et al., 2018	*Archaeopteryx*	Owen, 1863; Dames, 1884; Heller, 1959; Wellnhofer, 1974, 1988, 1993, 2009; Mayr et al., 2005; Wellnhofer and Röper, 2005; Tischlinger, 2009; Foth et al., 2014; Rauhut et al., 2018; Kundrát et al., 2019.
	Painten Formation	Germany	Late Jurassic	Tithonian	Foth and Rauhut, 2017	*Ostromia* (anchiornithine; possibly a troodontid; formerly Haarlem *Archaeopteryx*)	Foth and Rauhut, 2017
	Mörnsheim Formation	Germany	Late Jurassic	Tithonian	Foth and Rauhut, 2017	*Archaeopteryx*	Tischlinger, 2009; Kundrát et al., 2019
	La Pedrera de Rubies Lithographic Limestones Formation	Spain	Early Cretaceous	Barremian	Szwedo and Ansorge, 2015	*Noguerornis*, enantiornithines	Lacasa-Ruiz, 1989; Sanz et al., 1997
	Calizas de la Huérguina Formation	Spain	Early Cretaceous	Barremian	Buscalioni and Fregenal-Martínez, 2010	*Concornis*, *Eoalulavis*, *Iberomesornis*	Sanz and Bonaparte, 1992; Sanz and Buscalioni, 1992; Sanz et al., 1996, 2002; Sereno, 2000; Navalón et al., 2015
	Melovatskaya Formation	Russia	Late Cretaceous	Cenomanian	Kurochkin et al., 2007	*Cerebravis*	Kurochkin et al., 2007
	Csehbánya Formation	Hungary	Late Cretaceous	Santonian	Dyke and Ösi, 2010	*Bauxitornis*	Dyke and Ösi, 2010
	Grès à Reptiles Formation	France	Late Cretaceous	Campanian-Maastrichtian	Walker et al., 2007	*Gargantuavis*, *Martinavis*	Buffetaut, 1998; Walker et al., 2007
	"Fox-Amphoux basin"	France	Late Cretaceous	Maastrichtian?	Buffetaut et al., 1995	unnamed taxon	Buffetaut et al., 1995

TABLE 5 *continued*

Continent	Geological Unit	Country	Period	Age	Age Reference	Taxa	Reference
Europe	Sebeş Formation	Romania	Late Cretaceous	Maastrichtian	Brusatte et al., 2013	nests and bones of enantiornithines	Dyke et al., 2012
	"Hateg Basin"	Romania	Late Cretaceous	Maastrichtian	Wang et al., 2011	enantiornithines	Wang et al., 2011
	Maastricht Formation	Belgium	Late Cretaceous	Maastrichtian	Keutgen, 2018	*Ichthyornis*-like bird, *Asteriornis*	Dyke et al., 2002; Field et al., 2020
South America	Crato Formation	Brazil	Early Cretaceous	Aptian	de Souza Carvalho et al., 2015	enantiornithines; *Cratoavis* (valid?)	Naish et al., 2007; de Souza Carvalho et al., 2015
	Portezuelo Formation	Argentina	Early Cretaceous	Turonian-Coniacian	Agnolín et al., 2006	ornithuromorph	Agnolín et al., 2006
	Bajo de la Carpa Formation	Argentina	Late Cretaceous	Santonian	Fernández et al., 2013	*Neuquenornis*, *Patagopteryx*, nests with embryonic remains	Alvarenga and Bonaparte, 1992; Chiappe and Calvo, 1994; Schweitzer et al., 2002; Fernández et al., 2013
	Las Curtiembres Formation	Argentina	Late Cretaceous	Campanian	Novas et al., 2010	*Intiornis*	Novas et al., 2010
	Allen Formation	Argentina	Late Cretaceous	Campanian-Maastrichtian	Armas and Sánchez, 2015	*Limenavis*	Clarke and Chiappe, 2001
	Los Alamitos Formation	Argentina	Late Cretaceous	Campanian-Maastrichtian	Agnolín and Martinelli, 2009	*Alamitornis*	Agnolín and Martinelli, 2009
	Bauru Group	Brazil	Late Cretaceous	Campanian-Maastrichtian	Nava et al., 2015	enantiornithines	Nava et al., 2015
	Quiriquina Formation	Chile	Late Cretaceous	Campanian-Maastrichtian	Olson, 1992	*Neogaeornis*	Lambrecht, 1929; Olson, 1992; Mayr, 2016
	Lecho Formation	Argentina	Late Cretaceous	Maastrichtian	Walker and Dyke, 2009	*Elbretornis*, *Enantiornis*, *Lectavis*, *Martinavis*, *Yungavolucris*, *Soroavisaurus*	Walker, 1981; Chiappe, 1993; Walker et al., 2007; Walker and Dyke, 2009
	La Colonia Formation	Argentina	Late Cretaceous	Maastrichtian	Lawver et al., 2011	enantiornithines	Lawver et al., 2011
North America	Ashville Formation	Canada	Late Cretaceous	Cenomanian	Tokaryk et al., 1997	*Pasquiaornis*	Tokaryk et al., 1997

TABLE 5 *continued*

Continent	Geological Unit	Country	Period	Age	Age Reference	Taxa	Reference
North America	Belle Fourche Formation	Canada	Late Cretaceous	Cenomanian	Clarke, 2004	*Ichthyornis*-like material	Clarke, 2004
	Woodbine Formation	U.S.	Late Cretaceous	Cenomanian	Tykoski and Fiorillo, 2010	*Flexomornis*	Tykoski and Fiorillo, 2010
	Kaskapau Formation	Canada	Late Cretaceous	Turonian	Clarke, 2004	*Ichthyornis*-like material	Clarke, 2004
	"Canadian Arctic circle"	Canada	Late Cretaceous	Turonian	Bono et al., 2016	*Tingmiatornis*	Bono et al., 2016
	Mancos Shale Formation	U.S.	Late Cretaceous	Turonian	Clarke, 2004	*Ichthyornis*	Lucas and Sullivan, 1982; Clarke, 2004
	Austin Chalk Formation	U.S.	Late Cretaceous	Coniacian-Santonian	Clarke, 2004	*Ichthyornis*	Clarke, 2004
	Niobrara Formation	U.S.	Late Cretaceous	Coniacian-Campanian	Da Gama et al., 2014	*Apatornis*, *Baptornis*, *Hesperornis*, *Iaceornis*, *Ichthyornis*, *Parahesperornis*, hesperornithiforms	Marsh, 1872, 1877, 1880; Martin and Tate, 1976; Martin, 1984; Clarke, 2004; Bell and Chiappe, 2015; Field et al., 2018b
	Belly River Group	Canada	Late Cretaceous	Campanian	Longrich, 2009	ornithurines	Longrich, 2009
	Dinosaur Park Formation	Canada	Late Cretaceous	Campanian	Brown et al., 2013	enantiornithines	Buffetaut, 2010
	Northumberland Formation	Canada	Late Cretaceous	Campanian	McLachlan et al., 2017	*Maaqwi*	Morrison et al., 2005; McLachlan et al., 2017
	La Bocana Roja Formation	Mexico	Late Cretaceous	Campanian	Peecook and Sidor, 2015	*Alexornis*	Brodkorb, 1976
	Kaiparowits Formation	U.S.	Late Cretaceous	Campanian	Zanno et al., 2011	*Mirarce*	Atterholt et al., 2018
	Mooreville Chalk Formation	U.S.	Late Cretaceous	Campanian	Clarke, 2004	*Halimornis*, *Ichthyornis*	Chiappe et al., 2002; Clarke, 2004; Field et al., 2018b
	Two Medicine Formation	U.S.	Late Cretaceous	Campanian	Foreman et al., 2008	*Gettyia*	Atterholt et al., 2018

TABLE 5 *continued*

Continent	Geological Unit	Country	Period	Age	Age Reference	Taxa	Reference
North America	Pierre Shale	U.S.	Late Cretaceous	Campanian-Maastrichtian	Aotsuka and Sato, 2016	hesperornithiforms	Bell and Chiappe, 2015
	Frenchman Formation	Canada	Late Cretaceous	Maastrichtian	Martin et al., 2012	enantiornithines, hesperornithiforms, ornithurines	Longrich et al., 2011; Martin et al., 2012
	“Canadian Arctic Circle”	Canada	Late Cretaceous	Maastrichtian	Hou, 1999	*Canadaga*	Hou, 1999
	Hell Creek Formation	U.S.	Late Cretaceous	Maastrichtian	Fastovsky and Bercovici, 2016	*Avisaurus*, hesperornithiforms, ornithurines	Brett-Surman and Paul, 1985; Longrich et al., 2011
	Lance Formation	U.S.	Late Cretaceous	Maastrichtian	Elzanowski et al., 2000	ornithurines	Longrich et al., 2011
Africa	Maevarano Formation	Madagascar	Late Cretaceous	Maastrichtian	Rogers et al., 2013	*Vorona*, enantiornithines, *Rahonavis*?	Forster et al., 1996; O’Connor and Forster, 2010; Agnolín and Novas, 2013
Antarctica	López de Bertodano Formation	–	Late Cretaceous	Maastrichtian	Olivero et al., 2007	*Vegavis*, *Polarornis*; *Ichthyornis*-like material	Zinsmeister, 1985; Noriega and Tambussi, 1995; Chatterjee, 2000; Clark et al., 2005a
	Snow Hill Island Formation	–	Late Cretaceous	Maastrichtian	Cordes-Person, 2020	*Antarcticavis*; *Imperovator* (indeterminate deinonychosaurian material or nondromaeosaurid paravian)	Case et al., 2007; Turner et al., 2012; Ely and Case, 2019; Cordes-Person, 2020

plete skeleton (Xu and Wang, 2004b; Shen et al., 2017a, 2017b). *Jianianhualong* is only known from a single flattened specimen from the Yixian Formation, which preserves the first record of asymmetrical feathers in troodontids (Xu et al., 2017). *Sinornithoides* is known from the Aptian-Albian Ejinhoro Formation of Nei Mongol, China, based on a near complete skeleton (Russell and Dong, 1993). Across the border in Mongolia, unnamed Early Cretaceous troodontids have been reported, including the well-known "Early Cretaceous troodontid" MPC-D 100/44 and MPC-D 100/140 (Barsbold et al., 1987; Tsuihiji et al., 2016).

In northeastern China, the Middle Jurassic Bathonian Haifanggou Formation yields *Pedopenna* (Xu and Zhang, 2005), while the Late Jurassic Oxfordian Tiaojishan Formation yields *Anchiornis*, *Auronis*, *Caihong*, *Eosinopteryx*, *Serikornis*, and *Xiaotingia* (Xu et al., 2008, 2011a; Godefroit et al., 2013a, 2013b; Lefèvre et al., 2017; Hu et al., 2018). These taxa have been proposed as members of the Anchiornithinae, a controversial clade of long-tailed, early-diverging paravians. Anchiornithines were first described as early avialans, but their phylogenetic placement lacks consensus (Hu et al., 2009; Lee and Worthy, 2011; Xu et al., 2011a; Agnolín and Novas, 2013; Godefroit et al., 2013a, 2013b; Foth and Rauhut, 2017; Lefèvre et al., 2017; Pei et al., 2017b, in press). If they are troodontids as recovered in some recent works, they would be the oldest fossils of these animals (Hu et al., 2009). *Hesperornithoides*, from the Morrison Formation of Wyoming, is also a potential Jurassic troodontid (Hartman et al., 2019). Two Early Cretaceous taxa from the Yixian Formation, *Liaoningvenator* and *Yixianosaurus*, have been recovered as anchiornithines and are the only anchiornithine taxa besides *Ostromia* (previously an archaeopterygid) that have been found outside the Tiaojishan Formation (Cau et al., 2017; Foth and Rauhut, 2017; Shen et al., 2017b). However, the phylogenetic placement of *Yixianosaurus* remains controversial (Dececchi et al., 2012; Xu et al., 2013a; Cau et al., 2017; Foth and Rauhut, 2017; Lefèvre et al., 2017).

AVIALAE

The fossil record of stem birds (those members of Avialae falling outside the crown group Aves; alternatively crown group birds are referred to as Neornithes, with Aves consisting of stem and crown birds) has rapidly expanded since the 1980s (table 5). Prior to this, the record of Mesozoic birds consisted almost entirely of the Late Jurassic *Archaeopteryx* from the Solnhofen Limestone of southern Germany (Owen, 1863) and the Late Cretaceous "Odontornithes" (ornithurines *Ichthyornis* and the Hesperornithiformes) from marine deposits in North America (Marsh, 1880), with little to no evidence documenting the evolution of the avian postcranium from the primitive condition in *Archaeopteryx* to the nearly modern condition in *Ichthyornis* (fig. 1; table 5). Since the 1980s the number of species has more than doubled and the number of specimens has increased more than tenfold. In addition to the overwhelming collections uncovered in the Jehol Lagerstätte of northeastern China, important specimens have been discovered in Cretaceous deposits all over the world (O'Connor et al., 2011a) (fig. 1).

ASIA: The greatest concentration of non-avian avialan fossils is found in Asia. More than half of all known species of Cretaceous birds are from the Early Cretaceous Hauterivian - Aptian Jehol lagerstätten, preserved in northeastern China, which occurs in three successive formations (and their stratigraphic equivalents): the Huajiying, Yixian, and Jiufotang formations, deposited from about 131 to 120 Ma (Zhou and Zhang, 2006a; Pan et al., 2013). This includes the only lineage of long bony-tailed birds other than the Archaeopterygiformes, the Jeholornithiformes (Zhou and Zhang, 2002a); almost the entire record of non-ornithothoracine pygostylians, including the Sapeornithiformes, Confuciusornithiformes, and the Jinguofortisidae (Hou et al., 1995; Zhou and Zhang, 2002b; Wang et al., 2016b, 2018); and the earliest-known record of the Enantiornithes and Ornithuromorpha (together Ornithothoraces) in the Huajiying Formation (Zhang and

Zhou, 2000; Wang et al., 2014a, 2015). We adopt the node-based definition for the Ornithuromorpha because of the preference of our authors: Euornithes Sereno et al. 1998 is the stem-based definition. Two species of *Jeholornis* are currently recognized, *J. prima* and *J. palmapenis* (the holotype of "*J. curvipes*" is thought to be tampered) (O'Connor et al., 2012). The Sapeornithiformes is currently monospecific with all reported specimens purportedly ontogimorphs of *Sapeornis chaoyangensis* (Pu et al., 2013). *Jeholornis* and *Sapeornis* clades occur predominantly in the Jiufotang Formation with a few specimens also collected in the Yixian. The Confuciusornithiformes is much more diverse (*Eoconfuciusornis, Confuciusornis, Changchengornis,* and *Yangavis*: Wang and Zhou, 2018; Wang et al., 2019b). The early-diverging *Eoconfuciusornis zhengi* and another indeterminate confuciusornithiform have been reported from the Huajiying Formation (Zhang et al., 2008b; Navalón et al., 2018). Most confuciusornithiform specimens are referable to *Confuciusornis sanctus* and are found in the Yixian Formation with a few specimens from the Jiufotang. *C. dui* (Hou et al., 1999), *Changchengornis hengdaoziensis* (Chiappe et al., 1999), and *Yangavis confucii* (Wang and Zhou, 2018) are known only from single specimens. Enantiornithines and ornithuromorphs are found throughout the entirety of the Jehol Biota, with diversity increasing through time, peaking in the Jiufotang Formation. Currently, approximately 41 valid species of enantiornithines are recognized compared to approximately 19 species of ornithuromorphs. Diverse subclades are also recognized, such as the enantiornithine Pengornithidae (e.g., *Eopengornis, Chiappeavis*: O'Connor et al., 2016a), Bohaiornithidae (e.g., *Sulcavis, Longusunguis*: Wang et al., 2014b), and Longipterygidae (e.g., *Boluochia, Longipteryx*: O'Connor et al., 2011b), and the ornithuromorph lineage, the Hongshanornithidae (e.g., *Archaeornithura, Longicrusavis*: O'Connor et al., 2010). The Pengornithidae and Hongshanornithidae lineages persisted for the entire duration of the Jehol Biota (Wang et al., 2014a, 2015). Jehol equivalent deposits in nearby basins also preserve enantiornithines (e.g., Qiaotou, Dabeigou, and Yijinhuoluo formations).

The slightly younger Aptian Xiagou Formation in Gansu, northwestern China, has also produced a small diversity of enantiornithines (e.g., *Feitianius, Qiliania*: Ji et al., 2011; O'Connor et al., 2016b) and ornithuromorphs (*Jiuquanornis, Changmaornis*: Wang et al., 2013b) with a majority of the collected specimens assigned to the ornithuromorph *Gansus yumenensis* (You et al., 2006). The Late Cretaceous record consists of only two isolated specimens referable to the Enantiornithes: *Parvavis* from the Turonian-Santonian Jiangdihe Formation (Wang et al., 2014c) and an unnamed taxon from the upper Upper Cretaceous Qiupa Formation.

Fukuipteryx prima is the first nonornithothoracine pygostylian to be found outside of the Jehol Biota basins (Imai et al., 2019). Its partial skeleton as well as a single enantiornithine humerus have been reported from the Lower Cretaceous Tetori Group in Japan (Matsuoka et al., 2002; Imai et al., 2019) from the Barremian Kuwajima Formation and Aptian Kitadani Formation respectively. Confuciusornithiforms and enantiornithines have been reported in the North Korean Lower Cretaceous Sinuiju series (Gao et al., 2009). In southeastern Asia, Cenomanian (~99 Ma) age amber from Myanmar has recently become an unlikely major source of Cretaceous birds, recording a fauna of very small precocial enantiornithines including the taxon *Elektorornis* (Xing et al., 2016, 2017, 2019a,b,c). In Central Asia, a large number of fragments have been collected from the Turonian Bissekty Formation in Uzbekistan (Panteleev, 2018). These are apparently referable to enantiornithines and ornithuromorphs, including forms related to *Ichthyornis* (Kurochkin, 2000). The controversial and fragmentary enantiornithine taxon *Horezmavis* comes from Albian deposits of the Khodzhakul Formation, also in Uzbekistan (Kurochkin, 2000). A hesperornithiform, *Asiahesperornis*, has been described from numerous fragments collected from Maastrichtian deposits in Kazakhstan (Dyke et al., 2006). A few specimens have been collected in Russia including *Evgenavis* and *Mystiornis* from the Barremian Ilek Formation, both of uncertain phylogenetic affinity (Kurochkin et al., 2011; O'Connor et al., 2014), and *Hesperornis rossicus* from the Campanian Rybuskha Formation (Kurochkin, 2000). In western Asia, a single enantiornithine specimen (*Enantiophoenix*) has been collected from Cenomanian marine limestones in Lebanon (Dalla Vecchia and Chiappe, 2002).

Several early-diverging avialan skeletons as well as nests have been discovered in Mongolia. The enantiornithine *Holbotia* and the ornithuromorph *Ambiortus* were collected from the Hauterivian-Barremian Andaikhudag Formation in the Central Mongolian Altai, both preserving soft tissue (O'Connor and Zelenkov, 2013; Zelenkov and Averianov, 2016). All other specimens are from Late Cretaceous deposits. The early Late Cretaceous Javkhlant Formation has yielded enantiornithine embryos (Varricchio et al., 2015). The Campanian-Maastrichtian Barun Goyot Formation has produced several specimens of the enantiornithine *Gobipteryx* (Elzanowski, 1977) and the only known specimen of the ornithuromorph *Hollanda* (Bell et al., 2010). The Ukhaa Tolgod locality, which is attributed to the Campanian Djadokhta Formation, has produced a skull of the enantiornithine *Gobipteryx* (Chiappe et al., 2001) and the only known specimen of the ornithuromorph *Apsaravis* (Norell and Clarke, 2001; Clarke and Norell, 2002). The Tögrögiin Shiree locality of the Campanian Djadokhta Formation has yielded the enantiornithine *Elsornis*, which is represented by a partial articulated skeleton (Chiappe et al., 2007). Both the Barun Goyot and Djadokhta formations have also produced nests probably belonging to enantiornithines (Varricchio and Barta, 2015). Fragmentary hesperornithiforms including *Brodavis mongoliensis* and *Judinornis* and the enantiornithine *Gurilynia* were collected in the Maastrichtian Nemegt Formation (Kurochkin, 2000; Clarke and Norell, 2004).

The Oxfordian-aged anchiornithines were first described as early birds and this phylogenetic placement has been recovered by several independent studies (Xu et al., 2008, 2011a; Agnolín and Novas, 2013; Godefroit et al., 2013a; 2013b). However, until consensus is reached (see Pittman, et al., chapter 1), *Archaeopteryx* of Germany remains the oldest unequivocal bird (see Europe section below).

AUSTRALIA: Fragmentary enantiornithines are reported from the Barremian-Aptian Wonthaggi Formation (Close et al., 2009) and the Albian Toolebuc and Griman Creek formations (Molnar, 1986; Kurochkin and Molnar, 1997; Molnar, 1998; 1999). Contra Molnar (1999), reports of ornithuromorphs are likely misidentified enantiornithines (J. O'C., personal obs.).

EUROPE: Outside China, the greatest concentration of exceptionally well-preserved specimens of nonavian avialans occurs in the Early Cretaceous (Barremian) Las Hoyas lagerstätte (La Huerguina Formation) near Cuenca, Spain. These deposits have produced half a dozen enantiornithines, several of which represent distinct taxa (*Concornis*, *Eoalulavis*, and *Iberomesornis*), with most preserving at least some soft tissue (Sanz et al., 2002; Navalón et al., 2015). A pellet containing several juveniles and a perinate has also been collected (Sanz et al., 2001; Knoll et al., 2018). Two enantiornithine specimens (including the holotype of *Noguerornis*) have also been collected from the lithographic limestones of the Hauterivian-Barremian La Pedrera de Rúbies Formation near Montsec, Spain (Lacasa-Ruiz, 1988; Sanz et al., 1997; Szwedo and Ansorge, 2015). Fragmentary enantiornithines including the holotype of *Martinavis cruzyensis* and the ornithothoracine *Gargantuavis* have been collected from late Campanian–early Maastrichtian deposits in southern France (Buffetaut et al., 1995; Buffetaut, 1998; Walker et al., 2007). In Romania, an enantiornithine nesting colony that also preserved bones has been found in the Maastrichtian Sebeş Formation (Dyke et al., 2012), and an enantiornithine humerus has been described from Upper Cretaceous deposits in the

Hateg Basin (Wang et al., 2011). Several enantiornithine elements have been described from the Santonian Csehbánya Formation in Hungary, including a tarsometatarsus used to erect the taxon *Bauxitornis* (Dyke and Ösi, 2010). A cranial endocast inferred to be avialan (*Cerebavis*) was collected from Cenomanian deposits in European Russia (Kurochkin et al., 2007). Fragmentary remains of Hesperornithiformes are known from Campanian marine deposits of southern Sweden (Rees and Lindgren, 2005). A historically important specimen is *Enaliornis* from the Cambridge Greensand member of the West Melbury Marly Chalk Formation of southeast England. This specimen was one of the first Mesozoic avialans ever collected and is now considered a hesperornithomorph (Elzanowski and Galton, 1991).

South America: In 1981 the Enantiornithes was named from a large collection of isolated elements found in the Maastrichtian Lecho Formation of northwestern Argentina (Walker, 1981). Several taxa have been named, consisting of a few elements or less (e.g., *Enantiornis*, *Elbretornis*, and *Yungavolucris*) (Chiappe, 1993; Walker and Dyke, 2010). The partial skeletons of the avisaurid enantiornithine *Neuquenornis* (Chiappe and Calvo, 1994) and the early-diverging ornithuromorph *Patagopteryx* (Alvarenga and Bonaparte, 1992) were found soon after in the Santonian Bajo de la Carpa Formation of central Argentina, which has also yielded nests with embryonic remains (Schweitzer et al., 2002; Fernández et al., 2013). Fragmentary enantiornithines have been reported in the Campanian Las Curtiembres Formation of northwestern Argentina (*Intiornis*) (Novas et al., 2010) and the Upper Cretaceous La Colonia Formation of southern Argentina (Lawver et al., 2011). Fragmentary ornithuromorph taxa have also been published from the Campanian-Maastrichtian Allen Formation (*Limenavis*) (Clarke and Chiappe, 2001) and the similarly aged Los Alamitos Formation (*Alamitornis*) (Agnolín and Martinelli, 2009), both located in central Argentina. A partial ornithuromorph coracoid was described from the Turonian-Coniacian Portezuelo Formation, also in central Argentina (Agnolín et al., 2006). In Brazil several important enantiornithines have been described from the Lower Cretaceous Crato Formation (Naish et al., 2007; de Souza Carvalho et al., 2015). More recently a diverse but as yet undescribed enantiornithine avifauna is being excavated in the Campanian-Maastrichtian Bauru Group (Nava et al., 2015). *Neogaeornis*, from the Campanian-Maastrichtian Quiriquina Formation of Chile (Lambrecht, 1929), was identified as an early representative of Gaviiformes (loons) (Olson, 1992); however, it is based on a single tarsometatarsus and its identification as a crown bird is highly uncertain (Mayr, 2009, 2016).

North America: Only Late Cretaceous birds have been collected in North America. *Alexornis* (Enantiornithes) from the Campanian Roja (La Bocana Roja) Formation in Baja California is the only specimen known from Mexico (Brodkorb, 1976). In the United States, fragmentary remains of enantiornithines have been collected in the Campanian Kaiparowits (*Mirarce*) and Two Medicine (*Gettyia*) formations (Atterholt et al., 2018), the Campanian Mooreville Chalk (*Halimornis*) (Chiappe et al., 2002), and the Cenomanian Woodbine Formation (*Flexomornis*) (Tykoski and Fiorillo, 2010). The Maastrichtian Hell Creek Formation has yielded fragmentary remains of enantiornithines (*Avisaurus*), indeterminate (non-hesperornithiform or ichthyornithiform) ornithurines, and hesperornithiforms (Longrich et al., 2011). Hesperornithiforms have also been collected from the late Coniacian–early Campanian Smoky Hill Chalk Member of the Niobrara Formation and the Campanian-Maastrichtian Pierre Shale (Bell and Chiappe, 2015). Numerous specimens of the ornithurine *Ichthyornis* have been collected from the Smoky Hill Chalk Member of the Niobrara Formation, with additional remains found in Turonian and Campanian deposits belonging to the Mancos Shale, Mooreville Chalk, and other formations (Clarke, 2004). The fragmentary ornithurines *Apatornis* and *Iaceornis* are also known from the Smoky Hill Chalk Member (Clarke, 2004). The Maastrichtian

Lance Formation has also yielded indeterminate ornithurine fragments (Longrich et al., 2011).

Fragmentary specimens of enantiornithines and ornithuromorphs have been collected across Canada, reported in the Campanian Northumberland Formation (Nanaimo Group, from which the Ornithurine *Maaqwi* is reported) (Morrison et al., 2005; McLachlan et al., 2017) and Cenomanian Ashville Formation (Tokaryk et al., 1997), the latter including the hesperornithiform *Pasquiaornis*. An enantiornithine fragment has been reported from the Campanian Dinosaur Park Formation (Buffetaut, 2010), and the Campanian Belly River Group has produced a fragmentary fauna consisting primarily of ornithurine birds (Longrich, 2009). Enantiornithines, indeterminate ornithurines, and hesperornithiform fragments are reported from the Maastrichtian Frenchman Formation (Longrich et al., 2011; Martin et al., 2012). Fragmentary *Ichthyornis*-like material has been reported from the Turonian Kaskapau Formation and Cenomanian Belle Fourche Formation (Clarke, 2004). From within the Canadian Arctic circle two species have been named: *Tingmiatornis*, a large ornithurine from Turonian age deposits (Bono et al., 2016) and *Canadaga*, a Maastrichtian hesperornithiform (Hou, 1999).

AFRICA: Avialan remains are yet to be discovered on the African continent although a large number of avialan bones have been collected from the Maastrichtian Maevarano Formation in nearby Madagascar, consisting of a diversity of enantiornithines (O'Connor and Forster, 2010) as well as the ornithuromorph, *Vorona* (Forster et al., 1996). *Rahonavis* was also described as an avialan from this formation, but although this was supported by some subsequent analyses (Agnolín and Novas, 2013; Cau, 2018; Novas et al., 2018), *Rahonavis* has also recognized as a dromaeosaurid by several studies (Makovicky et al., 2005; Turner et al., 2012; Pei et al., in press).

ANTARCTICA: Latest Cretaceous deposits in Antarctica have produced some avialan remains, including the ornithurines *Vegavis* (Noriega and Tambussi 1995; Clarke et al. 2005), *Polarornis* (Chatterjee, 2002) and *Antarcticavis* (probable ornithurine; Cordes-Person et al., 2020). Preliminary descriptions have placed *Vegavis* in the Anatoidea (Clarke et al., 2005) and some cladistic analyses suggest this taxon may be an early stem-group anseriform (Agnolín et al., 2017; Worthy et al., 2017). However, others have argued that *Vegavis* falls outside the avian crown clade (Wang et al., 2014b; Mayr et al., 2018), so its status as a crown bird is contentious. *Polarornis* was described as a stem loon (Chatterjee, 2002), but the only available images of this specimen appear to be heavily reconstructed making any interpretations equivocal. *Antarcticavis* was described as an ornithuromorph that probably belongs to the Ornithurae (Cordes-Person, 2020). Some undescribed *Ichthyornis*-like material is also known (Zinsmeister, 1985).

EARLY FOSSIL RECORD OF CROWN BIRDS (AVES)

Much of our contemporary understanding of crown-bird macroevolution has come from large-scale molecular phylogenies, which are ever improving in light of the development of new sequencing technologies and analytical methods (Hackett et al., 2008; McCormack et al., 2013; Jarvis et al., 2014; Prum et al., 2015; Reddy et al., 2017; Kimball et al., 2019; see also Pittman, et al., chapter 1). However, the only direct evidence of crown-bird evolutionary history comes from the fossil record, placing a premium on the discovery of early fossil representatives of crown birds that can shed light on when (see Field et al.'s divergence time section in chapter 5) and where (see Ding et al.'s biogeography section, chapter 4) the major groups of crown birds originated.

Unfortunately, the earliest fossil record of crown birds is extremely sparse, as is the Late Cretaceous fossil record of the crownwardmost portion of the avialan stem group (fig. 1; table 5) (Mayr, 2016). The crownwardmost stem avialans known include classic Mesozoic taxa such as Ichthyornithiformes and Hesperornithiformes

(Marsh, 1880), both of which persisted into the terminal Maastrichtian (Dyke et al., 2002; Longrich et al., 2011; Dumont et al., 2016), as well as more poorly known marine taxa such as *Iaceornis* (Clarke, 2004), and the single specimen of the Campanian *Apsaravis* (Clarke and Norell, 2002), whose phylogenetic position is controversial and often unstable in recent analyses (Field et al., 2018a). Recent work on the anatomy and phylogeny of this portion of the avialan tree has revealed a multitude of anatomical plesiomorphies exhibited by these closest Mesozoic relatives of crown birds (e.g., in *Ichthyornis*, a strongly anteriorly projecting squamosal, primitive beak lacking a palatal shelf, extensive dentition throughout the upper and lower jaws; Field et al., 2018b). Clearly, our current knowledge of the closest-known stem-group relatives of crown birds must be incomplete: a range of hierarchically internested taxa crownward of Hesperornithiformes and Ichthyornithiformes must have existed, and their discovery will be necessary to document the acquisition of a fully crownlike avian skeleton. It is hoped that the coming years will reveal such fossils and clarify how, when, and where crown birds themselves originated.

The latest Cretaceous fossil record of crown birds is even more sparse. Total-clade loons (Gaviiformes) were long regarded as present in the latest Cretaceous on the basis of *Neogaeornis* (Olson, 1992) and *Polarornis* (Chatterjee, 2002), although the status of these taxa as gaviiforms is dubious (Mayr, 2016) and at least *Polarornis* may be closely related to, if not synonymous with, *Vegavis* (Clarke et al., 2016). Until recently, only one comparatively well-supported crown-bird fossil has emerged from the entirety of the Mesozoic and, even then, from within approximately one million years of the end-Cretaceous mass-extinction event (Noriega and Tambussi, 1995; Clarke et al., 2005). The phylogenetic position of this taxon, *Vegavis iaai*, is debated (Agnolín et al., 2017; Mayr et al., 2018), with recent analyses recovering it as an early stem-group anseriform (Worthy et al., 2017) and others questioning its validity as a crown bird (Mayr et al., 2018). Moreover, the stem lineages of the deepest clades within crown birds—Palaeognathae and Neognathae—are entirely unknown. This lack of stem palaeognaths and stem neognaths, which must have been present in the latest Cretaceous, has contributed to ongoing uncertainty regarding the antiquity of the avian crown group (Cracraft et al., 2015; Ksepka and Phillips, 2015; Mitchell et al., 2015; Prum et al., 2015; Berv and Field, 2018; see also Field et al.'s molecular rate variation section in chapter 5), precluding the application of a hard-minimum age for the avian root in node-dating analyses. Recently, the oldest clear evidence of a crown neognath was described from the Maastrichtian of Belgium (Field et al., 2020), and appears to represent an early galloanseran. This taxon, *Asteriornis maastrichtensis*, suggests that even earlier crown bird fossils are likely to be discovered from sediments in the Northern Hemisphere.

Although definitive representatives of Aves are exceedingly rare in Mesozoic sediments, isolated, often fragmentary remains from the latest Maastrichtian of North America (Hope, 2002; Longrich et al., 2011) may derive from crown-group birds. The only phylogenetic analysis to test the position of these specimens recovered several of them in a large polytomy with Aves and *Iaceornis*, crownward of Ichthyornithiformes and Hesperornithiformes. However, given the substantial presumed phylogenetic distance between these stem birds and Aves as discussed above, these isolated remains may instead be more likely to derive from the crownwardmost portion of the avian stem. With luck, continued exploration in the Late Cretaceous of North America may reveal more complete remains of these fragmentary avialans, and help clarify their phylogenetic affinities.

Beyond the Mesozoic, the earliest Paleocene fossil record of crown birds is also extremely sparse. Bird-producing lagerstätten comparable to the famous Eocene localities of Messel, Green River, and Fur have not been discovered in Paleocene sediments. Considering that a major diversification of crown birds, including Neoaves (which comprises >95% of extant avialan diversity) may have taken place within a narrow temporal window during the Paleocene (see Field et al.'s molecular rate variation section in chapter 5), avian fossils from this interval have strong potential to reveal important insights into the pattern and timing of the extant avian radiation, and will help shed light on the ancestral morphologies and biogeography of major avian lineages. With the exception of a handful of important fossil discoveries providing divergence time constraints across the bird tree of life (e.g., the earliest stem penguin *Waimanu*, the possible stem tropicbird *Australornis*, the earliest pelagornithid *Protodontopteryx* from New Zealand, as well as the stem mousebird *Tsidiiyazhi* from the southwestern United States (Slack et al., 2006; Mayr and Scofield, 2016; Ksepka et al., 2017; Mayr et al., 2019)), the early Paleocene avialan fossil record remains greatly undersampled with respect to subsequent epochs.

Importantly, the oldest of these discoveries, the stem-lineage mousebird *Tsidiiyazhi abini* from New Mexico (Ksepka et al., 2017) is approximately 62.5 million years old—dating to more than three million years after the end-Cretaceous mass extinction. Where are the diagnosable bird fossils closer in age to the K–Pg boundary? The Chicxulub asteroid impact 66.02 million years ago is hypothesized to have devastated avialan population sizes (Robertson et al., 2004; Field, 2017; Field et al., 2018a), which may help explain the rarity of birds in the lowermost Paleocene. Additionally, avialan body sizes are hypothesized to have been reduced in the wake of the K–Pg mass extinction event (Berv and Field, 2018), potentially adding a taphonomic bias against the preservation and discovery of birds from this time interval.

Furthermore, the early Cenozoic crown-bird fossil record is strongly biased towards remains from the northern hemisphere. Although considerable dissent regarding the biogeographic origins of crown birds and the major avian subclades is ongoing (Mayr, 2009; Claramunt and Cracraft, 2015; Cracraft and Claramunt, 2017; Mayr, 2017; Field and Hsiang, 2018; Saupe et al., 2019; see also Ding et al.'s biogeography section in chapter 4), analytical reconstructions have supported a scenario in which many lineages of crown birds originated in the southern hemisphere—specifically, South America and west Antarctica—and expanded northward following the end-Cretaceous mass extinction (Claramunt and Cracraft, 2015). If this scenario is accurate, then the scarcity of crown-bird fossils from the latest Cretaceous and earliest Paleocene may be at least partly explained by sparse sampling from relevant geographic regions (Claramunt and Cracraft, 2015).

DISCUSSION

The pennaraptoran fossil record has expanded phenomenally since they were first discovered in the mid 19th century, bringing about huge leaps in our understanding of the group. Archaeopterygiformes, anchiornithines, and scansoriopterygids tell us that the clade had originated by the Late Jurassic, with other pennaraptoran groups either unknown at that time as in oviraptorosaurians (Osmólska et al., 2004) or based on fragmentary specimens as in dromaeosaurids (Heckert and Foster, 2011). The anchiornithines are the best represented group of Jurassic paravians after Archaeopterygiformes, but their status as birds, troodontids, early-diverging deinonychosaurs, or sister to Paraves remains controversial, even though consensus for their near-avialan status is emerging (Pei et al., in press). The search for Jurassic-aged pennaraptorans should therefore remain a priority moving forward, both from lagerstätten that have recovered them already, like the Solnhofen Limestone of southern Germany and the Tiaojishan Formation of northern China, and from new localities. Although Konservat Lagerstätten are few and far between, it is heartening to note that new exposures containing Jehol and Yanliao biota fossils are cropping up across northern China with increasing collection efforts. They are also present, but undersampled in Mongolia, where only a few feathers have been excavated (Kurochkin, 2000). In general, the uneven nature of the pennaraptoran record, which is biased toward key formations like the Yixian and Djadokhta, needs to be better counterbalanced to ensure our understanding of this group is not being biased by potential local or regional factors. This is easier said than done, but a healthy awareness of this issue will at least help to minimize any chance of conflating separate evolutionary signals.

OVIRAPTOROSAURIA: Tooth-bearing early-diverging oviraptorosaurians like *Incisivosaurus* and *Caudipteryx* remain rare and oviraptorosaurians with more ancestral theropod body plans are expected in the Late Jurassic, but have not been found. This is potentially the most important priority for future work because it should shed more light on the evolution of the beak and the changes involved in skull specialization. Future finds of later-diverging taxa that could better characterize the caenagnathid and oviraptorid split would also be very useful, especially as early-diverging caenagnathids are not known from complete cranial material and include giant, evidently specialized forms like *Gigantoraptor* (Ma et al., 2017). Oviraptorosaurians and Scansoriopterygidae are currently exclusively Laurasian groups, but experience in other pennaraptoran groups, including those with a longer collection history, suggests that future Gondwanan finds are possible. Thus, efforts to seek such material whether in the field or in existing collections could be fruitful.

SCANSORIOPTERYGIDAE: Scansoriopterygids are among the least known early-diverging pennaraptorans because of their representation by a small pool of specimens. More specimens, particularly from adult growth stages, will be critical in solidifying the taxonomic status of the group and uncovering key events in their evolutionary history as well as their correct phylogenetic position. *Yi* preserves feathered, membranous wings that appear to be an alternative dinosaurian volant strategy to feathered, muscular wings (Xu et al., 2015a; Wang et al., 2019a). This astonishing discovery warrants extensive further study that will require additional soft-tissue-preserving specimens. Further discoveries are also needed to determine whether scansoriopterygids were a short-lived experiment or they persisted to the terminal Cretaceous like oviraptorosaurians.

DROMAEOSAURIDAE: Dromaeosaurids are among the most widely distributed pennaraptorans after birds. This, coupled with their generally more ground-based lifestyle compared with early birds (early birds could probably cross barriers more easily), provides the best opportunity to understand the impact of Mesozoic biogeography on pennaraptoran evolution. This is examined in the next chapter on coelurosaurian biogeography. Encouraging potential for further finds in underrepresented parts of Gondwana, e.g., the Wadi Milk Formation of Sudan and James Ross Island, Antarctica, underscores the importance of Dromaeosauridae in understanding pennaraptoran biogeography more generally. The reconstruction of flight capabilities in *Microraptor* makes microraptorines an obvious subclade to focus more attention on (Pei et al., in press). However, the unenlagiine *Rahonavis* also has similar flight potential, and so this clade should also be studied more intensively, especially given that it represents the only detection of nonavialan flight potential in Gondwana (Pei et al., in press).

TROODONTIDAE: Troodontids are thought to be a Laurasian clade, but the discovery of a possible troodontid tooth from the Kallamedu Formation of India (Goswami et al., 2013) justifies further search efforts to confirm this Gondwanan record and explore biogeographic differences among troodontids in more detail (see Ding et al., chapter 4). The taxonomic status of Anchiornithinae should be another study priority and will benefit from Jurassic nonavialan paravian finds, particularly from the Solnhofen and Tiaojishan as well as the sparse Early Cretaceous of North America. The discovery of more troodontid specimens with transitional anatomical features between longer-armed earlier-diverging forms and shorter-armed later-diverging forms (e.g. *Sinusonasus* and *Jianianhualong* (Xu et al., 2017)) would also shed more light on troodontid character evolution.

AVIALAE: Despite the incredible number of new specimens unearthed within the past four decades, there remain numerous major gaps in the fossil record of stem avialans. There is a 20 million year gap in the record between the 155–150 Ma *Archaeopteryx* and the beginning of the Jehol avifauna captured by the 131 Ma Huajiying Formation. Specimens from this 20 Ma gap are critical to understanding early skeletal transitions such as the evolution of the pygostyle and the evolution of the first avialan edentulous beak, let alone a host of other features like solidification of the pectoral girdle and plumage specialization. Notably, non-ornithothoracines are almost exclusively found in the Solnhofen limestones (Archaeopterygiformes) and in the Early Cretaceous Jehol lagerstätten, which may suggest early-diverging lineages went extinct fairly early, being unable to compete with ornithothoracines. No Mesozoic avialan has been collected from the African continent, despite its great potential (although remains are known from Madagascar). Globally, the Early Cretaceous record is far stronger than the Late Cretaceous record (mostly due to the Jehol Biota), but there are currently no Early Cretaceous avialan fossils known from North America. A major gap in the avialan fossil record consists of the conspicuous absence of fossils documenting the crownwardmost portion of the avian stem lineage, i.e., crownward of the Late Cretaceous ornithurine groups Hesperornithiformes, Ichthyornithiformes, and *Iaceornis*. Similarly, the earliest stages of crown-bird evolution are poorly known at present, and many of the greatest questions regarding the early evolutionary history of Aves will be resolved by new discoveries of crown birds from the Late Cretaceous and early Paleogene, including questions related to avialan survivorship, ecological selectivity, and recovery across the end-Cretaceous mass extinction. It is hoped that the coming years will yield avialan fossils filling the critical temporal and geographic gaps discussed above—and in the process, shed important new light on the Mesozoic and Cenozoic evolutionary history of avialan pennaraptorans.

ACKNOWLEDGMENTS

This paper arose from discussions at the International Pennaraptoran Symposium, held at the University of Hong Kong and supported by Kenneth H.C. Fung and First Initiative Foundation. This study was supported by the Research Grant Council of Hong Kong's General Research Fund (17103315 to M.P., X.X., and P.A.G.) and the National Science Foundation of China (41688103, 41120124002, and 91514302 to X.X.). It was also supported by Faculty of Science of the University of Hong Kong (to M.P.). M.A.N.'s support came from the American Museum of Natural History (Division of Vertebrate Paleontology), the Macaulay Family Endowment, and NSF Earth Sciences. D.J.F. is supported by UK Research and Innovation Future Leaders Fellowship MR/S032177/1.

REFERENCES

Agnolín, F.L., and A.G. Martinelli. 2007. Did oviraptorosaurs (Dinosauria: Theropoda) inhabit Argentina? Cretaceous Research 28: 785–790.

Agnolín, F.L., and A.G. Martinelli. 2009. Fossil birds from the Late Cretaceous Los Alamitos Formation, Río Negro Province, Argentina. Journal of South American Earth Sciences 27: 42–49.

Agnolín, F.L., and F.E. Novas. 2013. Avian ancestors: a review of the phylogenetic relationships of the theropods Unenlagiidae, Microraptoria, *Anchiornis* and Scansoriopterygidae, Dordrecht: Springer.

Agnolín, F.L., F.E. Novas, and G. Lio. 2006. Neornithine bird coracoid from the Upper Cretaceous of Patagonia. Ameghiniana 43: 245–248.

Agnolín, F.L., M.D. Ezcurra, D.F. Pais, and S.W. Salisbury. 2010. A reappraisal of the Cretaceous non-avian dinosaur faunas from Australia and New Zealand: evidence for their Gondwanan affinities. Journal of Systematic Palaeontology 8: 257–300.

Agnolín, F.L., F. Brissón Egli, S. Chatterjee, J.A. Garcia Marsà, and F.E. Novas. 2017. Vegaviidae, a new clade of southern diving birds that survived the K/T boundary. Science of Nature 104: 87.

Allain, R., and P. Taquet. 2000. A new genus of Dromaeosauridae (Dinosauria, Theropoda) from the Upper Cretaceous of France. Journal of Vertebrate Paleontology 20: 404–407.

Allain, R., R. Vullo, J. Le Loeuff, and J.F. Tournepiche. 2014. European ornithomimosaurs (Dinosauria, Theropoda): an undetected record. Geologica Acta 12: 127–135.

Alvarenga, H.M.F., and J.F. Bonaparte. 1992. A new flightless landbird from the Cretaceous of Patagonia. *In* K.C. Campbell, Jr. (editor), Papers in Avian Paleontology Honoring Pierce Brodkorb: 51–64. Los Angeles, CA: Natural History Museum of Los Angeles County.

An, W., et al. 2016. Detrital zircon dating and tracing the provenance of dinosaur bone beds from the Late Cretaceous Wangshi Group in Zhucheng, Shandong, East China. Journal of Palaeogeography 5: 72–99.

Anonymous. 1887. Discussion on *Ornithodesmus* and *Patricosaurus*. Quarterly Journal of the Geological Society of London 43: 219–220.

Antunes, M.T., and D. Sigogneau. 1992. La faune de petits dinosaures du Crétacé terminal du Portugal. Comuncações dos Serviços. Geológicos de Portugal 78: 49–62.

Aotsuka, K., and T. Sato. 2016. Hesperornithiformes (Aves: Ornithurae) from the Upper Cretaceous Pierre Shale, Southern Manitoba, Canada. Cretaceous Research 63: 154–169.

Armas, P., and M.L. Sánchez. 2015. Hybrid coastal edges in the Neuquén Basin (Allen Formation, Upper Cretaceous, Argentina). Andean Geology 42: 97–113.

Atterholt, J.A., J.H. Hutchison, and J.M.K. O'Connor. 2018. The most complete enantiornithine from North America and a phylogenetic analysis of the Avisauridae. PeerJ 6: e5910.

Averianov, A.O., and H.D. Sues. 2007. A new troodontid (Dinosauria: Theropoda) from the Cenomanian of Uzbekistan, with a review of troodontid records from the territories of the former Soviet Union. Journal of Vertebrate Paleontology 27: 87–98.

Bailleul, A.M., et al. 2019. An early Cretaceous enantiornithine (Aves) preserving an unlaid egg and probable medullary bone. Nature Communications 10 (1275): 1–10.

Balanoff, A.M., and M.A. Norell. 2012. Osteology of *Khaan mckennai* (Oviraptorosauria: Theropoda). Bulletin of the American Museum of Natural History 372: 1–77.

Balanoff, A.M., X. Xu, Y. Kobayashi, Y. Matsufune, and M.A. Norell. 2009. Cranial osteology of the theropod dinosaur *Incisivosaurus gauthieri* (Theropoda: Oviraptorosauria). American Museum Novitates 3651: 1–35.

Barclay, R.S., et al. 2015. High precision U–Pb zircon geochronology for Cenomanian Dakota Formation floras in Utah. Cretaceous Research 52A: 213–237.

Barsbold, R. 1974. Saurornithoididae, a new family of carnivorous dinosaurs from Central Asia and North America. Palaeontologica Polonica 30: 5–22.

Barsbold, R. 1981. Toothless dinosaurs of Mongolia. Joint Soviet-Mongolian Paleontological Expedition Transactions 15: 28–39.

Barsbold, R. 1983. Carnivorous dinosaurs from the Cretaceous of Mongolia. Sovmestnaâ Sovetsko-Mongolskaâ Paleontologičeskaâ Ekspediciâ, Trudy 19: 1–119.

Barsbold, R. 1986. Raubdinosaurier oviraptoren. *In* E.I. Vorobyeva (editor), Herpetologische Untersuchungen in der Mongolischen Volksrepublik: 210–223. Moscow: A.M. Severtsova.

Barsbold, R., H. Osmólska, and S.M. Kurzanov. 1987. On a new troodontid (Dinosauria, Theropoda) from the Early Cretaceous of Mongolia. Acta Palaeontologica Polonica. 30: 121–132.

Barsbold, R., H. Osmólska, M. Watabe, P.J. Currie, and K. Tsogtbaatar. 2000. A new oviraptorosaur (Dinosauria, Theropoda) from Mongolia: the first dinosaur with a pygostyle. Acta Palaeontologica Polonica 45: 97–106.

Bell, A.K., and L.M. Chiappe. 2015. A species-level phylogeny of the Cretaceous Hesperornithiformes (Aves: Ornithuromorpha): implications for body size evolution amongst the earliest diving birds. Journal of Systematic Palaeontology 14: 239–251.

Bell, P.R., and P.J. Currie. 2015. A high-latitude dromaeosaurid, *Boreonykus certekorum*, gen. et sp. nov. (Theropoda), from the upper Campanian Wapiti Formation, west-central Alberta. Journal of Vertebrate Palaeontology 36: e1034359.

Bell, A.K., et al. 2010. Description and ecologic analysis of *Hollanda luceria*, a Late Cretaceous bird from the Gobi Desert (Mongolia). Cretaceous Research 31: 16–26.

Berv, J.S., and D.J. Field. 2018. Genomic signature of an avian Lilliput effect across the K-Pg extinction. Systematic Biology 67: 1–13.

Bever, G.S., and M.A. Norell. 2009. The perinate skull of *Byronosaurus* (Troodontidae) with observations on the cranial ontogeny of paravian theropods. American Museum Novitates 3657: 1–51.

Bonde, N., and P. Christiansen. 2003. New dinosaurs from Denmark. Comptes Rendus Palevol 2: 13–26.

Bonnetti, C. et al. 2014. Sedimentology, stratigraphy and palynological occurrences of the late Cretaceous Erlian Formation, Erlian Basin, Inner Mongolia, People's Republic of China. Cretaceous Research 48: 177–192.

Bono, R.K., J.A. Clarke, J.A. Tarduno, and D. Brinkman. 2016. A large ornithurine bird (*Tingmiatornis arctica*) from the Turonian high arctic: climatic and evolutionary implications. Scientific Reports 6: 1–8.

Brinkman, D.L., R.L. Cifelli, and N.J. Czaplewski. 1998. First occurrence of *Deinonychus antirrhopus* (Dinosauria: Theropoda) from the Antlers Formation (Lower Cretaceous: Aptian-Albian) of Oklahoma. Oklahoma Geological Survey Bulletin 146: 1–27.

Brissón Egli, F., A.M. Aranciaga Rolando, F.L. Agnolín, and F.E. Novas. 2017. Osteology of the unenlagiid theropod *Neuquenraptor argentinus* from the Late Cretaceous of Patagonia. Acta Palaeontologica Polonica 62: 549–562.

Brett-Surman, M.K., and G.S. Paul. 1985. A new family of bird-like dinosaurs linking Laurasia and Gondwanaland. Journal of Vertebrate Paleontology 5 (2): 133–138.

Brodkorb, P. 1976. Discovery of a Cretaceous bird, apparently ancestral to the orders Coraciiformes and Piciformes (Aves: Carinatae). *In* S.L. Olson (editor), Collected papers in avian paleontology honoring the 90th birthday of Alexander Wetmore: 67–73. Washington D.C.: Smithsonian Institution Press.

Brown, C.M., D.C. Evans, N.E. Campione, L.J. O'Brien, and D.A. Eberth. 2013. Evidence for taphonomic size bias in the Dinosaur Park Formation (Campanian, Alberta), a model Mesozoic terrestrial alluvial-paralic system. Palaeogeography, Palaeoclimatology, Palaeoecology 372: 108–122.

Brusatte, S.L., et al. 2013. The osteology of *Balaur bondoc*, an island-dwelling dromaeosaurid (Dinosauria: Theropoda) from the Late Cretaceous of Romania. Bulletin of the American Museum of Natural History 374: 1–100.

Brusatte, S.L., G.T. Lloyd, S.C. Wang, and M.A. Norell. 2014. Gradual assembly of avian body plan culminated in rapid rates of evolution across the dinosaur-bird transition. Current Biology 24: 2386–2392.

Buffetaut, E. 1998. First evidence of enantiornithine birds from the Upper Cretaceous of Europe: postcranial bones from Cruzy (Herault, southern France). Oryctos 1: 131–136.

Buffetaut, E. 2010. A basal bird from the Campanian (Late Cretaceous) of Dinosaur Provincial Park (Alberta, Canada). Geological Magazine 147: 469–472.

Buffetaut, E., B. Marandat, and B. Sigé. 1986. Découverte de dents de deinonychosaures (Saurischia, Theropoda) dans le Crétacé supérieur du sud de la France. Comptes Rendus de l'Académie des Sciences 303: 1393–1396.

Buffetaut, E., J. Le Loeuff, P. Mechin, and A. Mechin-Salessy. 1995. A large French Cretaceous bird. Nature 377: 110.

Bureau of Geology and Mineral Resources of Jiangxi Province. 1984. Regional geology of Jiangxi Province. Beijing: Geological Publishing House.

Bureau of Geology and Mineral Resources of Guangdong Province. 1988. People's Republic of China, Ministry of Geology and Mineral Resources Geological Memoirs, Series 1 (9). Regional Geology of Guangdong Province. Beijing: Geological Publishing House.

Burnham, D.A., et al. 2000. Remarkable new birdlike dinosaur (Theropoda: Maniraptora) from the Upper Cretaceous of Montana. University of Kansas Paleontological Contributions 13: 1–14.

Buscalioni, A.D., and M.A. Fregenal-Martínez. 2010. A holistic approach to the palaeoecology of Las Hoyas Konservat-Lagerstätte (La Huérguina Formation, Lower Cretaceous, Iberian Ranges, Spain). Journal of Iberian Geology 36: 297–326.

Calvo, J.O., J.D. Porfiri, and A.W.A. Kellner. 2004. On a new maniraptoran dinosaur (Theropoda) from the Upper Cretaceous of Neuquén, Patagonia, Argentina. Arquivos do Museu Nacional, Rio de Janeiro 62: 549–566.

Calvo, J.O., J.D. Porfiri, B.J. Gonzalez-Riga, and A.W.A. Kellner. 2007. A new Cretaceous terrestrial ecosystem from Gondwana with the description of a new sauropod dinosaur. Anais da Academia Brasileira de Ciencias 79: 529–541.

Candeiro, C.R.A., A. Cau, F. Fanti, W.R. Nava, and F.E. Novas. 2012. First evidence of an unenlagiid (Dinosauria, Theropoda, Maniraptora) from the Bauru Group, Brazil. Cretaceous Research 37: 223–226.

Carpenter, K. 1979. Vertebrate fauna of the Laramie Formation (Maestrichtian), Weld County, Colorado. Contributions to Geology 17: 37–49.

Carpenter, K. 1982. Baby dinosaurs from the Late Cretaceous Lance and Hell Creek formations and a description of a new species of theropod. Contributions to Geology, University of Wyoming 20: 123–134.

Carvalho, I.D.S., et al. 2015 A new genus and species of enantiornithine bird from the Early Cretaceous of Brazil. Brazilian Journal of Geology 45: 161–171.

Case, J.A., J.E. Martin, and M. Reguero. 2007. A dromaeosaur from the Maastrichtian of James Ross Island and the Late Cretaceous Antarctic dinosaur fauna. *In* A.K. Cooper and C.R. Raymond (editors), Antarctica: a keystone in a changing world. Online proceedings of the 10th International Symposium on Antarctic Earth Science, USGS. [10.3133/of2007-1047.srp083]

Cau, A. 2018. The assembly of the avian body plan: a 160-million-year long process. Bollettino della Società Paleontologica Italiana 57: 1–25.

Cau, A., and P. Arduini. 2008. *Enantiophoenix electrophyla* gen. et sp. nov. (Aves, Enantiornithes) from the Upper Cretaceous (Cenomanian) of Lebanon and its phylogenetic relationships. Atti della Società Italiana di Scienze Naturali e del Museo Civico di Storia Naturale in Milano 149: 293–324.

Cau, A., and D. Madzia. 2018. Redescription and affinities of *Hulsanpes perlei* (Dinosauria, Theropoda) from the Upper Cretaceous of Mongolia. PeerJ 6: e4868.

Cau, A., T. Brougham, and D. Naish. 2015. The phylogenetic affinities of the bizarre Late Cretaceous Romanian theropod *Balaur bondoc* (Dinosauria, Maniraptora): dromaeosaurid or flightless bird? PeerJ 3: e1032.

Cau, A., et al. 2017. Synchrotron scanning reveals amphibious ecomorphology in a new clade of bird-like dinosaurs. Nature 552: 395–399.

Chang, S.C., H.C. Zhang, P.R. Renne, and Y. Fang. 2009. High-precision 40Ar/39Ar age for the Jehol Biota. Palaeogeography, Palaeoclimatology, Palaeoecology 280: 94–104.

Chang, S.C., K.Q. Gao, C.F. Zhou, and F. Jourdan. 2017. New chronostratigraphic constraints on the Yixian Formation with implications for the Jehol Biota. Palaeogeography, Palaeoclimatology, Palaeoecology 487: 399–406.

Chatterjee, S. 2002. The morphology and systematics of *Polarornis*, a Cretaceous loon (Aves: Gaviidae) from Antarctica. *In* Z.H Zhou and F.C Zhang (editors), Proceedings of the 5th symposium of the Society of Avian Paleontology and Evolution: 125–155. Beijing: Science Press.

Chiappe, L.M. 1993. Enantiornithine (Aves) tarsometatarsi from the Cretaceous Lecho Formation of northwestern Argentina. American Museum Novitates 3083: 1–27.

Chiappe, L.M., and J.O. Calvo. 1994. *Neuquenornis volans*, a new Late Cretaceous bird (Enantiornithes: Avisauridae) from Patagonia, Argentina. Journal of Vertebrate Paleontology 14: 230–246.

Chiappe, L.M., S. Ji, Q. Ji, and M.A. Norell. 1999. Anatomy and systematics of the Confuciusornithidae (Theropoda: Aves) from the Late Mesozoic of northeastern China. Bulletin of the American Museum of Natural History 242: 1–89.

Chiappe, L.M., M.A. Norell, and J.M. Clark. 2001. A new skull of *Gobipteryx minuta* (Aves: Enantiornithes) from the Cretaceous of the Gobi Desert. American Museum Novitates 3346: 1–15.

Chiappe, L.M., J.P. Lamb, Jr., and P.G.P. Ericson. 2002. New enantiornithine bird from the marine Upper Cretaceous of Alabama. Journal of Vertebrate Paleontology 22: 170–174.

Chiappe, L.M., et al. 2007. A new enantiornithine bird from the Late Cretaceous of the Gobi desert. Journal of Systematic Palaeontology 5: 193–208.

Chiappe, L.M., et al. 2014. A new specimen of the Early Cretaceous bird *Hongshanornis longicresta*: Insights into the aerodynamics and diet of a basal ornithuromorph. PeerJ. 2. e234.

Chiappe, L.M., et al. 2019a. Anatomy and flight performance of the early enantiornithine bird *Protopteryx fengningensis*: information from new specimens of the Early Cretaceous Huajiying Formation of China. The Anatomical Record: early view. [doi.org/10.1002/ar.24322]

Chiappe, L.M., et al. 2019b. New *Bohaiornis*-like bird from the Cretaceous of China: enantiornithine interrelationships and flight performance. PeerJ 7 (e7846): 1–50.

Chure, D.J. 1994. *Koparion douglassi*, a new dinosaur from the Morrison Formation (Upper Jurassic) of Dinosaur National Monument; the oldest troodontid (Theropoda: Maniraptora). Brigham Young University Geology Studies 40: 11–15.

Claramunt, S., and J. Cracraft. 2015. A new time tree reveals Earth history's imprint on the evolution of modern birds. Science Advances 1: e1501005.

Clark, J.M., M.A. Norell, and R. Barsbold. 2001. Two new oviraptorids (Theropoda: Oviraptorosauria), upper Cretaceous Djadokhta Formation, Ukhaa Tolgod, Mongolia. Journal of Vertebrate Paleontology 21: 209–213.

Clark, J.M., M.A. Norell, and T. Rowe. 2002. Cranial anatomy of *Citipati osmolskae* (Theropoda, Oviraptorosauria), and a reinterpretation of the holotype of *Oviraptor philoceratops*. American Museum Novitates 3364: 1–24.

Clarke, J.A. 2004. Morphology, phylogenetic taxonomy, and systematics of *Ichthyornis* and *Apatornis* (Avialae: Ornithurae). Bulletin of the American Museum of Natural History 286: 1–179.

Clarke, J.A., and L.M. Chiappe. 2001. A new carinate bird from the Late Cretaceous of Patagonia (Argentina). American Museum Novitates 3323: 1–23.

Clarke, J.A., and M.A. Norell. 2002. The morphology and phylogenetic position of *Apsaravis ukhaana* from the Late Cretaceous of Mongolia. American Museum Novitates 3387: 1–46.

Clarke, J.A., and M.A. Norell. 2004. New avialan remains and a review of the known avifauna from the Late Cretaceous Nemegt Formation of Mongolia. American Museum Novitates 3447: 1–12.

Clarke, J.A., C.P. Tambussi, J.I. Noriega, G.M. Erickson, and R.A. Ketcham. 2005. Definitive fossil evidence for the extant avian radiation in the Cretaceous. Nature 433: 305–308.

Clarke, J.A., et al. 2016. Fossil evidence of the avian vocal organ from the Mesozoic. Nature 538: 502–505.

Close, R.A., et al. 2009. Earliest Gondwanan bird from the Cretaceous of southeastern Australia. Journal of Vertebrate Paleontology 29: 616–619.

Cordes-Person, A., C. Acosta Hospitaleche, J. Case, and J. Martin. 2020. An enigmatic bird from the lower Maastrichtian of Vega Island, Antarctica. Cretaceous Research 108: 104314.

Cracraft, J., and S. Claramunt. 2017. Conceptual and analytical worldviews shape differences about global avian biogeography. Journal of Biogeography 44: 958–960.

Cracraft, J., et al. 2015. Response to Comment on "Whole-genome analyses resolve early branches in the tree of life of modern birds." Science 349: 1460.

Csiki, Z., and D. Grigorescu. 2005. A new theropod from Tustea: are there oviraptorosaurs in the Upper Cretaceous of Europe? Kaupia 14: 78.

Csiki, Z., V. Mátyás, S.L. Brusatte, and M.A. Norell. 2010. An aberrant island-dwelling theropod dinosaur from the Late Cretaceous of Romania. Proceedings of the National Academy of Sciences of the United States of America 107: 15357–15361.

Currie, P.J., and J.H. Peng. 1993. A juvenile specimen of *Saurornithoides mongoliensis* from the Upper Cretaceous of northern China. Canadian Journal of Earth Sciences 30: 2224–2230.

Currie, P.J. 1995. New information on the anatomy and relationships of *Dromaeosaurus albertensis* (Dinosauria: Theropoda). Journal of Vertebrate Paleontology 15: 576–591.

Currie, P.J. 2005. Theropods including birds. *In* P.J. Currie and E.B. Koppelhus (editors), Dinosaur Provincial Park: a spectacular ecosystem revealed: 367–397. Bloomington: Indiana University Press.

Currie, P.J., and A. Paulina-Carabajal. 2012. A new specimen of *Austroraptor cabazai* Novas, Pol, Canale, Porfiri and Calvo, 2008 (Dinosauria, Theropoda, Unenlagiidae) from the Latest Cretaceous (Maastrichtian) of Río Negro, Argentina. Ameghiniana 49: 662–667.

Currie, P.J. and D. Evans. 2020. Cranial anatomy of new specimens of *Saurornitholestes langstoni* (Dinosauria, Theropoda, Dromaeosauridae) from the Dinosaur Park Formation (Campanian) of Alberta. The Anatomical Record: 303: 691–715.

Currie, P.J., and A.R. Jacobsen. 1995. An azhdarchid pterosaur eaten by a velociraptorine theropod. Canadian Journal of Earth Sciences 32: 922–925.

Currie, P.J., and D.J. Varricchio. 2004. A new dromaeosaurid from the Horseshoe Canyon Formation (Upper Cretaceous) of Alberta, Canada. *In* P.J. Currie, E.B. Koppelhus, M.A. Shugar, and J.L. Wright (editors), Feathered dinosaurs: 112–132. Bloomington: Indiana University Press.

Currie, P.J., S.J. Godfrey, and L. Nessov. 1993. New caenagnathid (Dinosauria: Theropoda) specimens from the Upper Cretaceous of North America and Asia. Canadian Journal of Earth Sciences 30: 2255–2272.

Currie, P.J., P. Vickers-Rich, and T.H. Rich. 1996. Possible oviraptorosaur (Theropoda, Dinosauria) specimens from the Early Cretaceous Otway Group of Dinosaur Cove, Australia. Alcheringa 20: 73–79.

Currie, P.J., G.F. Funston, and H. Osmólska. 2016. New specimens of the crested theropod dinosaur *Elmisaurus rarus* of Mongolia. Acta Palaeontologica Polonica 61: 143–157.

Czerkas, S.A., and A. Feduccia. 2014. Jurassic archosaur is a non-dinosaurian bird. Journal of Ornithology 155: 841–851.

Czerkas, S.A., and Q. Ji. 2002. A preliminary report on an omnivorous volant bird from northeast China. *In* S.J. Czerkas (editor), Feathered dinosaurs and the origin of flight: 127–135. Blanding, UT: Dinosaur Museum.

Czerkas, S.A., and C. Yuan. 2002. An arboreal maniraptoran from northeast China. *In* Czerkas, S.J. (editor), Feathered dinosaurs and the origin of flight: 63–95. Blanding, UT: Dinosaur Museum.

Da Gama, R.O.B.P., et al. 2014. Integrated paleoenvironmental analysis of the Niobrara Formation: Cretaceous Western Interior Seaway, northern Colorado. Palaeogeography, Palaeoclimatology, Palaeoecology 413: 66–80.

Dalla Vecchia, F.M., and L.M. Chiappe. 2002. First avian skeleton from the Mesozoic of northern Gondwana. Journal of Vertebrate Paleontology 22: 856–860.

de Souza Carvalho, I., et al. 2015. A Mesozoic bird from Gondwana preserving feathers. Nature Communications 6: 1–5.

Dalsätt, J., Z.H. Zhou, F.C. Zhang, and P.G.P. Ericson. 2006. Food remains in *Confuciusornis sanctus* suggest a fish diet. Naturwissenschaften 93: 444–446.

Dalsätt, J., P.G., Ericson, and Z.H. Zhou. 2014. A new Enantiornithes (Aves) from the Early Cretaceous of China. Acta Geologica Sinica 88: 1034–1040.

Dames, W. 1884. Ueber *Archaeopteryx*. Palaeontologische Abhandlungen 2: 119–196.

Dececchi, T.A., H.C.E. Larsson, and D. Hone. 2012. *Yixianosaurus longimanus* (Theropoda: Dinosauria) and its bearing on the evolution of Maniraptora and ecology of the Jehol Biota. Vertebrata PalAsiatica 50: 111–139.

Dececchi, T.A., H.C.E. Larsson, and M.B. Habib. 2016. The wings before the bird: an evaluation of flapping-based locomotory hypotheses in bird antecedents. PeerJ 4: e2159.

Delcourt, R., and O.N. Grillo. 2017. On maniraptoran material (Dinosauria: Theropoda) from Vale do Rio do Peixe formation, Bauru group, Brazil. Revista Brasileira de Paleontologia 17: 307–316.

DePalma, R.A., D.A. Burnham, L.D. Martin, P.L. Larson, and R.T. Bakker. 2015. The first giant raptor (Theropoda: Dromaeosauridae) from the Hell Creek Formation. Paleontological Contributions 14: 1–16.

Dingus, L., et al. 2008. The geology of Ukhaa Tolgod (Djadokhta Formation, Upper Cretaceous, Nemegt Basin, Mongolia). American Museum Novitates 3616: 1–40.

Dumont, M., et al. 2016. Synchrotron imaging of dentition provides insights into the biology of *Hesperornis* and *Ichthyornis*, the "last" toothed birds. BMC Evolutionary Biology 16: 178.

Dyke, G.J., and A. Ösi. 2010. A review of Late Cretaceous fossil birds from Hungary. Geological Journal 45: 434–444.

Dyke, G.J., D.V. Malakhov, and L.M. Chiappe. 2006. A re-analysis of the marine bird Asiahesperornis from northern Kazakhstan. Cretaceous Research 27: 947–953.

Dyke, G.J., M. Vremir, G. Kaiser, and D. Naish. 2012. A drowned Mesozoic bird breeding colony from the Late Cretaceous of Transylvania. Naturwissenschaften 99: 435–442.

Dyke, G.J., et al. 2002. Europe's last Mesozoic bird. Naturwissenschaften 89: 408–411.

Dyke, G.J., et al. 2013. Aerodynamic performance of the feathered dinosaur *Microraptor* and the evolution of feathered flight. Nature Communications 4: 2489.

Easter, J. 2013. A new name for the oviraptorid dinosaur '*Ingenia*' *yanshini* (Barsbold, 1981; preoccupied by Gerlach, 1957). Zootaxa 3737: 184–190.

Eaton, J.G., R.L. Cifelli, J.H. Hutchison, J.I. Kirkland, and J.M. Parrish. 1999. Cretaceous vertebrate faunas from the Kaiparowits Plateau, south-central Utah. *In* D.D. Gillette (editor), Vertebrate paleontology in Utah: 345–353. Salt Lake City: Utah Geological Survey.

Eberth, D.A. 2005. The geology. *In* P.J. Currie and E.B. Koppelhus (editors), Dinosaur Provincial Park: a spectacular ancient ecosystem revealed: 54–82. Bloomington: Indiana University Press.

Eberth, D.A., and D.R. Braman. 2012. A revised stratigraphy and depositional history for the Horseshoe Canyon Formation (Upper Cretaceous), southern Alberta plains. Canadian Journal of Earth Sciences, 49: 1053–1086.

Ely, R.C. and J.A. Case. 2019. Phylogeny of a new gigantic paravian (Theropoda: Coelurosauria:
Maniraptora) from the Upper Cretaceous of James Ross Island, Antarctica. Cretaceous Research 101: 1–16.

Elżanowski, A. 1974. Preliminary note on the palaeognthous bird from the Upper Cretaceous of Mongolia. Palaeontologia Polonica 30: 103–109.

Elżanowski, A. 1977. Skulls of *Gobipteryx* (Aves) from the Upper Cretaceous of Mongolia. Palaeontologica Polonica 37: 153–165.

Elżanowski, A., and P. Galton. 1991. Braincase of *Enaliornis*, an Early Cretaceous bird from England. Journal of Vertebrate Paleontology 11: 90–107.

Elżanowski, A., G.S. Paul, and T.A. Stidham. 2000. An avian quadrate from the Late Cretaceous Lance Formation of Wyoming. Journal of Vertebrate Paleontology 20: 712–719.

Evans, D.C., D.W. Larson, and P.J. Currie. 2013. A new dromaeosaurid (Dinosauria: Theropoda) with Asian affinities from the latest Cretaceous of North America. Naturwissenschaften 100: 1041–1049.

Evans, D.C., D.W. Larson, T.M. Cullen, and R.M. Sullivan. 2014. '*Saurornitholestes*' *robustus* is a troodontid (Dinosauria: Theropoda). Canadian Journal of Earth Sciences 51: 730–734.

Evans, D.C., T.M. Cullen, D.W. Larson, and A. Rego. 2017. A new species of troodontid theropod (Dinosauria: Maniraptora) from the Horseshoe Canyon Formation (Maastrichtian) of Alberta, Canada. Canadian Journal of Earth Sciences 54: 813–826.

Fanti, F., P.J. Currie, and D. Badamgarav. 2012. New specimens of *Nemegtomaia* from the Baruungoyot and Nemegt Formations (Late Cretaceous) of Mongolia. PLoS One 7: e31330.

Fanti, F., P.R. Bell, and R.L. Sissons. 2013. A diverse, high-latitude ichnofauna from the Late Cretaceous Wapiti Formation, Alberta, Canada. Cretaceous Research 41: 256-269.

Farke, A.A., W.D. Maxwell, R.L. Cifelli, and M.J. Wedel. 2014. A ceratopsian dinosaur from the Lower Cretaceous of Western North America, and the biogeography of Neoceratopsia. PLoS One 9: e112055.

Fastovsky, D.E., and A. Bercovici. 2016. The Hell Creek Formation and its contribution to the Cretaceous-Paleogene extinction: a short primer. Cretaceous Research 57: 368–390.

Fernández, M.S., et al. 2013. A large accumulation of avian eggs from the Late Cretaceous of Patagonia (Argentina) reveals a novel nesting strategy in Mesozoic birds. PLoS One 8: e61030.

Field, D.J. 2017. Big-time insights from a tiny bird fossil. Proceedings of the National Academy of Sciences of the United States of America 114: 7750–7752.

Field, D.J., and A.Y. Hsiang. 2018. A North American stem turaco, and the complex biogeographic history of modern birds. BMC Evolutionary Biology 18: 102.

Field, D.J., et al. 2018a. Early evolution of modern birds structured by global forest collapse at the end-Cretaceous mass extinction. Current Biology 28: 1825–1831.

Field, D.J., et al. 2018b. Complete *Ichthyornis* skull illuminates mosaic assembly of the avian head. Nature 557: 96–100.

Field, D.J. et al. 2020. Late Cretaceous neornithine from Europe illuminates the origins of crown birds. Nature 579: 397–401.

Fiorillo, A.R., P.J. Mccarthy, and P.P. Flaig. 2016. A multi-disciplinary perspective on habitat preferences among dinosaurs in a Cretaceous Arctic greenhouse world, North Slope, Alaska (Prince Creek Formation: Early Maastrichtian). Palaeogeography, Palaeoclimatology, Palaeoecology 441: 377–390.

Foreman, B.Z., R.R. Rogers, A.L. Deino, K.R. Wirth, and J.T. Thole. 2008. Geochemical characterization of bentonite beds in the Two Medicine Formation (Campanian, Montana), including a new 40Ar/39Ar age. Cretaceous Research 29: 373–385.

Forster, C.A., L.M. Chiappe, D.W. Krause, and S.D. Sampson. 1996. The first Cretaceous bird from Madagascar. Nature 382: 532–534.

Forster, C.A., S.D. Sampson, L.M. Chiappe, and D.W. Krause. 1998. The theropod ancestry of birds: new evidence from the Late Cretaceous of Madagascar. Science 279: 1915–1919.

Foster. J.R., and A.B. Heckert. 2011. Ichthyoliths and other microvertebrate remains from the Morrison Formation (Upper Jurassic) of northeastern Wyoming: a screen-washed sample indicates a significant aquatic component to the fauna. Palaeogeography, Palaeoclimatology, Palaeoecology 305: 264–279.

Foth, C., and O.W.M. Rauhut. 2017. Re-evaluation of the Haarlem *Archaeopteryx* and the radiation of maniraptoran theropod dinosaurs. BMC Evolutionary Biology 17: 236.

Frankfurt, N.G., and L.M. Chiappe. 1999. A possible oviraptorosaur from the Late Cretaceous of northwestern Argentina. Journal of Vertebrate Paleontology 19: 101–105.

Funston, G.F., and P.J. Currie. 2014. A previously undescribed caenagnathid mandible from the late Campanian of Alberta, and insights into the diet of *Chirostenotes pergracilis* (Dinosauria: Oviraptorosauria). Canadian Journal of Earth Sciences 51: 156–165.

Funston, G.F., and P.J. Currie. 2016. A new caenagnathid (Dinosauria: Oviraptorosauria) from the Horseshoe Canyon Formation of Alberta, Canada, and a reevaluation of the relationships of Caenagnathidae. Journal of Vertebrate Paleontology 36: e1160910.

Funston, G.F., W.S. Persons IV, G.J. Bradley, and P.J. Currie. 2015. New material of the large-bodied caenagnathid *Caenagnathus collinsi* from the Dinosaur Park Formation of Alberta, Canada. Cretaceous Research 54: 179–187.Funston, G.F., S.E. Mendonca, P.J. Currie, and R. Barsbold. 2017. Oviraptorosaur anatomy, diversity and ecology in the Nemegt Basin. Palaeogeography, Palaeoclimatology, Palaeoecology 494: 101–120.

Gao, C.L, and J.Y. Liu. 2005. A new avian taxon from Lower Cretaceous Jiufotang Formation of western Liaoning. Global Geology 24: 313–316.

Gao, K.Q. and Shubin, N.H. 2012. Late Jurassic salamandroid from western Liaoning, China. Proceedings of the National Academy of Sciences of the United States of America. 109: 5767-5772.

Gao, C.L., et al. 2008. A new basal lineage of Early Cretaceous birds from China and its implications on the evolution of the avian tail. Palaeontology 51: 775–791.

Gao, C.L., et al. 2012. A subadult specimen of the Early Cretaceous bird *Sapeornis chaoyangensis* and a taxonomic reassessment of sapeornithids. Journal of Vertebrate Paleontology 32: 1103–1112.

Gao, K.Q., Q.G. Li, M.R. Wei, H.U. Pak, and I. Pak. 2009. Early Cretaceous birds and pterosaurs from the Sinuiji Series, and geographic extension of the Jehol Biota into the Korean Peninsula. Journal of the Paleontological Society of Korea 25: 57–61.

Garrido, A.C. 2010. Estratigrafía del Grupo Neuquén, Cretácico Superior de la Cuenca Neuquina (Argentina): Nueva propuesta de ordenamiento litoestratigráfico: Revista del Museo Argentino de Ciencias Naturales 12: 121–177.

Gianechini, F.A., P.J. Makovicky, S. Apesteguía, and I. Cerda. 2018. Postcranial skeletal anatomy of the holotype and referred specimens of *Buitreraptor gonzalezorum* Makovicky, Apesteguía and Agnolín 2005 (Theropoda, Dromaeosauridae), from the Late Cretaceous of Patagonia. PeerJ 6: e4558.

Gilmore, C.W. 1924. A new coelurid dinosaur for the Belly River Cretaceous of Alberta. Bulletin of the Canadian Department of Mines Geological Survey 38: 1–12.

Gilmore, C.W. 1932. A new fossil lizard from the Belly River Formation of Alberta. Proceedings and Transactions of the Royal Society of Canada 26: 117–120.

Godefroit, P., P.J. Currie, H. Li, C. Shang, and Z. Dong. 2008. A new species of *Velociraptor* (Dinosauria: Dromaeosauridae) from the Upper Cretaceous of northern China. Journal of Vertebrate Paleontology 28: 432–438.

Godefroit, P., et al. 2013a. A Jurassic avialan dinosaur from China resolves the early phylogenetic history of birds. Nature 498: 359–362.

Godefroit, P., et al. 2013b. Reduced plumage and flight ability of a new Jurassic paravian theropod from China. Nature Communications 4: 1394.

Gong, E.P., L.H. Hou, and L.X. Wang. 2004. Enantiornithine bird with diapsidian skull and its dental development in the Early Cretaceous in Liaoning, China. Acta Geologica Sinica 78: 1–7.

Gong, E.P., L.D. Martin, D.A. Burnham, A.R. Falk, and L.H. Hou. 2012. A new species of *Microraptor* from the Jehol Biota of northeastern China. Palaeoworld 21: 81–91.

Goswami, A., G.V.R. Prasad, O. Verma, J.J. Flynn, and R.B.J. Benson. 2013. A troodontid dinosaur from the latest Cretaceous of India. Nature Communications 4: 1703.

Gradziński, R., and T. Jerzykiewicz. 1974a. Dinosaur- and mammal-bearing aeolian and associated deposits of the Upper Cretaceous in the Gobi Desert (Mongolia). Sedimentary Geology 12: 249–278.

Gradziński, R., and T. Jerzykiewicz. 1974b. Sedimentation of the Bayan Goryot Formation. *In* Z. Kielan-Jaworowska (editor), Results of the Polish-Mongolian Palaeontological Expeditions: 111–146. Warsaw: Palaeontologia Polonica.

Grellet-Tinner, G., and P. Makovicky. 2006. A possible egg of the dromaeosaur *Deinonychus antirrhopus*: phylogenetic and biological implications. Canadian Journal of Earth Sciences 43: 705–719.

Hackett, S.J., et al. 2008. A phylogenomic study of birds reveals their evolutionary history. Science 320: 1763–1768.

Han, G., et al. 2014. A new raptorial dinosaur with exceptionally long feathering provides insights into dromaeosaurid flight performance. Nature Communications 5: 4382.

Hartman, S., et al. 2019. A new paravian dinosaur from the Late Jurassic of North America supports a late acquisition of avian flight. PeerJ 7: e7247.

Hasegawa, H., R. Tada, N. Ichinnorov, and C. Minjin. 2009. Lithostratigraphy and depositional environments of the Upper Cretaceous Djadokhta Formation, Ulan Nuur Basin, southern Mongolia, and its paleoclimatic implication. Journal of Asian Earth Sciences 35: 13–26.

He, H.Y., et al. 2004. Timing of the Jiufotang Formation (Jehol Group) in Liaoning, northeastern China, and its implications. Geophysical Research Letters. 31: L12605.

He, T., X.L. Wang, and Z.H. Zhou. 2008. A new genus and species of caudipterid dinosaur from the Lower Cretaceous Jiufotang Formation of western Liaoning, China. Vertebrata Palasiatica 46: 178–189.

Heller, F. 1959. Ein dritter *Archaeopteryx*-Fund aus den Solnhofener Plattenkalken von Longenaltheim/Mfr. Erlanger Geologische Abhandlungen 31: 1–25.

Herman, A.B., R.A. Spicer, and T.E.V. Spicer. 2016. Environmental constraints on terrestrial vertebrate behaviour and reproduction in the high Arctic of the Late Cretaceous. Palaeogeography, Palaeoclimatology, Palaeoecology 441: 317–338.

Hoganson, J.W., and E.C. Murphy. 2002. Marine Breien Member (Maastrichtian) of the Hell Creek Formation in North Dakota: stratigraphy, vertebrate fossil record, and age. *In* J.H. Hartman, K.R. Johnson, and D.J. Nichols (editors), The Hell Creek Formation and the Cretaceous-Tertiary boundary in the northern Great Plains: an integrated continental record of the end of the Cretaceous: 247–269. Boulder: Geological Society of America.

Hope, S. 2002. The Mesozoic record of Neornithes (modern birds). *In* L.M. Chiappe, and L.M. Witmer (editors), Mesozoic birds: above the heads of dinosaurs: 339–388. Berkeley: University of California Press.

Hou, L.H. 1994 A Late Mesozoic bird from Inner Mongolia. Vertebrate PalAsiatica 32: 258–266.

Hou, L.H. 1996. The discovery of a Jurassic carinate bird in China. Chinese Science Bulletin 41: 1861–1864.

Hou, L.H. 1997a. Mesozoic Birds of China. Nantou: Phoenix Valley Aviary.

Hou, L.H. 1997b. A carinate bird from the Upper Jurassic of western Liaoning, China. Chinese Science Bulletin 42: 413–417.

Hou, L.H. 1999. New hesperornithid (Aves) from the Canadian Arctic. Vertebrata PalAsiatica 37: 228–233.

Hou, L.H., and Z. Liu. 1984. A new fossil bird from Lower Cretaceous of Gansu and early evolution of birds. Scientia Sinica Series B 27: 1296–1302.

Hou, L.H, and J.Y. Zhang. 1993. A new fossil bird from Lower Cretaceous of Liaoning. Vertebrata PalAsiatica 31: 217–224.

Hou, L.H., Z.H. Zhou, Y.C. Gu, and H. Zhang. 1995. *Confuciusornis sanctus*, a new Late Jurassic sauriurine bird from China. Chinese Science Bulletin 40: 1545–1551.

Hou, L.H., L.D. Martin, Z.H. Zhou, A. Feduccia, and F.C. Zhang. 1999a. A diapsid skull in a new species of the primitive bird *Confuciusornis*. Nature 399: 679–682.

Hou, L.H., L.D. Martin, Z.H. Zhou, and A. Feduccia. 1999b. *Archaeopteryx* to opposite birds - missing link from the Mesozoic of China. Vertebrata PalAsiatica 37: 88–95.

Hou, L.H., Z.H. Zhou, F.C. Zhang, and Y.C. Gu. 2002. Mesozoic Birds from Western Liaoning in China. Shenyang: Liaoning Science and Technology Publishing House.

Hou, L.H., L.M. Chiappe, F.C. Zhang, and C.M. Chuong. 2004. New Early Cretaceous fossil from China documents a novel trophic specialization for Mesozoic birds. Naturwissenschaften 91: 22–25.

Howse, S.C.B., and A.R. Milner. 1993. *Ornithodesmus*—a maniraptoran theropod dinosaur from the Lower Cretaceous of the Isle of Wight, England. Palaeontology 36: 425–437.

Hu, H., and J.M.K. O'Connor. 2017. First species of Enantiornithes from Sihedang elucidates skeletal development in Early Cretaceous enantiornithines. Journal of Systematic Palaeontology 15: 909–926.

Hu, D.Y., L.H. Hou, L.J. Zhang, and X. Xu. 2009. A pre-*Archaeopteryx* troodontid theropod from China with long feathers on the metatarsus. Nature 461: 640–643.

Hu, D.Y., L. Li, L.H. Hou, and X. Xu. 2010. A new sapeornithid bird from China and its implication for early avian evolution. Acta Geologica Sinica 84: 472–482.

Hu, D.Y., L. Li, L. Hou, and X. Xu. 2011. A new enantiornithine bird from the Lower Cretaceous of western Liaoning, China. Journal of Vertebrate Paleontology, 31: 154–161.

Hu, H., J.M.K. O'Connor, and Z.H. Zhou. 2015a. A new species of Pengornithidae (Aves: Enantiornithes) from the Lower Cretaceous of China suggests a specialized scansorial habitat previously unknown in early birds. PLoS One 10: e0126791.

Hu, D.Y., et al. 2015b. *Yuanjiawaornis viriosus*, gen. et sp. nov., a large enantiornithine bird from the Lower Cretaceous of western Liaoning, China. Cretaceous Research 55: 210–219.

Hu, D.Y., et al. 2018. A bony-crested Jurassic dinosaur with evidence of iridescent plumage highlights complexity in early paravian evolution. Nature Communications 9: 217.

Hwang, S.H., M.A. Norell, Q. Ji, and K.Q. Gao. 2002. New specimens of *Microraptor zhaoianus* (Theropoda: Dromaeosauridae) from Northeastern China. American Museum Novitates 3381: 1–44.

Imai, T., et al. 2019. An unusual bird (Theropoda, Avialae) from the Early Cretaceous of Japan suggests complex evolutionary history of basal birds. Communications Biology 2 (388): 1–11.

Jackson, F.D., and D.J. Varricchio. 2017. Paleoecological implications of two closely associated egg types from the Upper Cretaceous St. Mary River Formation, Montana. Cretaceous Research 79: 182–190.

Jarvis, E.D., et al. 2014. Whole-genome analyses resolve early branches in the tree of life of modern birds. Science 346: 1320–1331.

Jerzykiewicz, T., and D.A. Russell. 1991. Late Mesozoic stratigraphy and vertebrates of the Gobi Basin. Cretaceous Research 12: 345–377.

Ji, Q., and S.A. Ji. 1997. Protarchaeopterygid bird (*Protarchaeopteryx* gen. nov.)—fossil remains of archaeopterygids from China. Chinese Geology 238: 38–41.

Ji, Q., P.J. Currie, M.A. Norell, and S. Ji. 1998. Two feathered dinosaurs from northeastern China. Nature 393: 753–761.

Ji, Q., L. Chiappe, and S. Ji. 1999. A new Late Mesozoic confuciusornithid bird from China. Journal of Vertebrate Paleontology 19: 1–7.

Ji, Q., et al. 2005. First avialian bird from China. Geological Bulletin of China 24: 197–210.

Ji, Q. et al. 2002a. Discovery of an Avialae bird from China, *Shenzhouraptor sinensis* gen. et sp. nov. Geological Bulletin of China 21: 363–369.

Ji, Q., et al. 2002b. A new avialian bird – *Jixiangornis orientalis* gen. et sp. nov. – from the Lower Cretaceous of Western Liaoning, NE China. Journal of Nanjing University (Natural Sciences) 38: 723–736.

Ji, Q., J. Lü, X. Wei, and X. Wang. 2012. A new oviraptorosaur from the Yixian Formation of Jianchang, western Liaoning Province, China. Geological Bulletin of China 31: 2102–2107.

Ji, S.A., et al. 2011. A new, three-dimensionally preserved enantiornithian (Aves: Ornithothoraces) from Gansu Province, northwestern China. Zoological Journal of the Linnean Society 162: 201–219.

Jiang, X.J., et al. 2011. Dinosaur-bearing strata and K/T boundary in the Luanchuan-Tantou Basin of western Henan Province, China. Science China Earth Sciences 54: 1149.

Jin, F., et al. 2008. On the horizon of *Protopteryx* and the early vertebrate fossil assemblages of the Jehol Biota. Chinese Science Bulletin 53: 2820–2827.

Jinnah, J.A., et al. 2009. New 40Ar/39Ar and detrital zircon U-Pb ages for the Upper Cretaceous Wahweap and Kaiparowits formations on the Kaiparowits Plateau, Utah: implications for regional correlation, provenance, and biostratigraphy: Cretaceous Research 30: 287-299.

Keutgen, N. 2018. A bioclast-based astronomical timescale for the Maastrichtian in the type area (southeast Netherlands, northeast Belgium) and stratigraphic implications: the legacy of P.J. Felder. Netherlands Journal of Geosciences 97: 229–260.

Khidir, A., and O. Catuneanu. 2010. Reservoir characterization of Scollard-age fluvial sandstones, Alberta foredeep. Marine and Petroleum Geology 27: 2037–2050.

Kielan-Jaworowska, Z., and R. Barsbold. 1972. Narrative of the Polish-Mongolian paleontological expeditions. Paleontologica Polonica 27: 5–13.

Kim, K.S., et al. 2018. Smallest known raptor tracks suggest microraptorine activity in lakeshore setting. Scientific Reports 8: 16908.

Kimball, R.T., et al. 2019. A phylogenomic supertree of birds. Diversity 11: 109.

Kirkland, J.I., D. Burge, and R. Gaston. 1993. A large dromaeosaur (Theropoda) from the Lower Cretaceous of eastern Utah. Hunteria 2: 1–16.

Knoll, F., et al. 2018. A diminutive perinate European Enantiornithes reveals an asynchronous ossification pattern in early birds. Nature Communications 9: 1–9.

Ksepka, D.T., and M.J. Phillips. 2015. Avian diversification patterns across the K-Pg boundary: influence of calibrations, datasets, and model misspecification. Annals of the Missouri Botanical Garden 100: 300–328.

Ksepka, D.T., T. Stidham, and T. Williamson. 2017. Early Paleocene landbird supports rapid phylogenetic and morphological diversification of crown birds after the K-Pg mass extinction. Proceedings of the National Academy of Sciences of the United States of America 114: 8047–8052.

Kundrát, M., J. Nudds, B. Kear, J.C. Lü, and P. Ahlberg. 2019. The first specimen of *Archaeopteryx* from the Upper Jurassic Mörnsheim Formation of Germany. Historical Biology 31: 3–63.

Kurochkin, E.N., G.J. Dyke, S.V. Saveliev, E.M. Pervushov, and E.V. Popov. 2007. A fossil brain from the Cretaceous of European Russia and avian sensory evolution. Biological Letters 3: 309–313.

Kurochkin, E.N., N.V. Zelenkov, A.O. Averianov, and S.V. Leshchinskiy. 2011. A new taxon of birds (Aves) from the Early Cretaceous of western Siberia, Russia. Journal of Systematic Palaeontology 9: 109–117.

Kurochkin, E.N. 2000. Mesozoic birds of Mongolia and the former USSR. *In* M.J. Benton, M.A. Shishkin, D.M. Unwin, and E.N. Kurochkin (editors), The age of dinosaurs in Russia and Mongolia: 533–559. Cambridge: Cambridge University Press.

Kurochkin, E.N., and R.E. Molnar. 1997. New material of enantiornithine birds from the Early Cretaceous of Australia. Alcheringa: an Australasian Journal of Palaeontology 21: 291–297.

Kurumada, Y. et al. 2020. Calcite U-Pb age of the Cretaceous vertebrate-bearing Bayn Shire Formation in the Eastern Gobi Desert of Mongolia: usefulness of caliche for age determination. Terra Nova: early view. [doi.org/10.1111/ter.12456]

Kurzanov, S.M. 1976. Braincase structure in the carnosaur *Itemirus* n. gen. and some aspects of the cranial anatomy of dinosaurs. Paleontological Journal 10: 361–369.

Kurzanov, S.M. 1981. On the unusual theropods from the Upper Cretaceous of Mongolia. Iskopaemye Pozvonocnye Mongolii. Sovmestnaâ Sovetsko-Mongolskaâ Paleontologičeskaâ Ekspediciâ, Trudy 16: 39–50.

Kurzanov, S.M., and H. Osmólska. 1991. *Tochisaurus nernegtensis* gen. et sp. n., a new troodontid (Dinosauria, Theropoda) from Mongolia. Acta Palaeontologica Polonica 36: 69–76.

Lacasa-Ruiz, A. 1989. An Early Cretaceous fossil bird from Montsec Mountain (Lleida, Spain). Terra Nova 1: 45–46.

Lamanna, M.C., H.D. Sues, E.R. Schachner, and T.R. Lyson. 2014. A new large-bodied oviraptorosaurian theropod dinosaur from the latest Cretaceous of western North America. PLoS One 9: e92022.

Lambrecht, K. 1929. *Neogaeornis wetzeli* n. g. n. sp., der reste Kreidevogel der südlichen Hemispäre. Palaeontologische Zeitschrift 11: 121–129.

Lawver, D.R., and F.D. Jackson. 2017. An accumulation of turtle eggs with embryos from the Campanian (Upper Cretaceous) Judith River Formation of Montana. Cretaceous Research 69: 90–99.

Lawver, D.R., A.M. Debee, J.A. Clarke, and G.W. Rougier. 2011. A new enantiornithine bird from the Upper Cretaceous La Colonia Formation of Patagonia, Argentina. Annals of the Carnegie Museum 80: 35–42.

Leanza, H.A., S. Apesteguía, F.E. Novas, and M.S. de la Fuente. 2004. Cretaceous terrestrial beds from the Neuquén Basin (Argentina) and their tetrapod assemblages. Cretaceous Research 25: 61–87.

Lee, M.S.Y., and T.H. Worthy. 2011. Likelihood reinstates *Archaeopteryx* as a primitive bird. Biology Letters 8: 299–303.

Lee, S.J., et al. 2019. A new baby oviraptorid dinosaur (Dinosauria: Theropoda) from the Upper Cretaceous Nemegt Formation of Mongolia. PLoS One 14: e0210867.

Lefèvre, U., D.Y. Hu, F. Escuillié, G. Dyke, and P. Godefroit. 2014. A new long-tailed basal bird from the Lower Cretaceous of north-eastern China. Biological Journal of the Linnean Society 113: 790–804.

Lefèvre, U., et al. 2017. A new Jurassic theropod from China documents a transitional step in the macrostructure of feathers. Science of Nature 104 (9–10): 74.

Lehman, T.M. 1985. Stratigraphy, sedimentology, and paleontology of Upper Cretaceous (Campanian-Maastrichtian) sedimentary rocks in Trans-Pecos, Texas. Ph.D. dissertation, Department of Geological Sciences, University of Texas Austin.

Leidy, J. 1856. Notices of the remains of extinct reptiles and fishes discovered by Dr. F.V. Hayden in the badlands of the Judith River, Nebraska Territory. Proceedings of the Academy of Natural Sciences of Philadelphia 8: 72–73.

LeLoeuff, J., and E. Buffetaut. 1998. A new dromaeosaurid theropod from the Upper Cretaceous of southern France. Oryctos 1: 105–112.

LeLoeuff, J., E. Buffetaut, P. Mechin, and A. Mechin-Salessy. 1992. The first record of dromaeosaurid dinosaurs (Saurischia, Theropoda) in the Maastrichtian of southern Europe: palaeobiogeographical implications. Bulletin de la Société Géologique de France 163: 337–343.

Li, D.S., C. Sullivan, Z.H. Zhou, and F.C. Zhang. 2010a. Basal birds from China: a brief review. Chinese Birds 1: 83–96.

Li L., J.Q. Wang, and S.L. Hou. 2010b. A new species of *Confuciusornis* from Lower Cretaceous of Jianchung, Liaoning, China. Global Geology 29: 183–187.

Li, L., and S.L. Hou. 2011. Discovery of a new bird (Enantiornithines) from Lower Cretaceous in western Liaoning, China. Journal of Jilin University (Earth Science Edition) 41: 759–763.

Li, L., J.Q. Wang, and S.L. Hou. 2011. A new ornithurine bird (Hongshanornithidae) from the Jiufotang Formation of Chaoyang, Liaoning, China. Vertebrata PalAsiatica 49: 195–200.

Li, R.H., et al. 2008a. Behavioral and faunal implications of Early Cretaceous deinonychosaur trackways from China. Naturwissenschaften 95: 185–191.

Li, J.J., et al. 2008b. A new species of *Cathayornis* from the Lower Cretaceous of Inner Mongolia, China and its stratigraphic significance. Acta Geologica Sinica 82: 1115–1123.

Li L., J.Q. Wang, X. Zhang, and S.L. Hou. 2012. A new enantiornithine bird from the Lower Cretaceous Jiufotang Formation in Jinzhou area, western Liaoning Province, China. Acta Geologica Sinica 5: 1039–1044.

Li, Z.H., Z.H. Zhou, M. Wang, and J.A. Clarke. 2014. A new specimen of large-bodied basal enantiornithine *Bohaiornis* from the Early Cretaceous of China and the inference of feeding ecology in Mesozoic birds. Journal of Paleontology 88: 99–108.

Liang, X.Q. et al., 2009. Dinosaur eggs and dinosaur egg-bearing deposits (Upper Cretaceous) of Henan

Province, China: occurrences, palaeoenvironments, taphonomy and preservation. Progress in Natural Science 19: 1587–1601.

Lillegraven, J.A., and J.J. Eberle. 1999. Vertebrate faunal changes through Lancian and Puercan time in southern Wyoming. Journal of Paleontology 73: 691–710.

Liu, D., et al. 2017. Flight aerodynamics in enantiornithines: information from a new Chinese Early Cretaceous bird. PLoS One 12: e0184637.

Liu, D., L.M. Chiappe, Y.G. Zhang, F.J. Serrano, and Q.J. Meng. 2019. Soft tissue preservation in two new enantiornithine specimens (Aves) from the Lower Cretaceous Huajiying Formation of Hebei Province, China. Cretaceous Research 95: 191–207.

Liu, Y.Q., et al. 2012. Timing of the earliest known feathered dinosaurs and transitional pterosaurs older than the Jehol Biota. Palaeogeography Palaeoclimatology Palaeoecology 323–325: 1–12.

Lockley, M.G., J.J. Li, M. Matsukawa, and R.H. Li. 2012. A new avian ichnotaxon from the Cretaceous of Nei Mongol, China. Cretaceous Research 34: 84–93.

Longrich, N.R. 2008. A new, large ornithomimid from the Cretaceous Dinosaur Park Formation of Alberta, Canada: implications for the study of dissociated dinosaur remains. Palaeontology 51: 983–997.

Longrich, N.R. 2009. An ornithurine-dominated avifauna from the Belly River Group (Campanian, Upper Cretaceous) of Alberta, Canada. Cretaceous Research 30: 161–177.

Longrich, N.R., and P.J. Currie. 2009. A microraptorine (Dinosauria-Dromaeosauridae) from the Late Cretaceous of North America. Proceedings of the National Academy of Sciences of the United States of America 106: 5002–5007.

Longrich, N.R., P.J. Currie, and Z.M. Dong. 2010. A new oviraptorid (Dinosauria: Theropoda) from the Upper Cretaceous of Bayan Mandahu, Inner Mongolia. Palaeontology 53: 945–960.

Longrich, N.R., T. Tokaryk, and D.J. Field. 2011. Mass extinction of birds at the Cretaceous-Paleogene (K-Pg) boundary. Proceedings of the National Academy of Sciences of the United States of America 108: 15253–15257.

Longrich, N.R., K. Barnes, S. Clark, and L. Millar. 2013. Caenagnathidae from the Upper Campanian Aguja Formation of West Texas, and a revision of the Caenagnathinae. Bulletin of the Peabody Museum of Natural History 54: 23–49.

López-Conde, O.A., J. Sterli, M.L. Chavarría-Arellano, D.B. Brinkman, and M. Montellano-Ballesteros. 2018. Turtles from the Late Cretaceous (Campanian) of El Gallo Formation, Baja California, Mexico. Journal of South American Earth Sciences. 88: 639–699.

Lü, J.C., Y. Tomida, Y. Azuma, Z. Dong, and Y.N. Lee. 2004. New oviraptorid dinosaur (Dinosauria: Oviraptorosauria) from the Nemegt Formation of southwestern Mongolia. Bulletin of the National Science Museum (Tokyo), Series C (Geology and Paleontology) 30: 95–130.

Lü, J.C., et al. 2009. A preliminary report on the new dinosaurian fauna from the Cretaceous of the Ruyang Basin, Henan Province of central China. 고생물학회지 (Journal of the Paleontological Society of Korea) 25: 43–56.

Lü, J.C., L. Yi, H. Zhong, and X. Wei. 2013a. A new oviraptorosaur (Dinosauria: Oviraptorosauria) from the Late Cretaceous of southern China and its paleoecological implications. PLoS One 8: e80557.

Lü, J.C., et al. 2013b. Chicken-sized oviraptorid dinosaurs from central China and their ontogenetic implications. Naturwissenschaften 100: 165–175.

Lü, J.C., et al. 2017. High diversity of the Ganzhou oviraptorid fauna increased by a new "cassowary-like" crested species. Scientific Reports 7: 6393.

Lü, J.C. 2003. A new oviraptorosaurid (Theropoda: Oviraptorosauria) from the Late Cretaceous of southern China. Journal of Vertebrate Paleontology 22: 871–875.

Lü, J.C., and S.L. Brusatte. 2015. A large, short-armed, winged dromaeosaurid (Dinosauria: Theropoda) from the Early Cretaceous of China and its implications for feather evolution. Scientific Reports 5: 11775.

Lü, J.C., and B.K. Zhang. 2005. A new oviraptorid (Theropoda: Oviraptorosauria) from the Upper Cretaceous of the Nanxiong Basin, Guangdong Province of southern China. Acta Palaeontologica Sinica 44: 412–422.

Lü, J.C., Y. Tomida, Y. Azuma, Z.M. Dong, and Y.N. Lee. 2005. *Nemegtomaia* gen. nov., a replacement name for the oviraptorosaurian dinosaur *Nemegtia* Lü et al. 2004, a preoccupied name. Bulletin of the National Science Museum (Tokyo), Series C (Geology and Paleontology) 31: 51.

Lü, J.C., et al. 2007. New dromaeosaurid dinosaur from the Late Cretaceous Qiupa Formation of Luanchuan area, western Henan, China. Geological Bulletin of China 26: 777–786.

Lü, J.C., et al. 2010. A new troodontid (Theropoda: Troodontidae) from the Late Cretaceous of central China, and the radiation of Asian troodontids. Acta Palaeontologica Polonica 55: 381–388.

Lü, J.C., et al. 2015. A new oviraptorid dinosaur (Dinosauria: Oviraptorosauria) from the Late Cretaceous of southern China and its paleobiogeographical implications. Scientific Reports 5: 11490.

Lü, J.C., R.J. Chen, S.L. Brusatte, Y.X. Zhu, and C.Z. Shen. 2016. A Late Cretaceous diversification of Asian oviraptorid dinosaurs: evidence from a new species preserved in an unusual posture. Scientific Reports 6: 35780.

Lucas, S., and R. Sullivan. 1982. *Ichthyornis* from the Late Cretaceous Mancos Shale (Juana Lopez Member), northwestern New Mexico. Journal of Paleontology 56: 545–547.

Lucas, S.G. 2006. The *Psittacosaurus* biochron, Early Cretaceous of Asia. Cretaceous Research 27: 189–198.

Ma, W., et al. 2017. Functional morphology of a giant toothless mandible from a bird-like dinosaur: *Gigantoraptor* and the evolution of the oviraptorosaurian jaw. Scientific Reports 7: 16247.

Makovicky, P.J., and M.A. Norell. 2004. Troodontidae. In D.B. Weishampel, P. Dodson, and H. Osmólska (editors), The Dinosauria: 184-209. Berkeley: University of California Press.

Makovicky, P.J., and H.D. Sues. 1998. Anatomy and phylogenetic relationships of the theropod dinosaur *Microvenator celer* from the Lower Cretaceous of Montana. American Museum Novitates 3240: 1–27.

Makovicky, P.J., M.A. Norell, J.M. Clark, and T. Rowe. 2003. Osteology and relationships of *Byronosaurus jaffei* (Theropda: Troodontidae). American Museum Novitates 3402: 1–32.

Makovicky, P.J., Apesteguía, S., Agnolín, F.L. 2005. The earliest dromaeosaurid theropod from South America. Nature 437: 1007–1011.

Makovicky, P.J., L.E. Zanno, and T.A. Gates. 2015. The advent of North America's Late Cretaceous fauna revisited: insights from new discoveries and improved phylogenies. Journal of Vertebrate Paleontology, Program and Abstracts 35: 172–173.

Marsh, O.C. 1872. Description of *Hesperornis regalis*, with notices of four other new species of Cretaceous birds. Annals and Magazine of Natural History 10 (57): 212–217.

Marsh, O.C. 1877. Characters of the Odontornithes, with notice of a new allied genus. American Journal of Science 14: 85–87.

Marsh, O.C. 1880. Odontornithes: a monograph on the extinct toothed birds of North America. Washington, DC: Government Printing Office.

Martin, L.D. 1984. A new hesperornithid and the relationships of the Mesozoic birds. Transactions of the Kansas Academy of Science 87 (3/4): 141–150.

Martin, L.D., and J. Tate Jr. 1976. The skeleton of *Baptornis advenus* (Aves: Hesperornithiformes) *In* S.L. Olson (editor), Collected papers in avian paleontology honoring the 90th birthday of Alexander Wetmore: 35–66. Washington: Smithsonian Contributions to Paleobiology.

Martin, L.D., E. Kurochkin, and T. Tokaryk. 2012. A new evolutionary lineage of diving birds from the Late Cretaceous of North America and Asia. Palaeoworld 21: 59–63.

Martínez, R.D., and F.E. Novas. 2006. *Aniksosaurus darwini* gen. et sp. nov., a new coelurosaurian theropod from the early Late Cretaceous of central Patagonia, Argentina. Revista del Museo Argentino de Ciencias Naturales, nuevo serie 8: 243–259.

Matsuoka, H., N. Kusuhashi, T. Takada, and T. Setoguchi. 2002. A clue to the Neocomian vertebrate fauna: initial results from the Kuwajima 'Kaseki-kabe' (Tetori Group) in Shiramine, Ishikawa, central Japan. Memoirs of the Faculty of Science, Kyoto University, Series of Geology and Mineralogy 59: 33–45.

Matthew, W.D., and B. Brown. 1922. The family Deinodontidae, with notice of a new genus from the Cretaceous of Alberta. Bulletin of the American Museum of Natural History 46 (6): 367–385.

Mayr, G. 2009. Paleogene fossil birds. Berlin: Springer-Verlag.

Mayr, G. 2016. Avian evolution: the fossil record of birds and its paleobiological significance. Chichester: Wiley-Blackwell.

Mayr, G. 2017. Avian higher level biogeography: southern hemispheric origins or southern hemispheric relicts? Journal of Biogeography 44: 956–958.

Mayr, G., and R.P. Scofield. 2016. New avian remains from the Paleocene of New Zealand: the first early Cenozoic Phaethontiformes (tropicbirds) from the southern hemisphere. Journal of Vertebrate Paleontology 36: e1031343.

Mayr, G., B. Pohl, and D.S. Peters. 2005. A well-preserved *Archaeopteryx* specimen with theropod features. Science 310: 1483–1486.

Mayr, G., V.L. De Pietri, R.P. Scofield, and T.H. Worthy. 2018. On the taxonomic composition and phylogenetic affinities of the recently proposed clade Vegaviidae Agnolín et al., 2017—neornithine birds from the Upper Cretaceous of the southern hemisphere. Cretaceous Research 86: 178–185.

Mayr, G., V.L. De Pietri, L. Love, A. Mannering, and R.P. Scofield. 2019. Oldest, smallest and phylogenetically most basal pelagornithid, from the early Paleocene of New Zealand, sheds light on the evolutionary history of the largest flying birds. Papers in Palaeontology: early view. [doi.org/10.1002/spp2.1284]

McCormack, J.E., et al. 2013. A phylogeny of birds based on over 1,500 loci collected by target enrichment and high-throughput sequencing. PLoS One 8: e54848.

McLachlan, S.M.S., G. Kaiser, and N. Longrich. 2017. *Maaqwi cascadensis*: a large, marine diving bird (Avialae: Ornithurae) from the Upper Cretaceous of British Columbia, Canada. PLoS One 12: e0189473.

Milner, A. 2002. Theropod dinosaurs of the Purbeck Limestone Group, southern England. *In* A. Milner and D. Batten (editors), Life and environments in Purbeck times: 191–201. London: The Palaeontological Association.

Mitchell, K.J., A. Cooper, and M.J. Phillips. 2015. Comment on "Whole-genome analyses resolve early branches in the tree of life of modern birds." Science 349: 1460.

Molnar, R.E. 1986. An enantiornithine bird from the Lower Cretaceous of Queensland, Australia. Nature 322: 736–738.

Molnar, R.E. 1998. Old and new Cretaceous birds from Australia, and their implications. *In* T. Yukimitsu, T.H. Rich, and P. Vickers-Rich (editors), Second symposium on Gondwana dinosaurs: abstracts with programs: 18. Tokyo: National Science Museum.

Molnar, R.E. 1999. Avian tibiotarsi from the Early Cretaceous of Lightning Ridge, New South Wales. *In* Y. Tomida, T.H. Rich, and P. Vickers-Rich (editors), Proceedings of the second Gondwana dinosaur symposium: 197–209. Tokyo: National Science Museum of Tokyo.

Moran, K., et al. 2010. Attributes of the wood-boring trace fossil Asthenopodichnium in the Late Cretaceous Wahweap Formation, Utah, USA. Palaeogeography Palaeoclimatology Palaeoecology 297: 662–669.

Morschhauser, E.M., et al. 2009. Anatomy of the Early Cretaceous bird *Rapaxavis pani*, a new species from Liaoning Province, China. Journal of Vertebrate Paleontology 29: 545–554.

Morrison, K., G.J. Dyke, and L.M. Chiappe. 2005. Cretaceous fossil birds from Hornby Island (British Columbia). Canadian Journal of Earth Sciences 42: 2097–2101.

Motta, M., F.L. Agnolín, F. Brissón Egli, and F.E. Novas. 2020. New theropod dinosaur from the Upper Cretaceous of Patagonia sheds light on the paravian radiation in Gondwana. Science of Nature 107: 24.

Müller, R.D., et al. 2018. GPlates: building a virtual Earth through deep time. Geochemistry, Geophysics, Geosystems 19: 2243–2261.

Naish, D., and D.M. Martill. 2007. Dinosaurs of Great Britain and the role of the Geological Society of London in their discovery: basal Dinosauria and Saurischia. Journal of the Geological Society, London 164: 493–510.

Naish, D., S. Hutt, and D.M. Martill. 2001. Saurischian dinosaurs 2: theropods. *In* D.M. Martill and D. Naish (editors), Dinosaurs of the Isle of Wight: 242–309. Durham: The Palaeontological Association.

Naish, D., D.M. Martill, and I. Merrick. 2007. Birds of the Crato Formation. *In* D.M. Martill, D.M., G. Bechly, and R.F. Loveridge (editors), The Crato fossil beds of Brazil: window into an ancient world: 525–533. Cambridge University Press.

Nava, W.R., H. Alvarenga, L.M. Chiappe, and A.G. Martinelli. 2015. Three-dimensionally preserved cranial remains of enantiornithine birds from the Late Cretaceous of Brazil. Proceedings of the Congreso Latinoamericano de Paleontología de Vertebrados.

Navalón, G., J. Marugán-Lobón, L.M. Chiappe, J.L. Sanz, and A.D. Buscalioni. 2015. Soft-tissue and dermal arrangement in the wing of an Early Cretaceous bird: implications for the evolution of avian flight. Scientific Reports 5: 14864.

Navalón, G., et al. 2018. Diversity and evolution of the Confuciusornithidae: evidence from a new 131-million-year-old specimen from the Huajiying Formation in NE China. Journal of Asian Earth Sciences 152: 12–22.

Nessov, L.A. 1984. Upper Cretaceous pterosaurs and birds from Central Asia. Paleontologicheskii Zhurnal 1: 47–57.

Nessov, L.A., and L. Y. Borkin. 1983. New findings of birds' bones from the Cretaceous of Mongolia and Middle Asia. Trudy Zoologicheskogo Instituta 116: 108–110.

Nessov, L.A., and B.V. Prizemlin. 1991. A large advanced flightless marine bird of the order Hesperornithiformes of the Late Senonian of Turgai Strait: the first finding of the group in the USSR. Proceedings of the Zoological Institute, Leningrad 239: 85–107.

Norell, M.A., and J.A. Clarke. 2001. Fossil that fills a critical gap in avian evolution. Nature 409: 181–184.

Norell, M.A., and P.J. Makovicky. 1997. Important features of the dromaeosaur skeleton: information from a new specimen. American Museum Novitates 3215: 1–28.

Norell, M.A., and P.J. Makovicky. 1999. Important features of the dromaeosaurid skeleton II: information from newly collected specimens of *Velociraptor mongoliensis*. American Museum Novitates 3282: 1–45.

Norell, M.A., and P.J. Makovicky. 2004. Dromaeosauridae. *In* D.B. Weishampel, P. Dodson, and H. Osmólska (editors), The Dinosauria: 196–209. Berkeley: University of California Press.

Norell, M.A., J.M. Clark, L.M. Chiappe, and D. Dashzeveg. 1995. A nesting dinosaur. Nature 378: 774–776.

Norell, M.A., P.J. Makovicky, and J.M. Clark. 2000. A new troodontid theropod from Ukhaa Tolgod, Mongolia. Journal of Vertebrate Paleontology 20: 7–11.

Norell, M.A., J.M. Clark, and L.M. Chiappe. 2001. An embryonic oviraptorid (Dinosauria: Theropoda) from the Upper Cretaceous of Mongolia. American Museum Novitates 3315: 1–17.

Norell, M.A., et al. 2006. A new dromaeosaurid theropod from Ukhaa Tolgod (Ömnögov, Mongolia). American Museum Novitates 3545: 1–51.

Norell, M.A., et al. 2009. A review of the Mongolian Cretaceous dinosaur *Saurornithoides* (Troodontidae: Theropoda). American Museum Novitates 3654: 1–63.

Noriega, J.I., and C.P. Tambussi. 1995. A Late Cretaceous Presbyornithidae (Aves: Anseriformes) from Vega Island, Antarctic Peninsula: Paleobiogeographic implications. Ameghiniana 32: 57–61.

Novas, F., and F. Agnolín. 2004. *Unquillosaurus ceibalii* Powell, a giant maniraptoran (Dinosauria, Theropoda) from the Late Cretaceous of Argentina. Revista del Museo Argentino de Ciencias Naturales 6: 61–66.

Novas, F.E., and D. Pol. 2005. New evidence on deinonychosaurian dinosaurs from the Late Cretaceous of Patagonia. Nature 433: 858–861.

Novas, F.E., and P.F. Puerta. 1997. New evidence concerning avian origins from the Late Cretaceous of Patagonia. Nature 387: 390–392.

Novas, F.E., D. Pol, J.I. Canale, J.D. Porfiri, and J.O. Calvo. 2009. A bizarre Cretaceous theropod dinosaur from Patagonia and the evolution of Gondwanan dromaeosaurids. Proceedings of the Royal Society B, Biological Sciences 276: 1101–1007.

Novas, F.E., F.L. Agnolín, and C.A. Scanferla. 2010. New enantiornithine bird (Aves, Ornithothoraces) from the Late Cretaceous of NW Argentina. Comptes Rendus Palevol 9: 499–503.

Novas, F.E., F. Brissón Egli, F.L. Agnolín, F.A. Gianechini, and I. Cerda. 2018. Postcranial osteology of a new specimen of *Buitreraptor gonzalezorum* (Theropoda, Unenlagiidae). Cretaceous Research 83: 127–167.

O'Connor, P.M., and C.A. Forster. 2010. A Late Cretaceous (Maastrichtian) avifauna from the Maevarano Formation, Madagascar. Journal of Vertebrate Paleontology 30: 1178–1201.

O'Connor, J.M.K., and C. Sullivan. 2014. Reinterpretation of the Early Cretaceous maniraptoran (Dinosauria: Theropoda) *Zhongornis haoae* as a scansoriopterygid-like non-avian, and morphological resemblances between scansoriopterygids and basal oviraptorosaurs. Vertebrata PalAsiatica 52: 3–30.

O'Connor, J.M.K., and N.Z. Zelenkov. 2013. The phylogenetic position of *Ambiortus*: comparison with other Mesozoic birds from Asia. Paleontological Journal 47: 1270–1281.

O'Connor, J.M.K., K.Q. Gao, and L.M. Chiappe. 2010. A new ornithuromorph (Aves: Ornithothoraces) bird from the Jehol Group indicative of higher-level diversity. Journal of Vertebrate Paleontology 30: 311–321.

O'Connor, J.M.K., L.M. Chiappe, and A. Bell. 2011a. Pre-modern birds: avian divergences in the Mesozoic. *In* G.D. Dyke, and G. Kaiser (editors), Living dinosaurs: the evolutionary history of birds: 39–114. Hoboken, NJ: John Wiley & Sons.

O'Connor, J.M.K., Z.H. Zhou, and F.C. Zhang. 2011b. A reappraisal of *Boluochia zhengi* (Aves: Enantiornithes) and a discussion of intraclade diversity in the Jehol avifauna, China. Journal of Systematic Palaeontology 9: 51–63.

O'Connor, J.M.K., et al. 2009. Phylogenetic support for a specialized clade of Cretaceous enantiornithine birds with information from a new species. Journal of Vertebrate Paleontology 29: 188–204.

O'Connor, J.M.K., C.K. Sun, X. Xu, X.L. Wang, and Z.H. Zhou. 2012. A new species of *Jeholornis* with complete caudal integument. Historical Biology 24: 29–41.

O'Connor, J.M.K., et al. 2013. A new enantiornithine from the Yixian Formation with the first recognized avian enamel specialization. Journal of Vertebrate Paleontology 33: 1–12.

O'Connor, J.M.K., A. Averianov, and N.Z. Zelenkov. 2014. A confuciusornithiform (Aves: Pygostylia)-like tarsometatarsus from the Early Cretaceous of Siberia and a discussion of the evolution of avian hindlimb musculature. Journal of Vertebrate Paleontology 34: 647–656.

O'Connor, J.M.K., et al. 2016a. An enantiornithine with a fan-shaped tail, and the evolution of the rectricial complex in early birds. Current Biology 26: 114–119.

O'Connor, J.M.K., et al. 2016b. A new Early Cretaceous enantiornithine (Aves: Ornithothoraces) from northwestern China with elaborate tail ornamentation. Journal of Vertebrate Paleontology 36: e1054035.

O'Connor, J.M.K., M. Wang, and H. Hu. 2016c. A new ornithuromorph (Aves) with an elongate rostrum from the Jehol Biota, and the early evolution of rostralization in birds. Journal of Systematic Palaeontology 14: 939-948.

Olson, S.L. 1992. *Neogaeornis wetzeli* Lambrecht, a Cretaceous loon from Chile (Aves: Gaviidae). Journal of Vertebrate Paleontology 12: 122–124.

Oreska, M.P.J., M.T. Carrano, and K.M. Dzikiewicz. 2013. Vertebrate paleontology of the Cloverly Formation (Lower Cretaceous), I: faunal composition, biogeographic relationships, and sampling. Journal of Vertebrate Paleontology 33: 264–292.

Osborn, H.F. 1924. Three new Theropoda, *Protoceratops* zone, central Mongolia. American Museum Novitates 144: 1–12.

Osmólska, H. 1981. Coossified tarsometatarsi in theropod dinosaurs and their bearing on the problem of bird origins. Palaeontologica Polonica 42: 79–95.

Osmólska, H. 1982. *Hulsanpes perlei* n.g. n.sp. (Deinonychosauria, Saurischia, Dinosauria) from the Upper Cretaceous Barun Goyot Formation of Mongolia. Neues Jahrbuch für Geologie und Paläontologie, Monatshef 1982: 440–448.

Osmólska, H. 1987. *Borogovia gracilicrus* gen. et sp. n., a new troodontid dinosaur from the Late Cretaceous of Mongolia. Acta Palaeontologica Polonica 31: 133–150.

Osmólska, H., P.J. Currie, and R. Barsbold. 2004. Oviraptorosauria. *In* D.B. Weishampel, P. Dodson, and H. Osmólska (editors), The Dinosauria 165–183. Berkeley: University of California Press.

Ostrom, J.H. 1969. Osteology of *Deinonychus antirrhopus*, an unusual theropod dinosaur from the Lower Cretaceous of Montana. Bulletin of the Peabody Museum of Natural History 30: 1–165.

Owen, R. 1854. On some fossil reptilian and mammalian remains from the Purbecks. Quarterly Journal of the Geological Society, 10: 420–433.

Owen, R. 1863. On the *Archaeopteryx* of von Meyer, with a description of the fossil remains of a long-tailed species, from the lithographic stone of Solenhofen. Philosophical Transactions of the Royal Society of London 153: 33–47.

Pan, Y.H., J.G. Sha, Z.H. Zhou, and F.T. Fürsich. 2013. The Jehol Biota: definition and distribution of exceptionally preserved relicts of a continental Early Cretaceous ecosystem. Cretaceous Research 44: 30–38.

Pan, Y.H., et al. 2016. Molecular evidence of keratin and melanosomes in feathers of the Early Cretaceous bird *Eoconfuciusornis*. Proceedings of the National Academy of Sciences of the United States of America 113: E7900–E7907.

Panteleev, A.V. 2018. Morphology of the coracoid of Late Cretaceous enantiornithines (Aves: Enantiornithes) from Dzharakuduk (Uzbekistan). Paleontological Journal 52: 201–207.

Peecook B.R., and C.A. Sidor. 2015. The first dinosaur from Washington State and a review of Pacific Coast dinosaurs from North America PLoS ONE 10: e0127792.

Pei, R., Q. Li, Q. Meng, K.Q. Gao, and M.A. Norell. 2014. A new specimen of *Microraptor* (Theropoda: Dromaeosauridae) from the Lower Cretaceous of western Liaoning, China. American Museum Novitates 3821: 1–28.

Pei, R., et al. 2017a. Osteology of a new Late Cretaceous troodontid specimen from Ukhaa Tolgod, Ömnögovi Aimag, Mongolia. American Museum Novitates 3889: 1–47.

Pei, R., Q.G. Li, Q.J. Meng, M.A. Norell, and K.Q. Gao. 2017b. New specimens of *Anchiornis huxleyi* (Theropoda: Paraves) from the Late Jurassic of northeastern China. Bulletin of the American Museum of Natural History 411: 1–66.

Pei, R., et al. In press. Potential for powered flight neared by most close avialan relatives but few crossed its thresholds. Current Biology.

Perle, A., M.A. Norell, and J.M. Clark. 1999. A new maniraptoran theropod—*Achillobator giganticus* (Dromaeosauridae)—from the Upper Cretaceous of Burkhant, Mongolia. Ulan Bator, Mongolia: Geology and Mineralogy Chair, National Museum of Mongolia.

Persons, W.S., P.J. Currie, and M.A. Norell. 2014. Oviraptorosaur tail forms and functions. Acta Palaeontologica Polonica 59: 553–567.

Pittman, M., S.M. Gatesy, P. Upchurch, A. Goswami, and J.R. Hutchinson. 2013. Shake a tail feather: the evolution of the theropod tail into a stiff aerodynamic surface. PLoS One 8: e63115.

Pittman, M., R. Pei, Q.W. Tan, and X. Xu. 2015. The first dromaeosaurid (Dinosauria: Theropoda) from the Lower Cretaceous Bayan Gobi Formation of Nei Mongol, China. PeerJ 3: e1480.

Porfiri, J., J. Calvo, and D. dos Santos. 2011. A new small deinonychosaur (Dinosauria: Theropoda) from the Late Cretaceous of Patagonia, Argentina. Anais da Academia Brasileira de Ciências 83: 109–116.

Poust, A.W., C.L. Gao, D.J. Varricchio, J.L. Wu, and F.J. Zhang. 2020. A new microraptorine theropod from the Jehol Biota and growth in early dromaeosaurids. The Anatomical Record 303: 963–987.

Powell, J.E. 1979. Sobre una asociación de dinosaurios y otras evidencias de vertebrados del Cretácico Superior de la región de La Candelaria, Prov. de Salta, Argentina. Ameghiniana 16: 191–204.

Prum, R.O., et al. 2015. A comprehensive phylogeny of birds (Aves) using targeted next-generation DNA sequencing. Nature 526: 569–573.

Pu, H.Y., et al. 2013. A new juvenile specimen of *Sapeornis* (Pygostylia: Aves) from the Lower Cretaceous of Northeast China and allometric scaling of this basal bird. Paleontological Research 17: 27–38.

Pu, H.Y., et al. 2017. Perinate and eggs of a giant caenagnathid dinosaur from the Late Cretaceous of central China. Nature Communications 8: 14952.

Qiu, R., et al. 2019. A new caudipterid from the Lower Cretaceous of China with information on the evolution of the manus of Oviraptorosauria. Scientific Reports 9: 6431.

Quinney, A., F. Therrien, D.K. Zelenitsky, and D.A. Eberth. 2013. Palaeoenvironmental and palaeoclimatic reconstruction of the Upper Cretaceous (late Campanian-early Maastrichtian) Horseshoe Canyon Formation, Alberta, Canada. Palaeogeography, Palaeoclimatology, Palaeoecology 371: 26–44.

Rashid, D.J., et al. 2018. Avian tail ontogeny, pygostyle formation, and interpretation of juvenile Mesozoic specimens. Scientific Reports 8: 9014.

Rauhut, O.W.M., and C. Werner. 1995. First record of the family Dromaeosauridae (Dinosauria: Theropoda) in the Cretaceous of Gondwana (Wadi Milk Formation, northern Sudan). Paläontologische Zeitschrift 69: 475–489.

Rauhut, O.W.M., and A.C. Milner, Moore-Fay, S. 2010. Cranial osteology and phylogenetic position of the theropod dinosaur *Proceratosaurus bradleyi* (Woodward, 1910) from the Middle Jurassic of England. Zoological Journal of the Linnean Society 158: 155–195.

Rauhut, O.W.M, C. Foth, and H. Tischlinger. 2018. The oldest *Archaeopteryx* (Theropoda: Avialae): a new specimen from the Kimmeridgian/Tithonian boundary of Schamhaupten, Bavaria. PeerJ 6: e4191

Reddy, S., et al. 2017. Why do phylogenomic data sets yield conflicting trees? Data type influences the avian tree of life more than taxon sampling. Systematic Biology 66: 857–879.

Rees, J., and J. Lindgren. 2005. Aquatic birds from the Upper Cretaceous (Lower Campanian) of Sweden and the biology and distribution of hesperornithiforms. Palaeontology 48: 1321–1329.

Rich, T.H., P. Vickers-Rich, A. Constantine, T.F. Flannery, L. Kool, and N. van Klavaren. 1999. Early Cretaceous mammals from Flat Rocks, Victoria, Australia. Records of the Queen Victoria Museum 106: 1–35.

Roberts, E.M., A.L. Deino, and M.A. Chan. 2005. 40Ar/39Ar age of the Kaiparowits Formation, southern Utah, and correlation of contemporaneous Campanian strata and vertebrate faunas along the margin of the Western Interior Basin. Cretaceous Research 26: 307–318.

Robertson, D.S., M.C. McKenna, O.B. Toon, S. Hope, and J.A. Lillegraven. 2004. Survival in the first hours of the Cenozoic. Geological Society of America Bulletin 116: 760–768.

Rogers, R.R., C.C. Swisher III, and J.R. Horner. 1993. 40Ar/39Ar age and correlation of the nonmarine Two Medicine Formation (Upper Cretaceous), northwestern Montana, U.S.A. Canadian Journal of Earth Sciences 30: 1066–1075.

Rogers, R.R., et al. 2013. A new, richly fossiliferous member comprised of tidal deposits in the Upper Cretaceous Maevarano Formation, northwestern Madagascar. Cretaceous Research 44: 12–29.

Russell, D.A., and Z.M. Dong. 1993. A nearly complete skeleton of a new troodontid dinosaur from the Early Cretaceous of the Ordos Basin, Inner Mongolia, People's Republic of China. Canadian Journal of Earth Sciences 30: 2163–2173

Ryan, M.J., and A.P. Russell. 2001. Dinosaurs of Alberta (exclusive of Aves). *In* D.H. Tanke and K. Carpenter (editors), Mesozoic vertebrate life: new research inspired by the paleontology of Philip J. Currie: 279–297. Bloomington: Indiana University Press.

Ryan, M.J., P.J. Currie, and J.D. Gardner. 1998. Baby hadrosaurid material associated with unusually high abundance of *Troodon* teeth from the Horseshoe Canyon Formation, Upper Cretaceous, Alberta, Canada. Gaia 15: 123–133.

Sankey, J.T. 2001. Late Campanian southern dinosaurs, Aguja Formation, Big Bend, Texas. Journal of Paleontology 75: 208–215.

Sano, S.I., and A. Yabe. 2017. Fauna and flora of Early Cretaceous Tetori Group in central Japan: the clues to revealing the evolution of Cretaceous terrestrial ecosystem in East Asia. Palaeoworld 26: 253–267.

Sanz, J.L., and J.F. Bonaparte. 1992. A new order of birds (Class Aves) from the Lower Cretaceous of Spain. *In* J.J. Becker (editor), Papers in avian paleontology honoring Pierce Brodkorb. Natural History Museum of Los Angeles County Contributions in Science 36: 39–49.

Sanz, J.L., and A.D. Buscalioni. 1992. A new bird from the Early Cretaceous of Las Hoyas, Spain, and the early radiation of birds. Palaeontology 35: 829–845.

Sanz, J.L., et al. 1996. An Early Cretaceous bird from Spain and its implications for the evolution of avian flight. Nature 382: 442–445.

Sanz, J.L., et al. 1997. A nestling bird from the Lower Cretaceous of Spain: implications for avian skull and neck evolution. Science 276: 1543–1546.

Sanz, J.L., et al. 2001. An Early Cretaceous pellet. Nature 409: 998–999.

Sanz, J.L., B.P. Pérez-Moreno, L.M. Chiappe, and A.D. Buscalioni. 2002. The birds from the Lower Cretaceous of Las Hoyas (province of Cuenca, Spain). *In* L.M. Chiappe and L.M. Witmer (editors), Mesozoic birds: above the heads of dinosaurs: 209–229. Berkeley: University of California Press.

Saupe, E.E., et al. 2019. Climatic shifts drove major contractions in avian latitudinal distributions throughout the Cenozoic. Proceedings of the National Academy of Sciences of the United States of America 116: 12895–12900.

Schweitzer, M.H., et al. 2002. Late Cretaceous avian eggs with embryos from Argentina. Journal of Vertebrate Paleontology 22: 191–195.

Seeley, H. 1887. On a sacrum, apparently indicating a new type of bird, *Ornithodesmus cluniculus*, Seeley, from the Wealden of Brook. Quarterly Journal of the Geological Society of London 42: 206–211.

Senter, P., R. Barsbold, B.B. Britt, and D.A. Burnham. 2004. Systematics and evolution of Dromaeosauridae (Dinosauria, Theropoda). Bulletin of the Gunma Museum of Natural History 8: 1–20.

Senter, P., J.I. Kirkland, J. Bird, and J.A. Bartlett. 2010. A new troodontid theropod dinosaur from the Lower Cretaceous of Utah. PLoS One 5: e14329.

Senter, P., J.I. Kirkland, D.D. DeBlieux, S. Madsen, and N. Toth. 2012. New dromaeosaurids (Dinosauria: Theropoda) from the Lower Cretaceous of Utah, and the evolution of the dromaeosaurid tail. PLoS One 7: e36790.

Sereno, P.C. 1998. A rationale for phylogenetic definitions, with application to the higher-level taxonomy of Dinosauria. Neues Jahrbuch für Geologie und Palaeontologie Abhandlungen 210: 41–83.

Sereno, P.C. 2000. *Iberomesornis romerali* (Ornithothoraces, Aves) re-evaluated as an enantiornithine bird. Neues Jahrbuch für Geologie und Paläontologie Abhandlungen 215: 365–395.

Sereno, P.C. 2010. Taxonomy, cranial morphology, and relationships of parrot-beaked dinosaurs (Ceratopsia: *Psittacosaurus*). *In* M.J. Ryan, B.J. Chinnery-Allgeier, and D.A. Eberth (editors), New perspectives on horned dinosaurs: 21–58. Bloomington: Indiana University Press.

Sereno, P.C., and C.G. Rao. 1992. Early evolution of avian flight and perching: new evidence from the lower Cretaceous of China. Science 255: 845–848.

Shen, C.Z., et al. 2017a. A new troodontid dinosaur from the Lower Cretaceous Yixian Formation of Liaoning Province, China. Acta Geologica Sinica 91: 763–780.

Shen, C.Z., B. Zhao, C.L. Gao, J.C. Lü, and M. Kundrát. 2017b. A new troodontid dinosaur (*Liaoningvenator curriei* gen. et sp. nov.) from the Early Cretaceous Yixian Formation in Western Liaoning Province. Acta Geoscientica Sinica 38: 359–371.

Shuvalov, V.F. 2000. The Cretaceous stratigraphy and palaeobiogeography of Mongolia. *In* M.J. Benton, M.A. Shishkin, D.M. Unwin, and E.N. Kurochkin (editors), The age of dinosaurs in Russia and Mongolia: 256–278. Cambridge: Cambridge University Press.

Slack, K.E., et al. 2006. Early penguin fossils, plus mitochondrial genomes, calibrate avian evolution. Molecular Biology and Evolution 23: 1144–1155.

Sternberg, C.M. 1932. Two new theropod dinosaurs from the Belly River Formation of Alberta. Canadian Field Naturalist 46: 99–105.

Sternberg, C. 1945. Pachycephalosauridae proposed for domeheaded dinosaurs, *Stegoceras lambei* n. sp., described. Journal of Paleontology 19: 534–538.

Sues, H.D. 1978. A new small theropod dinosaur from the Judith River Formation (Campanian) of Alberta Canada. Zoological Journal of the Linnean Society 62: 381–400.

Sues, H.D., and A. Averianov. 2014. Dromaeosauridae (Dinosauria: Theropoda) from the Bissekty Formation (Upper Cretaceous: Turonian) of Uzbekistan and the phylogenetic position of *Itemirus medullaris* Kurzanov, 1976. Cretaceous Research 51: 225–240.

Sues, H.D., and A. Averianov. 2015. New material of *Caenagnathasia martinsoni* (Dinosauria: Theropoda: Oviraptorosauria) from the Bissekty Formation (Upper Cretaceous: Turonian) of Uzbekistan. Cretaceous Research 54: 50–59.

Sullivan, C., et al. 2014. The vertebrates of the Jurassic Daohugou Biota of northeastern China. Journal of Vertebrate Paleontology 34: 243–280.

Sullivan, R.M. 2006. *Saurornitholestes robustus*, n. sp. (Theropoda: Dromaeosauridae) from the Upper Cretaceous Kirtland Formation (De-NaZin Member), San Juan Basin, New Mexico. New Mexico Museum of Natural History and Science Bulletin 35: 253–256.

Sullivan, R.M., and S.G. Lucas. 2006. The Kirtlandian land-vertebrate "age"-faunal composition, temporal position and biostratigraphic correlation in the nonmarine Upper Cretaceous of western North America. New Mexico Museum of Natural History and Science Bulletin 35: 7–29.

Sullivan, R.M., S.E. Jasinski, and M.P.A. van Tomme. 2011. A new caenagnathid *Ojoraptorsaurus boerei*, n. gen., n. sp. (Dinosauria, Oviraptorosauria), from the Upper Cretaceous Ojo Alamo Formation (Naashoibito member), San Juan basin, New Mexico. Bulletin of the New Mexico Museum of Natural History and Science 53: 418–428.

Sweetman, S.C. 2004. The first record of velociraptorine dinosaurs (Saurischia, Theropoda) from the Wealden (Early Cretaceous, Barremian) of southern England. Cretaceous Research 25: 353–364.

Szwedo, J., and J. Ansorge. 2015. The first Mimarachnidae (Hemiptera: Fulgoromorpha) from Lower Cretaceous lithographic limestones of the Sierra del Montsec in Spain. Cretaceous Research 52: 390–401.

Tan, Q.W., H. Xing, Y.G. Hu, L. Tan, and X. Xu. 2015. New hadrosauroid material from the Upper Cretaceous Majiacun Formation of Hubei Province, central China. Vertebrata PalAsiatica 53: 245–264.

Tian, N., et al. 2015. New records of Jurassic petrified wood in Jianchang of western Liaoning, China and their palaeoclimate implications. Science China Earth Sciences 58: 2154–2164.

Tischlinger, H. 2009. Der achte *Archaeopteryx*—das Daitinger Exemplar. *Archaeopteryx* 27: 1–20.

Tokaryk, T.T., S.L. Cumbaa, and J.E. Storer. 1997. Early Late Cretaceous birds from Saskatchewan, Canada: the oldest diverse avifauna known from North America. Journal of Vertebrate Paleontology 17: 172–176.

Trujillo, K.C, and B.J. Kowallis. 2015. Recalibrated legacy 40Ar/39Ar ages for the Upper Jurassic Morrison Formation, Western Interior, U.S.A. Geology of the Intermountain West 2: 1–8.

Tsuihiji, T., et al. 2014. An exquisitely preserved troodontid theropod with new information on the palatal structure from the Upper Cretaceous of Mongolia. Naturwissenschaften 101: 131–142.

Tsuihiji, T., M. Watabe, R. Barsbold, and K. Tsogtbaatar. 2015. A gigantic caenagnathid oviraptorosaurian (Dinosauria: Theropoda) from the Upper Cretaceous of the Gobi Desert, Mongolia. Cretaceous Research 56: 60–65.

Tsuihiji, T., et al. 2016. New material of a troodontid theropod (Dinosauria: Saurischia) from the Lower Cretaceous of Mongolia, Historical Biology, 28: 128–138.

Tucker, R.T., L.E. Zanno, H.Q. Huang, and P.J. Makovicky. 2020. A refined temporal framework for newly discovered fossil assemblages of the upper Cedar Mountain Formation (Mussentuchit Member), Mussentuchit Wash, Central Utah. Cretaceous Research 110: 104834.

Turner, A.H., P.J. Makovicky, and M.A. Norell. 2007a. Feather quill knobs in the dinosaur *Velociraptor*. Science 317: 1721.

Turner, A.H., D. Pol, J.A. Clarke, G.M. Erickson, and M.A. Norell. 2007b. A basal dromaeosaurid and size evolution preceding avian flight. Science 317: 1378–1381.

Turner, A.H., S.H. Hwang, and M.A. Norell. 2007c. A small derived theropod from Öösh, Early Cretaceous, Baykhangor Mongolia. American Museum Novitates 3557: 1–27.

Turner, A.H., D. Pol, and M.A. Norell. 2011. Anatomy of *Mahakala omnogovae* (Theropoda: Dromaeosauridae), Tögrögiin Shiree, Mongolia. American Museum Novitates 3722: 1–66.

Turner, A.H., P.J. Makovicky, and M.A. Norell. 2012. A review of dromaeosaurid systematics and paravian phylogeny. Bulletin of the American Museum of Natural History 371: 1–206.

Tykoski, R.S., and A.R. Fiorillo. 2010. An enantiornithine bird from the lower middle Cenomanian of Texas. Journal of Vertebrate Paleontology 30: 288–292.

van der Reest, A.J., and P.J. Currie. 2017. Troodontids (Theropoda) from the Dinosaur Park Formation, Alberta, with a description of a unique new taxon: implications for deinonychosaur diversity in North America. Canadian Journal of Earth Sciences 54: 919–935.

van Itterbeeck, J., D.J. Horne, P. Bultynck, and N. Vandenberghe. 2005. Stratigraphy and palaeoenvironment of the dinosaur-bearing Upper Cretaceous Iren Dabasu Formation, Inner Mongolia, People's Republic of China. Cretaceous Research 26: 699–725.

Varricchio, D.J., and D.E. Barta. 2015. Revisiting Sabath's "larger avian eggs" from the Gobi Cretaceous. Acta Palaeontologica Polonica 60: 11–25.

Varricchio, D.J., and F.D. Jackson. 2004. A phylogenetic assessment of prismatic dinosaur eggs from the Cretaceous Two Medicine Formation of Montana. Journal of Vertebrate Paleontology 24: 931–937.

Varricchio, D.J., and F.D. Jackson. 2016. Reproduction in Mesozoic birds and evolution of the modern avian reproductive mode. Auk 133: 654–684.

Varricchio, D.J., A.M. Balanoff, and M.A. Norell. 2015. Reidentification of avian embryonic remains from the Cretaceous of Mongolia. PLoS One 10: e0128458.

Walker, C.A. 1981. New subclass of birds from the Cretaceous of South America. Nature 292: 51–53.

Walker, C.A., and G.J. Dyke. 2009. Euenantiornithine birds from the Late Cretaceous of El Brete (Argentina). Irish Journal of Earth Sciences 27: 15–62.

Walker, C.A., E. Buffetaut, and G.J. Dyke. 2007. Large euenantiornithine birds from the Cretaceous of southern France, North America and Argentina. Geological Magazine 144: 977–986.

Wang, M., and D. Liu. 2015. Taxonomical reappraisal of Cathayornithidae (Aves: Enantiornithes). Journal of Systematic Palaeontology 14: 29–47.

Wang, M., and Z.H. Zhou. 2018. A new confuciusornithid (Aves: Pygostylia) from the Early Cretaceous increases the morphological disparity of the Confuciusornithidae. Zoological Journal of the Linnean Society 185: 417–430.

Wang, M., and Z.H. Zhou. 2019. A new enantiornithine (Aves: Ornithothoraces) with completely fused premaxillae from the Early Cretaceous of China. Journal of Systematic Palaeontology 17: 1299–1312.

Wang, L.L., et al. 2013c. SIMS U-Pb zircon age of Jurassic sediments in Linglongta, Jianchang, western Liaoning: constraint on the age of oldest feathered dinosaurs. Chinese Science Bulletin 58: 1346–1353.

Wang, M., J.M.K. O'Connor, N.Z. Zelenkov, and Z.H. Zhou. 2014b. A new diverse enantiornithine family (Bohaiornithidae fam. nov.) from the Lower Cretaceous of China with information from two new species. Vertebrata PalAsiatica 52: 31–76.

Wang, M., Z.H. Zhou, and G.H. Xu. 2014c. The first enantiornithine bird from the Upper Cretaceous of China. Journal of Vertebrate Paleontology 34: 135–145.

Wang, M., J.M.K. O'Connor, and Z.H. Zhou. 2014d. A new robust enantiornithine bird from the Lower Cretaceous of China with scansorial adaptations. Journal of Vertebrate Paleontology 34: 657–671.

Wang, M., H. Hu, and Z.H. Li. 2014e. A new small enantiornithine bird from the Jehol Biota, with implications for early evolution of avian skull morphology. Journal of Systematic Palaeontology 14: 481–497.

Wang, M., et al. 2015a. The oldest record of ornithuromorpha from the early Cretaceous of China. Nature Communications 6: 6987.

Wang, M., D.Q. Li, J.M.K. O'Connor, Z.H. Zhou, and H.L. You. 2015b. Second species of enantiornithine bird from the Lower Cretaceous Changma Basin, northwestern China with implications for the taxonomic diversity of the Changma avifauna. Cretaceous Research 55: 56–65.

Wang, M., X.L. Wang, Y. Wang, and Z.H. Zhou. 2016b. A new basal bird from China with implications for morphological diversity in early birds. Scientific Reports 6: 1–12.

Wang M., Z.H. Zhou, and S. Zhou. 2016c. A new basal ornithuromorph bird (Aves: Ornithothoraces) from the Early Cretaceous of China with implication for morphology of early Ornithuromorpha. Zoological Journal of the Linnean Society 176: 207–223.

Wang, M., J.M.K. O'Connor, Y.H. Pan, and Z.H. Zhou. 2017. A bizarre Early Cretaceous enantiornithine bird with unique crural feathers and an ornithuromorph plough-shaped pygostyle. Nature Communications 8: 14141.

Wang, M., T.A. Stidham, and Z.H. Zhou. 2018. A new clade of basal Early Cretaceous pygostylian birds and developmental plasticity of the avian shoulder girdle. Proceedings of the National Academy of Sciences of the United States of America 115: 10708–10713.

Wang, M., J.M.K. O'Connor, X. Xu, and Z.H. Zhou. 2019a. A new Jurassic scansoriopterygid and the loss of membranous wings in theropod dinosaurs. Nature 569: 256–259.

Wang, M., J.M.K. O'Connor, and Z.H. Zhou. 2019b. A taxonomical revision of the Confuciusornithiformes (Aves: Pygostylia). Vertebrata PalAsiatica 57: 1–37.

Wang, M., J.M.K. O'Connor, A.M. Bailleul, and Z.H. Li. 2019c. Evolution and distribution of medullary bone: evidence from a new Early Cretaceous enantiornithine bird. National Science Review: nwz214.

Wang, M., J.M.K. O'Connor, S. Zhou, and Z.H. Zhou. 2019d. New toothed Early Cretaceous ornithuromorph bird reveals intraclade diversity in pattern of tooth loss. Journal of Systematic Palaeontology: early view. [doi.org/10.1080/14772019.2019.1682696]

Wang, S., C. Sun, C. Sullivan, and X. Xu. 2013a. A new oviraptorid (Dinosauria: Theropoda) from the Upper Cretaceous of southern China. Zootaxa 3640: 242–257.

Wang, S., S.K. Zhang, C. Sullivan, and X. Xu. 2016a. Elongatoolithid eggs containing oviraptorid (Theropoda, Oviraptorosauria) embryos from the Upper Cretaceous of southern China. BMC Evolutionary Biology 16: 67.

Wang, X., et al. 2010b. A new enantiornithine bird from the Early Cretaceous of Western Liaoning, China. Condor 112: 432–437.Wang, X., G.J. Dyke, V. Codrea, P. Godefroit, and T. Smith. 2011. A euenantiornithine bird from the Late Cretaceous Haţeg Basin of Romania. Acta Palaeontologica Polonica 56: 853–857.

Wang, X.L., et al. 2014a. Insights into the evolution of rachis dominated tail feathers from a new basal enantiornithine (Aves: Ornithothoraces). Biological Journal of the Linnean Society 113: 805–819.

Wang, X.R., et al. 2010a. New species of Enantiornithes (Aves: Ornithothoraces) from the Qiaotou Formation in Northern Hebei, China. Acta Geologica Sinica 84: 247–256.

Wang, X.R., Q. Ji, F.F. Teng, and K.M. Jin. 2013d. A new species of *Yanornis* (Aves: Ornithurae) from the Lower Cretaceous strata of Yixian, Liaoning Province. Geological Bulletin of China 32: 601–606.

Wang, X.R., L.M. Chiappe, F.F. Teng, and Q. Ji. 2013e. *Xinghaiornis lini* (Aves: Ornithothoraces) from the Early Cretaceous of Liaoning: an example of evolutionary mosaic in early birds. Acta Geologica Sinica (English Edition) 87: 686–689.

Wang Y.M., J.M.K. O'Connor, D.Q. Li, and H.L. You. 2013f. Previously unrecognised ornithuromorph bird diversity in the Early Cretaceous Changma Basin, Gansu Province, northwestern China. PLoS ONE 8: e77693.

Wang, Y.M., J.M.K. O'Connor, D.Q. Li, and H.L. You. 2013b. Previously unrecognized ornithuromorph bird diversity in the Early Cretaceous Changma Basin, Gansu Province, northwestern China. PLoS One 8: e77693.

Wang, Y., et al., 2016d. A new Jehol enantiornithine bird with three-dimensional preservation and ovarian follicles. Journal of Vertebrate Paleontology 36: e1054496.

Wei, X.F., H.Y. Pu, L. Xu, D. Liu, and J.C. Lü. 2013. A new oviraptorid dinosaur (Theropoda: Oviraptorosauria) from the Late Cretaceous of Jiangxi Province, Southern China. Acta Geologica Sinica (English edition) 87: 899–904.

Weishampel, D.B., and C.M. Jianu. 1996. New theropod dinosaur material from the Hateg Basin (Late Cretaceous, Western Romania). Neues Jahrbuch für Geologie und Paläontologie, Abhandlungen 200: 387–404.

Weishampel, D.B., et al. 2004. Dinosaur distribution. *In* D.B. Weishampel, P. Dodson, and H. Osmólska (editors), The Dinosauria: 517–606. Berkeley: University of California Press.

Wellnhofer P. 1974. Das fünfte Skelettexemplar von *Archaeopteryx*. Palaeontographica A147: 169–216.

Wellnhofer, P. 1993. Das siebte Exemplar von *Archaeopeteryx* aus den Solnhofener Schichten. *Archaeopteryx* 11: 1–48.

Wellnhofer, P. 2009. *Archaeopteryx*: the icon of evolution, München: Verlag Dr. Friedrich Pfeil.

Wellnhofer, P, and M. Röper. 2005. Das neunte *Archaeopteryx*-Exemplar von Solnhofen. *Archaeopteryx* 23: 3–21.

Worthy, T.H., F.J. Degrange, W.D. Handley, and M.S.Y. Lee. 2017. The evolution of giant flightless birds and novel phylogenetic relationships for extinct fowl (Aves, Galloanseres). Royal Society Open Science 4: 170975.

Xing, L.D., et al. 2016. Mummified precocial bird wings in mid-Cretaceous Burmese amber. Nature Communications 7: 12089.

Xing, L.D., et al. 2017. A mid-Cretaceous enantiornithine (Aves) hatchling preserved in Burmese amber with unusual plumage. Gondwana Research 49: 264–277.

Xing, L.D., et al. 2019a. A new enantiornithine with unusual pedal proportions found in amber. Current Biology 29: 2396–2401.

Xing, L.D., R.C. McKellar, J.M.K. O'Connor, K.C. Niu, and H.J. Mai. 2019b. A mid-Cretaceous enantiornithine foot and tail feather preserved in Burmese amber. Scientific Reports 9 (15513): 1–8.

Xing, L.D., et al. 2019c. A fully feathered enantiornithine foot and wing fragment preserved in mid-Cretaceous Burmese amber. Scientific Reports 9 (927): 1–9.

Xu, G.L., Y.S. Yang, and S.Y. Deng. 1999. First discovery of Mesozoic bird fossils in Hebei province and its significance. Regional Geology of China 18: 444–448.

Xu, L., et al. 2011. A new ornithomimid dinosaur with North American affinities from the Late Cretaceous Qiupa Formation in Henan Province of China. Cretaceous Research 32: 213–222.

Xu, L., et al. 2012a. Discovery and significance of the Cretaceous system in Ruyang Basin, Henan Province. Geological Review 58: 601–613.

Xu, X. 2020. Filamentous integuments in nonavialan theropods and their kin: advances and future perspectives for understanding the evolution of feathers. In C. Foth, C. and O.W.M. Rauhut (editors), The evolution of feathers: 67–78. Cham, Switzerland: Springer.

Xu, X., and F.L. Han. 2010. A new oviraptorid dinosaur (Theropoda: Oviraptorosauria) from the Upper Cretaceous of China. Vertebrata PalAsiatica 48: 11–18.

Xu, X., and M.A. Norell. 2004. A new troodontid dinosaur from China with avian-like sleeping posture. Nature 431: 838–841.

Xu, X., and Z.C. Qin. 2017. A new tiny dromaeosaurid dinosaur from the Lower Cretaceous Jehol Group of western Liaoning and niche differentiation among the Jehol dromaeosaurids. Vertebrata PalAsiatica 55: 129–144.

Xu, X., and X. Wang. 2003. A new maniraptoran dinosaur from the Early Cretaceous Yixian Formation of western Liaoning. Vertebrata PalAsiatica 41: 195–202.

Xu, X., and X. Wang. 2004a. A new dromaeosaur (Dinosauria: Theropoda) from the Early Cretaceous Yixian Formation of Western Liaoning. Vertebrata PalAsiatica 42: 111–119.

Xu, X., and X.L. Wang. 2004b. A new troodontid (Theropoda: Troodontidae) from the Lower Cretaceous Yixian Formation of western Liaoning, China. Acta Geologica Sinica (English edition) 78: 22–26.

Xu, X., and F. Zhang. 2005. A new maniraptoran dinosaur from China with long feathers on the metatarsus. Naturwissenschaften 92: 173–177.

Xu, X., X.L. Wang, and X.C. Wu. 1999. A dromaeosaurid dinosaur with a filamentous integument from the Yixian Formation of China. Nature 401: 252–255.

Xu, X., Z.H. Zhou, and X.L. Wang. 2000. The smallest known non-avian theropod dinosaur. Nature 408: 705–708.

Xu, X., Y.N. Cheng, X.L. Wang, and C.H. Chang. 2002a. An unusual oviraptorosaurian dinosaur from China. Nature 419: 291–293.

Xu, X., M.A. Norell, X.L. Wang, P.J. Makovicky, and X.C. Wu. 2002b. A basal troodontid from the Early Cretaceous of China. Nature 415: 780–784.

Xu, X., et al. 2003. Four-winged dinosaurs from China. Nature 421: 335–340

Xu, X., Q.W. Tan, J.M. Wang, X.J. Zhao, and L. Tan. 2007. A gigantic bird-like dinosaur from the Late Cretaceous of China. Nature 447: 844–847.

Xu, X., et al. 2008. A new feathered maniraptoran dinosaur fossil that fills a morphological gap in avian origin. Chinese Science Bulletin 54: 430–435.

Xu, X., et al. 2009. A new feathered maniraptoran dinosaur fossil that fills a morphological gap in avian origin. Chinese Science Bulletin 54: 430–435.

Xu, X., X.T. Zheng, and H.L. You. 2010a. Exceptional dinosaur fossils show ontogenetic development of early feathers. Nature 464: 1338–1341.

Xu, X., et al. 2010b. A new dromaeosaurid (Dinosauria: Theropoda) from the Upper Cretaceous Wulansuhai Formation of Inner Mongolia, China. Zootaxa 2403: 1–9.

Xu, X., H.L. You, K. Du, and F.L. Han. 2011a. An *Archaeopteryx*-like theropod from China and the origin of Avialae. Nature 475: 465–470.

Xu, X., Q.W. Tan, C. Sullivan, F.L. Han, and D. Xiao. 2011b. A short-armed troodontid dinosaur from the Upper Cretaceous of Inner Mongolia and its implications for troodontid evolution. PLoS One 6: 1–12.

Xu, X., et al. 2012b. The taxonomy of the troodontid IVPP V10597 reconsidered. Vertebrata PalAsiatica 50: 140–150.

Xu, X., C. Sullivan, and S. Wang. 2013a. The systematic position of the enigmatic theropod dinosaur *Yixianosaurus longimanus*. Vertebrata PalAsiatica 51: 169–183.

Xu, X., et al. 2013b. A new oviraptorid from the Upper Cretaceous of Nei Mongol, China, and its stratigraphic implications. Vertebrata PalAsiatica 51: 85–101.

Xu, X., et al. 2015a. A bizarre Jurassic maniraptoran theropod with preserved evidence of membranous wings. Nature 521: 70–73.

Xu, X., et al. 2015b. The taxonomic status of the Late Cretaceous dromaeosaurid *Linheraptor exquisitus* and its implications for dromaeosaurid systematics. Vertebrata PalAsiatica 53: 29–62.

Xu, X., et al. 2017. Mosaic evolution in an asymmetrically feathered troodontid dinosaur with transitional features. Nature Communications 8: 14972.

Yao, X., et al. 2015. *Caenagnathasia* sp. (Theropoda: Oviraptorosauria) from the Iren Dabasu Formation (Upper Cretaceous: Campanian) of Erenhot, Nei Mongol, China. Vertebrata PalAsiatica 53: 291–298.

Yin, Y.L., R. Pei, and C.F. Zhou. 2018. Cranial morphology of *Sinovenator changii* (Theropoda: Troodontidae) on the new material from the Yixian Formation of western Liaoning, China. PeerJ 6: e4977.

You, H.L., et al. 2006. A nearly modern amphibious bird from the Early Cretaceous of northwestern China. Science 312: 1640–1643.

You, H.L., et al. 2010. A second Cretaceous ornithuromorph bird from the Changma Basin, Gansu Province, northwestern China. Acta Palaeontologica Polonica 55: 617–625.

Yu, J.X., S.Z. Mao, M.R. Sun, and S.Y. Sun. 1981. The Late Cretaceous dinoflagellates and acritarchs from Sansui Basin of Guandong province. Oil and Gas Geology 2: 254–266.

Yu, Y., et al. 2018. A new caenagnathid dinosaur from the Upper Cretaceous Wangshi Group of Shandong, China, with comments on size variation among oviraptorosaurs. Scientific Reports 8: 5030.

Yuan, C.X. 2010. A new genus and species of Sapeornithidae from Lower Cretaceous in Western Liaoning, China. Acta Geologica Sinica 82: 48–55.

Zanno, L.E., and S.D. Sampson. 2005. A new oviraptorosaur (Theropoda, Maniraptora) from the Late Cretaceous (Campanian) of Utah. Journal of Vertebrate Paleontology 25: 897–904.

Zanno, L.E., D.J. Varricchio, P.M. O'Connor, A.L. Titus, and M.J. Knell. 2011. A new troodontid theropod, *Talos sampsoni* gen. et sp. nov., from the Upper Cretaceous Western Interior Basin of North America. PLoS One 6: e24487.

Zelenkov, N.Z., and A.O. Averianov. 2016. A historical specimen of enantiornithine bird from the Early Cretaceous of Mongolia representing a new taxon with a specialized neck morphology. Journal of Systematic Palaeontology 14: 319–338.

Zhang, F.C., and Z.H. Zhou. 2000. A primitive enantiornithine bird and the origin of feathers. Science 290: 1955–1960.

Zhang, F.C, Z.H. Zhou, L.H. Hou, and G. Gu. 2001. Early diversification of birds: evidence from a new opposite bird. Chinese Science Bulletin 46: 945–950.

Zhang, F.C., Z.H. Zhou, and X. Xu. 2002. A juvenile coelurosaurian theropod from China indicates arboreal habits. Naturwissenschaften 89: 394–398.

Zhang, F.C., Z.H. Zhou, and M.J. Benton. 2008b. A primitive confuciusornithid bird from China and its implications for early avian flight. Science in China, D: Earth Sciences 51: 625–639.

Zhang, F.C., Zhou, Z.H., Xu, X., Wang, X., Sullivan, C. 2008a. A bizarre Jurassic maniraptoran from China with elongate ribbon-like feathers. Nature 455: 1105–1108.

Zhang, F.C., P.G.P. Ericson, Z.H. Zhou. 2004. Description of a new enantiornithine bird from the Early Cretaceous of Hebei, northern China. Canadian Journal of Earth Science 41: 1097–1107.

Zhang, Y.G., L.F. Zhang, J.J. Li, and Z.H. Li. 2010. New discovery and flying skills of *Cathayornis* from the Lower Cretaceous strata of the Otog Qi in Inner Mongolia, China. Geological Bulletin of China 29: 988–992.

Zhang, Z.H., L.M. Chiappe, G. Han, and A. Chinsamy. 2013. A large bird from the Early Cretaceous of China: new information on the skull of enantiornithines. Journal of Vertebrate Paleontology 33: 1176–1189.

Zhang, Z. et al. 2006. The first Mesozoic heterodactyl bird from China. Acta Geologica Sinica 80: 631–635.

Zhang, Z., et al. 2009. Diversification in an Early Cretaceous avian genus: evidence from a new species of *Confuciusornis* from China. Journal of Ornithology 150: 783–790.

Zheng, X.T., Z.H. Zhang, and L.H. Hou. 2007. A new enantiornithine bird with four long rectrices from the Early Cretaceous of northern Hebei, China. Acta Geologica Sinica 81: 703–708.

Zheng, X.T., X. Xu, H.L. You, Q. Zhao, and Z.M. Dong. 2009. A short-armed dromaeosaurid from the Jehol Group of China with implications for early dromaeosaurids evolution. Proceedings of the Royal Society of London B 277: 211–217.

Zheng, X.T., J.M.K. O'Connor, X.L Wang, X.M. Zhang, and Y. Wang. 2014. New information on Hongshanornithidae (Aves: Ornithuromorpha) from a new subadult specimen. Vertebrata PalAsiatica 52: 217–232.

Zheng, X.T., et al. 2013. Preservation of ovarian follicles reveals early evolution of avian reproductive behaviour. Nature 495: 507–511.

Zheng, X.T., et al. 2017. Exceptional preservation of soft tissue in a new specimen of *Eoconfuciusornis* and its biological implications. National Science Review 4: 441–452.

Zheng, X.T, J.M.K. O'Connor, X.L. Wang, Y. Wang, and Z.H. Zhou. 2018. Reinterpretation of a previously described Jehol bird clarifies early trophic evolution in the Ornithuromorpha. Proceedings of the Royal Society of London B 285: rspb.2017.2494.

Zhou, Z.H. 1995. Discovery of a new enantiornithine bird from the Early Cretaceous of Liaoning, China. Vertebrata PalAsiatica 33: 99–113.

Zhou, Z.H. 2002. A new and primitive enantiornithine bird from the Early Cretaceous of China. Journal of Vertebrate Paleontology 22: 49–57.

Zhou, Z.H., and L.H. Hou. 2002. The discovery and study of Mesozoic birds in China. *In* L.M. Chiappe and L.M. Witmer (editors), Mesozoic birds: above the heads of dinosaurs: 160–183. Berkeley: University of California Press.

Zhou, Z.H., and Wang, Y. 2010. Vertebrate diversity of the Jehol Biota as compared with other lagerstätten. Science China Earth Sciences 53: 1894–1907.

Zhou, Z.H., and F.C. Zhang. 2001. Two new ornithurine birds from the Early Cretaceous of western Liaoning, China. Chinese Science Bulletin 46: 1258–1264.

Zhou, Z.H., and F.C. Zhang. 2002a. A long-tailed, seed-eating bird from the Early Cretaceous of China. Nature 418: 405–409.

Zhou, Z.H., and F.C. Zhang. 2002b. Largest bird from the Early Cretaceous and its implications for the earliest avian ecological diversification Naturwissenschaften 89: 34–38.

Zhou, Z.H., and F.C. Zhang. 2003a. Anatomy of the primitive bird *Sapeornis chaoyangensis* from the Early Cretaceous of Liaoning, China. Canadian Journal of Earth Sciences 40: 731–747.

Zhou, Z.H., and F.C. Zhang. 2003b. *Jeholornis* compared to *Archaeopteryx*, with a new understanding of the earliest avian evolution. Naturwissenschaften 90: 220–225.

Zhou, Z.H., and F.C. Zhang. 2005. Discovery of an ornithurine bird and its implication for Early Cretaceous avian radiation. Proceedings of the National Academy of Sciences of the United States of America 102: 18998–19002.

Zhou, Z.H., and F.C. Zhang. 2006a. Mesozoic birds of China—a synoptic review. Vertebrata PalAsiatica 44: 74–98.

Zhou, Z.H., and F.C. Zhang. 2006b. A beaked basal ornithurine bird (Aves, Ornithurae) from the Lower Cretaceous of China. Zoologica Scripta 35: 363–373.

Zhou, Z.H, F. Jin, and J.Y. Zhang. 1992. Preliminary report on a Mesozoic bird from Liaoning, China. Chinese Science Bulletin 37: 1365–1368.

Zhou, Z.H., F.C. Zhang, and Z.H. Li. 2009. A new basal ornithurine bird (*Jianchangornis microdonta* gen. et sp. nov.), from the Lower Cretaceous of China. Vertebrata PalAsiatica 4: 299–310.

Zhou, Z.H., Zhang, F.C. and Li, Z.H. 2010. A new Lower Cretaceous bird from China and tooth reduction in early avian evolution. Proceedings of the Royal Society B 277: 219–227.

Zhou, S., Z.H. Zhou, and J.M.K. O'Connor. 2012. A new basal beaked ornithurine bid from the Lower Cretaceous of western Liaoning, China. Vertebrata PalAsiatica 50: 9–24.

Zhou, Z.H., X.L. Wang, F.C. Zhang, and X. Xu. 2000. Important features of *Caudipteryx*—evidence from two nearly complete new specimens. Vertebrata PalAsiatica 38: 241–254.

Zhou, Z.H., J.A. Clarke, F.C Zhang, and O. Wings. 2004. Gastroliths in *Yanornis*: an indication of the earliest radical diet-switching and gizzard plasticity in the lineage leading to living birds? Naturwissenschaften 91: 571–574.

Zhou, Z.H, J.A. Clarke, and F.C Zhang. 2008. Insight into diversity, body size and morphological evolution from the largest Early Cretaceous enantiornithine bird. Journal of Anatomy 212: 565–577.

Zhou, S., Z.H. Zhou, and J.M.K. O'Connor. 2013. Anatomy of the basal ornithuromorph bird *Archaeorhynchus spathula* from the Early Cretaceous of Liaoning, China. Journal of Vertebrate Paleontology 33: 141–152.

Zhou, S., J.M.K. O'Connor, and M. Wang. 2014a. A new species from an ornithuromorph (Aves: Ornithothoraces) dominated locality of the Jehol Biota. Chinese Science Bulletin 59: 5366–5378.

Zhou, S., Z.H. Zhou, and J.M.K. O'Connor. 2014b. A new piscivorous ornithuromorph from the Jehol Biota. Historical Biology 26: 608–618.

Zinsmeister, W.J. 1985. 1985 Seymour Island expedition. Antarctic Journal of the United States 20: 41–42.

Chapter 3

The Impact of Unstable Taxa in Coelurosaurian Phylogeny and Resampling Support Measures for Parsimony Analyses

DIEGO POL[1] AND PABLO A. GOLOBOFF[2]

ABSTRACT

Paleontological datasets often have large amounts of missing entries that result in multiple most parsimonious trees. Highly incomplete and conflictive taxa produce a collapsed strict consensus and several methods have been developed for identifying these unstable or rogue taxa in optimal trees derived from phylogenetic analyses. In addition to decreasing consensus resolution, incomplete or conflictive taxa can also severely affect the support values of phylogenetic analysis in paleontological datasets. Here, we explore a protocol for the identification of taxa that decrease jackknife support values in parsimony analysis. The taxa identified are excluded from majority rule jackknife trees, revealing nodes that have either low or high support irrespective of the uncertainties in the placement of unstable taxa. A recently published dataset of coelurosaurian relationships based on 164 taxa and 853 characters is explored using this protocol; our protocol detects a total of 40 unstable taxa as the most detrimental for node supports. Major clades that are well supported in the reduced jackknife tree include Coelurosauria, Maniraptoriformes, Compsognathidae, Ornithomimosauria, Alvarezsauroidea, Therizinosauria, Oviraptorosauria. Clades with moderate support instead include Maniraptora, Pennaraptora, Paraves, Dromaeosauridae, Troodontidae, Anchiornithinae, and early-diverging clades of Avialae.

INTRODUCTION

Morphological datasets that include a large number of extinct taxa are usually characterized by copious amounts of missing entries. The abundance of missing data in these datasets has been regarded as problematic for phylogenetic analyses, since the early days of quantitative cladistics (Gauthier, 1986; Wilkinson and Benton, 1995). The presence of taxa with abundant missing entries has been linked to searches that find multiple optimal trees in parsimony analyses and the related computational difficulties of dealing with thousands of trees (which were very problematic for early phylogenetic software). A subsequent problem in these cases is how the multiple optimal trees can be efficiently summarized given that the strict consensus is usually highly collapsed due to the alternative positions of wildcard or rogue taxa. The role of reduced consensus methods (Wilkinson, 1994) has become increasingly important in recent years, and several methods have been proposed and implemented for detecting rogue taxa in a collection of optimal trees (Goloboff et al., 2008; Pol and Escapa, 2009; Goloboff and Szumik, 2015).

---

[1] CONICET, Museo Paleontológico Egidio Feruglio, Trelew, Argentina.
[2] CONICET, Unidad Ejecutora Lillo (UEL), S.M. Tucumán, Argentina.

A second level of problems introduced by the presence of copious missing entries is related to their influence in support values. It is commonly the case that highly incomplete taxa can be more easily placed in alternative positions than more complete taxa. This obviously affects not only the support with which a taxon is placed in the phylogenetic tree but also the support values of many adjacent nodes (Wilkinson, 1996; Wilkinson et al., 2000). The empirical outcome of this is that paleontological datasets are also characterized by the presence of low support values for most of the nodes recovered in the consensus tree. Some methods exist for assessing the role of rogue taxa for parsimony measures such as Bremer or decay support (e.g., double decay; Wilkinson et al., 2000). Also, alternative resampling methods that do not eliminate characters and thus produce lower estimates of support only in the presence of actual character conflict have been explored (e.g. the "nozeroweight" option for resampling in TNT, used by Pei et al., in press). Recently, however, most efforts have been focused on the development of ways to detect wildcard taxa that decrease bootstrap support (Pattengale et al., 2011; Aberer and Stamatakis, 2011; Aberer et al., 2013).

Here, we explore the application of a more detailed protocol that identifies unstable taxa that decrease support measures, based on resampling procedures (i.e., jackknife or bootstrap) implemented with a script for TNT (Goloboff et al., 2008), that combines several of the options for identifying rogue taxa that already exist in that program. We employ this procedure for a comprehensive phylogenetic analysis of Coelurosauria, using the Theropod Working Group (TWiG) matrix published by Pei et al. (in press). This dataset has an extensive taxon sampling (164 taxa), and therefore provides an ideal case for testing the impact of fragmentary taxa on support measures. In particular, the TWiG dataset includes a dense sampling of pennaraptoran coelurosaurians that have been the focus of recent systematic debates, including the interrelationships of some of its major clades as well as the affinities of some small but conflictive groups such as scansoriopterygids (Xu et al., 2011, 2015, 2017; Turner et al., 2012; Agnolín and Novas, 2013; O'Connor and Sullivan, 2014) and unenlagiines (Turner et al., 2007; Turner et al., 2012; Agnolín and Novas, 2013; Brusatte et al., 2014). The application of the new protocol allows analyzing the varying degrees of clade support within this group and distinguishing between low support caused by fragmentary taxa, and low support due to underlying character conflict and/or lack of sufficient phylogenetic data.

MATERIALS AND METHODS

Phylogenetic Analysis

The phylogenetic dataset (Pei et al., in press) has 164 taxa scored across 853 characters and its parsimony analysis is best carried out using the "New Technology Searches" option in TNT (Goloboff et al., 2008). This strategy was applied in a first phase until 50 hits to minimum length were achieved (command: *xmult = hits 50;*), resulting in trees of 3424 steps. The application of traditional heuristic searches (multiple replicates of Wagner trees followed by TBR branch swapping) is possible, but then finding optimal trees requires longer search times than new technology searches. The strict consensus of this analysis is well resolved, with two relatively large polytomies at the base of Avialae and in Dromaeosauridae (fig. 1). These polytomies are caused by four unstable taxa that take multiple positions among the MPTs (i.e., *Yurgovuchia*, *Acheroraptor*, *Velociraptor osmolskae*, and *Archaeopteryx* Haarlem). Ten other taxa are also identified as unstable by IterPCR (Pol and Escapa, 2009) applied to the MPTs, as implemented in TNT (see Goloboff and Szumik, 2015). Ignoring all the unstable taxa results in a well-resolved, strict reduced-consensus tree (see resolved nodes in fig. 1).

It is important to note that the unstable taxa are pruned from the trees, but they are *not* eliminated from the matrix or the tree searches at any point. The elimination of taxa from the trees amounts to representing those parts of the results that are more useful, while eliminating taxa from the matrix amounts to ignoring the evidence (in the form of character combinations) provided by those taxa (see discussion in Goloboff and Szumik, 2015: 100–101, and fig. 6).

Resampling Support Measures

In this paper we compare jackknife support values obtained using the default settings in TNT (including all taxa and using group frequencies on the majority rule consensus) with jackknife frequencies obtained with the same procedure but on a reduced majority rule consensus tree (ignoring the alternative position of unstable taxa).

We opted for this comparison for the sake of simplicity to highlight the effect of unstable taxa on resampling support measures. However, we note that there are alternative ways for summarizing resampling measures, such as GC frequencies (rather than raw frequencies) and/or measuring frequencies for the nodes present in the strict consensus of the MPTs (rather than those appearing in the majority rule consensus of the resampling procedure).

The frequencies of the majority rule consensus obtained after performing a default jackknife analysis on the dataset of Pei et al. (in press) are low for most nodes. A raw frequency majority rule tree of the jackknife analysis is highly collapsed and has only 68 nodes, only 33 of which have support values above 75% (fig. 2). The jackknife majority rule tree shows a large polytomy at the base of Pennaraptora that involves the relationships of 38 terminal taxa and six moderately supported clades. Two important clades of Paraves (Dromaeosauridae and Avialae) are collapsed into the large early-diverging polytomy of Pennaraptora. The frequencies of the groups resolved in the reduced consensus (fig. 1) can be calculated for groups with frequency below 50%, but even in this case, the support values of Dromaeosauridae and Avialae are very low when all the remaining taxa are included in the summary tree. This situation, in which many clades of interest are collapsed in the majority rule tree derived from the resampling replicates, is in fact a common result in paleontological datasets (in particular when they are constructed using an extensive taxon-sampling regime).

Identifying Unstable Taxa for Resampling Support Analysis

A resampling procedure (e.g., jackknife or bootstrap) normally involves conducting at least 100 pseudoreplicates. In each of these replicates the characters of the original matrix are resampled at random so that a modified (perturbed) matrix is obtained and a tree search is conducted on this modified matrix (fig. 3). The difference between alternative resampling support measures is simply how the resampling of characters is performed (e.g., bootstrap, jackknife, symmetric; Farris et al., 1996; Goloboff et al., 2003). Regardless of how this is done, the tree search conducted for each pseudoreplicate results in a set of most parsimonious trees and, therefore, after finishing the 100 pseudoreplicates, there are 100 sets of most parsimonious trees.

As noted previously (Goloboff et al., 2003; Simmons and Freudenstein, 2011), some phylogenetic software (e.g., PAUP) calculates the bootstrap/jackknife frequencies by weighting groups according to their frequency within each pseudoreplicate, which can easily produce inappropriate estimates of support. This problem is prevented if the results for each individual pseudoreplicate are instead summarized by means of a strict consensus. Thus, TNT automatically calculates the strict consensus of the optimal trees for each pseudoreplicate, subsequently deriving the bootstrap/jackknife frequencies from the majority rule consensus tree of the 100 strict consensuses (each representing one pseudoreplicate; see fig. 3). Problems similar to those resulting from weighting groups according to their frequency within pseudoreplicates occur if a single tree is found or saved during the search for each pseudoreplicate (Goloboff and Pol 2005), with the possibility of bias in tree searches

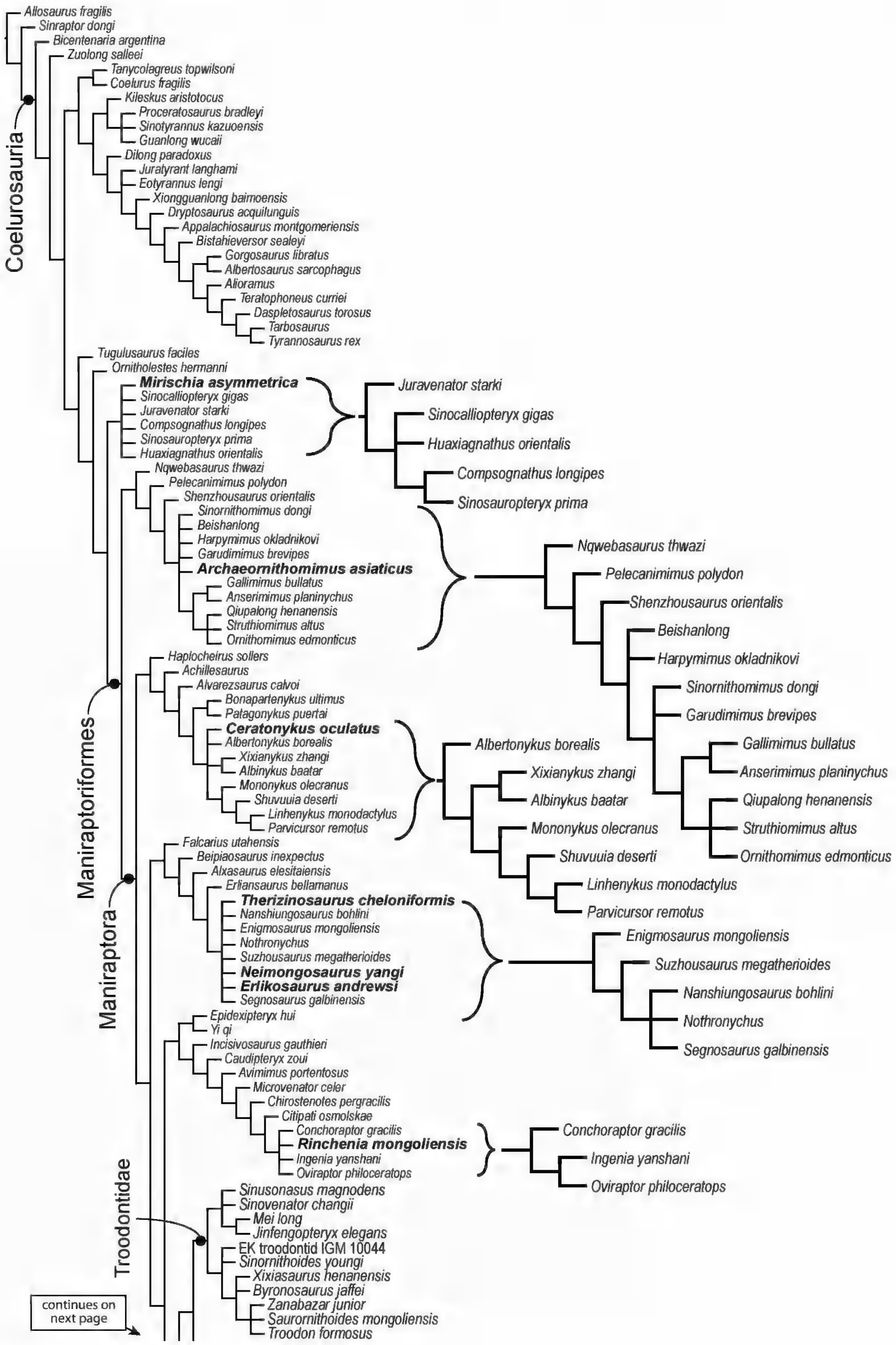
Allosaurus fragilis
Sinraptor dongi
Bicentenaria argentina
Zuolong salleei
Tanycolagreus topwilsoni
Coelurus fragilis
Kileskus aristotocus
Proceratosaurus bradleyi
Sinotyrannus kazuoensis
Guanlong wucaii
Dilong paradoxus
Juratyrant langhami
Eotyrannus lengi
Xiongguanlong baimoensis
Dryptosaurus acquilunguis
Appalachiosaurus montgomeriensis
Bistahieversor sealeyi
Gorgosaurus libratus
Albertosaurus sarcophagus
Alioramus
Teratophoneus curriei
Daspletosaurus torosus
Tarbosaurus
Tyrannosaurus rex
Coelurosauria
Tugulusaurus faciles
Ornitholestes hermanni
Mirischia asymmetrica
Sinocalliopteryx gigas
Juravenator starki
Compsognathus longipes
Sinosauropteryx prima
Huaxiagnathus orientalis
Juravenator starki
Sinocalliopteryx gigas
Huaxiagnathus orientalis
Compsognathus longipes
Sinosauropteryx prima
Nqwebasaurus thwazi
Pelecanimimus polydon
Shenzhousaurus orientalis
Sinornithomimus dongi
Beishanlong
Harpymimus okladnikovi
Garudimimus brevipes
Archaeornithomimus asiaticus
Gallimimus bullatus
Anserimimus planinychus
Qiupalong henanensis
Struthiomimus altus
Ornithomimus edmonticus
Nqwebasaurus thwazi
Pelecanimimus polydon
Shenzhousaurus orientalis
Beishanlong
Harpymimus okladnikovi
Sinornithomimus dongi
Garudimimus brevipes
Gallimimus bullatus
Anserimimus planinychus
Qiupalong henanensis
Struthiomimus altus
Ornithomimus edmonticus
Maniraptoriformes
Haplocheirus sollers
Achillesaurus
Alvarezsaurus calvoi
Bonapartenykus ultimus
Patagonykus puertai
Ceratonykus oculatus
Albertonykus borealis
Xixianykus zhangi
Albinykus baatar
Mononykus olecranus
Shuvuuia deserti
Linhenykus monodactylus
Parvicursor remotus
Albertonykus borealis
Xixianykus zhangi
Albinykus baatar
Mononykus olecranus
Shuvuuia deserti
Linhenykus monodactylus
Parvicursor remotus
Maniraptora
Falcarius utahensis
Beipiaosaurus inexpectus
Alxasaurus elesitaiensis
Erliansaurus bellamanus
Therizinosaurus cheloniformis
Nanshiungosaurus bohlini
Enigmosaurus mongoliensis
Nothronychus
Suzhousaurus megatherioides
Neimongosaurus yangi
Erlikosaurus andrewsi
Segnosaurus galbinensis
Enigmosaurus mongoliensis
Suzhousaurus megatherioides
Nanshiungosaurus bohlini
Nothronychus
Segnosaurus galbinensis
Epidexipteryx hui
Yi qi
Incisivosaurus gauthieri
Caudipteryx zoui
Avimimus portentosus
Microvenator celer
Chirostenotes pergracilis
Citipati osmolskae
Conchoraptor gracilis
Rinchenia mongoliensis
Ingenia yanshani
Oviraptor philoceratops
Conchoraptor gracilis
Ingenia yanshani
Oviraptor philoceratops
Troodontidae
Sinusonasus magnodens
Sinovenator changii
Mei long
Jinfengopteryx elegans
EK troodontid IGM 10044
Sinornithoides youngi
Xixiasaurus henanensis
Byronosaurus jaffei
Zanabazar junior
Saurornithoides mongoliensis
Troodon formosus
continues on next page

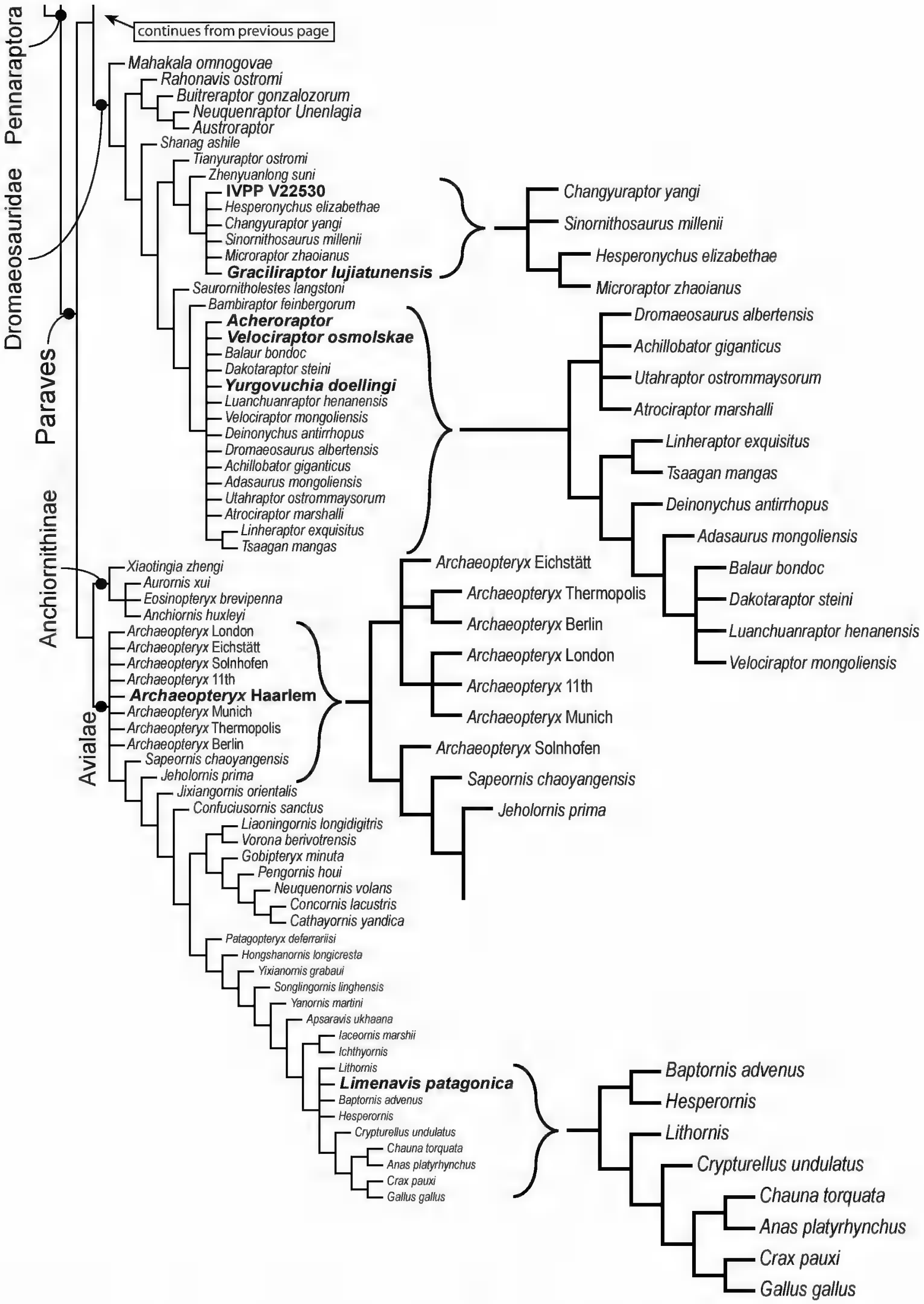
Pennaraptora
Dromaeosauridae
Paraves
Anchiornithinae
Avialae
continues from previous page
Mahakala omnogovae
Rahonavis ostromi
Buitreraptor gonzalozorum
Neuquenraptor Unenlagia
Austroraptor
Shanag ashile
Tianyuraptor ostromi
Zhenyuanlong suni
IVPP V22530
Hesperonychus elizabethae
Changyuraptor yangi
Sinornithosaurus millenii
Microraptor zhaoianus
Graciliraptor lujiatunensis
Saurornitholestes langstoni
Bambiraptor feinbergorum
Acheroraptor
Velociraptor osmolskae
Balaur bondoc
Dakotaraptor steini
Yurgovuchia doellingi
Luanchuanraptor henanensis
Velociraptor mongoliensis
Deinonychus antirrhopus
Dromaeosaurus albertensis
Achillobator giganticus
Adasaurus mongoliensis
Utahraptor ostrommaysorum
Atrociraptor marshalli
Linheraptor exquisitus
Tsaagan mangas
Xiaotingia zhengi
Aurornis xui
Eosinopteryx brevipenna
Anchiornis huxleyi
Archaeopteryx London
Archaeopteryx Eichstätt
Archaeopteryx Solnhofen
Archaeopteryx 11th
Archaeopteryx Haarlem
Archaeopteryx Munich
Archaeopteryx Thermopolis
Archaeopteryx Berlin
Sapeornis chaoyangensis
Jeholornis prima
Jixiangornis orientalis
Confuciusornis sanctus
Liaoningornis longidigitris
Vorona berivotrensis
Gobipteryx minuta
Pengornis houi
Neuquenornis volans
Concornis lacustris
Cathayornis yandica
Patagopteryx deferrariisi
Hongshanornis longicresta
Yixianornis grabaui
Songlingornis linghensis
Yanornis martini
Apsaravis ukhaana
Iaceornis marshii
Ichthyornis
Lithornis
Limenavis patagonica
Baptornis advenus
Hesperornis
Crypturellus undulatus
Chauna torquata
Anas platyrhynchus
Crax pauxi
Gallus gallus
Changyuraptor yangi
Sinornithosaurus millenii
Hesperonychus elizabethae
Microraptor zhaoianus
Dromaeosaurus albertensis
Achillobator giganticus
Utahraptor ostrommaysorum
Atrociraptor marshalli
Linheraptor exquisitus
Tsaagan mangas
Deinonychus antirrhopus
Adasaurus mongoliensis
Balaur bondoc
Dakotaraptor steini
Luanchuanraptor henanensis
Velociraptor mongoliensis
Archaeopteryx Eichstätt
Archaeopteryx Thermopolis
Archaeopteryx Berlin
Archaeopteryx London
Archaeopteryx 11th
Archaeopteryx Munich
Archaeopteryx Solnhofen
Sapeornis chaoyangensis
Jeholornis prima
Baptornis advenus
Hesperornis
Lithornis
Crypturellus undulatus
Chauna torquata
Anas platyrhynchus
Crax pauxi
Gallus gallus

FIG. 1. Strict consensus for the dataset of Pei et al., in press. Details of nodes resolved in the reduced consensus tree are shown, after excluding the 14 taxa that are unstable among the MPTs by the IterPCR implementation of TNT (Goloboff and Szumik, 2015). Taxa in bold in the strict consensus are the unstable taxa detected by IterPCR.

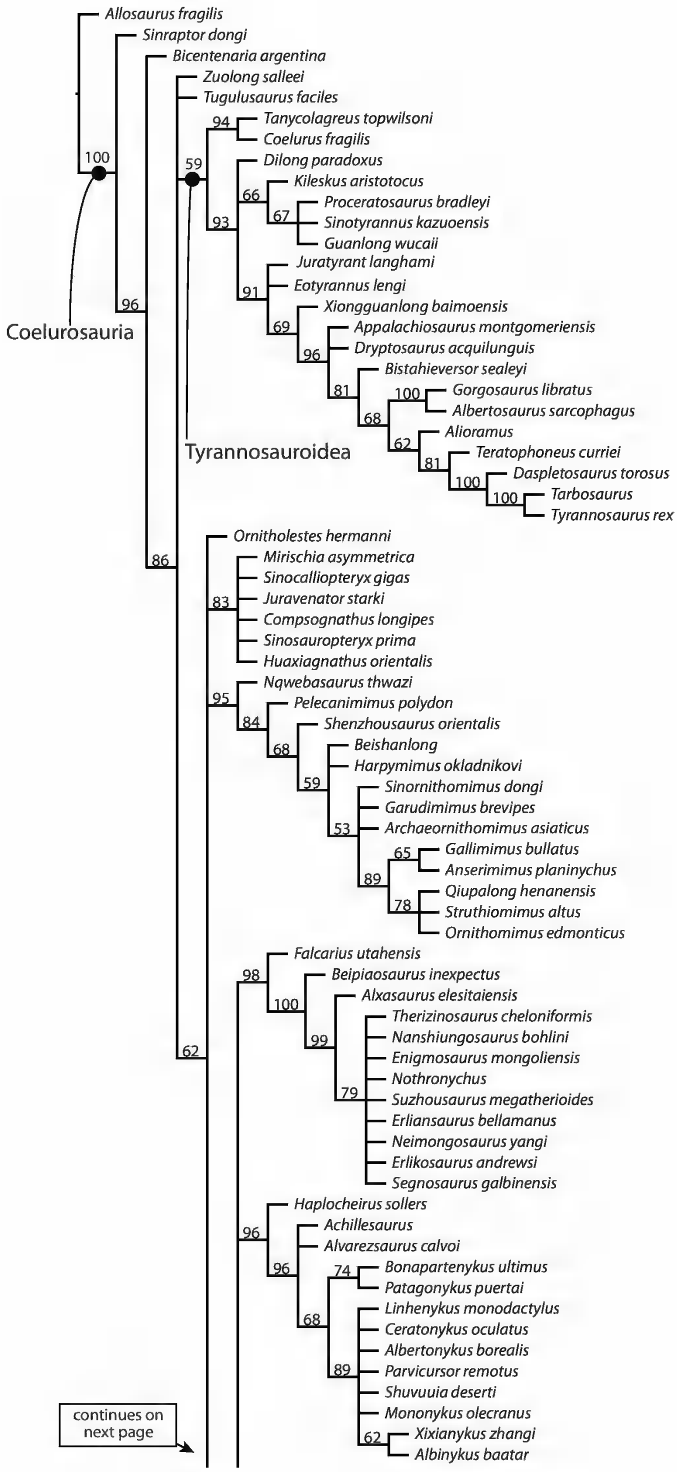
Allosaurus fragilis
Sinraptor dongi
Bicentenaria argentina
Zuolong salleei
Tugulusaurus faciles
94
Tanycolagreus topwilsoni
Coelurus fragilis
100
59
Dilong paradoxus
Kileskus aristotocus
66
Proceratosaurus bradleyi
67
Sinotyrannus kazuoensis
93
Guanlong wucaii
Juratyrant langhami
Eotyrannus lengi
91
Xiongguanlong baimoensis
96
69
Appalachiosaurus montgomeriensis
Coelurosauria
96
Dryptosaurus acquilunguis
Bistahieversor sealeyi
81
100
Gorgosaurus libratus
Albertosaurus sarcophagus
68
Alioramus
62
Tyrannosauroidea
Teratophoneus curriei
81
Daspletosaurus torosus
100
100
Tarbosaurus
Tyrannosaurus rex
Ornitholestes hermanni
Mirischia asymmetrica
86
Sinocalliopteryx gigas
83
Juravenator starki
Compsognathus longipes
Sinosauropteryx prima
Huaxiagnathus orientalis
Nqwebasaurus thwazi
95
Pelecanimimus polydon
84
Shenzhousaurus orientalis
68
Beishanlong
Harpymimus okladnikovi
59
Sinornithomimus dongi
Garudimimus brevipes
53
Archaeornithomimus asiaticus
65
Gallimimus bullatus
Anserimimus planinychus
89
Qiupalong henanensis
78
Struthiomimus altus
Ornithomimus edmonticus
Falcarius utahensis
98
Beipiaosaurus inexpectus
100
Alxasaurus elesitaiensis
Therizinosaurus cheloniformis
62
99
Nanshiungosaurus bohlini
Enigmosaurus mongoliensis
Nothronychus
79
Suzhousaurus megatherioides
Erliansaurus bellamanus
Neimongosaurus yangi
Erlikosaurus andrewsi
Segnosaurus galbinensis
Haplocheirus sollers
Achillesaurus
96
Alvarezsaurus calvoi
96
74
Bonapartenykus ultimus
Patagonykus puertai
Linhenykus monodactylus
68
Ceratonykus oculatus
Albertonykus borealis
89
Parvicursor remotus
Shuvuuia deserti
Mononykus olecranus
62
Xixianykus zhangi
continues on next page
Albinykus baatar

FIG. 2. Absolute frequency jackknife tree for the dataset of Pei et al. (in press) including all taxa as obtained in TNT.

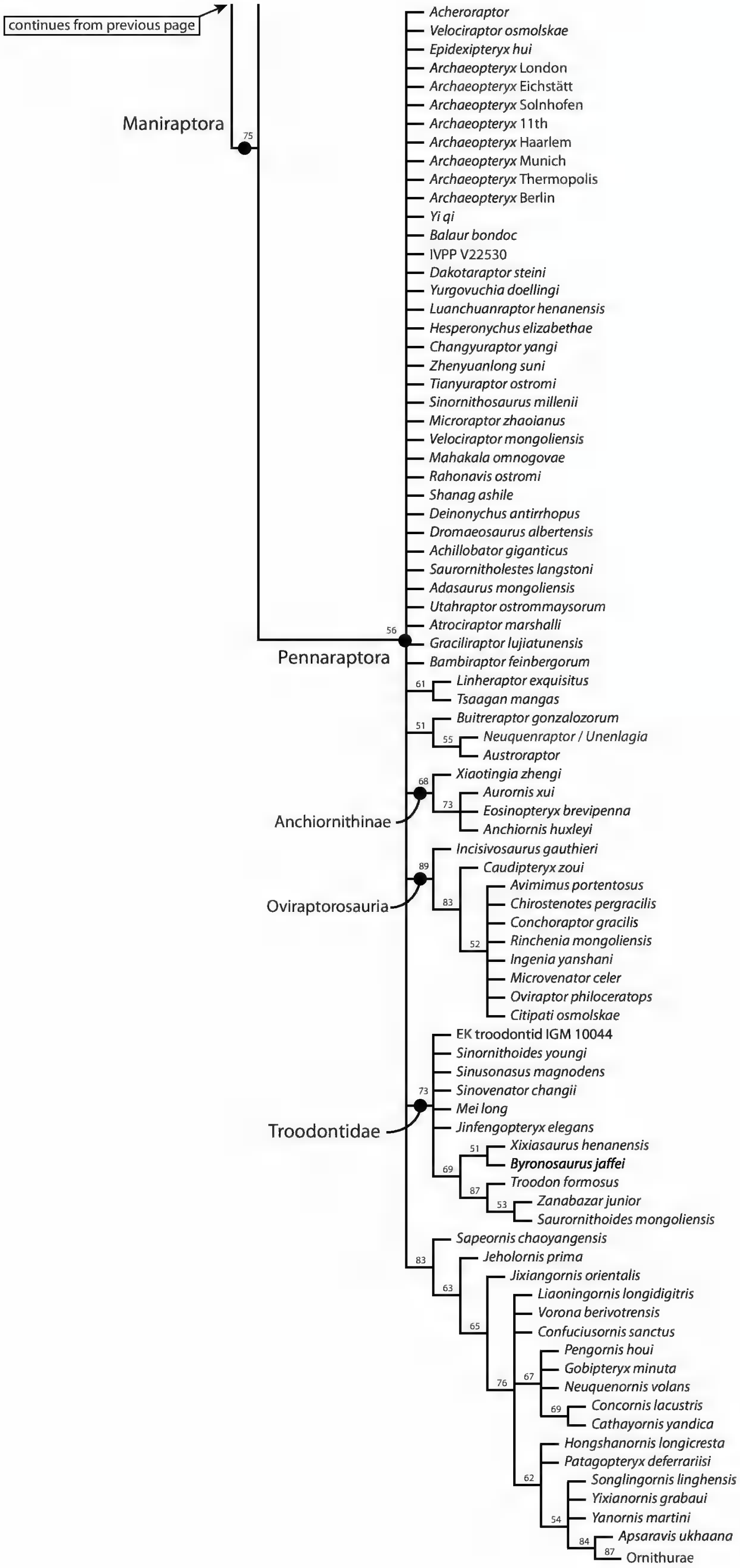
continues from previous page
Maniraptora
75
Acheroraptor
Velociraptor osmolskae
Epidexipteryx hui
Archaeopteryx London
Archaeopteryx Eichstätt
Archaeopteryx Solnhofen
Archaeopteryx 11th
Archaeopteryx Haarlem
Archaeopteryx Munich
Archaeopteryx Thermopolis
Archaeopteryx Berlin
Yi qi
Balaur bondoc
IVPP V22530
Dakotaraptor steini
Yurgovuchia doellingi
Luanchuanraptor henanensis
Hesperonychus elizabethae
Changyuraptor yangi
Zhenyuanlong suni
Tianyuraptor ostromi
Sinornithosaurus millenii
Microraptor zhaoianus
Velociraptor mongoliensis
Mahakala omnogovae
Rahonavis ostromi
Shanag ashile
Deinonychus antirrhopus
Dromaeosaurus albertensis
Achillobator giganticus
Saurornitholestes langstoni
Adasaurus mongoliensis
Utahraptor ostrommaysorum
Atrociraptor marshalli
56
Pennaraptora
Graciliraptor lujiatunensis
Bambiraptor feinbergorum
61
Linheraptor exquisitus
Tsaagan mangas
51
Buitreraptor gonzalozorum
55
Neuquenraptor / Unenlagia
Austroraptor
68
Anchiornithinae
Xiaotingia zhengi
73
Aurornis xui
Eosinopteryx brevipenna
Anchiornis huxleyi
89
Oviraptorosauria
Incisivosaurus gauthieri
83
Caudipteryx zoui
52
Avimimus portentosus
Chirostenotes pergracilis
Conchoraptor gracilis
Rinchenia mongoliensis
Ingenia yanshani
Microvenator celer
Oviraptor philoceratops
Citipati osmolskae
73
Troodontidae
EK troodontid IGM 10044
Sinornithoides youngi
Sinusonasus magnodens
Sinovenator changii
Mei long
Jinfengopteryx elegans
69
51
Xixiasaurus henanensis
Byronosaurus jaffei
87
Troodon formosus
53
Zanabazar junior
Saurornithoides mongoliensis
83
Sapeornis chaoyangensis
63
Jeholornis prima
65
Jixiangornis orientalis
76
Liaoningornis longidigitris
Vorona berivotrensis
Confuciusornis sanctus
67
Pengornis houi
Gobipteryx minuta
Neuquenornis volans
69
Concornis lacustris
Cathayornis yandica
62
Hongshanornis longicresta
Patagopteryx deferrariisi
54
Songlingornis linghensis
Yixianornis grabaui
Yanornis martini
84
Apsaravis ukhaana
87
Ornithurae

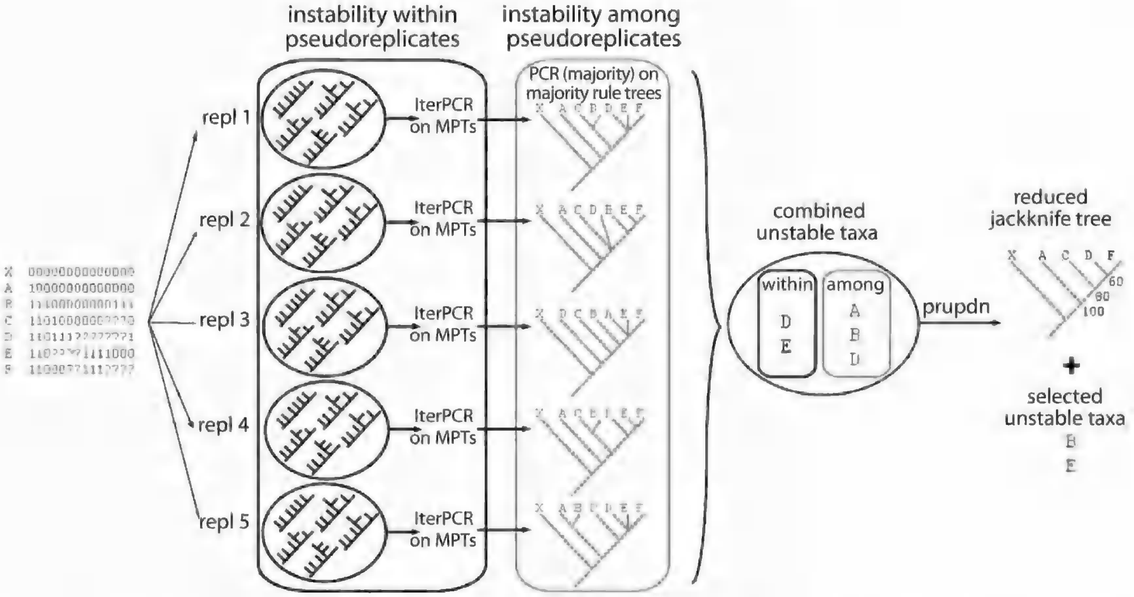

FIG. 3. Resampling support protocol indicating the steps in which the analysis of unstable taxa is applied, as implemented in the TNT script *pcrjak.run* (see http://www.lillo.org.ar/phylogeny/tnt/scripts/pcrjak.run).

(Goloboff and Simmons 2014) exacerbating the problem. The best assessments of support, therefore, are obtained when multiple trees are found for each pseudoreplicate, and they are summarized by a strict consensus tree. The multiple trees for each pseudoreplicate can be found during resampling either explicitly (by actual searches) or implicitly (i.e., finding a single tree approaching optimality, then collapsing groups lost on TBR rearrangements producing equally optimal trees; see Goloboff et al., 2008).

The identification of taxa that affect resampling support measures can be approached in several ways. Some authors (Wilkinson, 1996; Pattengale et al., 2011; Aberer and Stamatakis, 2011; Aberer et al., 2013) have analyzed a single combined set of topologies, derived from all the pseudoreplicates. This is made more difficult when the results for each of the individual pseudoreplicates are summarized by means of a strict consensus: the unstable taxa cannot be identified a posteriori of the calculation of the strict consensus. To illustrate the problem, consider a dataset with a terminal with a missing entry in every single character. If the strict consensus is produced from the multiple trees for each pseudoreplicate, every one of those will be a complete bush. Subsequent pruning of terminals from those trees cannot produce an improved resolution; rather, the terminals must be pruned from the original tree(s) for each pseudoreplicate, not from their (full) strict consensuses.

In the original analysis of Pei et al. (in press), the strategy used to cope with the problem just discussed had been: (1) using a fixed sequence of random seeds to produce the pseudoreplicate datasets and saving a single binary tree per pseudoreplicate; (2) using approximate methods to identify the effect on the majority rule of different taxon prunings in the resulting set of binary trees; and (3) once a set of unstable taxa is identified, the pseudoreplicate datasets are generated again with the same sequence of random seeds and the binary trees are collapsed by applying the implicit TBR-collapsing described above on the resampled dataset. This avoids having to search again for a large number of pseudoreplicate datasets; the optimal trees will not change and they can simply be used to collapse (via TBR) those groups that are unsupported by the pseudoreplicate.

A Combined Method for Detecting Instability

The present paper explores an alternative way to deal with the problem that unstable taxa cannot be identified from the strict consensus resulting from the multiple trees produced by every pseudoreplicate, taking advantage of the fact that the scripting facilities offered by TNT make it possible to easily explore different combinations of methods to summarize trees, and to identify potential candidates for pruning.

The main difference of the approach explored here is that it conducts two separate evaluations for unstable taxa, carried out first as the pseudoreplicate datasets are generated and analyzed, and then again on the resulting strict consensus trees. The first analysis aims to detect which taxa are commonly unstable among the most parsimonious topologies derived from a single pseudoreplicate. During each pseudoreplicate this evaluation is independently repeated and the MPTs of each pseudoreplicate are saved to temporary tree files (without collapsing) so that they do not have to be calculated again. The second analysis is conducted by analyzing the taxa that are unstable when comparing the 100 strict consensus trees derived from each of the replicates (fig. 3). This two-step procedure constitutes the major difference with previous approaches and provides a list of potentially unstable taxa that can decrease the support values in resampling measures. The final step consists of determining the optimal subset of unstable taxa that should be pruned to obtain an informative jackknife tree. Once the taxa are identified, they can be pruned from the trees saved for each pseudoreplicate for calculation of the reduced strict consensuses, followed by the majority rule consensus. We explore the implementation of this protocol for jackknife analysis, but equivalent implementations for bootstrap and symmetric resampling can be easily run through the use of an argument in the script used here (see below).

Taxon Instability within Pseudoreplicates: Given that for each pseudoreplicate a tree search and a strict consensus is performed, the detection of unstable taxa in this context is entirely equivalent to the problem of detecting unstable taxa for producing a reduced consensus. Therefore, we employ for this analysis the IterPCR method (Pol and Escapa, 2009) as implemented in TNT (Goloboff and Szumik, 2015). The taxa detected are in many cases known from highly incomplete specimens and have a large number of missing entries. These taxa, after the deletion of a few characters during the resampling procedures, become unstable in the tree search conducted in the perturbated dataset. Such taxa will create polytomies in the strict consensus tree that will obscure the relationships of the stable taxa in the analysis of a given pseudoreplicate. In our implementation, a taxon is added to a preliminary list of unstable taxa when it is detected as unstable in at least 15% of the pseudoreplicates (although this threshold value can be changed as an argument of the script in TNT).

Taxon Instability among Pseudoreplicates: The second analysis of taxon instability is conducted using the 100 strict consensus trees derived from each of the pseudoreplicates. The taxa that are unstable among these strict consensus trees are in many cases terminals that have a conflicting combination of characters and that are depicted in alternative positions depending on the combination of characters left in the perturbated dataset after the random deletion of certain characters. This procedure is performed using a modified version of the IterPCR script (Pol and Escapa, 2009) in which triplets are regarded as in agreement if they show the same resolution in more than half the topologies analyzed. This differs from the original implementation that counted agreement in triplets only when all the topologies shared the same resolution. This follows the logic of majority rule reduced consensus trees (Wilkinson, 1996) given that this is the method used for obtaining absolute frequencies for the jackknife support analysis. The set of taxa detected as unstable among the strict consensus trees derived from the 100 replicates is added to a preliminary list of unstable taxa.

OPTIMAL SET OF UNSTABLE TAXA: The final step consists of determining which of the taxa in the preliminary list affect the jackknife values in a significant way. Their effect on the resampling support values is then evaluated with the command *prupdn* (implemented by P.A.G.) in TNT ver 1.5 (Goloboff and Catalano, 2016). The preliminary list of unstable taxa is input to this command, which evaluates different combinations of prunes to improve the majority rule consensus. For each combination the command *prupdn* evaluates an optimality function *E*:

$$E = (P + \sum jak) / (T - 2)$$

where *jak* are the jackknife support values of each node of the pruned tree, *P* is a penalty for pruning taxa, and *T* is the number of taxa with least possible prunings. The penalty factor (*P*) is a function of the number of taxa removed (*R*) and a scaling factor (*F*) that can be adjusted between 0 and 100, with $P = 100\, R\, (1 - F^2)$. Using $F = 1$ results in no penalization for pruning taxa ($P = 0$) and selects the combination that maximizes the sum of support values of the reduced jackknife tree. Using values of $F > 1$ will penalize the pruning of taxa and values of $F < 1$ will favor the pruning of taxa. Further options of this command can be found in the TNT documentation (Goloboff and Catalano, 2016).

Note that the *prupdn* command evaluates *E* for a large number of combinations of prunes (the number of combinations to try is somewhat reduced by using groups with a high frequency as "separators" [see TNT documentation], but it is still a large number). This is why it is important to produce a preliminary list of taxa potentially affecting support values, found by more approximate methods that do not use an explicit optimality criterion, instead of pruning all combinations of all taxa. In the present implementation, that preliminary list is obtained by applying IterPCR to improve the strict consensus for the results of individual pseudoreplicates, and a modified IterPCR that evaluates triplet frequency for the majority rule tree of the consensuses resulting from all the pseudoreplicates. It would be easy to modify the script used here so that alternative ways to produce preliminary lists of prunes are used (e.g., with the TNT commands chkmoves, prunnelsen, or prunmaj).

IMPLEMENTATION: The entire procedure is implemented in *pcrjak.run* (see http://www.lillo.org.ar/phylogeny/tnt/scripts/pcrjak.run), a TNT script that takes as input the dataset and performs the jackknife pseudoreplicates, applies the two successive steps of identification of unstable taxa (within and among replicates), and then identifies the optimal set of unstable taxa that can be pruned in order to maximize the function *E* (see above).

To run the script, the user needs to call the script giving the data matrix name as the first argument (e.g., *pcrjak datafile.tnt;*). The default option is to use the jackknife resampling method, but this can be changed giving a second argument. For example, *pcrjak datafile.tnt boot;* will perform the same procedure on the data matrix *datafile.tnt* using the bootstrap resampling method.

The outputs of the script are two files. First, a graphical tree (*pcrjak.svg*) that shows the reduced jackknife tree with their absolute frequency values (after ignoring the position of the unstable taxa). Second, a plain text file (*pcrjak.out*) in which the same tree is depicted (in text format) followed by the list of the selected unstable taxa and the lists of taxa that are unstable within and among pseudoreplicates. We recommend using the command-based version of TNT (either for Windows, Mac, or Linux) so that all temporary tree files are deleted automatically.

RESULTS

Applying the above-described protocol for the TWiG dataset results in the identification of 35 taxa that decrease the jackknife support values. When the positions of these taxa are ignored for constructing the majority rule tree (reduced majority rule consensus tree; Wilkinson, 1996), a total of 104 nodes are recovered in this tree (in comparison to the 68 nodes present in the jackknife tree when all the taxa are included). The reduced jackknife tree (fig. 4) has an average support value of 77%, showing that numerous clades of coelurosaurian theropods are well supported within the context of the TWiG dataset. The support of the 36 nodes retrieved in the reduced jackknife analysis that are absent from the complete jackknife analyses was obscured only by the alternative positions of unstable taxa.

The protocol implemented identified 33 taxa that are unstable within the jackknife pseudoreplicates and 55 taxa that are unstable among the 100 strict consensuses of the jackknife pseudoreplicates (table 1). These two sets of unstable taxa are only partially overlapping and share 22 taxa (*Graciliraptor, Atrociraptor, Utahraptor, Saurornitholestes, Shanag, Austroraptor, Hesperonychus, Luanchuanraptor, Yurgovuchia*, IVPP V22530, *Archaeopteryx* Haarlem, IGM 10044, *Iaceornis, Limenavis, Liaoningornis, Erlikosaurus, Enigmosaurus, Nanshiungosaurus, Ceratonykus, Beishanlong, Mirischia, Velociraptor osmolskae*). The partial overlap among these taxon sets shows that taxa that are unstable within trees found in pseudoreplicates are not necessarily unstable in the strict consensuses among pseudoreplicates. Out of the combined set of 66 unstable taxa detected by this procedure, the command *prupdn* found that 35 taxa (table 1) are the ones that maximize the optimality function *E* and therefore more markedly decrease jackknife support values. The composition of these 35 taxa highlights the importance of the two-step procedure for identifying unstable taxa: five of them are unstable only within the trees from each pseudoreplicate, 14 of them are unstable only among the strict consensuses derived from each pseudoreplicate, and finally 16 taxa listed above were detected as unstable both within and among pseudoreplicates.

Many of the taxa detected as unstable are known from incomplete specimens, in particular those detected to vary within pseudoreplicates, having an average of 85% of missing entries. Taxa detected as unstable among pseudoreplicates have an average of 76% of missing entries (slightly larger than the 65% average across the entire dataset). The amount of missing entries, however, does not unequivocally indicate instability, given that several taxa detected as unstable have a percentage of missing entries that is below the overall average for the dataset (15 of the taxa that are unstable among pseudoreplicates and 3 of the taxa that are unstable within). Similarly, there are five taxa with >90% missing entries that are not unstable among jackknife trees. The distribution of missing entries among terminal taxa across time (fig. 5; gray circles) shows that taxa detected as unstable in jackknife trees within (fig. 5; green triangles) or among (fig. 5; blue squares) pseudoreplicates, as well as the subset selected by the *prupdn* command (fig. 5; solid red circles) include some taxa that are fairly well known (e.g., *Ornitholestes, Sinovenator, Sinosauropteryx*), for which the instability likely derives from character conflict more than from absence of information.

Below we discuss the results that arise from the jackknife analysis based on reduced majority rule consensus for several clades of coelurosaurian theropods, contrasting with those obtained when all the taxa are included in the support trees and when the results of the jackknife analysis are summarized using the majority rule consensus (as in the default option of TNT).

COELUROSAURIA: The monophyly of Coelurosauria has high support, but the taxon sampling includes few non-coelurosaurian theropods. *Tugulusaurus* is detected as unstable and causing low supports at the base of Coelurosauria in the jackknife analysis including all taxa (fig. 2). Ignoring this taxon in the reduced jackknife consensus (fig. 4) resolves *Zuolong* as the sister group of the clade formed by Maniraptorifomes and Tyrannosauroidea (although still with low support 66%; fig. 4). Multiple subclades within Tyrannosauroidea are well supported (>90%) in both the complete jackknife tree and the reduced jackknife trees (figs. 2, 4).

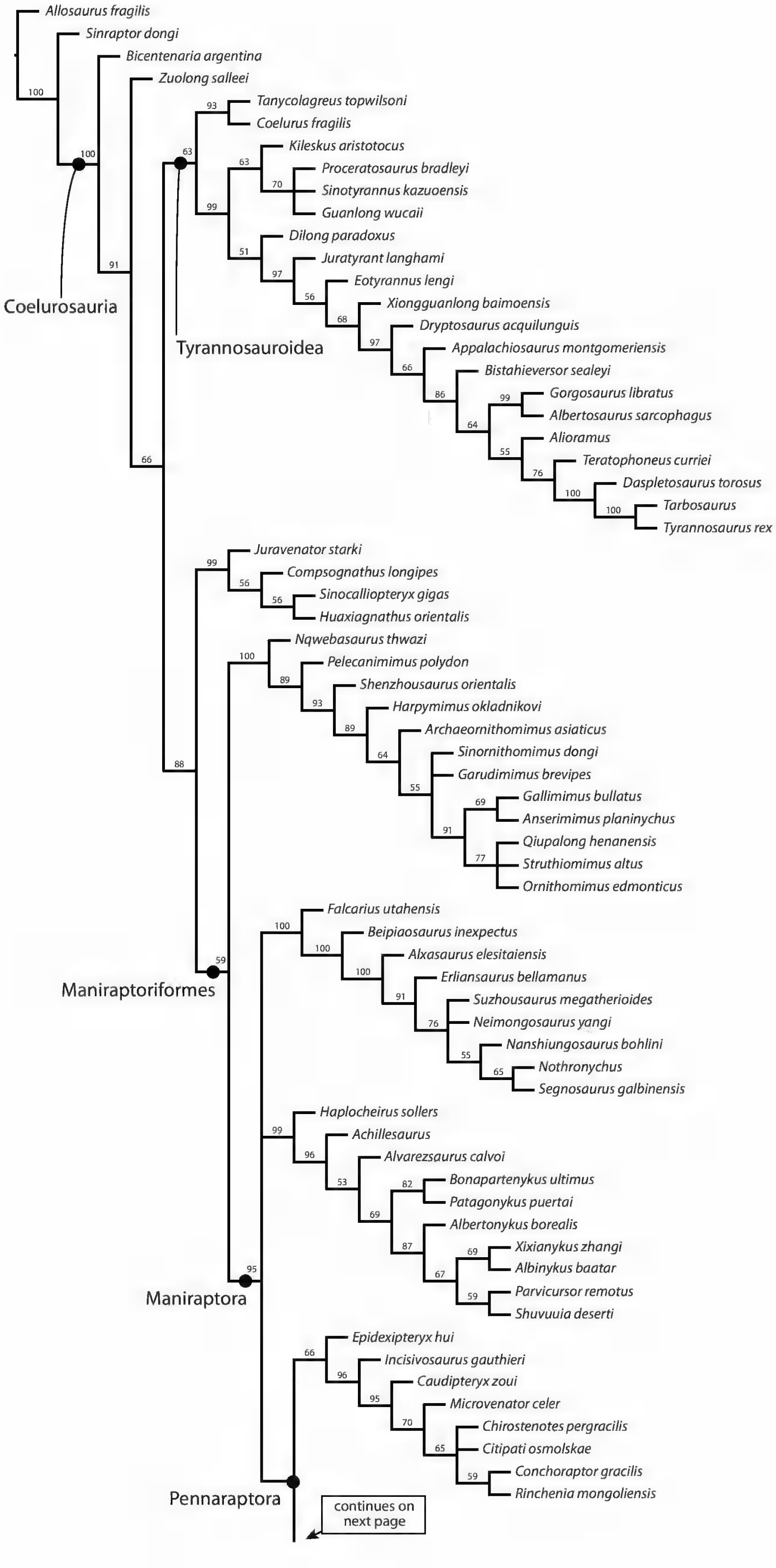
Allosaurus fragilis
Sinraptor dongi
Bicentenaria argentina
Zuolong salleei
Tanycolagreus topwilsoni
Coelurus fragilis
Kileskus aristotocus
Proceratosaurus bradleyi
Sinotyrannus kazuoensis
Guanlong wucaii
Dilong paradoxus
Juratyrant langhami
Eotyrannus lengi
Xiongguanlong baimoensis
Dryptosaurus acquilunguis
Appalachiosaurus montgomeriensis
Bistahieversor sealeyi
Gorgosaurus libratus
Albertosaurus sarcophagus
Alioramus
Teratophoneus curriei
Daspletosaurus torosus
Tarbosaurus
Tyrannosaurus rex
Juravenator starki
Compsognathus longipes
Sinocalliopteryx gigas
Huaxiagnathus orientalis
Nqwebasaurus thwazi
Pelecanimimus polydon
Shenzhousaurus orientalis
Harpymimus okladnikovi
Archaeornithomimus asiaticus
Sinornithomimus dongi
Garudimimus brevipes
Gallimimus bullatus
Anserimimus planinychus
Qiupalong henanensis
Struthiomimus altus
Ornithomimus edmonticus
Falcarius utahensis
Beipiaosaurus inexpectus
Alxasaurus elesitaiensis
Erliansaurus bellamanus
Suzhousaurus megatherioides
Neimongosaurus yangi
Nanshiungosaurus bohlini
Nothronychus
Segnosaurus galbinensis
Haplocheirus sollers
Achillesaurus
Alvarezsaurus calvoi
Bonapartenykus ultimus
Patagonykus puertai
Albertonykus borealis
Xixianykus zhangi
Albinykus baatar
Parvicursor remotus
Shuvuuia deserti
Epidexipteryx hui
Incisivosaurus gauthieri
Caudipteryx zoui
Microvenator celer
Chirostenotes pergracilis
Citipati osmolskae
Conchoraptor gracilis
Rinchenia mongoliensis
Coelurosauria
Tyrannosauroidea
Maniraptoriformes
Maniraptora
Pennaraptora

continues on next page

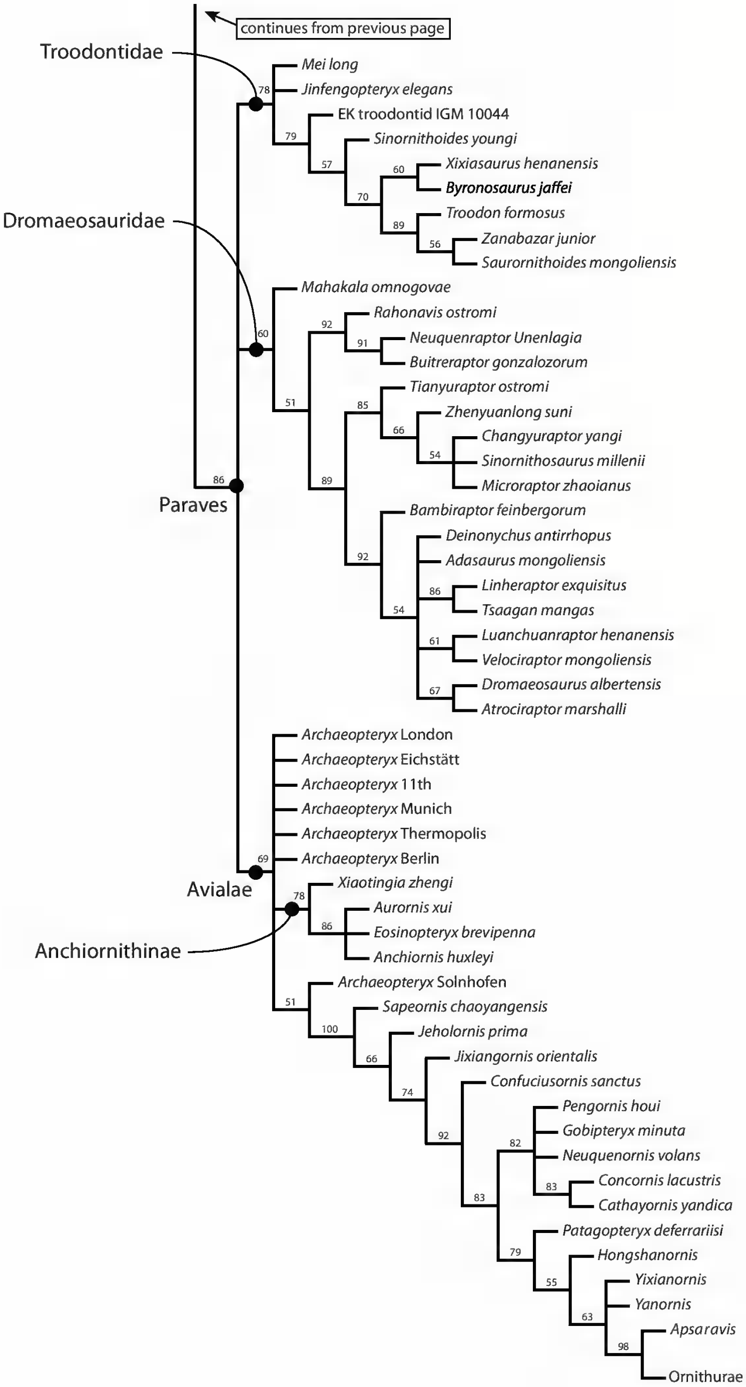
continues from previous page
Troodontidae
Dromaeosauridae
Paraves
Avialae
Anchiornithinae
78
Mei long
Jinfengopteryx elegans
79
EK troodontid IGM 10044
57
Sinornithoides youngi
70
60
Xixiasaurus henanensis
Byronosaurus jaffei
89
Troodon formosus
56
Zanabazar junior
Saurornithoides mongoliensis
60
Mahakala omnogovae
51
92
Rahonavis ostromi
91
Neuquenraptor Unenlagia
Buitreraptor gonzalozorum
89
85
Tianyuraptor ostromi
66
Zhenyuanlong suni
54
Changyuraptor yangi
Sinornithosaurus millenii
Microraptor zhaoianus
86
92
Bambiraptor feinbergorum
54
Deinonychus antirrhopus
Adasaurus mongoliensis
86
Linheraptor exquisitus
Tsaagan mangas
61
Luanchuanraptor henanensis
Velociraptor mongoliensis
67
Dromaeosaurus albertensis
Atrociraptor marshalli
69
Archaeopteryx London
Archaeopteryx Eichstätt
Archaeopteryx 11th
Archaeopteryx Munich
Archaeopteryx Thermopolis
Archaeopteryx Berlin
78
Xiaotingia zhengi
86
Aurornis xui
Eosinopteryx brevipenna
Anchiornis huxleyi
51
Archaeopteryx Solnhofen
100
Sapeornis chaoyangensis
66
Jeholornis prima
74
Jixiangornis orientalis
92
Confuciusornis sanctus
83
82
Pengornis houi
Gobipteryx minuta
Neuquenornis volans
83
Concornis lacustris
Cathayornis yandica
79
Patagopteryx deferrariisi
55
Hongshanornis
63
Yixianornis
Yanornis
98
Apsaravis
Ornithurae

FIG. 4. Absolute frequency jackknife tree for the dataset of Pei et al. (in press) obtained by the script *pcrjak. run*, ignoring the alternative positions of 35 taxa detected as unstable in the support analysis that decrease jackknife values.

TABLE 1

Taxa detected as unstable within and among jackknife pseudoreplicates and those selected by *prupdn* as unstable taxa decreasing support in jackknife support analysis

Unstable among jackknife pseudoreplications	Unstable within jackknife pseudoreplicates	Selected by *prupdn* as unstable taxa
–	*Acheroraptor*	*Acheroraptor*
Achillobator	–	*Achillobator*
Adasaurus	–	–
–	*Albinykus*	–
Archaeopteryx Haarlem	*Archaeopteryx* Haarlem	*Archaeopteryx* Haarlem
Atrociraptor	*Atrociraptor*	–
Austroraptor	*Austroraptor*	*Austroraptor*
Avimimus	–	*Avimimus*
Balaur	–	*Balaur*
–	*Baptornis*	–
Beishanlong	*Beishanlong*	*Beishanlong*
Buitreraptor	–	–
Byronosaurus	–	–
Ceratonykus	*Ceratonykus*	*Ceratonykus*
Changyuraptor	–	–
Compsognathus	–	–
Dakotaraptor	–	*Dakotaraptor*
Dromaeosaurus	–	–
Enigmosaurus	*Enigmosaurus*	*Enigmosaurus*
Erlikosaurus	*Erlikosaurus*	*Erlikosaurus*
Graciliraptor	*Graciliraptor*	*Graciliraptor*
Hesperonychus	*Hesperonychus*	*Hesperonychus*
–	*Hesperornis*	–
Iaceornis	*Iaceornis*	–
IGM 10044	IGM 1044	–
Ingenia	–	*Ingenia*
IVPP V22530	IVPP V22530	IVPP V22530
Jinfengopteryx	–	–
Liaoningornis	*Liaoningornis*	*Liaoningornis*
Limenavis	*Limenavis*	–
Linhenykus	–	*Linhenykus*
Linheraptor	–	–
–	*Lithornis*	–
Luanchuanraptor	*Luanchuanraptor*	–
Mei	–	–
Mirischia	*Mirischia*	*Mirischia*
Mononykus	–	*Mononykus*
Nanshiungosaurus	*Nanshiungosaurus*	–
Neimongosaurus	–	–
–	*Neuquenornis*	–
Ornitholestes	–	*Ornitholestes*

TABLE 1 *continued*

Unstable among jackknife pseudoreplications	Unstable within jackknife pseudoreplicates	Selected by *prupdn* as unstable taxa
Oviraptor	–	*Oviraptor*
–	*Patagopteryx*	–
Rahonavis	–	–
–	*Rinchenia*	–
Saurornithoides	–	–
Saurornitholestes	*Saurornitholestes*	*Saurornitholestes*
Shanag	*Shanag*	*Shanag*
Sinornithoides	–	–
Sinosauropteryx	–	*Sinosauropteryx*
Sinovenator	–	*Sinovenator*
Sinusonasus	–	*Sinusonasus*
–	*Songlingornis*	*Songlingornis*
Suzhousaurus	–	–
–	*Therizinosaurus*	*Therizinosaurus*
Troodon	–	–
Tsaagan	–	–
Tugulusaurus	–	*Tugulusaurus*
Unenlagia	–	–
Utahraptor	*Utahraptor*	*Utahraptor*
–	*Vorona*	*Vorona*
Velociraptor osmolskae	*Velociraptor osmolskae*	*Velociraptor osmolskae*
Xixiasaurus	–	–
Yi	–	*Yi*
Yurgovuchia	*Yurgovuchia*	*Yurgovuchia*
Zanabazar	–	–

MANIRAPTORIFORMES: This clade had low support (62%; fig. 2) and its early-diverging nodes were collapsed in the jackknife analysis including all the taxa, but the reduced jackknife analysis reveals high support (88%) for the node including compsognathids, ornithomimosaurians, and later-diverging coelurosaurians. The reduced jackknife tree also resolves compsognathids as earlier diverging than ornithomimosaurians, although with low support (59%; fig. 4). This improvement is a consequence of the unstable position of *Ornitholestes* and two compsognathids (the highly incomplete *Mirischia* and the better-known *Sinosauropteryx*) that were unstable within many replicates. The monophyly of both Compsognathidae and Ornithomimosauria are highly supported in the reduced jackknife tree (99% and 100%; fig. 4).

The support of Maniraptora is moderate in the jackknife based on the complete taxon set (75%; fig. 2), but increases to 95% in the reduced jackknife tree. This difference is due to the unstable behavior of pennaraptorans of uncertain affinities that are excluded from the reduced jackknife tree (see below). The monophyly of the two earliest-diverging branches (Alvarezsauroidea and Therizinosauria) is also extremely well supported (>90%) in both the complete jackknife tree and the reduced jackknife trees (figs. 2, 4).

PENNARAPTORA: The difference in the complete jackknife tree and the reduced jackknife trees in this clade is the largest of the analysis (figs. 2, 4). A high-order polytomy is present when all the taxa are included and poorly supported groups are collapsed. Pennaraptora has moderate support in the reduced tree (78%; fig.

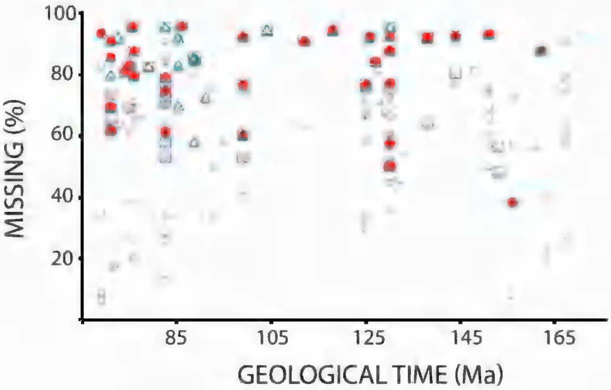

FIG. 5. Distribution of missing data in terminal taxa of the TWiG dataset (Pei et al., in press) through geological time. Each point represents a terminal taxon, vertical axis represents percentage of missing data in the matrix, and horizontal axis represents age of the terminal taxon (in millions of years). The graph represents all terminal taxa (gray circles), taxa identified as unstable within each pseudoreplicate (green triangles), taxa identified as unstable among the strict consensuses of pseudoreplicates (blue squares), and subset of taxa identified as unstable by the *prupdn* command (solid red circles).

4) and resolves the scansoriopterygid *Epidexipteryx* and oviraptorosaurians as the sister group of Paraves. Oviraptorosaurians are well supported in the reduced jackknife tree (96%; fig. 4) as well as in the complete jackknife tree (89%; fig. 2). Support within this clade is low even when unstable oviraptorids are excluded (e.g., *Oviraptor*, *Ingenia*), except for the early-diverging position of *Incisivosaurus* within this clade. One of the unstable taxa excluded from the reduced jackknife tree that resolves Pennaraptora is the bizarre scansoriopterygid *Yi qi*, reflecting the conflictive history of hypotheses about scansoriopterygid affinities (Zhang et al., 2008; Turner et al., 2012; Agnolín and Novas, 2013; Godefroit et al., 2013).

PARAVES: In the jackknife tree including all taxa, Paraves has very low support, but this clade is retrieved in the reduced jackknife tree with a relatively high nodal support (86%; fig. 4). The relationships between the three main paravian clades (Dromaeosauridae, Troodontidae, Avialae) are weakly supported in the reduced jackknife tree, demonstrating the lack of strong support for the topology retrieved in the MPTs (fig. 1), in which Deinonychosauria is depicted as monophyletic. The lack of support for the relationships of the three major clades of paravians is not caused by unstable taxa but instead due to character conflict in this dataset.

Dromaeosauridae is collapsed in the jackknife tree including all taxa and has low support (60%; fig. 4) when unstable taxa are pruned from the jackknife trees. The internal relationships of Dromaeosauridae also have relatively low supports, such as the nodes within Microraptoria and within Eudromaeosauria. The only nodes that are well supported in Dromaeosauridae are Microraptoria, Eudromaeosauria, and the node that clusters these two clades (89%–92%; fig. 4). Additionally, the support for Unenlagiinae and for the sister group relationship of *Buitreraptor* and *Unenlagia*/*Neuquenraptor* are also well supported (>90%; fig. 4) when the unstable *Austroraptor* is excluded. These well-supported dromaeosaurid nodes were completely collapsed in the jackknife tree including all the taxa, so that unstable dromaeosaurids obscured the support of these nodes. These support values are obtained after pruning a total of 11 dromaeosaurids (out of the 31 included in this matrix), identified as unstable by the *prupdn* command (i.e., *Saurornitholestes*, *Graciliraptor*, *Hesperonychus*, *Shanag*, *Zhenyuanlong*, *Dakotaraptor*, *Yurgov-*

uchia, Austroraptor, Achillobator, IVPP V22530, *and Utahraptor*). Dromaeosaurids concentrate the largest number of unstable taxa among all coelurosaurian clades in this dataset, and it is worth noting that some of these taxa are among the most complete of the 31 pruned taxa.

In contrast to Dromaeosauridae, Troodontidae is retrieved as moderately supported (73%; fig. 2) in the jackknife tree when all the taxa are included. The support for this node increases marginally (78%; fig. 4) in the reduced jackknife tree, after the exclusion of *Sinusonasus* and *Sinovenator.* As in the case of Dromaeosauridae, the internal relationships of troodontids have generally low support (56–89%; fig. 4).

Anchiornithinae is recovered in the jackknife tree when all the taxa are included (68%; fig. 2) and when the unstable taxa are pruned (78%; fig. 4). The early-diverging position of *Xiaotingia* is also present in both trees, although pruning the unstable taxa increases the support value from 73% (fig. 2) to 96% (fig. 4). Note that none of the anchiornithines are pruned in the reduced jackknife tree, so this increase is caused by non-anchiornithine taxa that influence the results of the jackknife analysis of this node.

The analysis of Pei et al. (in press) retrieves Anchiornithinae as the sister group of Avialae in the MPTs. The sister group relationship of Anchiornithinae and Avialae occurs with frequency below 50% in the complete jackknife tree, but occurs in the reduced jackknife tree with moderate support (69%; fig. 4). The affinities of anchiornithines are one of the most contentious issues in paravian systematics and vary significantly in previous analyses depending on the taxon and character sampling schemes (see Agnolín and Novas, 2013; Brusatte et al., 2014; Xu et al., 2015, 2017; Foth and Rauhut, 2017; Hu et al., 2018). This conflict is clearly not determined by unstable taxa within this clade but is affected by unstable taxa of other clades (e.g., dromaeosaurids and avialans) and the presence of character conflict (Xu and Pol, 2012).

Finally, Avialae is retrieved only in the reduced jackknife tree with low support (<50%; fig. 4), which is partially caused by the scoring of *Archaeopteryx* at the specimen level. After pruning the Haarlem specimen that was identified as highly unstable, most specimens of *Archaeopteryx* are in a polytomy at the base of Avialae in the reduced jackknife tree (fig. 4). Previous authors have noted the presence of character conflict related to the affinities of *Archaeopteryx* with early-diverging avialans (Xu et al., 2011; Turner et al., 2012; Xu and Pol, 2012; Godefroit et al., 2013) and this character conflict is present in the analyzed dataset. Combining all the specimens into a single composite terminal taxon does not result in high support for the position of *Archaeopteryx* at the base of Avialae. After combining all the specimens into a single OTU and running the *pcrjak* script the support for Avialae (*Archaeopteryx* + later-diverging birds) is still extremely low (53%). The low support retrieved in the reduced jackknife trees for the position of *Archaeopteryx* at the early-diverging node of Avialae reflects the presence of the character conflict noted by previous authors. The node formed by *Sapeornis* and later-diverging avialans is retrieved as monophyletic with moderately high support (83%; fig. 2) and maximal values are obtained after pruning unstable taxa (100%; fig. 4). Within avialans, some unstable taxa are pruned (e.g., *Vorona, Liaoningornis, Songlingornis, Limenavis*), but these are involved in small polytomies in the complete jackknife tree (fig. 2).

CONCLUSIONS

The protocol implemented for producing reduced jackknife trees reveals that a large number of coelurosaurian clades are well supported in the latest version of the TWiG dataset (Pei et al., in press) when unstable taxa are pruned from the trees found during the resampling procedure. The unstable taxa that decrease nodal support are detected in both the optimal trees within individual jackknife pseudoreplicates and among the strict consensuses of the different jackknife pseudoreplicates. The two-step approach used here for parsimony analysis is automated in a script for TNT (Goloboff et al., 2008) and differs from previous attempts to identify unstable taxa and to produce well-resolved trees in resampling procedures of nodal support (e.g., bootstrap/jackknife; Wilkinson, 1996; Pattengale et al., 2011; Aberer and Stamatakis, 2011; Aberer et al., 2013).

Previous support analyses on the TWiG dataset resulted in highly collapsed jackknife trees, which were largely influenced by the presence of fragmentary and/or conflictive taxa that hide nodal support for multiple clades. A total of 31 unstable taxa are identified as the most influential for obscuring nodal support. Although some of these taxa are fragmentary, others have a comparatively low amount of missing entries and suggest character conflict is also a cause of their instability. Major clades that are well supported in the reduced jackknife tree include Coelurosauria, Maniraptoriformes, Compsognathidae, Ornithomimosauria, Alvarezsauroidea, Therizinosauria, Oviraptorosauria. Other clades, in turn, have moderate to low support even when unstable taxa are pruned from the resampling trees: Maniraptora, Pennaraptora, Paraves, Dromaeosauridae, Troodontidae, Anchiornithinae, and early-diverging nodes of Avialae.

Reduced jackknife analysis as explored here not only reveals well-supported clades but (more importantly) also highlights specific terminal taxa producing low support of surrounding clades (due to character conflict or lack of enough phylogenetic information). This helps to identify taxa or areas of the phylogeny that require further research efforts in data collection based on comparative anatomical studies.

ACKNOWLEDGMENTS

This study was possible thanks to the International Pennaraptoran Dinosaur Symposium held at the University of Hong Kong and supported by Kenneth H.C. Fung and First Initiative Foundation. This study was supported by the Proyecto de Unidad Ejecutora from CONICET (PUE0070 to P.A.G). TNT is made freely available thanks to the Willi Hennig Society.

REFERENCES

Aberer, A., and A. Stamatakis. 2011. A simple and accurate method for rogue taxon identification. IEEE BIBM 2011, Atlanta, GA, November 2011.

Aberer, A., Krompas, D., and Stamatakis, A. 2013. Pruning rogue taxa improves phylogenetic accuracy: an efficient algorithm and webservice. Systematic Biology 62: 162–166.

Agnolín, F.L., and F.E. Novas. 2013. Avian ancestors: A review of the phylogenetic relationships of the theropods Unenlagiidae, Microraptoria, *Anchiornis* and Scansoriopterygidae. Dordrecht: Springer.

Brusatte, S.L., G.T. Lloyd, S.C. Wang, and M.A. Norell. 2014. Gradual assembly of avian body plan culminated in rapid rates of evolution across the dinosaur-bird transition. Current Biology 24 (20): 2386–2392.

Farris, J.S., V.A. Albert, M. Källersjö, D. Lipscomb, and A.G. Kluge. 1996. Parsimony jackknifing outperforms neighbor-joining. Cladistics 12: 99–124.

Foth, C., and O.W.M. Rauhut. 2017. Re-evaluation of the Haarlem *Archaeopteryx* and the radiation of maniraptoran theropod dinosaurs. BMC Evolutionary Biology 17: 236.

Gauthier, J.A. 1986. Saurischian monophyly and the origin of birds. *In* K. Padian (editor), The origin of birds and the evolution of flight: 1–55. San Francisco: California Academy of Science.

Godefroit, P., et al. 2013. A Jurassic avialan dinosaur from china resolves the early phylogenetic history of birds. Nature 498: 359–362.

Goloboff, P.A., and S.A. Catalano. 2016. TNT version 1.5, including a full implementation of phylogenetic morphometrics. Cladistics 32 (3): 221–238.

Goloboff, P.A., and D. Pol. 2005. Parsimony and bayesian phylogenetics. *In* V. Albert (editors), Parsimony, phylogeny, and genomics: 148–159. Oxford: Oxford University Press.

Goloboff, P.A., and M.P. Simmons. 2014. Bias in tree searches and its consequences for measuring group supports. Systematic Biology 63 (6): 851–861.

Goloboff, P.A., and C.A. Szumik. 2015. Identifying unstable taxa: efficient implementation of triplet-based measures of stability, and comparison with Phyutility and RogueNaRok. Molecular Phylogenetics and Evolution 88: 93–104.

Goloboff, P.A., et al. 2003. Improvements to resampling measures of group support. Cladistics 19: 324–332.

Goloboff, P.A., J.S. Farris, and K.C. Nixon. 2008. TNT, a free program for phylogenetic analysis. Cladistics 24 (5): 774–786.

Hu, D.Y., et al. 2018. A bony-crested Jurassic dinosaur with evidence of iridescent plumage highlights complexity in early paravian evolution. Nature Communications 9: 217.

O'Connor, J.M.K., and C. Sullivan. 2014. Reinterpretation of the Early Cretaceous maniraptoran (Dinosauria: Theropoda) *Zhongornis haoae* as a scansoriopterygid-like non-avian, and morphological resemblances between scansoriopterygids and basal oviraptorosaurs. Vertebrata PalAsiatica 52 (1): 3–30.

Pattengale N., Aberer, A., Swenson, K., Stamatakis, A., and B. Moret. 2011. Uncovering hidden phylogenetic consensus in large datasets. IEEE/ACM Transactions on Computational Biology and Bioinformatics (TCBB) 8: 902–911.

Pei, R., et al. In press. Potential for powered flight neared by most close avialan relatives but few crossed its thresholds. Current Biology.

Pol, D., and I.H. Escapa. 2009. Unstable taxa in cladistic analysis: identification and the assessment of relevant characters. Cladistics 25: 515–527.

Simmons, M.P., and J.V. Freudenstein. 2011. Spurious 99% bootstrap and jackknife support for unsupported clades. Molecular Phylogenetics and Evolution 61: 177–191.

Turner, A.H., S.H. Hwang, and M.A. Norell. 2007. A small derived theropod from Öösh, early Cretaceous, Baykhangor Mongolia. American Museum Novitates 3557: 1–27.

Turner, A.H., P.J. Makovicky, and M.A. Norell. 2012. A review of dromaeosaurid systematics and paravian phylogeny. Bulletin of the American Museum of Natural History 371: 1–206.

Wilkinson, M., 1994. Common cladistic information and its consensus representation: reduced Adams and reduced cladistic consensus trees and profiles. Systematic Biology 43: 343–368.

Wilkinson, M. 1996. Majority rule reduced consensus and their use in bootstrapping. Molecular Biology and Evolution 13: 437–444.

Wilkinson, M., and M.J. Benton. 1995. Missing data and rhynchosaur phylogeny. Historical Biology 10: 137–150.

Wilkinson, M., J.L. Thorley, and P. Upchurch. 2000. A chain is no stronger than its weakest link: double decay analysis of phylogenetic hypotheses. Systematic Biology 49: 754-776.

Xu, X., You, H.L., Du, K., and F.L. Han. 2011. An *Archaeopteryx*-like theropod from China and the origin of Avialae. Nature 475: 465–470.

Xu, X., and D. Pol. 2013. *Archaeopteryx*, paravian phylogenetic analyses, and the use of probability-based methods for palaeontological datasets. Journal of Systematic Palaentology 12: 323–334.

Xu, X., et al. 2015. A bizarre Jurassic maniraptoran theropod with preserved evidence of membranous wings. Nature 521: 70.

Xu, X., et al. 2017. Modular evolution in an asymmetrically feathered troodontid with transitional features. Nature Communications 8: 14972.

Zhang, F.C., Z.H. Zhou, X. Xu, X.L. Wang, and C. Sullivan. 2008. A bizarre Jurassic maniraptoran from China with elongate ribbon-like feathers. Nature 455: 1105–1108.

Chapter 4

The Biogeography of Coelurosaurian Theropods and Its Impact on Their Evolutionary History

ANYANG DING,[1] MICHAEL PITTMAN,[1] PAUL UPCHURCH,[2] JINGMAI O'CONNOR,[3]
DANIEL J. FIELD,[4] AND XING XU[3]

ABSTRACT

The Coelurosauria are a group of mostly feathered theropods that gave rise to birds, the only dinosaurians that survived the Cretaceous-Paleogene extinction event and are still found today. Between their first appearance in the Middle Jurassic up to the end Cretaceous, coelurosaurians were party to dramatic geographic changes on the Earth's surface, including the breakup of the supercontinent Pangaea, and the formation of the Atlantic Ocean. These plate tectonic events are thought to have caused vicariance or dispersal of coelurosaurian faunas, influencing their evolution. Unfortunately, few coelurosaurian biogeographic hypotheses have been supported by quantitative evidence. Here, we report the first, broadly sampled quantitative analysis of coelurosaurian biogeography using the likelihood-based package BioGeoBEARS. Mesozoic geographic configurations and changes are reconstructed and employed as constraints in this analysis, including their associated uncertainties. We use a comprehensive time-calibrated coelurosaurian evolutionary tree produced from the Theropod Working Group phylogenetic data matrix. Six biogeographic models in the BioGeoBEARS package with different assumptions about the evolution of spatial distributions are tested against geographic constraints. Our results statistically favor the DIVALIKE+J and DEC+J models, which allow vicariance and founder events, supporting continental vicariance as an important factor in coelurosaurian evolution. Ancestral range estimation indicates frequent dispersal events via the Apulian route (connecting Europe and Africa during the Early Cretaceous) and the Bering land bridge (connecting North America and Asia during the Late Cretaceous). These quantitative results are consistent with commonly inferred Mesozoic dinosaurian dispersals and continental-fragmentation-induced vicariance events. In addition, we recognize the importance of Europe as a dispersal center and gateway in the Early Cretaceous, as well as other vicariance events such as those triggered by the disappearance of land bridges.

---

[1] Vertebrate Palaeontology Laboratory, Division of Earth and Planetary Science, the University of Hong Kong, Hong Kong.

[2] Department of Earth Sciences, University College London, London.

[3] Key Laboratory of Vertebrate Evolution and Human Origins, Institute of Vertebrate Paleontology & Paleoanthropology, Beijing; and CAS Center for Excellence in Life and Paleoenvironment, Beijing.

[4] Department of Earth Sciences, University of Cambridge, Cambridge.

INTRODUCTION

Coelurosauria is a clade of later-diverging theropod dinosaurians that includes Tyrannosauroidea, Compsognathidae, Ornithomimosauria, Alvarezsauroidea, Therizinosauria, Oviraptorosauria, Dromaeosauridae, Troodontidae, and Avialae (Brusatte et al., 2014). A large portion of coelurosaurians were feathered, while some of them, mainly members of Avialae, acquired powered flight ability (Xu et al., 2014). Most coelurosaurian clades lived from the Middle Jurassic to the end of the Cretaceous, with only a subset of avialan taxa (Aves) surviving the Cretaceous-Paleogene (K-Pg) extinction event (Xu et al., 2014). During the late Mesozoic, coelurosaurians and other dinosaurians lived through dramatic geographic changes (Upchurch et al., 2002): plate tectonic activity caused continents to break apart to form new oceans and seas, produced intermittent reconnections, and prompted fluctuations in sea level that further modified paleogeographic relationships (Condie, 1997). These geographic configurations and changes are presumed to have affected coelurosaurian populations and faunas, impacting their pattern and tempo of evolution (Benton and Harper, 2013). Evaluating this impact is crucial if we are to fully understand the most significant events in coelurosaurian evolution, including the acquisitions of herbivory and early theropod flight.

Biogeographic studies focus on the geography-dependent processes that lead to alterations in faunal distributions and speciation (Benton and Harper, 2013). Four of the most fundamental biogeographic processes are: (1) *dispersal*, when a fauna expands its distribution range; (2) *regional extinction*, when the distribution shrinks; (3) *sympatry*, when speciation happens within the ancestral distribution range of the fauna: and (4) *vicariance*, when speciation takes place due to the separation of two populations by a geographic barrier (Sereno, 1999a; Upchurch et al., 2002; Sanmartín and Ronquist, 2004). These processes play important roles in organismal evolution and are sensitive to geographic conditions.

Numerous biogeographic hypotheses have been proposed for clades within Coelurosauria, though the vast majority of these are narratives (by the definition of Ball (1975): 409) because they tend to read the fossil record literally. A few studies (e.g., Loewen et al. 2013) have applied quantitative phylogenetic biogeographic analyses to groups such as Tyrannosauroidea, but the majority of coelurosaurian subclades, and the group as a whole, have not been investigated using such approaches. At present, therefore, much of our knowledge of coelurosaurian biogeographic history comes from studies of Dinosauria as a whole (e.g., Bonaparte 1986; Upchurch et al. 2002; O'Donovan et al. 2018). To address these deficits, we perform the first quantitative biogeographic analysis focused on the Coelurosauria as a whole.

MESOZOIC PALEOGEOGRAPHY

The paleogeography of Pangaea provides an important backdrop to the evolution of coelurosaurians, and information on this topic is required in order to support the geographic constraints we apply in our biogeographic analyses. Below, therefore, we briefly outline key aspects of Mesozoic paleogeography.

The Mesozoic witnessed the breakup of the supercontinent Pangaea and the establishment of global geography close to the modern arrangement (Scotese, 2001). However, narrow land bridges connecting isolated landmasses did appear during short time intervals, and shallow epicontinental seas existed throughout the Mesozoic, especially within Laurasian landmasses (Poropat et al., 2016)

During the early Mesozoic all continents were joined together to form Pangaea, although the Laurasia-Gondwana connection was present only between North America and (Africa + South America) (Smith et al., 2004). The breakup of Pangaea began during the Middle Jurassic, starting with the separation of North America from South America, together with the opening of the Northern Atlantic Ocean (Bardet et al., 2014). The complete separation of Laurasia and Gondwana dates back to the Kimmeridgian stage of the Late Jurassic (Gaina et al., 2013). Rifting and sea floor spreading among Africa, Indo-Madagascar, and Antarctica began later, during the Tithonian (Seton et al., 2012). The Turgai Sea existed between Asia and Europe throughout the late Mesozoic (especially the Late Cretaceous), although intermittent land connections occurred because of sea level fluctuations (Baraboshkin et al., 2003; Smith et al., 2004). During the Late Jurassic and earliest Cretaceous, Gondwana gradually separated into two large continents comprising South America + Africa (Samafrica) and Antarctica + Indo-Madagascar + Australia (East Gondwana) (Eagles and König, 2008). However, the sequence and timing of the breakup of Gondwana remain controversial (e.g., Sereno et al., 2004; Krause et al., 2006; Krause et al., 2007; Upchurch, 2008; Ali and Krause, 2011) and several workers have proposed that South America and Antarctica maintained a contact via Patagonia and the West Antarctic Peninsula throughout some or all of the Cretaceous (see review in Poropat et al. (2016)). During the earliest Cretaceous, the Apulian route was established (Zarcone et al., 2010). This connection between southwestern Europe and northwestern Africa was the first between Laurasia and Gondwana after the breakup of Pangaea (Ezcurra and Agnolín, 2012). The land connection between eastern North America and western Europe finally disappeared with the full establishment of the North Atlantic Ocean in the Barremian or Aptian (Seton et al., 2012). Later, in the late Aptian and Albian stages, the Bering land bridge connected northeastern Asia and northwestern North America for the first time (Plafker and Berg, 1994). This land bridge was probably absent during the Cenomanian-Santonian, but was potentially reestablished in the late Campanian and perhaps the Maastrichtian (Brikiatis, 2014). The Western Interior Seaway separating North America into eastern and western portions (known as Appalachia and Laramidia respectively) was present throughout much of the Late Cretaceous until a possible reconnection during the Maastrichtian (Smith et al., 2004; Farke and Phillips, 2017). Africa and South America separated from each other at the end of the Albian Stage, after the isolation of Indo-Madagascar during the Aptian Stage (Eagles and König, 2008). India separated from Madagascar during the latest Cretaceous (Plafker and Berg, 1994). By the end of the Cretaceous, global geography had a configuration that resembled the modern one, though Africa and India did not collide with Eurasia, and the Patagonia-Antarctica connection might not have been severed, until the Cenozoic (Matthews et al., 2016).

GEOGRAPHIC AND TEMPORAL DISTRIBUTION OF COELUROSAURIANS

Most known fossil coelurosaurians are from Laurasia (1083 occurrences recorded at the time of writing in the Paleobiology Database, https://paleobiodb.org/), with only a few occurrences in Gondwana (59 recorded in the Paleobiology Database). Currently, the earliest-known coelurosaurians are the proceratosaurids *Proceratosaurus* (von Huene, 1926) and *Kileskus* (Averianov et al., 2010) from the Bathonian stage of the Middle Jurassic of southern England and central Russia respectively. The earliest-diverging coelurosaurians are *Bicentenaria* from Argentina (Novas et al., 2012), *Coelurus* from North America (Marsh, 1879), and *Zuolong* from China (Choiniere et al., 2010a). The occurrences of tyrannosauroids during the Middle Jurassic and early-diverging paravians during the early Late Jurassic (e.g., *Anchiornis*) imply that major lineages of coelurosaurians were established by the Middle to Late Jurassic (Rauhut et al., 2010; Choiniere et al., 2012). Some authors have argued that the clades, including Compsognathidae, Tyrannosauroidea, and Maniraptoriformes, probably originated during or even before the Middle Jurassic (Rauhut et al., 2010), and so predate the separation of Laurasia and Gondwana. The currently known geographic and temporal distributions of the major coelurosaurian clades Tyrannosauroidea, Compsognathidae, Ornithomimosauria, Alvarezsauroidea, Therizinosauria, Oviraptorosauria, Dromaeosauridae, Troodontidae, and Avialae are discussed in more detail below.

TYRANNOSAUROIDEA: Tyrannosauroids include the infamous *Tyrannosaurus rex* and its closest relatives (Brusatte et al., 2010). Early-diverging Jurassic tyrannosauroids had a wide distribution in Laurasia as indicated by *Guanlong* from Asia (Xu et al., 2006), *Juratyrant* from Europe (Brusatte and Benson, 2013), and *Stokesosaurus* from North America (Benson, 2008). It is inferred that dispersal events within Laurasian landmasses occurred during that period of time (Rauhut et al., 2010). On the other hand, tyrannosaurids are known mostly from the Late Cretaceous of Asia and western North America (Brusatte et al., 2010). The existence of closely related taxa in both Asia and western North America just before the end of the Cretaceous, as in other coelurosaurian clades, may suggest faunal exchange events between these landmasses at that time (Brusatte et al., 2010). Traditionally, it was thought that tyrannosauroids were restricted to Laurasian landmasses, including North America, Europe, and Asia, but Gondwanan material challenges this (Benson et al., 2010). The Australian occurrence of a possible tyrannosauroid is inferred based on a late Early Cretaceous pubis described in 2010 (Benson et al.), although the material's affinity to megaraptorids was proposed later (Novas et al., 2013). Some authors (Novas et al., 2013; Porfiri et al., 2014, 2018) put megaraptorids within Tyrannosauroidea, which may imply a wider distribution of the clade within Gondwanan landmasses.

COMPSOGNATHIDAE: Compsognathids are comparatively small early-diverging coelurosaurians known from the Late Jurassic to Early Cretaceous (Hwang et al., 2004). Laurasian compsognathids occur in North America (Osborn, 1903), Europe (Göhlich and Chiappe, 2006), and Asia (Hwang et al., 2004), but only one Gondwanan taxon, *Mirischia*, from the Albian of South America is known (Naish et al., 2004). Since *Mirischia* is the youngest and latest-diverging compsognathid, a dispersal event from Laurasia to Gondwana seems likely, most probably from Europe to South America, via Africa (Naish et al., 2004). If this in fact occurred, later-diverging compsognathids are expected to be found in Africa in the future.

ORNITHOMIMOSAURIA: The slender "ostrich-like" ornithomimosaurians are known only from the Cretaceous period (Xu et al., 2011a). Ornithomimosaurians are found in all Laurasian landmasses, with most frequent occurrences in Asia (Xu et al., 2011a). *Nqwebasaurus* from South Africa is the earliest-diverging ornithomimosaurian and also the only one from Gondwana (De Klerk et al., 2000; Choiniere et al., 2012). Given the close relationship between *Nqwebasaurus* and early-diverging Laurasian ornithomimosaurians, the clade is inferred to have achieved a wide distribution before the breakup of Pangaea (Allain et al., 2014). The Late Cretaceous North American ornithomimids, including *Ornithomimus* and *Struthiomimus*, form a monophyletic group (Xu et al., 2011a). This phylogenetic and geographic pattern has been explained by a single dispersal event from Asia to North America via the Bering land bridge during the latest Cretaceous (Ji et al., 2003; Liyong et al., 2012).

ALVAREZSAUROIDEA: Alvarezsauroids are known for their small, later-diverging forms that have especially large first fingers (Xu et al., 2011b). Until recently, alvarezsauroids were known only from the Late Cretaceous, including earlier-diverging forms from South America (e.g., *Alvarezsaurus*: Bonaparte 1991) and later-diverging forms from Asia and North America (e.g., *Mononykus*: Altangerel et al., 1993; and *Albertonykus*: Longrich and Currie, 2009a). This led to a South American origin being proposed for the clade (Longrich and Currie, 2009a). The discovery of the early-diverging alvarezsauroid *Haplocheirus* from the Late Jurassic of China overturned this origin hypothesis (Choiniere et al., 2010b). On the basis of a quantitative analysis (Xu et al., 2011b), it was later proposed that if alvarezsauroids originated in central Asia shortly before the breakup of Pangea, a dispersal from Asia to South America probably occurred before the Late Cretaceous, most likely via Europe and Africa. This dispersal hypothesis is also supported by two recently discovered Early Cretaceous alvarezsauroids from China (Xu et al., 2018a). A distal tibiotarsus from Romania is the only suspected record of the group in Europe (Naish and Dyke, 2004), and no African records are yet known. The dispersal of Patagonian alvarezsaurids to Asia has become a consensus recently (Xu et al., 2011b; Averianov and Sues, 2017). An additional Late Cretaceous dispersal event from Asia to North America has been inferred to explain the occurrence of the Late Cretaceous North American alvarezsaurid *Albertonykus*, which is closely related to Asian forms (Longrich and Currie, 2009a; Agnolín et al., 2012).

THERIZINOSAURIA: Therizinosaurians are a Cretaceous coelurosaurian clade that evolved herbivory, as also seen in Ornithomimosauria and Oviraptorosauria (Zanno and Makovicky, 2011). Most therizinosaurians are from the Cretaceous of Asia, especially China and Mongolia (Zanno, 2010). The earliest-diverging therizinosaurian, *Falcarius* from the Barremian of Utah, potentially indicates a vicariance event resulting from the separation of North America and Asia during the Early Cretaceous, or a dispersal of early-diverging therizinosaurians from North America to Asia via the controversial land connections proposed across the proto-Atlantic and Turgai Sea (Zanno, 2010). More fossil evidence, such as earlier and/or confirmed European records are required to address this issue further. The other non-Asian therizinosaurians are later-diverging forms from the early Late Cretaceous of North America (e.g., *Nothronychus*) whose ancestors potentially dispersed from Asia via the Bering land bridge during its establishment in the later stages of the Early Cretaceous (Kirkland and Wolfe, 2001; Zanno, 2010; Fiorillo and Adams, 2012). This dispersal event has received further support in the form of a potential therizinosaurian track found in Alaska, which is on one side of the modern Bering Strait (Fiorillo and Adams, 2012; Fiorillo et al., 2018).

OVIRAPTOROSAURIA: Oviraptorosaurians are known for the preservation of evidence of their brooding behavior, and include later-diverging forms with short, elaborate skulls (Clark et al., 2001). Early-diverging oviraptorosaurians, including *Incisivosaurus*, caudipterygids and *Avimimus*, are solely Asian taxa that lived before the Late Cretaceous (Funston and Currie, 2016). Later-diverging taxa have parrotlike beaks, with or without bony skull crests, and have been divided into two subclades, Caenagnathidae and Oviraptoridae (Lü et al., 2015). Whereas known oviraptorids are restricted to Asia, the Caenagnathidae include both North American and Asian taxa (Xu et al., 2007; Funston and Currie, 2016). The presence of *Microvenator* in North America during the late Early Cretaceous is probably attributable to a dispersal event of early-diverging oviraptorosaurians from Asia via the Bering land bridge (Makovicky and Sues, 1998). Like several other coelurosaurian clades, the Late Cretaceous caenagnathids spread across Asia and North America (Funston and Currie, 2016).

DROMAEOSAURIDAE: Dromaeosaurids together with troodontids are the closest relatives of birds (Turner et al., 2012). Dromaeosaurids and troodontids have a hyperextendable second toe, while dromaeosaurids include taxa with rodlike tails comprising caudal vertebrae bound by elongated prezygapophyses (Turner et al., 2012). Dromaeosaurids have a broad geographic distribution across Laurasia and Gondwana throughout the Cretaceous (Turner et al., 2012). Laurasian taxa include early-diverging forms such as *Mahakala* (Turner et al., 2007) as well as later-diverging ones such as the renowned *Velociraptor* (Osborn et al., 1924). Early-diverging dromaeosaurids from Gondwanan landmasses, including *Rahonavis*, *Buitreraptor*, *Neuquenraptor*, and *Austroraptor*, form a single clade (Turner et al., 2012), but alternative relationships have been proposed (Novas et al., 2018). This may indicate a vicariance event due to the separation of Laurasia and Gondwana during the Middle

Jurassic (Makovicky et al., 2005; Novas and Pol, 2005). Antarctic occurrences of dromaeosaurids were also inferred from some pedal fossil fragments, which, together with other Gondwanan taxa, might imply a cosmopolitan distribution of the clade before the breakup of Pangea (Case et al., 2007). Although Jurassic teeth from Laurasia have been referred to Dromaeosauridae (Goodwin et al., 1999; Vullo et al., 2014), more substantial fossil evidence is needed to confirm this important early record. The establishment of the Bering land bridge during the later stages of the Early Cretaceous and again in the latest Cretaceous has been proposed as a potential explanation of the flourishing of the Velociraptorinae in Asia and the occurrences of microraptorines (*Hesperonychus*) in North America (Longrich and Currie, 2009b; Turner et al., 2012). Faunal exchange between Europe and Asia is also thought to have occurred during the Cretaceous based on the close relationship between the European dromaeosaurid *Balaur* and other Laurasian dromaeosaurids (Csiki et al., 2010; Brusatte et al., 2013). While flight capabilities have been proposed in the microraptorine *Microraptor*, these relate to flights of relatively short distances and probably did not affect the dispersal ability of dromaeosaurids over continental scales, but perhaps came into play in archipelago settings (Chatterjee and Templin, 2007).

TROODONTIDAE: Troodontids can be distinguished from dromaeosaurids by their numerous, closely packed teeth (Currie, 1987). Most of these close avialan relatives are from Asia (Lü et al., 2010). North American occurrences of the clade are restricted to *Geminiraptor* from the Early Cretaceous of Utah (Senter et al., 2010) and several later-diverging taxa from the Late Cretaceous (Leidy, 1856; Zanno et al., 2011). While the occurrence of later-diverging North American troodontids, represented by *Troodon*, can be attributed to a dispersal from Asia via the Bering land bridge during the Campanian and Maastrichtian stages of the Late Cretaceous (Dodson et al., 2004), *Geminiraptor* and abundant teeth referred to troodontids from Europe indicate that multiple dispersal events might have happened within Laurasia even before the Late Cretaceous (Senter et al., 2010). The first reported Gondwanan troodontid was based on a tooth found in the Late Cretaceous of India, with this occurrence reflecting either a dispersal event from Laurasia, or a much wider distribution of the clade before the breakup of Pangea (Goswami et al., 2013). However, this identification should be considered as provisional. Even though troodontids have reasonably diagnostic teeth among theropods, this record would be more convincing with additional confirmatory skeletal material (Makovicky and Norell, 2004).

AVIALAE: This clade includes early birds and their modern descendants (Padian, 2004). By the Late Cretaceous avialans had achieved a global geographic distribution (Brocklehurst et al., 2012). The controversial Late Jurassic early-diverging paravians, the anchiornithines, proposed as both early-diverging birds and troodontids, were previously known only from Liaoning, China (Godefroit et al., 2013), but have recently been confirmed in Europe (*Ostromia*) (Foth and Rauhut, 2017). This might indicate a Late Jurassic dispersal event from Asia to Europe (Foth and Rauhut, 2017), given that *Archaeopteryx*, the most widely accepted oldest and earliest-diverging bird, is from Germany (Wellnhofer, 2009; Foth et al., 2014). The second oldest avifaunas are in the Early Cretaceous Hauterverian-Barremian, during which the later-diverging clades Ornithuromorpha and Enantiornithes first appear, and are found in China (Zhou and Zhang, 2006) and in Mongolia (O'Connor and Zelenkov, 2013; Zelenkov and Averianov, 2016), where both clades are represented, as well as in Spain, where only enantiornithines have been found (Sanz, 1990; Sanz et al., 1995; Sanz et al., 1996). Until recently, the only recognized Cretaceous non-ornithothoracines were from the Hauterverian-Aptian Jehol Biota (*Jeholornis* with its long bony tail and early-diverging pygostylians such as *Sapeornis* and *Confuciusornis*; Zhou and Zhang, 2006) although recently a non-ornithothoracine pygostylian was recovered from the

Aptian Kitadani Formation in Japan (Imai et al., 2019). Slightly younger deposits have yielded enantiornithines with an even wider distribution, present in Brazil (de Souza Carvalho et al., 2015) and Australia (Close et al., 2009), with the earliest hesperornithiforms preserved in late Albian deposits in the U.K. (Galton and Martin, 2002). During the Late Cretaceous, enantiornithines and later-diverging ornithuromorphs (ornithurines) had a global distribution, with records in Asia (e.g., *Gobipteryx*), South America (e.g., *Patagopteryx*), North America (e.g., *Ichthyornis*), Europe (e.g., *Baptornis*), Madagascar (*Vorona*), and Antarctica (*Vegavis*) (Elzanowski, 1974; Martin and Bonner, 1977; Alvarenga and Bonaparte, 1992; Forster et al., 1996; Clarke, 2004; Clarke et al., 2005).

Theropod flight appeared in the Middle or Late Jurassic at the latest (Xu et al., 2014), but the exact time(s) when powered flight was acquired is still under debate (Brocklehurst et al., 2012; Allen et al., 2013; Zheng et al., 2013; Xu et al., 2014; Dececchi et al., 2016). Modern avialan flight ability varies widely from species to species (Tobalske et al., 2003). Some extant birds are flightless, while others (like terns, e.g., *Sterna*) are capable of migrating across oceans (Tobalske et al., 2003). Given the general absence of functionally informative soft tissue evidence in avialan fossils, the dispersal ability of Mesozoic avialans is even harder to estimate than modern birds, providing major challenges to biogeographic analysis of this clade. However, the distribution of Late Cretaceous taxa such as the enantiornithine *Martinavis*, found in North and South America and in Europe (Walker et al., 2007), if in fact all specimens have been correctly referred to a single genus, may suggest at least some taxa were able to disperse long distances, and were unrestricted in their dispersal relative to nonavialan dinosaurians.

Ancestral Crown Avialan Biogeography

The Mesozoic biogeographic history of coelurosaurians set the stage for early spatial distribution patterns of crown birds. Although the stunning diversity of living birds and their easily observable nature would seem to simplify robust biogeographic inferences for their major extant subclades, deep crown bird biogeography has emerged as one of the most contentious issues in contemporary avialan macroevolution (Cracraft and Claramunt, 2017; Mayr, 2017; Field and Hsiang, 2018; Saupe et al., 2019).

Opposing views on crown bird historical biogeography relate to the observation that their early Cenozoic fossil record frequently reveals unforeseen complexity in the distributions of major clades. For example, many major clades of extant birds are restricted to vestiges of Gondwana (South America, Africa, and Australasia). As a result, quantitative ancestral biogeographic reconstructions invariably infer a Gondwanan origin for crown birds, and for many of the deepest nodes within the avian tree of life (fig. 5) (Cracraft, 2001; Claramunt and Cracraft, 2015). However, the earliest known fossil stem group representatives of many such "Gondwanan" clades derive from the Paleogene of the northern hemisphere, entirely outside the modern geographic distributions of their crown clades, casting doubt on what the ancestral geographic distributions for these groups really were. This holds true for clades currently restricted to Africa, such as Musophagiformes (Field and Hsiang, 2018) and Coliiformes (Houde and Olson, 1992; Mayr and Peters, 1998; Mayr, 2001; Zelenkov and Dyke, 2008; Ksepka and Clarke, 2009, 2010a); Madagascar, such as Leptosomiformes (Mayr, 2002a, 2002b, 2008); South America, such as Cariamiformes (Mourer-Chauviré and Cheneval, 1983; Peters, 1995; Mourer-Chauviré, 1999; Mayr, 2000, 2002b; Mourer-Chauviré, 2006) and Opisthocomiformes (Mayr and De Pietri, 2014); and Australasia, such as Podargiformes (Nesbitt et al., 2011; Mayr, 2015). Indeed, the dynamic nature of crown bird biogeography is further evinced by the early Old World fossil record of clades presently restricted to the New World such as hummingbirds (Trochilidae) (Karhu, 1988; 1992; 1999; Mayr, 2003, 2004; Bochenski and Bochenski, 2008; Louchart et al.,

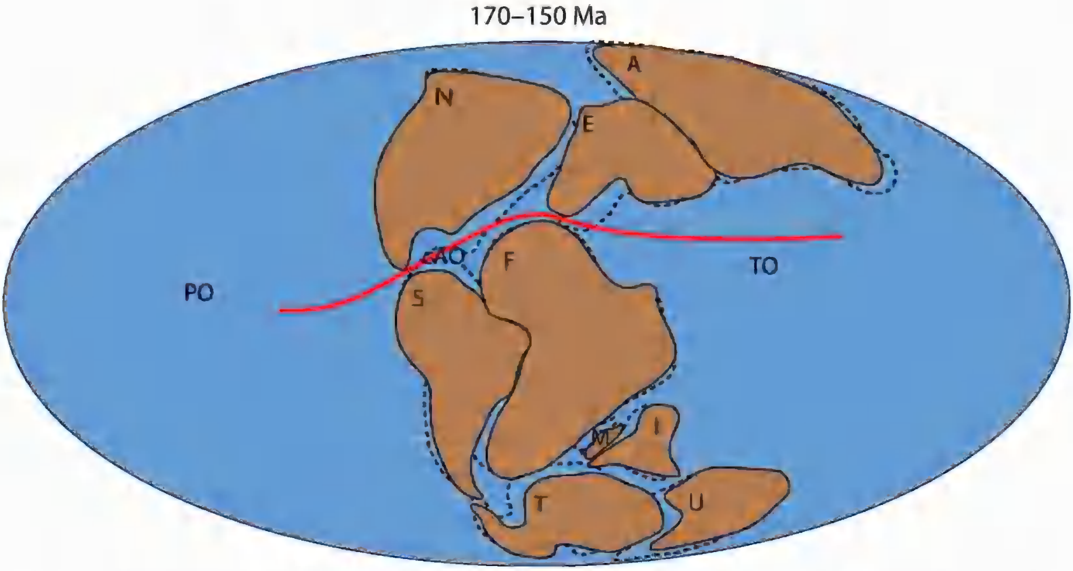

FIG. 1. Hypothesis 1, Laurasia-Gondwana vicariance event during the Late Jurassic. The separation between Laurasia and Gondwana was established in the Kimmeridgian Stage. The red line denotes the approximate position of the hypothesized biogeographical barrier: the central Atlantic Ocean (cAO) and Tethys Ocean (TO); Dotted lines denote paleogeography at 170 Ma, while solid lines denote it at 150 Ma. Paleomap after (Matthews et al., 2016). Abbreviations: **A,** Asia; **cAO,** central Atlantic Ocean; **E,** Europe; **F,** Africa; **I,** India; **M,** Madagascar; **N,** North America; **PO,** Pacific Ocean; **S,** South America; **T,** Antarctica; **TO,** Tethys Ocean; **U,** Australia.

2008), and the early New World fossil record of clades presently restricted to the Old World such as the roller + ground roller clade (Coracii) (Mayr et al., 2004; Clarke et al., 2009; Ksepka and Clarke, 2010b).

Inclusion of early Cenozoic crown bird fossils in biogeographic analyses therefore has potential to erode confidence in erstwhile robust analytical reconstructions of crown bird historical biogeography (fig. 5). Moreover, as the evolutionary timescale of crown birds has come into clearer focus (Feduccia, 2014; Jarvis et al., 2014; Prum et al., 2015; Berv and Field, 2018; Field, et al., on timing the extant avian radiation, this volume), attempts to reconcile the "trans-Antarctic" distributions of many groups of crown birds through Gondwanan vicariance (Cracraft, 2001) have emerged as untenable since Gondwanan breakup was largely complete by the time crown birds arose (Mayr, 2009). Recently, the hypothesis that large-scale climatic changes throughout the Cenozoic were implicated in driving major contractions in the distributions of "tropical" avian clades gained support from quantitative ecological and environmental modeling (Saupe et al., 2019). Additionally, the oldest crown-bird fossil yet identified, *Asteriornis*, comes from the latest Cretaceous of Belgium (Field et al., 2020). As a result, the true biogeographic origins of crown birds may be best regarded as uncertain at present; only future fossil discoveries of the earliest crown birds from the latest Cretaceous and earliest Cenozoic have potential to shed direct light on ancestral biogeographic distributions of crown birds (Field and Hsiang, 2018). As such, this article will not treat the biogeographic history of crown birds (the "living coelurosaurians") and will instead focus solely on the Mesozoic biogeography of the major nonavialan coelurosaurian clades.

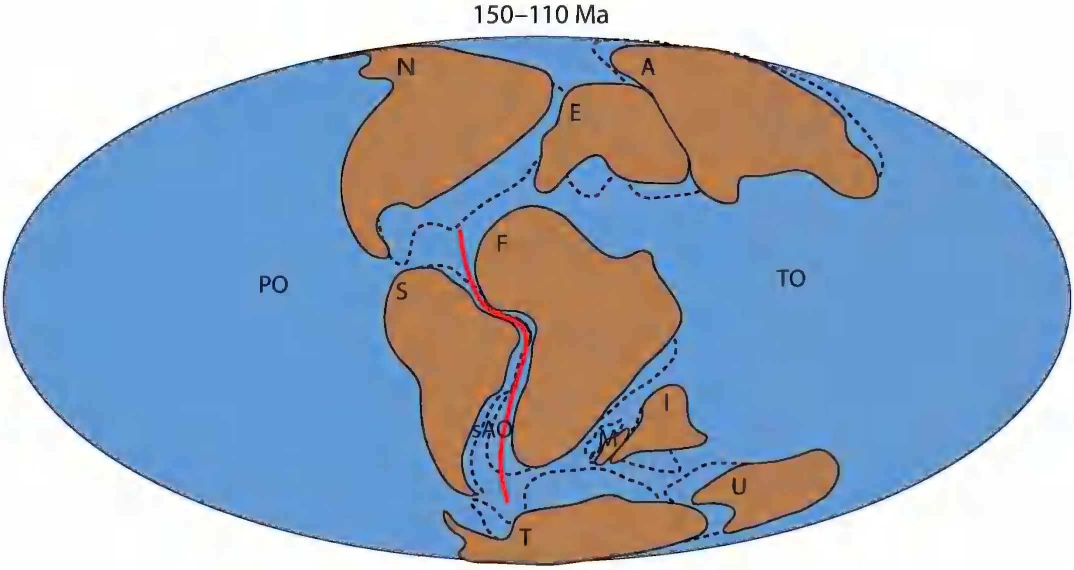

FIG. 2: Hypothesis 2, South America-Africa vicariance event during the late Early Cretaceous. The separation between South America and Africa was established in the Albian Stage. The red line denotes the approximate position of the hypothesized biogeographical barrier: the south Atlantic Ocean (sAO); Dotted lines denote paleogeography at 150 Ma, while solid lines denote it at 110 Ma. Paleomap after (Matthews et al., 2016). Abbreviations: **A,** Asia; **E,** Europe; **F,** Africa; **I,** India; **M,** Madagascar; **N,** North America; **PO,** Pacific Ocean; **S,** South America; **sAO,** south Atlantic Ocean; **T,** Antarctica; **TO,** Tethys Ocean; **U,** Australia.

MAJOR COELUROSAURIAN BIOGEOGRAPHIC HYPOTHESES

Besides the clade-level biogeographic hypotheses summarized above (see Geographic and Temporal Distribution of Coelurosaurians), analyses of dinosaurian biogeography as a whole, including coelurosaurians, have given varying emphasis to particular biogeographic processes, namely vicariance events, regional extinction events, and dispersal events.

Many authors attach particular importance to vicariance events because of the global continental fragmentation that occurred during the late Mesozoic (Sereno, 1999b; Upchurch et al., 2002; Choiniere et al., 2012). The Middle Jurassic occurrences of tyrannosauroids (e.g., *Kileskus* and *Proceratosaurus*) and Late Jurassic avialans (e.g., *Archaeopteryx* and possible avialan *Anchiornis* [also proposed as a troodontid]), are consistent with the idea that major coelurosaurian lineages were established at least before the Late Jurassic (Rauhut et al., 2010; Choiniere et al., 2012). Together with several early-diverging coelurosaurian Gondwanan occurrences (e.g., *Bicentenaria* from South America and *Nqwebasaurus* from Africa), a geographically widespread distribution of coelurosaurian lineages before the breakup of Pangaea has been inferred, which makes vicariance possible upon separation of the continents (Choiniere et al., 2012). Proposed continental scale vicariance events include the Laurasia-Gondwana separation during the Late Jurassic (as shown in fig. 1: Hypothesis 1) and the final disconnection of South America and Africa during the Early Cretaceous (as shown in fig. 2: Hypothesis 2) (Sereno, 1999b). Possible vicariance-induced phylogenetic patterns have been identified in the distributions of maniraptoran lineages (Makovicky et al., 2005) and Ornithomimosauria (De Klerk et al., 2000). However, other workers have seen continental-scale vicariance as a rare occurrence, and argue that regional extinctions were primarily responsible for late Meso-

TABLE 1

Biogeographic hypotheses tested in this study

Number	Hypothesis
1	Laurasia-Gondwana vicariance event during the Kimmeridgian Stage of the Late Jurassic (Sereno, 1999a; Choiniere et al., 2012).
2	South America-Africa vicariance event during the Albian stage of the Early Cretaceous (Sereno, 1999a).
3	Late Early Cretaceous Europe-Africa faunal exchange via the Apulian route (Naish et al., 2004; Ezcurra and Agnolín, 2011; Dal Sasso et al., 2016). Modified to include dispersal events of both directions.
4	Cretaceous North America-Asia faunal exchanges relating to Early and Late Cretaceous establishments of the Bering land bridge (Sereno, 1999a; Dodson et al., 2004; Zanno, 2010).

zoic dinosaurian distributions. This latter view is often based on the observation that vicariancelike repeated area relationships can also be explained by regional extinction events and that many clades were widespread early in their evolutionary history and seem to become more geographically restricted subsequently (Sereno, 1997; 1999a; Barrett et al., 2011; Benson et al., 2012; Carrano et al., 2012). Most authors agree that intercontinental dispersal played a key role in creating dinosaurian (coelurosaurian) biogeographic patterns (Bonaparte, 1986; Sereno, 1999b; Brusatte et al., 2013; Dunhill et al., 2016). Such dispersal events are implied from the fossil record and phylogenetic relationships. Faunal dispersal events in both directions via the Early Cretaceous Apulian route were inferred by different authors: faunal assemblages from the Santana Formation of northern South America that are similar to Laurasian ones suggest possible Asian dinosaurian dispersal to Africa via Europe (Naish et al., 2004); and the presence of Gondwanan faunas in Europe indicates dispersal events in the opposite direction (Ezcurra and Agnolín, 2012; Dal Sasso et al., 2016). These ideas are unified here as an Africa-Europe faunal exchange hypothesis (Hypothesis 3), as shown in figure 3. Frequent dispersal events within coelurosaurian lineages (including Tyrannosauroidea, Therizinosauria, and Dromaeosauridae), enabled by the Bering land bridge are well documented and accepted (Makovicky and Sues, 1998; Ji et al., 2003; Dodson et al., 2004; Longrich and Currie, 2009a; Brusatte et al., 2010; Zanno, 2010; Turner et al., 2012), as discussed in the last section (see Geographic and Temporal Distribution of Coelurosaurians) (Hypothesis 4: fig. 4): this includes the impacts of both the Early Cretaceous and Late Cretaceous establishments of the land bridge.

The dinosaurian biogeographic hypotheses we propose to test in this study include the existing hypotheses outlined above, as well as ones that we have modified or developed ourselves (table 1). Existing hypotheses are mostly based on narrative or qualitative approaches, which have limited their accuracy as well as their ability to undergo statistical testing. To address this issue, a quantitative biogeographic method with multiple biogeographic models is implemented in this study.

METHODOLOGY

Quantitative biogeographic methods are mainly used for inferring the ancestral geographic distributions of species and clades, as well as the biogeographic processes that produced the observed species distribution. Quantitative analyses require phylogenetic trees of the target clades and some models or assumptions about the evolution of faunal distribution (Ronquist and Sanmartín, 2011). A statistical framework, including parsimony (to a wider extent) and likelihood, is used for formulating an analysis (Ronquist, 1997; Ree, 2005; Landis et al., 2013; Matzke, 2013).

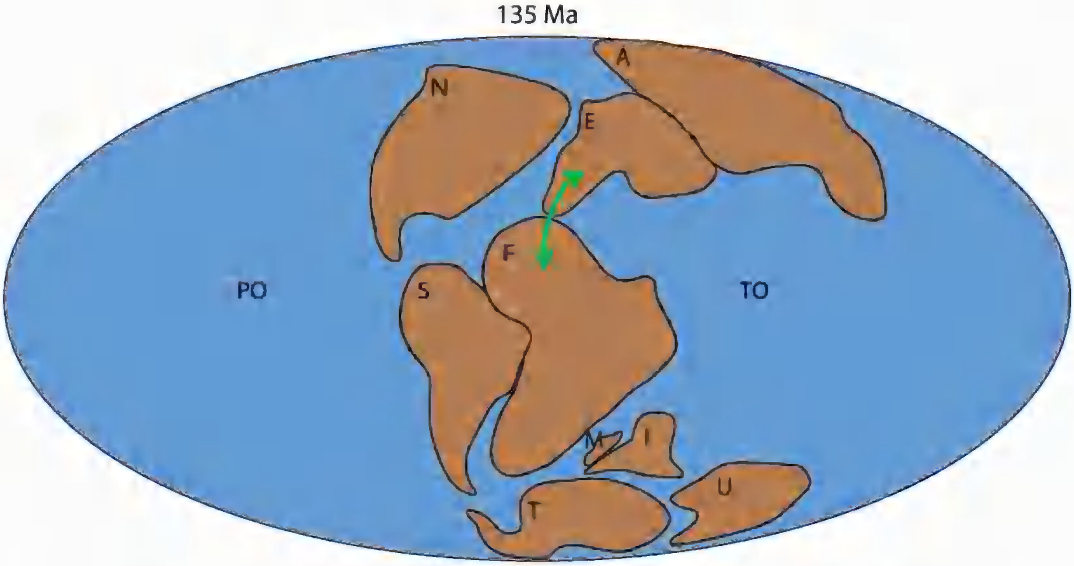

FIG. 3. Hypothesis 3, late Early Cretaceous Europe-Africa faunal exchange via the Apulian route. The green arrowed lines denote the approximate dispersal directions and dispersal routes; Solid lines denote paleogeography at 135 Ma. Paleomap after (Matthews et al., 2016). Abbreviations: **A,** Asia; **E,** Europe; **F,** Africa; **I,** India; **M,** Madagascar; **N,** North America; **PO,** Pacific Ocean; **S,** South America; **T,** Antarctica; **TO,** Tethys Ocean; **U,** Australia.

These historical biogeographic methods are analogous to phylogenetic analysis for inferring character evolution, in that the characters of the taxa are replaced with geographic distributions (Ree, 2005). Therefore, they share similar statistical frameworks, with parsimony, likelihood, and Bayesian methods, all of which are applied in different quantitative biogeographic techniques (Ronquist, 1997; Ree, 2005; Landis et al., 2013). Although the debate on the justification of different statistical frameworks in phylogenetic methods is heated (Goloboff et al., 2018a, 2018b; O'Reilly et al., 2018), the selection of methodological approach is more straightforward and constrained than in historical biogeography. To date, no single method has yet been shown to have better performance in historical biogeographic analyses. Validation of the plethora of biogeographic techniques is beyond the scope of this project, though this work should be a priority in the future.

In most analytical approaches the whole geographic range of interest is divided into multiple smaller areas and taxa are assigned to one or more of these areas. Faunal distribution evolution models are simplified versions of biogeographic processes that operate on the defined geographical areas (Ronquist, 1997; Ree, 2005; Landis et al., 2013; Matzke, 2013). For example, a dispersal event for a taxon corresponds to an increase in the number of distribution areas at a node and/or along a branch in a taxon phylogeny. Other distribution evolution models include regional extinction, sympatry, vicariance, and founder-event speciation (the latter occurring when one of the two daughter lineages of an ancestor acquires a different area to that ancestor, usually through dispersal across a barrier). Different quantitative biogeographic methods take different models into consideration, which directly affect the results obtained (Matzke, 2013). Thus, a multimodel approach is recommended for more accurate identification of biogeographical patterns.

The first widely used quantitative biogeographic analysis approach was dispersal-vicari-

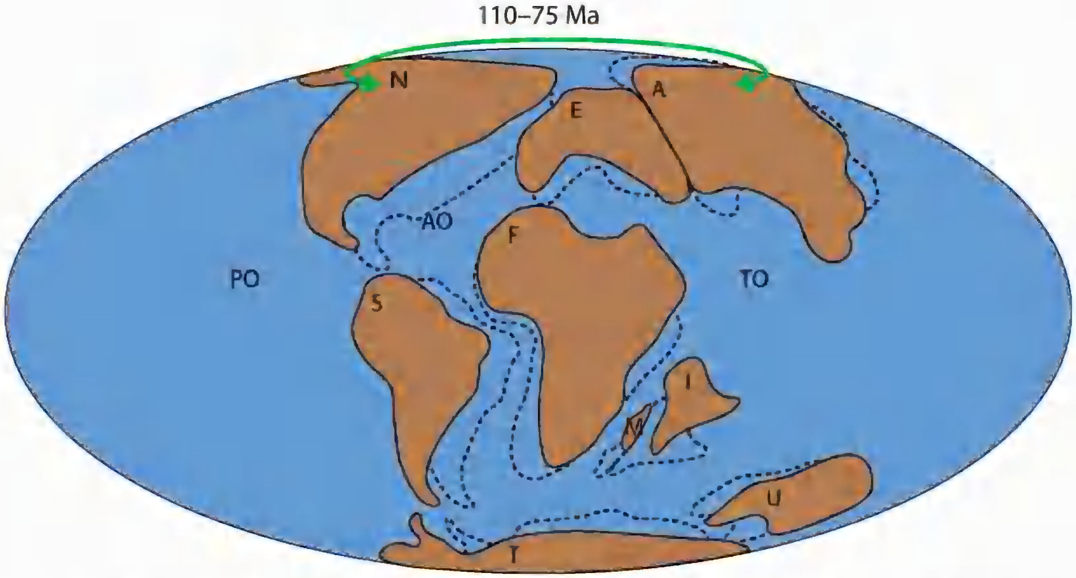

FIG. 4. Hypothesis 4, Cretaceous North America–Asia faunal exchanges. This includes both the Early and Late Cretaceous establishments of the Bering land bridge. The green arrowed line denotes the approximate dispersal directions and route. Dotted lines denote paleogeography at 110 Ma, solid lines denote paleogeography at 75 Ma. Paleomap after (Matthews et al., 2016). Abbreviations: **A,** Asia; **AO,** Atlantic Ocean; **E,** Europe; **F,** Africa; **I,** India; **M,** Madagascar; **N,** North America; **PO,** Pacific Ocean; **S,** South America; **T,** Antarctica; **TO,** Tethys Ocean; **U,** Australia.

ance analysis or DIVA (Ronquist, 1997), as implemented in the program FigTree. This parsimony-based approach utilizes phylogenetic character optimization methods and models dispersal, extinction, and vicariance events. Each event is assigned with a cost (the cost of dispersal and regional extinction events is 1 while the cost of vicariance events is 0). The overall biogeographic history with the lowest cost is favored (Ronquist, 1997). However, the time dimension is not considered in the analysis. Subsequently, a likelihood framework was introduced in the form of the dispersal-extinction cladogenesis model (DEC) by assigning dispersal and extinction rates as free parameters, which can vary to give different overall likelihoods (Ree and Smith, 2008). Subset sympatry (one of the daughter lineages lives in a subset of the ancestral range, while the other continues to occupy the whole ancestral range) and a limited form of vicariance (one of the daughter lineages occupies only one ancestral area, while the other occupies the rest of the ancestral range) are permitted, but widespread sympatry or vicariance are prohibited. By varying free parameter values, the ancestral state is reconstructed by maximizing the overall likelihood of the whole biogeographic process. This approach incorporates information on the branch lengths in phylogenetic trees (i.e., evolutionary time is taken into consideration). Historical geographic changes can also be incorporated into the analysis using this method (Ree and Smith, 2008). Finally, in order to enhance the computational speed of biogeographic analysis, the program BayArea was developed with a Bayesian approach based on a likelihood framework, in which vicariance was prohibited (Landis et al., 2013).

In this project, we adopt the R package, BioGeoBEARS (Matzke, 2013), for analyzing coelurosaurian biogeography. Likelihood versions of the biogeographic models in DIVA, DEC, and BayArea are incorporated into BioGeoBEARS, which allows the results of several models to be more easily compared. DEC is the original dispersal-extinction cladogenesis model (Ree and Smith, 2008). DIVALIKE is a likelihood version of dispersal-vicariance analysis (Ronquist, 1997). Unlike DEC, the DIVALIKE model disallows subset sympatry, but permits widespread vicariance (i.e., two daughter lineages divide up the ancestral range and both share more than one area). BAYAREALIKE is a likelihood-based version of BayArea (Landis et al., 2013). In BAYAREALIKE, the two daughter lineages of a given ancestor inherit the same area distribution as that ancestor. As a consequence, the BAYAREALIKE model allows widespread sympatry (i.e., for any ancestral range occupying more than one area, a daughter lineage copies it), which is prohibited in both the DEC and DIVALIKE models. Like BayArea, BAYAREALIKE also disallows vicariance events. All three models assume narrow sympatry (i.e., spontaneous range copying of single area ancestral ranges) and set dispersal and regional extinction rate as free parameters. In BioGeoBEARS, founder events are included as a separate range-switching process (termed the J parameter), which can be considered as a rapid dispersal event. This creates three new variants of the three models, giving a total of six possible model comparisons per biogeographic dataset: DEC, DIVALIKE, BAYAREALIKE, DEC+J, DIVALIKE+J, and BAYAREALIKE+J (Matzke, 2013). Standard statistical comparison with natural log of the process likelihood (LnL) and the Akaike information criterion (AIC) can be performed to identify the model(s) that best fits the data

Applying BioGeoBEARS has three notable advantages over existing methods: (1) different models are compared based on the same dataset (as mentioned above); (2) geological time spans are considered in calculating the likelihood of faunal distribution evolution; and (3) paleogeographic constraints can be implemented to inform the analysis about area connectedness during the Mesozoic. At this stage, these three features cannot be achieved by any current software based on a parsimony framework or Bayesian approach.

BioGeoBEARS considers time in calculating the likelihood of faunal distribution evolution. All things being equal, a biogeographic event should have a higher probability of occurring over a longer period of time. This time span, which is the branch length of each lineage, is taken into consideration within the likelihood framework through the relationship:

$$P_{ij}(t) = \exp(-Q_{ij}{}^{*}t)$$

Where P is the event likelihood, Q is the universal event rate (dispersal, local extinction, vicariance, founder event) and t is the branch length (Matzke, 2013). Although assigning one universal rate value to each biogeographic event is still overly simplistic, the consideration of time, which is not achievable within a parsimony framework at this time, remains an important advantage over other current methods of analysis.

BioGeoBEARS allows paleogeographic constraints with known temporal ranges to be incorporated into an analysis (Matzke, 2013). This ensures that dispersals between areas that are connected or separated are assigned different dispersal probabilities despite one universal dispersal rate. To do so, dispersal multipliers are introduced, whose product with the universal dispersal rate will be the new regional dispersal rate used to calculate the likelihood of the dispersal event in question. The dispersal multipliers for connected geographic ranges are set to 1 while those for separated ranges are set to 0.000001 (a low value does not rule out such dispersal events but implies that they are highly unlikely). Here, we follow the protocol of Poropat et al. (2016). When dealing with regions that are separated by shallow seas or uncertain geographic barriers, the value 0.5 is assigned to the dispersal multiplier between those regions, which act as our starting (or normal) constraints (see Poropat et al., 2016, for further details).

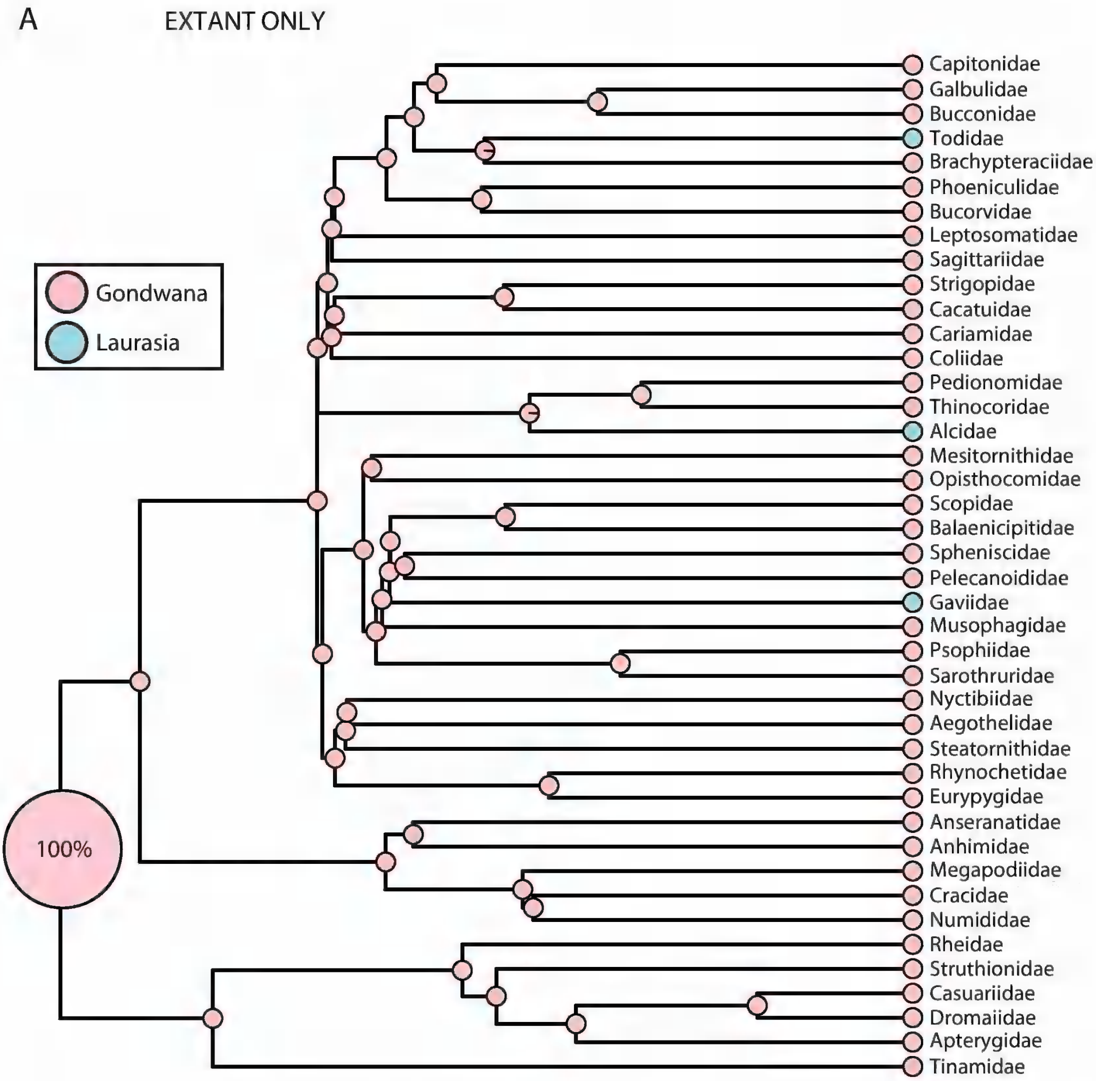
A
EXTANT ONLY
Gondwana
Laurasia
100%
Capitonidae
Galbulidae
Bucconidae
Todidae
Brachypteraciidae
Phoeniculidae
Bucorvidae
Leptosomatidae
Sagittariidae
Strigopidae
Cacatuidae
Cariamidae
Coliidae
Pedionomidae
Thinocoridae
Alcidae
Mesitornithidae
Opisthocomidae
Scopidae
Balaenicipitidae
Spheniscidae
Pelecanoididae
Gaviidae
Musophagidae
Psophiidae
Sarothruridae
Nyctibiidae
Aegothelidae
Steatornithidae
Rhynochetidae
Eurypygidae
Anseranatidae
Anhimidae
Megapodiidae
Cracidae
Numididae
Rheidae
Struthionidae
Casuariidae
Dromaiidae
Apterygidae
Tinamidae

Within each analysis, the overall likelihood of reproducing the dataset given the model is computed, and the overall biogeographic process with the maximum probability (likelihood) will be the best-fit result. The Akaike information criterion (AIC) and natural log of the process likelihood (LnL) are calculated to infer the quality of data fit. A smaller AIC and a larger (less negative) LnL indicate a better fit of the data given the model tested.

We divide land areas on the Earth's surface into eight geographic units, namely Africa, Asia, Australia, Europe, India, Madagascar, North America, and South America (although there are no taxa from India or Australia in our dataset). Each taxon is assigned to the areas according to data reviewed above in Geographic and Temporal Distributions of Coelurosaurians. These data were obtained by referring back to holotype descriptions and other literature (the dataset is available in the appendix of this paper).

The coelurosaurian phylogenetic tree with time calibration applied in the analysis is a maximum agreement subtree of a recent analysis of the Theropod Working Group (TWiG)

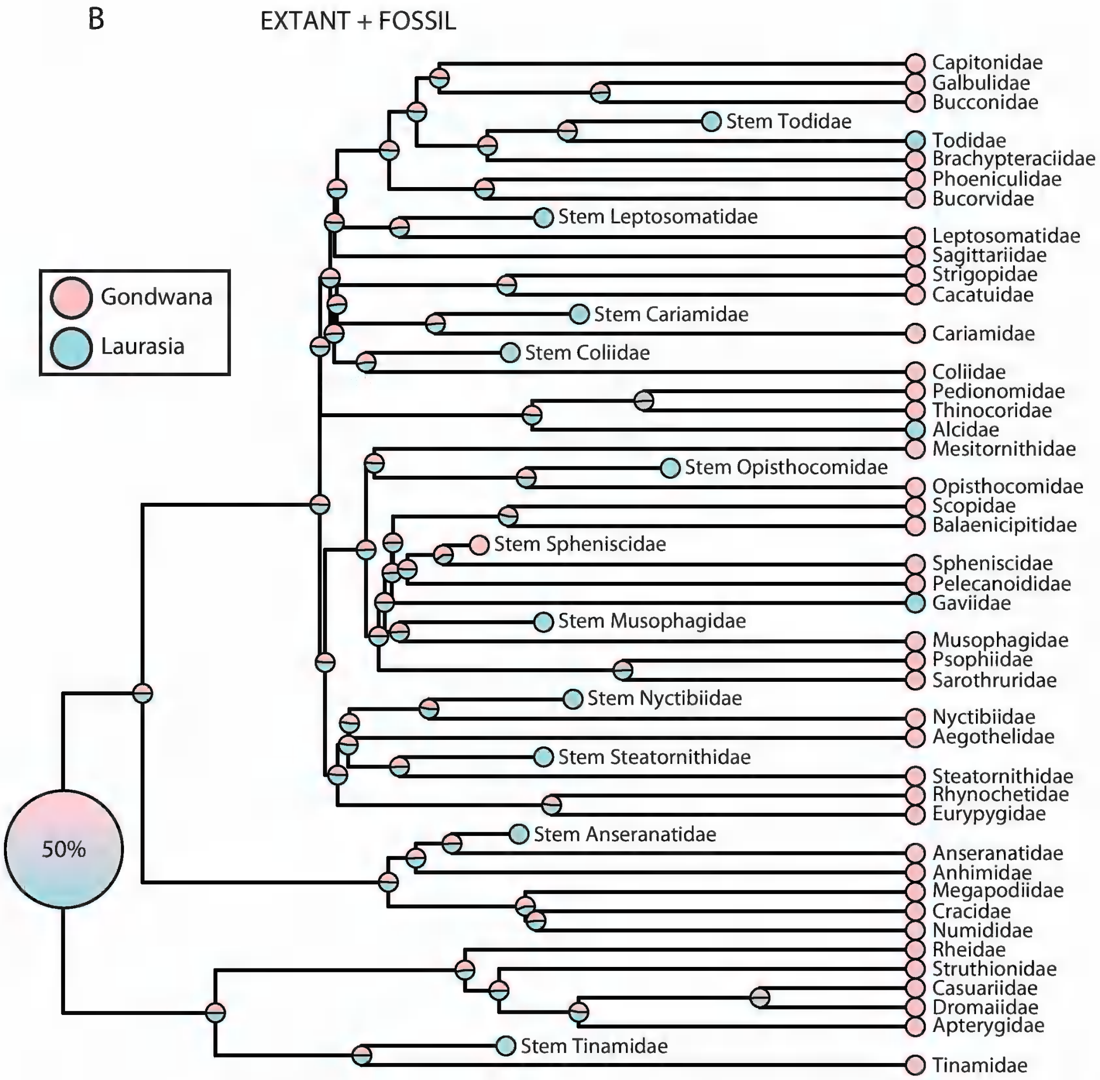
B
EXTANT + FOSSIL
Gondwana
Laurasia
50%
Capitonidae
Galbulidae
Bucconidae
Stem Todidae
Todidae
Brachypteraciidae
Phoeniculidae
Bucorvidae
Stem Leptosomatidae
Leptosomatidae
Sagittariidae
Strigopidae
Cacatuidae
Stem Cariamidae
Cariamidae
Stem Coliidae
Coliidae
Pedionomidae
Thinocoridae
Alcidae
Mesitornithidae
Stem Opisthocomidae
Opisthocomidae
Scopidae
Balaenicipitidae
Stem Spheniscidae
Spheniscidae
Pelecanoididae
Gaviidae
Stem Musophagidae
Musophagidae
Psophiidae
Sarothruridae
Stem Nyctibiidae
Nyctibiidae
Aegothelidae
Stem Steatornithidae
Steatornithidae
Rhynochetidae
Eurypygidae
Stem Anseranatidae
Anseranatidae
Anhimidae
Megapodiidae
Cracidae
Numididae
Rheidae
Struthionidae
Casuariidae
Dromaiidae
Apterygidae
Stem Tinamidae
Tinamidae

FIG. 5. Illustration (*opposite page and above*) of conflict between "extant only" biogeographic reconstructions for crown birds, and the crown bird fossil record (modified from Field and Hsiang, 2018). **A,** Extant-only reconstructions infer a Gondwanan origin of crown birds with strong probability, whereas **B,** identical analyses incorporating the earliest fossil stem group representatives infer a markedly less robustly supported result.

phylogenetic matrix (see Brusatte et al., 2014, for further details). The paleogeographic constraints are those used by Xu et al. (2018a), as modified from those summarized by Poropat et al. (2016) by better constraining the opening and closing of the Russian Platform Sea between Asia and Europe during the Jurassic (Xu et al., 2018b). They are represented by 23 dispersal multiplier matrices corresponding to 23 time slices from the Middle Jurassic to the Late Cretaceous. Four analyses with "starting", "relaxed", "harsh", or "no paleogeographic constraints" were carried out. Relaxed constraints set all 0.5 dispersal multiplier values to 1, harsh constraints set all 0.5 dispersal multipliers to 0.000001. These analyses were repeated for all six biogeographic models giving a total of 24 comparisons.

TABLE 2

Relative performance of the six biogeographic models under the unconstrained and three palaeogeographically constraint conditions

Abbreviations: **Alt,** alternative model; null, null model; **LnL,** natural log of the process likelihood; **p-value,** p-value of the likelihood ratio test; **AIC,** Akaike information criterion.

Analysis		Alternative	Null	LnL_{alt}	LnL_{null}	AIC_{alt}	AIC_{null}	p-value
Unconstrained	1	DEC+J	DEC	-177.3	-241.8	360.6	487.6	6.60E-30
	2	DIVALIKE+J	DIVALIKE	-177.2	-232.8	360.5	469.7	5.30E-26
	3	BAYAREALIKE+J	BAYAREALIKE	-179.9	-294.6	365.8	593.3	7.60E-52
Starting	1	DEC+J	DEC	-263	-278.4	532	560.9	2.80E-08
	2	DIVALIKE+J	DIVALIKE	-261.8	-275.1	529.6	551.9	2.60E-07
	3	BAYAREALIKE+J	BAYAREALIKE	-282.9	-317	571.7	638.1	1.30E-16
Relaxed	1	DEC+J	DEC	-262.7	-277.5	531.4	558.9	5.70E-08
	2	DIVALIKE+J	DIVALIKE	-261.4	-273.9	528.8	551.9	5.70E-07
	3	BAYAREALIKE+J	BAYAREALIKE	-278.1	-318.5	562.2	641	2.50E-19
Harsh	1	DEC+J	DEC	-338.1	-344.8	682.3	693.5	0.0003
	2	DIVALIKE+J	DIVALIKE	-372.5	-383	751	770.1	4.60E-06
	3	BAYAREALIKE+J	BAYAREALIKE	-311.4	-329.7	628.7	663.4	1.40E-09

RESULTS

The relative fit of the 24 analyses to the data are summarized in table 2, with the corresponding parameter values listed in table 3.

As shown in table 2, the AIC and LnL values indicate that the unconstrained analysis performs “better” than the constrained ones, an expected result for three reasons: first, without geographic constraints, the dispersal rate remains constant between any two geographic areas throughout coelurosaurian evolutionary history. Under these conditions, unlikely dispersal events will not be prohibited or penalized, and will have the same probability of occurring as paleogeographically more plausible dispersals. For example, Asian taxa may be able to directly disperse to South America, which to a large extent simplifies the biogeographic processes. As a result, the overall likelihood of the unconstrained processes should be expected to be higher than the constrained ones because of oversimplification of the biogeographic processes. Second, vicariance events can take place whenever a fauna is distributed across more than one geographic area. Since the overall dispersal rate is low between continents, any fauna having cross-continent biogeographic ranges is separated by “geographic barriers” as understood by the statistical framework. Due to the high flexibility for vicariance events in an unconstrained analysis, low-probability regional extinction events will frequently be replaced by “must-happen” vicariance, which boosts the overall process likelihood (in models that allow vicariance, the vicariance rate is set close to 1).

TABLE 3

Parameter values for the six biogeographic models under the unconstrained and three palaeogeographically constraint conditions

Abbreviations: **LnL,** natural log of the process likelihood; **d,** dispersal rate; **e,** regional extinction rate; **j,** founder-event rate; **AIC,** Akaike information criterion; **AICweight,** Akaike information criterion weight.

Model	LnL	d	e	j	AIC	AICweight
Unconstrained						
DEC	-241.8	0.001	0.0021	0	487.6	1.20E-28
DEC+J	-177.3	1.00E-12	1.00E-12	0.023	360.6	0.47
DIVALIKE	-232.8	0.0012	2.00E-09	0	469.7	9.50E-25
DIVALIKE+J	-177.2	1.00E-12	1.00E-12	0.024	360.5	0.49
BAYAREALIKE	-294.6	0.0011	0.015	0	593.3	1.40E-51
BAYAREALIKE+J	-179.9	1.00E-12	1.00E-12	0.024	365.8	0.035
Starting						
DEC	-278.4	0.014	0.0084	0	560.9	1.30E-07
DEC+J	-263	0.0083	0.0059	0.1	532	0.23
DIVALIKE	-275.1	0.016	0.0077	0	554.1	3.70E-06
DIVALIKE+J	-261.8	0.0099	0.0062	0.1	529.6	0.77
BAYAREALIKE	-317	0.013	0.022	0	638.1	2.10E-24
BAYAREALIKE+J	-282.9	0.0013	0.015	0.051	571.7	5.50E-10
Relaxed						
DEC	-277.5	0.011	0.0081	0	558.9	2.30E-07
DEC+J	-262.7	0.0068	0.0059	0.083	531.4	0.21
DIVALIKE	-273.9	0.013	0.0075	0	551.9	7.90E-06
DIVALIKE+J	-261.4	0.0083	0.0062	0.082	528.8	0.79
BAYAREALIKE	-318.5	0.011	0.022	0	641	3.50E-25
BAYAREALIKE+J	-278.1	0.0063	0.0082	0.12	562.2	4.50E-08
Harsh						
DEC	-344.8	0.021	0.0086	0	693.5	8.60E-15
DEC+J	-338.1	0.015	0.0072	0.082	682.3	2.40E-12
DIVALIKE	-383	0.023	0.008	0	770.1	2.00E-31
DIVALIKE+J	-372.5	0.015	0.0065	0.1	751	2.70E-27
BAYAREALIKE	-329.7	0.0056	0.024	0	663.4	2.90E-08
BAYAREALIKE+J	-311.4	0.0037	0.019	0.049	628.7	1

Third, founder events, as a fast version of dispersal, will be more frequently applied in an unconstrained analysis. A founder event is similar to instant range switching of an ancestral state, which shares the same rate as a dispersal event. In an unconstrained analysis, it not only mimics the process of dispersal, but also does not need low-probability regional extinction events to account for taxa that occupy just a single area. Therefore, founder events can accommodate any taxon that occupies an area that differs from its ancestral state, and this will be more statistically favorable than the estimate of vicariance events to explain the observed distributions. The large LnL contrasts between models with (+J models) and without founder-event speciation are also expected because of the statistical preference for models that include this parameter. The predicted high likelihoods achieved by the unconstrained analyses are confirmed in table 2 where the LnL values for all six biogeographic models are less negative than those in any constrained analyses. Thus, in spite of the low AIC and high LnL values, the results of the unconstrained analysis should be treated with caution because they do not consider paleogeographic constraints. The absence of such information relevant to the direction and probability of faunal dispersal is ultimately likely to lead to less accurate estimations of dispersal events, e.g., direct dispersal events from Asia to South America across the Mesozoic Pacific Ocean.

Within the constrained analyses, the starting and relaxed constraints give results that agree on the most preferred model, DIVALIKE+J, while the harsh constraints suggest a preference for BAYAREALIKE+J. Here, we accept DIVALIKE+J as the best-supported model based on the following reasons:

1. DIVALIKE+J is preferred in the analysis with the starting constraints, which to our knowledge best reflects Mesozoic geography. Such model preference is also supported in the analysis with the relaxed constraints.
2. The ancestral area estimations proposed by the DIVALIKE+J model yield more plausible interpretations of evolutionary history and biogeographic processes for coelurosaurians. This will be discussed in more detail in the Discussion.
3. The results of the BAYAREALIKE+J model (including the one under the harsh geographic constraints) estimate several occurrences of ancestors that were present solely in South America and Asia during the Cretaceous. Such ancestral area estimates are not realistic since the two continents were separated by large oceans during that time (Scotese, 2001) and it is highly unlikely that faunal exchange ever happened. Events of this type are frequent in the BAYAREALIKE+J model, because a high value (nearly 1) is assigned to the widespread sympatry process rate. Some authors (Poropat et al., 2016; Xu et al., 2018b) interpret such unlikely ancestral distributions as resulting from the impacts of uneven sampling of the fossil record. In reality, such widespread sympatry cannot happen without faunal exchange across these areas, but this is neglected in the model. The unrealistic results and oversimplified biogeographic processes justify the rejection of this model.
4. The harsh biogeographic constraints might not accurately reflect paleogeography and the true dispersal capabilities of coelurosaurians. The reason is that they treat all uncertain connections and shallow seas as geographic barriers, which largely isolates the individual continents throughout the Cretaceous. The harsh constraints could therefore be underestimating the dispersal ability of coelurosaurians. Analogous to the modern Madagascan fauna (Ali and Huber, 2010), coelurosaurians—particularly small ones, with or without aerodynamic capabilities—might have been

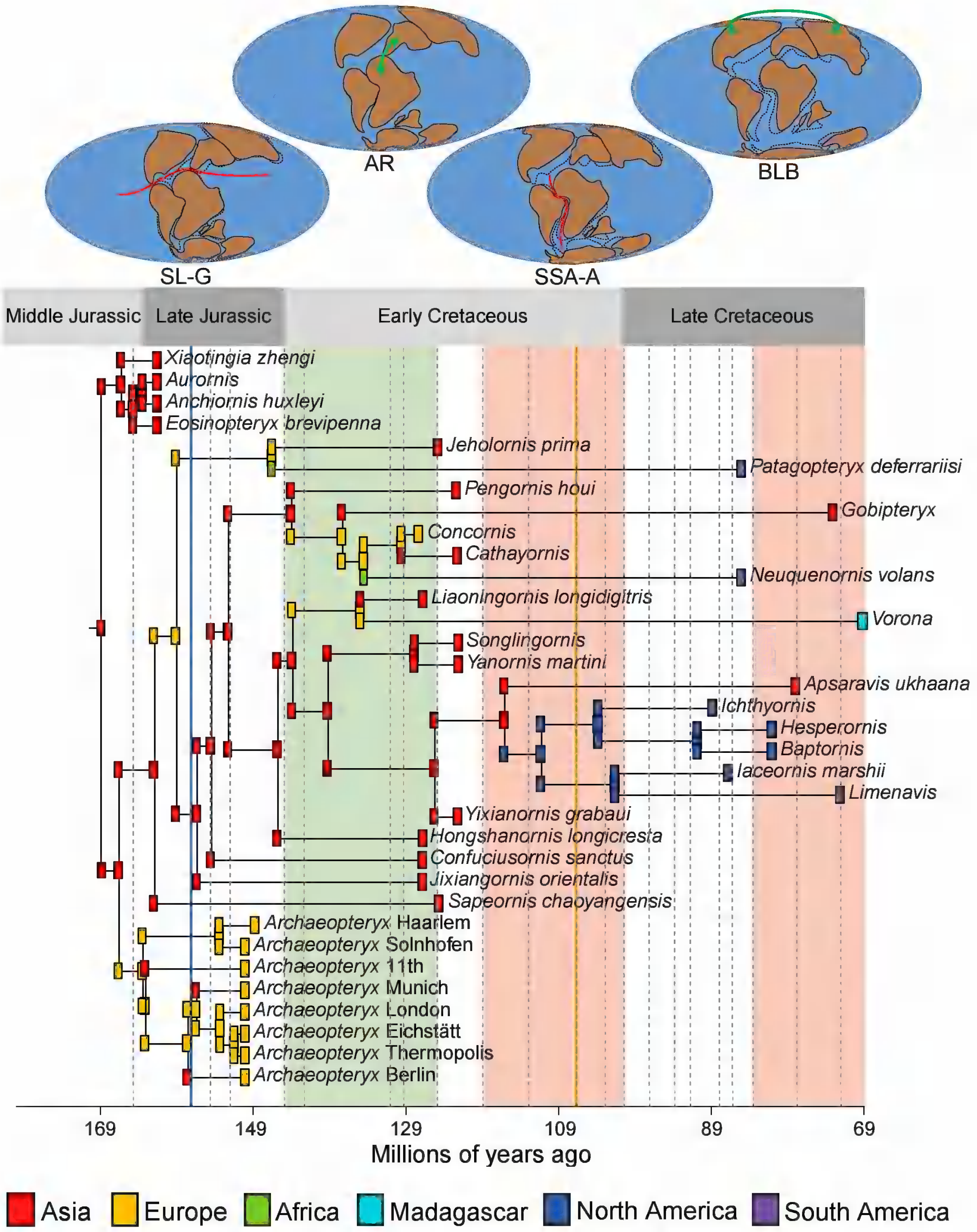

FIG. 6. Ancestral area estimation applying the DIVALIKE+J model with starting constraints to a dated coelurosaurian phylogeny (*above and following two pages*). Green shading denotes the period when the Apulian route (AR) connected northeast Africa and southwest Europe, while red shadings denote Bering land bridge (BLB) connections. The blue line denotes the time of separation between Laurasia and Gondwana (SL-G), while the yellow line denotes the time of separation between South America and Africa (SSA-A).

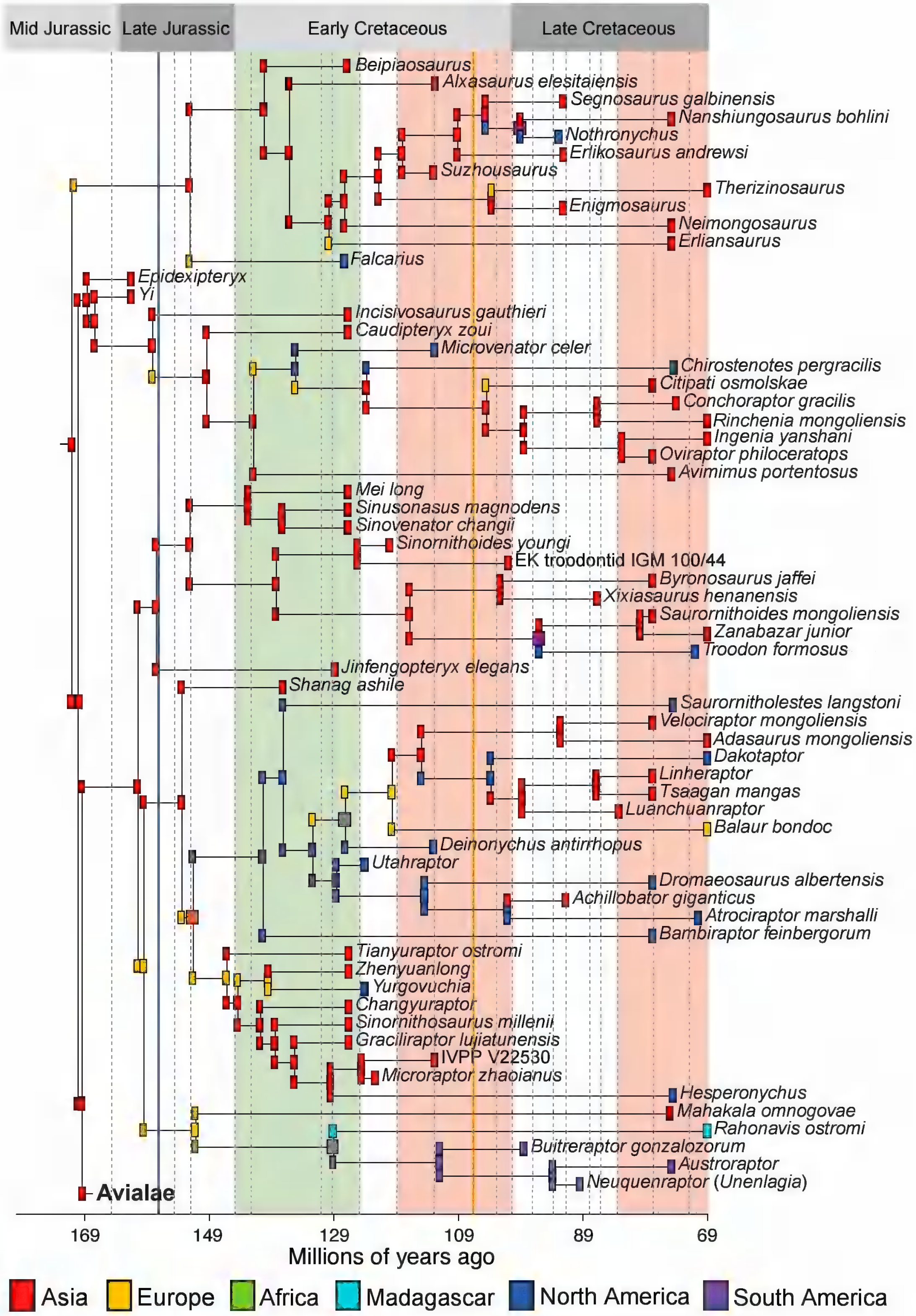
Mid Jurassic
Late Jurassic
Early Cretaceous
Late Cretaceous
Beipiaosaurus
Alxasaurus elesitaiensis
Segnosaurus galbinensis
Nanshiungosaurus bohlini
Nothronychus
Erlikosaurus andrewsi
Suzhousaurus
Therizinosaurus
Enigmosaurus
Neimongosaurus
Erliansaurus
Falcarius
Epidexipteryx
Yi
Incisivosaurus gauthieri
Caudipteryx zoui
Microvenator celer
Chirostenotes pergracilis
Citipati osmolskae
Conchoraptor gracilis
Rinchenia mongoliensis
Ingenia yanshani
Oviraptor philoceratops
Avimimus portentosus
Mei long
Sinusonasus magnodens
Sinovenator changii
Sinornithoides youngi
EK troodontid IGM 100/44
Byronosaurus jaffei
Xixiasaurus henanensis
Saurornithoides mongoliensis
Zanabazar junior
Troodon formosus
Jinfengopteryx elegans
Shanag ashile
Saurornitholestes langstoni
Velociraptor mongoliensis
Adasaurus mongoliensis
Dakotaptor
Linheraptor
Tsaagan mangas
Luanchuanraptor
Balaur bondoc
Deinonychus antirrhopus
Utahraptor
Dromaeosaurus albertensis
Achillobator giganticus
Atrociraptor marshalli
Bambiraptor feinbergorum
Tianyuraptor ostromi
Zhenyuanlong
Yurgovuchia
Changyuraptor
Sinornithosaurus millenii
Graciliraptor lujiatunensis
IVPP V22530
Microraptor zhaoianus
Hesperonychus
Mahakala omnogovae
Rahonavis ostromi
Buitreraptor gonzalozorum
Austroraptor
Neuquenraptor (Unenlagia)
Avialae
169
149
129
109
89
69
Millions of years ago
Asia
Europe
Africa
Madagascar
North America
South America

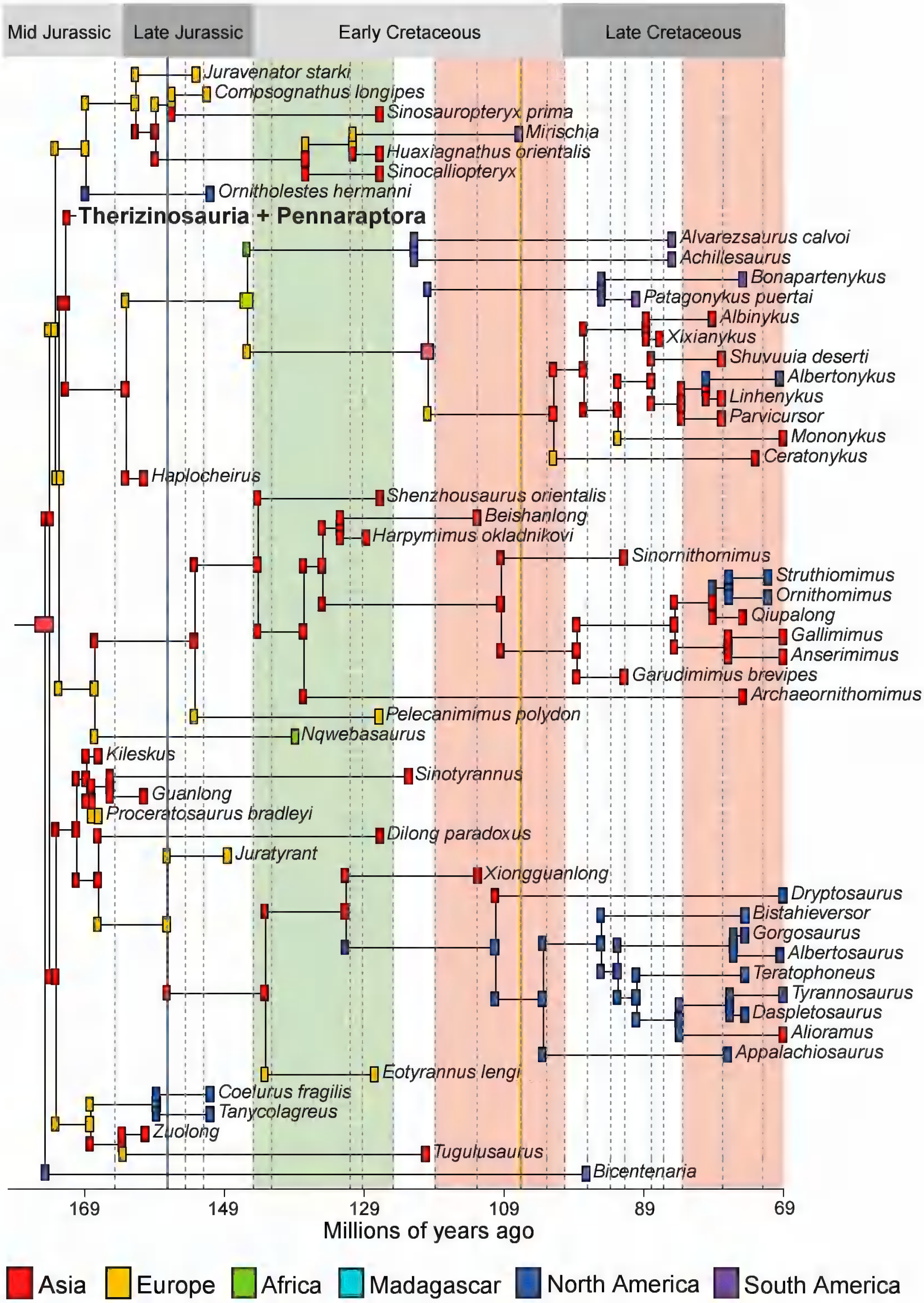
Mid Jurassic
Late Jurassic
Early Cretaceous
Late Cretaceous
Juravenator starki
Compsognathus longipes
Sinosauropteryx prima
Mirischia
Huaxiagnathus orientalis
Sinocalliopteryx
Ornitholestes hermanni
Therizinosauria + Pennaraptora
Alvarezsaurus calvoi
Achillesaurus
Bonapartenykus
Patagonykus puertai
Albinykus
Xixianykus
Shuvuuia deserti
Albertonykus
Linhenykus
Parvicursor
Mononykus
Ceratonykus
Haplocheirus
Shenzhousaurus orientalis
Beishanlong
Harpymimus okladnikovi
Sinornithomimus
Struthiomimus
Ornithomimus
Qiupalong
Gallimimus
Anserimimus
Garudimimus brevipes
Archaeornithomimus
Pelecanimimus polydon
Nqwebasaurus
Kileskus
Sinotyrannus
Guanlong
Proceratosaurus bradleyi
Dilong paradoxus
Juratyrant
Xiongguanlong
Dryptosaurus
Bistahieversor
Gorgosaurus
Albertosaurus
Teratophoneus
Tyrannosaurus
Daspletosaurus
Alioramus
Appalachiosaurus
Eotyrannus lengi
Coelurus fragilis
Tanycolagreus
Zuolong
Tugulusaurus
Bicentenaria
169
149
129
109
89
69
Millions of years ago
Asia
Europe
Africa
Madagascar
North America
South America

capable of crossing relatively narrow channels or shallow waterways over geological time scales.

In the various constrained analyses, the +J models still perform better than non+J models, although the differences are not as large as in the unconstrained analysis (as suggested by p-values in table 2). This phenomenon also occurs because founder-event speciation, as an alternative explanation for area switching, is statistically more favorable than other forms of dispersal. With the implementation of paleogeographic constraints, this flexibility is to some extent restricted and vicariance events are preferred if no feasible dispersal route is allowed, thereby reducing the likelihood gap of +J models and corresponding non+J models. However, which particular events happened during coelurosaurian evolution, whether founder events or dispersals, cannot be determined by these analyses.

In the analyses with the starting and relaxed constraints, the DIVALIKE+J and the DEC+J models perform nearly equally well with close AIC and LnL values. Both of the models allow narrow vicariance and founder events, while DIVALIKE+J allows widespread vicariance but DEC+J allows subset sympatry. Because nearly all taxa in our analysis occupy only single geographic areas and large-scale connections of these units were absent after the breakup of Pangaea, biogeographic processes that result in widespread ancestral species probably did not play a major role in coelurosaurian evolution. This might explain the similar results of the DIVALIKE+J and DEC+J models. The ancestral area estimates of the two models also provide similar interpretations of biogeographic history. Because the DIVALIKE+J model is slightly favored in terms of AIC and LnL values, we use its results in our discussion of coelurosaurian biogeography (fig. 6). The results of the starting constraints are used as the basis of our discussion here because they represent the most conservative paleogeography among the three constraints (starting, relaxed, and harsh).

DISCUSSION

Our results show that the major biogeographic processes during coelurosaurian evolution include intercontinental dispersals, regional extinctions, continent-scale vicariance events, and continental-scale founder events. While dispersal and extinction are part of all six BioGeoBEARS models, the support for the DIVALIKE+J model in particular indicates important roles for vicariance and founder-event speciation in coelurosaurian evolution. In contrast, the BAYAREALIKE models, which do not allow vicariance, are not supported except when particularly stringent (harsh) paleogeographic constraints are imposed. However, on a continental scale, founder events at ancestral nodes, although statistically preferred, become similar to within-lineage dispersal events from a biological point of view. Hence, no absolute or relative frequencies of founder events can be inferred from our results. As our area units are at the continental scale, our results cannot capture intracontinental or island-scale biogeographic patterns.

Our results confirm that continental-scale vicariance was probably an important biogeographic process influencing coelurosaurian evolution. This is consistent with many qualitative assessments in the literature (Fastovsky et al., 1996; Sereno, 1999b; Makovicky et al., 2005; Choiniere et al., 2012), and also agrees with a quantitative analysis of dinosaurian biogeography (Upchurch et al., 2002). Most workers recognized the importance of continental fragmentation in producing geographic barriers during the late Mesozoic, including the separation of Laurasia and Gondwana, the opening of the north Atlantic and the isolation of Gondwanan landmasses. Such vicariance events are seen in our results (fig. 6): for example, vicariance induced by the Middle Jurassic breakup of Pangaea led to the occurrence of the early-diverging coelurosaurian *Bicentenaria* in South America and other early-diverging taxa in Laurasia (Hypothesis 1). Similar vicariance patterns are also recognized within other terrestrial faunas living at that time, such as

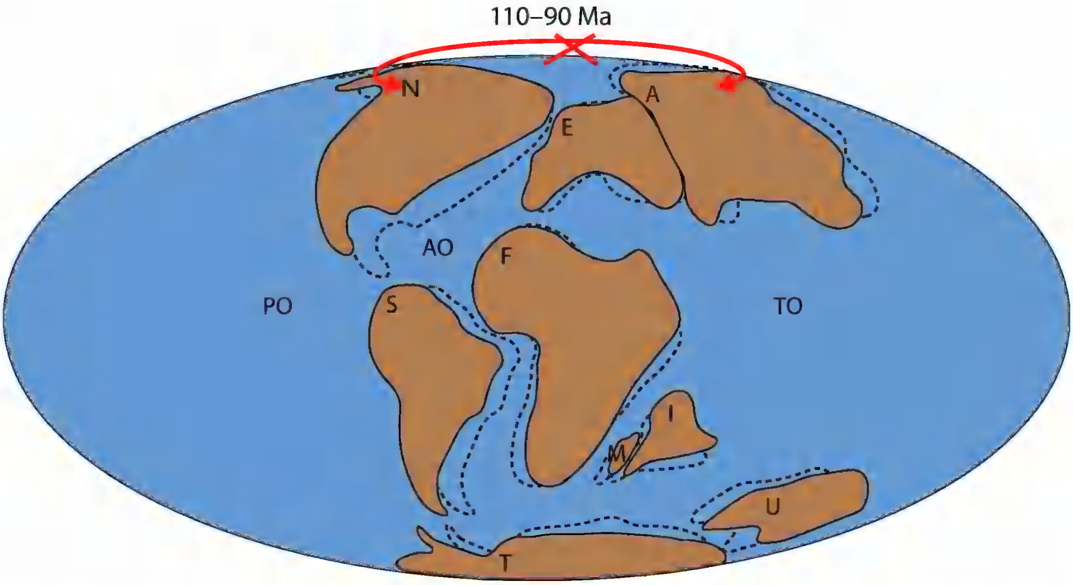

FIG. 7. Hypothesis 5, North America-Asia vicariance event caused by the breakdown of the Bering land bridge during the early Late Cretaceous. The marine barrier between northeast Asia and northwest North America was re-established in the Cenomanian Stage. The red X denotes the approximate position of the hypothesized biogeographical barrier (Bering Strait); Dotted lines denote paleogeography at 110 Ma, while solid lines denote it at 90 Ma. Paleomap after (Matthews et al., 2016). Abbreviations: **A,** Asia; **AO,** Atlantic Ocean; **E,** Europe; **F,** Africa; **I,** India; **M,** Madagascar; **N,** North America; **PO,** Pacific Ocean; **S,** South America; **T,** Antarctica; **TO,** Tethys Ocean; **U,** Australia.

turtles (Joyce et al., 2016), dryolestoid mammals and eilenodontine sphenodontians (Makovicky et al., 2005). However, we also note additional vicariance events that have not figured prominently in previous studies. An example of the latter is the apparent impact of the destruction of land bridges such as that across the Bering Strait (Hypothesis 5, fig. 7), which could explain the occurrence of *Nothronychus* in North America and *Nanshiungosaurus* in Asia (fig. 6). Ephemeral land bridges that reconnect separate areas after continental fragmentation were established from time to time throughout the Cretaceous, enabling intercontinental faunal dispersals. After the loss of these land bridges, the continents became isolated from one another once again and dispersed populations were separated by an oceanic barrier, which eventually caused vicariance. Such vicariance events are observed in the Therizinosauria and Troodontidae after the disappearance of the Bering land bridge during the early Late Cretaceous (fig. 7), and also within the Alvarezsauroidea after the loss of the Apulian route during the mid-Early Cretaceous.

Besides vicariance, the impact of other biogeographic processes on coelurosaurian evolution can also be recognized in our results. As suggested by multiple authors (Sereno, 1999b; Brusatte et al., 2013; Dunhill et al., 2016), dispersal played a major role in shaping coelurosaurian biogeography. The establishment of the Bering land bridge enabled direct Asia-North America dispersal without a transit via Europe. This dispersal route is the most frequently used by coelurosaurians as inferred from our results. Single dispersal events during the first establishment of the Bering land bridge in the late Early Cretaceous (fig. 4) potentially explain the Asian occurrence of the dromaeosaurid *Achillobator* and the North American occurrences of the troodontid *Troodon* and the dromaeosaurid *Dakotaraptor* (fig. 6). Our results therefore partially support

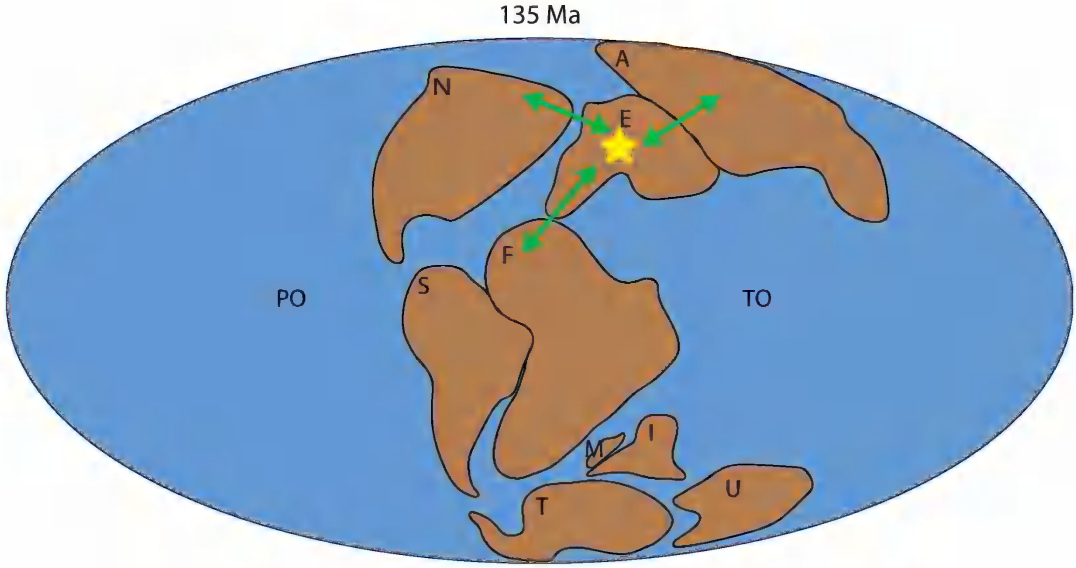

FIG. 8. Europe as a dispersal center and geographical gateway, especially during the Early Cretaceous. The green arrowed lines denote possible dispersal directions and approximate dispersal routes; Solid lines denote paleogeography at 135 Ma. Paleomap after (Matthews et al., 2016). Abbreviations: **A,** Asia; **E,** Europe; **F,** Africa; **I,** India; **M,** Madagascar; **N,** North America; **PO,** Pacific Ocean; **S,** South America; **T,** Antarctica; **TO,** Tethys Ocean; **U,** Australia.

Hypothesis 4 (fig. 4, table 1). Furthermore, the North American occurrence of the alvarezsaurid *Albertonykus* and the ornithomimids *Struthiomimus* and *Ornithomimus* as well as the Asian occurrence of the tyrannosaurid *Alioramus* can be attributed to ancestral dispersal via the Bering land bridge during its second connection in the latest Cretaceous (fig. 4). Thus, together, our results support Hypothesis 4 in full (table 1), indicating that the two episodes of connection across the Bering Strait probably facilitated important faunal exchanges that produced most of the Asia–North America coelurosaurian occurrences throughout the Cretaceous. However, we also support the Apulian route as important for coelurosaurian faunal exchange (Hypothesis 3, fig. 3), an idea that has been somewhat neglected in previous studies. It appears to account for the South American occurrence of the Early Cretaceous compsognathid *Mirischia* and the Late Cretaceous avialans *Patagopteryx* and *Neuquenornis*, while their closest relatives were present in Asia (although multiple intercontinental dispersals probably took place) (fig. 6). The formation of the Apulian route in the late Early Cretaceous marked the first Laurasia-Gondwana connection after the breakup of Pangaea during the Middle Jurassic (fig. 3). Other taxa are believed to have crossed from Gondwana to Laurasia via this route in the Cretaceous, including carcharodontosaurids (Brusatte et al., 2009), and rebbachisaurid (Sereno et al., 2007) and titanosaurian sauropods (Dal Sasso et al., 2016). If earlier-diverging coelurosaurian taxa from Gondwana were not derived from vicariance induced by Pangaean breakup, they most probably arrived from Laurasian landmasses. Although such “Laurasian arrival” hypotheses have been suggested (Naish et al., 2004; Foth and Rauhut, 2017), these biogeographic events were not linked by these authors to the only feasible Laurasia-Gondwana dispersal route known in the Early Cretaceous. In our results, many inferred dispersal events via the Apulian route explain South American coelurosaurian occurrences of their Laurasian relatives, but discoveries of closely related African taxa are lacking. Therefore, new African coelurosaurian discoveries will be crucial for testing Apulian route dispersal events.

Related to the impacts of the Apulian route and trans-Turgai land bridges, our analyses indicate that Europe might have been both a dispersal center and a geographical gateway in coelurosaurian evolution, especially before the Barremian (fig. 8). Although only having a few coelurosaurian occurrences, Europe forms all or part of the geographic range for many ancestral nodes in our results (fig. 6). Several lineages are inferred to have had early-diverging forms in Europe and then dispersed to other continents, while faunas from other lineages disperse from one continent to another via Europe. In the former case, ancestral faunas might have migrated from Europe to North America before the full establishment of the North Atlantic Ocean (e.g., early-diverging coelurosaurians, such as *Ornitholestes* and the Compsognathidae). They might also have migrated from Europe to Asia when terrestrial routes existed across the Turgai Sea (e.g., Compsognathidae as evidenced by the ancestral area estimations for the *Sinosauropteryx* lineage), and to Africa via the Apulian route during the Early Cretaceous (e.g., Ornithomimosauria as evident from *Nqwebasaurus*), and from there to other Gondwanan landmasses. Even without these Cretaceous land bridges, Europe is likely to have played a central role in coelurosaurian dispersal. In particular, ancestral faunas might have migrated between Asia and North America via Europe (e.g., Asia to North America dispersal in *Coelurus*), and from Laurasia to Gondwanan landmasses via Europe before the breakup of Gondwana (e.g., Asia to South America via Europe in alvarezsauroids, consistent with the results of Xu et al., 2018a, on alvarezsauroid biogeography). This conclusion is also consistent with the result found by Dunhill et al. (2016) that European dinosaurians had strong direct connections with those in adjacent continents during the Jurassic and Early Cretaceous. In addition, these authors demonstrated a high degree of connectivity between North America and Asia, Asia and Africa, and Africa and North America during the Early Cretaceous (Dunhill et al., 2016), which can be explained by faunal exchange events via Europe as a dispersal gateway. For example, Laurasian continents shared similar ankylosaurian (Ősi, 2005), hadrosauroid (Prieto-Marquez et al., 2006; Dalla Vecchia, 2009), non-dinosaurian archosaurian (Ezcurra and Agnolín, 2012) and gobiconodontid mammalian (Cuenca-Bescós and Canudo, 2003) faunas, implying faunal exchange among Europe, Asia, and North America. There were also European and Gondwanan faunas that were closely related (Dalla Vecchia, 2003; Gheerbrant and Rage, 2006), including spinosaurid theropods (Charig and Milner, 1997; Ruiz-Omeñaca et al., 2005), sauropods (Canudo et al., 2008), and thereuodontid mammals (Kielan-Jaworowska et al., 2004), that can be attributed to faunal exchanges via the Apulian route. Some Pangaean faunas, including spinosaurid theropods from Asia (Buffetaut et al., 2008), titanosaurian sauropods from Asia and North America (Salgado et al., 1997; Wilson, 2002), and crocodyliforms from Asia (Wu and Sues, 1996), had their closest relatives in Gondwana, and probably arrived from southern continents via Europe. Thus, the events estimated here for European coelurosaurians and their relatives elsewhere, are probably part of a widespread pattern imposed on multiple terrestrial clades by Pangaean fragmentation and the subsequent creation and destruction of key land bridges.

Finally, our results also imply that regional extinction played an important role in coelurosaurian evolution, as suggested by Sereno (1999b). Given frequent dispersals, continental-scale extinction events are necessary to account for the single-area-unit distributions of most coelurosaurian taxa. That regional extinction and dispersal were of comparable importance throughout coelurosaurian evolution is indicated by the similar values of the extinction and dispersal rates obtained in the analyses (table 3).

CONCLUSIONS

There are several uncertainties in our analyses that we should bear in mind. The major ones include: the quality of the fossil record, the accuracy of paleogeographic reconstructions; errors in phylogenetic tree topology and node dating; spatiotemporal sampling biases; and our lack of definitive knowledge of the dispersal abilities of different coelurosaurian clades. Although the phylogenetic tree used here is better sampled than any examined in previous analyses of coelurosaurian biogeography, no single tree includes all known taxa. Phylogenies also change as new morphological data become available, which could then alter estimates of biogeographic events and processes. New fossil discoveries from continents with rare or previously unknown records of particular clades are likely to modify our conclusions in the future (e.g., by changing tree topology, taxon ranges, origin dates, and so on, which in turn could favor other biogeographic patterns and processes). The accuracy of our results is also affected by as yet unquantified preservation biases, which will distort the observed spatial and temporal distributions of coelurosaurians (Upchurch et al., 2011). The second major uncertainty is regarding coelurosaurian dispersal ability. Coelurosaurian body sizes vary by six orders of magnitude, so their dispersal probability across narrow seaways may vary significantly. Avialans and probably some nonavialan paravians developed powered flight ability, which may have freed them from the constraints of conventional terrestrial dispersal corridors. However, these abilities are still not well understood. Future analyses will need to better quantify dispersal ability if we are to move away from the uniform dispersal probabilities assumed in this study, although Mesozoic avialans do not appear to have had the ability to cross expansive oceans using their own flight capabilities (Allen et al., 2013). One group of comparable flying vertebrates is pterosaurs. Although this clade had different biogeographic patterns from other Mesozoic terrestrial vertebrates, quantitative biogeographic analysis revealed little vicariance and dispersal signal, but high levels of sympatry, which indicates rare cross-ocean range-switching events possibly enabled by powered flight (Upchurch et al., 2015). However, such a lack of statistical support for vicariance among pterosaurs might also be attributable to fossil sampling biases. Therefore, a separate and more focused biogeographic analysis of Mesozoic avialans, combined with investigation of the dispersal abilities of various modern bird clades, should be the next step in tackling this issue. Despite these uncertainties, our results demonstrate that continental dispersal, extinction, vicariance, and founder-events were important biogeographic processes during coelurosaurian evolution. Major dispersal corridors included the Apulian route and the Bering land bridge, and Europe might have been an important dispersal center and gateway for coelurosaurians before the mid-Early Cretaceous.

ACKNOWLEDGMENTS

We thank Kenneth H.C. Fung and First Initiative Foundation for their support of the International Pennaraptoran Dinosaur Symposium, which was the catalyst for this chapter. A.D.'s participation in this project was supported by undergraduate student funds from a General Research Fund grant (17103315) awarded to M.P. by the HK Research Grants Council. A.D. was also supported by funding from the HKU MOOC course *Dinosaur Ecosystems* (awarded to M.P.) and from Jason R. Ali of HKU's Department of Earth Sciences; he is also thanked for his input in project discussions. D.J.F. is supported by UK Research and Innovation Future Leaders Fellowship MR/S032177/1. We thank the reviewers James Clark and Fernando Novas, whose critical comments helped to improve the article.

REFERENCES

Agnolín, F.L., J.E. Powell, F.E. Novas, and M. Kundrát. 2012. New alvarezsaurid (Dinosauria, Theropoda) from uppermost Cretaceous of north-western Patagonia with associated eggs. Cretaceous Research 35: 33–56.

Ali, J.R., and M. Huber. 2010. Mammalian biodiversity on Madagascar controlled by ocean currents. Nature 463: 653.

Ali, J.R., and D.W. Krause. 2011. Late Cretaceous bioconnections between Indo-Madagascar and Antarctica: refutation of the Gunnerus Ridge causeway hypothesis. Journal of Biogeography 38: 1855–1872.

Allain, R., R. Vullo, J. Le Loeuff, and J.-F. Tournepiche. 2014. European ornithomimosaurs (Dinosauria, Theropoda): an undetected record. Geologica Acta: an International Earth Science Journal 12 (2): 127–135.

Allen, V., K.T. Bates, Z. Li, and J.R. Hutchinson. 2013. Linking the evolution of body shape and locomotor biomechanics in bird-line archosaurs. Nature 497: 104.

Altangerel, P., M.A. Norell, L.M. Chiappe, and J.M. Clark. 1993. Flightless bird from the Cretaceous of Mongolia. Nature 362: 623.

Alvarenga, H.M., and J.F. Bonaparte. 1992. A new flightless land bird from the Cretaceous of Patagonia. Papers in Avian Paleontology. Natural History Museum of Los Angeles County, Science Series 36: 51–64.

Averianov, A., and H.D. Sues. 2017. The oldest record of Alvarezsauridae (Dinosauria: Theropoda) in the Northern Hemisphere. PLoS One 12 (10): e0186254.

Averianov, A., S. Krasnolutskii, and S. Ivantsov. 2010. A new basal coelurosaur (Dinosauria: Theropoda) from the Middle Jurassic of Siberia. Proceedings of the Zoological Institute of the Russian Academy of Sciences 314: 42–57.

Ball, I.R. 1975. Nature and formulation of biogeographical hypotheses. Systematic Biology 24: 407–430.

Baraboshkin, E.Y., A.S. Alekseev, and L.F. Kopaevich. 2003. Cretaceous palaeogeography of the north-eastern Peri-Tethys. Palaeogeography, Palaeoclimatology, Palaeoecology 196: 177–208.

Bardet, N., et al. 2014. Mesozoic marine reptile palaeobiogeography in response to drifting plates. Gondwana Research 26: 869–887.

Barrett, P.M., R.B. Benson, T.H. Rich, and P. Vickers-Rich. 2011. First spinosaurid dinosaur from Australia and the cosmopolitanism of Cretaceous dinosaur faunas. Biology Letters 7: 933–936.

Benson, R.B. 2008. New information on *Stokesosaurus*, a tyrannosauroid (Dinosauria: Theropoda) from North America and the United Kingdom. Journal of Vertebrate Paleontology 28: 732–750.

Benson, R.B., P.M. Barrett, T.H. Rich, and P. Vickers-Rich. 2010. A southern tyrant reptile. Science 327: 1613–1613.

Benson, R.B., T.H. Rich, P. Vickers-Rich, and M. Hall. 2012. Theropod fauna from southern Australia indicates high polar diversity and climate-driven dinosaur provinciality. PLoS One 7: e37122.

Benton, M., and D.A. Harper. 2013. Introduction to paleobiology and the fossil record: John Wiley & Sons.

Berv, J.S., and D.J. Field. 2018. Genomic signature of an avian Lilliput effect across the K-Pg Extinction. Systematic Biology 67: 1–13.

Bochenski, Z., and Z.M. Bochenski. 2008. An Old World hummingbird from the Oligocene: a new fossil from Polish Carpathians. Journal of Ornithology 149: 211–216.

Bonaparte, J.F. 1986. History of the terrestrial Cretaceous vertebrates of Gondwana. *In* Bonaparte, J.F. (editor), Evolucion de los Vertebrados Mesozoicos: 63-95. Mendoza: IV Congreso Argentino de Paleontología y Biostratigrafía, Mendoza, Actas.

Bonaparte, J.F. 1991. Los vertebrados fósiles de la Formación Río Colorado, de la ciudad de Neuquén y cercanías, Cretácico superior, Argentina. Revista del Museo Argentino de Ciencias Naturales "Bernardino Rivadavia" e Instituto Nacional de Investigacion de Las Ciencias. Paleontologia 4(3): 15–123.

Brikiatis, L. 2014. The De Geer, Thulean and Beringia routes: key concepts for understanding early Cenozoic biogeography. Journal of Biogeography 41: 1036–1054.

Brocklehurst, N., P. Upchurch, P.D. Mannion, and J.M.K. O'Connor. 2012. The completeness of the fossil record of Mesozoic birds: implications for early avian evolution. PloS One 7: e39056.

Brusatte, S.L., and R.B. Benson. 2013. The systematics of Late Jurassic tyrannosauroid theropods from Europe and North America. Acta Palaeontologica Polonica 58: 47–54.

Brusatte, S.L., et al. 2009. The first definitive carcharodontosaurid (Dinosauria: Theropoda) from Asia and the delayed ascent of tyrannosaurids. Naturwissenschaften 96: 1051–1058.

Brusatte, S.L., et al. 2010. Tyrannosaur paleobiology: new research on ancient exemplar organisms. Science 329: 1481–1485.

Brusatte, S.L., et al. 2013. The osteology of *Balaur bondoc*, an island-dwelling dromaeosaurid (Dinosauria: Theropoda) from the Late Cretaceous of Romania. Bulletin of the American Museum of Natural History 374: 1–100.

Brusatte, S.L., G.T. Lloyd, S.C. Wang, and M.A. Norell. 2014. Gradual assembly of avian body plan culminated in rapid rates of evolution across the dinosaur-bird transition. Current Biology 24: 2386–2392.

Buffetaut, E., V. Suteethorn, H. Tong, and R. Amiot. 2008. An Early Cretaceous spinosaurid theropod from southern China. Geological Magazine 145: 745–748.

Canudo, J.I., R. Royo-Torres, and G. Cuenca-Bescós. 2008. A new sauropod: *Tastavinsaurus sanzi* gen. et sp. nov. from the Early Cretaceous (Aptian) of Spain. Journal of Vertebrate Paleontology 28: 712–731.

Carrano, M.T., R.B. Benson, and S.D. Sampson. 2012. The phylogeny of Tetanurae (Dinosauria: Theropoda). Journal of Systematic Palaeontology 10: 211–300.

Case, J.A., J.E. Martin, and M. Reguero. 2007. A dromaeosaur from the Maastrichtian of James Ross Island and the Late Cretaceous Antarctic dinosaur fauna. Open-File Report 2007-1047-SRP-083, U.S. Geological Survey and the National Academies.

Charig, A.J., and A.C. Milner. 1997. *Baryonyx walkeri*, a fish-eating dinosaur from the Wealden of Surrey. Bulletin Natural History Museum Geology Series 53: 11–70.

Chatterjee, S., and R.J. Templin. 2007. Biplane wing planform and flight performance of the feathered dinosaur *Microraptor gui*. Proceedings of the National Academy of Sciences of the United States of America 104: 1576–1580.

Choiniere, J.N., C.A. Forster, and W.J. de Klerk. 2012. New information on *Nqwebasaurus thwazi*, a coelurosaurian theropod from the Early Cretaceous Kirkwood Formation in South Africa. Journal of African Earth Sciences 71: 1–17.

Choiniere, J.N., J.M. Clark, C.A. Forster, and X. Xu. 2010a. A basal coelurosaur (Dinosauria: Theropoda) from the Late Jurassic (Oxfordian) of the Shishugou Formation in Wucaiwan, People's Republic of China. Journal of Vertebrate Paleontology 30: 1773–1796.

Choiniere, J.N., et al. 2010b. A basal alvarezsauroid theropod from the early Late Jurassic of Xinjiang, China. Science 327: 571–574.

Claramunt, S., and J. Cracraft. 2015. A new time tree reveals Earth history's imprint on the evolution of modern birds. Science Advances 1: e1501005.

Clark, J.M., M.A. Norell, and R. Barsbold. 2001. Two new oviraptorids (Theropoda: Oviraptorosauria), Upper Cretaceous Djadokhta Formation, Ukhaa Tolgod, Mongolia. Journal of Vertebrate Paleontology 21: 209–213.

Clarke, J.A. 2004. Morphology, phylogenetic taxonomy, and systematics of *Ichthyornis* and *Apatornis* (Avialae: Ornithurae). Bulletin of the American Museum of Natural History 286: 1–179.

Clarke, J.A., C.P. Tambussi, J.I. Noriega, G.M. Erickson, and R.A. Ketcham. 2005. Definitive fossil evidence for the extant avian radiation in the Cretaceous. Nature 433: 305.

Clarke, J.A., D.T. Ksepka, N.A. Smith, and M.A. Norell. 2009. Combined phylogenetic analysis of a new North American fossil species confirms widespread Eocene distribution for stem rollers (Aves, Coracii). Zoological Journal of the Linnean Society 157: 586–611.

Close, R.A., et al. 2009. Earliest Gondwanan bird from the Cretaceous of southeastern Australia. Journal of Vertebrate Paleontology 29: 616–619.

Condie, K.C. 1997. Plate tectonics and crustal evolution: New York: Elsevier.

Cracraft, J. 2001. Avian evolution, Gondwana biogeography and the Cretaceous-Tertiary mass extinction event. Proceedings of the Royal Society B, Biological Sciences 268: 459–469.

Cracraft, J., and S. Claramunt. 2017. Conceptual and analytical worldviews shape differences about global avian biogeography. Journal of Biogeography 44: 958–960.

Csiki, Z., M. Vremir, S.L. Brusatte, and M.A. Norell. 2010. An aberrant island-dwelling theropod dinosaur from the Late Cretaceous of Romania. Proceedings of the National Academy of Sciences of the United States of America 107: 15357–15361.

Cuenca-Bescós, G., and J.I. Canudo. 2003. A new gobiconodontid mammal from the Early Cretaceous of Spain and its palaeogeographic implications. Acta Palaeontologica Polonica 48: 575–582.

Currie, P.J. 1987. Bird-like characteristics of the jaws and teeth of troodontid theropods (Dinosauria, Saurischia). Journal of Vertebrate Paleontology 7: 72–81.

Dal Sasso, C., G. Pierangelini, F. Famiani, A. Cau, and U. Nicosia. 2016. First sauropod bones from Italy offer new insights on the radiation of Titanosauria between Africa and Europe. Cretaceous Research 64: 88–109.

Dalla Vecchia, F.M. 2003. Observations on the presence of plant-eating dinosaurs in an oceanic carbonate platform. Natura Nascosta 27: 14–27.

Dalla Vecchia, F.M. 2009. *Tethyshadros insularis*, a new hadrosauroid dinosaur (Ornithischia) from the Upper Cretaceous of Italy. Journal of Vertebrate Paleontology 29: 1100–1116.

De Klerk, W.J., C.A. Forster, S.D. Sampson, A. Chinsamy, and C.F. Ross. 2000. A new coelurosaurian dinosaur from the Early Cretaceous of South Africa. Journal of Vertebrate Paleontology 20: 324–332.

de Souza Carvalho, I., et al. 2015. A Mesozoic bird from Gondwana preserving feathers. Nature Communications 6: 1–5.

Dececchi, T.A., H.C.E. Larsson, and M.B. Habib. 2016. The wings before the bird: an evaluation of flapping-based locomotory hypotheses in bird antecedents. PeerJ 4: e2159.

Dunhill, A.M., J. Bestwick, H. Narey, and J. Sciberras. 2016. Dinosaur biogeographical structure and Mesozoic continental fragmentation: a network-based approach. Journal of Biogeography 43: 1691–1704.

Eagles, G., and M. König. 2008. A model of plate kinematics in Gondwana breakup. Geophysical Journal International 173: 703–717.

Elzanowski, A. 1974. Preliminary note on the palaeognathous bird from the Upper Cretaceous of Mongolia. Acta Palaeontologia Polonica 30: 103–109.

Ezcurra, M.D., and F.L. Agnolín. 2012. A new global palaeobiogeographical model for the Late Mesozoic and Early Tertiary. Systematic Biology 61 (4): 553–566.

Farke, A.A., and G.E. Phillips. 2017. The first reported ceratopsid dinosaur from eastern North America (Owl Creek Formation, Upper Cretaceous, Mississippi, USA). PeerJ 5: e3342.

Fastovsky, D.E., D.B. Weishampel, and A. Charig. 1996. The evolution and extinction of the dinosaurs. Cambridge: Cambridge University Press.

Feduccia, A. 2014. Avian extinction at the end of the Cretaceous: assessing the magnitude and subsequent explosive radiation. Cretaceous Research 50: 1–15.

Field, D.J., and A.Y. Hsiang. 2018. A North American stem turaco, and the complex biogeographic history of modern birds. BMC Evolutionary Biology 18: 102.

Field, D.J., et al. 2020. Late Cretaceous neornithine from Europe illuminates the origins of crown birds. Nature 579: 397–401.

Fiorillo, A.R., and T.L. Adams. 2012. A therizinosaur track from the Lower Cantwell Formation (Upper Cretaceous) of Denali National Park, Alaska. Palaios 27: 395–400.

Fiorillo, A.R., et al. 2018. An unusual association of hadrosaur and therizinosaur tracks within Late Cretaceous rocks of Denali National Park, Alaska. Scientific Reports 8: 11706.

Forster, C.A., L.M. Chiappe, D.W. Krause, and S.D. Sampson. 1996. The first Cretaceous bird from Madagascar. Nature 382: 532.

Foth, C., and O.W. Rauhut. 2017. Re-evaluation of the Haarlem *Archaeopteryx* and the radiation of maniraptoran theropod dinosaurs. BMC Evolutionary Biology 17 (1): 236.

Foth, C., H. Tischlinger, and O.W. Rauhut. 2014. New specimen of *Archaeopteryx* provides insights into the evolution of pennaceous feathers. Nature 511: 79–82.

Funston, G.F., and P.J. Currie. 2016. A new caenagnathid (Dinosauria: Oviraptorosauria) from the Horseshoe Canyon Formation of Alberta, Canada, and a reevaluation of the relationships of Caenagnathidae. Journal of Vertebrate Paleontology 36: e1160910.

Gaina, C., et al. 2013. The African plate: A history of oceanic crust accretion and subduction since the Jurassic. Tectonophysics 604: 4–25.

Galton, P.M., and L.D. Martin. 2002. *Enaliornis*, an Early Cretaceous hesperornithiform bird from England, with comments on other Hesperornithiformes. *In* L.M. Chiappe and L.M. Witmer (editors), Mesozoic birds: above the heads of dinosaurs: 317–338. Berkeley: University of California Press.

Gheerbrant, E., and J.-C. Rage. 2006. Paleobiogeography of Africa: how distinct from Gondwana and Laurasia? Palaeogeography, Palaeoclimatology, Palaeoecology 241: 224–246.

Godefroit, P., et al. 2013. A Jurassic avialan dinosaur from China resolves the early phylogenetic history of birds. Nature 498: 359–362.

Göhlich, U.B., and L.M. Chiappe. 2006. A new carnivorous dinosaur from the Late Jurassic Solnhofen archipelago. Nature 440: 329.

Goloboff, P.A., A. Torres Galvis, and J.S. Arias. 2018a. Parsimony and model-based phylogenetic methods for morphological data: comments on O'Reilly et al. Palaeontology 61: 625–630.

Goloboff, P.A., A. Torres, and J.S. Arias. 2018b. Weighted parsimony outperforms other methods of phylogenetic inference under models appropriate for morphology. Cladistics 34: 407–437.

Goodwin, M.B., et al. 1999. Mesozoic continental vertebrates with associated palynostratigraphic dates from the northwestern Ethiopian Plateau. Journal of Vertebrate Paleontology 19: 728–741.

Goswami, A., G. Prasad, O. Verma, J. Flynn, and R. Benson. 2013. A troodontid dinosaur from the latest Cretaceous of India. Nature Communications 4: 1703.

Houde, P., and S.L. Olson. 1992. A radiation of coly-like birds from the early Eocene of North America (Aves: Sandcoleiformes new order). *In* K.E. Campbell (editor), Papers in avian paleontology honoring Pierce Brodkorb: 137–160. Natural History Museum of Los Angeles County, Science Series.

Hwang, S.H., M.A. Norell, J. Qiang, and G. Keqin. 2004. A large compsognathid from the Early Cretaceous Yixian Formation of China. Journal of Systematic Palaeontology 2: 13–30.

Imai, T., et al. 2019. An unusual bird (Theropoda, Avialae) from the Early Cretaceous of Japan suggests complex evolutionary history of basal birds. Communications Biology 2: 399.

Jarvis, E.D., et al. 2014. Whole-genome analyses resolve early branches in the tree of life of modern birds. Science 346: 1320–1331.

Ji, Q., et al. 2003. An early ostrich dinosaur and implications for ornithomimosaur phylogeny. American Museum Novitates 3420: 1–19.

Joyce, W.G., M. Rabi, J.M. Clark, and X. Xu. 2016. A toothed turtle from the Late Jurassic of China and the global biogeographic history of turtles. BMC Evolutionary Biology 16: 236.

Karhu, A. 1988. A new family of swift-like birds from the Paleogene of Europe. Paleontologicheskii Zhurnal 3: 78–88.

Karhu, A. 1992. Morphological divergence within the order Apodiformes as revealed by the structure of the humerus. *In* K.E. Campbell (editor), Papers in avian paleontology honoring Pierce Brodkorb: 379–384. Los Angeles: Natural History Museum of Los Angeles County, Science Series.

Karhu, A. 1999. A new genus and species of the family Jungornithidae (Apodiformes) from the Late Eocene of the Northern Caucasus, with comments on the ancestry of hummingbirds. *In* S.L. Olson (editor), Avian paleontology at the close of the 20th century. Proceedings of the 4th international meeting of the Society of Avian Paleontology and Evolution: 207–216. Washington, D.C.: Smithsonian Contributions to Paleobiology.

Kielan-Jaworowska, Z., R.L. Cifelli, and Z.-X. Luo. 2004. Mammals from the age of dinosaurs: origins, evolution, and structure: Columbia University Press.

Kirkland, J.I., and D.G. Wolfe. 2001. First definitive therizinosaurid (Dinosauria; Theropoda) from North America. Journal of Vertebrate Paleontology 21: 410–414.

Krause, D.W., et al. 2006. Late Cretaceous terrestrial vertebrates from Madagascar: implications for Latin American biogeography. Annals of the Missouri Botanical Garden 93: 178–208.

Krause, D.W., S.D. Sampson, M.T. Carrano, and P.M. O'Connor. 2007. Overview of the history of discovery, taxonomy, phylogeny, and biogeography of *Majungasaurus crenatissimus* (Theropoda: Abelisauridae) from the Late Cretaceous of Madagascar. Journal of Vertebrate Paleontology 27 (S2): 1–20.

Ksepka, D.T., and J.A. Clarke. 2009. Affinities of *Palaeospiza bella* and the phylogeny and biogeography of mousebirds (Coliiformes). Auk 126: 245–259.

Ksepka, D.T., and J.A. Clarke. 2010a. New fossil mousebird (Aves: Coliiformes) with feather preservation provides insight into the ecological diversity of an Eocene North American avifauna. Zoological Journal of the Linnean Society 160: 684–706.

Ksepka, D.T., and J.A. Clarke. 2010b. *Primobucco mcgrewi* (Aves: Coracii) from the Eocene Green River Formation: new anatomical data from the earliest constrained record of stem rollers. Journal of Vertebrate Paleontology 30: 215–225.

Landis, M.J., N.J. Matzke, B.R. Moore, and J.P. Huelsenbeck. 2013. Bayesian analysis of biogeography when the number of areas is large. Systematic Biology 62: 789–804.

Leidy, J. 1856. Notice of remains of extinct reptiles and fishes, discovered by Dr. FV Hayden in the Bad Lands of the Judith River, Nebraska Territory. Proceedings of the Academy of Natural Sciences of Philadelphia 8: 72–73.

Liyong, J., C. Jun, and P. Godefroit. 2012. A new basal ornithomimosaur (Dinosauria: Theropoda) from the early Cretaceous Yixian formation, Northeast China. Bernissart Dinosaurs and Early Cretaceous Terrestrial Ecosystems: 467.

Loewen, M.A., R.B. Irmis, J.J. Sertich, P.J. Currie, and S.D. Sampson. 2013. Tyrant dinosaur evolution tracks the rise and fall of Late Cretaceous oceans. PLoS One 8: e79420.

Longrich, N.R., and P.J. Currie. 2009a. *Albertonykus borealis*, a new alvarezsaur (Dinosauria: Theropoda) from the Early Maastrichtian of Alberta, Canada: implications for the systematics and ecology of the Alvarezsauridae. Cretaceous Research 30: 239–252.

Longrich, N.R., and P.J. Currie. 2009b. A microraptorine (Dinosauria-Dromaeosauridae) from the Late Cretaceous of North America. Proceedings of the National Academy of Sciences of the United States of America 106: 5002–5007.

Louchart, A., N. Tourment, J. Carrier, T. Roux, and C. Mourer-Chauviré. 2008. Hummingbird with modern feathering: an exceptionally well-preserved Oligocene fossil from southern France. Naturwissenschaften 95: 171–175.

Lü, J., et al. 2010. A new troodontid theropod from the Late Cretaceous of central China, and the radiation of Asian troodontids. Acta Palaeontologica Polonica 55: 381–388.

Lü, J., et al. 2015. A new oviraptorid dinosaur (Dinosauria: Oviraptorosauria) from the Late Cretaceous of southern China and its paleobiogeographical implications. Scientific Reports 5: 11490.

Makovicky, P.J., and M.A. Norell. 2004. Troodontidae. *In* D.B. Weishampel, P. Dodson, and H. Osmólska (editors), The Dinosauria: 184–195.

Makovicky, P.J., and H.-D. Sues. 1998. Anatomy and phylogenetic relationships of the theropod dinosaur *Microvenator celer* from the Lower Cretaceous of Montana. American Museum Novitates 3240: 1–27.

Makovicky, P.J., S. Apesteguía, and F.L. Agnolín. 2005. The earliest dromaeosaurid theropod from South America. Nature 437: 1007.

Marsh, O.C. 1879. Notice of new Jurassic reptiles. American Journal of Science 108: 501–505.

Martin, L.D., and O. Bonner. 1977. An immature specimen of *Baptornis advenus* from the Cretaceous of Kansas. Auk: 787–789.

Matthews, K.J., et al. 2016. Global plate boundary evolution and kinematics since the late Paleozoic. Global and Planetary Change 146: 226–250.

Matzke, N.J. 2013. Probabilistic historical biogeography: new models for founder-event speciation, imperfect detection, and fossils allow improved accuracy and model-testing. Ph.D. dissertation, University of California, Berkeley. Online resource.

Mayr, G. 2000. New or previously unrecorded avian taxa from the Middle Eocene of Messel (Hessen, Germany). Mitteilungen aus dem Museum für Naturkunde in Berlin. Geowissenschaftliche Reihe 3: 207–219.

Mayr, G. 2001. New specimens of the Middle Eocene fossil mousebird *Selmes absurdipes* Peters 1999. Ibis 143: 427–434.

Mayr, G. 2002a. A new species of *Plesiocathartes* (Aves:? Leptosomidae) from the middle Eocene of Messel, Germany. PaleoBios 22: 10–20.

Mayr, G. 2002b. Avian Remains from the Middle Eocene of the Geiseltal (Sachsen-Anhalt, Germany). *In* Z. Zhou and F. Zhang (editors), Proceedings of the 5th symposium of the Society of Avian Paleontology and Evolution, Beijing, 1–4 June 2000: 77–96. Beijing: Science Press.

Mayr, G. 2003. Phylogeny of early Tertiary swifts and hummingbirds (Aves: Apodiformes). Auk 120: 145–151.

Mayr, G. 2004. Old World fossil record of modern-type hummingbirds. Science 304: 861–864.

Mayr, G. 2008. The Madagascan "Cuckoo-Roller" (Aves: Leptosomidae) is not a roller–notes on the phylogenetic affinities and evolutionary history of a "living fossil." Acta Ornithologica 43: 226–230.

Mayr, G. 2009. Paleogene fossil birds. Berlin: Springer.

Mayr, G. 2015. Eocene fossils and the early evolution of frogmouths (Podargiformes): further specimens of *Masillapodargus* and a comparison with *Fluvioviridavis*. Palaeobiodiversity and Palaeoenvironments 95: 587–596.

Mayr, G. 2017. Avian higher level biogeography: southern hemispheric origins or southern hemispheric relicts? Journal of Biogeography 44: 956–958.

Mayr, G., and D. Peters. 1998. The mousebirds (Aves: Coliiformes) from the Middle Eocene of Grube Messel (Hessen, Germany). Senckenbergiana Lethaea 78 (1–2): 179–197.

Mayr, G., and V.L. De Pietri. 2014. Earliest and first Northern Hemispheric hoatzin fossils substantiate Old World origin of a "neotropic endemic." Naturwissenschaften 101: 143–148.

Mayr, G., C. Mourer-Chauviré, and I. Weidig. 2004. Osteology and systematic position of the Eocene Primobucconidae (Aves, Coraciiformes sensu stricto), with first records from Europe. Journal of Systematic Palaeontology 2: 1–12.

Mourer-Chauviré, C. 1999. Les relations entre les avifaunes du Tertiaire inférieur d'Europe et d'Amérique du Sud. Bulletin de la Société Géologique de France 170: 85–90.

Mourer-Chauviré, C. 2006. The avifauna of the Eocene and Oligocene phosphorites du Quercy (France): an updated list. Strata 1 (13): 135–149.

Mourer-Chauviré, C., and J. Cheneval. 1983. Les Sagittariidae fossiles (Aves, Accipitriformes) de l'Oligocène des phosphorites du Quercy et du

Miocène inférieur de Saint-Gérand-le-Puy. Geobios 16: 443–459.

Naish, D., and G.J. Dyke. 2004. *Heptasteornis* was no ornithomimid, troodontid, dromaeosaurid or owl: the first alvarezsaurid (Dinosauria: Theropoda) from Europe. Neues Jahrbuch für Geologie und Palaontologie 7: 385–401.

Naish, D., D.M. Martill, and E. Frey. 2004. Ecology, systematics and biogeographical relationships of dinosaurs, including a new theropod, from the Santana Formation (? Albian, Early Cretaceous) of Brazil. Historical Biology 16: 57–70.

Nesbitt, S.J., D.T. Ksepka, and J.A. Clarke. 2011. Podargiform Affinities of the Enigmatic *Fluvioviridavis platyrhamphus* and the Early Diversification of Strisores ("Caprimulgiformes" + Apodiformes). PLoS One 6: e26350.

Novas, F.E., and D. Pol. 2005. New evidence on deinonychosaurian dinosaurs from the Late Cretaceous of Patagonia. Nature 433: 858.

Novas, F.E., M.D. Ezcurra, F.L. Agnolín, D. Pol, and R. Ortíz. 2012. New Patagonian Cretaceous theropod sheds light about the early radiation of Coelurosauria. Revista del Museo Argentino de Ciencias Naturales 14: 57–81.

Novas, F.E., F.L. Agnolín, M.D. Ezcurra, J. Porfiri, and J.I. Canale. 2013. Evolution of the carnivorous dinosaurs during the Cretaceous: the evidence from Patagonia. Cretaceous Research 45: 174–215.

Novas, F.E., F.B. Egli, F.L. Agnolín, F.A. Gianechini, and I. Cerda. 2018. Postcranial osteology of a new specimen of *Buitreraptor gonzalezorum* (Theropoda, Unenlagiidae). Cretaceous Research 83: 127–167.

O'Connor, J.K., and N.Z. Zelenkov. 2013. The phylogenetic position of *Ambiortus*: comparison with other Mesozoic birds from Asia. Paleontological Journal 47: 1270–1281.

O'Donovan, C., A. Meade, and C. Venditti. 2018. Dinosaurs reveal the geographical signature of an evolutionary radiation. Nature Ecology and Evolution 2: 452.

O'Reilly, J.E., M.N. Puttick, D. Pisani, and P.C. Donoghue. 2018. Probabilistic methods surpass parsimony when assessing clade support in phylogenetic analyses of discrete morphological data. Palaeontology 61: 105–118.

Osborn, H.F. 1903. *Ornitholestes hermanni*, a new compsognathoid dinosaur from the Upper Jurassic. Bulletin of the American Museum of Natural History 19 (12): 459–464.

Osborn, H.F., P.C. Kaisen, and G. Olsen. 1924. Three new Theropoda, *Protoceratops* zone, central Mongolia. American Museum Novitates 144: 1–12.

Ősi, A. 2005. *Hungarosaurus tormai*, a new ankylosaur (Dinosauria) from the Upper Cretaceous of Hungary. Journal of Vertebrate Paleontology 25: 370–383.

Padian, K. 2004. Basal Avialae. *In* D.B. Weishampel, P. Dodson, and H. Osmólska (editors), The Dinosauria: 210–231. Berkeley: University of California Press.

Peters, D.S. 1995. *Idiornis tuberculata* n. spec., ein weiterer ungewöhnlicher Vogel aus der Grube Messel (Aves: Gruiformes: Cariamidae: Idiornithinae). *In* D.S. Peters (editor), Acta Palaeornithologica: 107–119. Frankfurt: Courier Forschungsinstitut Senckenberg.

Plafker, G., and H.C. Berg. 1994. Overview of the geology and tectonic evolution of Alaska. *In* The geology of Alaska: 989–1021. Boulder, CO: Geological Society of America.

Porfiri, J.D., et al. 2014. Juvenile specimen of *Megaraptor* (Dinosauria, Theropoda) sheds light about tyrannosauroid radiation. Cretaceous Research 51: 35–55.

Porfiri, J.D., R.D.J. Valieri, D.D. Santos, and M.C. Lamanna. 2018. A new megaraptoran theropod dinosaur from the Upper Cretaceous Bajo de la Carpa Formation of northwestern Patagonia. Cretaceous Research 89: 302–319.

Poropat, S.F., et al. 2016. New Australian sauropods shed light on Cretaceous dinosaur palaeobiogeography. Science Reports 6: 34467.

Prieto-Marquez, A., R. Gaete, G. Rivas, Á. Galobart, and M. Boada. 2006. Hadrosauroid dinosaurs from the Late Cretaceous of Spain: *Pararhabdodon isonensis* revisited and *Koutalisaurus kohlerorum*, gen. et sp. nov. Journal of Vertebrate Paleontology 26: 929–943.

Prum, R.O., et al. 2015. A comprehensive phylogeny of birds (Aves) using targeted next-generation DNA sequencing. Nature 526: 569–573.

Rauhut, O.W., A.C. Milner, and S. Moore-Fay. 2010. Cranial osteology and phylogenetic position of the theropod dinosaur *Proceratosaurus bradleyi* (Woodward, 1910) from the Middle Jurassic of England. Zoological Journal of the Linnean Society 158 (1): 155–195.

Ree, R.H. 2005. Detecting the historical signature of key innovations using stochastic models of character evolution and cladogenesis. Evolution 59: 257–265.

Ree, R.H., and S.A. Smith. 2008. Maximum likelihood inference of geographic range evolution by dispersal, local extinction, and cladogenesis. Systematic Biology 57: 4–14.

Ronquist, F. 1997. Dispersal-vicariance analysis: a new approach to the quantification of historical biogeography. Systematic Biology 46: 195–203.

Ronquist, F., and I. Sanmartín. 2011. Phylogenetic methods in biogeography. Annual Review of Ecology, Evolution, and Systematics 42: 441–464.

Ruiz-Omeñaca, J.I., J.I. Canudo, P. Cruzado-Caballero, P. Infante, and M. Moreno-Azanza. 2005. Baryonychine teeth (Theropoda: Spinosauridae) from the Lower Cretaceous of La Cantalera (Josa, NE Spain). Kaupia 14: 59–63.

Salgado, L., R.A. Coria, and J.O. Calvo. 1997. Evolution of titanosaurid sauropods: phylogenetic analysis based on the postcranial evidence. Ameghiniana 34: 3–32.

Sanmartín, I., and F. Ronquist. 2004. Southern hemisphere biogeography inferred by event-based models: plant versus animal patterns. Systematic Biology 53: 216–243.

Sanz, J. 1990. Los reptiles mesozoicos del registro español. [Madrid]: Museo Nacional de Ciencias Naturales: Consejo Superior de Investigaciones Científicas.

Sanz, J.L., L.M. Chiappe, and A.D. Buscalioni. 1995. The osteology of *Concornis lacustris* (Aves, Enantiornithes) from the Lower Cretaceous of Spain and a reexamination of its phylogenetic relationships. American Museum Novitates 3133: 1–23.

Sanz, J.L., et al. 1996. An Early Cretaceous bird from Spain and its implications for the evolution of avian flight. Nature 382: 442.

Saupe, E.E., et al. 2019. Climatic shifts drove major contractions in avian latitudinal distributions throughout the Cenozoic. Proceedings of the National Academy of Sciences of the United States of America 116: 12895–12900.

Scotese, C.R. 2001. Paleomap project. Online resource (http://www.scotese.com/).

Senter, P., J.I. Kirkland, J. Bird, and J.A. Bartlett. 2010. A new troodontid theropod dinosaur from the Lower Cretaceous of Utah. PloS One 5: e14329.

Sereno, P.C. 1997. The origin and evolution of dinosaurs. Annual Review of Earth and Planetary Sciences 25: 435–489.

Sereno, P.C. 1999a. Dinosaurian biogeography: vicariance, dispersal and regional extinction. National Science Museum Monographs 15: 249–257.

Sereno, P.C. 1999b. The evolution of dinosaurs. Science 284: 2137–2147.

Sereno, P.C., J.A. Wilson, and J.L. Conrad. 2004. New dinosaurs link southern landmasses in the Mid-Cretaceous. Proceedings of the Royal Society of London B, Biological Sciences 27: 1325–1330.

Sereno, P.C., et al. 2007. Structural extremes in a Cretaceous dinosaur. PLoS One 2: e1230.

Seton, M., et al. 2012. Global continental and ocean basin reconstructions since 200 Ma. Earth-Science Reviews 113: 212–270.

Smith, A.G., D.G. Smith, and B.M. Funnell. 2004. Atlas of Mesozoic and Cenozoic coastlines. Cambridge: Cambridge University Press.

Tobalske, B., T. Hedrick, K. Dial, and A. Biewener. 2003. Comparative power curves in bird flight. Nature 421: 363.

Turner, A.H., D. Pol, J.A. Clarke, G.M. Erickson, and M.A. Norell. 2007. A basal dromaeosaurid and size evolution preceding avian flight. Science 317: 1378–1381.

Turner, A.H., P.J. Makovicky, and M.A. Norell. 2012. A review of dromaeosaurid systematics and paravian phylogeny. Bulletin of the American Museum of Natural History 371: 1–206.

Upchurch, P. 2008. Gondwanan break-up: legacies of a lost world? Trends in Ecology and Evolution 23: 229–236.

Upchurch, P., C.A. Hunn, and D.B. Norman. 2002. An analysis of dinosaurian biogeography: evidence for the existence of vicariance and dispersal patterns caused by geological events. Proceedings of the Royal Society of London Series B, Biological Sciences 269: 613–621.

Upchurch, P., P.D. Mannion, R.B. Benson, R.J. Butler, and M.T. Carrano. 2011. Geological and anthropogenic controls on the sampling of the terrestrial fossil record: a case study from the Dinosauria. Geological Society, London, Special Publications 358: 209–240.

Upchurch, P., B. Andres, R.J. Butler, and P.M. Barrett. 2015. An analysis of pterosaurian biogeography: implications for the evolutionary history and fossil record quality of the first flying vertebrates. Historical Biology 27: 697–717.

von Huene, B.F. 1926. LX.—On several known and unknown reptiles of the order Saurischia from England and France. Journal of Natural History 17: 473–489.

Vullo, R., et al. 2014. Palaeontology of the Purbeck-type (Tithonian, Late Jurassic) bonebeds of Chassiron (Oléron Island, western France). Comptes Rendus Palevol 13: 421–441.

Walker, C.A., E. Buffetaut, and G.J. Dyke. 2007. Large euenantiornithine birds from the Cretaceous of southern France, North America and Argentina. Geological Magazine 144: 977–986.

Weishampel, D.B., P. Dodson, and H. Osmólska (editors). 2004. The Dinosauria. Berkeley: University of California Press.

Wellnhofer, P. 2009. *Archaeopteryx*: the icon of evolution München: Verlag Dr. Friedrich Pfeil.

Wilson, J. 2002. Sauropod dinosaur phylogeny: critique and cladistic analysis. Zoological Journal of the Linnean Society 136: 215–275.

Wu, X.C., and H.D. Sues. 1996. Anatomy and phylogenetic relationships of *Chimaerasuchus paradoxus*, an unusual crocodyliform reptile from the Lower Cretaceous of Hubei, China. Journal of Vertebrate Paleontology 16: 688–702.

Xu, L., et al. 2011a. A new ornithomimid dinosaur with North American affinities from the Late Cretaceous Qiupa Formation in Henan Province of China. Cretaceous Research 32: 213–222.

Xu, X., et al. 2006. A basal tyrannosauroid dinosaur from the Late Jurassic of China. Nature 439: 715–718.

Xu, X., Q.W. Tan, J.M. Wang, X.J. Zhao, and L. Tan. 2007. A gigantic bird-like dinosaur from the Late Cretaceous of China. Nature 447: 844–847.

Xu, X., et al. 2011b. A monodactyl nonavian dinosaur and the complex evolution of the alvarezsauroid hand. Proceedings of the National Academy of Sciences of the United States of America 108: 2338–2342.

Xu, X., et al. 2014. An integrative approach to understanding bird origins. Science 346: 1341–1351.

Xu, X., et al. 2018a. Two Early Cretaceous fossils document transitional stages in alvarezsaurian dinosaur evolution. Current Biology 28: 2853–2860.

Xu, X., et al. 2018b. A new Middle Jurassic diplodocoid suggests an earlier dispersal and diversification of sauropod dinosaurs. Nature Communications 9: 2700.

Zanno, L.E. 2010. A taxonomic and phylogenetic reevaluation of Therizinosauria (Dinosauria: Maniraptora). Journal of Systematic Palaeontology 8: 503–543.

Zanno, L.E., and P.J. Makovicky. 2011. Herbivorous ecomorphology and specialization patterns in theropod dinosaur evolution. Proceedings of the National Academy of Sciences of the United States of America 108: 232–237.

Zanno, L.E., D.J. Varricchio, P.M. O'Connor, A.L. Titus, and M.J. Knell. 2011. A new troodontid theropod, *Talos sampsoni* gen. et sp. nov., from the Upper Cretaceous Western Interior Basin of North America. PloS One 6: e24487.

Zarcone, G., et al. 2010. A possible bridge between Adria and Africa: new palaeobiogeographic and stratigraphic constraints on the Mesozoic palaeogeography of the Central Mediterranean area. Earth-Science Reviews 103 (3–4): 154–162.

Zelenkov, N.V., and G.J. Dyke. 2008. The fossil record and evolution of mousebirds (Aves: Coliiformes). Palaeontology 51: 1403–1418.

Zelenkov, N.V., and A.O. Averianov. 2016. A historical specimen of enantiornithine bird from the Early Cretaceous of Mongolia representing a new taxon with a specialized neck morphology. Journal of Systematic Palaeontology 14: 319–338.

Zheng, X.T., et al. 2013. Hind wings in basal birds and the evolution of leg feathers. Science 339: 1309–1312.

Zhou, Z.H., and F.C. Zhang. 2006. Mesozoic birds of China – a synoptic review. Vertebrata PalAsiatica 44: 74–98.

APPENDIX

LOCALITY, FORMATION AND AGE DATA FOR STUDY TAXA

Taxon	**Modern Locality**	**Formation and Age**
Achillesaurus	Paso Córdova, Río Negro Province, Argentina	Bajo de la Carpa Formation (86.3–83.6 Ma)
Achillobator giganticus	Burkhant, Dornogov, Mongolia	Bayan Shireh Formation (100.5–83.6 Ma)
Adasaurus mongoliensis	Bugin Tsav, Omnogov, Mongolia	Nemegt Formation (72.1–66.0 Ma)
Albertonykus	*Albertosaurus* bonebed, Dry Island Buffalo Jump Provincial Park, Alberta, Canada	Horseshoe Canyon Formation (72.1-66.0 Ma)
Albertosaurus sarcophagus	Kneehills Creek, Alberta, Canada	Horseshoe Canyon Formation (73–66.0 Ma)
Albinykus	Khugenetslavkant, Dornogov, Mongolia	Javkhlant Formation (86.3–72.1 Ma)
Alioramus	Nogon Tsav, Bayankhongor, Mongolia	Nogon Tsav Formation (72.1–66.0 Ma)
Alvarezsaurus calvoi	Boca del Sapo, Universidad Nacional del Comahue, Neuquén, Argentina	Bajo de la Carpa Formation (86.3–83.6 Ma)
Alxasaurus elesitaiensis	Elesitai, Nei Mongol, China	Bayan Gobi Formation (125–100.5 Ma)
Anchiornis huxleyi	Jianchang, Liaoning, China	Tiaojishan Formation (163.5–157.3 Ma)
Anserimimus planinychus	Bugin Tsav, Omnogov, Mongolia	Nemegt Formation (72.1–66.0 Ma)
Appalachiosaurus	Montgomery County, AL	Demopolis Formation (78–76 Ma)
Apsaravis ukhaana	Camels Humps Amphitheater, Ukhaa Tolgod, Omnogov, Mongolia	Djadokhta Formation (83.6–72.1 Ma)
Archaeopteryx Berlin	Blumenberg quarry, Eichstätt, Bayern, Germany	Solnhofen Limestone (Altmühltal Formation) (152.1–148 Ma)
Archaeopteryx Eichstätt	Workerszell, Eichstätt, Bayern, Germany	Solnhofen Limestone (Altmühltal Formation) (152.1–148 Ma)
Archaeopteryx Haarlem (also thought to be an anchiornithine: *Ostromia*; possibly a troodontid)	Riedenburg, Bayern, Germany	Painten Formation (152.1–145 Ma)
Archaeopteryx London	Langenaltheim quarry, Bayern, Germany	Solnhofen Limestone (Altmühltal Formation) (152.1–148 Ma)
Archaeopteryx Munich	Langenaltheim quarry, Bayern, Germany	Solnhofen Limestone (Altmühltal Formation) (152.1–148 Ma)
Archaeopteryx Thermopolis	Solnhofen, Bayern, Germany	Solnhofen Limestone (Altmühltal Formation) (152.1–148 Ma)
Archaeopteryx Solnhofen	Altmühl Valley, Bayern, Germany	Solnhofen Limestone (Altmühltal Formation) (152.1–148 Ma)

APPENDIX *continued*

Taxon	**Modern Locality**	**Formation and Age**
Archaeopteryx 11th	Eichstätt, Bayern, Germany	Solnhofen Limestone (Altmühltal Formation) (152.1–148 Ma)
Archaeornithomimus asiaticus	Johnson Quarry, Iren Dabasu, Nei Mongol, China	Iren Dabasu Formation (83.6–66.0 Ma)
Atrociraptor marshalli	Dunphy, Alberta, Canada	Horseshoe Canyon Formation (73.5–67.5 Ma)
Aurornis	Jianchang, Liaoning, China	Tiaojishan Formation (163.5–157.3 Ma)
Austroraptor	Bajo de Santa Rosa locality, Río Negro, Argentina	Allen Formation (83.6–66.0 Ma)
Avimimus portentosus	Udan-Sayr, Omnogov, Mongolia	Djadokhta Formation (83.6–66.0 Ma)
Balaur bondoc	Sebeş Glod, Alba, Romania	Sebeş Formation (72.1–66.0 Ma)
Bambiraptor feinbergorum	13 km west of Bynum, MT	Two Medicine Formation (83.6–72.1 Ma)
Baptornis	Logan County, KS	Niobrara Formation (89.8–72.1 Ma)
Beipiaosaurus	Beipiao, Liaoning, China	Yixian Formation (129.4–124 Ma)
Beishanlong	White Ghost Castle, Yujingzi Basin, Gansu, China	Xinminbao Group (125–100.5 Ma)
Bicentenaria	Ezequiel Ramos Mexía Reservoir, Río Negro, Argentina	Candeleros Formation (100.5–93.9 Ma)
Bistahieversor	Pinabete Arroyo, San Juan County, NM	Fruitland Formation (77–72.1 Ma)
Bonapartenykus	Salitral Ojo de Agua, Río Negro, Argentina	Allen Formation (83.6–66.0 Ma)
Buitreraptor gonzalezorum	La Buitrera, Río Negro, Argentina	Candeleros Formation (100.5–97 Ma)
Byronosaurus jaffei	Ankylosaur Flats, Ukhaa Tolgod, Omnogov, Mongolia	Djadokhta Formation (83.6–72.1 Ma)
Cathayornis	Beishan Quarry, Boluochi, Liaoning, China	Jiufotang Formation (125–120 Ma)
Caudipteryx zoui	Sihetun, Beipiao, Liaoning, China	Yixian Formation (129.4–124 Ma)
Ceratonykus	Khermin Tsav, Omnogov, Mongolia	Barun Goyot Formation (76–70 Ma)
Changyuraptor	Jianchang, Liaoning, China	Yixian Formation (129.4–124 Ma)
Chirostenotes pergracilis	2 miles northeast of mouth, Little Sandhill Creek, Alberta, Canada	Dinosaur Park Formation (76.5–72.1 Ma)
Citipati osmolskae	Ankylosaur Flats, Ukhaa Tolgod, Omnogov, Mongolia	Djadokhta Formation (83.6–72.1 Ma)
Coelurus fragilis	Como Bluff, Albany County, WY	Morrison Formation (157.3–145 Ma)

APPENDIX *continued*

Taxon	**Modern Locality**	**Formation and Age**
Compsognathus longipes	Kelheim, Bayern, Germany	Solnhofen Limestone (Altmühltal Formation) (154–149 Ma)
Conchoraptor gracilis	Khermin Tsav, Omnogov, Mongolia	Barun Goyot Formation (76.0–72.1 Ma)
Concornis	Las Hoyas, Cuenca, Spain	Calizas de la Huérguina Formation (128.5–125 Ma)
Confuciusornis sanctus	Huanghuagou, Shangyuan, Liaoning, China	Yixian Formation (129.4–124 Ma)
Dakotaraptor	Bone Butte, Harding County, SD	Hell Creek Formation (72.1 – 66.0 Ma)
Daspletosaurus	right bank, Sand Creek, Alberta, Canada	Oldman Formation (77–72.1 Ma)
Deinonychus antirrhopus	Cashen Pocket, Big Horn County, MT	Cloverly Formation (125–100.5 Ma)
Dilong paradoxus	Lujiatun, Beipiao, Liaoning, China	Yixian Formation (129.4–124 Ma)
Dromaeosaurus albertensis	Little Sandhill Creek, Alberta, Canada	Dinosaur Park Formation (83.6–72.1 Ma)
Dryptosaurus	St. Georges, New Castle County, DE	Merchantville Formation (72.1–66.0 Ma)
EK troodontid IGM (SPS) 100/44	Khamareen Us, Dornogov, Mongolia	Barunbayaskaya Formation (105–97 Ma)
Enigmosaurus	Khara Khutul, Dornogov, Mongolia	Bayan Shireh Formation (100.5–83.6 Ma)
Eosinopteryx brevipenna	Jianchang, Liaoning, China	Tiaojishan Formation (163.5–157.3 Ma)
Eotyrannus lengi	Isle of Wight, England	Wessex Formation (129.4–125 Ma)
Epidexipteryx	Daohugou, Ningcheng, Nei Mongol, China	Tiaojishan Formation (168.3–155 Ma)
Erliansaurus	Sanhangobi, Nei Mongol, China	Iren Dabasu Formation (83.6–66.0 Ma)
Erlikosaurus andrewsi	Bayshin Tsav, Omnogov, Mongolia	Bayan Shireh Formation (100.5–83.6 Ma)
Falcarius	Crystal Geyser Quarry, Grand County, UT	Cedar Mountain Formation (129.4–125 Ma)
Gallimimus bullatus	Western Sayr, Nemegt, Omnogov, Mongolia	Nemegt Formation (72.1–66.0 Ma)
Garudimimus brevipes	Bayshin Tsav, Omnogov, Mongolia	Bayan Shireh Formation (100.5–83.6 Ma)
Gobipteryx	Ukhaa Tolgod, Omnogov, Mongolia	Djadokhta Formation (76–70 Ma)
Gorgosaurus libratus	Sand Creek, Alberta, Canada	Dinosaur Park Formation (77–72.1 Ma)

APPENDIX *continued*

Taxon	**Modern Locality**	**Formation and Age**
Graciliraptor lujiatunensis	Lujiatun village, Beipiao, Liaoning, China	Yixian Formation (129.4–124 Ma)
Guanlong	Wucaiwan, Xinjiang, China	Shishugou Formation (163.5–157.3 Ma)
Haplocheirus	Wucaiwan, Xinjiang, China	Shishugou Formation (163.5–157.3 Ma)
Harpymimus okladnikovi	Khuren-Dukh, Dornogov, Mongolia	Khuren Dukh Formation (132.6–125 Ma)
Hesperonychus	Cripple Creek, Alberta, Canada	Dinosaur Park Formation (76.5–72.1 Ma)
Hesperornis	Goblin Hollow, Logan County, KS	Niobrara Formation (89.8–72.1 Ma)
Hongshanornis longicresta	Shifo, Ningcheng, Nei Mongol, China	Yixian Formation (129.4–124 Ma)
Huaxiagnathus orientalis	Dabangou, Beipiao, Liaoning, China	Yixian Formation (129.4–124 Ma)
IVPP V22530	Elesita, Nei Mongol, China	Bayan Gobi Formation (125–100.5 Ma)
Iaceornis marshii	Smoky Hill River, 5 miles W Russell Springs, Logan County, KS	Niobrara Formation (89.8–83.6 Ma)
Ichthyornis	Watino, Alberta, Canada	Kaskapau Formation (93.9–83.6 Ma)
Incisivosaurus gauthieri	Lujiatun village, Beipiao, Liaoning, China	Yixian Formation (129.4–124 Ma)
Ingenia yanshani (Ajancingenia yanshini)	Khermin Tsav, Omnogov, Mongolia	Barun Goyot Formation (72.1–66.0 Ma)
Jeholornis prima	Dapingfang, Chaoyang, Liaoning, China	Jiufotang Formation (129.4–120 Ma)
Jinfengopteryx elegans	Longfengshan Hill, Hebei, China	Huajiying Formation (132.6–125 Ma)
Jixiangornis orientalis	Baicaigou, Toutai, Liaoning, China	Yixian Formation (129.4–124 Ma)
Juratyrant	Rope Lake Head / Freshwater Steps, Dorset, England, United Kingdom	Kimmeridge Clay Formation (152.1–145 Ma)
Juravenator starki	Stark Quarry, Schamhaupten, Bayern, Germany	Painten Formation (154–152.1 Ma)
Kileskus	Berezovsk Quarry, Krasnoyarsk, Russian Federation	Itat Formation (168.3–166.1 Ma)
Liaoningornis longidigitris	Southwest of Beipiao City, Liaoning, China	Yixian Formation (129.4–124 Ma)
Limenavis patagonica	Salitral Moreno, Río Negro, Argentina	Allen Formation (75.0–69.0 Ma)
Linhenykus	Gate Area, Bayan Mandahu, Nei Mongol, China	Wulansuhai Formation (83.6–72.1 Ma)
Linheraptor	Gate Area, Bayan Mandahu, Nei Mongol, China	Wulansuhai Formation (83.6–72.1 Ma)

APPENDIX *continued*

Taxon	Modern Locality	Formation and Age
Luanchuanraptor	Qiupa, Luanchuan Basin, Henan, China	Qiupa Formation (83.6–66.0 Ma)
Mahakala omnogovae	Tögrögiin Shiree, Omnogov, Mongolia	Djadokhta Formation (78.0–72.1 Ma)
Mei long	Lujiatun village, Beipiao, Liaoning, China	Yixian Formation (129.4–124 Ma)
Microraptor zhaoianus	Chaoyang, Liaoning, China	Jiufotang Formation (125–120 Ma)
Microvenator celer	Crooked Creek, Big Horn County, WY	Cloverly Formation (125–100.5 Ma)
Mirischia	Araripina region, Pernambuco, Brazil	Santana Formation (113–100.5 Ma)
Mononykus olecranus	Bugin Tsav, Omnogov, Mongolia	Nemegt Formation (72.1–66.0 Ma)
Nanshiungosaurus bohlini	Mazongshan, Gansu, China	Nanxiong Formation (83.6–66.0 Ma)
Neimongosaurus	Sanhangobi, Nei Mongol, China	Iren Dabasu Formation (83.6–66.0 Ma)
Neuquenornis volans	Boca del Sapo, Universidad Nacional del Comahue, Neuquén, Argentina	Bajo de la Carpa Formation (86.3–83.6 Ma)
Neuquenraptor/Unenlagia	Sierra del Portezuelo, Neuquén, Argentina	Portezuelo Formation (92–87 Ma)
Nothronychus	Big Water, Tropic Shale, UT	Tropic Shale Formation (96–89.8 Ma)
Nqwebasaurus	5 km west of Kirkwood, Eastern Cape, South Africa	Kirkwood Formation (145–132.6 Ma)
Ornitholestes hermanni	Bone Cabin Quarry, Albany County, WY	Morrison Formation (157.3–145 Ma)
Ornithomimus edmonticus	Red Deer River, Alberta, Canada	Horseshoe Canyon Formation (76.5–66.0 Ma)
Oviraptor philoceratops	Shabarakh Usu, Omnogov, Mongolia	Djadokhta Formation (83.6–72.1 Ma)
Parvicursor	Khulsan, Omnogov, Mongolia	Barun Goyot Formation (83.6–72.1 Ma)
Patagonykus puertai	Sierra del Portezuelo, Neuquén, Argentina	Portezuelo Formation (93.9–86.3 Ma)
Patagopteryx deferrariisi	Boca del Sapo, Universidad Nacional del Comahue, Neuquén, Argentina	Bajo de la Carpa Formation (86.3–83.6 Ma)
Pelecanimimus polyodon	Las Hoyas, Cuenca, Spain	La Huérguina Formation, (128.5–125 Ma)
Pengornis houi	Dapingfang, Chaoyang, Liaoning, China	Jiufotang Formation (125–120 Ma)
Proceratosaurus bradleyi	Minchinhampton reservoir, England	White Limestone Formation (168.3–166.1 Ma)
Qiupalong	Qiupa, Luanchuan Basin, Henan, China	Qiupa Formation (83.6–66.0 Ma)

APPENDIX *continued*

Taxon	Modern Locality	Formation and Age
Rahonavis ostromi	Mahajanga, Madagascar	Maevarano Formation (72.1–66.0 Ma)
Rinchenia mongoliensis	Altan Ula, Omnogov, Mongolia	Nemegt Formation (72.1–66.0 Ma)
Sapeornis chaoyangensis	Dapingfang, Chaoyang, Liaoning, China	Jiufotang Formation (129.4–120 Ma)
Saurornithoides mongoliensis	Shabarakh Usu, Omnogov, Mongolia	Djadokhta Formation (83.6–72.1 Ma)
Saurornitholestes langstoni	Steveville Railway Grade, Alberta, Canada	Dinosaur Park Formation (77–72.1 Ma)
Segnosaurus galbinensis	Amtgay, Omnogov, Mongolia	Bayan Shireh Formation (100.5–83.6 Ma)
Shanag ashile	Öösh, Ovorkhangai, Mongolia	Öösh Formation (145–129.4 Ma)
Shenzhousaurus orientalis	Sihetun, Beipiao, Liaoning, China	Yixian Formation (129.4–124 Ma)
Shuvuuia deserti	Ukhaa Tolgod, Omnogov, Mongolia	Djadokhta Formation (83.6–72.1 Ma)
Sinocalliopteryx	Hengdaozi, Sihetun, Liaoning, China	Yixian Formation (129.4–124 Ma)
Sinornithoides youngi	Huamuxiao, Ordos Basin, Nei Mongol, China	Ejinhoro Formation (139.8–100.5 Ma)
Sinornithomimus	Suhongtu, Ulan Suhai, Nei Mongol, China	Ulansuhai Formation (93.9–89.8 Ma)
Sinornithosaurus millenii	Sihetun, Beipiao, Liaoning, China	Yixian Formation (129.4–124 Ma)
Sinosauropteryx prima	Sihetun, Beipiao, Liaoning, China	Yixian Formation (129.4–124 Ma)
Sinotyrannus	Dachengzi, Kazuo, Liaoning, China	Jiufotang Formation (125–120 Ma)
Sinovenator changii	Yanzigou, Shanyuan, Liaoning, China	Yixian Formation (129.4–124 Ma)
Sinusonasus magnodens	Lujiatun village, Beipiao, Liaoning, China	Yixian Formation (129.4–124 Ma)
Songlingornis	Beishan Quarry, Boluochi, Liaoning, China	Jiufotang Formation (125–120 Ma)
Struthiomimus altus	Ross Coulee, Irvine, Alberta, Canada	Dinosaur Park Formation (76.5–66.0 Ma)
Suzhousaurus	Yujingzi Basin, Jiuquan, Gansu, China	Xinminbao Group (125–100.5 Ma)
Tanycolagreus	Cleveland-Lloyd Dinosaur Quarry, Emery County, UT	Morrison Formation (157.3–145 Ma)
Teratophoneus	Horse Mountain, UT	Kaiparowits Formation (77–72.1 Ma)
Therizinosaurus	Nemegt, Omnogov, Mongolia	Nemegt Formation (72.1–66.0 Ma)

APPENDIX *continued*

Taxon	**Modern Locality**	**Formation and Age**
Tianyuraptor ostromi	Dawangzhangzi, Lingyuan, Liaoning, China	Yixian Formation (129.4–124 Ma)
Troodon formosus	Steveville Railway Grade, Alberta, Canada	Dinosaur Park Formation (76–66 Ma)
Tsaagan mangas	Xanadu, Ukhaa Tolgod, Omnogov, Mongolia	Djadokhta Formation (83.6–72.1 Ma)
Tugulusaurus	Wuerho, Karamay, Xinjiang, China	Lianmugin Formation (122.5–99.7 Ma)
Tyrannosaurus rex	Crowsnest Pass, Alberta, Canada	Willow Creek Formation (72.1–66.0 Ma)
Utahraptor	Robert Gaston Quarry, Grand County, UT	Cedar Mountain Formation (128–120 Ma)
Velociraptor mongoliensis	Shabarakh Usu, Omnogov, Mongolia	Djadokhta Formation (83.6–72.1 Ma)
Vorona	Mahajanga, Madagascar	Maevarano Formation (72.1–66.0 Ma)
Xiaotingia zhengi	Daxishan, Linglongta, Jianchang Liaoning, China	Tiaojishan Formation (163.5–157.3 Ma)
Xiongguanlong	White Ghost Castle, Yujingzi Basin, Gansu, China	Xinminbao Group (125–100.5 Ma)
Xixianykus	Zhoujiagou, Yangcheng, Henan, China	Majiacun Formation (89.8–83.6 Ma)
Xixiasaurus henanensis	Songgou, Xixia, Nanyang, Henan, China	Majiacun Formation (89.8–83.6 Ma)
Yanornis martini	Dapingfang, Chaoyang, Liaoning, China	Jiufotang Formation (125–120 Ma)
Yi	Mutoudeng, Hebei, China	Tiaojishan Formation (168.3–155 Ma)
Yixianornis grabaui	Qianyang, Yixian, Liaoning, China	Jiufotang Formation (125–120 Ma)
Yurgovuchia	Don's Place, Grand County, UT	Cedar Mountain Formation (128–120 Ma)
Zanabazar junior	Bugin Tsav, Omnogov, Mongolia	Nemegt Formation (72.1–66.0 Ma)
Zhenyuanlong	Sihedang, Lingyuan, Liaoning, China	Yixian Formation (129.4–124 Ma)
Zuolong	Wucaiwan, Xinjiang, China	Shishugou Formation (163.5–157.3 Ma)

Chapter 5

Timing the Extant Avian Radiation: The Rise of Modern Birds, and the Importance of Modeling Molecular Rate Variation

DANIEL J. FIELD,[1] JACOB S. BERV,[2] ALLISON Y. HSIANG,[3] ROBERT LANFEAR,[4] MICHAEL J. LANDIS,[5] AND ALEX DORNBURG[6]

ABSTRACT

Unravelling the phylogenetic relationships among the major groups of living birds has been described as the greatest outstanding problem in dinosaur systematics. Recent work has identified portions of the avian tree of life that are particularly challenging to reconstruct, perhaps as a result of rapid cladogenesis early in crown bird evolutionary history (specifically, the interval immediately following the end-Cretaceous mass extinction). At face value this hypothesis enjoys support from the crown bird fossil record, which documents the first appearances of most major crown bird lineages in the early Cenozoic—in line with a model of rapid postextinction niche-filling among surviving avian lineages. However, molecular-clock analyses have yielded strikingly variable estimates for the age of crown birds, and conflicting inferences on the impact of the end-Cretaceous mass extinction on the extant bird radiation. This uncertainty has often been ascribed to a patchy avian fossil record, but the possibility of model misspecification in molecular divergence-time analyses represents an important and relatively underexplored alternative hypothesis. Here, we highlight the necessity of further developing and using models that account for coordinated variation in rates of molecular evolution across a phylogeny (e.g., molecular early burst) as a means of assessing support for a rapid post-Cretaceous radiation of crown birds. We discuss how relationships between life history and substitution rates can mislead divergence-time studies that do not account for directional changes in substitution rates over time, and suggest that these effects might have caused some of the variation in existing molecular date estimates for birds. We suggest multiple paths forward that could help resolve this and similar conflicts within other major eukaryotic clades.

---

[1] Department of Earth Sciences, University of Cambridge, Cambridge.
[2] Department of Ecology & Evolutionary Biology, Cornell University, Ithaca, NY.
[3] Department of Bioinformatics and Genetics, Swedish Museum of Natural History, Stockholm.
[4] Ecology and Evolution, Research School of Biology, Australian National University, Canberra.
[5] Department of Biology, Washington University in St. Louis, St. Louis, MO.
[6] North Carolina Museum of Natural Sciences, Raleigh, NC.

INTRODUCTION

While the relative contributions of an asteroid impact and severe environmental change from volcanism continue to be debated, there is no doubt the large dinosaurs met their demise at the end-Cretaceous (K-Pg) mass extinction, ~66 million years ago (Brusatte et al., 2015, references therein). The impact of this extinction event on smaller pennaraptoran dinosaurs—the theropod subclade comprising oviraptorosaurs, deinonychosaurs, and the bird lineage, Avialae—has been more difficult to assess, given a relatively sparse fossil record in the latest Cretaceous. However, recent work has indicated that at least five major clades of avialans survived into the terminal Maastrichtian (latest Cretaceous), and thus were likely subject to the K-Pg extinction event (Longrich et al., 2011; Field et al., 2018a; Agnolín et al., 2017). Latest Cretaceous representatives of these clades (Enantiornithes, Palintropiformes, Hesperornithes, Ichthyornithes, and the bird crown clade, Aves) are largely known from isolated, fragmentary fossils (Hope, 2002; Longrich et al., 2011; Dumont et al., 2016; Field et al., 2018a) and, with the exception of crown birds, all are entirely unknown from post-Cretaceous sediments. Assessing whether crownward stem birds (e.g., Enantiornithes) were completely exterminated at the K-Pg boundary is challenging, given the generally meagre Paleocene bird fossil record (Mayr, 2007, 2009, 2016; Field, 2017). Notably, some groups of Cretaceous archosauromorphs (e.g., choristoderes) and mammals (e.g., multituberculates) survived the K-Pg mass extinction, only to go extinct later in the Cenozoic (Evans and Hecht, 1993; Wilson, 2014), and it is possible that some representatives of crownward avialans survived the mass extinction event only to succumb later in the early Cenozoic (Mayr, 2007). Nonetheless, no definitively diagnosed stem bird fossils are known from sediments above the K-Pg boundary, and it seems likely that the only major clade of avialans to survive in ecologically significant numbers were crown birds themselves (Longrich et al., 2011; Mayr, 2016; Field, 2017; Ksepka et al., 2017; Field et al., 2018b, 2020).

Today, crown birds are among the most diverse major groups of tetrapods, with nearly 11,000 living species that occupy virtually every subaerial habitat on Earth (Gill and Donsker, 2018). However, due to their limited Late Cretaceous and early Paleocene fossil record (see Pittman, et al., chapter 2), assessing the timing of the extant avian radiation has been challenging. Fossils representing the earliest known stem-group representatives of many extant avian orders appear throughout the Paleogene, but many derive from a relatively small number of bird-bearing Lagerstätten (e.g., the Messel, Fur, and Green River formations; Mayr, 2009). As a result, the temporal origins of these lineages have been difficult to precisely verify, complicating efforts to assess whether any of them extended into the Cretaceous. To date, only two well-supported crown birds have been described from the Late Cretaceous: *Vegavis iaai* from the terminal Maastrichtian of Antarctica (Noriega and Tambussi, 1995; Clarke et al., 2005, Agnolín et al., 2017), and *Asteriornis maastrichtensis* from the terminal Maastrichtian of Belgium (Field et al., 2020). However, the phylogenetic position of *Vegavis* is unclear (Mayr et al., 2018), with a recent hypothesis finding it to be an early stem group anseriform (Worthy et al., 2017). This position would imply that at least three avian crown group divergences had occurred prior to the K-Pg boundary (i.e., the divergences between Palaeognathae and Neognathae, Galloanserae and Neoaves, and Galliformes and Anseriformes). However, exactly when these divergences would have taken place in the Late Cretaceous is unknown (fig. 1). In light of this uncertainty in the fossil record, molecular divergence-time approaches offer our only means for establishing a timeline for the deepest divergences within the avian crown group.

In general, molecular clock-based estimates of major extant avian clade ages often differ markedly from observed patterns in the fossil record. Early attempts to address the timing of interordinal divergences within crown birds often suggested that many, if not all, diver-

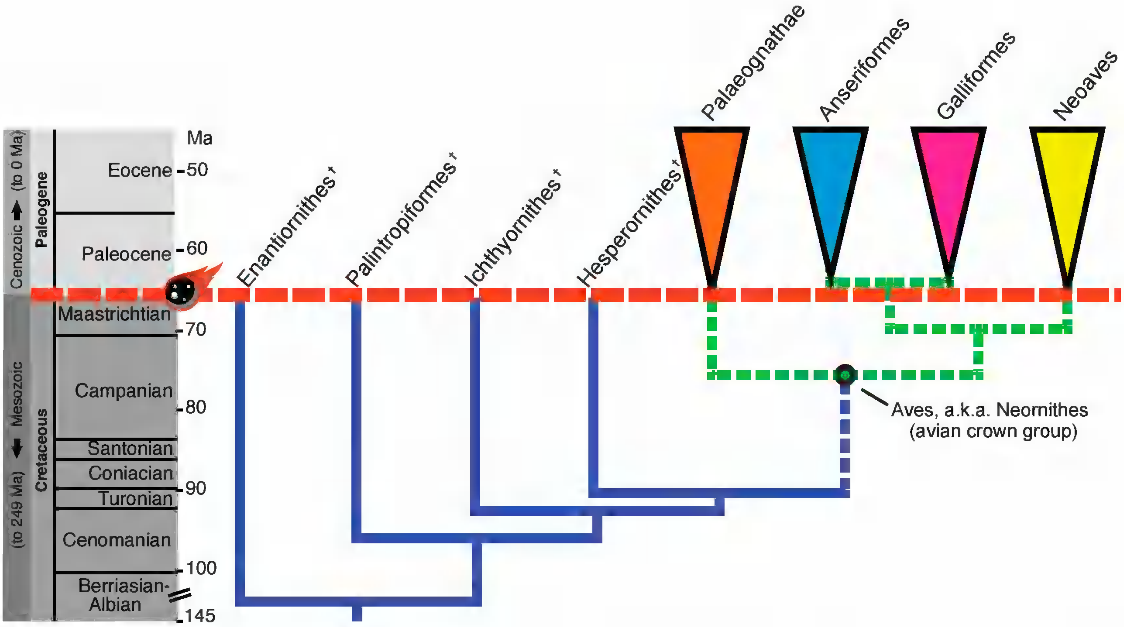
Palaeognathae
Anseriformes
Galliformes
Neoaves
Enantiornithes†
Palintropiformes†
Ichthyornithes†
Hesperornithes†
Cenozoic (to 0 Ma)
Mesozoic (to 249 Ma)
Paleogene
Cretaceous
Ma
Eocene
50
Paleocene
60
Maastrichtian
70
Campanian
80
Santonian
Coniacian
90
Turonian
Cenomanian
100
Berriasian-Albian
145
Aves, a.k.a. Neornithes (avian crown group)

FIG. 1. Schematic phylogeny and approximate divergence times of the major crownward stem bird lineages (blue) and the deepest extant clades within crown birds (green). Most recent common ancestor (MRCA) of crown birds indicated by green node. Dashed lines indicate extant lineages whose time-scaled branch lengths are debated. Divergence times illustrated for crown birds roughly follow those of Prum et al. (2015), and those of stem birds follow (Longrich et al., 2011). Stem bird phylogeny and scale modified from Field et al. (2018a), with stem bird topology following (Field et al., 2018b). K-Pg boundary indicated by dashed red line and asteroid at ~66 Ma.

gences between the ~40 extant avian orders (Gill and Donsker, 2018) took place during the Cretaceous (e.g., Cooper and Penny, 1997), substantiating arguments for a limited influence of the end-Cretaceous mass extinction on crown bird evolution. This interpretation stands in stark contrast to patterns in the crown bird fossil record, whereby virtually all of the earliest evidence for extant avian orders—with the exception of the deeply diverging Galloanserae (see mention of *Vegavis* and *Asteriornis* above)—is restricted to Cenozoic sediments (Mayr, 2009). What accounts for these dichotomous interpretations of avian evolutionary history? Have paleontologists simply failed to recover—or consistently failed to identify—a diverse range of neoavian remains from the Cretaceous (summarized by Brown et al., 2008)? Or have molecular-clock estimates of divergence times somehow failed to account for unrecognized patterns of genomic rate variation (Benton, 1999; Berv and Field, 2018)? These hypotheses are not mutually exclusive, but our ability to address the latter question is currently limited. Clarifying the extent to which these alternatives have affected our understanding of avian evolution is critical for accurately assessing the age of the extant avian radiation, and therefore our ability to correctly interpret how various events in Earth history—asteroid impacts, periods of climatic change, and major tectonic events among them—have influenced the evolution of birds. Moreover, this will allow us to understand whether extant bird orders arose slowly throughout the Late Cretaceous or whether they radiated rapidly in the early Cenozoic, which has important implications for how we understand the nature of major evolutionary radiations.

Discrepancies between Molecular Divergence Times and the Bird Fossil Record

Since the earliest attempts to date the age of the avian crown group using molecular divergence times (e.g., Cooper and Penny, 1997), the hypothesis of numerous ordinal-level divergences within Neoaves taking place in the Mesozoic has generally been supported in molecular clock studies (e.g., Brown et al., 2008; Pacheco et al., 2011; Haddrath and Baker, 2012; Crouch et al., 2018). This hypothesis has not been corroborated by the Cretaceous fossil record. All putative neoavian fossils thus far reported from the Mesozoic (Stidham, 1998; Hope, 2002) have instead been identified as stem group birds upon reevaluation (Dyke and Mayr, 1999; Longrich et al., 2011; Mayr et al., 2018). The elusiveness of Cretaceous neoavian fossils is consistent with the hypothesis of a largely post-Cretaceous diversification of crown Neoaves—perhaps no Cretaceous neoavians have been found because they simply had not yet originated at that point in Earth history. As Benton (1999) notes, this hypothesis is eminently testable, since the recovery of Cretaceous crown neoavian fossils would force a reevaluation of a model of explosive order-level neoavian divergences in the wake of the K-Pg. It is probably fair to say, however, that the current consensus among paleornithologists is that such discoveries are unlikely. The probability of crown neoavian fossil discoveries deep in the Cretaceous is presumably low, given the abundant preservation of noncrown avialans that have been recovered from Cretaceous sites around the world (see Pittman et al., chapter 2). Although conclusively "demonstrating" the absence of birds from deeper Mesozoic sediments presents a difficult epistemological problem (Sober, 2009), it appears more likely that the first appearances of major neoavian subclades in the early Cenozoic fossil record are simply a reflection of their early Cenozoic origins (Mayr, 2009, 2016; Longrich et al., 2011; Feduccia, 2014; Field, 2017; Ksepka et al., 2017).

In contrast to earlier molecular divergence-time analyses, the majority of large-scale phylogenomic divergence-time studies of birds in the last five years have inferred a post-Cretaceous radiation for the majority of the deep divergences within the avian crown group (i.e., divergences within crown Palaeognathae, crown Galloanserae, and crown Neoaves), with variable estimates of the age of the most recent common ancestor of crown birds, hereafter the avian MRCA (Jarvis et al., 2014; Claramunt and Cracraft, 2015; Prum et al., 2015). At first glance, these results—which are consistent with the Late Cretaceous avian fossil record—would appear to reflect more sophisticated analyses with better-justified fossil calibrations yielding more accurate divergence-time estimates. While this is undoubtedly true in part, the reality in its entirety is much less satisfying. As lingering discrepancies between the fossil record (indicating a largely post-Cretaceous radiation of birds) and loosely constrained molecular divergence-time estimates (largely advocating a Cretaceous radiation) have come into better focus, many divergence-time analyses have conditioned soft and hard maxima for internal fossil calibrations on the K-Pg boundary itself (Ericson et al., 2006; Jarvis et al., 2014; Prum et al., 2015). This approach largely precludes divergence-time estimates from exceeding the age of the K-Pg boundary, because explicit prior beliefs are used to constrain the outcome of these analyses (Warnock et al., 2015). While the resultant age estimates from such strongly constrained analyses may well be more accurate than those employing older soft maxima for deep neoavian divergences (and, based on their agreement with evidence from the bird fossil record, we would argue that they *are* indeed more accurate), this approach introduces problematic circularity into the process of inferring divergence times for the deepest nodes in the avian tree of life.

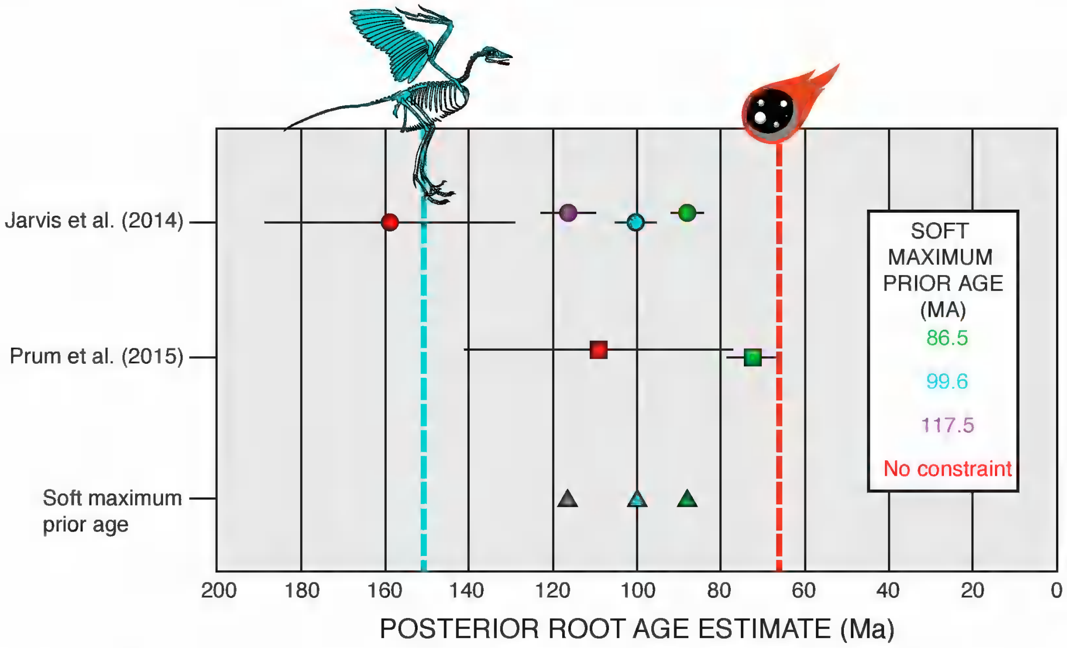

FIG. 2. Mean estimated ages of the crown bird MRCA (circles and squares ± 95% HPD intervals) are highly dependent on specified soft maximum prior age (triangles). Red circle and square indicate analyses run with no soft maximum age specified. Jarvis et al. (2014) results modified from Cracraft et al. (2015). Prum et al. (2015) results from the "top ten" nucleotide dataset (Berv and Field, 2018). Ages of *Archaeopteryx lithographica* (~155 Ma) and K-Pg boundary (~66 Ma) illustrated.

VARIABILITY AND CIRCULARITY OF CROWN BIRD ROOT AGE ESTIMATES

Estimated ages for the deepest nodes within the avian crown group, including the most recent common ancestor (MRCA) of living birds, have proven extremely sensitive to prior assumptions made about the maximum age of the MRCA. For example, Cracraft et al. (2015) applied 97.5% prior maximum age constraints of 86.5 Ma (following Benton and Donoghue, 2007), 99.6 Ma (following Jarvis et al., 2014), and 117.5 Ma (following Mitchell et al., 2015) to the Jarvis et al., (2014) molecular dataset. These analyses illustrated marked variability in the estimated number of pre-K-Pg order-level neoavian divergences (from a minimum of 1 under the 86.5 Ma constraint, to a maximum of 15 under the 117.5 Ma constraint). Such variability is to be expected, as the increased density of older ages within the prior age distribution elevates the probability of estimating older ages for clades throughout the tree (Dornburg et al., 2011; Warnock et al., 2012). Additional analyses by Cracraft et al. (2015), removing a specific soft maximum age for the MRCA and otherwise applying the same suite of parameters, resulted in age estimates for the crown bird MRCA in excess of 155 million years. Notably, this estimate is older than the oldest known and most stemward avialan, *Archaeopteryx lithographica* (fig. 2). This sensitivity underscores the sobering conclusion that, in the absence of informative priors, currently available molecular and fossil data, combined with our best model of their evolution, can shed very little light on the influence of the K-Pg mass extinction on avian evolution (fig. 3).

Given the almost complete absence of a Mesozoic crown bird fossil record (and, at the time of writing, the complete absence of any convincing Mesozoic neoavians), there is no strong evidence that can form the basis of a soft maximum age for the avian MRCA (Berv and Field, 2018; Pittman et al., on the fossil record,

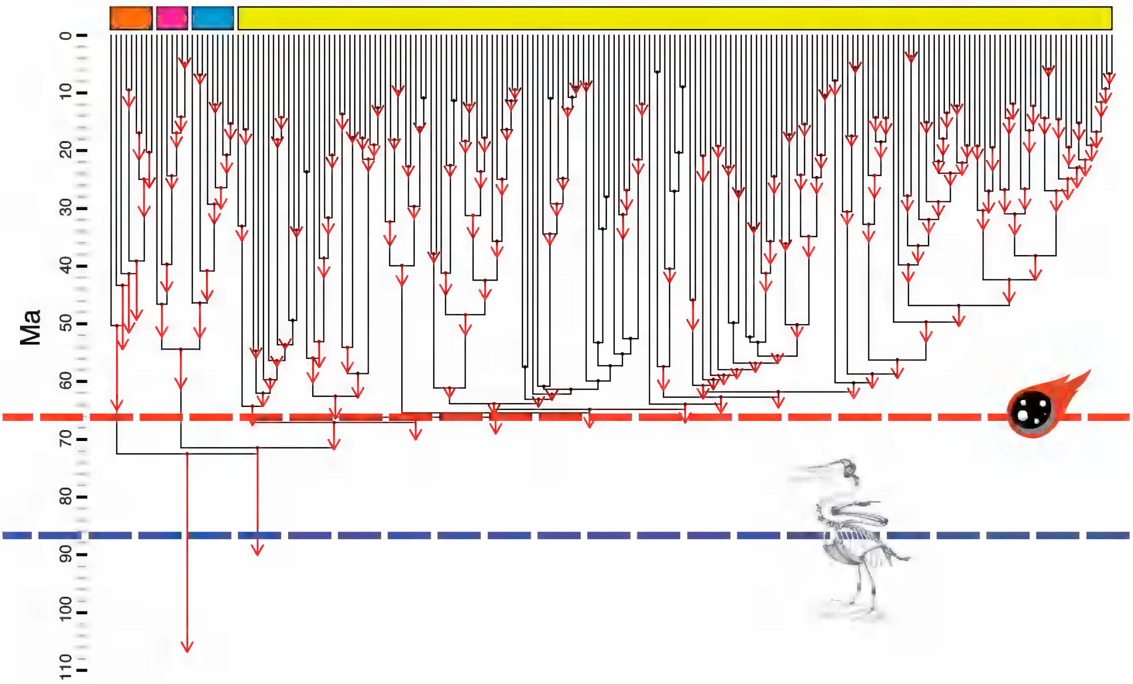

FIG. 3: Analytical influence of soft maximum prior selection on the avian evolutionary timescale (modified from Berv and Field, 2018). Colored boxes represent the major crown bird subclades and correspond to the color scheme from figure 1. Underlying black phylogeny represents the preferred time tree from Prum et al. (2015), applying a soft maximum age of 86.5 Ma for the crown bird MRCA. Red arrows illustrate shifts in estimated clade ages induced by removing this soft maximum prior, with other analytical parameters kept the same. The most severe branch length extensions occur on the deepest lineages of the tree (the lineages most likely to have crossed the K-Pg boundary). However, an important caveat is that the Paleogene calibrations in this analysis have soft maxima informed directly by the K-Pg boundary itself. K-Pg boundary denoted by red line and asteroid; age of the fossil avialan-rich Niobrara Formation "Niobrara Prior" indicated by blue dashed line. *Ichthyornis* reconstruction modified from Marsh (1880).

chapter 2). Nonetheless, we would argue that, because (1) the Cretaceous (144–66 Ma) avialan fossil record is relatively rich, (2) the oldest convincing crown bird, *Asteriornis*, derives from the extreme terminal Cretaceous ~66.7 Ma (Field et al., 2020), and (3) the earliest diverse crown-grade bird fossil assemblage is scarcely older than the K-Pg boundary (within 300,000 years of the boundary; Longrich et al., 2011), specifying soft maxima for the basal divergence within crown birds deep in the Cretaceous is likely unsound. For example, the 117.5 Ma soft maximum age constraint advocated by Mitchell et al. (2015) is 50 million years older than *Asteriornis* and *Vegavis*—a vast time span equivalent to 75% of the entire Cenozoic. Setting such a large prior age distribution has the intuitive consequence of widening the sampling of molecular divergences into deeper timescales (Dornburg et al., 2011; Warnock et al., 2012). Since soft maxima for the crown bird MRCA are extremely influential—even circular—in divergence-time analyses (figs. 2,3), we argue that assigning such ancient priors is extremely likely to yield inaccurately ancient divergence times for the MRCA of the avian crown group and its major subclades (a similar argument was made for mammals by Phillips, 2016).

Rapid post-Cretaceous Radiation as an Explanation for the 'Neoavian Comb'

The phylogenetic interrelationships of the major neoavian subclades have been notoriously challenging to disentangle, and a consensus regarding the higher order topology of Neoaves has yet to be reached (Pittman, et al., on systematics, chapter 1). Virtually all independent phylogenomic studies to date have supported differing neoavian topologies (Ericson et al., 2006; Hackett et al., 2008; McCormack et al., 2013; Jarvis et al., 2014; Prum et al., 2015; Reddy et al., 2017), although the most recent studies all tend to agree on roughly 10 major constituent subclades: Mirandornithes, Aequornithes, Charadriiformes, Gruiformes, Otidimorphae, Columbimorphae, Strisores, Phaethontimorphae, Telluraves, and the perpetually challenging-to-place, monotypic *Opisthocomus* (Reddy et al., 2017, Kimball et al., 2019). The lingering recalcitrance of neoavian relationships makes it a classic example of a difficult phylogenetic problem (the "neoavian comb," sensu Cracraft et al., 2004), and this recalcitrance has been hypothetically linked to rapid cladogenesis for some time (Ericson et al., 2006; Feduccia, 2014; Jarvis et al., 2014; Ksepka and Phillips, 2015; Prum et al., 2015; Suh, 2016, Musser et al., 2019; Kimball et al., 2019; Houde et al., 2020).

A scenario of rapid cladogenesis—such as that hypothesized to have occurred during post-K-Pg extinction recovery—provides a logical explanation for the distinctive combination of extremely short phylogenetic internodes and incomplete lineage sorting that may be responsible for the lack of a clear branching pattern for this portion of the bird tree of life. The combination of a deep timescale and short times between phylogenetic divergences render this scenario among the most challenging of phylogenetic problems for molecular evidence to disentangle (Degnan and Rosenberg, 2009; Townsend et al., 2012; Dornburg et al., 2017a, 2017b, 2018). Additionally, expectations based on other rapid evolutionary radiations suggest the possibility of high levels of gene flow among early diverging lineages (Meier et al., 2017). Indeed, if it is the case that early divergences among birds were associated with rampant incomplete lineage sorting and gene flow during a rapid early Cenozoic radiation (Suh, 2016), a clear bifurcating pattern may not exist in the first place (Hahn and Nakhleh, 2015). Regardless, the challenges of resolving the deepest avian divergences are consistent with what we should theoretically expect in a scenario of rapid postextinction avian cladogenesis in the earliest Cenozoic. Further, these challenges have profound implications for our ability to accurately estimate molecular divergence times using existing approaches.

Modeling Rate Variation: Among-Lineage Rate Variation versus Fast Early Rates

It has long been known that failing to properly account for substitution rate variation among lineages can fundamentally limit the accuracy of molecular dating analyses (Jukes and Holmquist, 1972; Radinsky, 1978; Vawter and Brown, 1986). Early studies of molecular divergence times relied on the assumption that the rate of evolution of a gene or locus can be characterized by a single rate, such as a mean rate, of character change (Bromham and Penny, 2003). However, it quickly became clear that substitution rates often vary substantially, even among closely related lineages (Li et al., 1987; Dornburg et al., 2014; Ho, 2014; Beaulieu et al., 2015; Moorjani et al., 2016). At the level of a gene or locus, site rate variation may be correlated with codon position, transition/transversion biases, or compositional biases toward certain bases (Kumar, 1996). As lineages shift their life histories in response to new ecological opportunities, this can further result in dramatic shifts in the substitution rates of entire loci (Martin and Palumbi, 1993; Bromham, 2002; Smith and Donoghue, 2008). It is not uncommon for clades to exhibit substitution rates varying by up to an order of magnitude for the same locus (Smith and

Donoghue, 2008; Dornburg et al., 2012); Berv and Field (2018) report a 20-fold difference between the fastest and slowest-evolving avian lineages. The consequences of failing to accurately model rates of character change—both across sites and across lineages—are intuitive. Overestimating substitution rates can lead to tree compression, biasing divergence times toward the present (Phillips, 2009; Ksepka and Phillips, 2015; Dornburg et al., 2017b). Conversely, underestimating molecular rates will drive tree expansion, in the worst-case scenario creating an artificial signature of an ancient pulse of diversification (Duchêne et al., 2017a). Developing models to correctly account for variation in substitution rates is an ongoing challenge in molecular dating (Drummond et al., 2006; Duchêne et al., 2014). However, further development of these models is made more challenging by the enormous number of factors that can influence substitution rates, including but not limited to aspects of molecular biology, physiology, life history, and population variation (Mooers and Harvey, 1994; Welch et al., 2008; Bromham, 2009; Lanfear et al., 2010a, 2014; Hodgkinson and Eyre-Walker, 2011).

Perhaps because of this complexity, most approaches to modeling substitution rate variation among lineages use sophisticated statistical models that largely ignore the biological causes and correlates of substitution rate variation, although there are notable exceptions (Lartillot and Poujol, 2010; Lartillot et al., 2016). If we are to time-calibrate the evolutionary history of birds, let alone all life, it will be important to consider instances where the most widely used models of substitution rate variation may be misleading. In particular, largely absent from current approaches to molecular divergence-time estimation are ways to account for another equally important, but less often appreciated, source of substitution rate variation: convergent, directional changes in lineage life history over time.

Modeling Rate Variation: Life-History Evolution and Mass Extinctions

The fossil record is rich in examples of rapid shifts in organismal size and form (Finarelli and Flynn, 2006; Evans et al., 2012; Bellwood et al., 2014; Huttenlocker, 2014; Near et al., 2014; Berv and Field, 2018). For major groups these shifts are particularly pervasive in the aftermath of mass extinction events (Twitchett, 2007; Friedman, 2010; Sibert et al., 2018). In these cases, the most recent common ancestors of survivors are often hypothesised to be relatively small bodied (Cardillo et al., 2005; He et al., 2010; Huttenlocker, 2014). Small-bodied organisms tend to have larger effective population sizes, shorter generation times, and lower absolute metabolic requirements relative to larger bodied relatives, all of which are predicted to buffer against the effects of the rapid environmental changes that are the hallmarks of mass extinctions (McKinney and Lockwood, 1999). These factors, as well as other life-history characters (below), are strongly correlated with rates of molecular evolution (Lynch and Walsh, 2007; Berv and Field, 2018).

The hypothesis of a "fast-running" molecular clock across mass extinction events was raised by Benton (1999); however, plausible drivers of such an acceleration have largely gone uninvestigated, and the hypothesis has not gained considerable traction (but see Lee et al., 2013; Berv and Field, 2018). This is unfortunate, as a growing body of literature examining correlations between molecular rates and life history offers a number of plausible and nonmutually exclusive macroevolutionary drivers that could have instigated a pulse of molecular evolution in the wake of the K-Pg mass extinction. In particular, for several major clades of vertebrates such as birds and mammals, numerous authors have confirmed a strong negative correlation between nucleotide substitution rate and body size, due to numerous size-linked biological and demographic factors that correlate with substitution rate (Martin and Palumbi, 1993; Dornburg et al., 2012; Nabholz et al., 2016; Berv and Field, 2018).

Birds may have exhibited elevated substitution rates in the wake of the K-Pg mass extinction for a number of reasons. First, and likely most importantly, smaller birds have shorter generation times on average, resulting in more genome copying events and thus more mutations and more substitutions per unit of time (Mooers and Harvey, 1994; Baer et al., 2007; Lehtonen and Lanfear, 2014). Generation time has been consistently shown to be strongly linked to substitution rates in taxa across the Tree of Life (Martin and Palumbi, 1993). Second, smaller birds have higher mass-specific metabolic rates on average, which may cause higher rates of DNA damage and thus higher mutation rates and higher substitution rates per unit of time (Mindell et al., 1996), although this hypothesis remains controversial because the mechanism linking metabolic rate to germline DNA damage remains unclear (Lanfear et al., 2007). Therefore, if K-Pg-surviving birds were relatively small bodied, relatively short generation times and higher mass specific metabolic rates would both be expected to result in high substitution rates in the wake of the K-Pg. Additionally, regardless of correlations between substitution rates and life history, lineages that survive mass extinction events are expected to have smaller effective population sizes in the early stages of postextinction recovery, which may itself cause a transient pulse of substitutions (Lanfear et al., 2014).

Following Berv and Field (2018), we suggest that a burst of rapid molecular evolution may have taken place early in the evolutionary history of crown birds. We refer to this phenomenon as an "epoch effect" (Lee and Ho, 2016), and suggest that such a cladewide substitution rate acceleration may be partially responsible for the enduring uncertainty in avian crown group age estimates as well as those for major crown bird subclades. It may be that the fast, early rates of crown birds were induced by selective extinction of larger species and/or size reduction among surviving lineages at the K-Pg extinction event (Twitchett, 2007), and suggest that this extinction-induced acceleration in the rate of molecular evolution may provide a plausible means of reconciling the incongruence between loosely constrained molecular divergence-time analyses and fossil-based estimates of divergence times in birds and other organisms.

PLAUSIBILITY OF AN 'ACCELERATED' MOLECULAR CLOCK EARLY IN CROWN BIRD HISTORY

BODY SIZE: Body size selectivity among K-Pg survivors may have accelerated the avian molecular clock. The evidence linking small body size to increased rates of molecular evolution raises a key question: How likely was the K-Pg to have acted as a filter on avian body size? Reductions in body size among survivors across mass extinction horizons, though often difficult to observe in clades lacking extensive pre- and postextinction fossil records, have been termed the "Lilliput effect" (Urbanek, 1993). Preliminary attempts to discern evidence for an avian Lilliput effect across the K-Pg based on fossil body size estimates (Field et al., 2013) and fossil calibrated ancestral body size reconstructions (Berv and Field, 2018) have yielded results consistent with transient body-size reduction across this mass extinction horizon (fig. 4). A Lilliput effect among avian survivors would, at least theoretically, have limited their total metabolic requirements in the early aftermath of the K-Pg, a calamitous interval during which the prospect of avian survival in itself may have been tenuous at best (Robertson et al., 2004, 2013; Longrich et al., 2011; Feduccia, 2014; Larson et al., 2016; Field et al., 2018b). Thus, if an avian Lilliput effect did take place, we would predict it to have induced a pulse of elevated substitution rates in the early Paleocene. This acceleration could cause currently available molecular-clock methods to dramatically underestimate the true substitution rates at the base of the avian tree of life, resulting in artificially ancient divergence time estimates for deep crown bird nodes as a consequence of tree extension (Berv and Field, 2018; fig. 4).

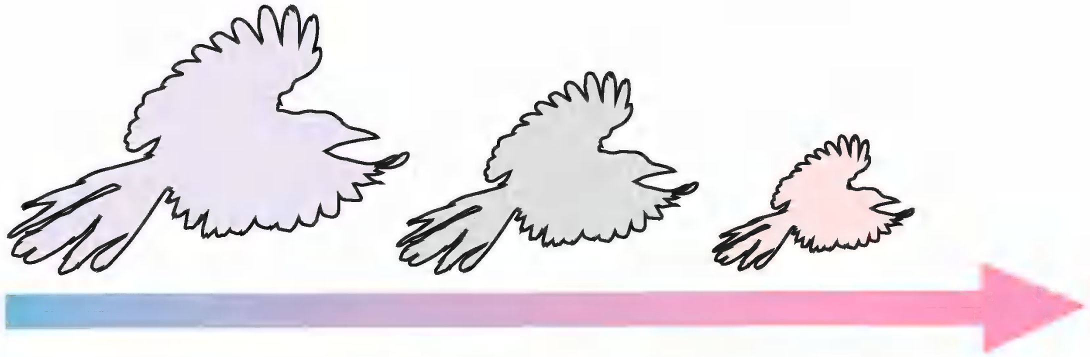

	Change in Body Size	Substitution Rate
Age at Sexual Maturity	Decrease	Increase
Incubation Time	Decrease	Increase
Fecundity	Increase	Increase
Mass-specific Metabolic Rate	Increase	Increase
Hatching Mass	Decrease	Increase
Growth Rate	Decrease	Increase
Longevity	Decrease	Increase

FIG. 4. Expected influence of avian body size decreases on life history variables linked to substitution rate for exon rich data (modified from Berv and Field, 2018). Reductions in avian body size are predicted to result in increased avian substitution rates.

Berv and Field (2018) confirmed a strong negative correlation between body size and nucleotide substitution rate across the avian crown group for a sample of exon-rich nucleotide data, consistent with the expectation that transitions toward smaller body size may induce accelerations in substitution rate (Martin and Palumbi, 1993; Nabholz et al., 2016; fig. 4). Ksepka and Phillips (2015) identified similar patterns, although the hypothesis of a Lilliput effect-induced rate acceleration was not investigated in that study. To investigate the potential for coordinated body size fluctuations to influence avian divergence-time estimates, Berv and Field (2018) first divided the avian crown group into seven major subclades. They then ran strict and relaxed clock divergence-time analyses, further subsampling "small," "median," and "large" sized species from each of those clades. When the age of the crown bird MRCA was estimated using a dataset of the smallest representatives from those seven major clades, an avian MRCA age of ~116 Ma was obtained (fig. 5). By contrast, analyses rerun using the largest representatives from the seven major clades resulted in a MRCA age of ~78 Ma (fig. 5). Finally, analyses run using "median-sized" taxa within those major clades yielded an intermediate avian MRCA age of ~95 Ma (fig. 5). These analyses clearly illustrate the potential for evolutionary perturbations in body size to induce branch length extensions and contractions. These results have profound implications for divergence-time analyses if the K-Pg extinction selected for small body size among boundary-crossing lineages.

POST-K-PG POPULATION SIZE: A collapse in post-K-Pg population sizes may have accelerated the avian molecular clock. The theoretical link between body size and rates of avian genomic substitution is strong, even if directly

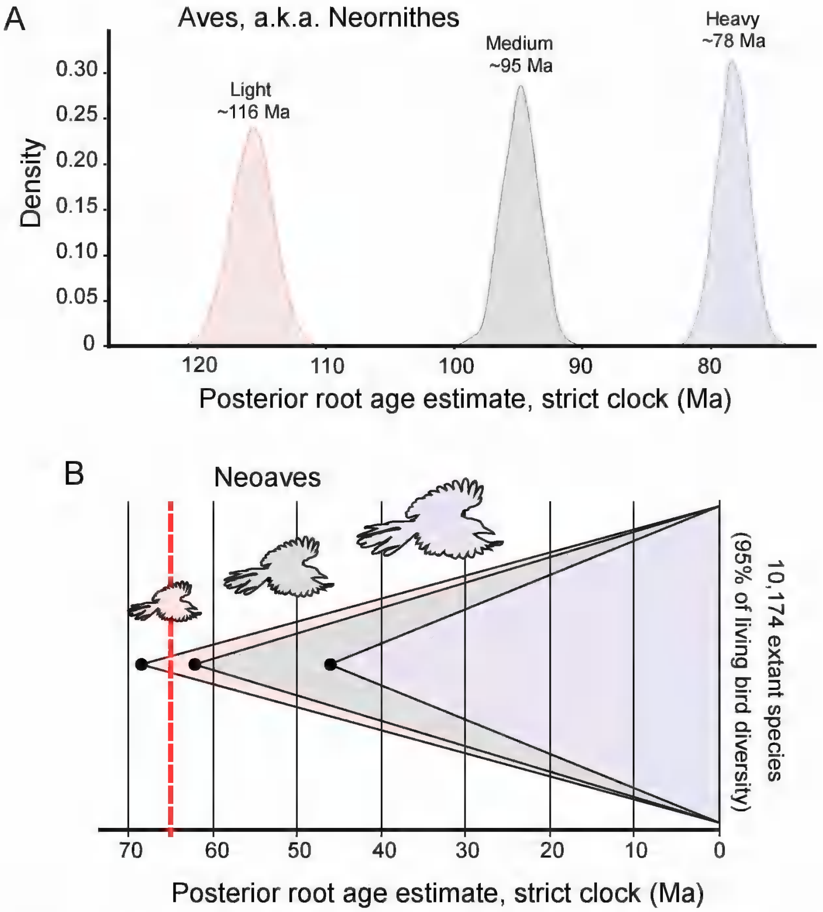

FIG. 5. The influence of body size on estimates of crown bird and neoavian clade ages from strict clock analyses (modified from Berv and Field, 2018). **A,** Results of body size partitioning on estimates of the age of the crown bird MRCA. The "heavy" body size partition (blue) yields a mean crown bird MRCA estimate ~17 million years younger than the "medium" body size partition, and ~38 million years younger than the "light" body size partition (pink). **B,** Results of body size partitioning on estimates of the age of the neoavian MRCA. "Heavy" body size partition yielded a neoavian MRCA estimate of ~46 Ma (blue), "medium" body size partition ~63 Ma (grey), "light" body size partition ~68 Ma (pink). Dashed red line corresponds to the K–Pg boundary.

modeling body size change across the K-Pg boundary is challenging in light of a sparse crown bird fossil record in the latest Cretaceous and earliest Cenozoic. But why is the fossil record during this interval so sparse? First, factors related to fossil preservation and recovery potential may conspire against the discovery of small-bodied fossils (Brown et al., 2013); thus, selectivity for reduced body size in the wake of the K-Pg may be partly responsible for a limited early Cenozoic record. However, a more important factor may have been the actual ecological rarity of birds triggered by the Chicxulub asteroid impact and its apocalyptic aftereffects (Robertson et al., 2004; Field et al., 2018b), which must have devastated population sizes even among surviving species. Such rarity—which can easily be misinterpreted as absence (Hull et al., 2015)—is likely also to blame for the limited bird fossil record during the first five million years of K-Pg recovery.

Could the devastation of population sizes in the wake of the K-Pg have exacerbated a substitution rate acceleration among birds? Theoretical work has established a negative relationship between population size and substitution rate when most mutations are slightly deleterious (Woolfit, 2009). For slightly deleterious mutations, the strength of drift scales negatively with effective population size (Kimura, 1968), leading to increases in substitution rates across lineages subjected to large reductions in effective population size (Ohta, 1973; Woolfit and Bromham, 2003; Lanfear et al., 2014). This may occur even when reductions in population size lead to a decline of absolute genetic diversity on microevolutionary scales within lineages. Depending on the relative interplay of these phenomena, dramatic changes in population sizes throughout Earth history may be associated with transient changes in substitution rates across the Tree of Life. If surviving lineages of birds—and indeed other organisms—across the K-Pg boundary suffered substantial and long-lasting reductions in their population sizes, then the relationship between drift and population size may have transiently increased nucleotide substitution rates in lineages surviving the K-Pg mass extinction. In combination with a probable Lilliput-effect-related acceleration of the molecular clock (Berv and Field, 2018), a population size-related acceleration would have increased the number of nucleotide substitutions in K-Pg boundary-crossing lineages, thereby increasing the lengths of the phylogenetic branches subtending many extant avian orders, and driving inevitable overestimates of the ages of these clades.

TREE PRIORS: MODELING LINEAGE DIVERSIFICATION AND TAXON SAMPLING

While the focus of the present article concerns the potential for underappreciated sources of systematic bias in inferences of substitution rates, the assumption of particular "tree priors" in divergence-time analyses is also germane, and deserves at least a brief discussion. Some avian divergence-time analyses have applied a Yule process tree prior (e.g., Jetz et al., 2012), which assumes that lineages branch at a constant birthrate without any chance of extinction (Yule, 1925). The assumptions of such a simple diversification model will clearly not be met for many clades. However, the potential effects of this kind of prior misspecification in divergence-time analyses are only beginning to receive more attention (Condamine et al., 2015). For example, given the assumption of a constant-rate Yule tree prior and a relaxed clock (as described in Drummond and Bouckaert, 2015), the interaction of these priors may result in a situation where the clock model is forced to fit slower or faster rates into branch lengths that are highly conditioned by the assumed tree prior. As such, it is possible that this type of prior misspecification may further confound both avian substitution rate and divergence-time estimates.

More complex tree priors (which, for example, allow for constant-rate extinction) are available, and are perhaps reasonable starting points (Nee et al., 1994; Mooers and Heard, 1997; Nee, 2001). However, a recent study (Claramunt and Cracraft, 2015) convincingly showed that the lineage-sampling fraction (i.e., the proportion of sampled taxa relative to the total number of extant lineages) can also have a significant and predictable effect on estimated avian divergence times (Yang and Rannala, 1997). By failing to account for incomplete sampling, the most-often used tree priors (Yule and birth-death) bias deep nodes to be older and young nodes to be younger (see supplemental materials in Claramunt and Cracraft, 2015). Stadler (2009) showed that we cannot empirically estimate both sampling probability together with birthrates and death rates: "One of these has to be known in order to estimate the other two." Thus, the sampling fraction can have a significant effect if it is small (Stadler, 2009), which is commonly the case for large-scale investigations of avian divergence times (Alfaro et al., 2009; Jarvis et al., 2014; Prum et al., 2015). Not only does the sampling fraction influence divergence-time estimates, but so does the sampling model. Taxa sampled to date backbone phylogenies are selected in a deliberately nonuniform manner to maximize diversity across the tree, enriching the tree for ancient branching events. Failing to account for diversified taxon sampling will bias birth and death estimates toward low speciation rates and near-zero death rates (Höhna et al., 2011), and thus will skew divergence-time estimates. Given the results of Claramunt and Cracraft (2015), we recommend that the birth-death-sampling tree prior (Stadler, 2009) be incorporated as the "null" tree prior for future investigations of avian divergence times relying on family-level (or similarly incomplete) sampling. Combined consideration of sampling fraction *and* the substitution rate biases discussed here will likely result in increasingly accurate and precise molecular age estimates for the crown bird MRCA. Correspondingly, we predict that more integrative models will shift age estimates for the age of crown birds later in the Cretaceous than have typically been recovered.

Biogeographic Dating to Bound Maximum Age Estimates

A sparse fossil record limits how reliably we can assign maximum ages for the deepest clades of modern birds in divergence-time analyses. However, maximum ages may be estimated under certain idealized paleogeographic and biogeographic conditions. As an example, a radiation endemic to a volcanic island is generally assumed to be younger than the island itself (Lerner et al., 2011). Biogeographic dating is the practice of time-calibrating trees based on plausible relationships among biogeography, paleogeography, and clade age (Ho et al., 2015; De Baets et al., 2016). Biogeographic dating operates under the premise that paleogeographic events—such as continental rifting or the rising of a mountain range—should influence when and where lineages diversify. If a paleogeographic event and a phylogenetic divergence are both congruent with a biogeographic disjunction and a hypothetical biogeographic scenario, then using that paleogeographic event's age to date the divergence event represents a means for establishing hypotheses of maximum clade ages.

There is no shortage of paleogeographic events that potentially influenced the diversification of crown bird lineages. Clades endemic to newly habitable islands or mountains have been used to impose hard maximum age constraints as described above, as with the reemergence of New Zealand (Cooper and Cooper, 1995; Landis et al., 2008) or with the uplift of the Andes (Hoorn et al., 2010). Similarly, new interregional dispersal corridors may serve as soft maximum age constraints for radiations within regions, such as the collision of the Sunda and Sahul Shelves (e.g., Lohman et al., 2011) that facilitated the Out-of-Australia oscine passerine radiation (Moyle et al., 2016; Oliveros et al., 2019). Vicariance calibrations are a third type of calibration that depict an ancestrally widespread lineage split into two descendant lineages by a newly formed geographical barrier. The final throes of Gondwanan vicariance during the Paleogene may explain some crown bird biogeographic disjunctions between South America and Australia, two continents that shared an Antarctic connection perhaps as recently as the Eocene (Scher and Martin, 2006; Near et al., 2015). While vicariance calibrations generate strong maximum and minimum age constraints, they are often the most difficult biogeographic scenarios to justify (Goswami and Upchurch, 2010; Kodandaramaiah, 2011). Although few such paleogeographic events are likely to bear directly upon the origins of the deepest crown bird nodes (e.g., Palaeognathae, Galliformes, Anseriformes, Neoaves) during the Early Paleogene, they are still indirectly useful. Maximum age constraints interspersed throughout the phylogeny may serve to limit the maximum age of a crown group— which may otherwise extend to implausibly ancient age estimates in the absence of maximum age constraints (fig. 5; Cracraft et al., 2015)—and thereby bound node age estimation errors.

In practice, there are two principal strategies for time-calibrating phylogenies with biogeography: prior-based node calibration methods and process-based inference methods. Biogeographic node calibration methods emulate a singular and specific biogeographic scenario (Ho et al., 2015; De Baets et al., 2016) in a manner similar to how fossil node calibrations are applied (Parham et al., 2011). However, an important distinction is that fossil priors are justified by asserting phylogenetic relationships between extant and fossil taxa based on morphological affinities, while biogeographic priors are justified by hypothesizing interactions among paleogeography, biogeography, and diversification that are often quite circumstantial. Correspondingly, in dating analyses for modern birds, biogeographic node calibrations are often critiqued as dubious because they invoke specific scenarios that fail to rule out alternative explanations (Claramunt and Cracraft, 2015; Gibb et al., 2015; Field and Hsiang, 2018). Because we generally do not know the true biogeographic history of any clade, process-based methods absorb this uncertainty into the broader inference problem. Process-based methods estimate not only divergence times, but also the full distribution of plausible biogeographic scenarios and palaeogeographic interactions that are compatible with the observed species ranges under a defined model of range evolution (Landis, 2017; Landis et al., 2018). Where prior-based methods are useful for their efficiency and simplicity, process-based methods are designed to handle the sources of historical uncertainty inherent to characterizing crown bird biogeography and diversification (Mayr, 2009, 2016; Claramunt and Cracraft, 2015; Prum et al., 2015; Berv and Field, 2018; Saupe et al., 2019).

Regardless of which biogeographic dating method is applied, the resultant divergence-time estimates should be viewed cautiously and critically. Lack of data on the ranges of extinct lineages can bias range reconstructions to reflect only present day distributions (Donoghue and Moore, 2003; Crisp et al., 2011; Friedman et al., 2013; Wood et al., 2013; Dornburg et al., 2015; Federman et al., 2015; Field and Hsiang, 2018; Saupe et al., 2019). However, these approaches can be used to provide expectations of what combination of biogeographic conditions and molecular rates would be necessary under alternative temporal hypotheses of diversification. In the case of birds, such approaches could be particularly useful in testing for congruence between biogeography and different hypotheses of clade age.

THE WAY FORWARD

There is evidently cause for concern that life-history-driven fluctuations in substitution rates can bias molecular-clock-based age estimates of crown bird divergences. The question becomes: where to go from here? One solution is the development of a time-heterogeneous clock model that can explicitly account for the pernicious K-Pg-related divergence-time errors introduced above. This model would be similar in its implementation to node dating—that is, at certain (user-defined) time slices, nodes, or branches, rates of evolution may be calibrated to increase or decrease, either suddenly or slowly, on the basis of independent evidence from the fossil record (e.g., in the case of birds, along the stem lineages of Palaeognathae, Neognathae, Galloanserae, and Neoaves). In practice, this concept may be encoded into an empirical prior that describes the acceleration and deceleration of molecular substitution rates over time, leveraging evidence from the fossil record of periodic trends in directional trait evolution (such as shifts in body size) and the co-evolutionary relationship between life history traits and molecular rates. However, such a model also poses the risk of high circularity depending on what is considered evidence by the investigator. In the case of the avian fossil record, limited information would simply lead to such a model reflecting the community's emerging prior beliefs and be no different than setting time constraints based on limited fossil data. This is not to say that such a model is without value, as even knowingly enforcing prior beliefs would generate expectations of the levels of heterotachy necessary to reconcile conflict between molecular and fossil-based age estimates.

An alternative solution is to develop molecular clock models that can integrate the complex correlational patterns between substitution rate and quantitative traits, like body size or other life history characters. Encouragingly, such models are already being developed (Lartillot and Poujol, 2010), providing a more sophisticated framework from which to account for the issues outlined above. This class of models could be further expanded to guide expectations of rate changes along specific branches of a given tree using advances in divergence dating that incorporate fossils as terminal taxa (Ronquist et al., 2012; Zhang et al., 2015) and mixed clock models that allow the degree of rate autocorrelation to fluctuate (Lartillot et al., 2016). By reconstructing ancestral states using fossil data (potentially incorporating expectations of preservation bias or temporal gaps), this would highlight where on a tree to expect changes in traits that might otherwise be masked by the absence of fossil taxa. Combining the expected distribution of trait states with an expectation of how strongly molecular rates correlate with these traits could guide the distributions of rates and times estimated for a given branch. While such a model is appealing, the computational burden of existing methods with the ability to model life history evolution currently limits their applicability in large-scale phylogenomic datasets (Berv and Field, 2018). In the case of avian phylogeny, this approach is also challenged by apparent body size decreases across the K-Pg influencing multiple lineages (Berv and Field, 2018). If such rapid changes occurred, they could render early small forms largely indiscernible in ancestral state reconstructions. Moreover, cladewide epoch effects are not likely to be exclusively restricted to periods of extinction recovery: recent investigations of cichlid genomes suggested an acceleration of molecular rates prior to the onset of the adaptive radiation of African rift lake cichlids, suggesting that periods of rapid molecular evolution may represent a precondition of adaptive radiation in some instances (Brawand et al., 2014). If this is true, then epoch effects could be commonly responsible for inducing large errors in divergence-time estimates. Further developments along these lines will certainly be fruitful for dating the Tree of Life as a whole, and it remains to be seen how such approaches could alter our understanding of early avian evolution.

In contrast to developing increasingly complex models, principles of phylogenetic experimental design offer a third approach: choosing markers that are not correlated with life history. Advocates of this approach have long argued that investigators use predictive frameworks for selecting loci of high utility for specific phylogenetic problems (Townsend, 2007; Townsend et al., 2012; Chen et al., 2015; Prum et al., 2015; Dornburg et al., 2016, 2017b; Bleidorn, 2017; Duchêne et al., 2017b). The use and development of these approaches has largely been restricted to tackling issues that arise when character states converge due to either substitution saturation (Dornburg et al., 2014; Theriot et al., 2015; Gilbert et al., 2018; Near et al., 2018) or biased patterns of nucleotide change (Borowiec et al., 2015; Romiguier et al., 2016; Dornburg et al., 2017a). However, selecting loci that do not depict a signature of directional change in molecular rates as a consequence of life history shifts is also an experimental design problem. For birds, assessing the strength of correlations between substitution rates and body sizes across loci, or among substitution types, could offer an additional criterion for selecting loci for divergence-time estimation (Smith et al., 2018). For example, it is well known that in mammals, substitutions that have occurred in CpG contexts display more clocklike behavior than most other types of substitution (Lanfear et al., 2010b). Further scrutinizing this candidate set of loci or substitutions to test against other major sources of error in divergence-time estimation such as substitution saturation (Phillips, 2009; Dornburg et al., 2014), high variance of site rates (Tinn and Oakley, 2008; Brandley et al., 2011), or clade-specific rate heterogeneity (Soltis et al., 2002; Dornburg et al.,

2012) should in principle lead to refined molecular clock estimates that could mitigate against the potential for "epoch effects" to mislead divergence-time analyses.

Regardless of whether these or other approaches are taken as the path forward for developing a better understanding of avian divergence times, it is important to consider that there is only one true history of paravian evolution. Given the currently wide-ranging estimates for the age of crown bird origins (fig. 2), there is still tremendous opportunity to unmask pathologies in our use of both molecular and paleontological data. It is our view that the evidence for organismal life histories that favored mass extinction survival and recovery, coupled with the strong correlation of these traits with molecular rates in markers commonly used for phylogenetics, suggest an underappreciated source of error for divergence-time estimation (Berv and Field, 2018). If life-history-associated shifts in molecular rates are responsible for systematically biasing age estimates for crown birds, then strategies such as those outlined above should all eventually converge on a similar range of age estimates. It is our hope that this review catalyses work testing this hypothesis.

CONCLUSIONS

An accurate understanding of the antiquity of the deepest crown bird nodes has broad implications for reconstructing the macroevolutionary history of modern birds. Assessing the interplay of the extant paravian radiation with major events in Earth history (e.g., Prum et al., 2015), periods of climatic upheaval (e.g., Claramunt and Cracraft, 2015), and potential episodes of vicariance (e.g., Cracraft, 2001) all fundamentally depend on reliable estimates of the age of the avian crown group and its major subclades. Moreover, estimates of diversification rates similarly depend on confident assessments of phylogenetic branch lengths. However, conflicts between paleontological evidence and molecular divergence-time estimates cast a long shadow of uncertainty over downstream inferences.

We propose that a driver of this conflict may be a failure to account for epoch effects in substitution rates caused by epoch effects in life history traits. If our hypothesis of elevated nucleotide evolution in the wake of the K-Pg mass extinction is correct, then this presents the exciting possibility that the resultant pulse of molecular evolution provided the genomic substrate for the rapid early Cenozoic diversification of modern avian lineages (Brawand et al., 2014). Lingering debates regarding the timing of deep evolutionary divergences within other major eukaryotic groups—such as major angiosperm subclades (e.g., Koenen et al., 2019), eutherian mammals (e.g., Phillips et al., 2016), acanthomorph fishes (e.g., Alfaro et al., 2018), and even crown Metazoa (e.g., Lee and Ho, 2016)—may additionally be related to similar epoch effects, suggesting that pulses of molecular evolution may often be associated with major evolutionary radiations. The development of divergence-time approaches capable of accommodating epoch effects, and simultaneously accounting for the interplay between molecular evolution and selection on life history parameters, would not only enable testing of this hypothesis but also more generally aid in establishing a more robust understanding of how major events in Earth history have influenced evolutionary patterns across the Tree of Life.

ACKNOWLEDGEMENTS

We thank M. Pittman and X. Xu for the invitation to discuss these ideas at the International Pennaraptoran Symposium and prepare this article. DJF gratefully acknowledges support from the Isaac Newton Trust, a UK Research and Innovation Future Leaders Fellowship (MR/S032177/1), and the Systematics Association. We thank J. Clark, F. Novas, T. Skawiński, and D. Cerni for comments on this manuscript.

REFERENCES

Agnolín, F.L., F.B. Egli, S. Chatterjee, J.A.G. Marsà, and F.E. Novas. 2017. Vegaviidae, a new clade of southern diving birds that survived the K/T boundary. Science of Nature 104: 87.

Alfaro, M.E., et al. 2009. Nine exceptional radiations plus high turnover explain species diversity in jawed vertebrates. Proceedings of the National Academy of Sciences of the United States of America 106: 13410–13414.

Alfaro, M.E., et al. 2018. Explosive diversification of marine fishes at the Cretaceous-Palaeogene boundary. Nature Ecology & Evolution 2: 688–696.

Baer, C.F., M.M. Miyamoto, and D.R. Denver. 2007. Mutation rate variation in multicellular eukaryotes: causes and consequences. Nature Reviews Genetics 8: 619–631.

Beaulieu, J.M., B.C. O'Meara, P. Crane, and M.J. Donoghue. 2015. Heterogeneous rates of molecular evolution and diversification could explain the Triassic age estimate for angiosperms. Systematic Biology 64: 869–878.

Bellwood, D.R., C.H.R. Goatley, S.J. Brandl, and O. Bellwood. 2014. Fifty million years of herbivory on coral reefs: fossils, fish and functional innovations. Proceedings of the Royal Society B, Biological Sciences 281: 20133046.

Benton, M.J. 1999. Early origins of modern birds and mammals: molecules vs. morphology. Bioessays 21: 1043–1051.

Benton, M.J., and P.C.J. Donoghue. 2007. Paleontological evidence to date the tree of life, Molecular Biology and Evolution 24(1): 26–53.

Berv, J.S., and D.J. Field. 2018. Genomic signature of an avian Lilliput effect across the K-Pg extinction. Systematic Biology 67: 1–13.

Bleidorn, C. 2017. Sources of error and incongruence in phylogenomic analyses. *In* C. Bleidorn (editor), Phylogenomics: 173–193. Cham: Springer.

Borowiec, M.L., E.K. Lee, J.C. Chiu, and D.C. Plachetzki. 2015. Extracting phylogenetic signal and accounting for bias in whole-genome data sets supports the Ctenophora as sister to remaining Metazoa. BMC Genomics 16: 987.

Brandley, M.C., et al. 2011. Accommodating heterogenous rates of evolution in molecular divergence dating methods: an example using intercontinental dispersal of *Plestiodon* (*Eumeces*) lizards. Systematic Biology 60: 3–15.

Brawand, D., et al. 2014. The genomic substrate for adaptive radiation in African cichlid fish. Nature 513: 375–381.

Bromham, L. 2002. Molecular clocks in reptiles: life history influences rate of molecular evolution. Molecular Biology and Evolution 19(3): 302–309.Bromham, L. 2009. Why do species vary in their rate of molecular evolution? Biology Letters 5: 401–404.

Bromham, L., and D. Penny. 2003. The modern molecular clock. Nature Reviews Genetics 4: 216–224.

Brown, C.M., D.C. Evans, N.E. Campione, L.J. O'Brien, and D.A. Eberth. 2013. Evidence for taphonomic size bias in the Dinosaur Park Formation (Campanian, Alberta), a model Mesozoic terrestrial alluvial-paralic system. Palaeogeography Palaeoclimatology Palaeoecology 372: 108–122.

Brown, J.W., J.S. Rest, J. García-Moreno, M.D. Sorenson, and D.P. Mindell. 2008. Strong mitochondrial DNA support for a Cretaceous origin of modern avian lineages. BMC Biology 6: 6.

Cardillo, M., et al. 2005. Multiple causes of high extinction risk in large mammal species. Science 309: 1239–1241.

Chen, M.Y., D. Liang, and P. Zhang. 2015. Selecting question-specific genes to reduce incongruence in phylogenomics: a case study of jawed vertebrate backbone phylogeny. Systematic Biology 64:1104–1120.

Claramunt, S., and J. Cracraft. 2015. A new time tree reveals Earth history's imprint on the evolution of modern birds. Science Advances 1(11): e1501005.

Clarke, J.A., C.P. Tambussi, J.I. Noriega, G.M. Erickson, and R.A. Ketcham. 2005. Definitive fossil evidence for the extant avian radiation in the Cretaceous. Nature 433: 305–308.

Condamine, F.L., N.S. Nagalingum, C.R. Marshall, and H. Morlon. 2015. Origin and diversification of living cycads: a cautionary tale on the impact of the branching process prior in Bayesian molecular dating. BMC Evolutionary Biology 15: 65.

Cooper, A., and R.A. Cooper. 1995. The Oligocene bottleneck and New Zealand biota: genetic record of a past environmental crisis. Proceedings of the Royal Society B: Biological Sciences 261: 293–302.

Cooper, A., and D. Penny. 1997. Mass survival of birds across the Cretaceous-Tertiary boundary: molecular evidence. Science 275: 1109–1113.

Cracraft, J. 2001. Avian evolution, Gondwana biogeography and the Cretaceous-Tertiary mass extinction event. Proceedings of the Royal Society B: Biological Sciences 268: 459–469.

Cracraft, J., et al. 2004. Phylogenetic relationships among modern birds (Neornithes). Assembling the Tree of Life: 468–489.

Cracraft, J., et al. 2015. Response to comment on "Whole-genome analyses resolve early branches in the tree of life of modern birds". Science 349: 1460.

Crisp, M.D., S.A. Trewick, and L.G. Cook. 2011. Hypothesis testing in biogeography. Trends in Ecology and Evolution 26: 66–72.

Crouch, N.M., K. Ramanauskas, and B. Igić. 2018. Tip-dating and the origin of Telluraves. Molecular Phylogenetics and Evolution 131: 55–63.

De Baets, K., A. Antonelli, and P.C.J. Donoghue. 2016. Tectonic blocks and molecular clocks. Philosophical Transactions of the Royal Society of London B: Biological Sciences 371(1699): rstb.2016.0098.

Degnan, J.H., and N.A. Rosenberg. 2009. Gene tree discordance, phylogenetic inference and the multispecies coalescent. Trends in Ecology and Evolution 24: 332–340.

Donoghue, M.J., and B.R. Moore. 2003. Toward an integrative historical biogeography. Integrative and Comparative Biology 43: 261–270.

Dornburg, A., J.M. Beaulieu, J.C. Oliver, and T.J. Near. 2011. Integrating fossil preservation biases in the selection of calibrations for molecular divergence time estimation. Systematic Biology 60: 519–527.

Dornburg, A., M.C. Brandley, M.R. McGowen, and T.J. Near. 2012. Relaxed clocks and inferences of heterogeneous patterns of nucleotide substitution and divergence time estimates across whales and dolphins (Mammalia: Cetacea). Molecular Biology and Evolution 29: 721–736.

Dornburg, A., J.P. Townsend, M. Friedman, and T.J. Near. 2014. Phylogenetic informativeness reconciles ray-finned fish molecular divergence times. BMC Evolutionary Biology 14: 169.

Dornburg, A., J. Moore, J.M. Beaulieu, R.I. Eytan, and T.J. Near. 2015. The impact of shifts in marine biodiversity hotspots on patterns of range evolution: evidence from the Holocentridae (squirrelfishes and soldierfishes). Evolution 69: 146–161.

Dornburg, A., J.N. Fisk, J. Tamagnan, and J.P. Townsend. 2016. PhyInformR: phylogenetic experimental design and phylogenomic data exploration in R. BMC Evolutionary Biology 16: 262.

Dornburg, A., et al. 2017a. New insights on the sister lineage of percomorph fishes with an anchored hybrid enrichment dataset. Molecular Phylogenetics and Evolution 110: 27–38.

Dornburg, A., J.P. Townsend, and Z. Wang. 2017b. Maximizing power in phylogenetics and phylogenomics: a perspective illuminated by fungal big data. Advances in Genetics 100: 1–47.

Dornburg, A., Z. Su, and J.P. Townsend. 2018. Optimal rates for phylogenetic inference and experimental design in the era of genome-scale datasets. Systematic Biology 68 (1): 145–156.Drummond, A.J., and R.R. Bouckaert. 2015. Bayesian evolutionary analysis with BEAST. Cambridge University Press.

Drummond, A.J., S.Y.W. Ho, M.J. Phillips, and A. Rambaut. 2006. Relaxed phylogenetics and dating with confidence. PLoS Biology 4: e88.

Duchêne, S., M. Molak, and S.Y.W. Ho. 2014. ClockstaR: choosing the number of relaxed-clock models in molecular phylogenetic analysis. Bioinformatics 30: 1017–1019.

Duchêne, D.A., X. Hua, and L. Bromham. 2017a. Phylogenetic estimates of diversification rate are affected by molecular rate variation. Journal of Evolutionary Biology 30: 1884–1897.

Duchêne, D.A., S, Duchêne, and S.Y.W. Ho. 2017b. New statistical criteria detect phylogenetic bias caused by compositional heterogeneity. Molecular Biology and Evolution 34: 1529–1534.

Dumont, M., et al. 2016. Synchrotron imaging of dentition provides insights into the biology of *Hesperornis* and *Ichthyornis*, the "last" toothed birds. BMC Evolutionary Biology 16:178.

Dyke, G.J., and G. Mayr. 1999. Did parrots exist in the Cretaceous period? Nature 399: 317–318.

Ericson, P.G.P., et al. 2006. Diversification of Neoaves: integration of molecular sequence data and fossils. Biology Letters 2: 543.

Evans, A.R., et al. 2012. The maximum rate of mammal evolution. Proceedings of the National Academy of Sciences of the United States of America 109: 4187–4190.

Evans, S.E., and M.K. Hecht. 1993. A history of an extinct reptilian clade, the Choristodera: longevity, Lazarus-taxa, and the fossil record. Evolutionary Biology 27: 323–338.

Federman, S., et al. 2015. The biogeographic origin of a radiation of trees in Madagascar: implications for the assembly of a tropical forest biome. BMC Evolutionary Biology 15: 216.

Feduccia, A. 2014. Avian extinction at the end of the Cretaceous: assessing the magnitude and subsequent explosive radiation. Cretaceous Research 50: 1–15.

Field, D.J. 2017. Big-time insights from a tiny bird fossil. Proceedings of the National Academy of Sciences of the United States of America 114: 7750–7752.

Field, D.J., and A.Y. Hsiang. 2018. A North American stem turaco, and the complex biogeographic history of modern birds. BMC Evolutionary Biology 18: 102.

Field, D.J., C. Lynner, C. Brown, and S.A. Darroch. 2013. Skeletal correlates for body mass estimation in modern and fossil flying birds. PLoS One 8(11): e82000.

Field, D.J., et al. 2018a. Complete *Ichthyornis* skull illuminates mosaic assembly of the avian head. Nature 557: 96–100.

Field, D.J., et al. 2018b. Early evolution of modern birds structured by global forest collapse at the end-Cretaceous mass extinction. Current Biology 28: 1825–1831.e2.

Field, D.J., et al. 2020. Late Cretaceous neornithine from Europe illuminates the origins of crown birds. Nature 579: 397–401.

Finarelli, J.A., and J.J. Flynn. 2006. Ancestral state reconstruction of body size in the Caniformia (Carnivora, Mammalia): the effects of incorporating data from the fossil record. Systematic Biology 55: 301–313.

Friedman, M. 2010. Explosive morphological diversification of spiny-finned teleost fishes in the aftermath of the end–Cretaceous extinction. Proceedings of the Royal Society B: Biological Sciences 277: 1675–1683.

Friedman, M., et al. 2013. Molecular and fossil evidence place the origin of cichlid fishes long after Gondwanan rifting. Proceedings of the Royal Society B: Biological Sciences 280: 20131733.

Gibb, G.C., et al. 2015. New Zealand passerines help clarify the diversification of major songbird lineages during the Oligocene. Genome Biology Evolution 7: 2983–2995.

Gilbert, P.S., J. Wu, M.W. Simon, J.S. Sinsheimer, and M.E. Alfaro. 2018. Filtering nucleotide sites by phylogenetic signal to noise ratio increases confidence in the Neoaves phylogeny generated from ultraconserved elements. Molecular Phylogenetics and Evolution 126: 116–128.

Gill, F., and D. Donsker. 2018. IOC world bird list (version 8.2). Online resource (https://www.worldbirdnames.org/).

Goswami, A., and P. Upchurch. 2010. The dating game: a reply to Heads (2010). Zoologica Scripta 39: 406–409.

Hackett, S.J., et al. 2008. A phylogenomic study of birds reveals their evolutionary history. Science 320: 1763–1768.

Haddrath, O., and A.J. Baker. 2012. Multiple nuclear genes and retroposons support vicariance and dispersal of the palaeognaths, and an Early Cretaceous origin of modern birds. Proceedings of the Royal Society of London B, Biological Sciences 279: 4617–4625.

Hahn, M.W., and L. Nakhleh. 2016. Irrational exuberance for resolved species trees. Evolution 70: 7-17.

He, W.H., et al. 2010. Controls on body size during the Late Permian mass extinction event. Geobiology 8: 391–402.

Ho, S.Y.W. 2014. The changing face of the molecular evolutionary clock. Trends in Ecology and Evolution 29: 496–503.

Ho, S.Y.W., et al. 2015. Biogeographic calibrations for the molecular clock. Biology Letters 11: 20150194.

Hodgkinson, A., and A. Eyre-Walker. 2011. Variation in the mutation rate across mammalian genomes. Nature Reviews Genetics 12: 756–766.

Höhna, S., T. Stadler, F. Ronquist, and T. Britton. 2011. Inferring speciation and extinction rates under different sampling schemes. Molecular Biology and Evolution 28: 2577–2589.

Hoorn, C., et al. 2010. Amazonia through time: Andean uplift, climate change, landscape evolution, and biodiversity. Science. 330: 927–931.

Hope, S. 2002. The Mesozoic radiation of Neornithes. *In* L.M. Chiappe and L. Witmer (editors), Mesozoic birds: above the heads of dinosaurs: 339–388. Berkeley: University of California Press.

Houde, P., E.L. Braun, and L. Zhou. 2020. Deep-time demographic inference suggests ecological release as driver of neoavian adaptive radiation. Diversity 12 (4): 164.

Hull, P.M., S.A.F. Darroch, and D.H. Erwin. 2015. Rarity in mass extinctions and the future of ecosystems. Nature 528: 345–351.

Huttenlocker, A.K. 2014. Body size reductions in nonmammalian eutheriodont therapsids (Synapsida) during the end-Permian mass extinction. PLoS One 9: e87553.

Jarvis, E.D., et al. 2014. Whole-genome analyses resolve early branches in the tree of life of modern birds. Science 346: 1320–1331.

Jetz, W., G.H. Thomas, J.B. Joy, K. Hartmann, and A.O. Mooers. 2012. The global diversity of birds in space and time. Nature 491: 444–448.

Jukes, T.H., and R. Holmquist. 1972. Evolutionary clock: nonconstancy of rate in different species. Science 177: 530–532.

Kimball, R.T., et al. 2019. A phylogenomic supertree of birds. Diversity 11: 109.

Kimura, M. 1968. Evolutionary rate at the molecular level. Nature 217: 624–626.

Kodandaramaiah, U. 2011. Tectonic calibrations in molecular dating. Current Zoology 57:116–124.

Koenen, E.J.M., et al. 2019. The origin and early evolution of the legumes are a complex paleopolyploid phylogenomic tangle closely associated with the Cretaceous-Paleogene (K-Pg) Boundary. BioRxiv 577957. [doi: https://doi.org/10.1101/577957]

Ksepka, D.T., and M.J. Phillips. 2015. Avian diversification patterns across the K-Pg boundary: influence of calibrations, datasets, and model misspecification. Annals of the Missouri Botanical Garden 100: 300–328.

Ksepka, D.T., T. Stidham, and T. Williamson. 2017. Early Paleocene landbird supports rapid phylogenetic and morphological diversification of crown birds after the K-Pg mass extinction. Proceedings of the National Academy of Sciences of the United States of America 114: 8047–8052.

Kumar, S. 1996. Patterns of nucleotide substitution in mitochondrial protein coding genes of vertebrates. Genetics 143: 537–548.

Landis, C.A., et al. 2008. The Waipounamu erosion surface: questioning the antiquity of the New Zealand land surface and terrestrial fauna and flora. Geological Magazine 145:173–197.

Landis, M.J. 2017. Biogeographic dating of speciation times using paleogeographically informed processes. Systematic Biology 66: 128–144.

Landis, M.J., W.A. Freyman, and B.G. Baldwin. 2018. Retracing the Hawaiian silversword radiation despite phylogenetic, biogeographic, and paleogeographic uncertainty. Evolution 72: 2343–2359.

Lanfear, R., J.A. Thomas, J.J. Welch, T. Brey, and L. Bromham. 2007. Metabolic rate does not calibrate the molecular clock. Proceedings of the National Academy of Sciences of the United States of America 104 (39): 15388–15393.

Lanfear, R., S.Y.W. Ho, D. Love, and L. Bromham. 2010a. Mutation rate is linked to diversification in birds. Proceedings of the National Academy of Sciences of the United States of America 107: 20423–20428.

Lanfear, R., J.J. Welch, and L. Bromham. 2010b. Watching the clock: studying variation in rates of molecular evolution between species. Trends in Ecology and Evolution 25: 495–503.

Lanfear, R., H. Kokko, and A. Eyre-Walker. 2014. Population size and the rate of evolution. Trends in Ecology and Evolution 29: 33–41.

Larson, D.W., C.M. Brown, and D.C. Evans. 2016. Dental disparity and ecological stability in bird-like dinosaurs prior to the end-Cretaceous mass extinction. Current Biology 26: 1325–1333.

Lartillot, N., and R. Poujol. 2010. A phylogenetic model for investigating correlated evolution of substitution rates and continuous phenotypic characters. Molecular Biology and Evolution 28: 729–744.

Lartillot, N., M.J. Phillips, and F. Ronquist. 2016. A mixed relaxed clock model. Philosophical Transactions of the Royal Society of London B, Biological Sciences 371 (1699): [doi/10.1098/rstb.2015.0132].

Lee, M.S.Y., and S.Y.W. Ho. 2016. Molecular clocks. Current Biology 26: R399–R402.

Lee, M.S.Y., Soubrier J., and G.D. Edgecombe. 2013. Rates of phenotypic and genomic evolution during the Cambrian Explosion. Current Biology 23: 1889–1895.

Lehtonen, J., and R. Lanfear. 2014. Generation time, life history and the substitution rate of neutral mutations. Biology Letters 10: 20140801.

Lerner, H.R.L., M. Meyer, H.F. James, M. Hofreiter, and R.C. Fleischer. 2011. Multilocus resolution of phylogeny and timescale in the extant adaptive radiation of Hawaiian honeycreepers. Current Biology 21: 1838–1844.

Li, W.H., M. Tanimura, and P.M. Sharp. 1987. An evaluation of the molecular clock hypothesis using mammalian DNA sequences. Journal of Molecular Evolution 25: 330–342.

Lohman, D.J., et al. 2011. Biogeography of the Indo-Australian Archipelago. Annual Review of Ecology, Evolution and Systematics 42: 205–226.

Longrich, N.R., T. Tokaryk, and D.J. Field. 2011. Mass extinction of birds at the Cretaceous-Paleogene (K-Pg) boundary. Proceedings of the National Academy of Sciences of the United States of America 108: 15253–15257.

Lynch, M., and B. Walsh. 2007. The origins of genome architecture (vol. 98). Sunderland: Sinauer Associates.

Marsh, O.C. 1880. Odontornithes: A monograph on the extinct toothed birds of North America. US Government Printing Office: 18.

Martin, A.P., and S.R. Palumbi. 1993. Body size, metabolic rate, generation time, and the molecular clock. Proceedings of the National Academy of Sciences of the United States of America 90: 4087–4091.

Mayr, G. 2009. Paleogene fossil birds. Berlin: Springer.

Mayr, G. 2016. Avian evolution: the fossil record of birds and its paleobiological significance. Chichester: Wiley-Blackwell.

Mayr, G. 2017. Avian higher level biogeography: southern hemispheric origins or southern hemispheric relicts? Journal of Biogeography 44 (4): 956–958.

Mayr, G., V.L. De Pietri, R.P. Scofield, and T.H. Worthy. 2018. On the taxonomic composition and phylogenetic affinities of the recently proposed clade Vegaviidae Agnolín et al., 2017—neornithine birds from the Upper Cretaceous of the Southern Hemisphere. Cretaceous Research 86: 178–185.

McCormack, J.E., et al. 2013. A phylogeny of birds based on over 1,500 loci collected by target enrichment and high-throughput sequencing. PLoS One 18(1): e54848.

McKinney, M.L., and J.L. Lockwood. 1999. Biotic homogenization: a few winners replacing many losers in the next mass extinction. Trends Ecology and Evolution 14: 450–453.

Meier, J.I., et al. 2017. Ancient hybridization fuels rapid cichlid fish adaptive radiations. Natural Communications 8: 14363.

Mindell, D.P., A. Knight, C. Baer and C.J. Huddleston. 1996. Slow rates of molecular evolution in birds and the metabolic rate and body temperature hypotheses. Molecular Biology and Evolution 13 (2): 422.

Mitchell, K.J., A. Cooper, and M.J. Phillips. 2015. Comment on "Whole-genome analyses resolve early branches in the tree of life of modern birds." Science 349: 1460.

Mooers, A.O., and P.H. Harvey. 1994. Metabolic rate, generation time, and the rate of molecular evolution in birds. Molecular Phylogenetics and Evolution 3:344–350.

Mooers, A.O., and S.B. Heard. 1997. Inferring evolutionary process from phylogenetic tree shape. Quarterly Review of Biology 72: 31–54.

Moorjani, P., C.E.G., Amorim, P.F. Arndt, and M. Przeworski. 2016. Variation in the molecular clock of primates. Proceedings of the National Academy of Sciences of the United States of America 113 (38): 10607–10612.

Moyle, R.G., et al. 2016. Tectonic collision and uplift of Wallacea triggered the global songbird radiation. Nature Communications 7: 12709.

Musser, G., D.T. Ksepka, and D.J. Field. 2019. New material of Paleocene-Eocene *Pellornis* (Aves: Gruiformes) clarifies the pattern and timing of the extant gruiform radiation. Diversity 11 (7): 102.

Nabholz, B., R. Lanfear, and J. Fuchs. 2016. Body mass-corrected molecular rate for bird mitochondrial DNA. Molecular Ecology 25: 4438–4449.

Near, T.J., et al. 2014. Boom and bust: ancient and recent diversification in bichirs (Polypteridae: Actinopterygii), a relictual lineage of ray-finned fishes. Evolution 68: 1014–1026.

Near, T.J., et al. 2015. Identification of the notothenioid sister lineage illuminates the biogeographic history of an Antarctic adaptive radiation. BMC Evolutionary Biology 15:109.

Near T.J., et al. 2018. Phylogenetic analysis of Antarctic notothenioids illuminates the utility of RADseq for resolving Cenozoic adaptive radiations. Molecular Phylogenetics and Evolution 129: 268–279.

Nee, S. 2001. Inferring speciation rates from phylogenies. Evolution 55: 661–668.

Nee, S., E.C. Holmes, R.M. May, and P.H. Harvey. 1994. Extinction rates can be estimated from molecular phylogenies. Philosophical Transactions of the Royal Society of London B: Biological Sciences 344: 77–82.

Noriega, J.I., and C.P. Tambussi. 1995. A Late Cretaceous Presbyornithidae (Aves: Anseriformes) from Vega Island, Antarctic Peninsula: paleobiogeographic implications. Ameghiniana 32:57–61.

Ohta, T. 1973. Slightly deleterious mutant substitutions in evolution. Nature 246: 96–98.

Oliveros, C.H., et al. 2019. Earth history and the passerine superradiation. Proceedings of the National Academy of Sciences 116: 7916–7925.

Pacheco, M.A., et al. 2011. Evolution of modern birds revealed by mitogenomics: timing the radiation and origin of major orders. Molecular Biology and Evolution 28: 1927–1942.

Parham, J.F., et al. 2011. Best practices for justifying fossil calibrations. Systematic Biology 61: 346–359.

Phillips, M.J. 2009. Branch-length estimation bias misleads molecular dating for a vertebrate mitochondrial phylogeny. Genetics 441: 132–140.

Phillips, M.J. 2016. Geomolecular dating and the origin of mammals. Systematic Biology 65: 546–557.

Prum, R.O., et al. 2015. A comprehensive phylogeny of birds (Aves) using targeted next-generation DNA sequencing. Nature 526: 569–573.

Radinsky, L. 1978. Do albumin clocks run on time? Science 200: 1182–1185.

Reddy, S., et al. 2017. Why do phylogenomic data sets yield conflicting trees? Data type influences the avian tree of life more than taxon sampling. Systematic Biology 66: 857–879.

Robertson, D.S., M.C. McKenna, O.B. Toon, S. Hope, and J.A. Lillegraven. 2004. Survival in the first hours of the Cenozoic. Geological Society of America Bulletin 116: 760–768.

Robertson, D.S., W.M. Lewis, P.M. Sheehan, and O.B. Toon. 2013. K-Pg extinction: reevaluation of the heat-fire hypothesis. Journal of Geophysical Research: Biogeosciences 118: 329–336.

Romiguier, J., et al. 2016. Phylogenomics controlling for base compositional bias reveals a single origin of eusociality in corbiculate bees. Molecular Biology and Evolution 33: 670–678.

Ronquist, F., et al. 2012. A total-evidence approach to dating with fossils, applied to the early radiation of the hymenoptera. Systematic Biology 61: 973–999.

Saupe, E.E., et al. 2019. Climatic shifts drove major contractions in avian latitudinal distributions throughout the Cenozoic. Proceedings of the National Academy of Sciences 116: 12895–12900.

Scher, H.D., and E.E. Martin. 2006. Timing and climatic consequences of the opening of Drake Passage. Science 312: 428–430.

Sibert, E., M. Friedman, P. Hull, G. Hunt, and R. Norris. 2018. Two pulses of morphological diversification in Pacific pelagic fishes following the Cretaceous-Palaeogene mass extinction. Proceedings of the Royal Society B, Biological Sciences 285: 20181194.

Smith, S.A., and M.J. Donoghue. 2008. Rates of molecular evolution are linked to life history in flowering plants. Science 322: 86–89.

Smith, S.A., J.W. Brown, and J.F. Walker. 2018. So many genes, so little time: a practical approach to divergence-time estimation in the genomic era. PLoS One 13: e0197433.

Sober, E. 2009. Absence of evidence and evidence of absence: evidential transitivity in connection with fossils, fishing, fine-tuning, and firing squads. Philosophical Studies 143: 63–90.

Soltis, P.S., D.E. Soltis, V. Savolainen, P.R. Crane, and T.G. Barraclough. 2002. Rate heterogeneity among lineages of tracheophytes: integration of molecular and fossil data and evidence for molecular living fossils. Proceedings of the National Academy of Sciences of the United States of America 99: 4430–4435.

Stadler, T. 2009. On incomplete sampling under birth-death models and connections to the sampling-based coalescent. Journal of Theoretical Biology 261: 58–66.

Stidham, T.A. 1998. A lower jaw from a Cretaceous parrot. Nature 396: 29–30.

Suh, A. 2016. The phylogenomic forest of bird trees contains a hard polytomy at the root of Neoaves. Zoologica Scripta 45: 50–62.

Theriot, E.C., M.P. Ashworth, T. Nakov, E. Ruck, and R.K. Jansen. 2015. Dissecting signal and noise in diatom chloroplast protein encoding genes with phylogenetic information profiling. Molecular Phylogenetics and Evolution 89: 28–36.

Tinn, O., and T.H. Oakley. 2008. Erratic rates of molecular evolution and incongruence of fossil and molecular divergence time estimates in Ostracoda (Crustacea). Molecular Phylogenetics and Evolution 48: 157–167.

Townsend, J.P. 2007. Profiling phylogenetic informativeness. Systematic Biology 56: 222–231.

Townsend, J.P., Su Z., and Y.I. Tekle. 2012. Phylogenetic signal and noise: predicting the power of a data set to resolve phylogeny. Systematic Biology 61: 835–849.

Twitchett, R.J. 2007. The Lilliput effect in the aftermath of the end-Permian extinction event. Palaeogeography Palaeoclimatology Palaeoecology 252: 132–144.

Urbanek, A. 1993. Biotic crises in the history of Upper Silurian graptoloids: A palaeobiological model. Historical Biology 7: 29–50.

Vawter, L., and W.M. Brown. 1986. Nuclear and mitochondrial DNA comparisons reveal extreme rate variation in the molecular clock. Science 234: 194–196.

Warnock, R.C.M., Z. Yang, and P.C.J. Donoghue. 2012. Exploring uncertainty in the calibration of the molecular clock. Biology Letters 8: 156–159.

Warnock, R.C.M., J.F. Parham, W.G. Joyce, T.R. Lyson, and P.C.J. Donoghue. 2015. Calibration uncertainty in molecular dating analyses: there is no substitute for the prior evaluation of time priors. Proceedings of the Royal Society B, Biological Sciences 282: 20141013.

Welch, J.J., O.R.P. Bininda-Emonds , and L. Bromham. 2008. Correlates of substitution rate variation in mammalian protein-coding sequences. BMC Evolutionary Biology 8: 53.

Wilson, G.P. 2014. Mammalian extinction, survival, and recovery dynamics across the Cretaceous-Paleogene boundary in northeastern Montana, USA. Geological Society of America Special Papers 503: 365–392.

Wood, H.M., N.J. Matzke, R.G. Gillespie, and C.E. Griswold. 2013. Treating fossils as terminal taxa in divergence time estimation reveals ancient vicariance patterns in the palpimanoid spiders. Systematic Biology 62: 264–284.

Woolfit, M. 2009. Effective population size and the rate and pattern of nucleotide substitutions. Biology Letters 5: 417–420.

Woolfit, M., and L. Bromham. 2003. Increased rates of sequence evolution in endosymbiotic bacteria and fungi with small effective population sizes. Molecular Biology and Evolution 20: 1545–1555.

Worthy, T.H., F.J. Degrange, W.D. Handley, and M.S.Y. Lee. 2017. The evolution of giant flightless birds and novel phylogenetic relationships for extinct fowl (Aves, Galloanseres). Royal Society Open Science 4 (10): 170975.

Yang, Z., and B. Rannala. 1997. Bayesian phylogenetic inference using DNA sequences: a Markov Chain Monte Carlo Method. Molecular Biology and Evolution 14: 717–724.

Yule, G.U. 1925. A mathematical theory of evolution, based on the conclusions of Dr. J. C. Willis, F.R.S. Philosophical Transactions of the Royal Society of London B, Biological Sciences 213: 21–87.

Zhang, C., T. Stadler, S. Klopfstein, T.A. Heath, and F. Ronquist. 2015. Total-evidence dating under the fossilized birth-death process. Systematic Biology 65: 228–249

SECTION 2. ANATOMICAL FRONTIERS

Chapter 6

Disparity and Macroevolutionary Transformation of the Maniraptoran Manus

SERGIO M. NEBREDA,[1] GUILLERMO NAVALÓN,[2] IRIS MENÉNDEZ,[3] TROND SIGURDSEN,[4] LUIS M. CHIAPPE,[5] AND JESÚS MARUGÁN-LOBÓN[6]

ABSTRACT

Multiple factors involved in the evolutionary transformation of the manus across the maniraptoran radiation, including its current morphology in modern birds, remain unexplored. Specifically, the morphological disparity of the manus has never been studied quantitatively, and there are no hypotheses about the possible mechanisms and constraints underlying its evolution. Morphological disparity is best studied with shape-analysis tools based on Procrustes methods, because they guarantee the independence of shape from size while depicting the results in expressive graphics. However, this methodology compares fixed configurations of coordinates, preventing their use in highly articulated and movable structures such as the maniraptoran manus. Here, we propose a new protocol, the one-dimensional Procrustes analysis (OPA), for transforming the chord lengths of these bones into unidimensional Cartesian coordinates, enabling treatment of the data under the operational advantages of the Procrustes methods. Our results applying this new method on a sample encompassing 174 maniraptoran dinosaurs manus, including 79 fossils (both avialan and nonavialan taxa) and 95 extant paleognathans and neognathans, document the morphological transition between early-diverging maniraptorans, nonavialan paravians, and birds over morphospace, highlighting an unexpectedly low disparity in the crown group when compared to early-diverging taxa. Within this transition, we show a common trend of proportional reduction and loss of distal elements, mostly in the minor and alular digits. Furthermore, our study reveals an allometric pattern characterizing manus morphological variation between early-diverging maniraptorans and enantiornithine avialans that disappears in crown birds and their closest early-diverging counterparts. This previously unnoticed allometric trend suggests a complex interplay of developmental, functional,

---

[1] Unidad de Paleontología, Departamento de Biología, Facultad de Ciencias, Universidad Autónoma de Madrid.

[2] Unidad de Paleontología, Departamento de Biología, Facultad de Ciencias, Universidad Autónoma de Madrid; and Department of Earth Sciences, University of Oxford, Oxford.

[3] Departamento de Geodinámica, Estratigrafía y Paleontología, Facultad de Ciencias Geológicas, Universidad Complutense de Madrid; and Departamento de Geología Sedimentaria y Cambio Medioambiental, Instituto de Geociencias (UCM, CSIC), Madrid.

[4] University of Southern California, Los Angeles.

[5] Dinosaur Institute, Natural History Museum of Los Angeles County, Los Angeles.

[6] Unidad de Paleontología, Departamento de Biología, Facultad de Ciencias, Universidad Autónoma de Madrid; and Dinosaur Institute, Natural History Museum of Los Angeles County, Los Angeles.

and historical constraints in the evolution of the maniraptoran manus.

INTRODUCTION

Modern birds are the only living representatives of the maniraptoran theropod radiation (Gauthier, 1986; Padian and Chiappe, 1998; Sereno, 1999; Zhou, 2004; Norell and Xu, 2005). One of the most intriguing events of the macroevolutionary transition leading to anatomically modern birds is the transformation of the archetypal grasping forelimb of nonavialan maniraptoran theropods into the forelimb of modern birds (fig. 1), which is largely enclosed in a soft-tissue airfoil and has limited grasping functions (Barta et al., 2018). This large morphological transition in proportion and size is often believed to have been fundamentally shaped by selective pressures related to the demanding biomechanical requirements of flight (Marden, 1994; Norberg, 1995). However, the great diversity of maniraptoran fossils found in recent decades is helping to mitigate such an exclusively adaptive view, given that aerial competence was probably acquired by taxa exhibiting non-modern forelimb morphologies (Xu et al., 2003, 2015; Barta et al., 2018; Wang et al., 2017, 2019; Pei et al., in press; Pittman et al., chapter 10; Dececchi et al., chapter 11; Larsson et al., chapter 12). Therefore, the history of the factors involved in shaping maniraptoran hand evolution is more complex than currently appreciated.

A miniaturization trend took place early in the lineage toward crown birds (Sereno, 1997; Carrano, 2006; Turner et al., 2007; Novas et al., 2012; Puttick et al., 2014; Lee et al., 2014). This trend was coupled with important quantitative changes in forelimb/hindlimb proportions (Dececchi and Larsson, 2013), yet the relative proportions of the skeletal elements of the forelimb (i.e., humerus, radius, ulna, carpals, metacarpals, and phalanges) changed very little (Middleton and Gatesy, 2000). However, it has been suggested that an increase in the morphological disparity of wing shapes occurred later within the avialan radiation, after the origin of active flight, which in turn triggered the evolution of different flight strategies (Serrano and Chiappe, 2017; Serrano et al., 2018, chapter 13). Because the wing's remiges and patagia are anchored in the skeletal elements of the hand and forearm, their shapes, proportions, and sizes may have contributed to such an increase in wing disparity (Nudds et al., 2007), although this assumption has never been tested quantitatively. Addressing the evolution of the morphospace-occupancy of the maniraptoran hand skeleton (manus) is important, as it establishes a critical bridge between paleobiology and the biological disciplines that seek to identify mechanisms underpinning macroevolutionary trends (e.g., molecular genetics and Evo-Devo; Raff, 1996, 2000).

The study of morphospace construction and the analysis of disparity are eminently mathematically quantifiable (McGhee, 1999), and most studies in vertebrate paleobiology have used bone ratios as a proxy for anatomy and ternary diagrams to build morphospaces and visualize disparity. Although this procedure is practical and easy to apply (e.g., Marugán-Lobón and Buscalioni, 2003), it is also analytically restrictive because ratios are highly limiting for statistical analyses (e.g., to study allometry; Rohlf and Marcus, 1993). In fact, geometric morphometrics (GM; Bookstein, 1991) is currently the optimal approach for understanding the evolution of morphological disparity, as it enables the separation of shape from size variation (Mitteroecker and Gunz, 2009; Marugán-Lobón et al., 2013a), which was impossible with "traditional morphometrics", namely, when working with absolute and/or relative lengths (Rohlf and Marcus, 1993). GM captures the geometry of forms as constellations of repeatable and corresponding points (often corresponding to primary homology positions), called landmarks. The Cartesian coordinates of these configurations are then compared in a multistep process, the generalized Procrustes analysis (GPA), which eliminates superfluous differences between the configurations due to position and orientation, together with the dif-

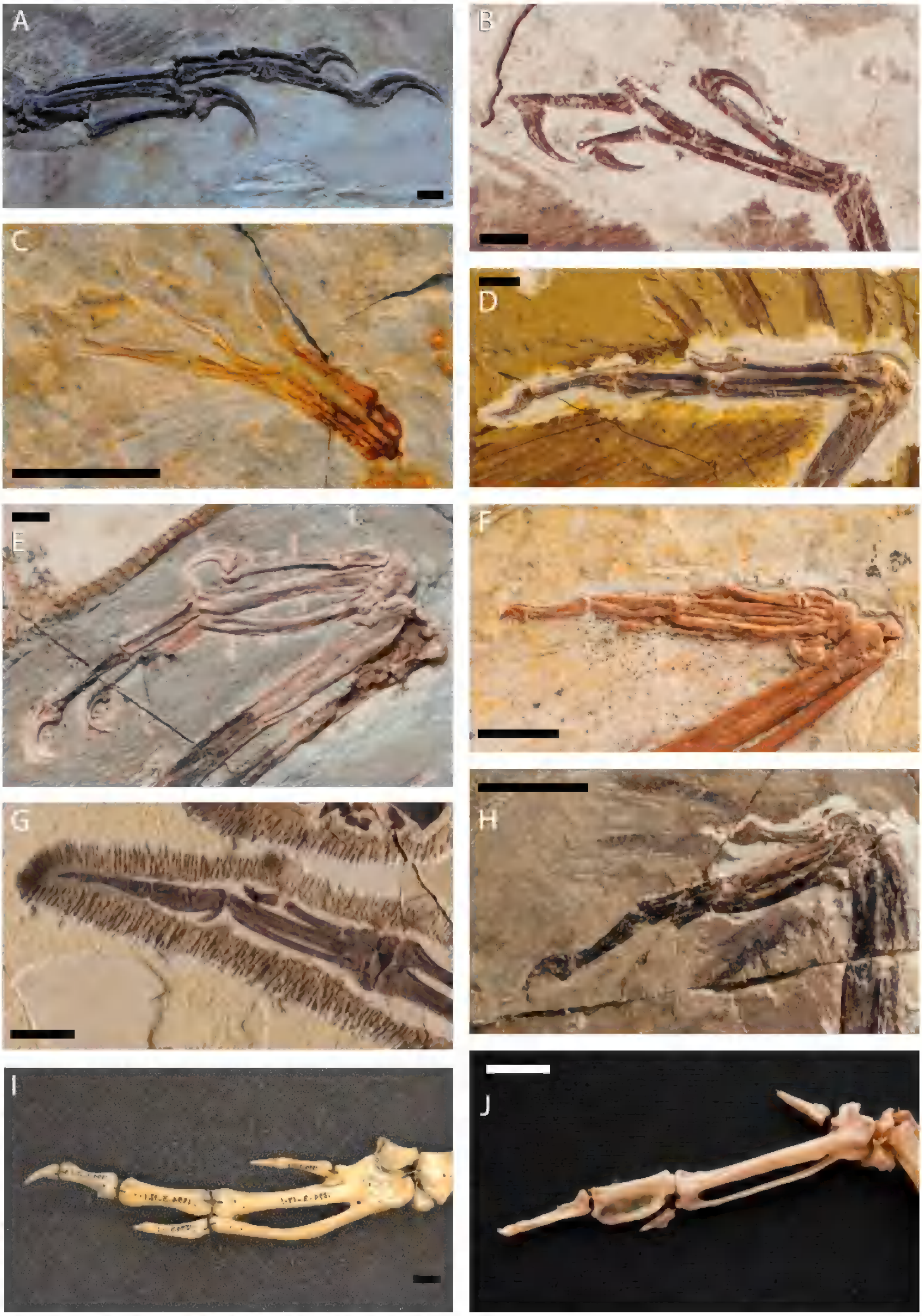

FIG. 1. Representative example of several maniraptorans hands, both fossil (A–H) and extant (I–J) specimens, illustrate the variability of shapes and sizes: **A.** *Zhenyuanlong*; **B.** *Anchiornis huxleyi*; **C.** *Zhongornis*; **D.** *Sapeornis chaoyangensis*; **E.** *Jeholornis*; **F.** *Zhouornis*; **G.** *Archaeorhynchus*; **H.** *Longipteryx*; **I.** *Struthio camelus*; **J.** *Falco tinnunculus*. Scale bars = 10 mm.

ferences due to isometric scaling between the forms (Gower, 1975). GPA calculates the centroid size for each configuration, a geometrically defined proxy for size that is calculated from the real distances between landmarks and rescales them to a standard called unit of centroid size. This key algebraic procedure of standardization was a breakthrough in morphometrics, as it makes size and shape orthogonal, securing the statistical independence between shape and size, and guaranteeing that any difference in shape between configurations associated with size (i.e., allometry) will never be spurious (Rohlf and Marcus, 1993; Mitteroecker and Gunz, 2009; Klingenberg, 2016).

Although the advantages of GM are widely recognized (e.g., Adams et al., 2013), there are certain limitations when applied to articulated skeletal structures. Specifically, the use of GM entails comparing configurations by superimposition to detect minimal differences between corresponding landmarks and, as a result, it requires working on integral structures that have no moveable or articulable parts. The reason is that with the Procrustes alignment of landmark configurations in articulated structures such as the manus, mobility and the ability to flex the digits implies that there are multiple possible spatial configurations between the elements (as many as the joints allow). Therefore, there will be as many configurations of landmarks of the same manus as there are possible positions between the digits, and this will drastically confuse interpretations derived from the method. Although criteria have been established to standardize the placement of moveable structures in one single position (e.g., Adams, 1999; Vidal-García et al., 2018), most choices are either arbitrary or may imply biologically inconsistent assumptions (Marugán-Lobón et al., 2013b). Moreover, the case of the maniraptoran manus is even more intricate given that early-diverging maniraptorans are known only from fossils and the manus elements are likely to be disarticulated or to be preserved in unnatural poses.

Here, we propose a simple morphometric protocol that allows exploiting the accessibility of longitudinal measurements from skeletons and fossils to obtain Procrustes data. Our method, from now on called one-dimensional Procrustes analysis (OPA), involves the transformation of longitudinal measurements of the elements of the manus into one-dimensional Cartesian coordinates, which can be aligned using the Procrustes criterion and analyzed using GM's standard multivariate tools (Dryden and Mardia, 1998), such as multivariate regression to assess allometry (Monteiro, 1999; Marugán-Lobón et al., 2013b). We applied this protocol to a large sample of maniraptoran dinosaur manus ranging from the Jurassic to the present. The objective of the present study was to analyze the morphological disparity of the maniraptoran manus in a macroevolutionary context, from the earliest-diverging taxa to the crown group (Aves), the present-day representatives of the clade. Within this context, the objective was to study the pattern of transformation of its shape understood as a set of proportional lengths of the conforming elements of the manus and its relationship with size (evolutionary allometry).

MATERIALS AND METHODS

Materials

In order to accurately capture the morphological transformation of the maniraptoran manus (fig. 1), we gathered data from a large sample of fossil and extant specimens (from early-diverging maniraptoran taxa to crown birds; fig. 2) with a complete autopod. The sampling of crown birds (Aves, equivalent to Neornithes here) was designed to cover the maximum morphological disparity in the distal region of the forelimb. We measured 174 speci-

FIG. 2. Random phylogenetic tree of the maniraptoran lineage out of the 100 trees used in this work, showing the topology of each member of the sample (N = 174), branch length, and time scale. Colour coding and schematic representations consistent in all figures. See supplemental figure for a large version of this figure that includes taxon names and a more detailed geological time scale (https://doi.org/10.5531/sd.sp.44).

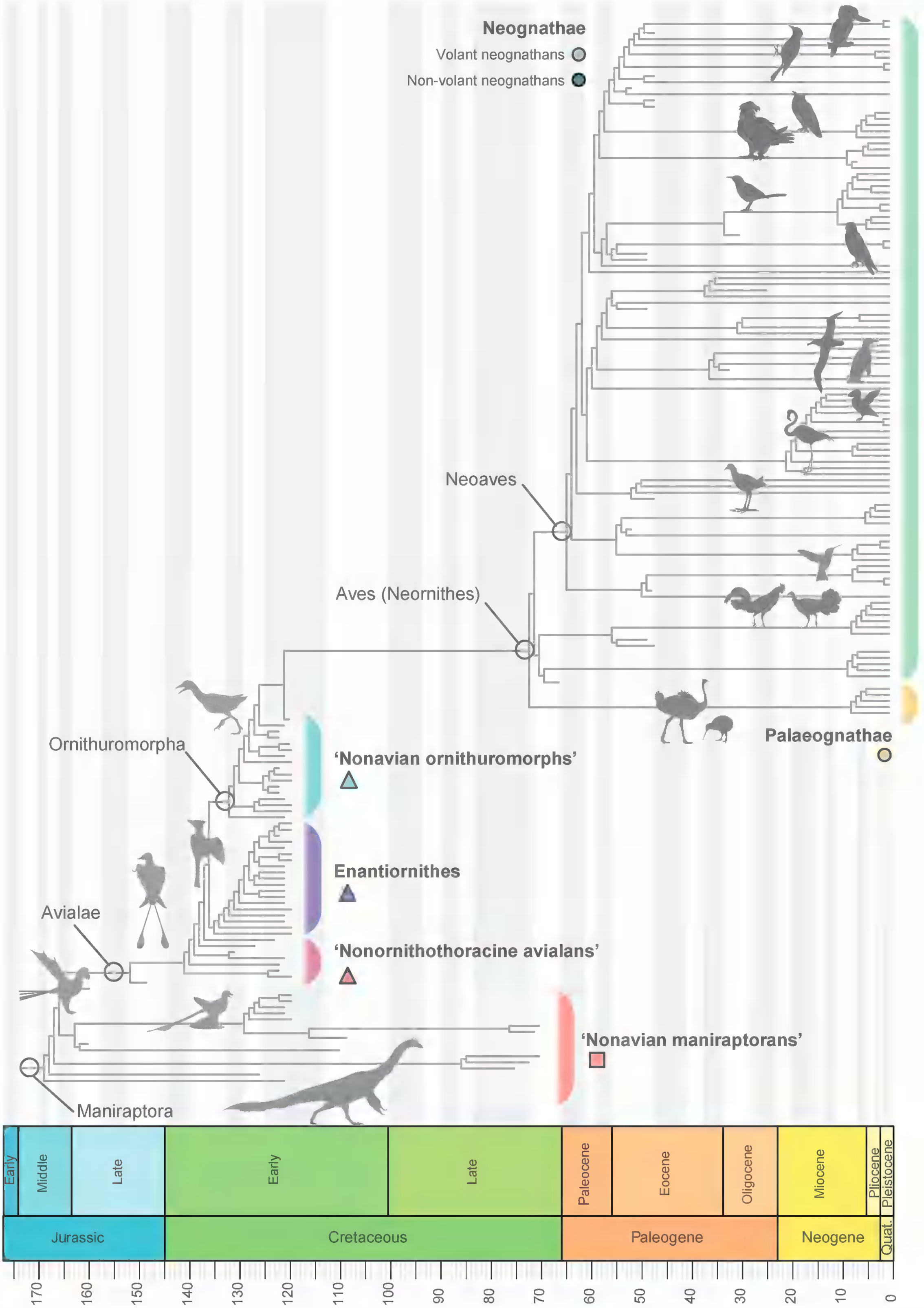
Neognathae
Volant neognathans ○
Non-volant neognathans ●
Neoaves
Aves (Neornithes)
Palaeognathae ○
Ornithuromorpha
'Nonavian ornithuromorphs' △
Enantiornithes ▲
Avialae
'Nonornithothoracine avialans' △
'Nonavian maniraptorans' ☐
Maniraptora
Early
Middle
Late
Early
Late
Paleocene
Eocene
Oligocene
Miocene
Pliocene
Pleistocene
Jurassic
Cretaceous
Paleogene
Neogene
Quat.
170
160
150
140
130
120
110
100
90
80
70
60
50
40
30
20
10
0

mens from the Natural History Museum of Los Angeles County (LACM) and Natural History Museum (NHMUK, Tring), as well as from high-definition photographs provided by one of the authors (L.M.C.) and the literature (pictures and published measurements). The total sample includes 16 specimens of nonavialan maniraptorans (Therizinosauria, Oviraptorosauria, Deinonychosauria, and Scansoriopterygidae), 44 early-diverging birds (nonornithothoracine taxa, Enantiornithes, and nonavian ornithuromorphs), and 114 crown birds (Palaeognathae and Neognathae, which includes Galloanserae and Neoaves, with fossil and extant taxa). All measured specimens are adults, except a juvenile enantiornithine (NIGP 130723; Chiappe et al., 2007) and the nonornithothoracine of uncertain affinities *Zhongornis* (DNHM D2456; Gao et al., 2008; Rashid et al., 2018; but see O'Connor & Sullivan 2014 about possible non-avialan theropod identity).

Manus Anatomy and Data Acquisition

The structure of the manus has changed dramatically during the transition from early-diverging maniraptorans to modern birds, with the reduction and loss of elements, fusions, and alterations in proportions (fig. 1). Therefore, the establishment of a homology framework for the identity of the digits of present-day birds with respect to their dinosaurian ancestors has been challenging (Wagner and Gauthier, 1999; Vargas and Wagner, 2009; Xu et al., 2009, 2011; Bever et al., 2011; Young et al., 2011; Xu and Mackem, 2013). Traditionally in paleontology and zoology the sequence of digits I-II-III has been considered to correspond to the alular, major and minor digits, in modern birds. This hypothesis has been supported mainly by fossil and morphological evidence and is supported by the embryological "frame shift" hypothesis (Wagner and Gauthier, 1999; Bever et al., 2011; Young et al., 2011). However, other embryological studies have proposed that the identity of the manual digits of modern birds is equivalent to the II-III-IV positions of the ancestral pentadactyl hand (i.e., the "lateral change" hypothesis; Xu et al., 2011). Although the debate continues, both hypotheses coincide in the homology of digit identities between the early-diverging maniraptoran and avian manus, thus allowing comparison. Furthermore, these hypotheses are congruent in that the morphogenesis (or condensation) of the digits and their identity is decoupled, thus allowing independent evolutionary changes (Wagner and Gauthier, 1999). Here, we followed the identity of avian digits as I-II-III, the ancestral condition in Theropoda in which digits IV and V are highly reduced (Gauthier, 1986; Xu et al., 2009). At the base of the maniraptoran clade (Gauthier, 1986) the autopod is elongated with a characteristic phalangeal formula of 2-3-4 (digits I-II-III, respectively). Digit II is normally the longest and digit I the shortest, and the wrist is characterized by the presence of a semilunate carpal that contacts the proximal portions of metacarpals (mc) I and II. In contrast, the autopod of crown birds (Aves), while still tridactyl, bears elements that have become fused and have changed their relative lengths as a result of reductions and/or losses of some of their phalanges. In modern groups, the general phalangeal formula is typically 1-2-1, with some exceptions with the formula 2-2-1 or 2-3-1 in forms that retain claws, such as some fowls (Galloanserae) or the ostrich (Struthionidae), respectively (Mayr, 2017). Here, the length of semilunate carpal in nonavialan maniraptorans was included in the measurement of mc-II to aid direct comparisons with avian forms in which these elements are fused (Middleton and Gatesy, 2000). We measured chord lengths of the hand bones of modern birds using calipers (by the authors S.M.N. and T.S.) and using the tpsDig2 software (Rohlf, 2017, v. 2.30) on digital images of the fossils forms (by first author, S.M.N.). The measurements represent the maximum length between the central points of the proximal and distal articulations between bones (chord lengths). For the ungual phalanges, we took the straight length from the central point of the articulation region to the bone tip (fig. 3).

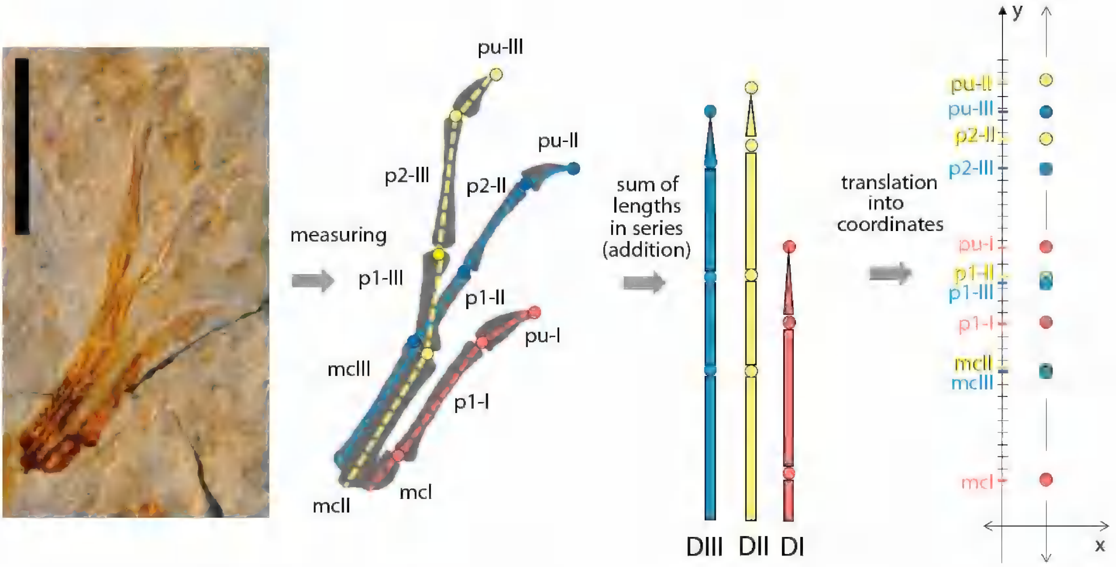

FIG. 3. Schematic representation of the one-dimensional Procrustes analysis (OPA) method carried out in the data processing, from lengthwise. Exampling manus belongs to the juvenile early-diverging avialan *Zhongornis* (DNHM D2456; Gao et al., 2008; Rashid et al., 2018).

Transformation to Procrustes Coordinate Data

OPA, the protocol to transform the linear measurements into Cartesian coordinates (fig. 3), starts from a baseline on a zeroed *x*-axis. Then, the length of metacarpal I yields the first *y*-coordinate value (fig. 3, red elements). Subsequently, the length of the first phalanx of digit I is added to the latter *y*-value, always with *x* set to 0. This yields a second *y*-coordinate that, in turn, corresponds to the sum of the lengths of metacarpal I plus the length of its first phalanx. The coordinate of the second phalanx is similarly attained by adding its chord length to the latter sum of lengths, yielding a third *y*-coordinate, thus giving the coordinates of the entire digit I. This procedure is repeated for digit II and III (fig. 3, yellow and blue elements respectively). Importantly, the phalangeal formula might be different given that there are evolutionary phalange losses (e.g., most modern forms lack unguals). This mismatch is solved by adding a repeated last coordinate (summing a length of zero could not be carried out because the software does not run with two equal coordinates, hence we added a negligible 0.01). This is equivalent to having two identical coordinates on top of each other at the tip of the affected digit. This adding of repeated landmarks allows performing the Procrustes superimposition with missing landmarks, without adding any extra information or variance to the data (Klingenberg, 2008).

The entire protocol (OPA) is unidimensional because there is only one coordinate axis with data. To separate size from shape and compare configurations we used a generalized Procrustes analysis (GPA; Gower, 1975), which uses the least-squares criterion to minimize, in a rigid way, the distance between corresponding landmarks among different configurations. This alignment uses the mean configuration as a reference for correcting the position and orientation of the configurations through superimposition and, in addition, rescales them to units of centroid size (CS). CS is an independent variable representing the scale or size of the configuration (it represents the real distances between the coordinates) and is calculated as the square root of the sum of the squared distances of all the coordinates (Bookstein, 1991). It is important to emphasize that working with coordinates that present values only on one axis implies that neither the translation nor the rotation steps are relevant for this study. The standardization of size of the coordinate data is particularly relevant, since it guarantees that the isometry (differences only in scale) are eliminated from the data (Gower, 1975), and the residuals of this analysis, the Procrustes coordinates, represent the different proportions of manus elements per specimen without size information. This "shape data" is used in downstream analyses, and we refer to it hereafter as manus shape.

Phylogenetic Hypothesis and Multivariate Statistics

We built an informal supertree (fig. 2) using Mesquite v. 3.40 (Maddison and Maddison, 2011) and based on the comprehensive phylogeny of Prum et al. (2015) for the relationships of birds within the crown group, Turner et al. (2012) for the relationships between early-diverging maniraptorans and Paraves, and O'Connor and Zhou (2012) as well as Wang and Lloyd (2016) for Mesozoic birds. The topology of the terminal branches not included in the previous studies was resolved with information on the specific groups. We calibrated the resulting tree using the R package Paleotree (Bapst, 2012), scaling the branches of taxa based on their stratigraphic range obtained from the Paleobiology Database (www.paleodb.org) and from the literature. To avoid zero-length branches we set a minimum branch length of 1 million years. We generated 100 trees using this method, which randomly assesses the first appearance dates (FADs) and last appearance dates (LADs) of each species inside the stratigraphic interval where they are assigned, generating 100 different tree distributions and solving randomly the polytomies that could not be resolved with the literature. See supplemental figure for a larger version of figure 2 that includes taxon names and a more detailed geological timescale (https://doi.org/10.5531/sd.sp.44). All of the following analyses were carried out in consideration of the phylogenetic relationships between all specimens in our sample.

We applied two of the main types of analysis from the custom statistical toolkit in GM (Bookstein, 1991), namely, principal components analysis (PCA), which allows us to reduce the dimensionality of the data and summarizes the differences (shape variance), and multivariate regression, a multivariate tool to test the relationship between shape variation (dependent variable) with the variation of any type of independent variable (Monteiro, 1999). This method is the most reliable for studying allometry in the context of shape analysis using size as the predictor or independent variable (e.g., Marugán-Lobón et al., 2013b; Mitteroecker et al., 2013). PCA generates an ordination that is generally interpreted as an empirical morphospace (Marugán-Lobón and Buscalioni, 2004) on which phylogeny can be mapped, including the reconstruction of the ancestral shapes represented by the nodes. This graph, called phylomorphospace, represents a reconstruction of the phylogenetic history of changes in shape, reflecting how different clades have evolved. We mapped a randomly selected tree from the population of the 100 trees we generated by means of weighted (i.e., including branch length information) squared-change parsimony (Maddison, 1991) into the PC1-3 morphospace using MorphoJ v. 1.06d (Klingenberg, 2011).

We also quantified mean manus shape disparity (Procrustes variance) and tested for statistically significant differences between groups using the function morphol.disparity in the R package geomorph v.3.0.7 (Adams and Otárola-Castillo, 2013). Specifically, we tested for differences between: (1) the stem and crown lineages, (2) all the main maniraptoran grades, and (3a) palaeognathans, all neognathans, (3b) only volant neognathans and non-volant neognathans to each other and to all the other main maniraptoran grades. The latter comparisons was triggered by the visual observation that flightless palaeognathans and neognathans seem to exhibit the most disparate manus morphologies among crown group birds. Because Procrustes variance provides information only about mean shape disparity within each group, we also calculated the convex hull volumes encapsulated by the manus morphologies of each of the groups in the tangent shape space defined by the first three principal components of manus shape. Convex hulls were computed as the smallest three-dimensional volume encompassing all the specimens within each group. Convex hull volumes were calculated using the convhull.volume function in the R package disparity (Guillerme, 2018).

Multivariate linear regression was performed between the manus shape variables (Procrustes data, as a dependent variable) and the log-transformed CS (log-CS) of the specimens (independent variable or predictor). In principle, the data cannot be considered independent because lineages are phylogenetically related (i.e., phylogenetic inertia). We therefore used phylogenetically informed regressions (phylogenetic generalized least squares, PGLS) to test the relationship between manus shape and manus size in all maniraptorans using the procD.pgls function in the R package geomorph v.3.0.7. All PGLS linear models included group category as an additional independent variable both to test for shape and size differences between clades and to test for group-specific allometries. We specifically tested for allometric differences between: (1) the stem and crown lineages, and (2) all the "grades" outlined in figure 2 (i.e., crown birds, early-diverging ornithuromorphs, enantiornithines, nonornithothoracine avialans, nonavialan maniraptorans). To test for group-specific allometries we conducted pairwise comparisons of slope vector angles and slope vector lengths between all the groups. PGLS regressions were repeated using all the corresponding 100 trees, and median and range values for all the main statistics (R^2, F, Z, P) were recorded, to address how differences in branch lengths affect our results. Furthermore, because log-CS and clade categories covary (table 1) we used type II (conditional) sums of squares to assess the statistical significance of all PGLS linear models (Adams and Collyer, 2018). Because our variables are unevenly dispersed across our phylogeny (e.g., different lineages exhibit different disparities of shape and size), which can severely reduce statistical power of linear models (Adams and Collyer, 2018), we used randomizing residuals in a permutation procedure (10,000 iterations implemented in geomorph v.3.0.6, Adams et al., 2018) to assess statistical significance for all PGLS regressions, as this has been shown to be more robust to group-clade aggregations (Adams and Collyer, 2018).

RESULTS

The first three main components of the PCA capture 92.62% of the total shape variance (i.e., proportional differences between the elements of the studied manus), which is graphically summarized in a 3D phylomorphospace (fig. 4). PC1 is clearly the dominant dimension, capturing as much as 63.38% of the total variance, while PC2 and PC3 capture 23.95% and 5.29%, respectively. PC1 describes the most notable morphological differences in the nonavialan-to-avialan transition, accounting for the differences in proportional lengths of the proximal elements of the manus with respect to the distal ones, namely, encompassing the proportional reduction and loss of phalanges in the lineage, toward crown birds. Along the PC1 axis, maniraptorans with proportionally shorter phalanges are grouped in the negative region, while those with autopods with proportionally more elongated phalanges are in the positive region (fig. 4). This distribution thus clearly separates some early-diverging avialans, nonavialan paravians and early-diverging maniraptorans, distributed exclusively in the positive region, from later-diverging nonavian avialans (Enantiornithes, early-diverging ornithuromorphs), ultimately polarizing the situation of Aves (Neornithes) in the negative region of PC1 due to their usual lack of distal phalanges. PC2 accounts for large changes in digit III, with only minor changes in digits I and II. Specifically, this axis describes the variation of the length of

TABLE 1

Differences in manus shape disparity between maniraptoran theropod groups

Pairwise comparisons of shape disparity (Procrustes variance) between **A.** crown and stem maniraptoran lineages; **B.** major maniraptoran grades. The comparison between major maniraptoran grades was also performed by dividing **C.** Aves between neognathans and palaeognathans and with **D.** neognathan birds further split in volant and non-volant taxa. Statistically significant values (*P* <0.05) are highlighted in bold. Numbered table columns correspond to the numbered clades in the table rows.

A	Crown
Stem	**<0.0001**

B	1	2	3	4
1. Nonornithothoracine avialans				
2. Enantiornithes	**0.016**			
3. Nonavialan maniraptorans	0.096	0.198		
4. Aves (Neornithes)	**0.009**	0.681	**0.047**	
5. Nonavian ornithuromorphs	**0.012**	0.721	0.137	0.975

C	1	2	3	4	5
1. Nonornithothoracine avialans					
2. Enantiornithes	**0.016**				
3. Nonavialan maniraptorans	0.096	0.197			
4. Neognathae	**0.006**	0.329	**0.024**		
5. Nonavian ornithuromorphs	**0.013**	0.718	0.135	0.69	
6. Palaeognathae	**0.035**	**6E-04**	**0.004**	**2E-04**	**3E-04**

D	1	2	3	4	5	6
1. Nonornithothoracine avialans						
2. Enantiornithes	**0.015**					
3. Nonavialan maniraptorans	0.094	0.192				
4. Volant neognathans	**0.004**	0.226	**0.017**			
5. Nonvolant neognathans	0.438	0.104	0.358	**0.04**		
6. Nonavian ornithuromorphs	**0.013**	0.713	0.134	0.568	0.089	
7. Palaeognathae	**0.036**	**4E-04**	**0.004**	**2E-04**	**0.034**	**3E-04**

digit III with respect to the other two digits; such variation is more pronounced in the more distal elements of digit III and separates taxa with digits I and II longer with respect to III in the positive region of this axis, from those with a digit III proportionally similar (or even longer) to the other two digits (I and II). Finally, PC3 describes changes in the proportional length of metacarpal I as compared with the length of the phalanx 1 of digit III, that is, when one increases in length the other decreases and vice versa. Manus with an elongated metacarpal I and a shorter phalanx 1 of digit III are located in the positive region, while those with a reduced metacarpal I and an

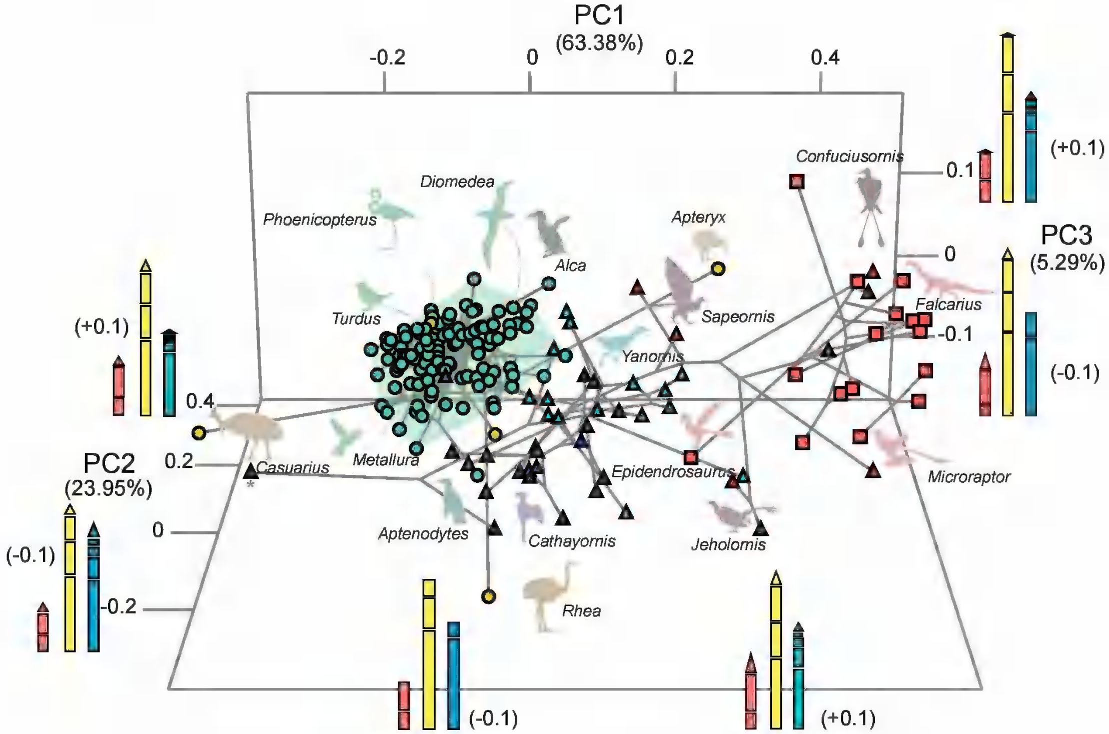

FIG. 4. Phylomorphospace of hand evolution in Maniraptora. Phylogeny mapped over the scores of the first three principal components of shape. Color coding is consistent with figure 2. Asterisk indicates juvenile enantiornithine NIGP 130723 (Chiappe et al. 2007).

elongated phalanx 1 of digit III are grouped in the negative region. Those that have similar relative lengths (such as the bulk of taxa within the crown group of birds) are distributed in the central region (fig. 4).

In the PC1-3 phylomorphospace, crown birds together with enantiornithes and early-diverging ornithuromorphs occupy a more central area of morphospace, clearly separated from the rest of the phylogenetically earlier-diverging taxa (non-ornithothoracine birds, scansoriopterygids, deinonychosaurs, and early-diverging maniraptorans), which occupy more peripheral positions (fig. 4). The latter are generally characterized by presenting more disparate manus morphologies, with distal elements proportionally more elongated with respect to the proximal (i.e., longer fingers). The greatest disparity lies mainly in the different relative lengths of digit III with respect to the other two digits. Likewise, there are certain taxa within these groups with very divergent manus from their parent clades, like the early-diverging birds *Jinguofortis perplexus* and *Sapeornis chaoyangensis*, whose manus display a reduced digit III more similar to that of ornithuromorphs, the paravian *Balaur bondoc* with a highly reduced digit III, or the non-ornithothoracine *Epidendrosaurus* (Scansoriopterygidae) and *Jeholornis curvipes* in which digit III is relatively long.

The rest of the dinosaurs studied cluster around a group consisting of Aves and its closest Mesozoic relatives (early-diverging ornithuromorphs and Enantiornithes) situated in the left region of morphospace. That these taxa are clustered separately from the rest of maniraptorans underscores their greater degree of morphological similarity (fig. 4). Enantiornithes and early-diverging ornithuromorphs have, however, more elongated digits than crown birds and differ between them in the relative length of digit III,

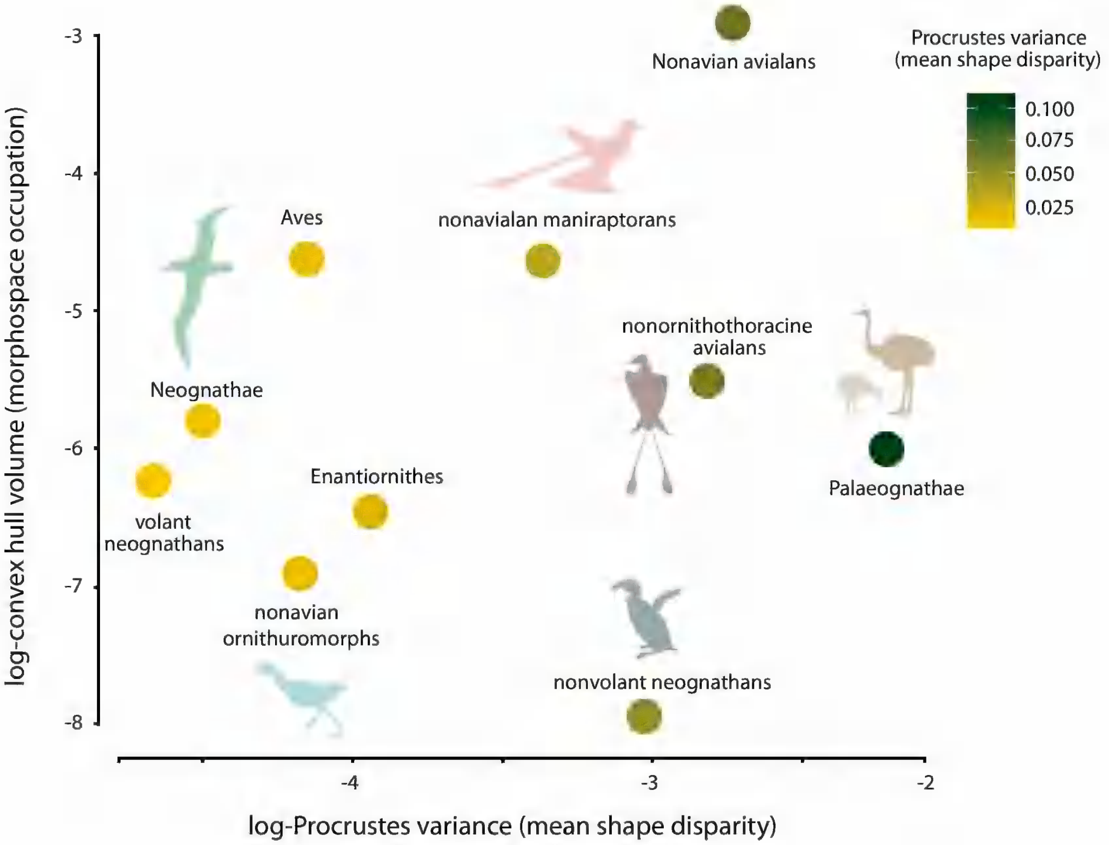

FIG. 5. Hand shape disparity (i.e., Procrustes variance) and morphospace occupation (i.e., convex hull volume) of the grades of Maniraptora.

which is generally longer in Enantiornithes (fig. 4). It is worth mentioning that the juvenile enantiornithine NIGP 130723 displays an incompletely ossified manus, thus leading to unusual proportions in which the distal elements are extremely reduced with respect to the proximal ones (even more than in crown birds); these proportions lead to significant differences between this taxon and the rest of the sample.

Interestingly, crown birds display very low manus disparity (fig. 5), all clustering in a very localized and reduced region of the morphospace, corresponding with manus morphologies with phalanges significantly shorter than those of their Mesozoic relatives. Palaeognathan taxa are an exception among the crown group in which the manus contains the greatest disparity (fig. 5), diverging substantially from one another and from the rest of the sample. These birds are nearly fingerless (e.g., *Casuarius bennetti*, situated in the lower left region of morphospace), with extremely small manus lacking digit III (e.g., *Apteryx australis*, situated in the upper right region of morphospace), or displaying large manus with slightly elongated, clawed digits, similar to those of Enantiornithes (e.g., *Struthio camelus* or *Rhea americana* in a more central region). Among the neognathans, Aequorlitornithes (seabirds, shorebirds, herons, cormorants and relatives) have some flightless forms diverging from their relatives, as in the case of the two penguins (*Spheniscus humboldti* and *Aptenodytes forsteri*), the Galapagos' cormorant (*Phalacrocorax harrisi*), and the great auk (*Alca impennis*) included in the sample.

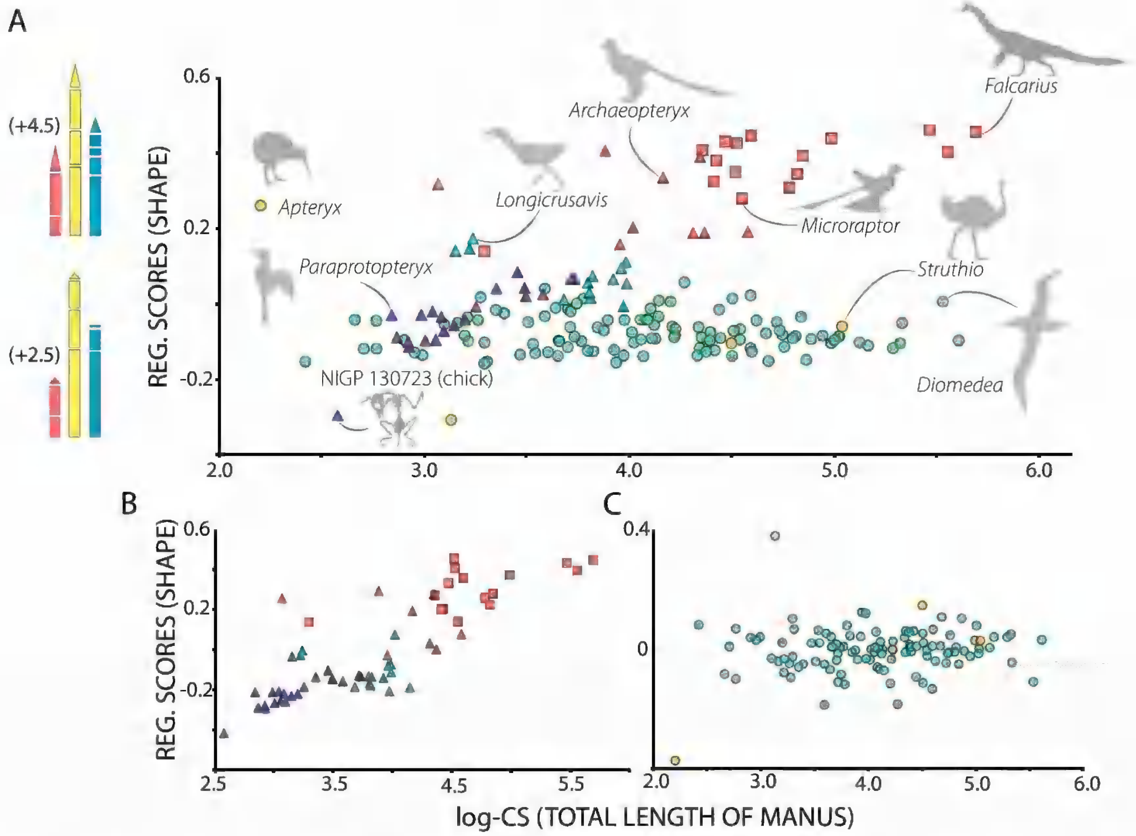

FIG. 6. Correlation between size and shape based on a multivariate regression. A significant correlation results in the existence of an allometric factor in the change of hand shape, significant in nonavialan maniraptorans. Among neognathans (in green tones) there is no allometry (i.e., shape changes occur regardless of size variation. Notice as well that variation is strikingly low). Below the main graph (**A**) dispersions **B** and **C** show the allometric and non-allometric trends, respectively.

Although differences in disparity are visible over morphospace, the pairwise statistical comparisons between the Procrustes disparities further corroborates significant differences in mean shape disparity between the crown and stem lineages, while revealing a drastic decrease in manus-shape morphological diversity in maniraptorans after the K-Pg (fig. 5, table 1). Non-ornithothoracine avialans (i.e., long tailed birds and early-diverging pygostylians) are significantly more disparate than all the other lineages of birds, excluding flightless crown birds, and exhibit higher manus mean disparity (although lower range of morphologies) than nonavialan maniraptorans. Furthermore, palaeognathans are more disparate than all the other lineages of avialan and nonavialan maniraptorans. Nonavialan maniraptorans, although more disparate than all the ornithothoracine lineages including crown birds, exhibit significant differences only in mean shape disparity with crown birds (but not with flightless taxa alone). Early-diverging ornithothoracine lineages, namely, enantiornithines and early-diverging ornithuromorphs, exhibit intermediate values of mean shape disparity, but these differences are not statistically significant. Furthermore, crown birds explore a larger range of morphologies than enantiornithines and early-diverging ornithuromorphs (lower values of convex hull volumes), although this observation is influenced by large

TABLE 2

Allometric differences between stem and crown lineages and between the four main grades of maniraptorans
Summary of statistics from the PGLS regression of hand shape as a function of log-CS and group **A.** stem/crown and **B.** maniraptoran grades. Median and range values (maximum and minimum) are summarized. Statistically significant values ($P < 0.05$) are highlighted in bold. R^2 is the observed proportion of shape (dependent variable) explained by differences in size and group (independent variables) in each of the PGLS regressions; F-values are a measure of the variance explained by each of the variables as compared with the error term (unexplained variance); Z are the standard deviates from the F-values obtained in the 1,000 sampling permutations and give a measure of the intensity of the effects of size, group, and interactions between both, on shape.

A. Between stem and crown

	R^2	**F**	**Z**	***P***
Log-CS	0.003 (0.002, 0.006)	0.463 (0.297, 1.020)	-0.406 (-0.852, 0.461)	0.653 (0.334, 0.799)
Group (stem/crown)	0.001 (0.001, 0.002)	0.218 (0.160, 0.322)	-1.129 (-1.455, -0.733)	0.86745 (0.764, 0.927)
Log-CS:group	0.04 (0.02, 0.06)	6.561 (3.939, 10.760)	2.484 (1.932, 2.986)	**0.004 (<0.001, 0.023)**

B. Between the main four grades of maniraptoran

	R^2	**F**	**Z**	***P***
Log-CS	0.004 (0.002, 0.006)	0.763 (0.362, 1.256)	0.273 (-0.554, 0.824)	0.401 (0.212, 0.71)
Group (grades)	0.119 (0.101, 0.150)	6.381 (5.172, 8.542)	3.673 (3.211, 4.078)	**>0.001 (>0.001, 0.001)**
Log-CS:group	0.108 (0.084, 0.150)	5.783 (4.305, 8.416)	3.287 (2.750, 3.747)	**>0.001 (>0.001, 0.008)**

differences in sample size. Similarly, flightless neognathans (penguins, flightless cormorant, and giant auk) exhibit high mean shape disparity.

A PGLS regression between manus shape (Procrustes coordinates) and size (log-CS) for the total sample is statistically significant but only captures 2.67% of variance (fig. 6, table 2), which represents a very low percentage of shape change explained by size (evolutionary allometry). However, from a visual inspection of the plot (fig. 6) it is evident that the allometric scaling between nonavians and avians is completely different, and such difference is confirmed by the statically significant differences between allometric vectors (table 2). In fact, when analyzed separately by groups, PGLS regression in early-diverging bird taxa explains up to 42.3% of the total variance (p <0.0001), whereas in Aves, the explained variance drops down to a negligible 0.5041% (p <0.0001). These striking results imply that maniraptoran manus shape differences are essentially non-allometric only in crown birds. The general allometric trend within the stem lineage equates small sized manus with relatively shorter digits (short phalanges with respect to metacarpals), very small claws, and a digit III that has lost the most distal elements (i.e., third phalanx and claw), in contrast with larger manus with relatively elongated digits (longer phalanges with respect to metacarpals), large ungual phalanges and a complete digit III (fig. 6). Few cases fall outside the general allometric trend with manus shapes that do not correspond to those expected by their size condition. In general, these outliers coincide with those observed in the PCA, such as the paleognathan *Apteryx australis* and *Casuarius bennetti*, and the early-diverging bird *Zhongornis*.

The range of values of the statistics from the PGLS regressions did not vary much due to differences in estimated branch lengths in our 100 trees (table 2). We thus picked only one tree for pairwise allometric comparisons between the five maniraptoran grades. The results largely

TABLE 3

Pairwise differences in pattern and strength of allometry between all the grades of maniraptorans studied

Significant p-values (<0.05) indicate differences in the **A.** strength (slope lengths) or pattern (slope angles) of allometry.

A. Strength of allometry

	Avialae	Enantiornithes	Maniraptora	Aves (Neornithes)	Ornithuromorpha
Avialae	1	0.056	0.4376	0.4209	0.9351
Enantiornithes	0.056	1	0.0556	**0.0026**	**0.021**
Maniraptora	0.4376	0.0556	1	**0.0083**	0.2431
Aves (Neornithes)	0.4209	**0.0026**	**0.0083**	1	0.2649
Ornithuromorpha	0.9351	**0.021**	0.2431	0.2649	1

P values of slope lengths = differences in the amount of shape change per unit of size change

B. Pattern of allometry

	Avialae	Enantiornithes	Maniraptora	Aves (Neornithes)	Ornithuromorpha
Avialae	1	**0.0327**	0.056	0.9936	0.9781
Enantiornithes	**0.0327**	1	0.9739	**0.0045**	**0.0178**
Maniraptora	0.056	0.9739	1	**0.008**	**0.013**
Aves (Neornithes)	0.9936	**0.0045**	**0.008**	1	0.9679
Ornithuromorpha	0.9781	**0.0178**	**0.013**	0.9679	1

P values of slope angles = differences in the pattern of the relationship between shape and size

confirm our observations by revealing only significant differences in the pattern and the strength of manus allometry between ornithuromorphs (both crown and stem) and the rest of the nonornithuromorph lineages, but nonsignificant differences between the crown (Aves) and early-diverging ornithuromophs, therefore substantiating that both groups share a common manus allometric pattern (table 3).

DISCUSSION

Morphological evolution needs to be studied quantitatively and at high taxonomical levels if we aim to map the variational limits of disparity and to determine which main factors underlie this disparity at macroevolutionary scales (Raff, 1996). However, this requires using approaches that allow preserving both the physical integrity of the structure and the information that pertains to the organization of the whole. Geometric morphometrics is one of those analytical methodologies, yet given the osteological complexity of certain anatomical structures, such as the maniraptoran manus, it is impossible to apply the method in its standard manner. In order to bridge this methodological gap, we have devised a simple protocol that translates traditional longitudinal measurements of hand bones into linear Cartesian coordinates, making them directly treatable under the scope of shape analysis based on Procrustes methods. Using OPA we have visually expressed the transition between early-diverging forms (e.g., therizinosaurians, oviraptorosaurians, and early-diverging paravians, including earliest-diverging birds), toward crown group birds, and how these compare with their closest relatives (early-diverging ornithuromorphs and enantiornithines). Given that this new way of treating data allows mapping evolutionary bone loss, we have not only shown that bone reduction and loss of phalanges are key morphological transformations, but also that the alular (I) and minor (III) digits are the most modified elements involved in the evolutionary transition of the manus from early-diverging maniraptorans to modern birds. Uniquely, using this method we have also unveiled two previously unreported aspects of the evolution of the manus in these dinosaurs. First, we have shown that there is a marked decrease of manus disparity stemming from changes in skeletal proportions along the maniraptoran lineage, which, unexpectedly, becomes minimal in neognathan birds. Secondly, we have revealed that in most early-diverging maniraptorans, morphological variation largely scales according to an equivalent allometric pattern. In fact, in crown birds and their early-diverging ornithuromorph relatives, the low structural variation of the manus is almost completely nonallometric, entailing an important evolutionary shift in the construction of manus variation.

The distribution of the main clades over morphospace shows a minimal overlap and effectively documents the stepwise acquisition of the modern avian manus across maniraptoran evolution. This ordination altogether epitomizes the view about the evolution of the avian manus along the dinosaur-bird transition, from a more typically "dinosaurian" grasping organization of early-diverging nonavialan maniraptorans (therizinosaurians and oviraptorosaurians), nonavialan paravians (deinonychosaurs and scansoriopterygids), and the earliest-diverging birds, to that of a more "avian" one visible in enantiornithines, early-diverging ornithuromorphs and crown birds. Effectively, the first dimension of variation accounts for the largest morphological change, namely, the proportional distal elongation to distal reduction of the digits' elements, showing even the loss of phalanges and the different phalangeal formulas in the lineage. This trend is one of the most relevant in the differential distribution of taxa across the phylomorphospace. The second and third dimensions show the two digits triggering this pattern (I and III). Interestingly, our results suggest that much of the evolution of the manus across the dinosaur-bird transition has occurred in an integrated way within a macroevolutionary trend of distal element reduction and loss, which is congruent with the fact that during the early stages of digit formation most proportional changes in phalanges are regulated as a system rather than individually (Kavanagh et al., 2013).

Previous studies proposed that the reduction and loss of the most distal elements of a winged manus may have been functionally adaptive, given that the mass and moment of inertia of the hand is reduced, making it more effective during active flight (Berg and Rayner, 1995; Bakker et al., 2013). Moreover, it has been proposed that the wide variety of manus morphologies of different early-diverging paravian taxa, such as the divergent scansoriopterygids, the first avialans (e.g., *Archaeopteryx*), and *Anchiornis* or *Microraptor*, could have triggered substantial flight experimentation prior to the acquisition of the modern avian manus (Xu et al., 2015; Brusatte, 2017; Wang et al., 2017, 2019). However, important morphological differences exist between crown and stem birds for which similar flight types have been inferred (e.g., *Sapeornis chaoyangensis* as a soaring bird aerodynamically similar to a screamer: Serrano and Chiappe (2017) and Serrano et al. (chapter 13); the enantiornithines *Concornis lacustris* and *Eoalulavis hoyasi*, functionally similar to small passerines or woodpeckers: Serrano et al., 2018; see Pittman et al., on early flight study, chapter 10). Our results show that the morphology of the manus in crown birds, compared with the wide range of morphologies in nonavialan forms, exhibits very low disparity in spite of its uniformity in species displaying different flight styles. In light of these results, it is likely that drivers other than flight were also at play during the morphological transformation of the manus from nonavialan maniraptorans to modern birds, despite highly diverse morphologies existing in the early stages of paravian evolution possibly related to experimentation of aerodynamic capabilities (as well as with a complex trade-off between aspects such as grasping, folding, and tegument support). Rather, it seems as if many different skeletal morphologies might have been functionally equivalent, entailing that other morphological traits, such as aspects of the manus shape not taken into account in this study, the proportions of the forelimb elements (Serrano et al., 2017), and/or the evolution of integumentary structures such as feathers or patagia (Navalón et al., 2015; Wang et al., 2017, 2019), are probably more relevant to understand the evolution of avian flight.

It is surprising that in spite of being the most speciose group of terrestrial vertebrates (more than 10,000 species) and displaying an enormous size range (from 5 cm and 1.8 g of the hummingbird bee, *Mellisuga helenae*, up to 3 meters and 180 kg in the ostrich, *Struthio camelus*) as well as a huge ecological and functional diversity, modern birds show such a strikingly low disparity in the proportions of their hand skeleton. From a paradigmatic standpoint, this low disparity could be interpreted as a result of the filtering effect of the K-Pg mass extinction that constrained the morphological variation available for the subsequent radiation during the Cenozoic. From a paleobiological point of view, this scenario is also congruent with the type of "bottom-up" trends whereby clades accumulate high morphological disparity during their early radiation and slow down as they diversify later (Foote, 1997). Interestingly, bottom-up trends are also explained as an outcome of early experimentation of development programs through geological time (Raff, 2000). However, at lower macroevolutionary scales, a remarkable exception in such trends is the high disparity of hand skeletal proportions and phalangeal formulas of paleognathan birds. Ratites are paraphyletic due to the position of the tinamous (e.g., Prum et al., 2015), the only modern palaeognathan with flying capabilities. The manus of these avians sometimes bears claws (*Struthio camelus* and *Rhea americana*), lacks phalanges in digit III (*Apteryx australis*), entirely lacks fingers (*Casuarius bennetti*), and can even have a morphology similar to that of flying neognathan (as the case of the tinamou, *Tinamus solitarius*). Members of these lineages have different ontogenetic trajectories (Faux and Field, 2017), possibly translating into their different manual morphologies and the absence of flight-related selective pressures eliminated a vital constraint, therefore favoring greater variability in forelimb elements. For instance, the emu (*Dromaius novaehollandie*) has greater variability in wing bones than any flying bird (Maxwell and Larsson, 2007). Among neognathans, specialized underwater divers such as the Galapagos cormorant (*Phalacrocorax harrisi*), the great auk (*Alca impennis*), and the penguins (*Spheniscus humboldti* and *Aptenodytes forsteri*) are also examples of higher disparity in different functional selective regimes.

Our results also showed that an important and common allometric trend explains a large portion of manus disparity in Mesozoic taxa, including Enantiornithes and the earlier-diverging maniraptoran lineages spectrum. This allometric trend is unambiguously truncated in early-diverging ornithuromorphs and crown birds, in which manus size and shape variation are completely decoupled (i.e., evolutionary allometry disappears). A similar pattern of allometric decoupling had been reported for the forelimb in the dinosaur-bird transition (Dececchi and Larsson, 2013), probably implying that the morphology of the manus first evolved as strongly integrated with the changes in body size that took place in the avialan stem lineage (Turner et al., 2007; Puttick et al., 2014; Lee et al., 2014). More strikingly, in light of the observed allometric pattern (fig. 6), modern avians have almost completely decoupled their manus proportions and size variation, a condition that appears to have started in early-diverging ornithuromorphs. Interestingly, the adult manus of the neognathans retains a skeletal morphology that is more similar to that of enantiornithines at early ontogenetic stages (see the manus of juvenile enantiornithine NIGP 130723 as example; Chiappe et al., 2007), hinting that their low disparity and variation, apart from the filtering effect of the K-Pg, may have also resulted from an heterochronic truncation of the primitive allometric pattern, similar to what happened with their skull (Bhullar et al., 2012). Thus, heterochrony may be a systemic process underlying many main features of the modern avian bauplan, including the manus.

CONCLUSIONS

We have proposed a new method (and named it one-dimensional Procrustes analysis, OPA), that allows transforming traditional morphometrics into unidimensional configurations of Cartesian coordinates that can be submitted to a Procrustes transformation and thereafter analyzed using the multivariate kit of geometric morphometrics. We applied the method to a large sample of maniraptoran dinosaurs, fossil and modern, and the obtained results are highly consistent with qualitative descriptions of the maniraptoran manus, thus further substantiating the applicability of the proposed morphometric protocol. Moreover, using this new protocol we have discovered that the elements evolving in the maniraptoran manus are mostly digits I and III, digit II (the central digit) being the least modified, and that much of the early stages of this evolutionary pattern are highly allometric. In contrast, we show that the transformation of the ancestral manus into that of crown group birds is not allometric (it is size independent) and that it encompasses a significant decrease of disparity, which is likely linked to heterochrony. Our morphometric proxy could be extrapolated to other articulated anatomical structures such as, but not restricted to, the manus of other dinosaurs, and other archosaurs and tetrapods in general, as well as for studies aiming at understanding other aspects of morphological evolution, such as the integration and modularity in articulated structures, which require reliable morphometric data for their statistics.

ACKNOWLEDGMENTS

The authors are grateful to the Editors for inviting us to participate in this landmark volume. Thanks to the collection curators, Kimball L. Garret (LACM) and Joanne Cooper and Judith White (NHMUK, Tring), and thanks to C. Klingenberg for inspiration on the transformation of linear measurements to Procrustes data. S.M.N. is supported by a FPI-UAM 2019 predoctoral grant from the Autonomous University of Madrid. G.N. was supported by a PG Scholarship/Studentship from the Alumni Foundation, University of Bristol, U.K.. I.M. was funded by a predoctoral grant from the Complutense University of Madrid (CT27/16-CT28/16). I.M. acknowledges project PGC2018-094955-A-I00 granted by the Spanish Ministerio de Ciencia, Innovación y Universidades. J.M.L. was funded by project CGL2013-42643P from MINECO (Spain).

REFERENCES

Adams, D.C. 1999. Methods for shape analysis of landmark data from articulated structures. Evolutionary Ecology Research 1: 959–970.

Adams, D.C., and M.L. Collyer. 2018. Phylogenetic ANOVA: Group-clade aggregation, biological challenges, and a refined permutation procedure. Evolution 72: 1204–1215.

Adams, D.C., and E. Otárola-Castillo. 2013. Geomorph: an R package for the collection and analysis of geometric morphometric shape data. Methods in Ecology and Evolution: 4: 393–399.

Adams, D.C., F.J. Rohlf, and D.E. Slice. 2013. A field comes of age: geometric morphometrics in the 21st century. Hystrix 24: 7–14.

Bakker, M.A.G. de, et al. 2013. Digit loss in archosaur evolution and the interplay between selection and constraints. Nature 500: 445–448.

Bapst, D.A. 2012. paleotree: an R package for paleontological and phylogenetic analyses of evolution. Methods in Ecology and Evolution 3: 803–807.

Barta, D.E., S.J. Nesbitt, and M.A. Norell. 2018. The evolution of the manus of early theropod dinosaurs is characterized by high inter- and intraspecific variation. Journal of Anatomy 232: 80–104.

Berg, C., and J.M.V. Rayner. 1995. The moment of inertia of bird wings and the inertial power requirement for flapping flight. Journal of Experimental Biology 198: 1655–1664.

Bever, G.S., J.A. Gauthier, and G.P. Wagner. 2011. Finding the frame shift: digit loss, developmental variability, and the origin of the avian hand. Evolution and Development 13: 269–279.

Bhullar, B.A.S., et al. 2012. Birds have paedomorphic dinosaur skulls. Nature 487: 223–226.

Bookstein, F.L. 1991. Morphometric tools for landmark data: geometry and biology. Cambridge: Cambridge University Press.

Brusatte, S.L. 2017. A Mesozoic aviary. Science 335: 792–794.

Carrano, M.T. 2006. Body size evolution in the Dinosauria. *In* M.T. Carrano, T.J. Gaudin, R.W. Blob, and J.R. Wible (editors), Amniote paleobiology: perspectives on the evolution of mammals, birds and reptiles: 225–257. Chicago: University of Chicago Press.

Chiappe, L.M., S.A. Ji, and Q. Ji. 2007. Juvenile birds from the Early Cretacous of China: implications for enantiornithine ontogeny. American Museum Novitates 3594: 1–46.

Dececchi, T.A., and H.C.E. Larsson. 2013. Body and limb size dissociation at the origin of birds: uncoupling allometric constraints across a macroevolutionary transition. Evolution 67: 2741–2752.

Dryden, I.L., and K.V. Mardia. 1998. Statistical shape analysis. Chichester: John Wiley.

Faux, C., and D.J. Field. 2017. Distinct developmental pathways underlie independent losses off light in ratites. Biology Letters 13: 20170234.

Foote, M. 1997. The evolution of morphological diversity. Annual Review of Ecology and Systematics 28: 129–152.

Gao, C., et al. 2008. A new basal lineage or early cretaceous birds from China and its implication on the evolution of the avian tail. Palaeontology 51: 775–791.

Gauthier, J.A. 1986. Saurischian monophyly and the origin of birds. *In* K. Padian (editor), The origin of birds and evolution of flight: 1–55. San Francisco: California Academy of Sciences Memoir.

Gower, J.C. 1975. Generalized Procrustes analysis. Psychometrika 40: 33–51.

Guillerme, T. 2018. disparity: a modular R package for measuring disparity. Methods in Ecology and Evolution 9: 1755–1763.

Kavanagh, K.D., et al. 2013. Developmental bias in the evolution of phalanges. Proceedings of the National Academy of Sciences of the United States of America 110: 18190–18195.

Klingenberg, C.P. 2008. Novelty and 'homology-free' morphometrics: what's in a name? Evolutionary Biology 35: 186–190.

Klingenberg, C.P. 2011. MorphoJ: an integrated software package for geometric morphometrics. Molecular Ecology Resources 11: 353–357.

Klingenberg, C.P. 2016. Size, shape and form: concepts of allometry in geometric morphometrics. Development Genes and Evolution 226: 113–137.

Lee, M.S.Y., A. Cau, D. Naish, and G.J. Dyke. 2014. Sustained miniaturization and anatomical innovation in the dinosaurian ancestors of birds. Science 345: 562–566.

Maddison, W.P. 1991. Squared-change parsimony reconstructions of ancestral states for continuous-valued characters on a phylogenetic tree. Systematic Zoology 40: 304–314.

Maddison, W.P., and D.R. Maddison. 2011. Mesquite: a modular system for evolutionary analysis, v. 2.73.

Marden, J.H. 1994. From damselflies to pterosaurs: how burst and sustainable flight performance scale with size. American Journal of Physiology 266: 1077–1084.

Marugán-Lobón, J., and A.D. Buscalioni. 2003. Disparity and geometry of the skull on Archosauria (Reptilia: Diapsida). Biological Journal of the Linnean Society 80: 67–88.

Marugán-Lobón, J., and Á.D. Buscalioni. 2004. Geometric morphometrics in macroevolution: morphological diversity of the skull in modern avian forms in contrast to some theropod dinosaurs. *In* A.M.T. Elewa (editors) Morphometrics: 157–173. Berlin: Springer.

Marugán-Lobón, J., D. Blanco Miranda, B. Chamero, and H. Martín-Abad. 2013a. On the importance of examining the relationship between shape data and biologically meaningful variables. An example studying allometry with geometric morphometrics. Spanish Journal of Palaeontology 28: 139–148.

Marugán-Lobón, J., L.M. Chiappe, and A.A. Farke. 2013b. The variability of inner ear orientation in saurischian dinosaurs: testing the use of semicircular canals as a reference system for comparative anatomy. PeerJ 1: e124.

Maxwell, E.E., and H.C.E. Larsson. 2007. Osteology and miology of the wing of the Emu (*Dromaius novaehollandiae*), and its bearing on the evolution of vestigial structures. Journal of Morphology 268: 423–441.

Mayr, G. 2017. Avian evolution: the fossil record of birds and its paleobiological significance. Frankfurt: Wiley Blackwell.

McGhee, G.R. 1999. Theoretical morphology: the concept and its applications. New York: Columbia University Press.

Middleton, K.M., and S.M. Gatesy. 2000. Theropod forelimb design and evolution. Zoological Journal of the Linnean Society 128: 149–187.

Mitteroecker, P., and P. Gunz. 2009. Advances in geometric morphometrics. Evolutionary Biology 36 (2): 235–247.

Mitteroecker, P., P. Gunz, S. Windhager, and K. Schaefer. 2013. A brief review of shape, form, and allometry in geometric morphometrics, with applications to human facial morphology. Hyxtrix 24: 59–66.

Monteiro, L.R. 1999. Multivariate regression models and geometric morphometrics: the search for causal factors in the analysis of shape. Systematic Biology 48: 192–199.

Navalón, G., J. Marugán-Lobón, L.M. Chiappe, J.L. Sanz, and A.D. Buscalioni. 2015. Soft-tissue and dermal arrangement in the wing of an Early Cretaceous bird: Implications for the evolution of avian flight. Scientific Reports 5: 14864.

Norberg, U.M. 1995. How a long tail and changes in mass and wing shape affect the cost for flight in animals. Functional Ecology 9: 48–54.

Norell, M., and X. Xu. 2005. Feathered dinosaurs. Annual Review of Earth and Planetary Sciences 33: 277–299.

Novas, F.E., M. Ezcurra, F.L. Agnolín, D. Pol, and R. Ortíz. 2012. New Patagonian Cretaceous theropod sheds light about the early radiation of Coelurosauria. Revista del Museo Argentino de Ciencias Naturales (n.s) 14: 57–81.

Nudds, R.L., G.J. Dyke, and J.M.V. Rayner. 2007. Avian brachial index and wing kinematics: putting movement back into bones. Journal of Zoology 272: 218–226.

O'Connor, J.M.K., and Z.H. Zhou. 2012. A redescription of *Chaoyangia beishanensis* (Aves) and a comprehensive phylogeny of Mesozoic birds. Journal of Systematic Palaeontology 11: 889–906.

O'Connor, J.M.K., and C. Sullivan. 2014. Reinterpretation of the Early Cretaceous maniraptoran (Dinosauria: Theropoda) *Zhongornis haoae* as a scansoriopterygid-like non-avian, and morphological resemblances between scansoriopterygids and basal oviraptorosaurs. Vertebrata Palasiatica 52: 3–30.

Padian, K., and L.M. Chiappe. 1998. The origin and early evolution of birds. Biological Reviews of the Cambridge Philosophical Society 73: 1–42.

Pei, R., et al. In press. Potential for powered flight neared by most close avialan relatives but few crossed its thresholds. Current Biology.

Prum, R.O., et al. 2015. A comprehensive phylogeny of birds (Aves) using targeted next-generation DNA sequencing. Nature 562: 569–573.

Puttick, M.N., G.H. Thomas, and M.J. Benton. 2014. High rates of evolution preceded the origin of birds. Evolution 68: 1497–1510.

Raff, R.A. 1996. The shape of life: genes, development, and the evolution of animal form. Chicago: University of Chicago Press.

Raff, R.A. 2000. Evo-devo: the evolution of a new discipline. Nature Reviews Genetics 1: 74–79.

Rashid, D.J., et al. 2018. Avian tail ontogeny, pygostyle formation, and interpretation of juvenile Mesozoic specimens. Scientific Reports 8: 9014.

Rohlf, F.J. 2017. TpsDig, version 2.30. Stony Brook: Department of Ecology and Evolution, State University of New York.

Rohlf, F.J., and L.F. Marcus. 1993. A revolution morphometrics. Trends in Ecology and Evolution 8: 129–132.

Sereno, P.C. 1997. The origin and evolution of dinosaurs. Annual Review of Earth and Planetary Sciences 25: 435–489.

Sereno, P.C. 1999. The evolution of dinosaurs. Science 284: 2137–2147.

Serrano, F.J., and L.M. Chiappe. 2017. Aerodynamic modelling of a Cretaceous bird reveals thermal soaring capabilities during early avian evolution. Journal of the Royal Society Interface 14: 20170182.

Serrano, F.J., P. Palmqvist, L.M. Chiappe, and J.L. Sanz. 2017. Inferring flight parameters of Mesozoic avians through multivariate analyses of forelimb elements in their living relatives. Paleobiology 43: 144–169.

Serrano, F.J., et al. 2018. Flight reconstruction of two European enantiornithines (Aves, Pygostylia) and the achievement of bounding flight in Early Cretaceous birds. Palaeontological Association 61: 359–368.

Turner, A.H., D. Pol, J.A. Clarke, G.M. Erickson, and M.A. Norell. 2007. A basal dromaeosaurid and size evolution preceding avian flight. Science 317: 1378–1381.

Turner, A.H., P.J. Makovicky, and M.A. Norell. 2012. A review of dromaeosaurid systematics and paravian phylogeny. Bulletin of the American Museum of Natural History 371: 1–206.

Vargas, A.O., and G.P. Wagner. 2009. Frame-shifts of digit identity in bird evolution and cyclopamine-treated wings. Evolution and Development 11: 163–169.

Vidal-García, M., L. Bandara, and J.S. Keogh. 2018. ShapeRotator: an R tool for standardized rigid rotations of articulated three-dimensional structures with application for geometric morphometrics. Ecology and Evolution 8: 4669–4675.

Wagner, G.P., and J.A. Gauthier. 1999. 1,2,3 = 2,3,4: a solution to the problem of the homology of the digits in the avian hand. Proceedings of the National Academy of Sciences of the United States of America 96: 5111–5116.

Wang, M., and G.T. Lloyd. 2016. Rates of morphological evolution are heterogeneous in Early Cretaceous birds. Proceeding of the Royal Society of London B, Biological Sciences 283: rspb.2016.0214.

Wang, X.L., et al. 2017. Basal paravian functional anatomy illuminated by high-detail body outline. Nature Communications 8: 14576.

Wang, M., J.M.K. O'Connor, X. Xu, and Z.H. Zhou. 2019. A new Jurassic scansoriopterygids and the loss of membranous wings in theropod dinosaurs. Nature 569: 256–259.

Xu, X., and S. Mackem. 2013. Tracing the evolution of avian wing digits. Current Biology 23: R538–R544.

Xu, X., Z.H. Zhou, X.L. Wang, X.W. Kuang, F.C. Zhang and X.K. Du. 2003. Four-winged dinosaurs from China. Nature 421: 335–340.

Xu, X., et al. 2009. A Jurassic ceratosaur from China helps clarify avian digit homologies. Nature 459: 940–944.

Xu, X., J. Choiniere, C. Sullivan, and F.L. Han. 2011. Comment on 'Embryological evidence identifies wing digits in birds as digits 1, 2, and 3.' Nature Precedings (Pre-publication research and preliminary findings). Online resource (npre.2011.6433.1).

Xu, X., et al. 2015. A bizarre Jurassic maniraptoran theropod with preserved evidence of membranous wings. Nature 521: 70–73.

Young, R.L., G.S. Bever, Z. Wang, and G.P. Wagner. 2011. Identity of the avian wing digits: problems resolved and unsolved. Developmental Dynamics 240: 1042–1053.

Zhou, Z.H. 2004. The origin and early evolution of birds: discoveries, disputes, and perspectives from fossil evidence. Naturwissenschaften 91: 455–471.

Chapter 7
Tooth vs. Beak: The Evolutionary Developmental Control of the Avian Feeding Apparatus

SHUO WANG,[1] JOSEF STIEGLER,[2] PING WU,[1] AND CHENG-MING CHUONG[1]

ABSTRACT

Recent discoveries of exquisitely preserved nonavialan and avialan theropod dinosaurs have not only prompted studies of theropod tooth morphologies, but have also provided information about the origin and early evolution of avian beaks. Recent studies on beak morphologies and morphogenesis in Darwin's finches have greatly improved our understanding of how avian beaks adapt to various ecological niches, but the question of how birds lost their teeth during the course of evolution has long been debated. Evolutionary developmental experiments performed on extant bird embryos bridge the gap between paleontological and neontological evidence, suggesting that the avian beak could have originated through heterochronic truncation of odontogenesis over evolutionary time. Here, we systematically review independently evolved regional and complete edentulism present in nonavialan and avialan theropod dinosaurs, and suggest that the tooth-reduction processes of different jaw bones are likely to be independently controlled. Through reviewing the recent advances of molecular regulations involved in tooth and avian beak morphogenic processes, we suggest that several molecules regulating the development of the avian beak also mediate the growth of keratinous rhamphothecae, and the divergence of odontogenic signalling pathways are likely to have accounted for both of these processes.

INTRODUCTION

Food is the main source of energy for the survival of animals. Therefore, the mechanisms by which food is ingested (feeding modes) play important roles in shaping animals' developmental patterns, morphogenetic processes, behaviors, and reproduction through their effects on metabolism (Temeles et al., 2010). Despite various feeding modes, the feeding apparatuses are relatively conserved among different clades of animals: most jawed vertebrates feed through teeth or beaks (Louchart and Viriot, 2011), while other mechanisms for feeding account for less than 1% of the diversity of feeding apparatuses of extant jawed vertebrates (Davit-Béal et al., 2009; Louchart and Viriot, 2011), including baleen (e.g., mysticete whales), sticky tongues (e.g., toads), and mouthparts designed for suction (e.g., seahorses). Note that throughout this review, we define "beak" as the edentulous, rigid bony mouthpart of all vertebrates that is used for eating, preening, fighting, etc., and the term "rhamphotheca" refers to the keratinous sheath that covers the bony beak.

---

[1] Department of Pathology, Keck School of Medicine, University of Southern California, Los Angeles.
[2] Department of Anatomical Sciences, Stony Brook University, Stony Brook, NY.

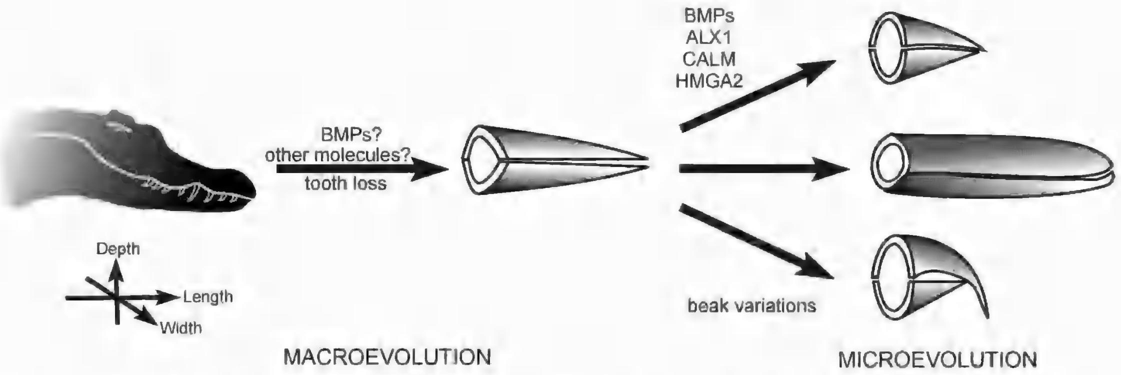

FIG. 1. Macroevolution and microevolution of avian beak from toothed ancestor's snout. The avian beak is inferred to have evolved from the snout of toothed nonavian dinosaurian ancestors through alterations to the signaling pathways involving bone morphogenetic proteins (BMPs) and other molecules. BMP, ALX homeobox protein 1 (ALX1), calcium-modulated protein (CALM) and high-mobility group AT-hook 2 (HMGA2) are all important molecules that regulate the diversity of beak shapes. Not to scale.

Birds account for almost 99.9% of extant beaked vertebrates (Meredith et al., 2014), and the remaining 0.1% are chelonians (Rhodin et al., 2017) and a few mammals (Thomas, 1889; Green, 1937; Manger et al., 1998; Musser and Archer, 1998; Davit-Béal et al., 2009). Avian beaks have many functions including preening, fighting, and courtship, in addition to feeding (Gill, 2006). Although they vary significantly in size, shape, curvature, and color, avian beaks share similar architectures: a thin keratinized epidermal layer, known as the rhamphotheca, covers the underlying bony bases in both upper and lower jaws (Gill, 2006). This prototype is highly adaptable as evidenced by a high degree of variation in beak function and morphology (Gill, 2006). The adaptability of the beak has been a major contributing factor in birds' successful adoption of various dietary and ecological niches (Mallarino et al., 2011; Bhullar et al., 2015).

In 1859, Darwin inferred the rapid evolution of avian beaks in response to environmental changes in *The Origin of Species* (Darwin, 1859). Only two years later, the discovery of *Archaeopteryx* skeletons (especially the London and Berlin specimens) demonstrated that the ancestor of modern birds was toothed (Owen, 1863a; 1863b; Evans, 1865; Dames, 1884; Howgate, 1984), raising the question of how the avian beak originated. Since then, the evolution and morphogenesis of the avian beak has attracted many biologists (Abzhanov et al., 2004; Podos and Nowicki, 2004; Wu et al., 2004a; Abzhanov et al., 2006; Wu et al., 2006; Genbrugge et al., 2011; Mallarino et al., 2011; Lamichhaney et al., 2015; Lamichhaney et al., 2016). While the diversity of extant birds provides an opportunity to understand the morphogenesis and microevolution of the beak (Abzhanov et al., 2004; Wu et al., 2004b; Wu et al., 2006; de Leon et al., 2010), the question of how beaked extant birds evolved from toothed ancestors has been poorly understood (Heilmann, 1927; Dilger, 1957; Zhou et al., 2009; Meredith et al., 2014). The recently discovered ontogenetic transition from tooth to beak in a Jurassic ceratosaurian theropod *Limusaurus inextricabilis* has shed new light on this question and transformed our understanding of the evolutionary origins of beaks (fig. 1; Wang et al., 2017b).

Here, we review the debate over the evolutionary origin of avian beaks, and comment on recent research advances that combine paleontological evidence with neontological experimental results. In the following two sections, we will review the molecular basis of tooth and beak development, respectively. In the fourth and the fifth sections, we will review the independently

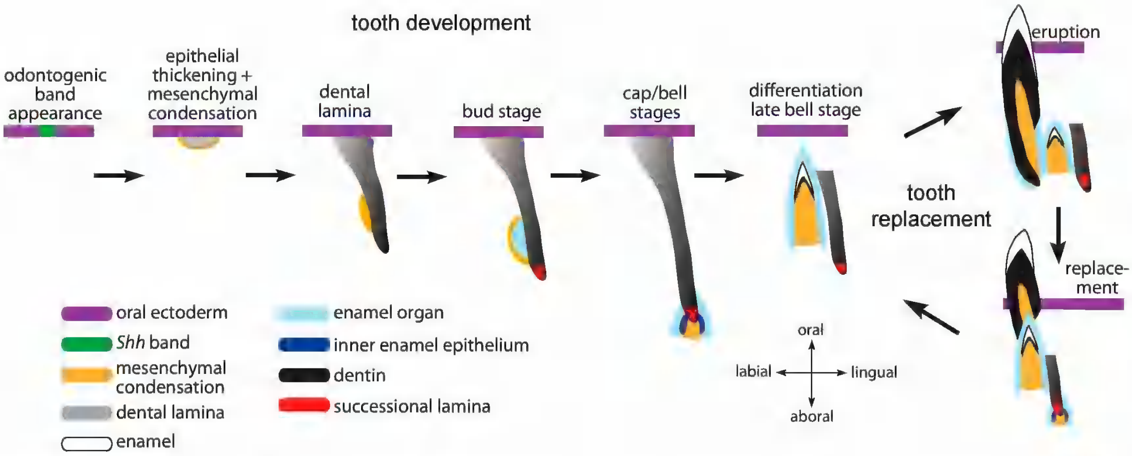
tooth development
odontogenic band appearance
epithelial thickening + mesenchymal condensation
dental lamina
bud stage
cap/bell stages
differentiation late bell stage
eruption
tooth replacement
replace-ment
oral
labial
lingual
aboral
oral ectoderm
Shh band
mesenchymal condensation
dental lamina
enamel
enamel organ
inner enamel epithelium
dentin
successional lamina

FIG. 2. Schematic drawing showing tooth developmental and replacement processes of archosaurs (modified from Richman and Handrigan, 2011; and Wu et al., 2013). Not to scale.

evolved instances of regional and complete edentulism in nonavialan and avialan theropod dinosaurs, respectively. The hypotheses of the evolutionary origin of avian beaks will then be briefly surveyed, from the classic paleontological hypotheses to recent evidences derived from the evolutionary developmental biology experiments. In the last section, we will briefly discuss the evolutionary significance of the avian beak, and comment on some recent advances clarifying the relationships between the emergence of the beak and craniofacial evolution in birds.

BIOLOGY OF TOOTH DEVELOPMENT AND REPLACEMENT

As an ectodermal organ, the development of teeth is regulated by sequential and reciprocal interactions between the epithelium and underlying mesenchyme (Thesleff, 2003). Although size, shape, and tooth count may vary among different taxa, the basic molecules and early signaling pathways of odontogenesis are essentially conserved across vertebrate phylogeny (Huysseune and Sire, 1998; Chen et al., 2000; Berkovitz and Shellis, 2016).

Knowledge of the molecular basis of tooth development comes primarily from the mouse (Thesleff, 2003). Prior to the initiation of tooth formation, the tooth-forming region is marked by a band expressing *Shh* (sonic hedgehog) and *Pitx2* (paired-like homeodomain transcription factor 2) (Jernvall et al., 2000; Cobourne et al., 2004; Fraser et al., 2006; Buchtová et al., 2008; Fraser et al., 2009; Smith et al., 2009; Richman and Handrigan, 2011), which are required for tooth formation (fig. 2; Chen et al., 2000). When tooth formation is initiated, the oral epithelium thickens and expresses BMPs (bone morphogenetic proteins) and FGFs (fibroblast growth factors) that lead to condensation of the oral mesenchyme (fig. 1), which activate a set of mesenchymal signals that then act on the epithelium and mediate the formation of placodes at each future tooth position (Thesleff, 2003; Jussila and Thesleff, 2012). During the tooth bud stage, the epithelium folds and invaginates into the underlying mesenchyme. This is followed by the cap stage during which the epithelium extends further into the condensing mesenchyme and wraps itself around the mesenchyme. The enamel knot, another signaling center that expresses multiple signaling molecules including BMPs, FGFs, WNT, and SHH that induce reciprocal signals from the mesenchyme, appears (Thesleff, 2003; Jernvall and Thesleff, 2012). Subsequently, the inner enamel epithelium and the mesenchyme differentiate into ameloblasts and odontoblasts at the epithelial-mesenchymal interface, secreting enamel and dentin matrices, respectively (Thesleff, 2003; Jernvall and Thesleff, 2012; Jussila and Thesleff, 2012).

Like other ectodermal organs such as hair, scales, and feathers, teeth undergo cyclic regeneration through which a new tooth is produced with possible phenotypic changes occurring during regeneration (Streelman et al., 2003; Jernvall and Thesleff, 2012; Wu et al., 2013). The maintenance of dental regeneration is made possible by a cluster of odontogenic stem cells (Huysseune and Thesleff, 2004; Whitlock and Richman, 2013; Wu et al., 2013; Tsai et al., 2016). Although cells with stem-cell properties were also identified in mouse molar dental pulp, follicle, and epithelium, they are used for continual tooth growth, and are not able to regenerate a new tooth after a tooth is lost. This results in a single generation of molars (Huang et al., 2009). For example, mouse incisors can grow continuously, as they are maintained by stem cells enriched at the labial incisor cervical loop (Harada et al., 1999, Renvoisé and Michon, 2014, Whitlock and Richman, 2013), but cannot regenerate the incisor if it is lost. Therefore, the mouse is not an ideal model for studying the cyclical tooth replacements in polyphyodonty vertebrates such as dinosaurs.

The dental lamina is an invagination of the oral epithelium into underlying mesenchyme, and its free aboral end is enriched in odontogenic stem cells that are highly proliferative (Smith et al., 2009; Wu et al., 2013). These stem cells form the successional lamina where the subsequent generations of teeth are differentiated (Huysseune, 2006; Jussila and Thesleff, 2012; Jussila et al., 2014). Therefore, the ability of the dental lamina to continuously differentiate into successional laminae is essential for the maintenance of tooth replacement (fig. 2). In taxa whose teeth can be replaced for many generations throughout life (polyphyodonty), such as reptiles and fishes, the successional lamina exists throughout life (Huysseune, 2006; Zahradnicek et al., 2012; Wu et al., 2013). Most mammals are diphyodont, they only replace their teeth once (Luo et al., 2004), and the successional lamina degenerates following the first tooth replacement (Järvinen et al., 2009; Richman and Handrigan, 2011; Buchtová et al., 2012; Buchtová et al., 2013; Whitlock and Richman, 2013; Dosedělová et al., 2015). Taken together, the existence of the successional lamina is directly related to the maintenance of tooth replacement (Jussila et al., 2014).

The frequency of tooth replacement depends on the division cycles of the odontogenic stem cells (Wu et al., 2013), which can be different among various vertebrate taxa and different ontogenetic stages of the same species. For instance, the primary teeth of mammals may be replaced at an interval of several months to decades (Berkovitz and Shellis, 2018), and in most cases their tooth family units consist of only one functional tooth. In contrast, some taxa (e.g., Chondrichthyes and Actinopterygii) can replace a whole set of teeth within a few days such that several replacement teeth can be found in the tooth family units (Peyer, 1968; Mochizuki and Fujui, 1983; Berkovitz and Shellis, 2016). Therefore, the replacement frequency of a given tooth position can be discerned from the exact tooth count of that tooth family unit (Wu et al., 2013).

The pattern of tooth replacement along the tooth row also varies among vertebrate taxa, which is more obvious in vertebrates with thecodonty as opposed to pleurodonty or acrodonty. In mammals, tooth replacement is highly regionally specific, with incisors (mesial teeth) replaced earlier than other antemolars (Berkovitz and Shellis, 2018). Much attention has been paid to mammal premolar replacement. Teeth are alternatively replaced in mammallike cynodonts with indeterminate cranial growth patterns (e.g., *Pachygenelus*) (Luo et al., 2004). The early-diverging clades of crown mammals have a rostrocaudally sequential replacement of premolars, which is the reverse alternate pattern of some, if not all, early-diverging trechnotherians (Luo et al., 2004). The replacement of premolars in most extant placentals is also sequential, either rostrocaudally (e.g., ungulates and carnivores) or caudorostrally (e.g., some insectivores) (Luo et al., 2004). In extant metatherians, only the ultimate premolar on each jaw quadrant is replaced (Cifelli and Muizon, 1998; Rougier et al., 1998; Luo et al., 2004). Therefore, the tooth replacement pattern has undergone several reversals and changes across the evolutionary history of mammals.

Most nonmammalian vertebrates are polyphyodont (Edmund, 1960), with early studies that address tooth replacement in these vertebrates dating to near the turn of the 19th century (Röse, 1893a; 1893b; Harrison, 1901; Woerdeman, 1919a; 1919b; 1921a; 1921b). These works identified an alternating tooth replacement pattern in nonmammalian vertebrates such that teeth arise and replace alternately at odd and even positions to form a wave. This pattern was defined as *Zahnreihen*, or "replacement waves," by Woerdeman (1921b; Edmund, 1960). A Zahnreihen consists of a series of adjacent teeth from different tooth family units that are roughly at the same developmental stage.

Two theories have been proposed to explain the alternating pattern of tooth replacement: one is the "wave-stimulation theory" and the other refers to a "zone of inhibition" (Richman and Handrigan, 2011). The "wave-stimulation theory" is based primarily on observations and is thus somewhat speculative, emphasizing that tooth growth and replacement are controlled by periodically expressed stimuli in the dental mesenchyme that pass distally from the mesial end of the tooth row (Edmund, 1960; 1962). Accordingly, new teeth are formed along the tooth rows in the same direction that the stimuli pass through, and the alternating tooth-replacement patterns are produced by the time intervals between multiple successive Zahnreihens coexisting at a given time (Edmund, 1960). While this theory is consistent with observations of replacement in some taxa (Cooper et al., 1970; Ziegler, 1971; Bolt and Demar, 1975; Hanai and Tsuihiji, 2019; He et al., 2018), it must be acknowledged that not all animals replace teeth in anteroposterior or posteroanterior orders and intraspecific order reversal is not rare (Miller and Radnor, 1970). The validity of this theory has been tested in both alligators and lizards through surgeries removing teeth and paradentium, and the results suggest that the recovery of teeth is not required for subsequent tooth initiation (Osborn, 1970; 1977; Westergaard and Ferguson, 1987, 1990; Buchtová et al., 2013; Brink et al., 2018). In some taxa, Zahnreihen may exist in immature individuals, but it has been suggested they are gradually broken down with increasing maturity (Miller and Radnor, 1970; Buchtová et al., 2013). This is probably related to cranial growth patterns as tooth replacement patterns are necessarily modified by cranial growth.

The theory of a "zone of inhibition" asserts that a developing tooth secretes some inhibitors into the surrounding paradentium, depressing the odontogenic process in neighboring tooth positions, and the growth of the neighboring teeth can start only after the predecessor between them stops growing (Osborn, 1971). The potential inhibitors have not been identified (Whitlock and Richman, 2013), yet surgical experiments in reptiles have demonstrated that tooth replacement is independently controlled by tooth family units rather than a global signal transmitting along the tooth rows (Brink et al., 2018). This is consistent with the observable variability in dental replacement patterns. Taken together, the available evidence suggests there is no clear common rule of vertebrate tooth-replacement patterns. The independent control of tooth replacement could be a prerequisite for regional tooth variation, replacement, and reduction in many vertebrates (Brink et al., 2018).

MOLECULAR BASIS FOR AVIAN BEAK MORPHOGENESIS

Avian beaks are formed from multiple facial prominences, each of which has a neural crest-derived mesenchymal core that is covered externally by an epithelial layer of ectoderm (Francis-West et al., 1998; Helms and Schneider, 2003; Richman and Lee, 2003). The upper beak comprises five prominences, including a fused frontonasal mass and paired maxillary and lateral nasal prominences (Romanoff, 1960; Wu et al., 2006). The lower beak is formed from two highly proliferating sites (one on each side) that are later fused into a single mandibular prominence (Romanoff, 1960; Wu et al., 2006). All prominences are coordinated with proportional sizes to produce a species-specific beak morphology (Abzhanov et al., 2004; Wu et al., 2004a; Wu et al., 2006). Transplantations of presumptive neural crest cells between quail and duck produced chimeric beak phenotypes, demonstrating that interspecific variations of beak morphogenesis can be guided by these cells (Schneider and Helms, 2003).

Beak morphogenesis consists of three major processes: the outgrowth of beak primordial mesenchyme (skeletal basis), the development of integument inside the oral cavity (oral mucosa) and the growth of the external keratinous sheath covering the snout (rhamphothecae). In chickens, beak growth starts by the end of embryonic day 5 (E5) and is marked by the initiation of the fused mandibular processes elongation (Romanoff, 1960). Later, the mesenchymal cell proliferation increases in the frontonasal mass, resulting in relatively faster growth of the upper beak than that of the lower beak (Romanoff, 1960). The mesenchymal cell proliferation centers are species specific, which constitute the structural basis of the species-specific beak morphotypes. Both chicken and duck have two mesenchymal cell proliferation centers in the frontal mass by E5, but they are fused at the subsequent developmental stages in chicken while they remain separated in duck (Wu et al., 2004a, 2006). It is unclear how this difference would give rise to the interspecific differences of beak morphologies.

Beak morphogenesis is regulated at both genomic and gene expression levels. At the genomic level, *ALX1* (ALX homeobox protein 1) encodes a transcription factor affecting craniofacial development demonstrated to be associated with beak shape diversity in Darwin's finches, while beak size is primarily controlled by a genomic region containing *HMGA2* (High-mobility group AT-hook 2) (fig. 1; (Lamichhaney et al., 2015, 2016). At the gene expression level, a recent study suggests that increased spatiotemporal activity of FGF and WNT could produce a completely fused premaxilla-dominated avian beak in contrast to the ancestral archosaurian forms that are characterized by paired abbreviated and rounded premaxillae (Bhullar et al., 2015). The interspecific morphological differences of avian beaks can also be modulated by BMP4, CALM (calcium-modulated protein, or calmodulin), FGF8, and WNT, which affect the proliferation activity of facial prominences (Abzhanov et al., 2004; Wu et al., 2004a, 2006). The information collectively suggests the emergence of a morphological novelty can be produced through manipulating the expression patterns of existing signals in addition to creating new regulatory networks (Wu et al., 2006; Bhullar et al., 2015).

Development of the rhamphotheca in extant birds is initiated by keratinization of epithelium from the anterior tips of both the premaxillae and dentaries at embryonic day 7 (E7) (Romanoff, 1960; Wu et al., 2006; Wang et al., 2017a), which then proceeds posteriorly to form complete horny sheaths covering the jaws (Wu et al., 2006; Hieronymus and Witmer, 2010). Avian rhamphothecae contain both alpha and beta keratins. Experiments show proper interactions between these keratins are necessary for normal formation of keratinous epidermal appendages (Wu et al., 2015). Variation in the spatial organization and interaction of alpha and beta keratins likely contribute to the morphological and structural diversity of avian beaks, but our current knowledge is limited to the chicken.

A recent study shows several molecules that regulate the morphogenesis of the beak, such as BMP4 and Noggin, are also involved in the growth of rhamphotheca (Wang et al., 2017a), and the overexpression of BMP4 in chicken embryos can produce rhamphotheca hypertrophy and/or ectopic beak keratin growth (Wang et al., 2017a). Although this has been suggested as a possible cause of odontogenic truncation (Wang et al., 2017a), the detailed signaling transductions that mediate the early truncation of odontogenesis, beak morphogenesis, and development of the keratinous rhamphotheca remain unclear.

TRACKING BEAK EVOLUTION IN NONAVIALAN DINOSAURS

Extant birds are toothless, but most of their nonavialan and avialan ancestors were toothed, suggesting the origin of rhamphotheca and tooth reduction are coupled (Wang et al., 2017a). Beaks evolved independently in ornithischians, sauropodomorph, and theropod dinosaurs, and appeared in many theropod clades in parallel with their appearance in birds (Wang et al., 2017a), with each independent evolution of a beak accompanied by some form of tooth reduction. In this section, we primarily document the presence of rhamphothecae with tooth reductions in theropod dinosaurs (fig. 3). Three types of tooth reduction are considered: (1) reduction of tooth number due either to the simplified shortening of the tooth row or that of the tooth-bearing elements; (2) reduction of tooth generations and the decrease of tooth replacement rate; and (3), reduction of tooth size compared to close relatives. Each form of reduction often occurs in conjunction with one or both of the others. We emphasize that all conditions discussed in this review are based on known specimens, and other conditions cannot be ruled out given the fact that new specimens continue to be discovered.

CERATOSAURIA: Though ontogenetic tooth reduction is common in extant vertebrates (Wang et al., 2017b), it is very rarely preserved in the fossil record. Ontogenetic reduction leading to edentulous adults has been reported in *Limusaurus* (Wang et al., 2017b), representing the only known example of edentulism in ceratosaurians. The youngest *Limusaurus* (presumed hatchlings) have one premaxillary, eight maxillary, and 12 dentary teeth on each side, whereas all teeth have been gradually lost, accompanied by a remodeling of the alveoli during the first two years of postnatal growth (Wang et al., 2017b). The presence of a single posteriorly positioned premaxillary tooth and an anteriorly edentulous dentary in some of the youngest *Limusaurus* suggests the tooth reduction of the upper jaw started from the anterior tip of the premaxilla (Wang et al., 2017b). The presence of only a single replacement tooth in the largest *Limusaurus* hatchlings suggests the cessation of normal tooth replacement is probably an indicator of tooth reduction (Wang et al., 2017a).

ORNITHOMIMOSAURIA: The evolution of ornithomimosaurians is characterized by the loss of dentition (Makovicky et al., 2004). Early-diverging ornithomimosaurians have teeth (Perez-Moreno et al., 1994; Ji et al., 2003 ; Kobayashi and Barsbold, 2005; Choiniere et al., 2012), but regional edentulism is present in all known toothed ornithomimosaurians (Wang et al., 2017a). Teeth are present in all known dentigerous elements of *Nqwebasaurus* and all elements of *Pelecanimimus* (Perez-Moreno et al., 1994), but the maxillary tooth row is shorter than that of the dentary in both taxa, and in *Nqwebasaurus* the maxillary tooth row ends anterior to the antorbital fenestra (Choiniere et al., 2012). In *Harpymimus* and *Shenzhousaurus*, teeth are restricted to the anterior end of the dentary and neither the premaxilla nor maxilla bear teeth (Ji et al., 2003; Kobayashi and Barsbold, 2005). A series of impressed neurovascular grooves characterizes the medial aspect of the anterior end of the dentary in *Harpymimus* suggesting this region may have also been covered by a rhamphotheca (Kobayashi and Barsbold, 2005). Besides the Early Cretaceous ornithomimosaurians, all known Late Cretaceous ornithomimosaurians have beaks that were covered with rhamphothecae (Kobayashi et al., 1999; Norell et al., 2001a; Kobayashi and Lü, 2003; Lee et al., 2014a). These data suggest the loss of dentition in ornithomimosaurs proceeds from posterior to anterior (Choiniere et al., 2012) and the edentulism of the upper jaw was achieved prior to that of the lower jaw. Microtomographic data of immature ornithomimosaurians are neces-

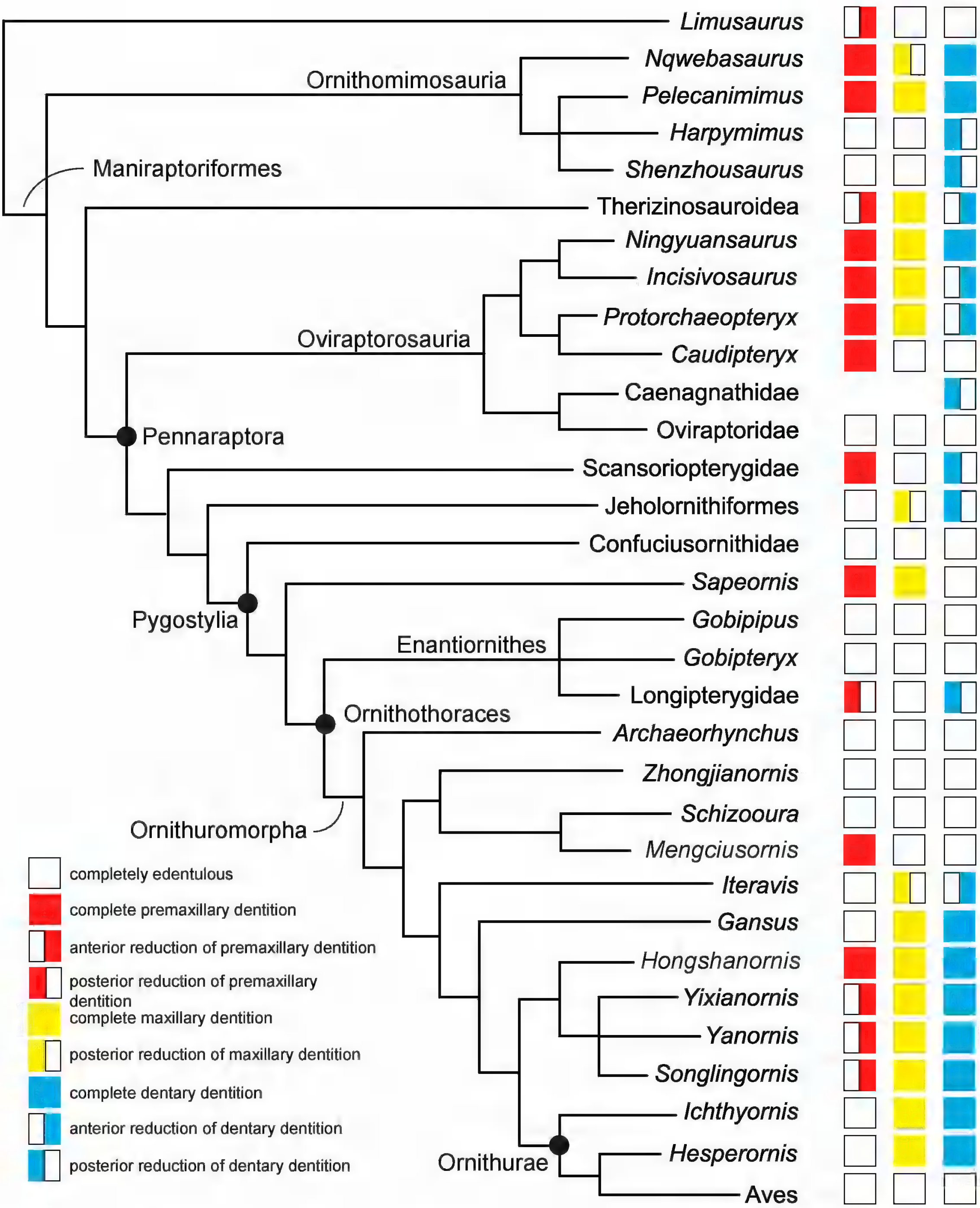
Limusaurus
Ornithomimosauria
Nqwebasaurus
Pelecanimimus
Harpymimus
Maniraptoriformes
Shenzhousaurus
Therizinosauroidea
Ningyuansaurus
Incisivosaurus
Protorchaeopteryx
Oviraptorosauria
Caudipteryx
Caenagnathidae
Pennaraptora
Oviraptoridae
Scansoriopterygidae
Jeholornithiformes
Confuciusornithidae
Sapeornis
Pygostylia
Gobipipus
Enantiornithes
Gobipteryx
Longipterygidae
Ornithothoraces
Archaeorhynchus
Zhongjianornis
Schizooura
Ornithuromorpha
Mengciusornis
completely edentulous
complete premaxillary dentition
anterior reduction of premaxillary dentition
posterior reduction of premaxillary dentition
complete maxillary dentition
posterior reduction of maxillary dentition
complete dentary dentition
anterior reduction of dentary dentition
posterior reduction of dentary dentition
Iteravis
Gansus
Hongshanornis
Yixianornis
Yanornis
Songlingornis
Ichthyornis
Ornithurae
Hesperornis
Aves

FIG. 3. Simplified phylogenetic hypothesis of theropod dinosaurs showing the tooth-reduction patterns in different clades (modified from Wang et al., 2014a, 2017a, 2019; and Zheng et al., 2018).

sary to investigate whether the evolutionary tooth reduction in this clade is heterochronically controlled.

Therizinosauria: The early-diverging therizinosaurians *Falcarius* and *Eshanosaurus* have fully toothed dentaries (Xu et al., 2001; Zanno, 2010). *Falcarius* also has maxillary teeth, but whether teeth are present in premaxillae is unknown (Zanno, 2010). The premaxillae and the anterior end of the dentaries are edentulous in all known therizinosauroids including embryos (Clark et al., 2004; Kundrát et al., 2008; Lautenschlager et al., 2013), but the dentary's edentulous region is shorter in *Jianchangosaurus* than that in other therizinosauroids (Pu et al., 2013a).

Oviraptorosauria: Similar to ornithomimosaurians, oviraptorosaurians are also characterized by a progressive loss of teeth throughout their evolutionary history (Osmólska et al., 2004; Wang et al., 2017a; Wang et al., 2018). All known noncaenagnathoid oviraptorosaurians are toothed. Early-diverging oviraptorosaurians including *Ningyuansaurus* (Ji et al., 2012), *Protarchaeopteryx* (Ji et al., 1998), and *Incisivosaurus* (Xu et al., 2002) have teeth in all dentigerous elements, but *Incisivosaurus* and *Protarchaeopteryx* start losing teeth from the anterior end of dentaries, and their maxillary and dentary teeth are remarkably reduced both in size and number relative to those in *Ningyuansaurus* (Xu et al., 2002; Balanoff et al., 2009). *Caudipteryx* has four premaxillary teeth, but its maxilla and dentary are edentulous (Ji et al., 1998; Zhou et al., 2000), indicating the dentary teeth would have been lost first in early-diverging oviraptorosaurians followed by maxillary teeth (fig. 3).

Small premaxillary teeth were reported in an as of yet undescribed specimen of the caenagnathid *Avimimus* (Watabe et al., 2000), and remain the only report of upper dentition in Caenagnathoidea, though some have cast doubt on this observation (Gregory Funston, personal commun., 2019). Structures that have been interpreted (Wang et al., 2018) as vestigial alveoli are present in dentaries in almost all known specimens of caenagnathids (Currie et al., 1993; Xu et al., 2007; Longrich et al., 2013; Funston and Currie, 2014; Lamanna et al., 2014; Bell et al., 2015; Tsuihiji et al., 2015; Yao et al., 2015; Tsuihiji et al., 2016). This suggests that dentary teeth were present at some point during the ontogeny of caenagnathids, and an ontogenetic tooth reduction comparable to that in *Limusaurus* is also present in caenagnathid oviraptorosaurians (Wang et al., 2017a, 2018). In small specimens of caenagnathids, posterior vestigial alveoli are smaller than the anterior ones (Wang et al., 2018), and the anterior tip of the dentary is edentulous as in *Incisivosaurus* and *Protarchaeopteryx*. This suggests the ontogenetic tooth reduction occurred from both the anterior and posterior ends of the dentary in caenagnathid oviraptorosaurians.

Through investigating histological sections of dentaries from a growth series of Caenagnathidae and prior studies of the ontogeny of interdental tissues, Funston et al. (2020) argued that the lingual grooves and ridges of caenagnathid dentaries that were interpreted as vestigial alveoli and interdental septa respectively (Wang et al., 2018) cannot have previously housed teeth during caenagnathid ontogeny. We agree with the histological observations of Funston et al. (2020), but we disagree that they negate a hypothesis of ontogenetic edentulism in Caenagnathidae and will respond to their critiques elsewhere.

All known oviraptorid dinosaurs are completely edentulous, including embryos (Norell et al., 1994, 2001b; Wang et al., 2016), and none bear any dentary structures suggestive of ontogenetic edentulism (fig. 3).

Scansoriopterygidae: Teeth are restricted to the premaxillae and anterior dentary in all known Scansoriopterygidae including *Epidendrosaurus* (Zhang et al., 2002) and *Yi* (Xu et al., 2015), but *Epidexipteryx* probably has maxillary teeth as well (Zhang et al., 2008a). The presence of more complete dentitions in Early Cretaceous oviraptorosaurians, Jurassic avialans, and deinonychosaurians indicates the condition in Scansoriopterygidae is an apomorphic reduction of the posterior dentition (Wang et al., 2017a).

TRACKING BEAK EVOLUTION IN THE EARLY EVOLUTION OF BIRDS

JEHOLORNITHIFORMES: All known specimens of *Jeholornis* lack premaxillary teeth (Zhou and Zhang, 2002; O'Connor et al., 2012; Zhou, 2015). Although teeth were initially described as absent from the upper jaws in *J. prima* (Zhou and Zhang, 2002; 2003a; O'Connor et al., 2012), a single tooth and an empty alveolus are present in the maxilla of *J. palmapenis* (O'Connor et al., 2012). An undescribed specimen of *Jeholornis* preserves a single maxillary tooth (Wang et al., 2017a), while another specimen (STM 3-32) has two maxillary teeth (Zhou, 2015). All known maxillary teeth of *Jeholornis* are restricted to the anterior portion of the maxilla below the ascending process. Teeth in the lower jaw are restricted to the anterior extent of the dentaries. Three small teeth were reported in the dentary of the holotype of *J. prima* (IVPP V13274) (Zhou and Zhang, 2002; 2003a), whereas only two are present in IVPP V13350 (Zhou and Zhang, 2003a). The dentaries of *J. palmapenis* and a possible *J. prima* are edentulous (Ji et al., 2002; O'Connor et al., 2012; Zhou, 2015). The dentition of *Jeholornis* has been significantly reduced in comparison to all known Jurassic paravians such as *Archaeopteryx* (Zhou and Zhang, 2003a; O'Connor et al., 2012), with complete edentulism occurring first in the premaxilla, while the maxilla and dentary experienced reductions proceeding from posterior to anterior.

The variability in the dentition of *Jeholornis* suggests the possibility of an ontogenetic reduction of the dentition in this taxon (Wang et al., 2017a), but this hypothesis cannot be tested at the present time since it is not clear whether available specimens of *Jeholornis* represent a growth series of a single species, and currently no high-resolution CT images are available to verify whether alveolar vestiges are present in these specimens.

CONFUCIUSORNITHIDAE: All known confuciusornithids are completely edentulous and show clear osteological correlations of rhamphotheca, and CT images have revealed no sign of a vestigial tooth or alveolus in *Confuciusornis* (Ji et al., 1999; Zhang et al., 2008b; Wang et al., 2017a; Wang and Zhou, 2018).

SAPEORNITHIFORMES: All known *Sapeornis* specimens have premaxillary and maxillary teeth when these dentigerous element are preserved, but dentary teeth are present only in some small specimens (Zhou and Zhang, 2003b). A recent study suggests the variation of dental formula in *Sapeornithiformes* is taphonomic (Wang et al., 2017c), however no hypothesis is offered to explain the relative tendency for dentary teeth to be lost while the upper dentition is retained within alveoli. All known specimens of *Sapeornis* from the Jiufotang Formation are hypothesized to represent a growth series of a single species *Sapeornis chaoyangensis* (Gao et al., 2012; Pu et al., 2013b), and the absence of dentary teeth in some specimens suggests that teeth have been lost from this taxon through ontogenetic truncation of odontogenesis as in *Limusaurus* and caenagnathids (Wang et al., 2017a).

Currently known specimens suggest edentulism first took place in the dentary, where dentition is reduced, followed by the posterior portion of the maxilla, and the premaxilla is the area from which teeth are least likely to be lost (Wang et al., 2017c). The dentary teeth, if present, are usually accompanied by two or three empty alveolar homologs anterior to these teeth (Wang et al., 2017a). Posterior to the last dentary tooth or alveolar homologs, a series of regularly distributed foramina are present on the lingula aspect of the dentary, which internally communicate with a canal that is hypothesized to represent a closed alveolar canal (Wang et al., 2017a). These lines of evidence collectively suggest dentary teeth of *Sapeornis* are reduced from both the posterior and anterior ends of the tooth row (fig. 3). The anterior end of the lower jaw is likely to have been covered by a horny rhamphotheca, and how the remaining few dentary teeth functioned in feeding is unclear.

ENANTIORNITHES: Pengornithids have numerous small teeth preserved in all dentigerous bones (Wang et al., 2014a; Hu et al., 2015; O'Connor et al., 2016), representing the primitive condition of Enantiornithes. Dental reductions begin in the maxilla and dentary in several enantiornithines such as *Cathayornis*, Bohaiornithidae, and Longipterygidae (Martin and Zhou, 1997; O'Connor and Dyke, 2010; Wang and Liu, 2016). Bohaiornithids can be distinguished from other enantiornithines in having anteriorly located large and robust subconical teeth (Wang et al., 2014b; Peteya et al., 2017), which probably represent functional compensation for the reduced tooth count in addition to the presence of gastroliths (Li et al., 2014). The teeth of Longipterygidae are further reduced compared to those seen in Bohaiornithidae. Large posteriorly recurved teeth are present only in the premaxilla and the anterior end of the dentary, while the maxillae are edentulous (Zhang et al., 2001; O'Connor et al., 2009; Li et al., 2012; Wang et al., 2017a). However, it is unclear whether the jaw bones of longipterygids were covered by rhamphothecae posteriorly.

Teeth are completely absent in *Gobipipus* and *Gobipteryx* (Elzanowski, 1976; Elzanowski, 1977; 1981; Chiappe et al., 2001; Kurochkin et al., 2013), representing the only known examples of edentulous enantiornithines (Zhou, 2015). *Gobipipus* is known only from embryonic specimens with edentulous jaw bones (Elzanowski, 1981; Kurochkin et al., 2013), but whether teeth are also absent in adults is unknown given the possibility of delayed tooth eruption (Wang et al., 2017d). *Gobipteryx* is known from postjuvenile specimens, and the presence of the acuminate occlusal margins of the beak and neurovascular foramina on the external surfaces of premaxilla and dentary all indicate the presence of horny rhamphothecae (Elzanowski, 1976; Chiappe et al., 2001; Wang et al., 2017a).

Teeth are also present in embryonic and neonatal enantiornithines (Sanz et al., 1997; Zhou and Zhang, 2004; Xing et al., 2017; Kaye et al., 2019). A Spanish Early Cretaceous neonatal enantiornithine bears four premaxillary teeth, at least five maxillary teeth, and eight dentary teeth (Sanz et al., 1997). An Early Cretaceous embryonic enantiornithine from China that has been only preliminarily described bears maxillary teeth, though the tooth count in each element is unclear (Zhou and Zhang, 2004). A single premaxillary tooth has been reported in an amber embedded enantiornithine hatchling (Xing et al., 2017), though the taxonomic affinities of this specimen are impossible to determine based only on the presence of the premaxillary tooth, because all known enantiornithines have at least three premaxillary teeth except *Gobipipus* and *Gobipteryx*, as has been mentioned above. The reason for the absence of maxillary and dentary teeth in this specimen may be taphonomic, since embryonic teeth are common for both extinct and extant toothed archosaurs (Westergaard and Ferguson, 1987; Westergaard and Ferguson, 1990; Sanz et al., 1997; Wang and Zhou, 2004; Zhou and Zhang, 2004; Kundrát et al., 2008), though an independent reduction of dentition is possible.

ORNITHUROMORPHA (INCLUDING AVES): Tooth reduction patterns are fairly complicated among Ornithuromorpha. *Archaeorhynchus*, *Schizooura*, and *Zhongjianornis* are completely edentulous in known specimens (Zhou and Zhang, 2006; Zhou et al., 2009, 2012, 2013; Wang and Zhou, 2016), and their beaks are inferred to have been covered with rhamphothecae. The condition in younger ontogenetic stages of these taxa is unknown. The Early Cretaceous *Yanornis*, *Yixianornis*, and *Songlingornis* all have dentigerous premaxillae, maxillae, and dentaries (Zhou and Zhang, 2001), but premaxillary teeth of these taxa are posteriorly located and the edentulous anterior tip of their upper jaws are thus inferred to be covered by rhamphothecae (Zhou and Zhang, 2001; Zhou, 2015). In *Gansus zheni* (Liu et al., 2014), *Iteravis* (Zhou et al., 2014), *Ichthyornis*, and *Hesperornis* (Marsh, 1875), the premaxillae are edentulous while the maxillary teeth are reduced to various degrees, and a rhamphotheca is therefore inferred to have covered at least the premaxilla in these taxa. Despite the apparent absence of dentition in hongshanornithids, the identification of teeth and alveoli in both the upper and lower jaws suggest this group is also toothed (O'Connor et al., 2010; Chiappe et al., 2014). The recently described *Mengciusornis* has four premaxillary teeth and an edentulous maxilla and dentary (Wang et al., 2019). This implies that the way ornithuromorphs reduced their dentition was more complicated than expected.

In addition to the various states of tooth reduction in premaxillae, maxillae, and dentaries, an edentulous "predentary" is present in some Ornithuromorpha (fig. 3). This intersymphyseal ossification is topologically similar to the predentary of ornithischian dinosaurs but is unlikely to be homologous with that element (O'Connor et al., 2010). Its presence is relatively common in extinct ornithurines and a likely homolog is present in Pelagornithidae (Mayr and Rubilar-Rogers, 2010), but it has been lost in all extant crown birds (Zhou and Martin, 2011; Bailleul et al., 2019). It is interesting that among ornithurines, the presence of the predentary always corresponds to the presence of anterior edentulism of the premaxillae (Zhou and Martin, 2011), and similar correspondence is also present in ornithischians. This indicates that the small triangular element anterior to the left dentary of *Mengciusornis* may not be the predentary given there are four premaxillary teeth present in this taxon (Wang et al., 2019).

All known Aves are completely edentulous throughout postnatal ontogeny, but epithelial thickenings presumably homologous to the dental lamina are temporarily present during embryonic stages in at least some taxa (Chen et al., 2000).

EVOLUTIONARY ORIGIN OF AVIAN BEAK

Early Understanding of Avian Tooth Loss

Scientific study of rudimentary avian dental structures can be traced back to the early 19th century when transiently present papillae were found in bird embryos that were suggested to be homologs of reptilian teeth (Cuvier, 1821; St. Hilarie, 1821). However, these were later discounted as dermal papillae, which are common for integumentary derivatives and therefore were ignored by academia for quite a while (Blanchard, 1860; Gardiner, 1884; Heilmann, 1927; Harris et al., 2006).

Before the mid-nineteenth century, the public understanding of the toothlessness of birds was so ingrained that the avian affinities of the first *Archaeopteryx* skeleton (London specimen) was questioned by many in academia (Wellnhofer, 2010). Hermann von Meyer, the German paleontologist who reported the isolated feather of *Archaeopteryx* (von Meyer, 1861; von Meyer, 1862), described the London specimen as "a feathered animal which differs from our birds essentially" (Wellnhofer, 2010). Richard Owen described *Archaeopteryx* as a bird despite many features that are reminiscent of reptiles, including the clawed wings and the elongate tail (Owen, 1863a). Owen dismissed the importance of a premaxilla with teeth preserved next to the pelvis, suggesting that it came from an unknown fish (Owen, 1863a).

It was not until the discoveries of *Hesperornis*, *Ichthyornis*, and the iconic Berlin *Archaeopteryx* in 1870s that most were convinced that early birds were toothed (Marsh, 1872a; 1872b; Dames, 1884). The presence of teeth in early birds unquestionably linked the beaked extant bird to a toothed reptilian ancestor (Gegenbaur, 1863; Cope, 1867). The question of how birds originated soon became a topic of contention in the natural sciences by the end of the 19th century. Thomas Huxley extensively compared *Archaeopteryx* with other reptiles and suggested that it was much closer to dinosaurs than to any other groups of reptiles (the dinosaur hypothesis) (Huxley, 1868; 1870). Indeed, the presence of teeth in *Archaeopteryx* gave Huxley and his followers high confidence that birds evolved from dinosaurs (Seeley, 1901; Nopcsa, 1907), but none of them published on the question of how birds lost their teeth during the course of evolution.

Gerhard Heilmann was the first person who dealt with this question, but only briefly in his book *The Origin of Birds*: "the oldest birds had teeth, but these, being no longer needed, were gradually lost, and the jaws were recovered with horny sheaths…the teeth that were lost, it would no more have been able to recover" (Heilmann, 1927: 139).

Heilmann did not answer the question of how birds lost their teeth, but crucially hypothesized that the degradation of avian teeth and the formation of beaks were coupled. In 1957, William Dilger further developed Heilmann's idea, and hypothesized that avian tooth loss was a response to weight-saving demands for the evolution of flight (Dilger, 1957). This explanation was influential for more than four decades, and influenced numerous studies of avian locomotion and/or diet (Feduccia, 1999; Zhou and Zhang, 2006; Zhou et al., 2009; Louchart and Viriot, 2011; Zanno and Makovicky, 2011; Zheng et al., 2011; Zheng et al., 2014; Wang et al., 2017c; O'Connor et al., 2018; Zheng et al., 2018). However, recent studies suggest the selection pressure favoring body mass reduction is unlikely to be a factor in the tooth reduction of early birds (Lautenschlager et al., 2013; Zhou et al., 2019).

Neo-Darwinian Interpretations of the Macroevolution of Avian Beaks

A recent comparative genomics study consisting of extant representatives of nearly all avian orders suggested that inactivation mutations of odontogenetic genes may account for the evolution of avian tooth reduction (Meredith et al., 2014). In contrast, a series of investigations suggested that early odontogenic signals are conserved in embryonic chicken (Kollar and Fisher, 1980; Chen et al., 2000; Mitsiadis et al., 2003), and a classic experiment even induced enameled dental structures through the recombination of chicken oral epithelium and mouse molar mesenchyme (Kollar and Fisher, 1980). Although this result was probably altered via contamination by mouse dental epithelium (Chen et al., 2000), rudimentary dental structures including local epithelial thickenings can be induced by replacing chick oral mesenchyme with skin mesenchyme or even mouse mesenchyme (Chen et al., 2000; Mitsiadis et al., 2003). These lines of evidence suggest avian oral epithelium can still respond to signals from oral mesenchyme in toothed amniotes, and mutations of odontogenic genes in extant birds alone cannot account for the evolution of avian tooth reduction. A separate study hypothesized that the arrest of tooth development in modern birds is probably due to loss of mesenchymal odontogenic signals in modern birds (Mitsiadis et al., 2003), and as reviewed above, avian evolution is marked by partial tooth reductions, demonstrating that other factors contributed to avian tooth loss prior to any inactivation of the necessary genetic architecture.

Epigenetic Evidence

Interactions between oral epithelium and mesenchyme are prerequisites for the initiation of odontogenic processes in vertebrates (Thesleff, 2003). The morphogenic processes of many chicken organs can be affected by an autosomal recessive mutation *talpid*^{2} (Abbott et al., 1959; Dvorak and Fallon, 1991). However, conical dental rudiments occur at the anterior tips of both the premaxillae and dentaries of embryonic *talpid*^{2} chicken mutants, which morphologically resemble the null-generation teeth of *Alligator* in topology and morphology (Harris et al., 2006). By comparing the odontogenic tissues of *talpid*^{2} mutant and wild-type chicken embryos, it has been suggested that the absence of avian teeth was due primarily to the loss of direct contact between oral epithelium and the underlying mesenchyme in modern birds, making the avian epithelium unable to induce odontogenic processes (Harris et al., 2006).

In addition to the epithelium-mesenchyme apposition, another phenomenon present in *talpid*^{2} chicken mutants is that their keratinization of epithelium is only restricted to the aboral aspect of the mouth (Harris et al., 2006; Louchart and Viriot, 2011). Because a non-keratinized oral epithelium is required for interaction with mesenchyme when initiating odontogenesis, the presence of dental rudiments in *talpid*^{2} mutants was suggested to be related to the absence of keratinized oral epithelium (Louchart and Viriot, 2011). In wild type chicken embryos, oral epithelium keratinization initiates penecontemporaneously with the cessation of the oral epithelial thickening (Wang et al., 2017a), further support this assertion. While these experiments demonstrate the expression of keratin in oral epithelium may have truncated odontogenic signals in embryonic birds, the absence of keratinization of oral epithelium still cannot maintain the growth of the tooth rudiments and no mineralized teeth have been successfully induced de novo in extant birds (Sire et al., 2008).

The ontogenetic tooth reduction present in *Limusaurus* and hypothesized for *Sapeornis* illustrates the importance of secondary tool and ontogenetic dietary changes in the evolution of edentulium, as tooth loss without secondary tools and corresponding dietary changes would likely be lethal. Secondary tools such as rhamphothecae, gizzard, or both, appear before the loss of teeth and take on functions normally served by the dentition such as food acquisition and mechanical digestion (Wang et al., 2017a).

Several molecules involved in the odontogenic signaling pathways, such as BMP4 (Bone morphogenesis protein 4) and its antagonist Noggin, also regulate the growth of rhamphotheca (Abzhanov et al., 2004; Wu et al., 2004a; Wu et al., 2006; Wang et al., 2017a). The overexpression of BMP4 could not only produce hypertrophic rhamphotheca and/or ectopic beak keratin growth (Wang et al., 2017a), but could also truncate normal odontogenic signaling pathways, resulting in a tooth agenesis (Hu et al., 2012; Vogel et al., 2014). Acceleration of postnatal growth of rhamphothecae could overgrow alveoli and would likely induce alveolar remodeling (Wang et al., 2017a). A single replacement tooth present inside a completely enclosed dentary alveolus in a hatchling *Limusaurus* suggests the remodeling of the alveolus must have been accomplished after the initiation of the development of the replacement tooth, and the normal epithelial-mesenchymal contact would have been cut off by occlusal enclosure of the alveolus, explaining why the growth of the replacement tooth was truncated. Taken together, the truncation of odontogenesis is a result, rather than the cause, of the growth of rhamphotheca, which is a process combining the divergence of odontogenic signaling pathways and the loss of epithelial-mesenchymal interactions (Wang et al., 2017a).

Based on these discoveries, a four-step scenario of avian beak evolution has been depicted based on the current evolutionary developmental evidence, which emphasizes the correlation between tooth reduction and rhamphotheca expansion (Wang et al., 2017a). This epigenetic interpretation explains the various tooth reduction patterns could be aroused by the random growth of ectopic beak keratin. During the evolution of birds, a postnatal expansion of rhamphotheca can be achieved progressively earlier in ontogeny through heterochrony (Wang et al., 2017a; Yang and Sander, 2018), resulting in the embryonic truncation of odontogenesis in extant birds.

DISCUSSION

Since the ancestors of all beaked tetrapods were toothed (Li et al., 2008; Davit-Béal et al., 2009; Zhou et al., 2009; Louchart and Viriot, 2011; Fraser et al., 2012; Meredith et al., 2014; Li et al., 2018), tooth reduction patterns must have directly impacted the independent origins and evolution of beaks.

Among various instances of regional edentulism occurring in theropods, the evolutionary tooth reductions are proceeded from the posterior ends of the maxillae and dentaries toward the rostrum (rostrad reduction) in some lineages of theropods (e.g. Ornithomimosauria and Scansoriopterygidae) as well as enantiornithine birds and the recently reported ornithuromorph *Mengciusornis*, whereas in *Limusaurus*, Therizinosauria, Oviraptorosauria, and Ornithuromorpha, tooth reduction proceeded from the rostral tips of the premaxillae and dentaries toward the pharynx (orad reduction). This suggests the tooth reduction seen in theropods was dominated by at least two different patterns (Louchart and Viriot, 2011). Other patterns, such as the centrally contracted tooth row present in early-diverging birds may combine the two (Wang et al., 2017a, 2017c). The orad tooth reduction pattern is likely to have played an important role in the origin of beaked crown birds. The replacement of teeth with a beak at the anterior portion of the rostrum reduces the functional primacy of teeth for food acquisition and enhances the potential for secondary tools such as beaks, gastric mills, crops, tongue specializations, etc. to take over other functions of teeth. In addition, a progressively earlier appearance of rhamphotheca through heterochronic development would have prompted the evolution of a beak (Wang et al., 2017a). In contrast, the enlarged anterior teeth present in many taxa that have experienced a rostrad tooth reduction pattern (e.g. Scansoriopterygidae, enantiornithine) suggest the remaining teeth are still functionally important for food acquisition.

It should be noted that in comparison to the condition of ancestral archosaurs and most non-avialan theropods, tooth replacement in theropods on the stem to birds is fairly diminished. Extant alligators have tooth family units each consisting of three teeth: one is the functional tooth, a second is the replacement tooth, and the third is a developing tooth bud connecting with the dental lamina (Wu et al., 2013). Tooth replacement in non-avialan theropod dinosaurs appears similar to most other archosaurs, but it can be observed only in a few taxa of Mesozoic birds (e.g. *Archaeopteryx* (Wellnhofer, 2009), *Ichthyornis* and *Hesperornis* (Martin and Stewart, 1977; Dumont et al., 2016)) and appears to be absent in most toothed avialan taxa, especially those with various tooth reductions. This suggests that reductions in frequency of tooth replacement and number of generations could be a prelude to regional and complete edentulism.

Although current evidence suggests teeth can be lost independently from different jaw bones, the correspondent edentulism of predentaries and premaxillae (at least the anterior tips) suggests the tooth reductions in the upper jaw are linked by some unknown mechanisms with those in the lower jaw. The independent regional tooth loss is not difficult to understand, given jaw bones are differentiated from different groups of neural crest cells (Helms and Schneider, 2003; Schneider and Helms, 2003). However, the question of how odontogenic signals in the upper jaws are connected with those in the lower jaws is worthy to investigate in the near future.

Tooth loss in early birds has long been regarded as a phenomenon driven by the evolution of flight and/or adaptation of herbivory diet (Dilger, 1957; Feduccia, 1999; Zhou et al., 2009; Zanno and Makovicky, 2011; Larson et al., 2016; Wang et al., 2017c; Zheng et al., 2018). However, some other studies demonstrated the body mass effect of tooth reduction is negligible in Mesozoic birds and suggested the edentulism is just in favor of the skull mechanics in addition to adapt herbivorous diet (Zanno and Makovicky, 2011; Lautenschlager et al., 2013; Zhou et al., 2019). The evolutionary success of crown birds is clearly unlikely to have been caused by a single factor, and various authors have suggested paedomorphic evolutionary developmental patterns (Bhullar et al., 2012), miniaturized body sizes (Lee et al., 2014b), improved flapping flight (Heers et al., 2018), a transition from omnivorous to herbivorous diet (Zanno and Makovicky, 2011) and a collapse of global forest and/or other environmental catastrophes (Larson et al., 2016; Field et al., 2018). Body miniaturization, various flight capabilities and dietary transitions are potential internal factors favoring crown-bird survivorship over other contemporaneous small theropods (Field et al., 2018). They constitute the raw materials that were selected by external elements such as regional and global climate and environmental changes.

Natural selection is not the only determinant of the direction of evolutionary change (Psujek and Beer, 2008). The premise for the presence of a new feature is that it must be created by existing developmental mechanisms or through modifications of existing developmental mechanisms, and its adaptation to a particular environmental niche is the result of natural selection (Psujek and Beer, 2008). The regional upregulation of BMP4 could not only create the modern form of avian beaks and prompt the growth of rhamphotheca (Bhullar et al., 2015; Wang et al., 2017a), but also likely mediates the truncation of odontogenic processes (Wang et al., 2017a). This suggests the cranial evolution of modern birds would have been regulated by common signaling pathways through which variations of different cranial elements are coordinated, and the various tooth reduction patterns seen in early birds may have linked with different beak and/or cranial growth strategies. During growth of dentigerous elements, the normal functions of tooth rows are maintained through enlargement and/or increase of replacement teeth, and the frequency of tooth replacement is usually high in the region where jaw bones grow rapidly. The loss of teeth apparently did not prevent the evolution of the avian skull, which in turn may have led to the avian craniofacial diversity. From this perspective, the slow and finite tooth replacement prior to the regional or complete edentulism in theropod dinosaurs on the line to birds could probably result from the unbalance of some signaling pathways involved in the cranial developmental processes. Investigations into the relationships between allometric craniofacial development, tooth replacement and growth of beak keratin would be worthwhile in the near future.

ACKNOWLEDGEMENTS

We thank M. Pittman (HKU) and X. Xu (IVPP) for organizing the International Pennaraptoran Dinosaur Symposium and supporting this work, Andrew Moore for providing references, and D. Field, F. Novas, and J. Clark for their helpful comments on the manuscript. This work is supported by the National Science Foundation of China (41602013) and the U.S. National Institutes of Health (AR47364, 60306) and HFSP (LT000728/2018).

REFERENCES

Abbott, U.K., L.W. Taylor, and H. Abplanalp. 1959. Studies with *talpid*^{2}, an embryonic lethal of the fowl. Journal of Heredity 50: 195–202.

Abzhanov, A., M. Protas, B.R. Grant, P.R. Grant, and C.J. Tabin. 2004. *Bmp4* and morphological variation of beaks in Darwin's finches. Science 305: 1462–1465.

Abzhanov, A., et al. 2006. The calmodulin pathway and evolution of elongated beak morphology in Darwin's finches. Nature 442: 563–567.

Bailleul, A.M., Z.H. Li, J.M.K. O'Connor, and Z.H. Zhou. 2019. Origin of the avian predentary and evidence of a unique form of cranial kinesis in cretaceous ornithuromorphs. Proceedings of the National Academy of Sciences of the United States of America 116: 24696–24706.

Balanoff, A.M., X. Xu, Y. Kobayashi, Y. Matsufune, and M.A. Norell. 2009. Cranial osteology of the theropod dinosaur *Incisivosaurus gauthieri* (Theropoda: Oviraptorosauria). American Museum Novitates 3651: 1–35.

Bell, P.R., P.J. Currie, and D.A. Russell. 2015. Large caenagnathids (Dinosauria, Oviraptorosauria) from the uppermost Cretaceous of Western Canada. Cretaceous Research 52: 101–107.

Berkovitz, B.K.B., and R.P. Shellis. 2016. The teeth of non-mammalian vertebrates. London: Academic Press.

Berkovitz, B.K.B., and R.P. Shellis. 2018. The teeth of mammalian vertebrates. London: Academic Press.

Bhullar, B.A.S., et al. 2012. Birds have paedomorphic dinosaur skulls. Nature 487: 223–226.

Bhullar, B.A.S., et al. 2015. A molecular mechanism for the origin of a key evolutionary innovation, the bird beak and palate, revealed by an integrative approach to major transitions in vertebrate history. Evolution 69: 1665–1677.

Blanchard, E. 1860. Observations sur le systeme dentaire chez les oiseaux. Comptes Rendus de l'Académie des Sciences 50: 540–542.

Bolt, J.R., and R. Demar. 1975. An explanatory model of the evolution of multiple rows of teeth in *Captorhinus aguti*. Journal of Paleontology 49: 815–832.

Brink, K.S., T. Grieco, and J.M. Richman. 2018. The dynamics of tooth cycling in polyphyodont vertebrates. Journal of Vertebrate Paleontology, Program and Abstracts: 33.

Buchtová, M., et al. 2008. Initiation and patterning of the snake dentition are dependent on Sonic Hedgehog signaling. Developmental Biology 319: 132–145.

Buchtová, M., J. Štembírek, K. Glocová, E. Matalová, and A.S. Tucker. 2012. Early regression of the dental lamina underlies the development of diphyodont dentitions. Journal of Dental Research 91: 491–498.

Buchtová, M., O. Zahradníček, S. Balková, and A.S. Tucker. 2013. Odontogenesis in the Veiled Chameleon (*Chamaeleo calyptratus*). Archives of Oral Biology 58: 118–133.

Chen, Y.P., et al. 2000. Conservation of early odontogenic signaling pathways in Aves. Proceedings of the National Academy of Sciences of the United States of America 97: 10044–10049.

Chiappe, L.M., M.A. Norell, and J.M. Clark. 2001. A new skull of *Gobipteryx minuta* (Aves: Enantiornithes) from the Cretaceous of the Gobi Desert. American Museum Novitates 3346: 1–15.

Chiappe, L.M., et al. 2014. A new specimen of the Early Cretaceous bird *Hongshanornis longicresta*: Insights into the aerodynamics and diet of a basal ornithuromorph. PeerJ 2: e234.

Choiniere, J.N., C.A. Forster, and W.J. de Klerk. 2012. New information on *Nqwebasaurus thwazi*, a coelurosaurian theropod from the Early Cretaceous Kirkwood Formation in South Africa. Journal of African Earth Sciences 71–72: 1–17.

Cifelli, R.L., and C. de Muizon. 1998. Tooth eruption and replacement pattern in early marsupials. Comptes Rendus de l'Académie des Sciences (Series IIA) Earth and Planetary Science 326: 215–220.

Clark, J.M., T. Maryanska, and R. Barsbold. 2004. Therizinosauroidea. *In* D.B. Weishampel, P. Dodson, and H. Osmólska (editors), The Dinosauria: 151–164. Berkeley: University of California Press.

Cobourne, M.T., I. Miletich, and P.T. Sharpe. 2004. Restriction of sonic hedgehog signalling during early tooth development. Development 131: 2875–2885.

Cooper, J.S., D.F.G. Poole, and R. Lawson. 1970. The dentition of agamid lizards with special reference to tooth replacement. Journal of Zoology 162: 85–98.

Cope, E.D. 1867. An account of the extinct reptiles which approached the birds. Proceedings of the Academy of Natural Sciences of Philadelphia 19: 234–235.

Currie, P.J., S.J. Godfrey, and L. Nessov. 1993. New caenagnathid (Dinosauria: Theropoda) specimens from the Upper Cretaceous of North America and Asia. Canadian Journal of Earth Sciences 30: 2255–2272.

Cuvier, G. 1821. Physiologie animale et anatomie. Analyse des Travaux de l'Académie Royale des Sciences, pendant l'année 1821, partie physique: 32–42.

Dames, W. 1884. Über *Archaeopteryx*. Palaeontologische Abhandlungen 2: 119–196.

Darwin, C. 1859. The origin of species by means of natural selection, 1st ed. London: John Murray.

Davit-Béal, T., A.S. Tucker, and J.-Y. Sire. 2009. Loss of teeth and enamel in tetrapods: Fossil record, genetic data and morphological adaptations. Journal of Anatomy 214: 477–501.

de Leon, L.F., E. Bermingham, J. Podos, and A.P. Hendry. 2010. Divergence with gene flow as facilitated by ecological differences: Within-island variation in Darwin's finches. Philosophical Transactions of the Royal Society B, Biological Sciences 365: 1041–1052.

Dilger, W.C. 1957. The loss of teeth in birds. Auk 74: 103–104.

Dosedělová, H., et al. 2015. Fate of the molar dental lamina in the monophyodont mouse. PLoS One 10: e0127543.

Dumont, M., et al. 2016. Synchrotron imaging of dentition provides insights into the biology of *Hesperornis* and *Ichthyornis*, the "last" toothed birds. BMC Evolutionary Biology 16: 178.

Dvorak, L., and J.F. Fallon. 1991. *Talpid*^{2} mutant chick limb has anteroposterior polarity and altered patterns of programmed cell death. Anatomical Record 231: 251–260.

Edmund, A.G. 1960. Tooth replacement phenomena in the lower vertebrates. Royal Ontario Museum Life Sciences Contribution 52.

Edmund, A.G. 1962. Sequence and rate of tooth replacement in the Crocodilia. Royal Ontario Museum Life Sciences Contribution 56: 1–42.

Elzanowski, A. 1976. Palaeognathous bird from the Cretaceous of Central Asia. Nature 264: 51–53.

Elzanowski, A. 1977. Skulls of *Gobipteryx* (Aves) from the Upper Cretaceous of Mongolia. Palaeontologia Polonica 37: 153–166.

Elzanowski, A. 1981. Embryonic bird skeletons from the Late Cretaceous of Mongolia. Palaeontologia Polonica 42: 147–179.

Evans, J. 1865. On portions of a cranium and of a jaw, in the slab containing the fossil remains of *Archaeopteryx*. Natural History Review 5: 415–421.

Feduccia, A. 1999. The origin and evolution of birds, New Haven, CT: Yale University Press.

Field, D.J., et al. 2018. Early evolution of modern birds structured by global forest collapse at the end-cretaceous mass extinction. Current Biology 28: 1825–1831.

Francis-West, P., R. Ladher, A. Barlow, and A. Graveson. 1998. Signalling interactions during facial development. Mechanisms of Development 75: 3–28.

Fraser, G.J., A. Graham, and M.M. Smith. 2006. Developmental and evolutionary origins of the vertebrate dentition: Molecular controls for spatio-temporal organisation of tooth sites in osteichthyans. Journal of Experimental Zoology B, Molecular and Developmental Evolution 306B: 183–203.

Fraser, G.J., et al. 2009. An ancient gene network is co-opted for teeth on old and new jaws. PLoS Biology 7: e1000031.

Fraser, G.J., R. Britz, A. Hall, Z. Johanson, and M.M. Smith. 2012. Replacing the first-generation dentition in pufferfish with a unique beak. Proceedings of the National Academy of Sciences of the United States of America 109: 8179–8184.

Funston, G.F., and P.J. Currie. 2014. A previously undescribed caenagnathid mandible from the Late Campanian of Alberta, and insights into the diet of *Chirostenotes pergracilis* (Dinosauria: Oviraptorosauria). Canadian Journal of Earth Sciences 51: 156–165.

Funston, G.F. et al. 2020. Histology of caenagnathid (Theropoda, Oviraptorosauria) dentaries and implications for development, ontogenetic edentulism, and taxonomy. Anatomical Record 303: 918–934.

Gao, C.L., et al. 2012. A subadult specimen of the Early Cretaceous bird *Sapeornis chaoyangensis* and a taxonomic reassessment of sapeornithids. Journal of Vertebrate Paleontology 32: 1103–1112.

Gardiner, E.G. 1884. Beiträge zur Kenntniss des Epitrichiums und der Bildung des Vogelschnabels. Archiv für Mikroskop. Anatomie 24: 289–338.

Gegenbaur, K. 1863. Vergleichend-anatomische Bemerkungen über das Fußskelet der Vögel. Archiv für Anatomie, Physiologie und Wissenschaftliche Medicin 1863: 450–472.

Genbrugge, A., et al. 2011. Ontogeny of the cranial skeleton in a Darwin's finch (*Geospiza fortis*). Journal of Anatomy 219: 115–131.

Gill, F.B. 2006. Ornithology, 3rd ed. New York: W. H. Freeman.

Green, H.L.H.H. 1937. The development and morphology of the teeth of *Ornithorhynchus*. Philosophical Transactions of the Royal Society of London B, Biological Sciences 228: 367–420.

Hanai, T., and T. Tsuihiji. 2019. Description of tooth ontogeny and replacement patterns in a juvenile *Tarbosaurus bataar* (Dinosauria: Theropoda) using CT-scan data. Anatomical Record 302: 1210–1225.

Harris, M.P., S.M. Hasso, M.W.J. Ferguson, and J.F. Fallon. 2006. The development of archosaurian first-generation teeth in a chicken mutant. Current Biology 16: 371–377.

Harrison, H.S. 1901 The development and succession of teeth in *Hatteria punctata*. Quarterly Journal of Microscopical Science 44: 161–219.

He, Y., P.J. Makovicky, X. Xu, and H. You. 2018. High-resolution computed tomographic analysis of tooth replacement pattern of the basal neoceratopsian *Liaoceratops yanzigouensis* informs ceratopsian dental evolution. Scientific Reports 8: 5870.

Heers, A.M., J.W. Rankin, and J.R. Hutchinson. 2018. Building a bird: Musculoskeletal modeling and simulation of wing-assisted incline running during avian ontogeny. Frontiers in Bioengineering and Biotechnology 6: 140.

Heilmann, G. 1927. The origin of birds, London: D. Appleton.

Helms, J.A., and R.A. Schneider. 2003. Cranial skeletal biology. Nature 423: 326–331.

Hieronymus, T.L., and L.M. Witmer. 2010. Homology and evolution of avian compound rhamphothecae. Auk 127: 590–604.

Howgate, M.E. 1984. The teeth of *Archaeopteryx* and a reinterpretation of the Eichstätt specimen. Zoological Journal of the Linnean Society 82: 654–660.

Hu, H., J.K. O'Connor, and Z.H. Zhou. 2015. A new species of Pengornithidae (Aves: Enantiornithes) from the Lower Cretaceous of China suggests a specialized scansorial habitat previously unknown in early birds. PLoS One 10: e0126791.

Hu, X., et al. 2012. Noggin is required for early development of murine upper incisors. Journal of Dental Research 91: 394–400.

Huxley, T.H. 1868. On the animals which are most nearly intermediate between birds and reptiles. Annals & Magazine of Natural History 2: 66–75.

Huxley, T.H. 1870. Further evidence of the affinity between the dinosaurian reptiles and birds. Quarterly Journal of the Geological Society 26: 12–31.

Huysseune, A. 2006. Formation of a successional dental lamina in the zebrafish (*Danio rerio*): support for a local control of replacement tooth initiation. International Journal of Developmental Biology 50: 637–643.

Huysseune, A., and J.-Y. Sire. 1998. Evolution of patterns and processes in teeth and tooth-related tissues in non-mammalian vertebrates. European Journal of Oral Sciences 106 (Suppl. 1): 437–481.

Huysseune, A., and I. Thesleff. 2004. Continuous tooth replacement: The possible involvement of epithelial stem cells. Bioessays 26: 665–671.

Järvinen, E., M. Tummers, and I. Thesleff. 2009. The role of the dental lamina in mammalian tooth replacement. Journal of Experimental Zoology B, Molecular and Developmental Evolution 312B: 281–291.

Jernvall, J., and I. Thesleff. 2012. Tooth shape formation and tooth renewal: Evolving with the same signals. Development 139 (19): 3487–3497.

Jernvall, J., S.V.E. Keränen, and I. Thesleff. 2000. Evolutionary modification of development in mammalian teeth: Quantifying gene expression patterns and topography. Proceedings of the National Academy of Sciences of the United States of America 97: 14444–14448.

Ji, Q., P.J. Currie, M.A. Norell, and S.A. Ji. 1998. Two feathered dinosaurs from northeastern China. Nature 393: 753–761.

Ji, Q., L.M. Chiappe, and S.A. Ji. 1999. A new Late Mesozoic confuciusornithid bird from China. Journal of Vertebrate Paleontology 19: 1–7.

Ji, Q., et al. 2002. Discovery of an avialae bird – *Shenzhouraptor sinensis* gen. et sp. nov – from China. Geological Bulletin of China 21: 363–369.

Ji, Q., et al. 2003 An early ostrich dinosaur and implications for ornithomimosaur phylogeny. American Museum Novitates 3420: 1–19.

Ji, Q., J.C. Lü, X.F. Wei, and X.R. Wang. 2012. A new oviraptorosaur from the Yixian Formation of Jianchang, Western Liaoning Province, China. Geological Bulletin of China 31: 2102–2107.

Jussila, M., and I. Thesleff. 2012. Signaling networks regulating tooth organogenesis and regeneration, and the specification of dental mesenchymal and epithelial cell lineages. Cold Spring Harbor Perspectives in Biology 4: a008425.

Jussila, M., X. Crespo Yanez, and I. Thesleff. 2014. Initiation of teeth from the dental lamina in the ferret. Differentiation 87: 32–43.

Kaye, T.G., et al. 2019. Fully fledged enantiornithine hatchling revealed by Laser-Stimulated Fluorescence supports precocial nesting behavior. Scientific Reports 9: 5006.

Kobayashi, Y., and R. Barsbold. 2005. Anatomy of *Harpymimus okladnikovi* Barsbold and Perle 1984 (Dinosauria, Theropoda) of Mongolia. *In* Carpenter, K. (editor) The carnivorous dinosaurs: 97–126. Indianapolis: Indiana University Press.

Kobayashi, Y., and J.C. Lü. 2003. A new ornithomimid dinosaur with gregarious habits from the Late Cretaceous of China. Acta Palaeontologia Polonica 48: 235–259.

Kobayashi, Y., et al. 1999. Palaeobiology: Herbivorous diet in an ornithomimid dinosaur. Nature 402: 480–481.

Kollar, E., and C. Fisher. 1980. Tooth induction in chick epithelium: expression of quiescent genes for enamel synthesis. Science 207: 993–995.

Kundrát, M., A.R.I. Cruickshank, T.W. Manning, and J. Nudds. 2008. Embryos of therizinosauroid theropods from the Upper Cretaceous of China: diagnosis and analysis of ossification patterns. Acta Zoologica 89: 231–251.

Kurochkin, E.N., S. Chatterjee, and K.E. Mikhailov. 2013. An embryonic enantiornithine bird and associated eggs from the Cretaceous of Mongolia. Paleontological Journal 47: 1252–1269.

Lamanna, M.C., H.-D. Sues, E.R. Schachner, and T.R. Lyson. 2014. A new large-bodied oviraptorosaurian theropod dinosaur from the Latest Cretaceous of western North America. PLoS One 9: e92022.

Lamichhaney, S., et al. 2015. Evolution of Darwin's finches and their beaks revealed by genome sequencing. Nature 518: 371–375.

Lamichhaney, S., et al. 2016. A beak size locus in Darwin's finches facilitated character displacement during a drought. Science 352: 470–474.

Larson, D.W., C.M. Brown, and D.C. Evans. 2016. Dental disparity and ecological stability in bird-like dinosaurs prior to the end-Cretaceous mass extinction. Current Biology 26: 1325–1333.

Lautenschlager, S., L.M. Witmer, P. Altangerel, and E.J. Rayfield. 2013. Edentulism, beaks, and biomechanical innovations in the evolution of theropod dinosaurs. Proceedings of the National Academy of Sciences of the United States of America 110: 20657–20662.

Lee, Y.-N., et al. 2014a. Resolving the long-standing enigmas of a giant ornithomimosaur *Deinocheirus mirificus*. Nature 515: 257–260.

Lee, M.S.Y., A. Cau, D. Naish, and G.J. Dyke. 2014b. Sustained miniaturization and anatomical innovation in the dinosaurian ancestors of birds. Science 345: 562–566.

Li, C., X.C. Wu, O. Rieppel, L.T. Wang, and L.J Zhao. 2008. An ancestral turtle from the Late Triassic of southwestern China. Nature 456: 497.

Li, C., N.C. Fraser, O. Rieppel, and X.C. Wu. 2018. A Triassic stem turtle with an edentulous beak. Nature 560: 476–479.

Li, L., J.Q. Wang, X. Zhang, and S.L. Hou. 2012. A new enantiornithine bird from the Lower Cretaceous Jiufotang Formation in Jinzhou Area, western Liaoning Province, China. Acta Geologica Sinica - English Edition 86: 1039–1044.

Li, Z.H., Z.H. Zhou, M. Wang, and J.A. Clarke. 2014. A new specimen of large-bodied basal Enantiornithine *Bohaiornis* from the Early Cretaceous of China and the inference of feeding ecology in Mesozoic birds. Journal of Paleontology 88: 99–108.

Liu, D., et al. 2014. An advanced, new long-legged bird from the Early Cretaceous of the Jehol Group (northeastern China): Insights into the temporal divergence of modern birds. Zootaxa 3884: 253–266.

Longrich, N.R., K. Barnes, S. Clark, and L. Millar. 2013. Caenagnathidae from the Upper Campanian Aguja Formation of West Texas, and a revision of the Caenagnathinae. Bulletin of the Peabody Museum of Natural History 54: 23–49.

Louchart, A., and L. Viriot. 2011. From snout to beak: The loss of teeth in birds. Trends in Ecology and Evolution 26: 663–673.

Luo, Z.X., Z. Kielan-Jaworowska, and R.L. Cifelli. 2004. Evolution of dental replacement in mammals. Bulletin of Carnegie Museum of Natural History 36: 159–175.

Makovicky, P.J., Y. Kobayashi, and P.J. Currie. 2004. Ornithomimosauria. *In* D.B. Weishampel, P. Dodson, and H. Osmólska (editors), The Dinosauria: 137–150. Berkeley: University of California Press.

Mallarino, R., et al. 2011. Two developmental modules establish 3D beak-shape variation in Darwin's finches. Proceedings of the National Academy of Sciences of the United States of America 108: 4057–4062.

Manger, P.R., L.S. Hall, and J.D. Pettigrew. 1998. The development of the external features of the platypus (*Ornithorhynchus anatinus*). Philosophical Transactions of the Royal Society of London B, Biological Sciences 353: 1115–1125.

Marsh, O.C. 1872a. Notice of a new reptile from the Cretaceous. American Journal of Science 4: 406.

Marsh, O.C. 1872b. Notice of a new and remarable fossil bird. American Journal of Science 4: 344.

Marsh, O.C. 1875. Odontornithes, or birds with teeth. American Naturalist 9: 625–631.

Martin, L.D., and J.D. Stewart. 1977. Teeth in *Ichthyornis* (Class: Aves). Science 195: 1331–1332.

Martin, L.D., and Z.H. Zhou. 1997. *Archaeopteryx*-like skull in Enantiornithine bird. Nature 389: 556.

Mayr, G., and D. Rubilar-Rogers. 2010. Osteology of a new giant bony-toothed bird from the Miocene of Chile, with a revision of the taxonomy of neogene pelagornithidae. Journal of Vertebrate Paleontology 30: 1313–1330.

Meredith, R.W., G.J. Zhang, M.T.P. Gilbert, E.D. Jarvis, and M.S. Springer. 2014. Evidence for a single loss of mineralized teeth in the common avian ancestor. Science 346: 1254390.

Miller, W.A., and C.J.P. Radnor. 1970. Tooth replacement patterns in young *Caiman sclerops*. Journal of Morphology 130: 501–509.

Mitsiadis, T.A., Y. Chéraud, P. Sharpe, and J. Fontaine-Pérus. 2003. Development of teeth in chick embryos after mouse neural crest transplantations. Proceedings of the National Academy of Sciences of the United States of America 100: 6541–6545.

Mochizuki, K., and S. Fujui. 1983. Development and replacement of upper jaw teeth in gobiid fish, *Sicyopterus japonicus*. Japanese Journal of Ichthyology 30: 27–36.

Musser, A.M., and M. Archer. 1998. New information about the skull and dentary of the Miocene platypus *Obdurodon dicksoni*, and a discussion of ornithorhynchid relationships. Philosophical Transactions of the Royal Society of London B, Biological Sciences 353: 1063–1079.

Nopcsa, F. 1907 Ideas on the origin of flight. Proceedings of the Zoological Society of London: 223–238.

Norell, M.A., et al. 1994. A theropod dinosaur embryo and the affinities of the flaming cliffs dinosaur eggs. Science 266: 779–782.

Norell, M.A., P.J. Makovicky, and P.J. Currie. 2001a. The beaks of ostrich dinosaurs. Nature 412: 873–874.

Norell, M.A., J.M. Clark, and L.M. Chiappe. 2001b. An embryonic oviraptorid (Dinosauria: Theropoda) from the Upper Cretaceous of Mongolia. American Museum Novitates 3315: 1–17.

O'Connor, J.K., and G. Dyke. 2010. A reassessment of *Sinornis santensis* and *Cathayornis yandica* (Aves: Enantiornithes). Records of the Australian Museum 62: 7–20.

O'Connor, J.K., et al. 2009. Phylogenetic support for a specialized clade of Cretaceous enantiornithine birds with information from a new species. Journal of Vertebrate Paleontology 29: 188–204.

O'Connor, J.K., K.Q. Gao, and L.M. Chiappe. 2010. A new ornithuromorph (Aves: Ornithothoraces) bird from the Jehol Group indicative of higher-level diversity. Journal of Vertebrate Paleontology 30: 311–321.

O'Connor, J.K., C.K. Sun, X. Xu, X.L. Wang, and Z.H. Zhou. 2012. A new species of *Jeholornis* with complete caudal integument. Historical Biology 24: 29–41.

O'Connor, J.K., et al. 2016. An enantiornithine with a fan-shaped tail, and the evolution of the rectricial complex in early birds. Current Biology 26: 114–119.

O'Connor, J.K., et al. 2018. First report of gastroliths in the Early Cretaceous basal bird *Jeholornis*. Cretaceous Research 84: 200–208.

Osborn, J.W. 1970. New approach to Zahnreihen. Nature 225: 343–346.

Osborn, J.W. 1971. The ontogeny of tooth succession in *Lacerta vivipara* Jacquin (1787). Proceedings of the Royal Society of London B, Biological Sciences 179: 261–289.

Osborn, J.W. 1977. The interpretation of patterns in dentitions. Biological Journal of the Linnean Society 9: 217–229.

Osmólska, H., P.J. Currie, and R. Barsbold. 2004. Oviraptorosauria. *In* D.B. Weishampel, P. Dodson, and H. Osmólska (editors), The Dinosauria: 165–183. Berkeley: University of California Press.

Owen, R. 1863a. III. On the *Archeopteryx* of von Meyer, with a description of the fossil remains of a long-tailed species, from the lithographic stone of Solenhofen. Philosophical Transactions of the Royal Society of London 153: 33–47.

Owen, R. 1863b. On the fossil remains of a long-tailed bird (*Archeopteryx macrurus* Ow.) from the lithographic slate of Solenhofen. Proceedings of the Royal Society of London 12: 272–273.

Perez-Moreno, B.P., et al. 1994. A unique multitoothed ornithomimosaur dinosaur from the Lower Cretaceous of Spain. Nature 370: 363–367.

Peteya, J.A., J.A. Clarke, Q.G. Li, K.Q. Gao, and M.D. Shawkey. 2017. The plumage and colouration of an enantiornithine bird from the Early Cretaceous of China. Palaeontology 60: 55–71.

Peyer, B. 1968. Comparative odontology. Chicago: University of Chicago Press.

Podos, J., and S. Nowicki. 2004. Beaks, adaptation, and vocal evolution in Darwin's finches. BioScience 54: 501–510.

Psujek, S., and R.D. Beer. 2008. Developmental bias in evolution: evolutionary accessibility of phenotypes in a model evo-devo system. Evolution and Development 10: 375–390.

Pu, H.Y., et al. 2013a. An unusual basal therizinosaur dinosaur with an ornithischian dental arrangement from northeastern China. PLoS One 8: e63423.

Pu, H.Y., et al. 2013b. A new juvenile specimen of *Sapeornis* (Pygostylia: Aves) from the Lower Cretaceous of northeast China and allometric scaling of this basal bird. Paleontological Research 17: 27–38.

Rhodin, A.G.J., et al. 2017. Turtles of the world-annotated ckecklist and atlas of taxonomy, synonymy, distribution, and conservation status (8th ed.). Chelonian Research Monographs 7: 1–291.

Richman, J.M., and G.R. Handrigan. 2011. Reptilian tooth development. Genesis 49: 247–260.

Richman, J.M., and S.H. Lee. 2003. About face: Signals and genes controlling jaw patterning and identity in vertebrates. BioEssays 25: 554–568.

Romanoff, A.L. 1960. The avian embryo: structural and functional development. New York: Macmillan Company.

Röse, C. 1893a. Über die zahnentwicklung der Krokodile. Gegenbaurs Morphologisches Jahrbuch 3: 195–228.

Röse, C. 1893b. Über die Zahnentwicklung von *Chamaeleon*. Anatomischer Anzeiger 9: 439–451.

Rougier, G.W., J.R. Wible, and M.J. Novacek. 1998. Implications of *Deltatheridium* specimens for early marsupial history. Nature 396: 459–463.

Sanz, J.L., et al. 1997. A nestling bird from the Lower Cretaceous of Spain: implications for avian skull and neck evolution. Science 276: 1543–1546.

Schneider, R.A., and J.A. Helms. 2003. The cellular and molecular origins of beak morphology. Science 299: 565–568.

Seeley, H.G. 1901. Dragons of the air: An account of extinct flying reptiles. New York: D. Appleton & Methuen.

Sire, J.-Y., S.C. Delgado, and M. Girondot. 2008. Hen's teeth with enamel cap: from dream to impossibility. BMC Evolutionary Biology 8: 246.

Smith, M.M., G.J. Fraser, and T.A. Mitsiadis. 2009. Dental lamina as source of odontogenic stem cells: evolutionary origins and developmental control of tooth generation in gnathostomes. Journal of Experimental Zoology B, Molecular and Developmental Evolution 312B: 260–280.

St. Hilarie, G. 1821. Sur le system dentaire des oiseaux. Annales Generales des Sciences Physiques 8: 373–380.

Streelman, J.T., J.F. Webb, R.C. Albertson, and T.D. Kocher. 2003. The cusp of evolution and development: a model of cichlid tooth shape diversity. Evolution and Development 5: 600–608.

Temeles, E.J., J.S. Miller, and J.L. Rifkin. 2010. Evolution of sexual dimorphism in bill size and shape of hermit hummingbirds (Phaethornithinae): A role for ecological causation. Philosophical Transactions of the Royal Society of London B, Biological Sciences 365: 1053–1063.

Thesleff, I. 2003. Epithelial-mesenchymal signalling regulating tooth morphogenesis. Journal of Cell Science 116: 1647–1648.

Thomas, O. 1889. On the dentition of *Ornithorhynchus*. Proceedings of the Royal Society of London 46: 126–131.

Tsai, S., et al. 2016. The molecular circuit regulating tooth development in crocodilians. Journal of Dental Research 95: 1501–1510.

Tsuihiji, T., M. Watabe, R. Barsbold, and K. Tsogtbaatar. 2015. A gigantic caenagnathid oviraptorosaurian (Dinosauria: Theropoda) from the Upper Cretaceous of the Gobi Desert, Mongolia. Cretaceous Research 56: 60–65.

Tsuihiji, T., M. Watabe, K. Tsogtbaatar, and R. Barsbold. 2016. Dentaries of a caenagnathid (Dinosauria: Theropoda) from the Nemegt Formation of the Gobi Desert in Mongolia. Cretaceous Research 63: 148–153.

Vogel, P., et al. 2014. Malformation of incisor teeth in *Grem2*$^{-/-}$ mice. Veterinary Pathology 52: 224–229.

von Meyer, H. 1861. Vogel-Feder und *Palpipes priscus* von Solenhofen. Neues Jahrbuch für Mineralogie, Geognosie, Geologie und Petrefakten-Kunde 1861: 561.

von Meyer, H. 1862. *Archaeopteryx lithographica* aus dem lithographischen Schiefer von Solnhofen. Palaeontographica 10: 53–56.

Wang, M., and D. Liu. 2016. Taxonomical reappraisal of Cathayornithidae (Aves: Enantiornithes). Journal of Systematic Palaeontology 14: 29–47.

Wang, M., J.K. O'Connor, S. Zhou, and Z.H. Zhou. 2019. New toothed early cretaceous ornithuromorph bird reveals intraclade diversity in pattern of tooth loss. Journal of Systematic Palaeontology: 1-15.

Wang, M., and Z.H. Zhou. 2016. A new adult specimen of the basalmost ornithuromorph bird *Archaeorhynchus spathula* (Aves: Ornithuromorpha) and its implications for early avian ontogeny. Journal of Systematic Palaeontology 14: 1–18.

Wang, M., and Z.H. Zhou. 2018. A new confuciusornithid (Aves: Pygostylia) from the Early Cretaceous increases the morphological disparity of the Confuciusornithidae. Zoological Journal of the Linnean Society 28: 1–14.

Wang, M., Z.H. Zhou, J.K. O'Connor, and N.V. Zelenkov. 2014b. A new diverse enantiornithine family (Bohaiornithidae fam. nov.) from the Lower Cretaceous of China with information from two new species. Vertebrata PalAsiatica 52: 31–76.

Wang, S., Q.Y. Zhang, and R. Yang. 2018. Reevaluation of the dentary structures of caenagnathid oviraptorosaurs (Dinosauria, Theropoda). Scientific Reports 8: 391.

Wang, S., S.K. Zhang, C. Sullivan, and X. Xu. 2016. Elongatoolithid eggs containing oviraptorid (Theropoda, Oviraptorosauria) embryos from the Upper Cretaceous of southern China. BMC Evolutionary Biology 16: 67.

Wang, S., et al. 2017a. Heterochronic truncation of odontogenesis in theropod dinosaurs provides insight into the macroevolution of avian beaks. Proceedings of the National Academy of Sciences of the United States of America 114: 10930–10935.

Wang, S., et al. 2017b. Extreme ontogenetic changes in a ceratosaurian theropod. Current Biology 27: 144–147.

Wang, X.L., and Z.H. Zhou. 2004. Pterosaur embryo from the Early Cretaceous. Nature 429: 621.

Wang, X.L., et al. 2014a. Insights into the evolution of rachis dominated tail feathers from a new basal enantiornithine (Aves: Ornithothoraces). Biological Journal of the Linnean Society 113: 805–819.

Wang, Y., et al. 2017c. A previously undescribed specimen reveals new information on the dentition of *Sapeornis chaoyangensis*. Cretaceous Research 74: 1–10.

Wang, X.L., et al. 2017d. Egg accumulation with 3D embryos provides insight into the life history of a pterosaur. Science 358: 1197–1201.

Watabe, M., D. Weishampel, R. Barsbold, K. Tsogtbataar, and S. Suzuki. 2000. New nearly complete skeleton of the bird-like theropod, *Avimimus*, from the Upper Cretaceous of the Gobi Desert, Mongolia. Journal of Vertebrate Paleontology 20: 77A.

Wellnhofer, P. 2009. *Archaeopteryx*: The icon of evolution, München: Verlag Dr. Friedrich Pfeil.

Wellnhofer, P. 2010. A short history of research on *Archaeopteryx* and its relationship with dinosaurs. *In* R.T.J. Moody, E. Buffetaut, D. Naish, and D.M. Martill (editors), Dinosaurs and other extinct saurians: a historical perspective: London: Geological Society Publishing House.

Westergaard, B., and M.W.J. Ferguson. 1987. Development of the dentition in *Alligator mississippiensis*. Later development in the lower jaws of embryos, hatchlings and young juveniles. Journal of Zoology 212: 191–222.

Westergaard, B., and M.W.J. Ferguson. 1990. Development of the dentition in *Alligator mississippiensis*: Upper jaw dental and craniofacial development in embryos, hatchlings, and young juveniles, with a comparison to lower jaw development. American Journal of Anatomy 187: 393–421.

Whitlock, J.A., and J.M. Richman. 2013. Biology of tooth replacement in amniotes. International Journal of Oral Science 5: 66–70.

Woerdeman, M.W. 1919a. Beiträge zur Entwicklungsgeschichte von Zähnen und Gebiss der Reptilien. I. Die Anlage und Entwicklung des embryonalen Gebisses als ganzes und seine Beziehung zur Zahnleiste. Archiv für Mikroskopische Anatomie 92: 104–182.

Woerdeman, M.W. 1919b. Beiträge zur Entwicklungsgeschichte von Zahnen und Gebiss der Reptilien. II. Ueber die Anlage des Ersatzgebisses und den Zahnwechsel (distichie- und matrix-Theorie). Archiv für Mikroskopische Anatomie 92: 183–230.

Woerdeman, M.W. 1921a. Beiträge zur Entwicklungsgeschichte von Zähnen und Gebiss der Reptilien. Beiträge V. Uëber der Mundhöhlendrüsen zum Zahnsystem. Archiv für Mikroskopische Anatomie 95: 396–413.

Woerdeman, M.W. 1921b. Beiträge zur Entwicklungsgeschichte von Zähnen und Gebiss der Reptilien. Beiträge IV. Uëber die Anlage und Ersatzgebiss der Zähnen. Archiv für Mikroskopische Anatomie 95: 265–395.

Wu, P., T.X. Jiang, S. Suksaweang, R.B. Widelitz, and C.M. Chuong. 2004a. Molecular shaping of the beak. Science 305: 1465–1466.

Wu, P., et al. 2004b. Evo-devo of amniote integuments and appendages. International Journal of Developmental Biology 48: 249–270.

Wu, P., T.X. Jiang, J.Y. Shen, R.B. Widelitz, and C.M. Chuong. 2006. Morphoregulation of avian beaks: Comparative mapping of growth zone activities and morphological evolution. Developmental Dynamics 235: 1400–1412.

Wu, P., et al. 2013. Specialized stem cell niche enables repetitive renewal of alligator teeth. Proceedings of the National Academy of Sciences of the United States of America 110: E2009–2018.

Wu, P., et al. 2015. Topographical mapping of α- and β-keratins on developing chicken skin integuments: functional interaction and evolutionary perspectives. Proceedings of the National Academy of Sciences of the United States of America 112: E6770–E6779.

Xing, L.D., et al. 2017. A mid-Cretaceous enantiornithine (Aves) hatchling preserved in Burmese amber with unusual plumage. Gondwana Research 49: 264–277.

Xu, X., X.J. Zhao, and J.M. Clark. 2001. A new therizinosaur from the Lower Jurassic Lower Lufeng Formation of Yunnan, China. Journal of Vertebrate Paleontology 21: 477–483.

Xu, X., Y.N. Cheng, X.L. Wang, and C.H. Chang. 2002. An unusual oviraptorosaurian dinosaur from China. Nature 419: 291–293.

Xu, X., Q.W. Tan, J.M. Wang, X.J. Zhao, and L. Tan. 2007. A gigantic bird-like dinosaur from the Late Cretaceous of China. Nature 447: 844–847.

Xu, X., et al. 2015. A bizarre Jurassic maniraptoran theropod with preserved evidence of membranous wings. Nature 521: 70–73.

Yang, T.R., and P.M. Sander. 2018. The origin of the bird's beak: New insights from dinosaur incubation periods. Biology Letters 14: 20180090.

Yao, X., et al. 2015. *Caenagnathasia* sp. (Theropoda: Oviraptorosauria) from the Iren Dabasu Formation (Upper Cretaceous: Campanian) of Erenhot, Nei Mongol, China. Vertebrata PalAsiatica 53: 291–298.

Zahradnicek, O., I. Horacek, and A.S. Tucker. 2012. Tooth development in a model reptile: Functional and null generation teeth in the gecko *Paroedura picta*. Journal of Anatomy 221: 195–208.

Zanno, L.E. 2010. Osteology of *Falcarius utahensis* (Dinosauria: Theropoda): Characterizing the anatomy of basal therizinosaurs. Zoological Journal of the Linnean Society 158 (1): 196–230.

Zanno, L.E., and P.J. Makovicky. 2011. Herbivorous ecomorphology and specialization patterns in theropod dinosaur evolution. Proceedings of the National Academy of Sciences of the United States of America 108: 232–237.

Zhang, F.C., Z.H. Zhou, L.H. Hou, and G. Gu. 2001. Early diversification of birds: evidence from a new opposite bird. Chinese Science Bulletin 46: 945–949.

Zhang, F.C., Z.H. Zhou, X. Xu, and X.L. Wang. 2002. A juvenile coelurosaurian theropod from China indicates arboreal habits. Naturwissenschaften 89: 392–398.

Zhang, F.C., Z.H. Zhou, X. Xu, X.L. Wang, and C. Sullivan. 2008a. A bizarre Jurassic maniraptoran from China with elongate ribbon-like feathers. Nature 455: 1105.

Zhang, F.C., Z.H. Zhou, and M.J. Benton. 2008b. A primitive confuciusornithid bird from China and its implications for early avian flight. Science in China Series D: Earth Sciences 51: 625–639.

Zheng, X.T., et al. 2011. Fossil evidence of avian crops from the Early Cretaceous of China. Proceedings of the National Academy of Sciences of the United States of America 108: 15904–15907.

Zheng, X.T., et al. 2014. New specimens of *Yanornis* indicate a piscivorous diet and modern alimentary canal. PLoS One 9: e95036–e95036.

Zheng, X.T., J.K. O'Connor, X.L. Wang, Y. Wang, and Z. Zhou. 2018. Reinterpretation of a previously described Jehol bird clarifies early trophic evolution in the Ornithuromorpha. Proceedings of the Royal Society B, Biological Sciences 285: 20172494.

Zhou, S., Z.H. Zhou, and J.K. O'Connor. 2012 A new basal beaked ornithurine bird from the Lower Cretaceous of Western Liaoning, China. Vertebrata PalAsiatica 50: 9–24.

Zhou, S., Z.H. Zhou, and J.K. O'Connor. 2013. Anatomy of the basal ornithuromorph bird *Archaeorhynchus spathula* from the Early Cretaceous of Liaoning, China. Journal of Vertebrate Paleontology 33: 141–152.

Zhou, S., J.K. O'Connor, and M. Wang. 2014. A new species from an ornithuromorph (Aves: Ornithothoraces) dominated locality of the Jehol Biota. Chinese Science Bulletin 59: 5366–5378.

Zhou, Y.C. 2015. Teeth morphology, teeth weight and dentition morphology of Mesozoic birds. Master's thesis, University of Chinese Academy of Sciences, Beijing.

Zhou, Y.C., C. Sullivan, and F.C. Zhang. 2019. Negligible effect of tooth reduction on body mass in Mesozoic birds. Vertebrata PalAsiatica 57: 38-50.

Zhou, Z.H., and L.D. Martin. 2011. Distribution of the predentary bone in Mesozoic ornithurine birds. Journal of Systematic Palaeontology 9: 25–31.

Zhou, Z.H., and F.C. Zhang. 2001. Two new ornithurine birds from the Early Cretaceous of western Liaoning, China. Chinese Science Bulletin 46: 1258–1264.

Zhou, Z.H., and F.C. Zhang. 2002. A long-tailed, seed-eating bird from the Early Cretaceous of China. Nature 418: 405–409.

Zhou, Z.H., and F.C. Zhang. 2003b. Anatomy of the primitive bird *Sapeornis chaoyangensis* from the Early Cretaceous of Liaoning, China. Canadian Journal of Earth Sciences 40: 731–747.

Zhou, Z.H., and F.C. Zhang. 2003a. *Jeholornis* compared to *Archaeopteryx*, with a new understanding of the earliest avian evolution. Naturwissenschaften 90: 220–225.

Zhou, Z.H., and F.C. Zhang. 2004. A precocial avian embryo from the Lower Cretaceous of China. Science 306: 653–653.

Zhou, Z.H., and F.C. Zhang. 2006. A beaked basal ornithurine bird (Aves, Ornithurae) from the Lower Cretaceous of China. Zoologica Scripta 35: 363–373.

Zhou, Z.H., X.L. Wang, F.C. Zhang, and X. Xu. 2000. Important features of *Caudipteryx*—evidence from two nearly complete new specimens. Vertebrata PalAsiatica 38: 241–254.

Zhou, Z.H, F.C. Zhang, and Z.H. Li. 2009. A new Lower Cretaceous bird from China and tooth reduction in early avian evolution. Proceedings of the Royal Society B, Biological Sciences 277: 219–227.

Ziegler, A.C. 1971. A theory of the evolution of therian dental formulas and replacement patterns. Quarterly Review of Biology 46: 226-249.

Chapter 8

Functional Morphology of the Oviraptorosaurian and Scansoriopterygid Skull

WAISUM MA,[1] MICHAEL PITTMAN,[2] STEPHAN LAUTENSCHLAGER,[1]
LUKE E. MEADE,[1] AND XING XU[3]

ABSTRACT

Oviraptorosauria and Scansoriopterygidae are theropod clades that include members suggested to have partially or fully herbivorous diets. Obligate herbivory and carnivory are two ends of the spectrum of dietary habits along which it is unclear how diet within these two clades might have varied. Clarifying their diet is important as it helps understanding of dietary evolution close to the dinosaur-bird transition. Here, diets are investigated by conventional comparative anatomy, as well as measuring mandibular characteristics that are plausibly indicative of the animal's feeding habit, with reference to modern herbivores that may also have nonherbivorous ancestry. In general, the skulls of scansoriopterygids appear less adapted to herbivory compared with those of oviraptorids because they have a lower dorsoventral height, a smaller lateral temporal fenestra, and a smaller jaw-closing mechanical advantage and they lack a tall coronoid process prominence. The results show that oviraptorid mandibles are more adapted to herbivory than those of caenagnathids, early-diverging oviraptorosaurians and scansoriopterygids. It is notable that some caenagnathids possess features like an extremely small articular offset, and low average mandibular height may imply a more carnivorous diet than the higher ones of other oviraptorosaurians. Our study provides a new perspective to evaluate different hypotheses on the diets of scansoriopterygids and oviraptorosaurians, and demonstrates the high dietary complexity among early-diverging pennaraptorans.

INTRODUCTION

Scansoriopterygidae is a clade of theropod dinosaurs only known from the Middle to Late Jurassic Haifanggou/Jiulongshan Formation (Zhang et al., 2002, 2008) and Tiaojishan Formation (Xu et al., 2015) of China. To date, only four species of scansoriopterygids have been reported: *Ambopteryx longibrachium* (Wang et al., 2019), *Epidendrosaurus ninchengensis* (Zhang et al., 2002), *Epidexipteryx hui* (Zhang et al., 2008) and *Yi qi* (Xu et al., 2015). The most iconic feature of scansoriopterygids is perhaps their elongated third manual digit (Czerkas and Yuan, 2002; Zhang et al., 2002, 2008; Xu et al., 2015). It is generally thought that scansoriopterygids had an arboreal lifestyle (Zhang et al., 2002). *Yi* even possesses a rodlike bone extending from its forelimbs, believed to have sup-

---

[1] School of Geography, Earth and Environmental Sciences, University of Birmingham, Birmingham, U.K.
[2] Vertebrate Palaeontology Laboratory, Division of Earth and Planetary Science, the University of Hong Kong, Hong Kong.
[3] Key Laboratory of Vertebrate Evolution and Human Origins, Institute of Vertebrate Paleontology & Paleoanthropology, Beijing; and CAS Center for Excellence in Life and Paleoenvironment, Beijing.

ported membranous wings, the only example among theropods (Xu et al., 2015). Despite having a bizarre body plan, scansoriopterygids share a number of cranial and postcranial osteological similarities with the theropod clades Oviraptorosauria and Avialae (Zhang et al., 2008; O'Connor and Sullivan, 2014). However, the phylogenetic placement of Scansoriopterygidae within Pennaraptora has been contentious: it has been placed at the base of Avialae (O'Connor and Sullivan, 2014) and as an early-diverging lineage within Oviraptorosauria (Agnolín and Novas, 2013; Brusatte et al., 2014; Pei et al., in press). Following the discovery of *Yi*, Scansoriopterygidae has also been recovered as a separate clade from Avialae and Oviraptorosauria, situated at the base of Paraves (Xu et al., 2015, 2017). However, this proposal involves a polytomy between Scansoriopterygidae, Avialae and Deinonychosauria (Xu et al., 2017).

Despite the unique osteology of scansoriopterygids and their importance in understanding the origins of birds and flight, the functional morphology of their skulls has yet to be studied in depth. Only *Epidexipteryx* and *Yi* preserve an articulated skull in lateral view (Zhang et al., 2008; Xu et al., 2015) and all scansoriopterygid fossils are preserved as fossil slabs (Czerkas and Yuan, 2002; Zhang et al., 2002, 2008; Xu et al., 2015) making three-dimensional modeling work difficult. Even for clades like Oviraptorosauria that have a number of taxa preserved in three dimensions, using these methods is still challenging as the sample size is heavily limited by time constraints and logistical difficulties associated with obtaining and restoring 3D models. Thus, analysis requiring 2D data is currently the most tenable for the study of cranial functional morphology in known scansoriopterygid specimens.

Scansoriopterygids and early-diverging oviraptorosaurians do not show obvious adaptations to either obligate herbivory or obligate carnivory, which has meant that their inferred diets remain controversial. The heavy-wear facets in the dentition of *Incisivosaurus* are an exception because they are a strong indicator of herbivory (Xu et al., 2002). Previous work on the dietary patterns among theropods inferred herbivory in both Scansoriopterygidae and Oviraptorosauria based on their osteological features (Zanno and Makovicky, 2011). Recent studies generally accept that at least some oviraptorosaurians were herbivorous (Xu et al., 2002; Longrich et al., 2010, 2013; Lü et al., 2013; Funston et al., 2016), whereas the diet of scansoriopterygids has not been commented on in other studies. As in modern bird groups and those of many other extant animals, it is likely that the diets of all scansoriopterygids and oviraptorosaurians were not entirely homogeneous, but displayed interclade, intraclade, and intraspecific variations.

A suite of differences in the mandibular morphology of caenagnathids and oviraptorids likely indicates distinct feeding styles and diets (Longrich et al., 2010, 2013; Funston and Currie, 2016; Ma et al., 2017, 2020). Most studies propose that oviraptorids had a herbivorous diet (Longrich et al., 2010, 2013; Lü et al., 2013), whereas the diet of caenagnathids is more controversial. The latter includes suggestions of a more predatory lifestyle (Funston and Currie, 2016) or alternatively a herbivorous diet consisting of plant materials softer than those consumed by oviraptorids (Longrich et al., 2013).

Investigating the dietary variation of closely related animals is challenging because their skull shape is usually very similar. Ancestral-state reconstruction analysis of herbivory-related anatomical characters (e.g., the possession of a downturned maxilla and/or dentary and the reduction of tooth count) has been effective in recovering broad patterns in the dietary evolution of theropods (Zanno and Makovicky, 2011), where "absence" or "presence" conditions for many of these characteristics are easily identified among a large sample of skulls with broad morphological and functional diversity. However, applying this method to differentiate the diets of oviraptorosaurians and scansoriopterygids is difficult because most of them possess these categorical "herbivorous characters," so uncovering patterns among these clades requires additional lines of evidence. Here we apply a conventional comparative anatomy approach coupled with a quantitative, functional approach to study the dietary variation patterns among scansoriopterygids and oviraptorosaurians.

Numerous independently evolved modern herbivores show converging functional adaptations (Stayton, 2006). A series of cranial and mandibular characteristics show a functional link with herbivory in some extant and/or extinct animals, including birds (Greaves, 1974; Freeman, 1979; Emerson, 1985; Hanken and Hall, 1993; Thomason, 1997; Barrett, 2001; Sacco and Van Valkenburgh, 2004; Metzger and Herrel, 2005; Kammerer et al., 2006; Stayton, 2006; Grubich et al., 2008; Samuels, 2009; Olsen, 2017; Navalón et al., 2018). This is based on the idea that herbivores are likely to develop functional convergence, despite the fact that they may not show substantial morphological similarities (Stayton, 2006). For example, modern herbivores usually have a larger jaw-closing mechanical advantage than their carnivorous sister taxon (Stayton, 2006; Samuels, 2009). Thus, an increase in mechanical advantage along a lineage likely suggests an increasing adaptiveness to herbivory. Here we apply six of these characters to scansoriopterygid and oviraptorosaurian skulls, interpreting their variation patterns in terms of different levels of mandibular adaptation to herbivory (see Methods). This is the first in-depth study of the functional morphology of the early-diverging pennaraptorans and promises to provide new insights into their dietary variation that can help to clarify dietary evolution near the origin of birds.

MATERIALS AND METHODS

Materials

Twenty-six pennaraptoran mandibles were studied firsthand and from the literature (table 1). High-resolution photographs in lateral view were taken in person or from the literature (table 1) and then measured with the software ImageJ. The study sample included all available and usable mandibles of scansoriopterygids (2) and oviraptorosaurians (15). It also included six early-diverging avialans and three dromaeosaurids for comparative purposes, especially because of the controversial phylogenetic placement of Scansoriopterygidae at present (see Introduction).

Comparative Anatomy

Standard comparative anatomy methods are used to study the morphology and functional implications of scansoriopterygid and oviraptorosaurian skulls.

Functional Analysis

The six mandibular characteristics included in the functional analysis are: (1) anterior jaw-closing mechanical advantage (AMA); (2) posterior jaw-closing mechanical advantage (PMA); (3) jaw-opening mechanical advantage (OMA); (4) relative articular offset (RAO); (5) relative maximum mandible height (MMH); and (6) relative average mandible height (AMH). All these characters involve only two-dimensional measurements, which allows us to maximize our sample size from the slab specimens available while at the same time obtaining meaningful insights into the dietary habits of these early-diverging pennaraptorans. For the selection of each mandibular characteristic we identify a rationale.

JAW-CLOSING MECHANICAL ADVANTAGE: Mechanical advantage refers to the ratio of the output force to the input force of a mechanical system. This is also equivalent to the ratio of the distance between the fulcrum and the effort (inlever) to the distance between the fulcrum and the load (outlever). Measuring the jaw-closing mechanical advantage (MA) allows us to compare the effectiveness of the jaw occlusal system of different mandibles. The value of MA is also likely to provide an indication of the diet of an animal. Animals that have a plant-based diet are likely to have a higher jaw-closing MA than their carnivorous sister taxa (sensu Stayton, 2006). In a mechanical system, there is a trade-off between

TABLE 1

List of specimens utilized in the functional analysis of this study

Institutional abbreviations: **AMNH,** American Museum of Natural History, New York; **BSP,** Bayerische Staatssammlung für Paläontologie und Geologie, Munich, Germany; **CM,** Carnegie Museum of Natural History, Pittsburgh, PA; **CMN,** Canadian Museum of Nature, Ottawa, Ontario, Canada; **DYM,** Dongyang Museum, Dongyang City, Zhejiang, China; **FIP,** Florida Institute of Paleontology, Dania Beach, FL; **HGM,** Henan Geological Museum, Zhengzhou, Henan, China; **IVPP,** Institute of Vertebrate Paleontology and Paleoanthropology, Beijing, China; **LH,** Long Hao Institute of Geology and Paleontology, Hohhot, Nei Mongol, China; **MPC,** Paleontological Center, Mongolian Academy of Sciences, Ulaanbaatar, Mongolia; **STM,** Shandong Tianyu Museum of Nature, Pingyi, Shandong, China; **TMP,** Royal Tyrrell Museum of Palaeontology, Drumheller, Alberta, Canada; **YPM,** Yale Peabody Museum, New Haven, CT.

Clade	Taxon	Specimen	Data source	Reference
Scansoriopterygidae	*Epidexipteryx hui*	IVPP V15471	Firsthand	(Zhang et al., 2008)
	Yi qi	STM 31-2	Firsthand	(Xu et al., 2015)
Early-diverging oviraptorosaurians	*Incisivosaurus gauthieri*	IVPP V13326	Firsthand	(Xu et al., 2002)
	Caudipteryx sp.	IVPP V12430	Firsthand	(Ji et al., 1998)
Caenagnathidae	*Gigantoraptor erlianensis*	LH V0011	Firsthand	(Xu et al., 2007; Ma et al., 2017)
	Anzu wyliei	CM 78000	Firsthand	(Lamanna et al., 2014)
	Caenagnathus collinsi	CMN 8776	Literature	(Currie et al., 1993)
	Chirostenotes pergracilis	TMP 2001.12.12	Literature	(Funston and Currie, 2014)
Oviraptoridae	*Oviraptor philoceratops*	AMNH 6517	Firsthand	(Osborn et al., 1924)
	Rinchenia mongoliensis	MPC-D 100/32A	Literature	(Funston et al., 2017)
	Citipati osmolskae	IGM 100/978	Firsthand	(Clark et al., 2002)
	Huanansaurus ganzhouensis	HGM41HIII-0443	Firsthand	(Lü et al., 2015)
	Tongtianlong limosus	DYM-2013-8	Firsthand	(Lü et al., 2016)
	Banji long	IVPP V16896	Firsthand	(Xu and Han, 2010)
	Khaan mckennai	IGM 100/973	Firsthand	(Balanoff and Norell, 2012)
	Jiangxisaurus ganzhouensis	HGM41HIII0421	Firsthand	(Wei et al., 2013)
	Nemegtomaia barsboldi	MPC-D 100/2112	Literature	(Lü et al., 2004)
Avialae	*Jeholornis prima*	Reconstruction	Literature	(Xu et al., 2011)
	Sapeornis chaoyangensis	Reconstruction of IVPP V13275 and V13276	Firsthand	(Zhou and Zhang, 2003)
	Confuciusornis sanctus	Reconstruction	Literature	(Martin et al., 1998)
	Archaeopteryx lithographica	Reconstruction of BSP 1999 I 50	Firsthand	(Martin et al., 1998)
	Xiaotinggia zhengi	Reconstruction of STM 27-2	Firsthand	(Xu et al., 2011)
	Anchiornis huxleyi	Reconstruction	Literature	(Xu et al., 2011)
Dromaeosauridae	*Dromaeosaurus albertensis*	AMNH 5356	Firsthand	(Currie, 1995)
	Deinonychus antirrhopus	Reconstruction of YPM 5210 and YPM 5232	Firsthand	(Ostrom, 1969)
	Bambiraptor feinbergi	Reconstruction of FIP001	Firsthand	(Burnham et al., 2000)

jaw-closing velocity and MA—they cannot be maximized at the same time (i.e., increasing the jaw-closing velocity would reduce the MA). Velocity is important to carnivores that feed on elusive prey. Thus, carnivores need to take a balance between velocity and bite force as both factors influence hunting success. In contrast, it is expected that herbivores tend to maximize their jaw-closing MA because velocity is not a determining factor in plant procurement (Stayton, 2006). Increasing the MA allows herbivores to produce a larger bite force with the same input muscle force, and so exploit a wider range of vegetation (i.e., hard-fibered plants). This pattern is commonly seen in modern animals: herbivorous bird taxa convergently show increased jaw-closing MA compared to their omnivorous/carnivorous counterparts (Olsen, 2017; Navalón et al., 2018). Similar functional convergence is also observed in extant herbivorous lizards (Stayton, 2006), rodents (Samuels, 2009), and bears (Sacco and Van Valkenburgh, 2004). In this study, two characteristics of jaw-closing MA are applied:

ANTERIOR JAW-CLOSING MECHANICAL ADVANTAGE: When measuring anterior jaw-closing mechanical advantage (AMA) (fig. 1A), the inlever is the distance from the midpoint of the articular glenoid to the midpoint of the adductor muscle attachment site (comprising the m. adductor mandibulae externus profundus [m. AMEP], m. adductor mandibulae externus medialis [m. AMEM], and m. adductor mandibulae externus superficialis [m. AMES]). The muscle-attachment sites were identified based on the reconstruction proposed by Holliday (2009). The outlever is defined as the distance between the midpoint of the articular glenoid and the most anterior point of the dentary or the tip of the first dentary tooth for toothed specimens. Oviraptorosaurians have a distinctive sliding joint that allows anteroposterior jaw movement (Clark et al., 2002), and thus measurements depending on glenoid location change as the jaw moves. The midpoint of the glenoid was chosen as the measurement point to facilitate comparisons with other taxa, although it should be noted that such measurements may not represent the full range of biomechanical performance of oviraptorosaurian jaws.

POSTERIOR JAW-CLOSING MECHANICAL ADVANTAGE: For the measurement of posterior mechanical advantage (PMA), the inlever is the same as that of AMA (fig. 1A). However, the outlever here refers to the distance between the midpoint of the articular glenoid and the most posterior point of the occlusal margin (fig. 1B). For toothed specimens, the most posterior occlusal point is defined as the tip of the most posterior dentary tooth (fig. 1B). For edentulous specimens, this point is marked as the posteriormost point of the beak along the dorsal margin of the dentary. The posterior extent of the rhamphotheca in these specimens is reconstructed with reference to the proposed examples in Ma et al. (2017), which in turn follow the rationale suggested in Hieronymus and Witmer (2010) and Lautenschlager et al. (2014).

JAW-OPENING MECHANICAL ADVANTAGE: In the calculation of jaw-opening mechanical advantage (OMA), the outlever refers to the distance between the midpoint of the articular glenoid and the anteriormost point of the mandible or the dorsal tip of the first tooth (fig. 1C). The inlever is measured from the midpoint of the articular glenoid to the posteriormost point of the retroarticular process (fig. 1C). The retroarticular process is the attachment point for the m. depressor mandibulae (m. DM), a muscle that is responsible for the jaw-opening action (Holliday, 2009).

OMA is related to the velocity of the jaw-opening action, with a smaller OMA indicating a faster jaw-opening action. Animals that feed on elusive prey would benefit from having a lower OMA, which increases the speed of the prey-capturing process. Thus, herbivores are likely to have a higher OMA than their carnivorous relatives. Previous studies on modern carnivorous lizards (Hanken and Hall, 1993), gars (Kammerer et al., 2006), and frogs (Emerson, 1985) indicate that skulls with a shorter retroarticular process have a higher jaw-opening speed, which suits the hunting of fast-moving prey.

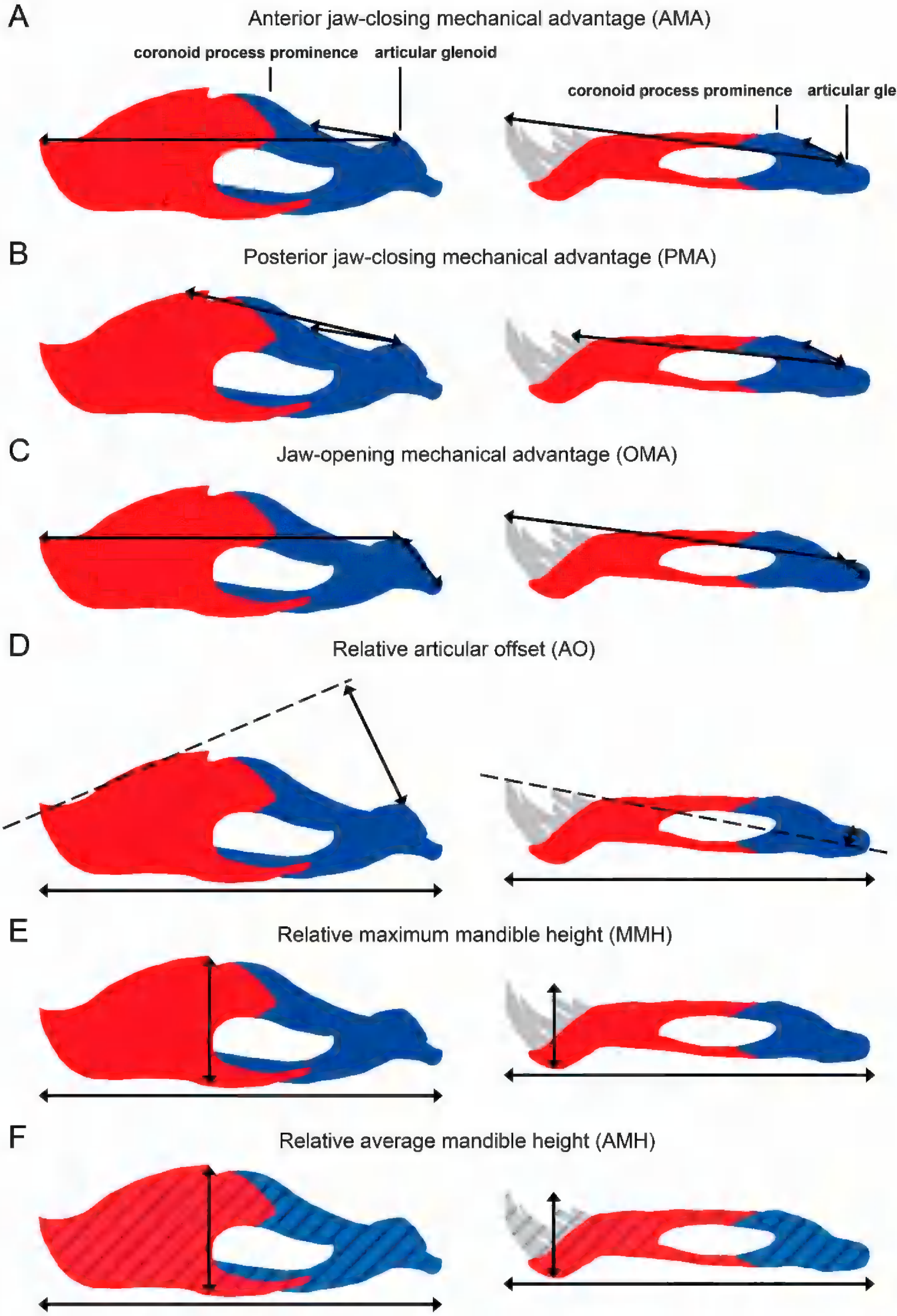
A
Anterior jaw-closing mechanical advantage (AMA)
coronoid process prominence
articular glenoid
coronoid process prominence
articular glenoid
B
Posterior jaw-closing mechanical advantage (PMA)
C
Jaw-opening mechanical advantage (OMA)
D
Relative articular offset (AO)
E
Relative maximum mandible height (MMH)
F
Relative average mandible height (AMH)

FIG. 1. Schematic diagram showing how the six functionally related mandibular characteristics were measured in the oviraptorosaurians and scansoriopterygids studied. **A.** Anterior jaw-closing mechanical advantage, AMA. **B.** Posterior jaw-closing mechanical advantage, PMA. **C.** Jaw-opening mechanical advantage, OMA. **D.** Relative articular offset, AO. **E.** Relative maximum mandible height, MMH. **F.** Relative average mandible height, AMH.

Relative Articular Offset: Relative articular offset (AO) is measured as the perpendicular distance between the tangent line of the occlusal margin and the midpoint of the articular glenoid, divided by the anteroposterior length of the mandible (fig. 1D). The purpose of dividing the articular offset by the total mandibular length is to make the measurement size independent, as body size varies among scansoriopterygids and oviraptorosaurians.

Differences in this character represent different modes of occlusion. A large AO suggests that different locations of the occlusal margin of the mandible contact with the upper jaw nearly simultaneously (Greaves, 1974). In contrast, a small AO suggests that different locations of the mandible occlude with the upper jaw at different instants, starting from the posteriormost point to the anterior tip (i.e., a "scissorlike" occlusal mode) (Greaves, 1974; Grubich et al., 2008). Herbivores usually have a large AO whereas carnivores tend to have a small one (Freeman, 1979; Thomason, 1997). This increases the effectiveness of the plant-cropping and meat-slicing procedures in herbivores and carnivores respectively (Freeman, 1979). This pattern can be observed extensively in both extant and extinct animals, such as ornithischian dinosaurs (Barrett, 2001), modern mammals (Greaves, 1974), and fish (Grubich et al., 2008).

Relative Maximum Mandible Height: Relative maximum mandible height (MMH) refers to the maximum height of the mandible divided by its total length (fig. 1E). To ensure the orientation of the mandibles are standardized when measurements are made, the horizon here refers to the "best fit" of the ventral margin of the mandible, as defined in the studies of therizinosaurian (Zanno et al., 2016) and oviraptorosaurian jaws (Ma et al., 2017). The height is measured as perpendicular to the horizon. This character relates to the stiffness of a mandible along the dorsoventral direction (the direction along which stress is applied on the jaw during occlusion). It is observed that animals with a feeding style that requires a larger bite force have a more robust mandible (i.e., a larger MMH) to resist the stress (Sacco and Van Valkenburgh, 2004). With an expected increase in MA and bite force in herbivores, having a stiffer mandible allows them to mitigate the stress experienced by the mandibles during plant cropping. Herbivorous bears are known to have a more rigid mandible than the nonherbivorous ones, a trait that may be linked to an increase in MA (Sacco and Van Valkenburgh, 2004). Different lineages of extant herbivorous lizards convergently show an increase in skull height, whereas their carnivorous counterparts have a relatively elongated skull (i.e., lower in height) (Metzger and Herrel, 2005). Extant rodents specialized in herbivory are observed to have a taller skull than the generalist herbivorous rodents (Samuels, 2009).

Relative Average Mandible Height: Relative average mandible height (AMH) can be obtained by dividing the average mandible height by the total mandible length (fig. 1F). Average mandible height is defined as the total area of the mandible in lateral view divided by its total mandible length. The total area of the mandible excludes the area of the external mandibular fenestra to ensure only the parts that contribute to jaw stiffness are considered. Based on the same principle as MMH, a larger AMH is likely to represent a stiffer jaw, which suggests a feeding style that requires a stronger bite. Thus, animals having a larger AMH are likely to be more adapted to herbivory.

Ancestral-State Reconstruction: Ancestral-state reconstruction of functional characters was conducted in the software Mesquite v. 3.4 with the function "Parsimony ancestral state reconstruction method" under "Trace character history" (Maddison and Maddison, 2018). This allows us to visualize the evolutionary trends of different characters in Pennaraptora, especially across those well-sampled lineages such as Oviraptoridae and Caenagnathidae. As there is no single phylogeny that includes all the pennaraptorans involved in the study, we have produced a hypothetical phylogenetic tree by integrating the trees of different pennaraptoran clades (Lü et al., 2017; Pei et al., in press).

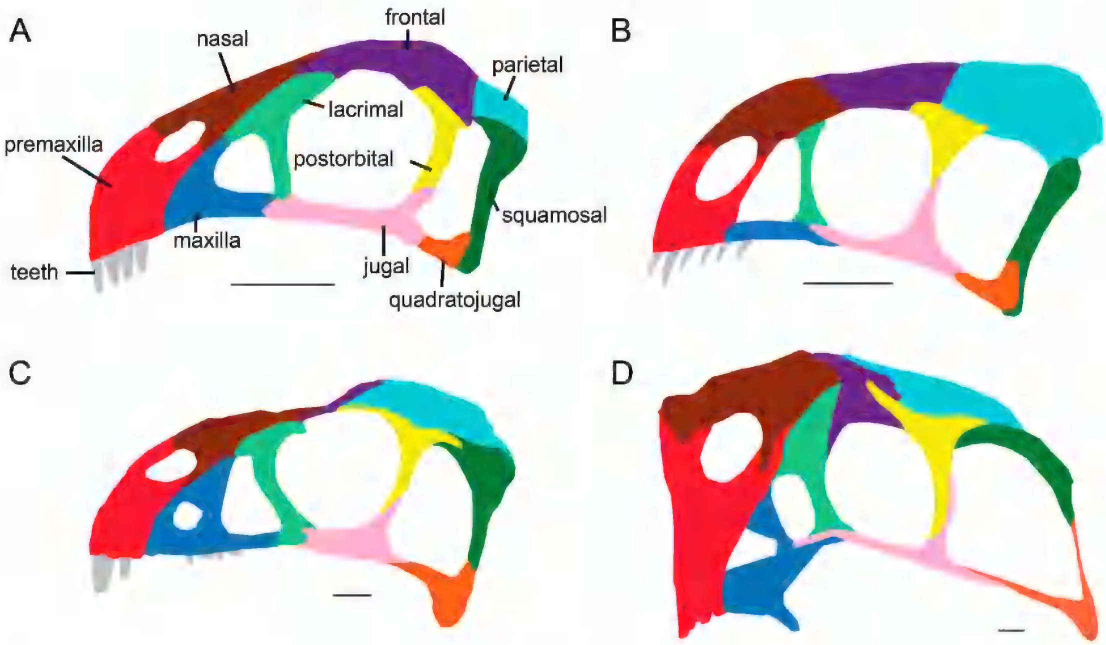

FIG. 2. Simplified drawings of the crania of early-diverging pennaraptorans. **A.** *Yi.* Qualitative reconstruction of STM 31-2, modified from Xu et al. (2015). **B.** *Epidexipteryx.* Qualitative reconstruction of IVPP V15471, modified from Zhang et al. (2008). **C.** *Incisivosaurus.* Qualitative reconstruction of IVPP V13326, modified from Xu et al. (2002). **D.** *Citipati.* Qualitative reconstruction of IGM 100/978, modified from Clark et al. (2002). Scale is 1 cm.

RESULTS

Comparative Anatomy

Cranium

The skulls of scansoriopterygids are short and high when compared with those of typical theropods (fig. 2). Scansoriopterygids share a similar skull shape to early-diverging oviraptorosaurians such as *Incisivosaurus* (fig. 2C) and *Caudipteryx* (O'Connor and Sullivan, 2014). The skulls of *Yi* and *Epidexipteryx* have a height of about 40% and 60% (Zhang et al., 2008) of their anteroposterior lengths respectively (fig. 2A, B). The height/length ratio of the skull of *Epidexipteryx* is comparable to those of some oviraptorids, such as *Banji*, *Citipati*, and *Khaan* (fig. 2B, D). However, some late-diverging oviraptorosaurians have a taller skull because of the presence of a tall crest (Lamanna et al., 2014; Funston et al., 2017; Lü et al., 2017). Oviraptorids, such as *Rinchenia*, have a skull length and height that are nearly identical (Tsuihiji et al., 2016: fig. 8). *Yi* was described with a crestlike structure above its nasal (Xu et al., 2015) that is lower than those of crested caenagnathids and oviraptorids (fig. 2D). However, cranial crests are not known in early-diverging oviraptorosaurians (fig. 2C). The dorsal margin of the external naris of scansoriopterygids is positioned at a comparable level to that of the antorbital fenestra, as in *Incisivosaurus* and possibly *Caudipteryx* (fig. 2A–C). In late-diverging oviraptorosaurians, the relative position of the external naris and antorbital fenestra is highly variable (Lü et al., 2017: fig. 6; Ma et al., 2020). When compared to scansoriopterygids and early-diverging oviraptorosaurians, late-diverging oviraptorosaurians generally have an elevated external naris (fig. 2). The orbit of scansoriopterygids is large relative to the lateral profile of the crania (about 25% of the total area of the crania in lateral view; fig. 2A, B). The relative size of the orbit is smaller in oviraptorosaurians (about 14% and 20% in oviraptorids and

Incisivosaurus respectively; fig. 2C, D). The orbit of scansoriopterygids and oviraptorosaurians are circular in shape (fig. 2), similar to those of closely related theropods like early-diverging avialans, therizinosaurians, and ornithomimosaurians. The lateral temporal fenestra of scansoriopterygids is smaller than their orbits in lateral view, unlike the condition in oviraptorosaurians where the two fenestrae are usually comparable in size (fig. 2). The lateral temporal fenestra of scansoriopterygids is longer dorsoventrally than anteroposteriorly (fig. 2), similar to those of typical theropods. This condition is also present in some oviraptorosaurians such as *Incisivosaurus*, *Tongtianlong*, and *Corythoraptor*. However, some oviraptorids have a more squarelike lateral temporal fenestra, including *Rinchenia*, *Conchoraptor*, and *Citipati* (fig. 2D). The upper jaw of scansoriopterygids is toothed, a condition absent in oviraptorids and caenagnathids but present in some early-diverging oviraptorosaurians including *Incisivosaurus*, *Caudipteryx*, and *Protarchaeopteryx*. *Yi* possesses at least four premaxillary teeth on each side whereas no maxillary tooth is visible in the only known specimen of *Yi* (Xu et al., 2015). *Epidexipteryx* has at least seven teeth on each side of its upper jaw (Zhang et al., 2008), although the exact number of premaxillary and maxillary teeth cannot be determined due to poor preservation. In general, toothed oviraptorosaurians seem to possess more teeth in their upper jaw than scansoriopterygids: *Incisivosaurus* has at least four and nine teeth on each side of the premaxilla and maxilla respectively (Balanoff et al., 2009); *Protarchaeopteryx* displays eight teeth on each side of its upper jaw (Ji et al., 1998). However, the maxilla of *Caudipteryx* is edentulous and each of its premaxillae possesses only four teeth (Ji et al., 1998). A heterodont condition with anterior teeth enlargement is present in both scansoriopterygids and toothed oviraptorosaurians. In scansoriopterygids, anterior premaxillary teeth are larger than the ones located more posteriorly (Zhang et al., 2008; Xu et al., 2015). This condition is especially evident in *Epidexipteryx*: its robust second premaxillary tooth is about 1.5× the lengths of the other teeth (Zhang et al., 2008: fig. 1). In comparison, the anterior enlargement of teeth is less obvious in *Yi* as the size difference between its teeth is not prominent. The dentition-variation patterns in *Incisivosaurus* and *Protarchaeopteryx* are slightly different from those of scansoriopterygids. The first premaxillary tooth of *Incisivosaurus* is the largest tooth, which is about double the length of the other teeth. In *Protarchaeopteryx*, the first four teeth seem to be comparable in their sizes but they are all longer than the more posterior ones (Ji et al., 1998: fig. 2).

Compared to oviraptorosaurians, the frontals of scansoriopterygids are relatively long in general (fig. 2). *Epidexipteryx*, *Yi*, and *Epidendrosaurus* have fairly long frontals, which make up approximately 40% of their skull lengths (the skull length of *Epidendrosaurus* is estimated from its mandible length) (Zhang et al., 2002: fig. 1; 2008: fig. 2; Xu et al., 2015: fig. 3). The relative length of the frontals of *Incisivosaurus* is longer than those of other oviraptorosaurians (about 20% of the skull length) (Xu et al., 2002; Balanoff et al., 2009), although it is still shorter than those of scansoriopterygids. In scansoriopterygids, the parietals are anteroposteriorly shorter than the frontals (Zhang et al., 2002: fig. 1; 2008: fig. 2; Xu et al., 2015: fig. 3). Both *Epidexipteryx* and *Epidendrosaurus* have a parietal/frontal ratio of approximately 0.8, whereas the ratio is about 0.25 for *Yi* (Zhang et al., 2002: fig. 1; 2008: fig. 2; Xu et al., 2015: fig. 3). In the early-diverging oviraptorosaurians *Incisivosaurus* and *Caudipteryx*, the lengths of parietals are similar to and shorter than the frontals respectively (Ji et al., 1998; Balanoff et al., 2009). However, in oviraptorids, the parietals are anteroposteriorly longer than the frontals (Osmolska et al., 2004).

Mandible

The overall shape of the mandible of scansoriopterygids is more similar to those of early-diverging oviraptorosaurians (especially

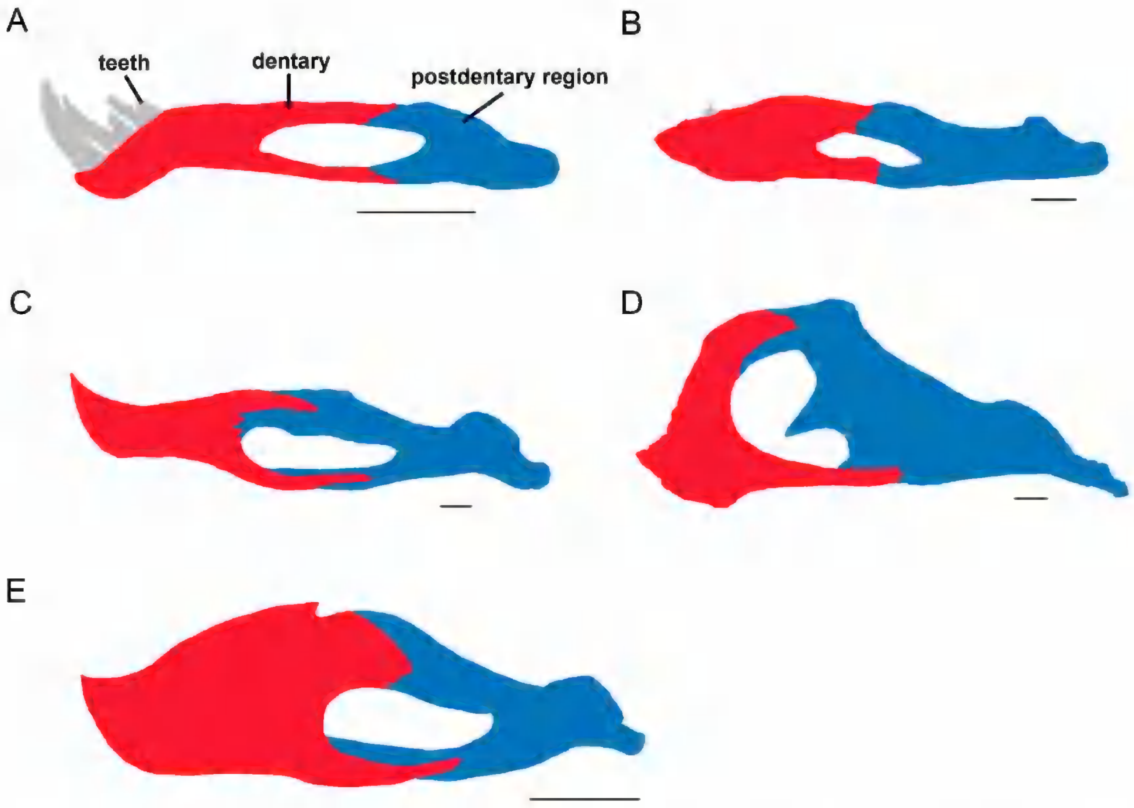

FIG. 3. Mandible of early-diverging pennaraptorans. **A.** *Epidexipteryx.* Qualitative reconstruction of IVPP V15471, modified from Zhang et al. (2008). **B.** *Incisivosaurus.* Qualitative reconstruction of IVPP V13326, modified from Xu et al. (2002). **C.** *Chirostenotes.* Qualitative reconstruction of TMP 2001.12.12, modified from Funston and Currie (2014). **D.** *Citipati.* Qualitative reconstruction of IGM 100/978, modified from Clark et al. (2002). **E.** *Gigantoraptor.* Qualitative reconstruction of LH V0011, modified from Ma et al. (2017). Scale is 1 cm in A–D; 10 cm in E.

Caudipteryx) and most caenagnathids (except *Gigantoraptor*) than the late-diverging ones (fig. 3A–C compared with 3D, E). The mandible of scansoriopterygids is shallow relative to those of oviraptorids (fig. 3A compared to 3D). Their dentary does not expand dorsoventrally posterior to the symphyseal region, in contrast to the condition in caenagnathids, oviraptorids, and *Avimimus*. The dentary of oviraptorosaurians is likely to be covered with rhamphotheca, as indicated by the presence of foramina and fossa on the outer surface of the dentary (Ma et al., 2017), whereas the condition in scansoriopterygids is unclear as no foramina are visible in known specimens.

The anterior portion of the dentary of scansoriopterygids is downturned (fig. 3A), as in theropods like oviraptorosaurians, ornithomimosaurians, therizinosaurians, and some early-diverging avialans (Zanno and Makovicky, 2013). Dentary teeth are present in *Epidexipteryx* (Zhang et al., 2008), *Epidendrosaurus* (Zhang et al., 2002) and *Yi* (Xu et al., 2015). In Oviraptorosauria, *Incisivosaurus* (Xu et al., 2002), *Protarchaeopteryx* (Ji et al., 1998), and *Ningyuansaurus* (Ji et al., 2012) are known to have dentary teeth. *Protarchaeopteryx*, *Incisivosaurus*, and *Ningyuansaurus* have at least seven (Ji et al., 1998), nine (Balanoff et al., 2009), and 14 (Ji et al., 2012) dentary teeth respectively. In scansoriopterygids, *Epidexipteryx*, *Yi*, and *Epidendrosaurus* have at least five (Zhang et al., 2008), three (Xu et al., 2015) and 12 (Zhang et al., 2002) dentary teeth respectively.

Scansoriopterygids and *Incisivosaurus* both possess unserrated teeth, whereas all the dentary teeth of *Protarchaeopteryx* are anteriorly and posteriorly serrated (Ji et al., 1998). The teeth of scansoriopterygids are generally straight (i.e., not recurved), although the distal margin of the first dentary tooth of *Epidexipteryx* appears to be curved (Zhang et al., 2008: fig. 1; Xu et al., 2015: fig. 1). Anterior enlargement of the dentary teeth is observed in scansoriopterygids (Zhang et al., 2002, 2008; Xu et al., 2015). This condition is especially obvious in *Epidexipteryx* as its first dentary tooth is about 2× the length of its third and fourth teeth (Zhang et al., 2008: fig. 1; fig. 3A). Due to missing teeth, it is unclear whether anterior teeth enlargement is also present in *Incisivosaurus* and *Protarchaeopteryx*, although the sizes of their preserved teeth do not show strong variation. The dentary teeth of scansoriopterygids are highly procumbent (Zhang et al., 2002, 2008; Xu et al., 2015), unlike the condition in *Incisivosaurus* where its teeth are only slightly procumbent (Balanoff et al., 2009; fig. 3A, B). In *Epidexipteryx*, the first dentary tooth is highly recurved and the more posterior teeth are relatively long and thin (Zhang et al., 2008: fig. 1; fig. 3A). In contrast, the preserved dentary teeth of *Incisivosaurus* (Balanoff et al., 2009) and *Protarchaeopteryx* (Ji et al., 1998) are more bulbous and none of them are recurved. The dentary teeth of *Epidexipteryx* are tightly packed, unlike those of *Incisivosaurus* where the distances between subsequent teeth are similar to half of the width of the teeth themselves (Xu et al., 2002: fig. 1e) (fig. 3A, B).

Scansoriopterygids do not possess a tall coronoid process prominence, unlike most oviraptorosaurians. Oviraptorids, in general, have a taller coronoid process prominence than other oviraptorosaurians (Ma et al., 2017). The shape of the external mandibular fenestra of scansoriopterygids is similar to those of early-diverging oviraptorosaurians and caenagnathids, which are all relatively long and dorsoventrally low (fig. 3A–C, E). This is different from the condition in oviraptorids, in which the external mandibular fenestra is more circular (fig. 3D). The articular glenoid of oviraptorosaurians is dorsally convex in lateral view, unlike that of scansoriopterygids where it is relatively flat (Zhang et al., 2008: figs. 1, 2; fig. 3).

FUNCTIONAL COMPARISON

Six functional characters were measured and subjected to ancestral-state reconstruction analysis using squared-change parsimony and a tree topology (fig. 4; table 2) based on Lü et al. (2017) and Pei et al. (in press). The reconstructed nodal value of mechanical advantage (MA) of the jaw-closing system (average of AMA and PMA) of scansoriopterygids (~0.179) is lower than those of oviraptorosaurians. MA varies largely within Oviraptorosauria: oviraptorids have the largest MA of ~0.311 whereas caenagnathids have a value of ~0.272. The MAs of early-diverging avialans and dromaeosaurids are smaller than those of oviraptorosaurians. Scansoriopterygids have a lower AMA than oviraptorosaurians. The AMAs of caenagnathids and early-diverging oviraptorosaurians are similar, which is ~0.190. Oviraptorids have the greatest AMA, which is ~0.267. Oviraptorids have the largest PMA among the studied taxa (~0.355). Caenagnathids and early-diverging oviraptorosaurians have PMAs of ~0.341 and ~0.291 respectively. The PMA of scansoriopterygids is smaller than that of oviraptorosaurians, which is ~0.202. PMA is always larger than AMA because when the position of the load moves from the front tip of the occlusal margin to the posteriormost point, the outlever decreases and eventually results in a larger MA. It is noteworthy that some taxa display a more significant variation in MA than others (i.e., percentage difference between AMA and PMA). The MA of scansoriopterygids shows the smallest increase among the studied taxa, which is only ~30.3%. The percentage increases in MA of oviraptorids is relatively small, which is ~33.0%. The

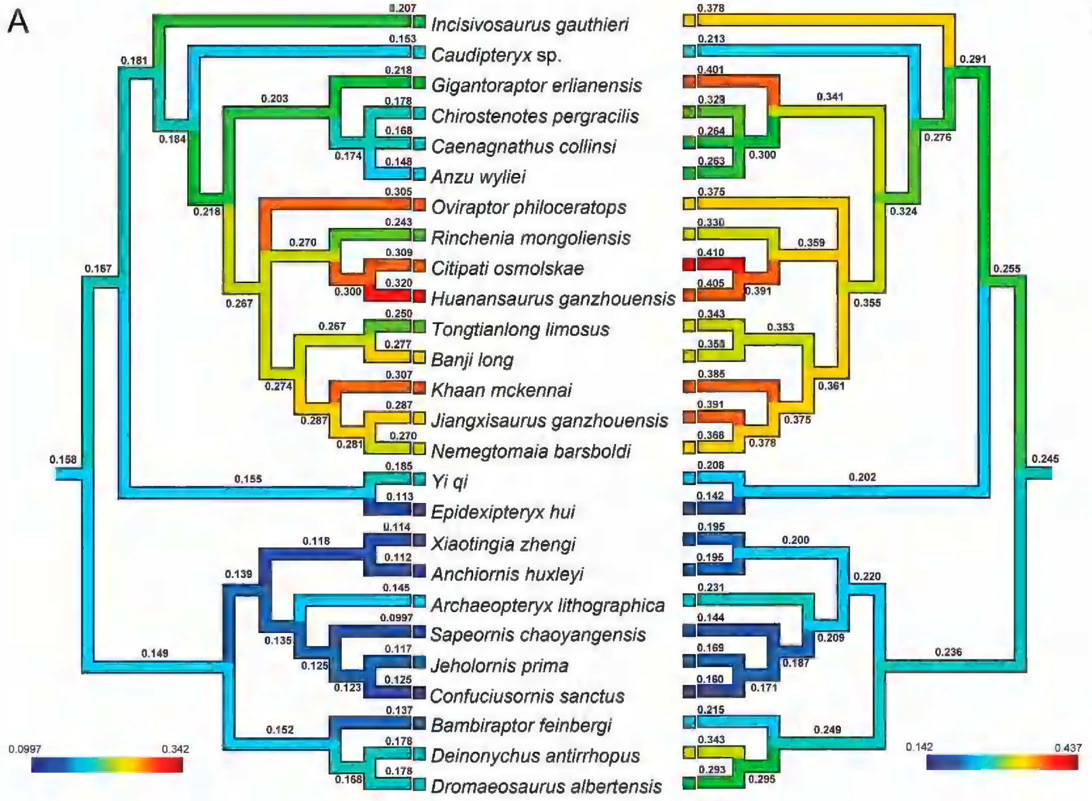

FIG. 4. Ancestral-state reconstruction (*above and following two pages*) of the six functional characters across Pennaraptora under squared-change parsimony (above and on next two pages). **A.** Anterior jaw-closing mechanical advantage, AMA. **B.** Posterior jaw-closing mechanical advantage, PMA. **C.** Jaw-opening mechanical advantage, OMA. **D.** Relative articular offset, AO. **E.** Relative maximum mandible height, MMH. **F.** Relative average mandible height, AMH. Tree topology based on Lü et al. (2017) and Pei et al. (in press). Reconstructed nodal values for select nodes are given in table 2.

percentage increase in MA in early-diverging oviraptorosaurians is ~60.8%, which is intermediate between those of oviraptorids and caenagnathids. Caenagnathids and dromaeosaurids show a large increase in MA of ~68.0% and ~63.8% respectively.

Ancestral-state reconstructions of MA reveal that there is an overall increase in AMA and PMA from early-diverging oviraptorosaurians to the oviraptorid lineage (AMA: from ~0.181 to ~0.267; PMA: from ~0.291 to ~0.355). Both AMA and PMA show an increasing trend along the oviraptorid lineage, whereas the caenagnathid lineage displays a decreasing trend (fig. 4). Paravians, in general, have relatively uniform AMAs, whereas their PMAs are more variable: members such as dromaeosaurids have an increased PMA.

The reconstructed opening mechanical advantage (OMA) of scansoriopterygids (~0.130) is lower than that of oviraptorosaurians. Early-diverging oviraptorosaurians and caenagnathids have a similar OMA (~0.185 & ~0.208 respectively). Oviraptorids have the highest OMA, which is ~0.264. Early diverging avialans and dromaeosaurids have a small OMA of ~0.103 and ~0.106 respectively. Ancestral-state reconstruction reveals an increase in OMA along the oviraptorosaurian lineage, whereas the OMA is relatively uniform among paravians (fig. 4).

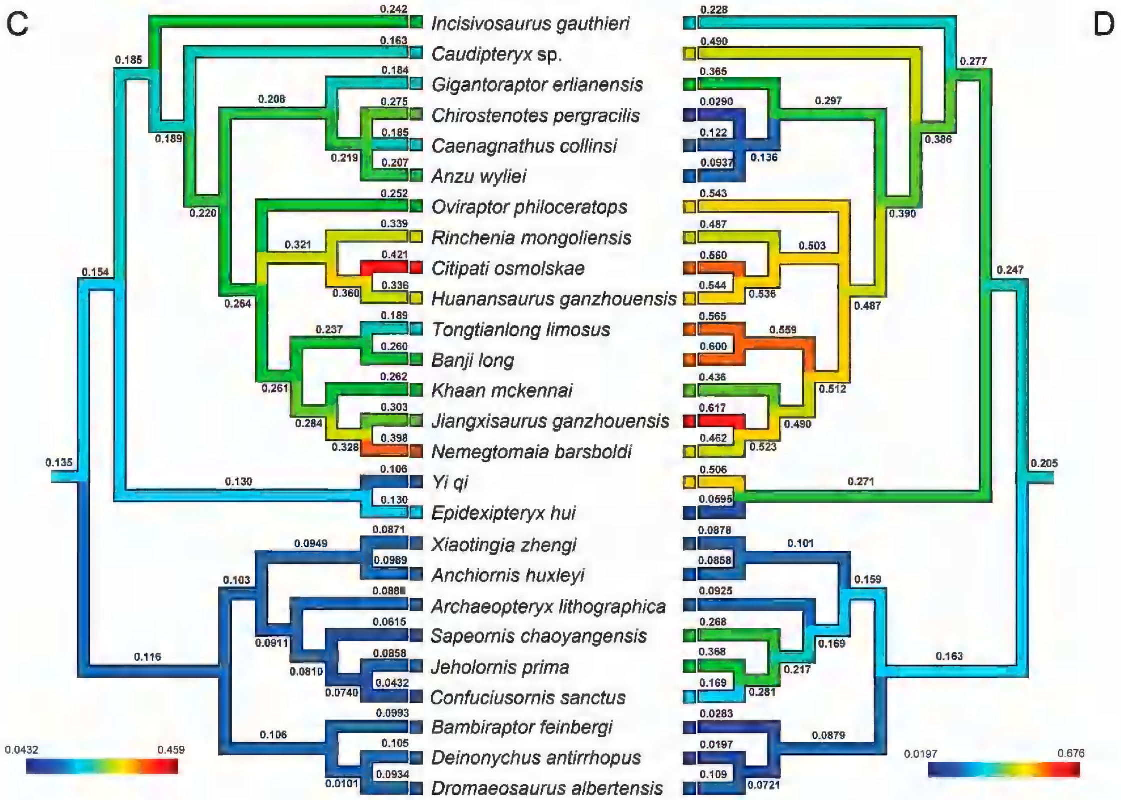
C
D
Incisivosaurus gauthieri
Caudipteryx sp.
Gigantoraptor erlianensis
Chirostenotes pergracilis
Caenagnathus collinsi
Anzu wyliei
Oviraptor philoceratops
Rinchenia mongoliensis
Citipati osmolskae
Huanansaurus ganzhouensis
Tongtianlong limosus
Banji long
Khaan mckennai
Jiangxisaurus ganzhouensis
Nemegtomaia barsboldi
Yi qi
Epidexipteryx hui
Xiaotingia zhengi
Anchiornis huxleyi
Archaeopteryx lithographica
Sapeornis chaoyangensis
Jeholornis prima
Confuciusornis sanctus
Bambiraptor feinbergi
Deinonychus antirrhopus
Dromaeosaurus albertensis
0.242
0.185
0.163
0.184
0.208
0.275
0.189
0.185
0.219
0.207
0.252
0.220
0.339
0.321
0.421
0.154
0.360
0.336
0.264
0.189
0.237
0.260
0.262
0.261
0.303
0.284
0.398
0.328
0.135
0.106
0.130
0.130
0.0871
0.0949
0.0989
0.103
0.0888
0.0615
0.0911
0.116
0.0858
0.0810
0.0432
0.0740
0.0993
0.106
0.105
0.0934
0.0101
0.0432
0.459
0.228
0.490
0.277
0.365
0.0290
0.297
0.386
0.122
0.0937
0.136
0.543
0.390
0.487
0.503
0.560
0.247
0.544
0.536
0.487
0.565
0.559
0.600
0.436
0.512
0.617
0.490
0.462
0.523
0.506
0.205
0.271
0.0595
0.0878
0.101
0.0858
0.159
0.0925
0.268
0.169
0.368
0.163
0.217
0.169
0.281
0.0283
0.0879
0.0197
0.109
0.0721
0.0197
0.676

The reconstructed relative articular offset (AO) of oviraptorids is ~0.488, which is the highest among the studied taxa. Scansoriopterygids, caenagnathids, noncaenagnathoid oviraptorosaurians, and early-diverging avialans have a much smaller AO than oviraptorids, which are only ~0.271, ~0.297, ~0.277, and ~0.159 respectively. However, it should be noted that *Gigantoraptor erlianensis* has a high AO (~0.365), which strongly deviates from those of other caenagnathids. If only caenagnathids diverging later than *Gigantoraptor* are considered, the nodal value drops to ~0.136. A high disparity in AO is also noticed among scansoriopterygids, e.g., the AO of *Yi* (~0.506) is about 10 times that of *Epidexipteryx* (~0.0595). Dromaeosaurids have the smallest AO, ~0.0879. Ancestral-state reconstruction shows an increasing trend in AO from early-diverging oviraptorosaurians to oviraptorids (fig. 4). In contrast, AO decreases across the caenagnathid lineage (fig. 4). Similar to oviraptorosaurians, the AOs among paravians also display high variability (fig. 4).

The relative maximum mandibular height (MMH) of scansoriopterygids and early-diverging oviraptorosaurians are similar, ~0.187 and ~0.188 respectively. The MMH of caenagnathids is ~0.266, with the value for *Gigantoraptor* the largest (~0.325). Oviraptorids have the highest MMH, ~0.320. The MMHs of early-diverging avialans and dromaeosaurids are both smaller than those of oviraptorosaurians and scansoriopterygids, which are ~0.127 and ~0.135 respectively. Similar patterns are also observed in the AMH measurements. The AMHs of scansoriopterygids and early-diverging oviraptorosaurians show similar values of ~0.129 and ~0.125 respectively. Caenagnathids have an AMH of ~0.152. As in average MMH, oviraptorids show the greatest average AMH value (~0.160). The AMH of early-diverging avialans and drom-

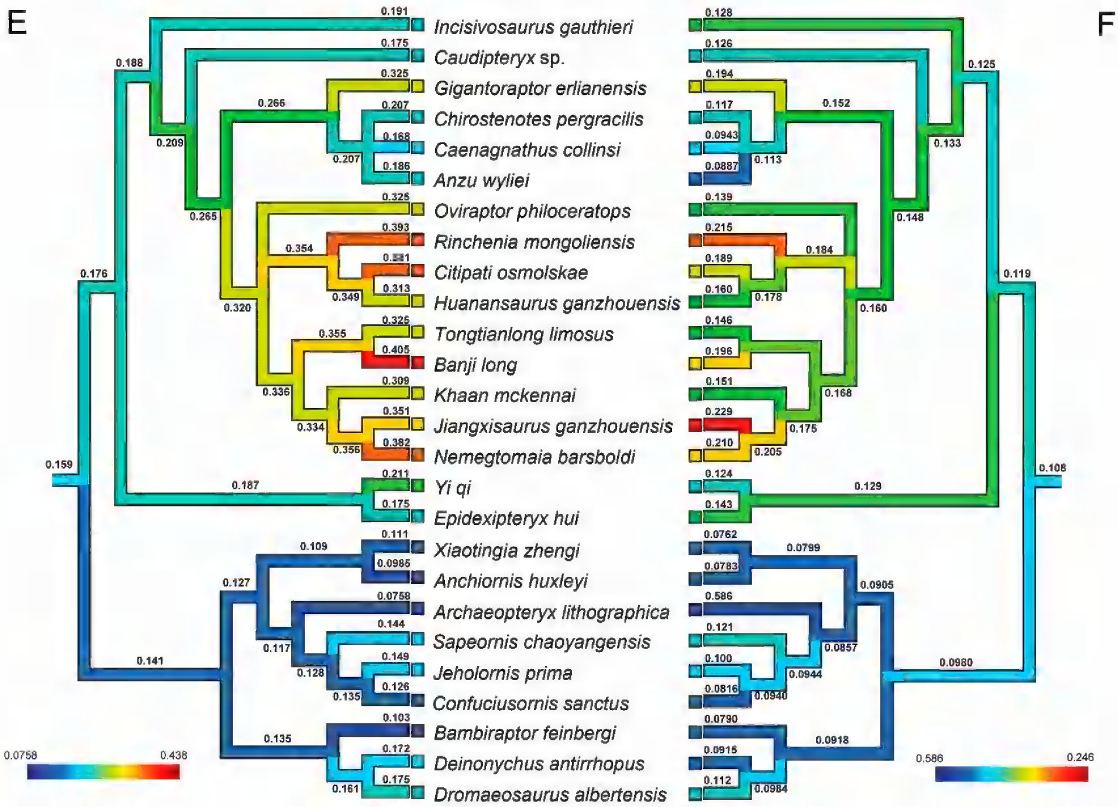

aeosaurids are ~0.0905 and ~0.0918 respectively, which are all smaller than those of oviraptorosaurians and scansoriopterygids.

Ancestral-state reconstructions show that there is an increase in MMH and AMH from early-diverging oviraptorosaurians to oviraptorids, and along oviraptorid lineage. For both MMH and AMH, there is a decreasing trend along Caenagnathidae, due to the large values of *Gigantoraptor* (fig. 4). The MMH and AMH of paravians are fairly similar without large variations (fig. 4).

DISCUSSION

The results of the functional comparison, with reference to comparative anatomy, suggest that different levels of adaptation to herbivory existed among early-diverging pennaraptorans. These variation patterns are likely to be indicative of the level of herbivory among these animals. Based on this inference, a number of dietary-related trends can be identified along different lineages of early-diverging pennaraptorans.

The most obvious pattern that can be inferred is that oviraptorids are likely to be more adapted to herbivory than other early-diverging pennaraptorans. Oviraptorids have the largest mean values for all the six characteristics compared to other early-diverging pennaraptorans (table 1). For all the six functional characteristics, the larger the value, the more likely the animal is to be adapted to herbivory (see Methods for detailed explanations). Oviraptorids have a large jaw-closing mechanical advantage (MA), a low jaw opening speed, an occlusal style similar to modern herbivores, and a rigid mandible. The large jaw-closing MA of oviraptorids favors the production of a large bite force, which facilitates plant cropping. However, this also increases the stress experienced by the jaw during jaw occlusion. Thus, increasing the rigidness of the jaw by

TABLE 2

Reconstructed nodal values of the six diet-related functional characteristics of the major clades of pennaraptorans

Abbreviations: **AMA,** anterior mechanical advantage; **AMH,** average mandibular height; **AO,** relative articular offset; **MA,** mechanical advantage; **MMH,** maximum mandibular height; **OMA,** jaw-opening mechanical advantage; **PMA,** posterior mechanical advantage.

Taxon	AMA	PMA	MA	% increase in MA	OMA	AO	MMH	AMH
Scansoriopterygids	0.155	0.202	0.179	30.3	0.130	0.271	0.187	0.129
Oviraptorosaurians (excluding scansoriopterygids)	0.181	0.291	0.236	60.8	0.185	0.277	0.188	0.125
Caenagnathids	0.203	0.341	0.272	68.0	0.208	0.297	0.266	0.152
Oviraptorids	0.267	0.355	0.311	33.0	0.264	0.487	0.320	0.160
Early-diverging avialans	0.139	0.220	0.180	58.3	0.103	0.159	0.127	0.0905
Dromaeosaurids	0.152	0.249	0.201	63.8	0.106	0.0879	0.135	0.0918

increasing its height is a likely adaptive outcome. Since animals with a high-level herbivorous diet are likely to rely less on hunting, they do not experience large selective pressure to increase the velocity of jaw movement for food procurement. Evidence from comparative anatomy also suggests that oviraptorids are likely to be more adapted to herbivory than other early-diverging pennaraptorans. Oviraptorids in general have a taller skull, a relatively larger lateral temporal fenestra, and a taller coronoid process prominence. Having a taller skull probably increases its rigidity and reduces the risk of bone fracturing during feeding (Metzger and Herrel, 2005; Samuels, 2009). The possession of a tall coronoid process prominence provides a larger area for inserting adductor muscles, increasing the jaw-adducting force (Nogueira et al., 2009; Lü et al., 2013; Ma et al., 2017). The crania of oviraptorids have relatively long parietals and a large lateral temporal fenestra compared to other early-diverging pennaraptorans. The expansion of the posterior region of the crania is likely to provide more space to accommodate thicker adductor muscles, which allow oviraptorids to produce a stronger bite. Evidence from both functional analysis and comparative anatomy consistently shows that the skulls of oviraptorids are well suited for feeding that requires a stronger bite force but less demand on speed than other early-diverging pennaraptorans, and its jaw occlusion is similar to that of modern herbivores. This suggests that oviraptorids are likely the most adapted to herbivory among early-diverging pennaraptorans, strengthening the hypothesis that oviraptorids included a large amount of plants in their diets (Longrich et al., 2013).

Scansoriopterygids appear to be less adapted to herbivory compared to oviraptorids, although scansoriopterygid stomach contents remain unknown. The mandibles of scansoriopterygids have a relatively low jaw-closing MA and lack a tall coronoid process prominence, in contrast to those of oviraptorids. Also, the mandible and crania of scansoriopterygids appear to be less robust due to their relatively long length. Scansoriopterygids have a smaller lateral temporal fenestra than oviraptorids, which probably constrains the space available for muscle attachment and reduces its bite force. If they were herbivorous to some degree, the adaptiveness of their skull to herbivory was probably similar to early-diverging oviraptorosaurians, which preserve direct evidence of herbivory (Ji et al., 1998, 2012;

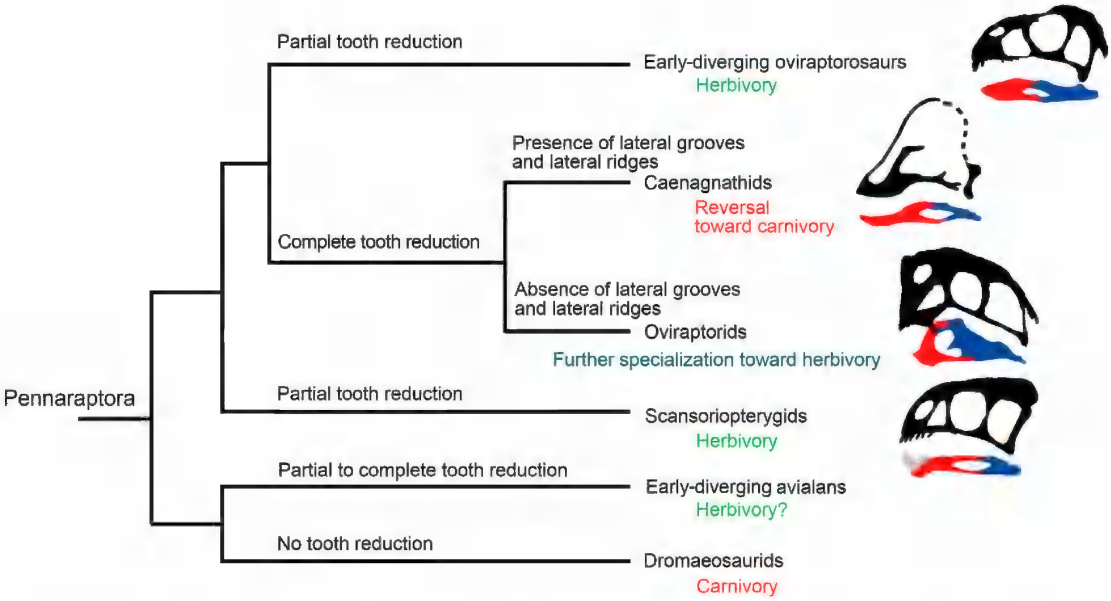
Partial tooth reduction
Early-diverging oviraptorosaurs
Herbivory
Presence of lateral grooves and lateral ridges
Caenagnathids
Reversal toward carnivory
Complete tooth reduction
Absence of lateral grooves and lateral ridges
Oviraptorids
Further specialization toward herbivory
Pennaraptora
Partial tooth reduction
Scansoriopterygids
Herbivory
Partial to complete tooth reduction
Early-diverging avialans
Herbivory?
No tooth reduction
Dromaeosaurids
Carnivory

FIG. 5. Patterns of tooth reduction and inferences of dietary evolution in Pennaraptora based on the results of the functional analysis (fig. 4). Tree topology based on Lü et al. (2017) and Pei et al. (in press). Skull drawings modified from Clark et al. (2002), Xu et al. (2002, 2011) and Lamanna et al. (2014).

Xu et al., 2002). The large relative articular offset in the mandible of *Yi* suggests a jaw-occlusal mode similar to extinct and extant herbivores (e.g., ornithischian dinosaurs and herbivorous mammals and fish), *Caudipteryx*, and oviraptorids. However, *Epidexipteryx* has a small relative articular offset that is comparable to those of late-diverging caenagnathids and dromaeosaurids. This suggests that the modes of occlusion might not be homogeneous within scansoriopterygids. The crania of scansoriopterygids also share a number of similarities with those of early-diverging oviraptorosaurians, such as their relative heights and sizes of cranial fenestra. It is noteworthy that scansoriopterygids have a low jaw-opening MA, which suggests that they have a more rapid jaw-opening movement than oviraptorosaurians. This may give them advantages during occasional hunting. In general, this functional and morphological evidence suggests that scansoriopterygids are unlikely to be as adapted to herbivory as oviraptorids, but their diets were probably similar to early-diverging oviraptorosaurians in being mostly made up of plants. Preserved scansoriopteryid stomach contents are unknown, but they will be essential in validating these findings to complement the direct dietary information currently known in early-diverging oviraptorosaurians.

Our results show that caenagnathids are more adapted to predation than other oviraptorosaurians and scansoriopterygids, implying a possible dietary reversal back to the typical carnivorous diet. Unlike oviraptorids, caenagnathids do not display apparent adaptations to herbivory—they have a smaller anterior jaw-closing mechanical advantage (AMA) and a less robust mandible than oviraptorids. Instead, caenagnathids show a number of features that facilitate a carnivorous feeding style. The extremely low relative articular offset of caenagnathids points to a more carnivorous diet compared to oviraptorids and early-diverging oviraptorosaurians. It is noteworthy that dromaeosaurids, which are dominated by carnivorous theropods, also have a very small relative articular offset that is comparable to caenagnathids. Caenagnathids also have a smaller opening mechanical advantage than oviraptorids, which can be interpreted as having a higher jaw-opening velocity for prey capture. Caenagnathids and dromaeosaurids have a high posterior mechanical advantage relative to their anterior mechanical advantage. This pattern can be interpreted as an indication of carnivory as carnivores usually have a "scissorlike" occlusal style (Greaves, 1974; Grubich et al., 2008), such that the posterior part of the dentary is also actively involved in food processing. The anteriormost tip of the mandibles of caenagnathids appears to be more recurved and sharper compared with those of oviraptorids. Having a pointed beak tip is favourable for slashing meat (Funston et al., 2016) and prey capturing—the tip allows bite force to be concentrated at one point for killing the prey effectively. The mandibles of caenagnathids are likely adapted to shearing action, which could actually benefit both cutting of foliage and meat (Funston and Currie, 2014; Ma et al., 2017). In modern carnivores, shearing is the dominant food-processing mechanism whereas crushing plays only a minor role (Sanson, 2016). The carnivorous affinity of caenagnathids is also supported by their postcranial anatomy. Although the recurved claws of oviraptorids have been considered an indication of carnivory (Osmolska et al., 2004), geometric morphometric analysis shows that oviraptorosaurian claws are morphologically similar to those of therizinosaurians (Lautenschlager, 2014), suggesting that the possession of recurved claws may not necessarily be a sign of carnivory. Despite this, the arctometatarsalian condition in caenagnathids suggests that they are more cursorial than oviraptorids, which is possibly linked to predation (Funston et al., 2016). The hands and feet of caenagnathids are also more elongated than those of oviraptorids, which shows grasping and prey capture ability that is not commonly seen in herbivorous dinosaurs (Longrich et al., 2013). It was hypothesized that their limbs may be suited for tree climbing or grasping of vegetation for feeding (Longrich et al., 2013). However, considering the mandibular features and postcranial anatomy of caenagnathids, it seems more likely that the limbs of caenagnathids are primarily adapted for predation. All this evidence suggests that caenagnathids are likely to have had an omnivorous diet that was more carnivorous than that of oviraptorids and possibly other oviraptorosaurians and scansoriopterygids.

Although the six functional characteristics were developed based on the fact that they have shown convergence in independently evolved modern herbivores, including birds, we still need to be careful when interpreting the results—distinct diets may share similar functional demands. Similar to herbivory, the evolution of a durophagous diet results in an animal's larger bite force with less selective pressure on the speed of food procurement compared with a nonherbivorous sister taxon. By solely considering the results of the functional analysis, one may conclude that oviraptorids were more specialized in durophagy than any other early-diverging pennaraptorans. Durophagy, in particular feeding on freshwater molluscs, has long been suggested as a feeding mode of oviraptorids (Barsbold, 1983). However, this hypothesis is weakly supported by their environmental preferences—oviraptorids are discovered mainly in arid environments, although they have also been found in fluvial deposits (Longrich et al., 2010, 2013; Funston et al., 2017). Freshwater molluscs are less likely to be abundant in drought-prone environments (García et al., 2010), and so it is doubtful that the skulls of oviraptorids are primarily adapted for consuming them. An herbivorous diet is a more probable hypothesis for the diet of oviraptorids. Despite this, we cannot rule out the possibility that oviraptorids occasionally included molluscs or other items in their diets, as their robust skulls may have allowed them to do so. The robust mandibles of parrots, which are morphologically similar to those of oviraptorosaurians (Longrich et al., 2010, 2013; Funston and Currie, 2014; Ma et al., 2017), are capable of procuring a wide range of food items including nuts, seeds, fruits, leaves, stems, and bark (Benavidez et al., 2018). We suggest that the highly specialized skulls of oviraptorids allowed them to consume not only tough vegetation, but also harder plant materials such as stems, seeds, and nuts. This might have provided them with an additional advantage in an arid environment, as plant materials (e.g., leaves, seeds) tend to be thicker and harder in a dry environment to prevent water loss (Jones, 2013).

Various degrees of tooth reduction can be observed among early-diverging pennaraptorans—early-diverging oviraptorosaurians, scansoriopterygids, and some early-diverging avialans exhibit partial tooth loss; late-diverging oviraptorosaurians (*Avimimus*, caenagnathids and oviraptorids) are edentulous; dromaeosaurids do not show tooth loss. An extensive study on tooth reduction in theropod dinosaurs clarified the mechanisms involved, suggesting that tooth reduction involves a series of transformations and further tooth reduction is associated with the formation of a more extensive rhamphotheca (Wang et al., 2017: fig. 4). The possession of a rhamphotheca has been demonstrated to have a stress mitigation effect on the skull (Lautenschlager et al., 2013). Developing a rhamphotheca is beneficial to herbivores as it reduces the risk of skull failure during plant procurement (Lautenschlager et al., 2013). This may explain why different dental anatomies are observed among late-diverging oviraptorosaurians—lingual grooves are present in some caenagnathids but absent in all known oviraptorids. Lingual grooves are likely to be vestigial alveoli (Wang et al., 2017) and their presence in caenagnathids suggests that rhamphothecae are likely to be less extensive in caenagnathids than in oviraptorids. The reason may be that oviraptorids are more specialized in herbivory, and hence they have experienced a larger selective pressure in increasing their skull stability.

Early-diverging members of several theropod lineages have evolved beaklike structures, and are likely to have undergone development of different morphological strategies in response to functional demands possibly related to dietary shifts (Lautenschlager et al., 2013). Early-diverging oviraptorosaurians experienced partial tooth reduction and developed a complete edentulous beak in their late-diverging forms. Instead of developing an edentulous beak like late-diverging oviraptorosaurians, the scansoriopterygid *Epidexipteryx* evolved a different dentition pattern: it has tightly packed mandibular teeth that are reminiscent of the shape of a beak. By possessing anteriorly enlarged and densely packed procumbent teeth, the dentary of *Epidexipteryx* is morphologically and possibly functionally similar to those of beaked oviraptorosaurians. Although Oviraptorosauria and Scansoriopterygidae are closely related clades, their members have shown distinct strategies in adapting to herbivory (observed or suspected), the former by developing an edentulous beak, the latter by modifying the size and the arrangement of teeth. This adds to the known diversity of mandibular morphology in theropod dinosaurs and highlights the innovations in the feeding apparatus accompanying the dietary shift by pennaraptorans closely related to avialans.

CONCLUSIONS

This study presents the first comprehensive analysis of the dietary habits of scansoriopterygids and oviraptorosaurians from both anatomical and functional perspectives, with reference to dietary patterns observed in extant animals. The results of the comparative anatomy and functional analyses consistently suggest that oviraptorid skulls are more adapted to herbivory than caenagnathids, early-diverging oviraptorosaurians, and scansoriopterygids. Scansoriopterygids are less adapted to herbivory than oviraptorids because they have a lower dorsoventral height, a smaller lateral temporal fenestra, a smaller jaw-closing mechanical advantage and lack a tall coronoid process prominence. Some caenagnathids possess features like an extremely small relative articular offset and small average mandible height that may imply a more carnivorous diet than those of other oviraptorosaurians. Our study provides a new perspective to evaluate various hypotheses on the diets of scansoriopterygids and oviraptorosaurians, and demonstrates the high dietary complexity among early-diverging pennaraptorans. Future work involving other approaches such as geochemical proxies of diet and 3D biomechanical modeling would provide additional opportunities to test these hypotheses. However, this study provides insights that are important to our understanding of the dietary evolution of theropods close to the origin of birds.

ACKNOWLEDGMENTS

This study was supported by funding for the HKU MOOC Dinosaur Ecosystems. We thank Kenneth H.C. Fung and First Initiative Foundation for their support of the International Pennaraptoran Dinosaur Symposium, which was the catalyst for this study.

REFERENCES

Agnolín, F.L., and F.E. Novas. 2013. Review of the phylogenetic relationships of the theropods Unenlagiidae, Microraptoria, Anchiornis and Scansoriopterygidae. Dordrecht: Springer.

Balanoff, A.M., and M.A. Norell. 2012. Osteology of *Khaan mckennai* (Oviraptorosauria: Theropoda). Bulletin of the American Museum of Natural History 372: 1–77.

Balanoff, A.M., X. Xu, Y. Kobayashi, Y. Matsufune, and M.A. Norell. 2009. Cranial osteology of the theropod dinosaur *Incisivosaurus gauthieri* (Theropoda: Oviraptorosauria). American Museum Novitates 3651: 1–35.

Barrett, P.M. 2001. Tooth wear and possible jaw action of *Scelidosaurus harrisonii* Owen and a review of feeding mechanisms in other thyreophoran dinosaurs. *In* K. Carpenter (editor), The armored dinosaurs: 25–52. Bloomington: Indiana University Press.

Barsbold, R. 1983. Carnivorous dinosaurs from the Cretaceous of Mongolia. Translation of "Khishchnye dinozavry mela Mongolii," in Transactions of the Joint Soviet-Mongolian Paleontological Expedition. Moscow: Nauka.

Benavidez, A., F.X. Palacio, L.O. Rivera, A.L. Echevarria, and N. Politi. 2018. Diet of Neotropical parrots is independent of phylogeny but correlates with body size and geographical range. Ibis 160: 742–754.

Brusatte, S.L., G.T. Lloyd, S.C. Wang, and M.A. Norell. 2014. Gradual assembly of avian body plan culminated in rapid rates of evolution across the dinosaur-bird transition. Current Biology 24: 2386–2392.

Burnham, D.A., et al. 2000. Remarkable new birdlike dinosaur (Theropoda: Maniraptora) from the Upper Cretaceous of Montana. University of Kansas Paleontological Contributions 13: 1–12.

Clark, J.M., M.A. Norell, and T. Rowe. 2002. Cranial anatomy of *Citipati osmolskae* (Theropoda, Oviraptorosauria), and a reinterpretation of the holotype of *Oviraptor philoceratops*. American Museum Novitates 3364: 1–24.

Currie, P.J. 1995. New information on the anatomy and relationships of *Dromaeosaurus albertensis* (Dinosauria: Theropoda). Journal of Vertebrate Paleontology 15: 576–591.

Currie, P.J., S.J. Godfrey, and L. Nessov. 1993. New caenagnathid (Dinosauria: Theropoda) specimens from the Upper Cretaceous of north America and Asia. Canadian Journal of Earth Sciences 30: 2255–2272.

Czerkas, S.A., and C. Yuan. 2002. An arboreal maniraptoran from northeast China. *In* S.J. Czerkas (editor), Feathered dinosaurs and the origin of flight, vol. 1: 63–95. Blanding, UT: Dinosaur Museum.

Emerson, S.B. 1985. Skull shape in frogs: correlations with diet. Herpetologica: 177–188.

Freeman, P.W. 1979. Specialized insectivory: beetle-eating and moth-eating molossid bats. Journal of Mammalogy 60: 467–479.

Funston, G.F., and P.J. Currie. 2014. A previously undescribed caenagnathid mandible from the late Campanian of Alberta, and insights into the diet of *Chirostenotes pergracilis* (Dinosauria: Oviraptorosauria). Canadian Journal of Earth Sciences 51: 156–165.

Funston, G.F., and P.J. Currie. 2016. A new caenagnathid (Dinosauria: Oviraptorosauria) from the Horseshoe Canyon Formation of Alberta, Canada, and a reevaluation of the relationships of Caenagnathidae. Journal of Vertebrate Paleontology 36: e1160910.

Funston, G.F., P.J. Currie, and M.E. Burns. 2016. New elmisaurine specimens from North America and their relationship to the Mongolian *Elmisaurus rarus*. Acta Palaeontologica Polonica 61: 159–173.

Funston, G.F., S.E. Mendonca, P.J. Currie, and R. Barsbold. 2017. Oviraptorosaur anatomy, diversity and ecology in the Nemegt Basin. Palaeogeography, Palaeoclimatology, Palaeoecology 494: 101–120.

García, N., A. Cuttelod, and D.A. Malak. 2010. The status and distribution of freshwater biodiversity in Northern Africa. Gland, Switzerland: IUCN.

Greaves, W. 1974. Functional implications of mammalian jaw joint position. Forma et Functio 7: 363–376.

Grubich, J.R., A.N. Rice, and M.W. Westneat. 2008. Functional morphology of bite mechanics in the great barracuda (*Sphyraena barracuda*). Zoology 111: 16–29.

Hanken, J., and B.K. Hall. 1993. The skull, vol. 3: functional and evolutionary mechanisms. Chicago: University of Chicago Press.

Hieronymus, T.L., and L.M. Witmer. 2010. Homology and evolution of avian compound rhamphothecae. Auk 127: 590–604.

Holliday, C.M. 2009. New insights into dinosaur jaw muscle anatomy. Anatomical Record 292: 1246–1265.

Ji, Q., P.J. Currie, M.A. Norell, and S.A. Ji. 1998. Two feathered dinosaurs from northeastern China. Nature 393: 753–761.

Ji, Q., J.C. Lü, X.F. Wei, and X.R. Wang. 2012. A new oviraptorosaur from the Yixian Formation of Jianchang, Western Liaoning Province, China. Regional Geology of China 12: 2102–2107.

Jones, H.G. (editor). 2013. Plants and microclimate: a quantitative approach to environmental plant physiology. Cambridge: Cambridge University Press.

Kammerer, C.F., L. Grande, and M.W. Westneat. 2006. Comparative and developmental functional morphology of the jaws of living and fossil gars (Actinopterygii: Lepisosteidae). Journal of Morphology 267: 1017–1031.

Lamanna, M.C., H.D. Sues, E.R. Schachner, and T.R. Lyson. 2014. A new large-bodied oviraptorosaurian theropod dinosaur from the latest Cretaceous of western North America. PLoS One 9: e92022.

Lautenschlager, S. 2014. Morphological and functional diversity in therizinosaur claws and the implications for theropod claw evolution. Proceedings of the Royal Society B, Biological Sciences 281: 20140497.

Lautenschlager, S., L.M. Witmer, P. Altangerel, and E.J. Rayfield. 2013. Edentulism, beaks, and biomechanical innovations in the evolution of theropod dinosaurs. Proceedings of the National Academy of Sciences of the United States of America 110: 20657–20662.

Lautenschlager, S., L.M. Witmer, P. Altangerel, L.E. Zanno, and E.J. Rayfield. 2014. Cranial anatomy of *Erlikosaurus andrewsi* (Dinosauria, Therizinosauria): new insights based on digital reconstruction. Journal of Vertebrate Paleontology 34: 1263–1291.

Longrich, N.R., P.J. Currie, and Z. Dong. 2010. A new oviraptorid (Dinosauria: Theropoda) from the Upper Cretaceous of Bayan Mandahu, Inner Mongolia. Palaeontology 53: 945–960.

Longrich, N.R., K. Barnes, S. Clark, and L. Millar. 2013. Caenagnathidae from the Upper Campanian Aguja Formation of West Texas, and a Revision of the Caenagnathinae. Bulletin of the Peabody Museum of Natural History 54: 23–49.

Lü, J.C., et al. 2013. Chicken-sized oviraptorid dinosaurs from central China and their ontogenetic implications. Naturwissenschaften 100: 165–175.

Lü, J.C., et al. 2017. High diversity of the Ganzhou Oviraptorid Fauna increased by a new "cassowary-like" crested species. Scientific Reports 7: 6393.

Lü, J.C., Y. Tomida, Y. Azuma, Z.M. Dong, and Y.N. Lee. 2004. New oviraptorid dinosaur (Dinosauria: Oviraptorosauria) from the Nemegt Formation of southwestern Mongolia. Bulletin of the National Science Museum Series C (Geology and Paleontology) 30: 95–130.

Lü, J.C., et al. 2015. A new oviraptorid dinosaur (Dinosauria: Oviraptorosauria) from the Late Cretaceous of southern China and its paleobiogeographical implications. Scientific Reports 5: 11490.

Lü, J.C., R.J. Chen, S.L. Brusatte, Y.X. Zhu, and C.Z. Shen. 2016. A Late Cretaceous diversification of Asian oviraptorid dinosaurs: evidence from a new species preserved in an unusual posture. Scientific Reports 6: 35780.

Ma, W., et al. 2017. Functional anatomy of a giant toothless mandible from a bird-like dinosaur: *Gigantoraptor* and the evolution of the oviraptorosaurian jaw. Scientific Reports 7: 16247.

Ma, W., S.L. Brusatte, J.C. Lü and M. Sakamoto. 2020. The skull evolution of oviraptorosaurian dinosaurs: the role of niche partitioning in diversification. Journal of Evolutionary Biology 33: 178–188.

Maddison, W.P., and D.R. Maddison. 2018. Mesquite: a modular system for evolutionary analysis. Version 3.4. Online resource (http://mesquiteproject.org).

Martin, L.D., Z. Zhou, L. Hou, and A. Feduccia. 1998. *Confuciusornis sanctus* compared to *Archaeopteryx lithographica*. Naturwissenschaften 85: 286–289.

Metzger, K.A., and A. Herrel. 2005. Correlations between lizard cranial shape and diet: a quantitative, phylogenetically informed analysis. Biological Journal of the Linnean Society 86: 422–435.

Navalón, G., J.A. Bright, J. Marugán-Lobón, and E.J. Rayfield. 2018. The evolutionary relationship among beak shape, mechanical advantage, and feeding ecology in modern birds. Evolution 73: 419–631.

Nogueira, M.R., A.L. Peracchi, and L.R. Monteiro. 2009. Morphological correlates of bite force and diet in the skull and mandible of phyllostomid bats. Functional Ecology 23: 715–723.

O'Connor, J.M.K., and C. Sullivan. 2014. Reinterpretation of the Early Cretaceous maniraptoran (Dinosauria: Theropoda) *Zhongornis haoae* as a scansoriopterygid-like non-avian, and morphological resemblances between scansoriopterygids and basal oviraptorosaurs. Vertebrata PalAsiatica 52: 3–30.

Olsen, A.M. 2017. Feeding ecology is the primary driver of beak shape diversification in waterfowl. Functional Ecology 31: 1985–1995.

Osborn, H.F., P.C. Kaisen, and G. Olsen. 1924. Three new Theropoda, *Protoceratops* zone, central Mongolia. American Museum Novitates 144: 1–12.

Osmólska, H., P.J. Currie, and R. Barsbold. 2004. Oviraptorosauria. *In* Weishampel, D.B., P. Dodson, and H. Osmolska (editors), The Dinosauria: 165–183. Berkeley: University of California Press.

Ostrom, J.H. 1969. Osteology of *Deinonychus antirrhopus*, an unusual theropod from the Lower Cretaceous of Montana. New Peabody Museum of Natural History, Yale University, Bulletin 30: 1–165.

Pei, R., et al. In press. Potential for powered flight neared by most close avialan relatives but few crossed its thresholds. Current Biology.

Sacco, T., and B. Van Valkenburgh. 2004. Ecomorphological indicators of feeding behaviour in the bears (Carnivora: Ursidae). Journal of Zoology 263: 41–54.

Samuels, J.X. 2009. Cranial morphology and dietary habits of rodents. Zoological Journal of the Linnean Society 156: 864–888.

Sanson, G. 2016. Cutting food in terrestrial carnivores and herbivores. Interface Focus 6: 20150109.

Stayton, C.T. 2006. Testing hypotheses of convergence with multivariate data: morphological and functional convergence among herbivorous lizards. Evolution 60: 824–841.

Thomason, J. 1997. Functional morphology in vertebrate paleontology. Cambridge: Cambridge University Press.

Tsuihiji, T., M. Watabe, K. Tsogtbaatar, and R. Barsbold. 2016. Dentaries of a caenagnathid (Dinosauria: Theropoda) from the Nemegt Formation of the Gobi Desert in Mongolia. Cretaceous Research 63: 148–153.

Wang, M., J.M.K. O'Connor, X. Xu, and Z.H. Zhou. 2019. A new Jurassic scansoriopterygid and the loss of membranous wings in theropod dinosaurs. Nature 569: 256–259.

Wang, S., et al. 2017. Heterochronic truncation of odontogenesis in theropod dinosaurs provides insight into the macroevolution of avian beaks. Proceedings of the National Academy of Sciences of the United States of America 114: 10930–10935.

Wei, X.F., H.Y. Pu, L. Xu, D. Liu, and J.C. Lü. 2013. A new oviraptorid dinosaur (Theropoda: Oviraptorosauria) from the Late Cretaceous of Jiangxi Province, Southern China. Acta Geologica Sinica (English edition) 87: 899–904.

Xu, X., and F.L. Han. 2010. A new oviraptorid dinosaur (Theropoda: Oviraptorosauria) from the Upper Cretaceous of China. Vertebrata PalAsiatica 48: 11–18.

Xu, X., Y.N. Cheng, X.L. Wang, and C.H. Chang. 2002. An unusual oviraptorosaurian dinosaur from China. Nature 419: 291–293.

Xu, X., Q.W. Tan, J.M. Wang, X.J. Zhao, and L. Tan. 2007. A gigantic bird-like dinosaur from the Late Cretaceous of China. Nature 447: 844–847.

Xu, X., H.L. You, K. Du, and F.L. Han. 2011. An *Archaeopteryx*-like theropod from China and the origin of Avialae. Nature 475: 465–470.

Xu, X., et al. 2015. A bizarre Jurassic maniraptoran theropod with preserved evidence of membranous wings. Nature 521: 70–73.

Xu, X., et al. 2017. Mosaic evolution in an asymmetrically feathered troodontid dinosaur with transitional features. Nature Communications 8: 14972.

Zanno, L.E., and P.J. Makovicky. 2011. Herbivorous ecomorphology and specialization patterns in theropod dinosaur evolution. Proceedings of the National Academy of Sciences of the United States of America 108: 232–237.

Zanno, L.E., and P.J. Makovicky. 2013. No evidence for directional evolution of body mass in herbivorous theropod dinosaurs. Proceedings of the Royal Society of London B, Biological Sciences 280: 20122526.

Zanno, L.E., K. Tsogtbaatar, T. Chinzorig, and T.A. Gates. 2016. Specializations of the mandibular anatomy and dentition of *Segnosaurus galbinensis* (Theropoda: Therizinosauria). PeerJ 4: e1885.

Zhang, F.C., Z.H. Zhou, X. Xu, and X.L. Wang. 2002. A juvenile coelurosaurian theropod from China indicates arboreal habits. Naturwissenschaften 89: 394–398.

Zhang, F.C., Z.H. Zhou, X. Xu, X.L. Wang, and C. Sullivan. 2008. A bizarre Jurassic maniraptoran from China with elongate ribbon-like feathers. Nature 455: 1105.

Zhou, Z.H., and F.C. Zhang. 2003. Anatomy of the primitive bird *Sapeornis chaoyangensis* from the Early Cretaceous of Liaoning, China. Canadian Journal of Earth Sciences 40: 731–747.

Chapter 9

Fossil Microbodies Are Melanosomes: Evaluating and Rejecting the "Fossilized Decay-Associated Microbes" Hypothesis

ARINDAM ROY,[1] CHRISTOPHER S. ROGERS,[2] THOMAS CLEMENTS,[3]
MICHAEL PITTMAN,[1] OLIVIER HABIMANA,[4] PETER MARTIN,[5] AND JAKOB VINTHER[6]

ABSTRACT

Melanosomes are membrane-bound organelles of varying geometry, commonly found within a range of vertebrate tissues, that contain the pigment melanin. Melanosomes have been identified in the fossil record in many exceptionally preserved fossils allowing reconstructions of the coloration of many extinct animals. However, these microstructures have also been interpreted as "microbial cells" or melanin-producing bacteria based on their geometric similarities to melanosomes. Here we test these two conflicting hypotheses experimentally. Our results demonstrate multiple lines of evidence that these fossil microbodies are indeed melanosomes: the geometry of decay-associated microbes differs significantly from fossil microbodies; fossil microbodies are very strongly localized to in vivo melanized tissues and are absent in tissues typically unmelanized in vivo, in all fossils examined regardless of lithology or age.

On the basis of these results, as well as a thorough review of existing literature on melaninlike pigments, we are able to rule out a bacterial origin for fossil microbodies associated with exceptional vertebrate fossils and demonstrate that fossil microbodies are in fact preserved melanosomes.

INTRODUCTION

Integumentary coloration and patterning are instrumental to comprehending an animal's life history and evolution (Burley et al., 1982; Butcher and Rohwer, 1989). Coloration is commonly utilized by animals for aposematic signals, crypsis, sociosexual selection and optimizing physiological functions (Cuthill et al., 2017). Pigmentary systems (including melanins, carotenoids and porphyrins) produce coloration through selective absorbance and reflectance of wavelengths of light (Hill and McGraw, 2006a; 2006b). Additionally, structural integumentary coloration is produced by scattering of different wavelengths of light due to nanoscale variations in refractive indices of the tissue constituents making up the integumen-

---

[1] Vertebrate Palaeontology Laboratory, Division of Earth and Planetary Science, the University of Hong Kong, Hong Kong.

[2] School of Biological, Earth and Environmental Sciences and Environmental Research Institute, University College Cork, Cork, Ireland.

[3] School of Geography, Earth and Environmental Sciences, University of Birmingham, Edgbaston, Birmingham, U.K.

[4] School of Biological Sciences, the University of Hong Kong, Hong Kong.

[5] Interface Analysis Centre, H.H. Wills Physics Laboratory, School of Physics, University of Bristol, Bristol, U.K.

[6] School of Earth Sciences, University of Bristol, Bristol, U.K.

tary structures (Prum, 1999). Melanin pigments are widespread among vertebrates and have garnered much interest within the paleontological community in the last decade (Vinther et al., 2008, 2010, 2015, 2020; Li et al., 2010, 2012; Clements et al., 2016; McNamara et al., 2016; Roy et al., 2020) especially because the identification of fossilized pigments has allowed the color of extinct organisms to be interpreted, which has provoked significant scientific and cultural interest (Vinther, 2015, 2020; Roy et al., 2020). What makes melanin especially important to fossil color reconstruction is its intrinsic synthesis as a metabolic product (rather than the result of dietary uptake, e.g., carotenoids), and its potential for preservation in various taxa across deep time (Vinther et al., 2008; Glass et al., 2012).

Melanin is most commonly found within vertebrates encased within lysosome-derived, membrane-bound and subcellular vesicles called melanosomes (Raposo et al., 2001). Melanosomes have been described in fossil fish (Lindgren et al., 2012; Tanaka et al., 2014; Clements et al., 2016; Gabbott et al., 2016), amphibians (McNamara et al., 2016, Rossi et al. 2019), marine reptiles (Lindgren et al., 2014), birds (Clarke et al., 2010; Pan et al., 2016; Gren et al., 2017; Zheng et al., 2017), nonavialan dinosaurs (Li et al., 2010, 2012; Zhang et al., 2010; Xu et al., 2015; Vinther et al., 2016; Hu et al., 2018) and mammals (Manning et al., 2019; Rossi et al., 2019).

Animal melanins create a spectrum of colors within a tissue by varying the ratio of dark-brown/black, produced by eumelanin, and rufous to buff, produced by pheomelanin (Vinther et al., 2008). Observations of extant mammalian and avian melanosomes show a geometrical continuum from spherical to "elongate-oblong" shapes. The elongate-oblong integumentary melanosomes that contain high relative proportions of eumelanin and have been termed "eumelanosomes," whereas spherical melanosomes are typically dominated by pheomelanin and are called "pheomelanosomes" (Hill and McGraw, 2006b). It is important to appreciate, though, that natural melanosomes will vary in composition and the eumelanosome/phaeomelanosome dichotomy is only crudely instructive in describing this observed variation.

The reconstruction of color patterns in ancient animals is a burgeoning field of paleontological research and is intricately linked with the geometry of melanin-bearing "melanosome-like microbodies" (Moyer et al., 2014; Lindgren et al., 2015; Schweitzer et al., 2015) preserved in fossils. Investigations into the distribution of melanosomes in fossils led to the identification of countershading in extinct animals allowing ecological and behavioral implications to be inferred (Vinther et al., 2016; Brown et al., 2017; Smithwick et al., 2017). However, the identity of such "microbodies" has been repeatedly called into question, with a counter view (Wuttke, 1983; Toporski et al., 2002; Moyer et al., 2014; Lindgren et al., 2015; Schweitzer et al., 2015) that interprets them as fossilized microbial cells, which they were traditionally identified as, prior to the work of Vinther et al. (2008). This traditional view has been challenged in several studies evaluating the evidence for these microbodies being melanosomes, based on four important characteristics: (1) geometric and spatial consistency with extant melanosomes (Vinther et al., 2008; Li et al., 2010; Zhang et al., 2010; Li et al., 2012); (2) concentration of microbodies in fossilized vertebrate tissues that originally contained melanosomes, i.e., feathers, eyes, and visceral organs (Vinther et al., 2008; Zhang et al., 2010; Gabbott et al., 2016); (3) preserved color patterns (Vinther et al., 2008); and (4) presence of chemical signatures of melanin-derived compounds in the microbodies (Glass et al., 2012 , 2013; Colleary et al., 2015).

Despite this body of direct and indirect evidence, a consensus regarding the identity of fossil microbodies has yet to be reached. Four main counterarguments have been posited in favor of the microbial identity of fossil micro-

TABLE 1

Melanosomes measured from feathers of modern birds

No..	Species sampled	Feather color	Sample size	Melanosome shape
1	*Tragopan* sp.	Black	162	Elongate rod
2	Sunbittern (*Eurypyga helias*)	Dark brown	100	Spherical/oblate
3	Turaco (species unknown)	Iridescent	144	Elongate rod
4	Palawan peacock-pheasant (*Polyplectron napoleonis*)	Iridescent	150	Elongate rod
5	Chicken (*Gallus gallus*)	Iridescent tructural	50	Oblong
6	Black-throated trogon (*Trogon rufus*)	Iridescent structural	50	Elongate rod
7	Bar-tailed trogon (*Apaloderma vittatum*)	Iridescent structural	60	Elongate rod
8	Eurasian kingfisher (*Alcedo atthis*)	Noniridescent structural	65	Oblong
9	Black-capped kingfisher (*Halcyon pileata*)	Noniridescent structural	70	Oblong
10	Blue cuckooshrike (*Coracina azurea*)	Noniridescent structural	80	Elongate rod/ oblong
11	Ivory-breasted pitta (*Pitta maxima*)	Noniridescent structural	70	Oblong
12	Rock dove (*Columba livia*)	Gray	150	Elongate rod
13	Victoria crowned pigeon (*Goura victoria*)	Gray	131	Spherical/oblong

bodies (Moyer et al., 2014; Lindgren et al., 2015; Schweitzer et al., 2015): (1) frameworks seen in fossil microbodies are formed because microbes align themselves in biofilms (Toporski et al., 2002; Moyer et al., 2014); (2) decay-related microbes readily colonize dead bodies and so would naturally be preserved and more readily visible than melanosomes, which would instead be encapsulated by fossilized keratin out of view (Toporski et al., 2002; Moyer et al., 2014; Schweitzer et al., 2015); (3) microbes are ubiquitous, fossilize easily, and are indistinguishable geometrically from melanosomes (Moyer et al., 2014; Schweitzer et al., 2015); and (4) certain microbes (bacteria and fungi) produce melanin pigments that may lead to erroneous chemical identification rather than the melanin in the tissues of the organism itself (Lindgren et al., 2015; Schweitzer et al., 2015). Herein, we test the validity of these arguments, by designing experiments to test the following hypotheses:

(1) Melanosomes and microbial cells are geometrically indistinguishable

(2) Microbes localize and align themselves in orientations akin to extant melanosomes

(3) Microbes fossilize easily and are thus ubiquitous throughout fossils

(4) Microbes are sources of melanin and there is a likelihood of extraneous preservation in fossils.

TABLE 2

Microbody samples measured from isolated fossil feather specimens

No.	Material	Accession code	Sample size	Microbody shape	Source
1	feather	LEUIG 115562	40	Elongate rod	Crato formation, Brazil
2	feather	SMF-ME 3850	60	Elongate rod	Grube Messel, Germany
3	feather	MORS-1003	32	Elongate rod	Island of Mors, Fur Formation, Denmark
4	feather	SMF-ME 3830 (microbody type 1)	54	Elongate rod/ oblong	Grube Messel, Germany
5	feather	SMF-ME 3830 (microbody type 2)	31	Oblong/spherical	Grube Messel, Germany
6	feather	SMF-ME 3800B	40	Elongate rod/ oblong	Grube Messel, Germany
7	feather	SMF-ME 3721	30	Elongate rod	Grube Messel, Germany
8	feather	SMF-ME 3719A	40	Elongate rod	Grube Messel, Germany
9	feather	SMF-ME 3815	40	Elongate rod	Grube Messel, Germany

TABLE 3

Fossilised feather specimens associated with skeletal material, used for sampling and measurement of microbodies

No.	Specimen	Accession code	Sample size	Microbody shape	Taxon	Source
1	Danekræ 200	MGUH 28.929	40	Elongate rod	Aves	Fur, Denmark
2	*Eocypselus vincenti*	MHUG 26729	40	Elongate rod/ oblong	Aves	Fur, Denmark
3	*Eocoracias* sp.	Un-accessioned	35	Elongate rod/ oblong	Aves	Grube Messel, Germany
4	Unknown feather with tail	FUM-N 2275	34	Elongate rod	Aves	Fur, Denmark
5	*Hassiavis laticauda*	HLMD-ME 9047a	50	Elongate rod	Aves	Grube Messel, Germany
6	*Messelirrisor halcyrostris*	SMF-ME 10987b	40	Elongate rod	Aves	Grube Messel, Germany
7	Unknown (with head crest)	HLMD-ME 15634a	50	Elongate rod/ oblong	Aves	Grube Messel, Germany
8	*Anchiornis huxleyi* (microbody type 1)	BMNHC PH828	40	Spherical/ oblate	Avialae	Liaoning, China
9	*Anchiornis huxleyi* (microbody type 2)	BMNHC PH828	40	Elongate rod/ oblong	Avialae	Liaoning, China
10	*Microraptor gui*	BMNHC PH881	50	Elongate rod/ oblong	Dromaeosauridae	Liaoning, China

TABLE 4

Fossil anuran specimens used for sampling and measurement of microbodies

No.	Specimen	Accession code	Sample size	Microbody shape	Taxon	Material	Formation
1	*Pelobates* sp.	PW 2005-5034LS_ GDKE	60	Spherical/oblate	Anuran tadpole	Skin	Enspel, Germany
2	Pipidae	MU 41-13	50	Spherical/oblate	Anura	Skin	Mush valley, Ethiopia
3	*Paleobatrachus* sp.	SMF-ME 11390a	70	Spherical/oblate	Anura	Skin	Messel, Germany

MATERIALS AND METHODS

Sampling of Melanosome Geometry through Scanning Electron Microscopy

Modern melanosomes were extracted from the feathers of 13 extant birds (table 1) and the skin and liver of *Xenopus* sp. Melanin extracts and tissue samples from decay experiments were air dried, affixed to aluminium stubs with double-sided carbon tape, and sputter-coated with gold. Fossil microbody samples were measured from SEM images of exceptionally preserved specimens (tables 2–4). Modern melanosomes and fossil microbodies were imaged at an accelerating voltage of 5–15 keV using a Hitachi 3500N SEM. Melanosomes and microbodies were measured using Image J v.1.52 (Schneider et al., 2012).

Decay Experiments to Investigate the Geometry of Microbial Cells

Actuopalaeontological laboratory experiments (Valentine, 1989; Kowalewski, 1999; Briggs and Crowther, 2008; Sansom, 2014; Zuschin and Ebner, 2015) modeling decay under submerged, freshwater lacustrine, marine, and estuarine conditions, were carried out on a range of specimens: (1) isolated feathers (table 5), (2) bird carcasses (table 6) and (3) clawed frog (*Xenopus* sp.) tadpole carcasses (table 7). Chicken (*Gallus gallus*) and golden pheasant (*Chrysolophus pictus*) feathers were chosen for this experiment due to their availability and range of colors as well as their prior experimental use to facilitate comparisons with these studies (Ichida et al., 2001; Moyer et al., 2014; Schweitzer et al., 2015). Recently deceased bird carcasses were provided by the Royal Society for the Prevention of Cruelty to Animals (RSPCA).

Isolated feathers and bird carcasses were placed in individually sealed vessels of two sizes, 250 ml and 1 L, filled with either pond water or mineral water with estuarine sediment. Within 250 ml glass jars, isolated feathers were submerged in: (1) 180 ml of pond water, sparing amounts of pond sediment (<5 g), and small amounts of algal material, and (2) 180 ml of mineral water with fresh sediment (30 g) collected from the Severn estuary mudflats. The isolated feather decay experiments were conducted over two- and four-week intervals. Whole carcasses of two British Dipper (*Cinclus cinclus gularis*) and Eurasian Kingfisher (*Alcedo atthis*) were placed in separate 1 L containers. One specimen of *C. gularis* was submerged in 750 ml of pond water (<5 g sediment/container). The other *C. gularis* and *A. atthis* carcasses were submerged in 120 g (wet weight) of estuarine sediment and 750 ml of mineral water. All three carcasses were secured underwater using a plastic mesh. One feather was sampled from each whole bird carcass at several locations (head and neck, back, breast, wings, flank, abdomen and tail) at one- and two-week intervals. Additionally, *Xenopus* sp. tadpoles, euthanized in accordance with Schedule 1 of the United Kingdom Animals (Scientific Procedures) Act (1986), were

TABLE 5

Treatments, sample sizes and bacterial morphotypes observed in isolated feather decay experiments
(* measured from Ichida et al., 2001: fig. 6)

No.	Isolated feathers	Decay time	Treatments	Sample size	Bacterial morphotypes
1	Keratin digesting bacteria	4 weeks	*	35	baciliform, coccoid, coccobaciliform
2	Black chicken feather	2 weeks	Estuarine sediment + mineral water	42	baciliform, coccoid
3	Black chicken feather	2 weeks	Pond water	100	baciliform, coccoid, flagellated vibrio, fusiform
4	White chicken feather	2 weeks	Pond water	45	baciliform, coccoid
5	Variegated golden pheasant feather	2 weeks	Pond water	80	baciliform, coccoid, vibrio, actinomycetes
6	Black chicken feather	4 weeks	Pond water	68	baciliform, coccoid, actinomycetes
7	White chicken feather	4 weeks	Pond water	28	baciliform, coccoid
8	Variegated golden pheasant feather	4 weeks	Pond water	49	baciliform, coccoid, coccobaciliform vibrio, actinomycetes
9	Black chicken feather	4 weeks	Cyanobacterial tank	111	baciliform, coccoid
10	White chicken feather	4 weeks	Cyanobacterial tank	45	baciliform, coccoid

submerged in small 43 ml sealed containers filled with 32 ml of pond water. Three tadpoles (~3 cm long) were sampled after 1, 2, and 5 days of decay. Each individual sealed container was maintained at 22.5° C ± 0.1° C within a temperature-controlled incubator. Isolated feathers were also placed at the bottom of a tank (35 cm × 24 cm × 22 cm) containing artificial sea water, cyanobacterial blooms as well as a variety of marine microflora and fauna that had grown and stabilized over a period of more than six months. Feathers were harvested from the tanks after four weeks. The temperature for the cyanobacterial tank experiment was maintained between 20°–26° C.

All the tissue samples were fixed using 10% neutral buffered formalin (for 30 minutes) and dehydrated using standard histological techniques (Suvarna et al., 2019). Samples were critical point dried (using CO_2 gas), mounted on aluminum stubs using double-sided carbon tape and sputter-coated with gold. The stubs were imaged using a Hitachi S-3500N SEM.

MEASUREMENTS AND STATISTICAL DATA ANALYSIS

Length, diameter, and aspect ratio (length ÷ diameter) of melanosomes ($n = 1521$), microbodies from exceptionally preserved fossils ($n = 927$) and microbial cells from decay experiments ($n = 2117$) were measured. These measurements were pooled into three categories based on their source. The raw data are available at Dryad (https://doi.org/10.5061/dryad.xgxd254dj). Statistical tests were employed to better understand the extent of geometrical overlap between melanosomes, fossil microbodies, and decay-associated microbes.

The datasets were first standardized and the residuals were examined for normality using the Kolmogorov-Smirnov (KSL) and Shapiro-Wilk (S-W) goodness-of-fit tests (Yap and Sim, 2011) using JMP, 14.0 (SAS Institute Inc., 1989–2019). Secondly, since the residuals for all three categories have significant departures from normality ($p < 0.001$), we opted for nonparametric analytical methods (Lehmann, 2006) of comparing

TABLE 6

Treatments, sample sizes and bacterial morphotypes observed in bird carcass associated feather decay experiments

(– indicates no microbial growth)

Bird carcass	Treatment	Feather location	Feather color	Sample size	Decay time	Bacterial morphotypes
British Dipper (*Cinclus cinclus gularis*) #1	Pond water	Head & neck	Black	58	1 week	Baciliform, coccoid, coccobaciliform
		Shoulder	Black	86	1 week	Baciliform, club-rod
		Breast	Black-tipped white	31	1 week	Baciliform, vibrio, spirochaete
		Flank	Grayish black	27	1 week	Baciliform
British Dipper (*Cinclus cinclus gularis*) #2	Estuarine sediment + mineral water	Head & neck	Black	–	1 week	–
		shoulder	Black	-	1 week	–
		Breast	Black-tipped white	43	1 week	Baciliform
		Flank	greyish black	19	1 week	Baciliform, actinomycetes
Eurasian Kingfisher (*Alcedo atthis*)	Estuarine sediment + mineral water	Head (back)	Gray	94	1 week	Baciliform, coccoid, coccobaciliform, actinomycetes
		Shoulder	Greenish blue	35	1 week	Baciliform
		Abdomen	White & ginger with black tip	–	1 week	–
		Tail	Pale blue	95	1 week	Baciliform
British Dipper #1	Pond water	Head & neck	Black	112	2 weeks	Baciliform, coccobaciliform, actinomycetes
		Shoulder	Black	61	2 weeks	Baciliform, coccobaciliform, actinomycetes
		Breast	Black-tipped white	52	2 weeks	Baciliform, coccobaciliform,
		Flank	Grayish black	115	2 weeks	Baciliform, coccoid, coccobaciliform
British Dipper #2	Estuarine sediment + mineral water	Head & neck	Black		2 weeks	Baciliform, club rod
		shoulder	black	75	2 weeks	Baciliform, coccoid, coccobaciliform
		breast	Black-tipped White	80	2 weeks	Baciliform, club rod
		Flank	Grayish black	41	2 weeks	Baciliform, coccoid, fusiform, actinomycetes

TABLE 6 *continued*

Bird carcass	Treatment	Feather location	Feather color	Sample size	Decay time	Bacterial morphotypes
Eurasian Kingfisher	Estuarine sediment + mineral water	Head (back)	Gray	–	2 weeks	–
		Shoulder	Greenish blue	106	2 weeks	Baciliform, fusiform, actinomycetes
		Abdomen	White & ginger with black tip	97	2 weeks	Baciliform, coccoid, actinomycetes
		Tail	Pale blue	42	2 weeks	Baciliform

medians, followed by multiple comparisons (Neuhäuser and Bretz, 2001; for nonpooled analyses using rarefied taxonomic groups, see appendix 1 in the online supplement at: doi.org/10.5531/sd.sp.44). Additionally, principal components analysis (PCA), which has been previously used to separate characteristic ToF-SIMS peaks in the chemical discrimination of fossilized melanin pigments (Colleary et al., 2015), has also been utilized in this study to further visualize the differences between each category's geometrical space. In parallel to pairwise comparisons and PCA, we also log-transform and reexpress the two initial independent variables into two new parameters:

Shape = log (length) + log (diameter) (1)
Size = log (length) – log (diameter) (2)

While shape parameter (1) serves as an estimate of the area, a size parameter (2) captures an estimate of aspect ratio, both of which can adequately characterize regular shapes. Since one of the major questions investigated by this study is the possibility of discriminating between our three sources of data, two statistical methods, discriminant analysis and logistic regression, could potentially be of interest. To accurately capture the estimates of area and aspect ratio, length and diameter were operationalized into variables, i.e., size and shape. However, none of the categories seem to show normal distribution as evidenced by low goodness-of-fit values from KSL test and Normal quantile plots. Since normality of factor distributions is an important assumption for discriminant analysis applied to categorize melanosome types (Li et al., 2010, 2012; Hu et al., 2018), it cannot be applied in this case. Hence, logistic regression, which does not assume any normality of distribution in fitting a nominal multilevel response to independent explanatory variables, was the method of choice. The sources of the data were categorized into three response levels (modern melanosomes, fossil microbodies, and decay-associated microbes) of the dependent variable "Type" (Y, Response). (1) and (2) then become the independent predictor variables (X, Factors). Nominal logistic regression of the two predictor variables (1) and (2) were performed on "Type" first individually to examine the cumulative probability plots and then multinomially to estimate the probabilities of choosing one of the three response levels as a smooth function of the independent explanatory variables.

SURVEY OF BEDDING PLANES IN EXCEPTIONALLY PRESERVED FOSSILS

The matrix of seven exceptionally preserved fossils were investigated using a Zeiss Sigma HD VP Field Emission SEM (FE-SEM) to assess the prevalence of microbodies present in the matrix (table 8). Areas of the fossil likely to be heavily melanized in life (e.g., eyes, feather barb/barbules) were marked with copper tape pointers. A 3×3 grid with nine centered points, each at a vertical

TABLE 7

Treatments, sample sizes and bacterial morphotypes observed in tadpole decay experiments

Xenopus Tadpole	Treatment	Sample size	Decay time	Bacterial morphotypes
#1	Pond water	183	1 day	Baciliform, coccoid, coccobaciliform, vibrio, streptobacilli
#2	Pond water	124	2 days	Baciliform, coccoid, coccobaciliform, streptobacilli

and horizontal distance of 100 μm apart were set up at the rear ends of the copper tape pointer in the matrix. In each specimen a total area of 8748 μm^2 of the matrix was scanned for microbodies.

RESULTS

Decay Experiments on Isolated Feathers and Carcasses

Isolated chicken (*Gallus gallus*) and golden pheasant (*Chrysolophus pictus*) feather samples decayed in pond water, yielded microbial growth after one week and two weeks of decay respectively. SEM images revealed microbial activity on the surface of barbs, barbules, and the rachis of feathers after one and two weeks of decay in brackish and freshwater conditions. The major bacterial morphotypes observed include rod-shaped, spherical, helical, commashaped, and stalked subspherical forms (table 5). One black feather that had decayed for two weeks using sediment inoculum showed randomly oriented bacterial cells with diverse geometry, ranging from bacilliform and coccoid cells to stalked spherical forms. Some of the bacilliform cells were captured in a state of division (fig. 4K).

After one and two weeks of decay, the major bacterial morphotypes observed on the isolated feathers also appear on feathers removed from the whole bird carcasses (fig. 4H–K, table 6). The *Xenopus* tadpoles showed a dense accumulation of bacterial and fungal growth on the wrinkled and partially degraded epidermis after one and two days of decay. After five days the tadpole body had completely disintegrated, so microbes could not be visualized. The morphotypes of microbes observed include rod-shaped and subspherical cells often forming chainlike or three-dimensional multicellular aggregate structures (fig. 4I, table 7).

Statistical Appraisal of the Geometrical Similarity in Melanosomes, Fossil Microbodies, and Decay-Associated Microbial Consortia

KSL and S-W goodness-of-fit tests for the residuals for all three categories show statistically significant deviation from normal distributions, necessitating the use of nonparametric tests. Thus, to avoid violating the normality assumptions for one-way analysis of variance (ANOVA), Wilcoxon/Kruskal Wallis (rank sums) was opted for, which independently demonstrated that for all three variables—length, diameter, and aspect ratio—the null hypothesis (H_0: samples originate from identical populations) was rejected in favor of the alternative hypothesis (H_A: samples originate from dissimilar populations). Multiple pairwise comparisons to further scrutinize the differences between the three categories, the Steel-Dwass method (a nonparametric alternative to the parametric Tukey-Kramer test) exhibited significant differences ($p < 0.0001$) between all possible pairs (modern melanosomes; fossil microbodies, fossil microbodies; decay-associated microbes, modern melanosomes; decay associated microbes) for all three variables. The Hodges-Lehmann statistic (an estimate of the median of the difference) indicates the extent of the differences between the pair (table 9).

The observations from the significant Steel-Dwass test ($p < 0.05$) show that when all three of the parameters are used to make pairwise com-

TABLE 8

Specimens used in survey of bedding planes for preserved microbes

No.	Specimen	Accession code	Taxon	Location
1	Isolated feather	IVPP V15388B	Avialae	Jehol Group, N.E. China
2	Isolated feather	MORS-1003	Aves	Fur Formation, Denmark
3	*Antigonia* sp.	Unaccessioned	Actinopterygii	Ølst formation, Denmark
4	*Esconicthys apopyris*	ROM56792	Dipnoi	Mazon Creek, IL
5	*Acanthodes* sp.	PF11509	Acanthodii	Mazon Creek, IL
6	*Acanthodes* sp.	ROM56807	Acanthodii	Mazon Creek, IL
7	*Bandringa rayi*	ROM56789A	Chondrichthyes	Mazon Creek, IL

TABLE 9

Steel-Dwass multiple comparison tests with the Hodges-Lehmann statistics
(* indicates significant differences)

	Pairwise comparisons		p Value	Hodges-Lehmann
Length	Modern melanosomes	Fossil microbodies	<.0001*	-0.112000
	Fossil microbodies	Decay-associated microbes	<.0001*	-0.358000
	Modern melanosomes	Decay-associated microbes	<.0001*	-0.463000
Diameter	Modern melanosomes	Fossil microbodies	<.0001*	-0.071000
	Fossil microbodies	Decay-associated microbes	<.0001*	-0.156000
	Modern melanosomes	Decay-associated microbes	<.0001*	-0.229000
Aspect ratio	Modern melanosomes	Decay-associated microbes	<.0001*	0.4592003
	Fossil microbodies	Decay-associated microbes	0.0006*	0.2450064
	Modern melanosomes	Fossil microbodies	0.0003*	0.2753790

parisons between modern melanosomes and fossil microbodies, the values of Hodges-Lehmann statistic are the least. Lower values of the Hodges-Lehmann statistic indicate that there is very little difference between the two categories. Additionally, the pairwise relative differences between the other two categories (fossil microbodies and decay-associated microbes; modern melanosomes and decay-associated microbes) elicit the largest values for Hodges-Lehmann statistic indicating that these pairs are very different from each other.

Secondly, PCA also provides further evidence of the distinction between the three categories using the same variables: length, diameter, and aspect ratio. The two-main principal components accounted for 83.84% of the total variance, with PC1 and PC2 accounting for a variance of 43.28% and 40.56% respectively. PC1 was positively correlated with long-axis description parameter, whereas PC2 was negatively correlated with short-axis description parameter (see table 10 for eigenvalues and loadings). The score plot (fig. 1), revealed the presence of two main

TABLE 10

Importance of components and component score coefficients' matrix obtained from PCA

	PC1	PC2	PC3	PC4
Standard deviation	1.3155	1.2737	0.7550	0.2778
Proportion of variance	0.4328	0.4056	0.1425	0.0193
Cumulative proportion	0.4328	0.8382	0.9807	1.0000

	PC1	PC2
Length	0.9469427	0.0569732
Diameter	0.2407538	-0.8809818
Aspect ratio	0.6956320	0.6941172
Type	0.5403630	-0.6008939

groupings, one composed of microbial cells and the other composed of fossils and melanosome microbodies. Results indicate that microbial cells are highly variable in terms of long-axis measurements, and larger in short-axis measurement parameters. Melanosomes and fossil microbodies were, unlike bacterial cells, better described as having the smaller short-axis and moderate long-axis measurements.

Finally, individual logistic fits of "Type" against shape (χ^2 = 56.070, p <0.0001) and size (χ^2 = 2607.614, p <0.0001) both show statistical significance (fig. 2). Better model fit is exhibited by size (R^2 = 0.2730) compared to shape (R^2 = 0.0059); therefore, size is more important in classification of the collected data into modern melanosomes, fossil microbodies, and decay-associated microbodies. This receives further support through the misclassification rate, which is comparatively lower for size (33.03%) than for shape (52.46%). When shape and size, taken together, were regressed against Type, the logistic fit was still statistically significant (χ^2 = 2757.983, p <0.0001), the model fit improves (R^2 = 0.2887) and the misclassification rate drops to 32.31%. Lack-of-fit test for the combined logistic regression is also statistically significant (χ^2 = 6769.544, p ≈ 1), also suggesting that the model fit is quite good. Given that there are three response levels to the dependent variable Type, a misclassification rate cutoff for statistically nonsignificant classification would be 66%. Thus, the results show that we can indeed classify the collected geometrical data based on the source, i.e., melanosomes from modern animals, microbodies from fossils and microbial cells associated with decay of tissues.

SURVEY OF FOSSIL-BEARING BEDDING PLANES

All fossils exhibited localization of microbodies to the tissues and organs that were melanin bearing in life (fig. 3; see also figs. S3–S9 in the online supplement at: doi.org/10.5531/sd.sp.44). Organic microbodies preserved in three dimensions appear in the feather from the Fur Formation (MORS-1003), but the adjacent matrix sampled in the 3 × 3, 100 μm grid yielded no microbodies either as organic structures or impressions (see fig. S9 in appendix 2 in the online supplement at: doi.org/10.5531/sd.sp.44). The same was the case for the feather from Jehol Group (IVPP V15388B), although the microbodies here were preserved only as impressions (see fig. S8 in appendix 2 in the online supplement at: doi.org/10.5531/sd.sp.44). Microbodies in the feathers were furthermore aligned along the barb and barbule axes. The eyes of all Mazon Creek specimens examined in this study and *Antigonia* sp. (Bonde, 1997) from the Fur Formation (see figs. S4–S9 in appendix 2 in the online supplement: doi.org/10.5531/sd.sp.44) display clusters or layers of distinct oblong and oblate microbodies. Like the feathers

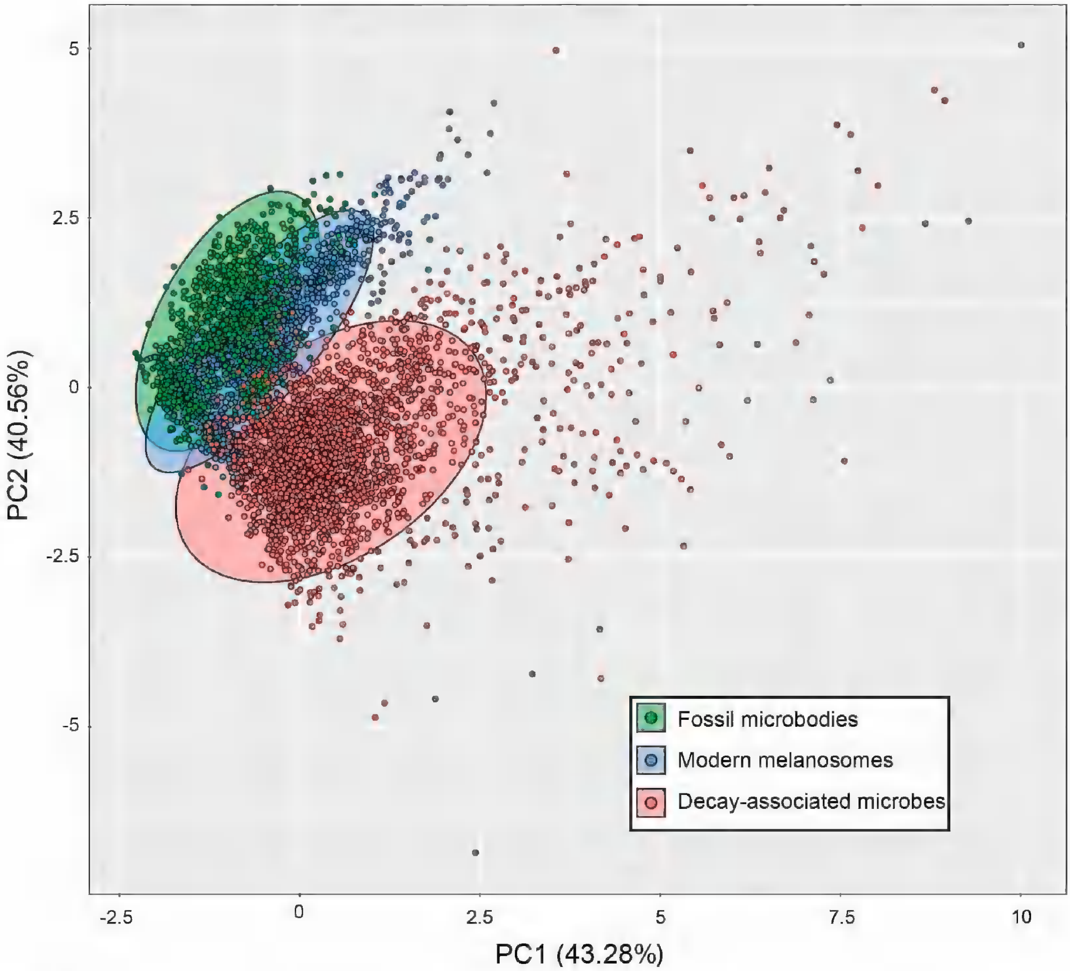

FIG. 1. PCA plot with PC1 and PC2 as axes establishes the presence of two main groupings, one composed of microbial cells and the other composed of intermingled fossils and melanosome microbodies populations; 95% confidence intervals shown by colored ellipses.

examined, the systematic survey of the adjacent matrix yielded no microbodies. Pockets of pyrite framboids appear quite frequently in the matrix but are easily distinguishable from coccoid bacterial cells by their less rounded, regular crystalline facets and framboidal habits.

DISCUSSION

Decay Experiments

The results of the decay experiments demonstrate that geometrically diverse microbes colonize isolated feathers and carcasses (fig. 4). While some microbes do overlap with melanosomes in shape, their size distribution is broader and exceeds the range of sizes observed in melanosomes (fig. 1). Bacterial cells in our experiments are not observed to concentrate or align themselves along barbs or barbule axes like melanosomes in any of our experiments, allowing the rejection of the hypothesis that microbes align like elongate melanosomes in modern avian feathers. Decay microbes typically populated areas of the feather that were sheltered and relatively secluded from strong flow regimes (therefore, efficacious for attachment an establishment of biofilms, e.g., at platelike barbule surfaces, junction

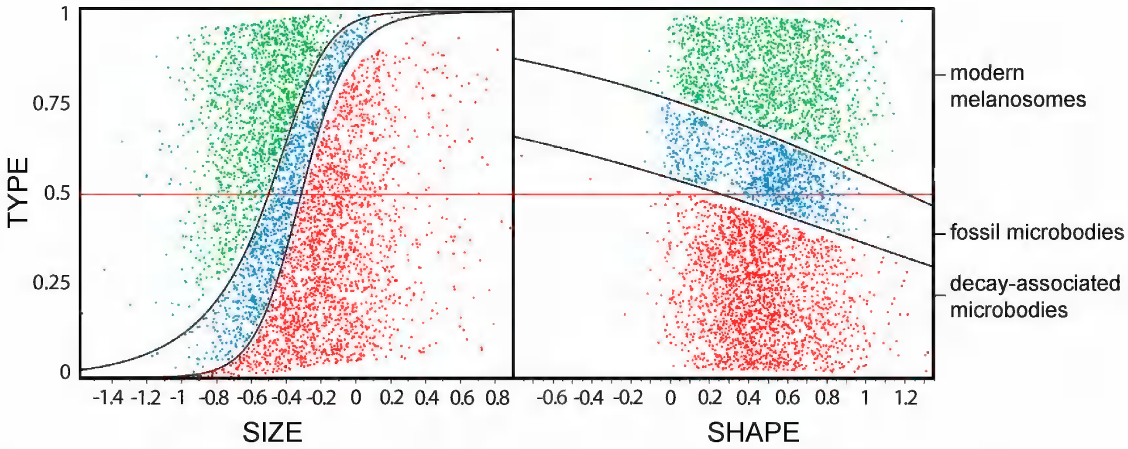

FIG. 2. Logistic fits of "type" against size ($\chi^2 = 2607.614$, $p < 0.0001$) and shape ($\chi^2 = 56.070$, $p < 0.0001$) both statistically significant. Size ($R^2 = 0.2730$) compared with shape ($R^2 = 0.0059$) is more important in classification of the collected data into modern melanosomes, fossil microbodies, and decay-associated microbodies.

points between the barbs and rachis, and regions between consecutive barbules). The microbial aggregates were not affected by pigmentation or lack of it, but there are alternate views (Peteya et al., 2017). If the bacterial identity of the microbodies associated with fossil soft tissue is assumed to be true, then the sources of these microbes would have to be an amalgamation of nonsaprotrophic bacteria, obligate and facultative saprotrophic bacteria from the external environment, and endogenous intestinal flora released to surrounding environment by degradation of the integument in the carcass. Studies have illustrated how bacterial communities fluctuate over seasons and temperature regimes (Dickson et al., 2011), and as a result they should encompass a large variety of shapes and sizes, as opposed to more uniform melanosomes and microbodies. Additionally, melanosomes are concentrated in certain tissues and are often structured in a distinct fashion such as alignment of oblong melanosomes along the axes in the feather cortex or barbules (Vinther et al., 2008; Vinther et al., 2010), features also not observed in decay bacteria.

Spherical and subspherical shapes are the most conducive shapes for any membrane-bound structure exposed to osmotic pressure (Jiang et al., 2015), as would be the case for both microbes and subcellular organelles like melanosomes. Moreover, the bacterial samples are a mixed assemblage of geometries. Even if only the rod and spherical shapes are considered, size differences extend over a broad range (a scenario akin to measuring a considerable number of objects of dissimilar sizes), while melanosomes are characteristically more uniform and overlap with fossil microbodies in our PCA plots.

STATISTICAL ANALYSES OF MICROBODY GEOMETRY

Nonparametric comparisons and PCA of microbody geometry demonstrate that fossil microbodies and microbial cells are significantly dissimilar in shape and size. If the fossil microbodies measured represent melanosomes, differences in geometry between modern melanosomes and fossil microbodies could be due to alteration of melanosome size during diagenesis (Colleary et al., 2015). It has recently been proposed that non-integumentary melanosomes in fossils can be redistributed due to weak lakebed currents and can potentially bias reconstructions of the colors of fossil vertebrates (McNamara et al., 2018). The range of melanosome geometry present in vertebrate tissues has yet to

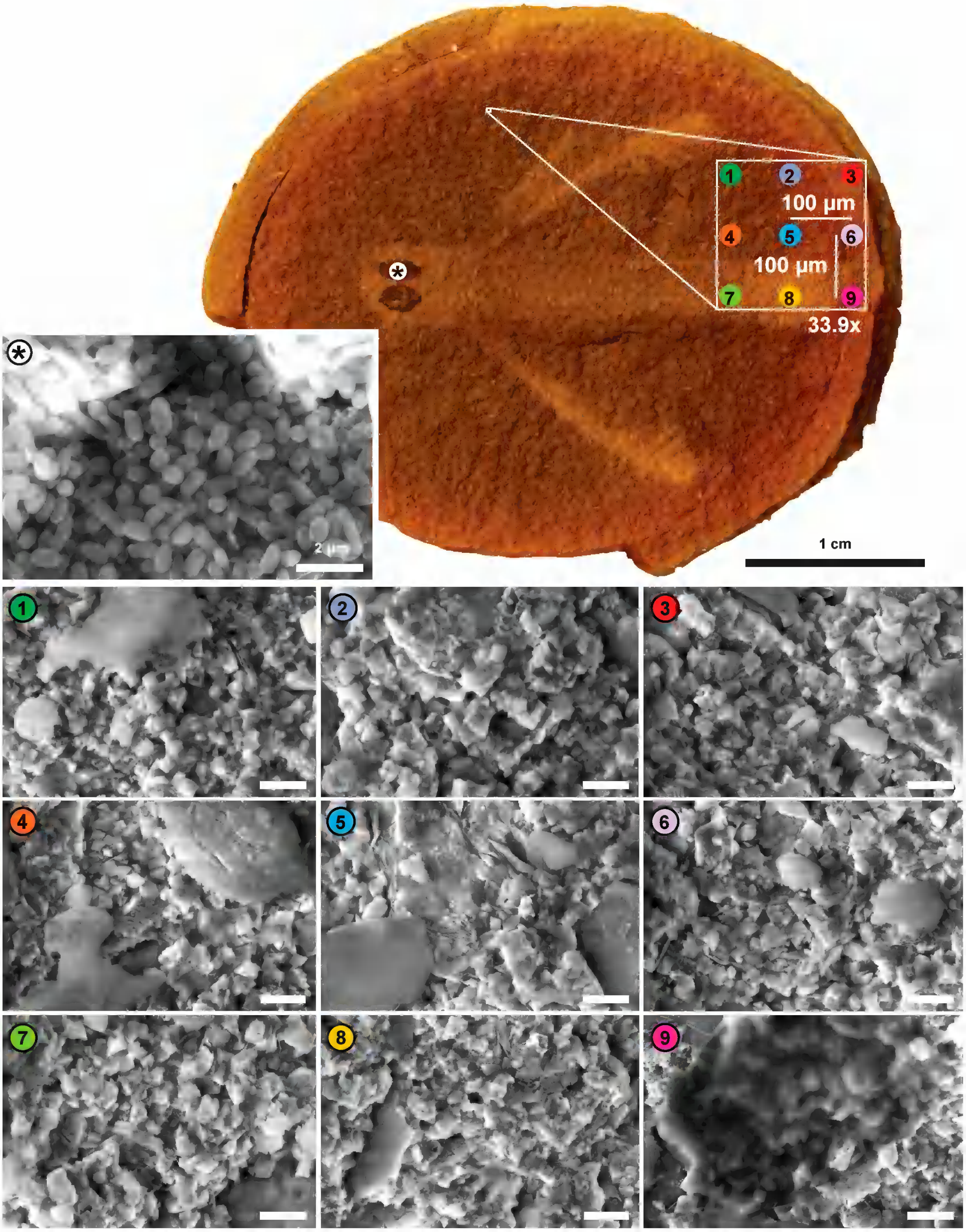

FIG. 3. SEM bedding plane survey for microbodies in the 300 Myr old lungfish *Esconicthys apopyris* (ROM56792), from Mazon Creek, Illinois. The asterisk indicates the region within the outline of the eye, which contains a fabric of microbodies (inset). By contrast, none of the grid points (1–9) show any evidence of such microbodylike structures in the matrix. Scale bars on images = 5 µm.

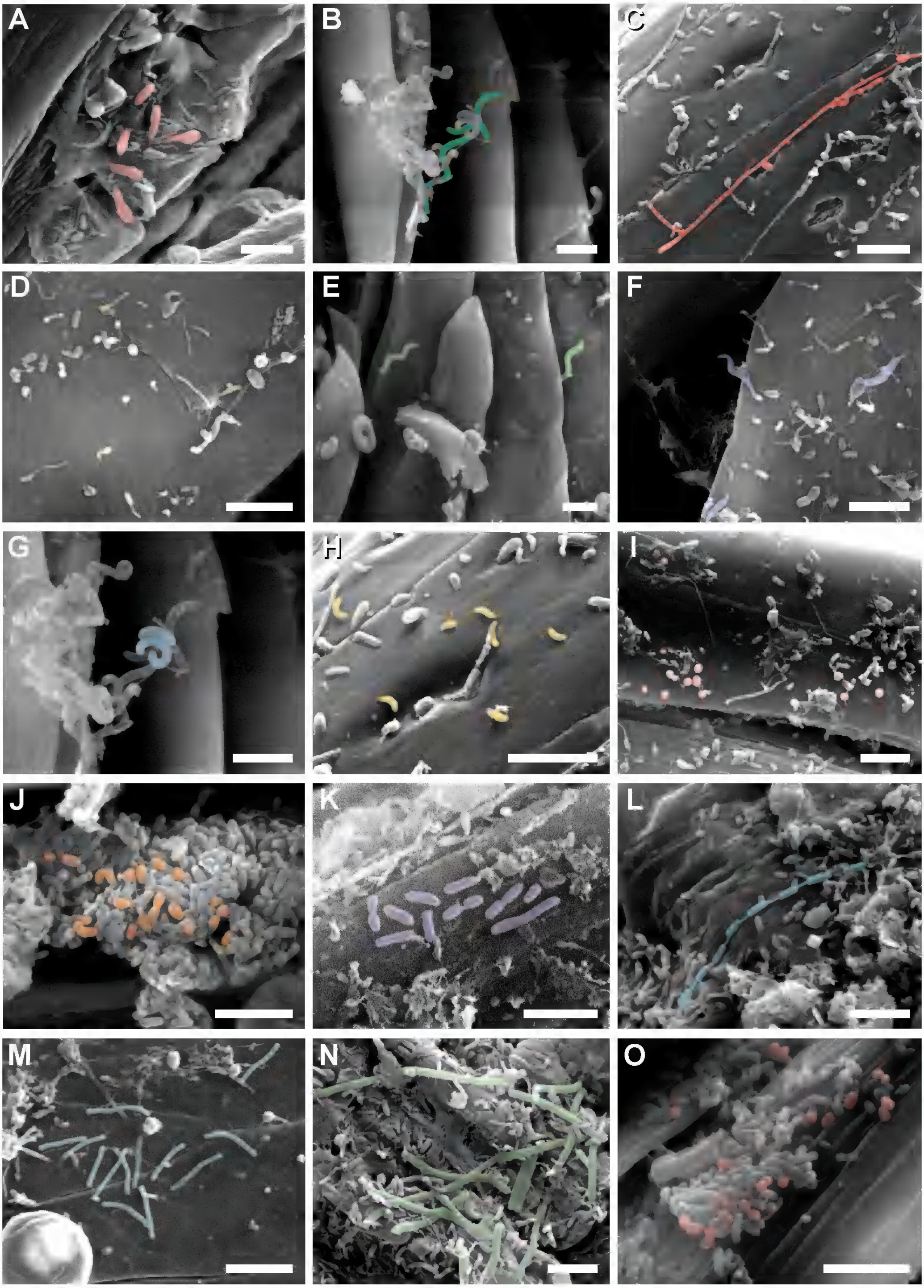

FIG. 4. A wide range of bacterial morphotypes observed in the decay experiments. Bacteria are shown in false colors in the SEM images: **A,** Club rods; **B, E,** spirochaetes; **C, N,** actinomycetes; **D,** flagellated vibrio; **F,** fusiform **G, H,** curved vibrio; **I, J, O,** cocci and coccobacilli; and **K, M,** bacilli; **L,** streptobacilli. Scale bars = 5 μm.

be comprehensively cataloged, although variation in melanosome geometry between tissues and organs is expected to be minimal relative to the geometrical diversity of decay bacteria. Thus, the potential movement of internal melanosomes around the carcass during decay is unlikely to result in consortia of fossil microbodies superficially similar to a community of decay bacteria.

Investigation of Bedding Planes in Exceptionally Preserved Fossils

We surveyed fossil vertebrate material from a range of Lagerstätte localities in which vertebrates are preserved with soft tissues, such as the Cretaceous Jehol Biota from Liaoning, China (Zhang et al., 2010; Chang et al., 2011), the Carboniferous Mazon Creek of Illinois (Clements et al., 2016; Gabbott et al., 2016) and the Eocene Fur and Ølst formations of Denmark (Vinther et al., 2008; Pedersen et al., 2011; Lindgren et al., 2012; Field et al., 2013). These samples represent a multitude of paleoenvironments with varied diagenetic regimes, permitting a robust investigation of the distribution of fossil microbodies. None of the fossil bedding planes investigated showed evidence for microbodies in the surrounding matrix or in tissues that were not originally melanin bearing—fundamentally, fossil microbodies are restricted to specific tissues within the fossil. The lack of microbodies outside of melanin-bearing tissues has also been noted in other studies (Clements et al., 2016; Gabbott et al., 2016). Our findings therefore reject the bacterial hypothesis since decay-associated microbes would be expected to be ubiquitous on the carcass as well as the adjacent sediment, and not restricted to specific tissues. Thus, it can be concluded that it is not common for microbes to fossilize, and particularly not as three-dimensional organic microbodies.

Rare examples of microbes are known from the fossil record, these are mainly restricted to occurrences in which the microbes were entombed alive in rapidly forming cements, such as calcium phosphates (Xiao and Knoll, 1999; Briggs et al., 2005), manganese carbonate (Lozano and Rossi, 2012), amber (Cano and Borucki, 1995; Girard et al., 2009), and chert (Qu et al., 2017). Soft-tissue replacement by authigenic minerals such as calcium phosphate is relatively common in fossil Lagerstätten and generally replicates intestinal tracts (Butterfield, 2002; Vannier et al., 2014), muscle tissue (Briggs et al., 2005; Parry et al., 2015; Wilson et al., 2016; Young et al., 2017), and skin (McNamara et al., 2009; Navalon et al., 2015). Calcium phosphate can preserve tissue and eukaryotic cellular-level fidelity, however, despite the contribution microbes make to the formation of diagenetic and sedimentary calcium phosphate (Briggs, 2003; Crosby and Bailey, 2012), there are few convincing examples of fossilized microbes in this medium (Xiao and Knoll, 1999; Briggs et al., 2005). Examples of microbes that are preserved within manganese carbonates of cave stromatolites are assumed to be due to young ages of the rocks and their lack of diagenesis (Lozano and Rossi, 2012). Silica chert is the most persistent medium for microbial preservation; with bacterial and cyanobacterial fossils documented in rocks from the Archaean (Westall et al., 2001). While cherts commonly preserve microbes, there are limitations to this medium for preservation because precipitation rates vary: increased precipitation through intertidal exposure and the fluctuating conditions will affect the bacterial consortia preserved and intervals with less rapid precipitation often lack microbes altogether (Knoll and Golubic, 1979). Observations of modern hydrothermal systems (Jones et al., 2001, 2004) show that silicification may alter bacterial geometry markedly and may not capture key anatomical features that would allow for confident diagnosis. Thus, even the best taphonomic settings for microbial preservation lead to unreliable and inconsistent preservation of microbes. Most importantly, we know of no microbes fossilized in sedimentary environments that otherwise give way to carbonaceous preservation of cellular organelles like melanosomes.

MELANINS BEYOND THE METAZOA: NOT ALL THAT IS BLACK, BROWN, OR RED IS EUMELANIN/PHEOMELANIN

Two prior publications (Lindgren et al., 2015; Schweitzer et al., 2015) have proposed alternative scenarios in which the microbial consortia colonizing decaying carcasses assist in (1) exceptional preservation of carbonaceous films in highly flattened fossils; and (2) the exogenous secretion of extracellular polymeric substances (EPS) and/or melanin by some microbial consortia, in turn, facilitates preservation of these microbial cells, which are being misinterpreted as melanosomes (contra: integumentary melanosomes are the primary cause of preservation of soft tissues in the form of carbonaceous films). However, our review of the literature rules out these alternatives. The term "melanin" has been used rather loosely for several diverse chemical entities. Several attempts to classify these chemicals over the last five decades have occurred (Marks and Seabra, 2001; Prota, 2012), but an all-encompassing definition remains elusive. There are furthermore classes of complex molecules formed from degradation of proteins, sugars, and lipids through Maillard reactions called melanoidins, thought to be involved in kerogen formation (Larter and Douglas, 1980) and are suspected to form inside mollusc shells from their organic shell matrix (Collins et al., 1992). These molecules are, however, compositionally disparate from eu- and pheomelanin. The major enzymes catalysing the synthesis of melanins are tyrosinases, laccases, polyketide synthases, 4-hydroxyphenylacetic acid hydroxylase, and *p*-hydroxyphenylpyruvate oxidase.

The forms of melanin most common to vertebrates—eumelanin and pheomelanin—originate from branches of the catabolic pathway for the amino acids tyrosine and phenylalanine through the action of tyrosinases (Borovansky and Riley, 2011). Forms of melanin more commonly associated with microbial systems are allomelanin and pyomelanin. Allomelanin, also known as 1,8-dihydroxynapthalene (DHN) melanins, is a varied group produced from the precursor Acetyl-CoA via a pathway called pentaketide pathway (Langfelder et al., 2003) via polymerization through action of polyketide synthases, laccases, 4-hydroxyphenylacetic acid hydroxylase (Plonka and Grabacka, 2006), and through oxidation of catecholamines (Wang et al., 1995, 1996). Pyomelanin is produced via part of the tyrosine/phenylalanine catabolism pathway followed by the oxidation and polymerization of homogentisic acid (HGA) through the enzyme *p*-hydroxyphenylpyruvate oxidase (Plonka and Grabacka, 2006).

Several bacterial strains produce allomelanin and pyomelanin. Strains of *Streptomyces* from various environments, marine sources (Vasanthabharathi et al., 2011; Sivaperumal et al., 2014), field soils (Dastager et al., 2006), and limestone quarries (Quadri and Agsar, 2012) are reported to produce melanin/melanoid compounds. These compounds act as alternatives for conventional electron acceptors (Turick et al., 2002), act to prevent UV damage (Plonka and Grabacka, 2006; Gao and Garcia-Pichel, 2011), or enable survival in nutrient-deficient (Chatfield and Cianciotto, 2007; Zheng et al., 2013) and/or hostile environments (Gessler et al., 2014). However, there are instances of microorganisms producing eumelanin/pheomelanin (or slightly similar chemical entities) that function analogously to those of allomelanin and pyomelanin. An *Aeromonas media* strain "WS" isolated from lacustrine settings has been shown to produce elevated levels of melanin (from L-3,4-dihydroxyphenylalanine precursor) (Wan et al., 2007). Other species such as *Marinomonas mediterranea* have been known to possess a two-component melanogenic system, utilizing both tyrosinase (Lopez-Serrano et al., 2002, 2004) and laccase mediated pathways (Solano, 2014), indicating a potential for highly adaptive melanin synthesis.

Strains of *Bacillus*-producing melanin contain active tyrosinases and they become heavily pigmented in the presence of L-tyrosine in the media (Aghajanyan et al., 2005; Drewnowska et al., 2015). *Bacillus subtilis* also synthesizes a brown pigment related to melanin for sporulation, but this process is catalyzed by a laccase-related protein named cot A (Barnett and Hageman, 1983). *Vibrio cholerae* has been reported to produce pyomelanin but switches to eumelanin under stress conditions, like elevated temperatures, hyperosmotic medium, and starvation (Plonka and Grabacka, 2006). One hypertoxic mutant strain of *V. cholerae* HTX-3 has even been described to make pheomelanin (Ivins and Holmes, 1980; 1981). *Streptomyces antibioticus* (a spore-bearing filamentous bacterium) produces eumelanin in which the operon *melC* controls melanin production. The main factor inducing the expression of the *MelC* protein is the amino acid methionine (Chen et al., 1992; Chen et al., 1993). Contrary to the synthesis of animal melanin within well-confined subcellular compartments, bacterial melanin formation usually takes place by autooxidation and subsequent polymerization of the precursors secreted outside the cell (Plonka and Grabacka, 2006).

Fungal melanins are a diverse group of negatively charged, high-molecular-weight hydrophobic pigments (Pombeiro-Sponchiado et al., 2017). Although these pigments are quite common in fungi, their production is limited to certain growth stages on the mycelia, spore formation, or in response to wounding (Bell and Wheeler, 1986). Allomelanin (DHN-melanin) is frequent in ascomycetous fungi and some fungi imperfecti except *Aspergillus niger* and basidiomycetes (Wheeler, 1983). The ascomycete fungi *Cryptococcus neoformans*, a parasite of the central nervous system, produces melanin precursors 3,4-dihydroxyphenylalanine (DOPA) and catecholamines (Wang et al., 1995; Wang et al., 1996) but the chemical nature of the pigments (eumelanin or otherwise) remain contentious (Liu et al., 1999). Basidiomycetes like *Agaricus bisporus* contain a very active tyrosinase enzyme and produce eumelanin from a γ-glutaminyl-4-hydroxybenzene precursor (Solano, 2014), but the process does not take place within the mycelium. Unlike animal melanin, fungal melanin predominantly occurs either as electron-dense granules in extracellular secretions or is deposited within the outermost layer of the chitinous cell wall.

MICROBIAL MELANIN NEITHER YIELDS MELANOSOMELIKE BODIES NOR IS CHEMICALLY IDENTICAL TO ANIMAL MELANINS

While the literature is replete with evidence of microorganisms synthesizing allomelanin and pyomelanin, evidence for microbial synthesis of eumelanin and pheomelanin is limited. Melanin synthesis by *V. cholerae* is of particular interest because of the reported switch from pyomelanin to eumelanin production during conditions of stress. The genetic mechanisms for reported production of pheomelanin by the strain *V. cholerae* HTX-3, however, are still pending investigation. The fact that the amino acid methionine is needed to induce the expression of *MelC* protein in *S. antibioticus* is peculiar. Methionine, which forms an integral part of the prokaryotic protein translation machinery, is one of the less abundant amino acids in the prokaryotic metabolome (Pasamontes and Garcia-Vallve, 2006), thus indicating a tightly controlled melanogenic pathway activated only during certain situations (Plonka and Grabacka, 2006).

Fungal melanins perform the same functions as bacterial melanins and are known products that offset stressful environments. Melanization offers defense against UV light and ionizing radiation, and resistance to heat or cold and activity of inorganic antimicrobial compounds, such as silver nitrate (Plonka and Grabacka, 2006). A particularly extreme form of this is observed in certain fungal species, such as *Cladosporium spp.*, *Alternaria alternata*, *Aureobasidium pullulans*, and *Hormocornis resinae*, found on the walls of the damaged reactors in Chernobyl, which overproduce melanin to withstand elevated levels of ionizing radiation (Dadachova and Casadevall, 2008; Gessler et al., 2014).

However, none of the aforementioned extremophilic microbes carrying out melanin synthesis have been reported to colonize environs like decaying feathers or carcasses. Additionally, their mode of secretion either extracellularly or as thin peripheral sheets would not lead to melanosomelike microbodies, which are solidly packed with melanin (apart from some iridescent feathers with hollow melanosomes (Durrer, 1977), which would still have a thicker wall of melanin than those microbes produce. Furthermore, as shown here, these microbes would have different modes of growth and geometry than melanosomes do.

Although it could be argued that the confusion in the differentiation between fossilized microbodies and microbial cells was brought about using biased qualitative-based imaging analysis methods, the current study demonstrates that semiquantitative analysis led to a promising deconvolution of the studied bodies. We acknowledge that body dimensions were manually recorded during SEM image analysis in the hope that future method developments will include automated and standardized image analysis for the interpretation of SEM data from fossils of interest. While semiquantitative analyses of nonfossilized microbodies led to clear distinctions between melanosomes and bacterial bodies, one should also take into account the possibility of artifacts during SEM preparations, and the challenges of properly attributing three-dimensionality to bodies from two-dimensional micrographs. Future differentiation experiments should consider using other methods that allow for proper three-dimensional quantification of microbodies, which would then validate the evidence presented in this study.

Criteria for Fossil Melanin/Melanosome Identification

Since microbes have clear ethological, compositional, and geometrical differences to metazoan melanosomes it is pertinent to evaluate the means of identifying melanin/melanosomes from the fossil record. Melanosomes can be identified by several lines of evidence:

They are localized to certain tissues: In vertebrates, melanosomes are present in the skin and epidermal appendages, such as scales, hair, and feathers (Vinther et al. 2015; Colleary et al., 2015) while some organs, like the eyes, liver, peritoneum, and parts of the nervous system (McNamara et al., 2018; Rossi et al. 2019) have these localized to them. Hence, if the melanosomes form distinct associations that resemble the outline of a feather, liver, or eye, this conforms to a melanosome interpretation.

They may be aligned or layered within said tissues: Melanosomes are oriented in specific directions in different tissues or may be arranged into different layers and this organization has a critical biological function in extant animals (Maia et al., 2012), thus allowing their reliable identification even in fossilized soft tissues. They are likely to occur only in recalcitrant tissues and rarely in exceptionally preserved organs such as the eye. In many soft tissues, decay will result in collapse and potential dispersal of any layers or organization.

Certain taxa may have a limited melanosome geometry: Exemplified in amphibians, the integumentary melanosomes are generally oblate in shape and intermediate between pheomelanosomes and eumelanosomes seen in birds and mammals. Mammals appear to exhibit a more limited diversity of melanosome shape compared to birds (Li et al., 2014), which utilize melanosomes to produce more diverse colors such as structural iridescence and gray, in which the melanosome geometry may play a role in the self-assembly into these conformations (Maia et al., 2012). Very little is known about the true extent of melanosome geometry and arrangements extending across different tissues and taxa; work to address these knowledge gaps in modern animals is currently underway. However, despite the true variety of melanosome geometry being unknown, it is unlikely this variety would exceed that observed in microbes.

Chemical analyses can identify melanin signatures: The most reliable method for identifying melanin in extant samples (Wakamatsu and Ito, 2002) is through permanganate oxidation of eumelanin and hydriodic acid reductive hydrolysis of pheomelanin. This method has been applied to quantify molecularly intact melanin in Jurassic coleoid ink but is otherwise too destructive for most fossil samples preserving melanin. Another confounding factor is that fossil melanin is diagenetically altered. Other methods provide signatures for melanin such as time of flight–secondary ion mass spectrometry (ToF-SIMS), which provides spectra of molecular ionized fragments that can be visually compared (Lindgren et al., 2012, 2014), or using principal component analyses (Colleary et al., 2015). Colleary et al. (2015) showed that fossil and fresh melanin are distinct in ToF-SIMS, but that artificial maturation experiments yield signatures more similar to fossil spectra. Pyrolysis-GCMS (Py-GCMS) is also valuable for analyzing small amounts of fossil tissue, which yield a suite of distinct markers (Dzierzega-Lecznar et al., 2012; Brown et al., 2017) and the diagenetic alteration of these can also be studied with Py-GCMS (Glass et al., 2012, 2013).

Melanosomes have a distinct geometry: As reviewed herein and presented elsewhere (Vinther et al., 2008, 2010, 2016; Li et al., 2010, 2012), melanosomes present themselves as microstructures with a very distinct geometrical range and have distinct size variation within tissues (Rossi et al., 2019). Their fossilization potential is high, as they have been confidently diagnosed from sample fossil tissues as old as Carboniferous (300 Myr) (Clements et al., 2016; Gabbott et al., 2016) and can leave impressions in the matrix cement when secondarily oxidized.

In total, several lines of evidence are available to detect melanin, and only a subset of these is necessary to diagnose its presence. While a single piece of evidence is persuasive by itself, separate lines of evidence (congruence) make the judgment stronger and this is generally advocated. It has been argued that chemical analyses are warranted in every instance because microbes and melanosomes are indistinguishable (Lindgren et al., 2012, 2014, 2015). Given the evidence presented here, this perspective cannot be justified based on those assumptions. To simply diagnose the preservation of melanin or melanosomes, identifying their distinct microbodies and observing their presence in tissues that are known to be melanin bearing is adequate as separate lines of evidence on which to make a judgment. This allows for diagnosis of melanosomes even when they are not preserved organically, but only as impressions. However, sometimes melanosome geometries are lost, and the melanin has merged into a solid mass (Carney et al., 2012). In these instances, chemical analyses may be helpful in providing a complementary line of evidence in addition to patterns of distribution (Brown et al., 2017). Likewise, if melanosomes are found outside a tissue that is assumed to be melanin bearing, then chemical analyses may be advisable (Vinther et al., 2016).

There is still much to be learnt about the relative stability and survival of melanins through diagenesis and geological time; a question also remains as to whether eumelanin and pheomelanin have different survival potentials. Chemical surveys should aim to synthesize evidence in larger frameworks rather than targeting single specimens for the sake of diagnosing it as melanin bearing or not (Gren et al., 2017).

CONCLUSIONS

The results of this study demonstrate that the interpretation of microbodies in fossil vertebrate tissues as microbes (Moyer et al., 2014; Lindgren et al., 2015; Schweitzer et al., 2015) cannot be justified and that they conform to melanosomes in terms of shape and size. During decay experiments, microbes are not localized to melanin-bearing tissues, nor do they exhibit the ordered arrangement common to extant melanosomes. Conversely, in fossil material, the microbodies are restricted to tissues known to be melanosome rich in vivo. The microbodies are not present in the adjacent matrix or continuously across boundaries of melanized and unmelanized tissues—contradicting a bacterial diagnosis. The geometry (Ivins and Holmes, 1980; 1981; Chen et al., 1992, 1993), mode of secretion (Plonka and Grabacka, 2006; Solano, 2014), and chemical composition (Wang et al., 1995; Wang et al., 1996; Plonka and Grabacka, 2006) of melanin-synthesizing microbes would also negate any conflation with melanosomes.

Based on our results, we reject all four of our original hypotheses: (1) melanosomes and microbial cells are geometrically indistinguishable; (2) microbes localize and align themselves in orientations akin to extant melanosomes; (3) microbes fossilize easily and are thus ubiquitous throughout fossils; and (4) microbes are sources of melanin and there is a likelihood of extraneous preservation in fossils. The rejection of hypotheses 1–4 strongly upholds the interpretation of fossil microbodies as melanosomes. Additionally, as multiple lines of evidence support melanosome identification, we suggest that only a subset of these evidence sources are necessary for the interpretation of fossil melanin and its use in inferring tissue identity, structure, evolution, and color.

ACKNOWLEDGMENTS

We would like to thank Bel Deering of the RSPCA West Hatch Animal Centre (Taunton, U.K.) for providing us with carcasses of deceased birds for our decay studies. We thank the Royal Ontario Museum, Toronto, Canada. the Field Museum of Natural History, Chicago, the Lauer Foundation PSE and the Burpee Museum, Rockford, IL, for their loans of Mazon Creek fossil material to T.C. We would also like to thank Klara Norden (Department of Ecology and Evolutionary Biology, Princeton University, NJ.), Jaeike W. Faber (Department of Medical Biology, Amsterdam Cardiovascular Sciences, Amsterdam UMC, University of Amsterdam, Amsterdam, The Netherlands) and Frane Babarović (Department of Animal and Plant Sciences, University of Sheffield, Sheffield, U.K.) for modern melanosome samples, Fiann Smithwick (School of Earth Sciences, University of Bristol, Bristol, U.K.) for fossil microbody samples from the Grube Messel Lagerstätte, and David Marshall (School of Earth Sciences, University of Bristol) for assistance regarding the collection of sediment inocula from the Severn Estuary. Further thanks to Michael Benton (School of Earth Sciences, University of Bristol), Stuart Kearns (School of Earth Sciences, University of Bristol) and Zhang Fucheng (Institute of Geology and Paleontology, Linyi University, Linyi, China) for access to the fossil feather specimen IVPP V15388B; and to John Bacon-Shone (Faculty of Social Sciences, the University of Hong Kong, Hong Kong SAR, China) for helping A.R. with the statistical analysis. Evan Saitta (Field Museum, Chicago, IL), Benjamin Moon and Tom Stubbs (School of Earth Sciences, University of Bristol) are thanked for discussions and suggestions. This study was supported by funds from the Bob Savage Memorial Fund (School of Earth Sciences, University of Bristol) to A.R., Hong Kong Ph.D. Fellowship 2017-18 (PF16-09281) to A.R., and a Royal Society Research Grant RG15042 to J.V. Conference presentations made by A.R. helped to improve the study and were supported by the Palaeontological Association Postgraduate Travel Fund (Grants-in-Aid scheme) and a University of Bristol Alumni Foundation Travel Grant.

REFERENCES

Aghajanyan, A.E., et al. 2005. Isolation, purification and physicochemical characterization of water-soluble *Bacillus thuringiensis* melanin. Pigment Cell & Melanoma Research 18: 130–135.

Barnett, T.A., and J.H. Hageman. 1983. Characterization of a brown pigment from *Bacillus subtilis* cultures. Canadian Journal of Microbiology 29: 309–315.

Bell, A.A., and M.H. Wheeler. 1986. Biosynthesis and functions of fungal melanins. Annual Review of Phytopathology 24: 411–451.

Bonde, N.C. 1997. An Upper Paleocene *Antigonia*-like fish from Denmark: and its relations to other advanced teleosteans. Bulletin of the Geological Society of Denmark 9710-0100.

Borovansky, J., and P.A. Riley. 2011. Melanins and melanosomes: biosynthesis, structure, physiological and pathological functions. Weinheim: Wiley-VCH.

Briggs, D.E.G. 2003. The role of decay and mineralization in the preservation of soft-bodied fossils. Annual Review of Earth and Planetary Sciences 31: 275–301.

Briggs, D.E.G., and P.R. Crowther. 2008. Palaeobiology II. Oxford: John Wiley & Sons.

Briggs, D.E.G., R.A. Moore, J.W. Shultz, and G. Schweigert. 2005. Mineralization of soft-part anatomy and invading microbes in the horseshoe crab *Mesolimulus* from the Upper Jurassic Lagerstatte of Nusplingen, Germany. Proceedings of the Royal Society B, Biological Sciences 272: 627–632.

Brown, C.M., et al. 2017. An exceptionally preserved three-dimensional armored dinosaur reveals insights into coloration and Cretaceous predator-prey dynamics. Current Biology 27: 2514–2521.

Burley, N., G. Krantzberg, and P. Radman. 1982. Influence of colour-banding on the conspecific preferences of zebra finches. Animal Behaviour 30: 444–455.

Butcher, G.S., and S. Rohwer. 1989. The evolution of conspicuous and distinctive coloration for communication in birds. *In* D.M. Power (editor), Current Ornithology, vol. 6: 51–108. Boston: Springer.

Butterfield, N.J. 2002. *Leanchoilia* guts and the interpretation of three-dimensional structures in Burgess Shale-type fossils. Paleobiology 28: 155–171.

Cano, R., and M. Borucki. 1995. Revival and identification of bacterial spores in 25- to 40-million-year-old Dominican amber. Science 268: 1060–1064.

Carney, R.M., J. Vinther, M.D. Shawkey, L. D'Alba, and J. Ackermann. 2012. New evidence on the colour and nature of the isolated *Archaeopteryx* feather. Nature Communications 3: 637.

Chang, M.M., P.J. Chen, Y. Wang, and Y.Q. Wang. 2011. The Jehol fossils: the emergence of feathered dinosaurs, beaked birds and flowering plants, London: Academic Press.

Chatfield, C.H., and N.P. Cianciotto. 2007. The secreted pyomelanin pigment of *Legionella pneumophila* confers ferric reductase activity. Infection and Immunity 75: 4062–4070.

Chen, L.Y., W.M. Leu, K.T. Wang, and Y.H. Lee. 1992. Copper transfer and activation of the *Streptomyces* apotyrosinase are mediated through a complex formation between apotyrosinase and its *trans*-activator MelC1. Journal of Biological Chemistry 267: 20100–20107.

Chen, L.Y., M.Y. Chen, W.M. Leu, T.Y. Tsai, and Y.H. Lee. 1993. Mutational study of *Streptomyces* tyrosinase *trans*-activator MelC1. MelC1 is likely a chaperone for apotyrosinase. Journal of Biological Chemistry 268: 18710–18716.

Clarke, J.A., et al. 2010. Fossil evidence for evolution of the shape and color of penguin feathers. Science 330: 954–957.

Clements, T., et al. 2016. The eyes of *Tullimonstrum* reveal a vertebrate affinity. Nature 532: 500–503.

Colleary, C., et al. 2015. Chemical, experimental, and morphological evidence for diagenetically altered melanin in exceptionally preserved fossils. Proceedings of the National Academy of Sciences of the United States of America 112: 12592–12597.

Collins, M.J., P. Westbroek, G. Muyzer, and J.W. de Leeuw. 1992. Experimental evidence for condensation reactions between sugars and proteins in carbonate skeletons. Geochimica et Cosmochimica Acta 56: 1539–1544.

Crosby, C.H., and J.V. Bailey. 2012. The role of microbes in the formation of modern and ancient phosphatic mineral deposits. Frontiers in Microbiology 3: 241.

Cuthill, I.C., et al. 2017. The biology of color. Science 357: eaan0221.

Dadachova, E., and A. Casadevall. 2008. Ionizing radiation: how fungi cope, adapt, and exploit with the help of melanin. Current Opinion in Microbiology 11: 525–531.

Dastager, S.G., et al. 2006. Seperation, identification and analysis of pigment (melanin) production in *Streptomyces*. African Journal of Biotechnology 5: 1131–1134.

Dickson, G.C., R.T. Poulter, E.W. Maas, P.K. Probert, and J.A. Kieser. 2011. Marine bacterial succession as a potential indicator of postmortem submersion interval. Forensic Science International 209: 1–10.

Drewnowska, J.M., M. Zambrzycka, B. Kalska-Szostko, K. Fiedoruk, and I. Swiecicka. 2015. Melanin-like pigment synthesis by soil *Bacillus weihenstephanensis* isolates from Northeastern Poland. PLoS One 10: e0125428.

Durrer, H. 1977 Schillerfarben der vogelfeder als evolutionsproblem. Denkschriften der Schweizerischen Naturforschenden Gesellschaft 91: 1–127.

Dzierzega-Lecznar, A., S. Kurkiewicz, and K. Stepien. 2012. Detection and quantitation of a pheomelanin component in melanin pigments using pyrolysis-gas chromatography/tandem mass spectrometry system with multiple reaction monitoring mode. Journal of Mass Spectrometry 47: 242–245.

Field, D.J., et al. 2013. Melanin concentration gradients in modern and fossil feathers. PLoS One 8: e59451.

Gabbott, S.E., et al. 2016. Pigmented anatomy in Carboniferous cyclostomes and the evolution of the vertebrate eye. Proceedings of the Royal Society B, Biological Sciences 283: rspb.2016.1151.

Gao, Q., and F. Garcia-Pichel. 2011. Microbial ultraviolet sunscreens. Nature Reviews Microbiology 9: 791–802.

Gessler, N.N., A.S. Egorova, and T.A. Belozerskaia. 2014. Melanin pigments of fungi under extreme environmental conditions Prikladnaia Biokhimiia i Mikrobiologiia 50: 125–134.

Girard, V., et al. 2009. Taphonomy and palaeoecology of mid-Cretaceous amber-preserved microorganisms from southwestern France. Geodiversitas 31: 153–162.

Glass, K., et al. 2012. Direct chemical evidence for eumelanin pigment from the Jurassic period. Proceedings of the National Academy of Sciences of the United States of America 109: 10218–10223.

Glass, K., et al. 2013. Impact of diagenesis and maturation on the survival of eumelanin in the fossil record. Organic Geochemistry 64: 29–37.

Gren, J.A., et al. 2017. Molecular and microstructural inventory of an isolated fossil bird feather from the Eocene Fur Formation of Denmark. Palaeontology 60: 73–90.

Hill, G.E., and K.J. McGraw. 2006a. Bird coloration, vol. 2: function and evolution. Cambridge: Harvard University Press.

Hill, G.E., and K.J. McGraw. 2006b. Bird coloration, vol. 1: mechanisms and measurements. Cambridge: Harvard University Press.

Hu, D.Y., et al. 2018. A bony-crested Jurassic dinosaur with evidence of iridescent plumage highlights complexity in early paravian evolution. Nature Communications 9: 217.

Ichida, J.M., et al. 2001. Bacterial inoculum enhances keratin degradation and biofilm formation in poultry compost. Journal of Microbiological Methods 47: 199–208.

Ito, S. & Wakamatsu, K. (2003). Quantitative analysis of eumelanin and pheomelanin in humans, mice, and other animals: a comparative review. Pigment Cell Research 16: 523–531.

Ivins, B.E., and R.K. Holmes. 1980. Isolation and characterization of melanin-producing (mel) mutants of *Vibrio cholerae*. Infection and Immunity 27: 721–729.

Ivins, B.E., and R.K. Holmes. 1981. Factors affecting phaeomelanin production by a melanin-producing (mel) mutant of *Vibrio cholerae*. Infection and Immunity 34: 895–899.

Jiang, C., P.D. Caccamo, and Y.V. Brun. 2015. Mechanisms of bacterial morphogenesis: evolutionary cell biology approaches provide new insights. Bioessays 37: 413–425.

Jones, B., R.W. Renaut, and M.R. Rosen. 2001. Taphonomy of silicified filamentous microbes in modern geothermal sinters—implications for identification. Palaios 16: 580–592.

Jones, B., K.O. Konhauser, R.W. Renaut, and R.S. Wheeler. 2004. Microbial silicification in Iodine Pool, Waimangu geothermal area, North Island, New Zealand: implications for recognition and identification of ancient silicified microbes. Journal of the Geological Society 161: 983–993.

Knoll, A.H., and S. Golubic. 1979. Anatomy and taphonomy of a Precambrian algal stromatolite. Precambrian Research 10: 115–151.

Kowalewski, M. 1999. Actuopaleontology: the strength of its limitations. Acta Palaeontologica Polonica 44: 452–454.

Langfelder, K., M. Streibel, B. Jahn, G. Haase, and A.A. Brakhage. 2003. Biosynthesis of fungal melanins and their importance for human pathogenic fungi. Fungal Genetics and Biology 38: 143–158.

Larter, S.R., and A.G. Douglas. 1980. Melanoidins—kerogen precursors and geochemical lipid sinks—a study using pyrolysis-gas chromatography (Pgc). Geochimica et Cosmochimica Acta 44: 2087–2095.

Lehmann, E.L. 2006. Nonparametrics: statistical methods based on ranks. New York: Springer.

Li, Q., et al. 2010. Plumage color patterns of an extinct dinosaur. Science 327: 1369–1372.

Li, Q., et al. 2012. Reconstruction of *Microraptor* and the evolution of iridescent plumage. Science 335: 1215–1219.

Li, Q., et al. 2014. Melanosome evolution indicates a key physiological shift within feathered dinosaurs. Nature 507: 350–353.

Lindgren, J., et al. 2012. Molecular preservation of the pigment melanin in fossil melanosomes. Nature Communications 3: 824.

Lindgren, J., et al. 2014. Skin pigmentation provides evidence of convergent melanism in extinct marine reptiles. Nature 506: 484–488.

Lindgren, J., et al. 2015. Interpreting melanin-based coloration through deep time: a critical review. Proceedings of the Royal Society B, Biological Sciences 282: rspb.2015.0614.

Liu, L.D., K. Wakamatsu, S. Ito, and P.R. Williamson. 1999. Catecholamine oxidative products, but not melanin, are produced by *Cryptococcus neoformans* during neuropathogenesis in mice. Infection and Immunity 67: 108–112.

Lopez-Serrano, D., A. Sanchez-Amat, and F. Solano. 2002. Cloning and molecular characterization of a SDS-activated tyrosinase from *Marinomonas mediterranea*. Pigment Cell and Melanoma Research 15: 104–111.

Lopez-Serrano, D., F. Solano, and A. Sanchez-Amat. 2004. Identification of an operon involved in tyrosinase activity and melanin synthesis in *Marinomonas mediterranea*. Gene 342: 179–187.

Lozano, R.P., and C. Rossi. 2012. Exceptional preservation of Mn-oxidizing microbes in cave stromatolites (El Soplao, Spain). Sedimentary Geology 255: 42–55.

Maia, R., R.H. Macedo, and M.D. Shawkey. 2012. Nanostructural self-assembly of iridescent feather barbules through depletion attraction of melanosomes during keratinization. Journal of the Royal Society Interface 9: 734–743.

Manning, P.L., et al. 2019. Pheomelanin pigment remnants mapped in fossils of an extinct mammal. Nature Communications 10: 2250.

Marks, M.S., and M.C. Seabra. 2001. The melanosome: membrane dynamics in black and white. Nature Reviews Molecular Cell Biology 2: 738–748.

McNamara, M.E., et al. 2009. Soft-tissue preservation in Miocene frogs from Libros, Spain: insights into the genesis of decay microenvironments. Palaios 24: 104–117.

McNamara, M.E., et al. 2016. Fossilization of melanosomes via sulfurization. Palaeontology 59: 337–350.

McNamara, M.E., et al. 2018. Non-integumentary melanosomes can bias reconstructions of the colours of fossil vertebrates. Nature Communications 9: 2878.

Moyer, A.E., et al. 2014. Melanosomes or microbes: testing an alternative hypothesis for the origin of microbodies in fossil feathers. Scientific Reports 4: 4233.

Navalón, G., J. Marugan-Lobon, L.M. Chiappe, J. Luis Sanz, and A.D. Buscalioni. 2015. Soft-tissue and dermal arrangement in the wing of an Early Cretaceous bird: implications for the evolution of avian flight. Scientific Reports 5: 14864.

Neuhäuser, M., and F. Bretz. 2001. Nonparametric all-pairs multiple comparisons. Biometrical Journal: Journal of Mathematical Methods in Biosciences 43: 571–580.

Pan, Y., et al. 2016. Molecular evidence of keratin and melanosomes in feathers of the Early Cretaceous bird *Eoconfuciusornis*. Proceedings of the National Academy of Sciences of the United States of America 113: E7900–E7907.

Parry, L.A., P. Wilson, D. Sykes, G.D. Edgecombe, and J. Vinther. 2015. A new fireworm (Amphinomidae) from the Cretaceous of Lebanon identified from three-dimensionally preserved myoanatomy. BMC Evolutionary Biology 15: 256.

Pasamontes, A., and S. Garcia-Vallve. 2006. Use of a multi-way method to analyze the amino acid composition of a conserved group of orthologous proteins in prokaryotes. BMC Bioinformatics 7: 257.

Pedersen, G.K., et al. 2011. Molerområdets geologi – sedimenter, fossiler, askelagog glacialtektonik. Geologisk Tidsskrift: 41–135.

Peteya, J.A., J.A. Clarke, Q.G. Li, K.Q. Gao, and M.D. Shawkey. 2017. The plumage and colouration of an enantiornithine bird from the Early Cretaceous of China. Palaeontology 60: 55–71.

Plonka, P.M., and M. Grabacka. 2006. Melanin synthesis in microorganisms—biotechnological and medical aspects. Acta Biochimica Polonica 53: 429–443.

Pombeiro-Sponchiado, S.R., G.S. Sousa, J.C.R. Andrade, H.F. Lisboa, and R.C.R. Gonçalves. 2017. Production of melanin pigment by fungi and its biotechnological applications. *In* M. Blumenberg (editor), Melanin: 47–75. London: InTech.

Prota, G. 2012. Melanins and melanogenesis. San Diego: Academic Press.

Prum, R.O. 1999. The anatomy and physics of avian structural colours. *In* N. Adams and R. Slotow (editors), Proceedings of the 22nd International Ornithological Congress 16–22 August 1998, Durban, "Making rain for African ornithology": 1633–1653. Johannesburg: BirdLife South Africa.

Qu, Y.G., et al. 2017. Carbonaceous biosignatures of diverse chemotrophic microbial communities from chert nodules of the Ediacaran Doushantuo Formation. Precambrian Research 290: 184–196.

Quadri, S.R., and D. Agsar. 2012. Detection of melanin producing thermo-alkaliphilic *Streptomyces* from limestone quarries of the Deccan traps. World Journal of Science and Technology 2: 8–12.

Raposo, G., D. Tenza, D.M. Murphy, J.F. Berson, and M.S. Marks. 2001. Distinct protein sorting and localization to premelanosomes, melanosomes, and lysosomes in pigmented melanocytic cells. Journal of Cell Biology 152: 809–824.

Rossi, V., M.E. McNamara, S.M. Webb, S. Ito, and K. Wakamatsu. 2019. Tissue-specific geometry and chemistry of modern and fossilized melanosomes reveal internal anatomy of extinct vertebrates. Proceedings of the National Academy of Sciences of the United States of America: 201820285.

Roy, A., M. Pittman, E.T. Saitta, T.G. Kaye, and X. Xu. 2020. Recent advances in amniote palaeocolour reconstruction and a framework for future research. Biological Reviews 95: 22–50.

Sansom, R.S. 2014. Experimental decay of soft tissues. Paleontological Society Papers 20: 259–274.

Schneider, C.A., W.S. Rasband, and K.W. Eliceiri. 2012. NIH Image to ImageJ: 25 years of image analysis. Nature Methods 9: 671–675.

Schweitzer, M.H., J. Lindgren, and A.E. Moyer. 2015. Melanosomes and ancient coloration re-examined: a response to Vinther 2015. Bioessays 37: 1174–1183.

Sivaperumal, P., K. Kamala, R. Rajaram, and S.S. Mishra. 2014. Melanin from marine *Streptomyces* sp. (MVCS13) with potential effect against ornamental fish pathogens of *Carassius auratus* (Linnaeus, 1758). Biocatalysis and Agricultural Biotechnology 3: 134–141.

Smithwick, F.M., R. Nicholls, I.C. Cuthill, and J. Vinther. 2017. Countershading and stripes in the theropod dinosaur *Sinosauropteryx* reveal heterogeneous habitats in the Early Cretaceous Jehol Biota. Current Biology 27: 3337–3343.

Solano, F. 2014. Melanins: skin pigments and much more—types, structural models, biological functions, and formation routes. New Journal of Science 2014: 1–28.

Suvarna, K., C. Layton, and J. Bancroft. 2019. Bancroft's theory and practice of histological techniques. Amsterdam: Elsevier.

Tanaka, G., et al. 2014. Mineralized rods and cones suggest colour vision in a 300 Myr-old fossil fish. Nature Communications 5: 5920.

Thibaudeau, G. & Altig, R. (2012). Coloration of anuran tadpoles (Amphibia): development, dynamics, function, and hypotheses. ISRN Zoology 2012: 1–16.

Toporski, J.K.W., et al. 2002. Morphologic and spectral investigation of exceptionally well-preserved bacterial biofilms from the Oligocene Enspel formation, Germany. Geochimica et Cosmochimica Acta 66: 1773–1791.

Turick, C.E., L.S. Tisa, and F. Caccavo Jr. 2002. Melanin production and use as a soluble electron shuttle for Fe(III) oxide reduction and as a terminal electron acceptor by *Shewanella algae* BrY. Applied and Environmental Microbiology 68: 2436–2444.

Valentine, J.W. 1989. How good was the fossil record? Clues from the Californian Pleistocene. Paleobiology 15: 83–94.

Vannier, J., J. Liu, R. Lerosey-Aubril, J. Vinther, and A.C. Daley. 2014. Sophisticated digestive systems in early arthropods. Nature Communications 5: 3641.

Vasanthabharathi, V., R. Lakshminarayanan, and S. Jayalakshmi. 2011. Melanin production from marine *Streptomyces*. African Journal of Biotechnology 10: 11224–11234.

Vinther, J. 2015. A guide to the field of palaeo colour—melanin and other pigments can fossilise: reconstructing colour patterns from ancient organisms can give new insights to ecology and behaviour. Bioessays 37: 643–656.

Vinther, J. 2016. Fossil melanosomes or bacteria? A wealth of findings favours melanosomes: melanin fossilises relatively readily, bacteria rarely, hence the need for clarification in the debate over the identity of microbodies in fossil animal specimens. Bioessays 38: 220–225.

Vinther, J. 2020. Reconstructing vertebrate paleocolor. Annual Reviews of Earth and Planetary Sciences 48: 14.1–14.31.

Vinther, J., D.E.G. Briggs, R.O. Prum, and V. Saranathan. 2008. The colour of fossil feathers. Biology Letters 4: 522–525.

Vinther, J., D.E.G. Briggs, J. Clarke, G. Mayr, and R.O. Prum. 2010. Structural coloration in a fossil feather. Biology Letters 6: 128–131.

Vinther, J., et al. 2016. 3D camouflage in an ornithischian dinosaur. Current Biology 26: P2456–2462.

Wakamatsu, K., and S. Ito. 2002. Advanced chemical methods in melanin determination. Pigment Cell and Melanoma Research 15: 174–183.

Wan, X., et al. 2007. Isolation of a novel strain of *Aeromonas media* producing high levels of DOPA-melanin and assessment of the photoprotective role of the melanin in bioinsecticide applications. Journal of Applied Microbiology 103: 2533–2541.

Wang, Y.L., P. Aisen, and A. Casadevall. 1995. *Cryptococcus neoformans* melanin and virulence: mechanism of action. Infection and Immunity 63: 3131–3136.

Wang, Y.L., P. Aisen, and A. Casadevall. 1996. Melanin, melanin "ghosts," and melanin composition in *Cryptococcus neoformans*. Infection and Immunity 64: 2420–2424.

Westall, F., et al. 2001. Early Archean fossil bacteria and biofilms in hydrothermally-influenced sediments from the Barberton greenstone belt, South Africa. Precambrian Research 106: 93–116.

Wheeler, M.H. 1983. Comparisons of fungal melanin biosynthesis in Ascomycetous, imperfect and Basidiomycetous fungi. Transactions of the British Mycological Society 81: 29–36.

Wilson, P., L.A. Parry, J. Vinther, G.D. Edgecombe, and S. Gabbott. 2016. Unveiling biases in soft-tissue phosphatization: extensive preservation of musculature in the Cretaceous (Cenomanian) polychaeteRollinschaeta myoplena(Annelida: Amphinomidae). Palaeontology 59: 463–479.

Wuttke, M. 1983. Weichteil-Erhaltung'durch lithifizierte Mikroorganismen bei mittel-eozänen Vertebraten aus den Ölschiefern der 'Grube Messel'bei Darmstadt. Senckenbergiana Lethaea 64: 509–527.

Xiao, S., and A.H. Knoll. 1999. Fossil preservation in the Neoproterozoic Doushantuo phosphorite Lagerstatte, South China. Lethaia 32: 219–240.

Xu, X., et al. 2015. A bizarre Jurassic maniraptoran theropod with preserved evidence of membranous wings. Nature 521: 70–73.

Yap, B.W., and C.H. Sim. 2011. Comparisons of various types of normality tests. Journal of Statistical Computation and Simulation 81: 2141–2155.

Young, F.J., J. Vinther, and X.G. Zhang. 2017. Onychophoran-like myoanatomy of the Cambrian gilled lobopodian *Pambdelurion whittingtoni*. Palaeontology 60: 27–54.

Zhang, F.C., et al. 2010. Fossilized melanosomes and the colour of Cretaceous dinosaurs and birds. Nature 463: 1075–1078.

Zheng, H., C.H. Chatfield, M.R. Liles, and N.P. Cianciotto. 2013. Secreted pyomelanin of *Legionella pneumophila* promotes bacterial iron uptake and growth under iron-limiting conditions. Infection and Immunity 81: 4182–4191.

Zheng, X.T., et al. 2017. Exceptional preservation of soft tissue in a new specimen of *Eoconfuciusornis* and its biological implications. National Science Review 4: 441–452.

Zuschin, M., and C. Ebner. 2015. Actuopaleontological characterization and molluscan biodiversity of a protected tidal flat and shallow subtidal at the northern Red Sea. Facies 61: 5.

SECTION 3. EARLY-FLIGHT STUDY: METHODS, STATUS, AND FRONTIERS

Chapter 10

Methods of Studying Early Theropod Flight

MICHAEL PITTMAN,[1] ASHLEY M. HEERS,[2] FRANCISCO J. SERRANO,[3] DANIEL J. FIELD,[4]
MICHAEL B. HABIB,[5] T. ALEXANDER DECECCHI,[6] THOMAS G. KAYE,[7]
AND HANS C.E. LARSSON[8]

ABSTRACT

The study of early theropod flight involves avialans as well as other pennaraptorans. It requires the study of anatomy that is familiar to the modern ornithologist, but also very different and alien. Early theropod flight therefore necessitates study methods that can incorporate what we know about sophisticated powered and unpowered flight in living birds while being mindful of the differences between them and the earliest theropod flyers. In this chapter we will survey key methods and approaches, covering their best-practice applications along the timeline of early theropod flight evolution and priorities for future method development.

INTRODUCTION

Locomotion plays a central role in the lives of most vertebrates, and reconstructing locomotor behaviors of extinct taxa is key to understanding some major evolutionary transitions—for example, the origin of walking tetrapods or swimming whales. But how do we reconstruct locomotion in extinct taxa when it is very difficult to compare them to modern forms?

When trying to decipher early theropod flight, researchers are faced with substantial anatomical differences between modern flying birds like pigeons and early birds like *Archaeopteryx* as well as their closely related nonavialan relatives. In particular, extant volant birds have a large keel on the sternum, which anchors two main flight muscles, the pectoralis for downstroke and the supracoracoideus for upstroke (George and Berger, 1966). Though the supracoracoideus is in a ventral position, it is

---

[1] Vertebrate Palaeontology Laboratory, Division of Earth and Planetary Science, the University of Hong Kong, Hong Kong.

[2] College of Natural and Social Sciences, California State University, Los Angeles.

[3] Dinosaur Institute, Natural History Museum of Los Angeles County, Los Angeles; and Real Academia Ciencias Exactas, Físicas y Naturales, Madrid.

[4] Department of Earth Sciences, University of Cambridge, Cambridge.

[5] Dinosaur Institute, Natural History Museum of Los Angeles County, Los Angeles.

[6] Division of Natural Sciences, Mount Marty College, Yankton, SD.

[7] Foundation for Scientific Advancement, Sierra Vista, AZ.

[8] Redpath Museum, McGill University, Montreal.

able to elevate and supinate (Poore et al., 1997a; Tobalske and Biewener, 2008) the wing because it loops through a donut-shaped triosseal canal and attaches to the dorsal surface of the humerus, similar to a pulley. *Archaeopteryx*, in contrast, has no triosseal canal and no ossified sternum, but some early avialans and possibly volant nonavialan pennaraptorans have either feature or both in an incipient form (Zhou and Zhang, 2002; Xu et al., 2003; Baier et al., 2007; Dyke et al., 2013; Zheng et al., 2014; Pei et al., in press). Consequently, at least some of the flight muscles of many early avialans and suspected volant nonavialan pennaraptorans were probably not very large, and would have had different configurations compared with extant birds. What does that mean in terms of the locomotor capacity of early birds and some nonavialan pennaraptorans?

The study of early theropod flight engages tailored methodologies with their own emphases to address the spectrum of form-function differences along the line of descent from the first theropod flyers to modern living ones. Theropod aerial locomotion seems to have multiple origins, the study of which involves anatomy that is very different to modern birds. At the other end of the theropod flight timeline, the origin of avian flight involves looking at a much more refined set of flight-related avian features that allowed birds to adopt different flight styles, but not the sophisticated powered flight of living birds. In this chapter we will survey key methods and approaches adopted in studying early theropod flight, detailing their best practice applications to the facets of this iconic field of pennaraptoran paleontology.

FORM-FUNCTION RELATIONSHIPS

Substantial efforts to characterize the morphology of early pennaraptoran theropods and investigate their relationship with flight function continue to greatly advance our knowledge of early theropod flight. This ranges from numerous studies assessing the functional morphology of single taxa (Navalón et al., 2015; Xu et al., 2015; Wang et al., 2017) to work focusing on one or a few anatomical features, such as feathers and/or wings (e.g., Burgers and Chiappe, 1999; Nudds and Dyke, 2010; Chiappe et al. 2019), tails (e.g., Gatesy and Dial, 1996; Gatesy, 2001; Pittman et al., 2013), the shoulder (e.g., Jenkins, 1993; Baier et al., 2007; Navalón et al., 2018), or the supracoracoideus muscle (e.g., Poore et al., 1997b). Recent efforts to leverage the locomotor variation among nearly 11,000 living species (Prum et al., 2015; Gill and Donsker, 2017) using large-scale datasets to characterize aspects of the avian flight apparatus have begun to bear fruit. New analytical techniques are showing that yet more high-fidelity flight-related soft-tissue details are hidden in the very best preserved pennaraptorans, especially those from China (Falk et al., 2016; Wang et al., 2017; see Serrano et al., chap. 13). Advancements in early flight studies have greatly benefited from the evolutionary context provided by a range of detailed phylogenetic analyses, the details of which are provided by Pittman et al. in chapter 2.

LARGE-SCALE AVIAN ANATOMICAL DATASETS: Seminal datasets like those by Greenewalt (1975) or Hartman (1961) have been extremely helpful in informing our understanding of early theropod flight (e.g., Dececchi et al., 2016; Pei et al., in press), but their use has generally fallen out of favor in recent times. The reason for this may be that these datasets are often created from amalgamations of other datasets or sources, so that specific specimens are rarely scored for all relevant measurements (Hartman, 1961; Greenewalt, 1975). A new generation of studies has begun to broach this data gap to quantify anatomical variation for key modules of the flight apparatus by using large comparative samples that draw on the majority of avian higher-order subclades. These studies have begun to yield form-function relationships that may provide new lines of investigation into early flight. This includes work on the furcula (Close and Rayfield, 2012) as well as on flight feathers (Feo et al., 2015) and skeletal proportions (Field et al., 2013; Serrano et al., 2015).

Feathers are among the most characteristic avian specializations, but quantitative compari-

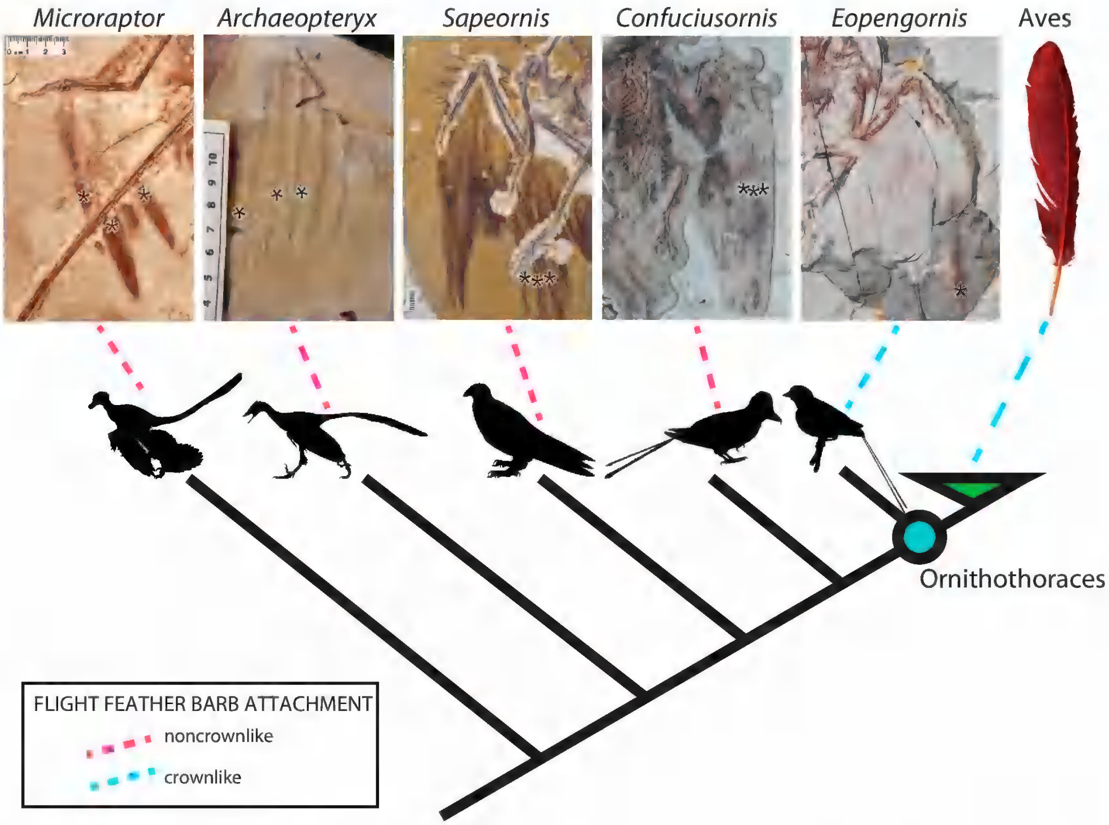

FIG. 1. Flight feather morphology across paravian phylogeny (modified from Feo et al., 2015). Early-diverging taxa (indicated by dashed pink lines) exhibit flight feather trailing edges characterized by narrow angles of barb-to-rachis attachment. The crownlike condition (broad angles of barb-to-rachis trailing edge attachment; blue dashed lines) arose on the internode subtending Ornithothoraces, and may have conferred a more flexible trailing edge of the wing during flight in order to increase feather-to-feather contact and maintenance of a coherent wing surface in flight during active downstrokes. Silhouettes from phylopic.org.

sons between flight-feather morphology in living and extinct total-clade birds are hampered by the rarity of intact fossil feathers and the preservation difficulty posed by their flexible feather vanes. A large comparative dataset examining feather-barb geometry was successfully generated and used to characterize macroevolutionary patterns in barb arrangement across the crown bird tree of life (Feo et al., 2015). Among other observations, this study observed that crown birds exhibit characteristic barb-to-rachis attachment angles on the leading and trailing edges of flight feathers (Feo et al., 2015). Primary feather barbs on a wing's leading edge that cut into the air during flight connect to the rachis at narrow attachment angles, providing a relatively inflexible airfoil for stability during flight, whereas barbs on the trailing edge of flight feathers connect to the rachis at broad angles of attachment, providing a more flexible vane in order to maintain a coherent wing surface through feather-to-feather contact. These patterns are generally conserved across crown birds. In contrast to this pattern, deinonychosaurians, like *Microraptor*, and early-diverging volant avialans, like *Archaeopteryx*, *Confuciusornis*, and *Sapeornis*, exhibit trailing edge barbs with angles of attachment indistinguishable from the narrow angles of attachment of leading-edge barbs (fig. 1), suggesting that the trailing-edge vane flexibility—and associated benefits for maintaining a coherent trailing edge of the wing during flight—did not exist in these taxa (Feo et al., 2015). By contrast, more crownward avialans (e.g., Enantiornithes) appear to have exhibited the crownlike trailing-edge condition, suggesting that broad angles of trailing-edge barb-to-rachis attachment arose on the internode-subtending Ornithothoraces and were inherited by the ancestors of crown birds (fig. 1). This work suggests that despite an early origin of flight-feather asymmetry (Feduccia and Tordoff, 1979), "modern" flight feathers arose at a later-diverging point in paravian evolutionary history than previously recognized. Other aspects of feather morphology, such as emargination and its ability to offset the cost of slow flight also appear to have been later developments in avian evolution (van Oorschot et al., 2017), further stressing how the feathers of extant taxa are not identical to those of the earliest avialans.

Body mass is one of the most critical parameters in flight studies (Norberg, 2002; Videler, 2005; Pennycuick, 2008; Tennekes, 2009). In light of differing body mass estimates, inferences of a particular fossil taxon's flight potential could differ radically. The dependence of functional inferences on body mass places a premium on the attainment of accurate and precise estimates of fossil body size in paravians. Recent work aimed at improving methods for paravian body size estimation has focused on the development of multivariate and bivariate equations for body size estimation based on avian skeletal proportions (Field et al., 2013; Serrano et al., 2015). In addition to providing scaling equations for the estimation of mean body size in crown birds and nonavian avialans from skeletal measurements, these studies represent the first avian skeletal studies to explicitly provide equations for 95% prediction intervals on body mass estimates, providing better-informed constraints on uncertainty in fossil avialan body size estimates and their resulting functional hypotheses (fig. 2). Used with caution, these constraints can potentially have comparable benefits in more morphologically disparate nonavialan paravians. An encouraging development to emerge from such scaling studies is that relatively robust estimates of body mass can be reconstructed from the mostly fragmentary, isolated elements typically preserved in the avialan fossil record (fig. 2) (Louchart et al., 2009; Longrich et al., 2011; Brocklehurst et al., 2012; Field, 2017). Of 13 skeletal measurements investigated, 11 yielded especially high correlations with body size ($R^2 > 0.9$). Moreover, scaling equations for several elements (e.g., femur length; fig. 3) scale uniformly for both flying and flightless extant birds, suggesting that these measurements are particularly appropriate for estimating body size in extinct taxa for which flying potential is uncertain (e.g., nonavian avialans). However, it is important to be mindful of how anatomical differences between extant and extinct taxa may affect results. Beyond the obvious relationship between body mass and flying potential, body mass is strongly associated with a host of important physiological, ecological, and biomechanical parameters (Schmidt-Nielsen, 1984; Rayner, 1988; Pollock and Shadwick, 1994; Brown, 1995; Ahlborn, 2000; Gillooly et al., 2001; Gillooly et al., 2002; Campione and Evans, 2012; Smith, 2012; Berv and Field, 2018), parameters that underscore the importance of robustly estimating body size in paleobiological studies of extinct fossil taxa.

HIDDEN FLIGHT-INFORMATIVE FOSSILIZED SOFT TISSUE DATA: Newly available analytical techniques in modern paleontology have enabled more attention to be given to the discovery of fossil soft tissues, including soft tissues directly related to flight capability and performance. The feather impressions found in *Archaeopteryx* was the key evidence used to suggest that early birds were flight capable (Wellnhofer, 2009). Raking light for *Archaeopteryx* feather impressions has now given way to direct microscopic analysis of feathers, such as the Chinese feathered dinosaurs. Barbs are easily visualized with white light but

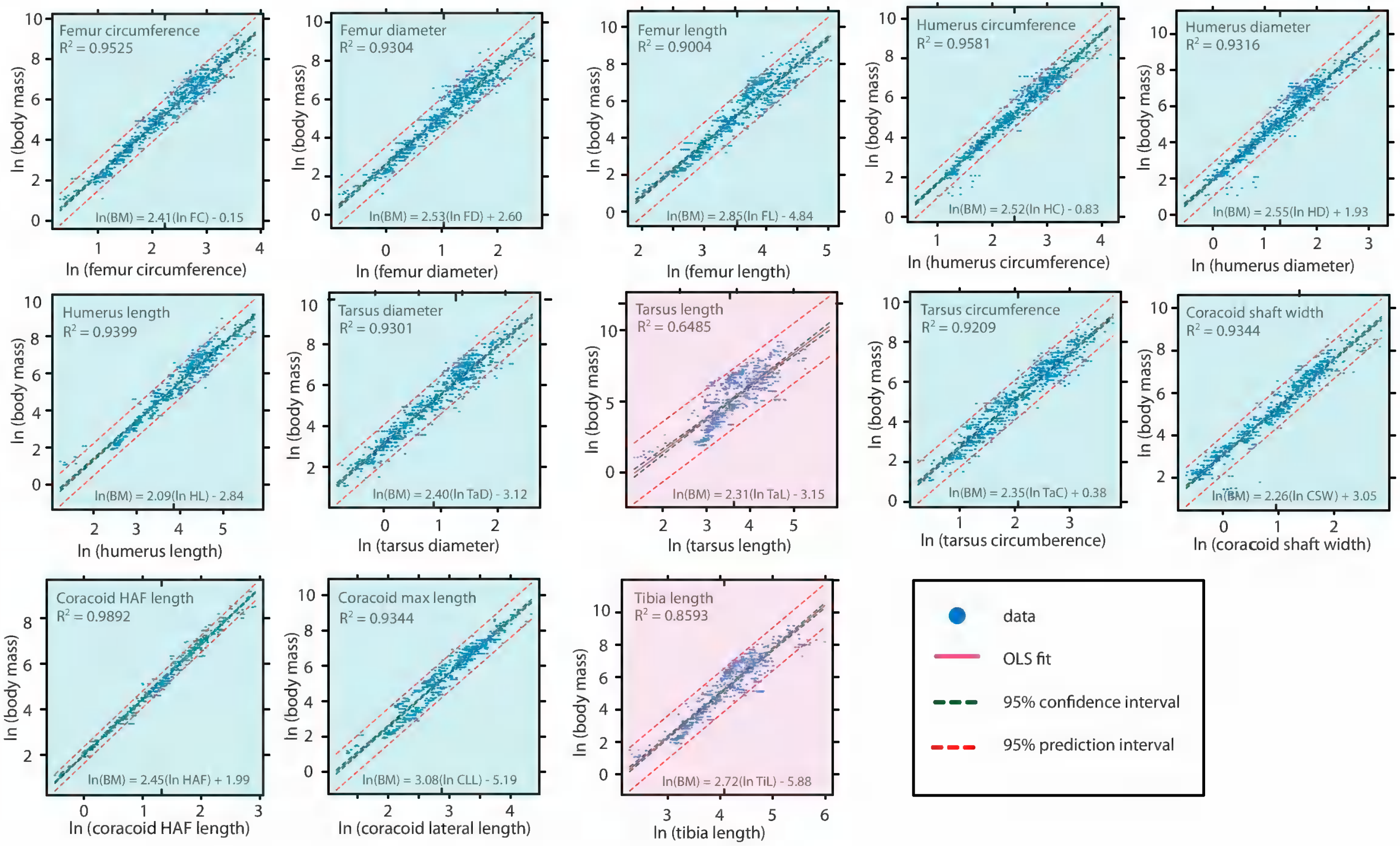

FIG. 2. Bivariate scaling equations for crown birds for 13 skeletal measurements, including 95% prediction intervals (modified from Field et al., 2013). Equations with R^2 >0.9 are highlighted in blue; equations with R^2 <0.9 are highlighted in pink.

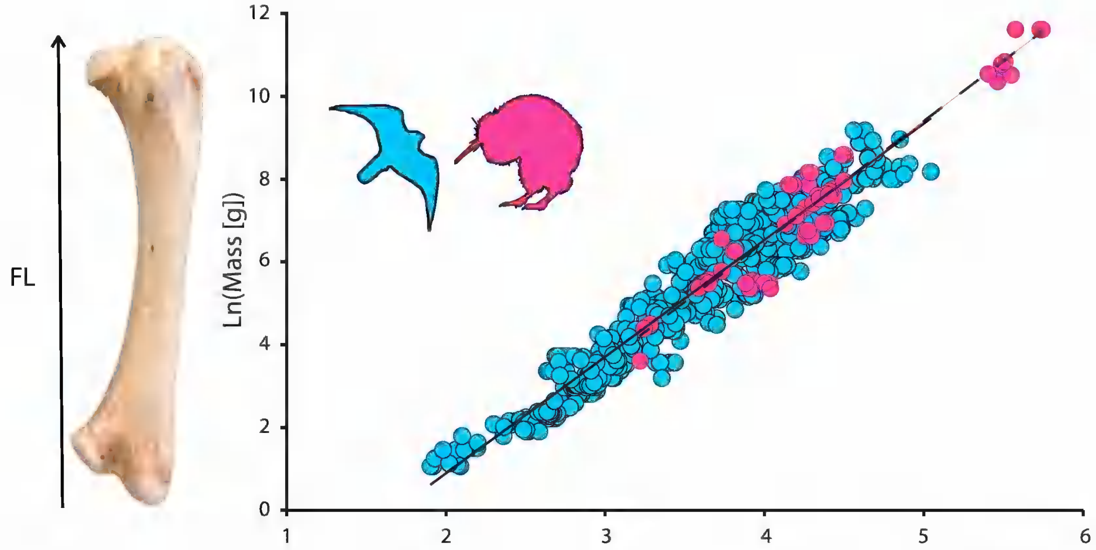

FIG. 3. Example of a bivariate scaling equation for femur length (D.J. Field, unpublished data) illustrating virtually invariant scaling equations for flying (blue) and flightless (pink) extant bird taxa. Datasets such as this will be useful for estimating live body mass for extinct avialans with unknown flying potential.

laser-stimulated fluorescence (LSF) is now capable of bringing out barbule structure by fluorescing sediment matrix to backlight nonfluorescent carbon films comprising fossil feathers (Kaye et al., 2015, 2019; Wang et al., 2017; to a lesser extent under UV: Hone et al., 2010). This application of LSF has important potential in reappraising known fossil feather diversity (Lefèvre, 2020; Xu 2020) and testing ideas of the evolution of feather rigidity and integrity that directly impact reconstructions of early flight. Neutron imaging also has the potential to contribute meaningful new data in the study of fossil feathers. While synchrotron elemental analysis has trouble with atomic numbers below silicon (Brown and Waychunas, 2004), neutrons work best on carbon and other lower atomic number elements. This makes it a unique elemental technique compared to alternatives for imaging soft tissues.

The UV lamp has now advanced to high power near UV wavelength lasers capable of fluorescing virtually all minerals. This allows clarifying osteology (Tischlinger and Unwin, 2004; Foth et al., 2014; Rauhut et al., 2018) and has produced the first quantifiable body outline of the early-diverging paravian *Anchiornis* (Wang et al., 2017) (see Pittman et al., chapters 1 and 2). The latter study revealed the wing's leading edge shape as well as arrangement of the feathers from the leading to trailing edge, providing the refined direct data of wing span and lift (= wing) surface (Wang et al., 2017). In chapter 13 of this volume, Serrano et al. used direct nonfeather-based soft-tissue data to refine calculations of flight performance using mechanically informed morphospace analysis for the first time.

The increasingly common use of nondestructive imaging in the study of the mostly skeletal portions of fossil birds provides an opportunity to develop augmented imaging protocols that can visualize and document preserved soft tissues, even before preparation (sensu Abel et al., 2012. and Schilling et al., 2014). Alternative imaging approaches like neutron imaging and proven soft-tissue imaging methods like LSF all have a role to play in this area. However, new analytical techniques also have a role in further curating existing specimens, such as by clarifying the integrity of suspect fossils. For example, the extent of prior repair work can be clarified using regular and synchrotron x-rays (Rowe et al., 2001; Cau et al., 2017) and fluorescence imaging like LSF and UV (Kaye et al., 2015; Eklund et al., 2018).

Theropod Early Flight Performance

In-depth functional morphology knowledge of many of the earliest flying theropods as well as evolutionary context afforded by an impressive legacy of phylogenetic analyses (see chapter 1) has provided the basis for efforts to estimate early theropod flight performance. Our knowledge of flight performance of early birds has dramatically increased in recent years, including the reconstruction of flight styles that we are familiar with today, such as thermal soaring (Serrano and Chiappe, 2017), as well as support for powered flight potential in a number of nonavialan theropod taxa (Pei et al., in press). Herein we cover three of the most powerful approaches available: mechanically informed morphospace analysis, first-principles-based modeling and interactive musculoskeletal modeling and simulation.

Mechanically Informed Morphospace Analysis: In the previous section, body mass (M_b) was mentioned as a key variable known to influence flight in living birds and this is also true of wing span (B) and lift (= wing) surface (S_L) (Norberg, 2002; Videler, 2005; Pennycuick, 2008; Tennekes, 2009). Using a conservative approach that recognizes the statistical, phylogenetic, ecological, and taphonomic sources of error associated with early bird fossils, these key flight variables can be used to infer flight performance in early birds. By carefully selecting forelimb and hind-limb measurements for each early-diverging taxon, multiple regressions can be obtained that minimize these sources of error as well as predictive error (Serrano et al., 2015, 2017). Reliable estimates of M_b, B, and S_L from this approach enable direct comparisons between early and modern birds in morphospaces that include these variables. Fine estimates of B and S_L can also be obtained from outline reconstruction in well-preserved feathered fossils (Wellnhofer, 2009; Chiappe et al., 2014).

Morphospaces relating M_b with B and/or the length of the deltopectoral crest of the humerus (DPC) allow the flapping pattern of early birds to be approximated (Serrano and Chiappe, 2017). For a given M_b and B, modern birds that fly with alternating flapping and gliding periods have shorter DPCs than birds with a stricter flapping pattern. Based on lever theory (Alexander, 2003), the latter birds have higher mechanical advantage for moving the wing faster—hence flapping it more frequently—than the former ones. This approach provided support for a flight pattern less dominated by wing flapping in the early-diverging pygostylian *Sapeornis* (Serrano and Chiappe, 2017). In a similar way, estimations showed that enantiornithines *Concornis* and *Eoalulavis* had short wings in relation to their body mass and DPC, suggesting that they flew strictly using flapping flight with no gliding phases in steady flight (Serrano et al., 2018). In such a study, a combined analysis of the three basic variables allowed bounding flight to be specifically inferred in *Concornis* and *Eoalulavis*.

Valuable information about flying behavior of extinct birds also can be obtained from the calculation of the wing loading (i.e., $WL = M_b/S_L$) and the aspect ratio ($AR = B^2/S_L$). While AR provides information relative to drag and thrust (Rayner, 1993; Swaddle and Lockwood, 2003; Meseguer and Sanz-Andres, 2007; Shyy et al., 2008), the WL provides information about the flight speed and turn radius (Von Mises, 1945; Norberg, 2002; Tennekes, 2009). In the case of *Sapeornis*, the relatively low AR of its wings indicated a continental (= thermal) soaring capacity instead of dynamic soaring (Serrano and Chiappe, 2017). In other cases, the low values of AR and WL estimated for *Junornis* and *Orienantius* suggested that these enantiornithines may have been capable of rapid takeoff and tight turns (Liu et al., 2017, 2019).

In many cases the aerial inferences obtained from morphospaces can be validated by constructing aerodynamic models based on the estimates of M_b, B, and S_L. Such models allow the checking of the power margin during flapping flight and gliding patterns. This type of analysis supported conclusions that early birds like *Sapeornis* and *Gretcheniao* were incapable of generating sufficient power for sustaining prolonged flapping flight (Serrano and Chiappe, 2017; Chiappe et al. 2019), and also that *Concornis* and *Eoalulavis* could improve their efficiency of transport switching from continuous flapping to bounding (Serrano et al., 2018).

First-Principles-Based Modeling: These approaches to estimating flight performance rely on fundamental properties of aerodynamics and morphology that apply to all flying systems. They typically utilize a comparative framework, because calculations of exact performance values in fossil taxa are difficult to make with precision without a very large number of variables that are often not directly observable in fossils. The relative differences in performance, however, can often be robustly inferred using first principles approaches.

In the context of flight origins and evolution, modeling is often best approached from a dynamics perspective. Reconstructing kinematics with confidence requires a more species-specific approach, such as simulation or range-of-motion analysis from analogous living taxa (see Interactive Musculoskeletal Modeling and Simulation Method below). Typically, dynamics models must still make some kinematic assumptions. More conservative kinematic assumptions will yield more robust conclusions regarding dynamics. As an example, in our recent work on microraptorine flight dynamics (see Dececchi et al., chapter 11), we made only two kinematic assumptions: (1) the hind limbs generated the launch prior to the wing being engaged, (2) there was a sufficient range of motion to generate a viable flight stroke for climb out. For all taxa, we used only configurations in which the hind limbs (and therefore hind wings, where present) were held under the body in a vertical configuration. The first of these assumptions is conservative because the use of the stance limbs to engage takeoff is a universal trait of flying animals. The second assumption is conservative because it requires only that there be at least one motion set that provides sufficient wing amplitude for flight. This is therefore more conservative than specifying a particular flight stroke. Lift from the hindwings, in this configuration, potentially contributes to stability and control during flight, as the lift would be oriented laterally, rather than upward. It would not contribute to weight support or thrust, which we assume comes only from the forelimbs (and potentially the tail, but only for pitch authority).

Modeling approaches of this kind are particularly useful for determining those variables that have a particularly large effect on the performance outcome of interest. In the case of our microraptorine flight performance work, we found that maximal wing loading and specific lift capacity are strong criteria for evaluating flight performance in a comparative dataset of fossil taxa. These two criteria were devised from theoretical and in vivo work on extant avians and present easily testable benchmarks that accurately model the minimal thresholds needed to discern volant from flightless taxa (Meunier, 1951; Marden, 1987; Livezey, 1992; Guillemette and Ouellet, 2005)

For example, for taxa without complete primary feathers preserved, feather length was modeled on closely related taxa and wing area was calculated based on the methods presented in Dececchi et al. (2016). Geometric measurements were all taken using standard digital calipers. Wingspan was taken as 2.1× the summation of the lengths of the humerus, ulna and metacarpal II, and the longest distal primary (Dececchi et al., 2016). Wing chord was taken as 65% of the longest distal primary length (Dececchi et al., 2016). Wing loading is based on body weight estimated as per above (kg) over wing area (cm^2). Specific lift, here used as the lift force generated in the vertical plane is based on Marden's model (Marden, 1987). This model has been suggested to underestimate maximum vertical force produced (Buchwald and Dudley, 2010), thus these values may represent a conservative estimate of force produced in these taxa. Specific lift = FMR × Po,m × (L/P) where FMR is the flight muscle ratio, which is assigned at a constant value of 10% of body weight across all taxa examined. This is at the lower range of the values seen in volant birds and is likely a significant overestimation for all nonparavian taxa based on recent 3D modeling work (Allen et al., 2013). The methods used here will help us to refine these estimates by producing more accurate body-outline reconstructions that place quantitative constraints on musculature. Po,m is the maximum muscle mass-specific power output based on values from extant birds. As Po,m is unknown for nonavialan theropods, three separate calculations were made that span the range of Po,m values that could have reasonably been expected (225, 250, and 287 $\mathrm{Wkg^{-1}}$). However, we use the two extremes (225 and 287 $\mathrm{Wkg^{-1}}$) to reconstruct minimum and maximum flying ability. We assume that all thrust is lift generated, and so the estimates of required power for flight essentially relate to the power that must be exerted against drag to generate sufficient lift for flight. Drag can contribute to thrust, but this is a relatively sophisticated dynamic, and lift-generated thrust dominates in living flying animals in the size range relevant to our study. The value of 225 $\mathrm{Wkg^{-1}}$ was suggested by Marden (1994) as the mean value for burst flight in birds. Work by Guillemette and Ouellet (2005) suggested that a range between 225 and 250 $\mathrm{Wkg^{-1}}$ more accurately mimics values seen in the Common Eider, a bird with short wings that displays some of the highest wing-loading values seen in extant birds, two features that resemble the condition seen in the extinct taxa examined here. The value of 287 $\mathrm{Wkg^{-1}}$ was based on the values calculated for Chukar partridges (Askew et al., 2001), a short burst flight taxon previously used as a model for early flight in theropods. Our work here will help refine these estimates and help us constrain these values even further. L/P is calculated from:

$$\log10\ (L/P) = -0.440\ \log10\ \text{muscle mass} + 0.845\ \log10\ (\text{wingspan}/2) - 2.239$$

To improve optimization of the data we screened the coelurosaurians based on their presence of vaned feathers, which are integral to the production of aerodynamic forces; terminals for which feather condition is unknown were considered to have the same state as their ancestor, which is the condition predicted by our recent phylogenetic hypothesis (Pei et al., in press). If a taxon showed both wing-loading values below 2.5 $\mathrm{gcm^{-2}}$ (which has been estimated to be the upper limit for flight in extant birds: Meunier, 1951; Guillemette and Ouellet, 2005) as well as the potential to generate lift values more than 9.8 $\mathrm{Nkg^{-1}}$, we suggest that this taxon has the potential to achieve takeoff and powered flight. We use linear parsimony to reconstruct wing loading and specific lift values over our tree topology. In this project we use the upper and lower limits recovered for *Microraptor* to see whether this affects the results of surrounding nodes, if at all. We will also consider tail area and shape, mostly for its role in determining the center of lift and providing pitch stability, adopting the approach previously utilized by one of the authors (MBH – see Han et al., 2015). In chapter 11, Dececchi et al. develop this approach further by presenting the first ontogenetic trajectory of flight and flapping-related behaviors in the nonavialan theropod *Microraptor*, which are directly compared to similar curves produced for extant birds (Heers and Dial, 2012).

INTERACTIVE MUSCULOSKELETAL MODELING AND SIMULATION: This method has been widely used to study human locomotion, and adapted for use with extant animals such as chimpanzees (O'Neill et al., 2013) and extinct animals such as *Tyrannosaurus rex* (Hutchinson et al., 2005) and *Mussaurus* (Otero et al., 2017). Musculoskeletal modeling and simulation use programs like SIMM (Software for Interactive Musculoskeletal Modeling; Musculographics, Inc., http://www.musculographics.com/) and OpenSim (http://opensim.stanford.edu/) (Delp et al., 2007) to construct digital, musculoskeletal models and then simulate different behaviors to analyze muscle function or determine, for example, whether muscles would

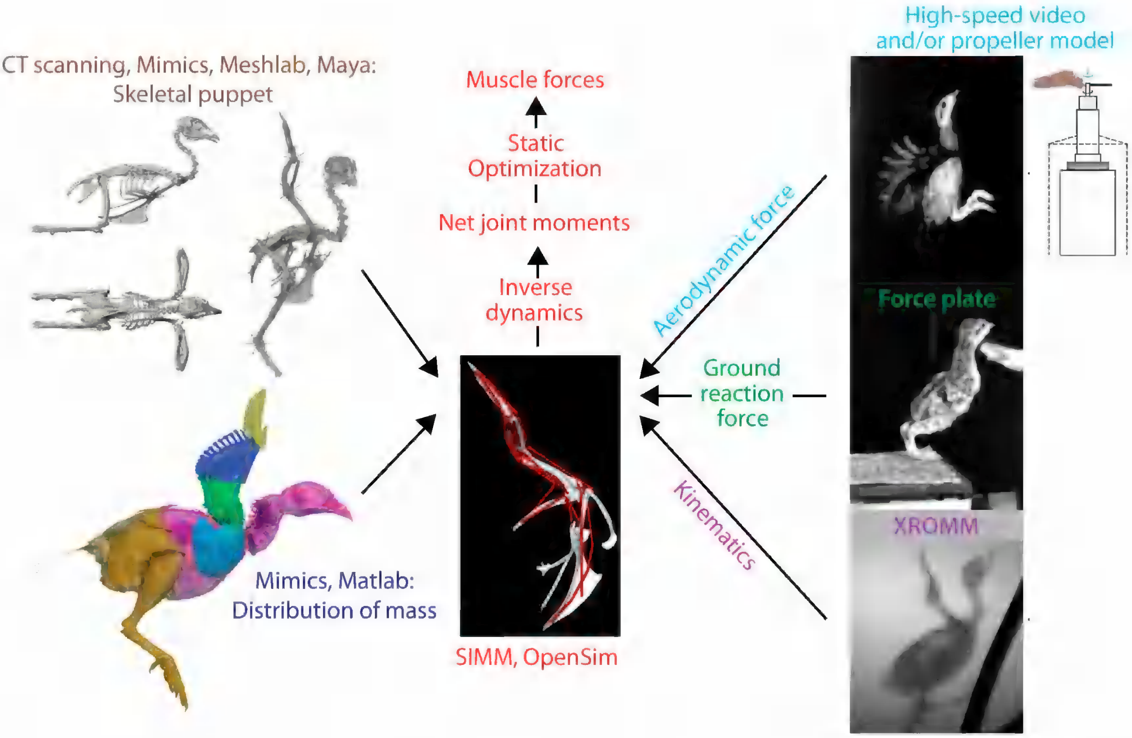
CT scanning, Mimics, Meshlab, Maya:
Skeletal puppet
Muscle forces
Static Optimization
Net joint moments
Inverse dynamics
High-speed video and/or propeller model
Aerodynamic force
Force plate
Ground reaction force
Kinematics
XROMM
Mimics, Matlab: Distribution of mass
SIMM, OpenSim

FIG. 4. Interactive musculoskeletal modeling and simulation involves 4 steps: (1) Computed tomography (CT) scanning, (2) dissection, (3) measurement of kinematics, and (4) measurement of all external forces. Modified from Heers, et al., 2016, 2018.

be strong enough to perform a particular behavior. For extant animals, musculoskeletal modeling involves four steps (fig. 4):

1. Computed Tomography Scanning: CT scanning of the animal in question, to construct a skeletal "puppet." This three-step process involves:

Isolating Skeletal Elements: Importing CT slices into programs such as Mimics (Materialise, Inc., Leuven, Belgium) or Osirix/Horos (Rosset et al., 2004), and using a density threshold to isolate skeletal elements (e.g., wing bones in a bird), which are then saved as three-dimensional objects (e.g., .obj files).

Constructing a Hierarchical Joint Coordinate System: This is often done by importing the skeletal elements into Maya (Autodesk; http://autodesk.com/) to align and link bones together through joints. A "zero" or resting position and coordinate systems for each joint must be defined. Joint-coordinate systems (Grood and Suntay, 1983) are typically defined anatomically, either based on the anatomy of the bones articulating at the joint or based on the morphology of the joint itself, though they can also be defined kinematically (i.e., joint location and axes of rotation can be calculated based on how bones are translated and rotated about each other during locomotion).

Determining Mass Distribution: Once the skeletal "puppet" is constructed, the distribution of mass must be quantified for each moveable body segment. Mimics, for example, can be used to digitally segment the animal into hind limb, trunk, brachial, antebrachial, and manual segments, depending on the animal and behavior in question. Each segment includes all tissues associated with that segment (bones, muscles, skin, fat, etc.). Assuming a tissue density of 1060 kgm^{-3}, a custom script (Allen et al. 2013) can then calculate the mass, centre of mass, and inertial tensor for each body segment, based on its volume. These values determine the inertial properties of each moveable segment.

2. Dissection: This is done to add representations of muscles to the skeletal model. Model muscles, added in SIMM, are specified by:

Muscle Geometry: Origin(s), insertion(s), and path(s) between them. "Via points" or "wrapping objects" can be added to prevent the muscle from passing through bone.

Muscle Architecture: Optimal fibre length (typically taken as the length of muscle fascicles at rest: Zajac, 1989) and average pennation angle, which are important determinants of muscle strain (changes in length) and stress (force per unit physiological cross-sectional area).

Maximum Isometric Muscle Force: This is calculated from the physiological cross-sectional area of the muscle (area perpendicular to muscle fibres).

Tendon Slack Length: This is the length beyond which a muscle's tendons begin resisting stretch and producing force; this essentially specifies how much force is produced actively, by muscle fibers contracting, versus passively, by tendon(s) being stretched. Tendon slack length is calculated using an algorithm (Manal and Buchanan, 2004) that analyzes the shortening and lengthening behavior of muscle-tendon units over a large range of motion.

For more complex (dynamic) simulations, physiological properties such as maximal contractile velocity, force-velocity relationships, and activation-deactivation dynamics are included as well.

3. Measurement of Joint Kinematics: For some animals and behaviors, this is accomplished with high-speed visible light video. For birds and/or behaviors involving rapid movement, this may require X-ray Reconstruction of Moving Morphology (www.xromm.org).

4. Measurement of All External Forces Acting on the Animal: In addition to gravity, this may include ground reaction, aerodynamic, and/or hydrodynamic forces. Ground reaction forces are recorded by force plates, whereas fluid dynamic forces may be calculated using techniques like PIV (particle image velocimetry) (Tobalske and Dial, 2007) and "propeller models" (Heers et al., 2011; Dial et al., 2012), or measured using newly developed Aerodynamic Force Platforms (Lentink et al., 2015). For each force, a magnitude, direction, and location must be provided. Magnitude, direction, and sometimes location vary through a stroke or stride cycle.

In short, steps 1 and 2 result in the construction of an anatomical (musculoskeletal) model, and steps 3 and 4 involve collecting kinematic and kinetic data, which are required for simulation. Once a musculoskeletal model is constructed and the necessary experimental data are collected, various types of simulations can be performed in OpenSim:

Muscle Moment Arms: At the most basic level, the musculoskeletal model and joint kinematics can be used to calculate muscle moment arms through a stroke or stride cycle. The moment arm of a muscle indicates (a) what action it would perform if it were activated, and (b) how effective it would be at performing that action, because a muscle's ability to transform force into bone movement depends both on muscle force (which is proportional to muscle size) and the length of the muscle's moment arm. Thus, musculoskeletal models are useful tools for predicting muscle function(s).

Static Simulations: These take simulations one step further by calculating the timing and level of muscle activations during the movement of interest. First, *inverse dynamics* uses the musculoskeletal model, kinematics, and external loads provided to calculate the net joint moments that would be required to produce the simulated motion. A *static optimization* routine then resolves the net moments into individual muscle moments (muscle force times muscle moment arm) at each time step by minimizing the sum of squared muscle activations. This type of simulation can be used for a variety of purposes—for example, to compare simulated muscle activations with activations recorded in vivo and thereby validate a model, to more explicitly determine muscle function (which depends not only on muscle moment arms, but also on muscle activation and joint kinematics), or to determine whether the modeled muscles are strong enough to drive various behaviors. One disadvantage of static simulations is that they consider each time step independently, and cannot account for time-dependent physiological properties such as force-velocity relationships or activation-deactivation dynamics. At this point in time, OpenSim's static optimization routine also assumes that tendons are rigid, and thus does not account for the storage and release of elastic energy. These two limitations must be addressed for behaviors involving rapid limb movements, such as flapping or jumping (see Heers et al., 2018).

Dynamic Simulations: Unlike static simulations, dynamic simulations account for time-dependent properties but require extensive knowledge of muscle physiology and can be difficult to work with. One type of dynamic simulation is forward dynamics. When muscle activations are known (e.g., previously measured using electromyography), they can be used to predict what type of locomotor behavior would result, given the animal's musculoskeletal anatomy and the muscle activations. Forward dynamics can thus be used to validate a model (does the behavior I'm trying to model actually occur with the given inputs?), and to compare or predict how muscle anatomy and activation affect locomotion (does locomotor behavior/performance differ because muscle anatomy and/or activations differ?).

Together, musculoskeletal modeling and simulation provide a dynamic, three-dimensional, whole-body perspective on locomotion in living animals, by analyzing how the skeleton, muscles, and feathers (which produce external, i.e., aerodynamic, forces) all work together during locomotion. Once a modeling and simulation approach has been worked out, additional questions that would be impossible to answer working solely with live animals can be explored. For example, anatomical features (e.g., bony processes, joint morphology, muscle size), as well as kinematic (i.e., the wing stroke) and/or kinetic (i.e., aerodynamic force production) properties can be altered to assess their effects on locomotion or muscle performance. Musculoskeletal modeling and simulation thus allow for a more explicit examination of form-function relationships, by allowing anatomical, kinematic, kinetic, and/or physiological features to be individually adjusted and their effects on locomotion determined. Consequently, this approach is also one of the most quantitative methods for reconstructing locomotion in extinct animals.

For extinct animals, modeling and simulation procedures are similar but require more assumptions. These assumptions must be analyzed through sensitivity analyses and validated by comparison with models of living homologs or analogs (Hutchinson, 2011). For example, step 1 requires assumptions about the distribution of mass and about joint anatomy, because the soft-tissue components of joints are usually not preserved. For step 2, although the geometry of some muscles can be reconstructed based on muscle scars and phylogenetic bracketing, muscle size, architecture, and physiology must always be extrapolated based on knowledge of living counterparts. Joint kinematics (step 3) and external forces (step 4) must also be inferred, potentially by phylogenetic bracketing coupled with analyses of joint range of motion and body size scaling. For all such inferences, it is probably best to analyze a range of possible anatomical, kinematic, and kinetic inputs (i.e., conduct a sensitivity analysis), which results in a range of "answers" to questions but reflects the uncertainty in these types of analyses and can highlight results that are robust to modeling or simulation assumptions. Regardless of how many models or simulations are considered, the modeling and simulation procedure must be validated by comparison with similar models and simulations of living animals. Locomotor capabilities are known in living animals, and the degree to which a musculoskeletal model and simulation can mimic those capabilities indicates our level of confidence in the modeling and simulation of locomotion in extinct animals.

Musculoskeletal modeling and simulation have been used to study posture and locomotor capacity (i.e., running speed) of theropods such as *Tyrannosaurus rex* (Hutchinson et al., 2005), and efforts are currently underway to apply this approach to the evolution of avian flight (Heers and Carney, 2017). For example, by simulating a range of potential flapping kinematics in key taxa like *Archaeopteryx* and in earlier and later diverging forms, we can assess which behaviors were potentially possible at different evolutionary stages and examine how evolutionary changes in morphology might have facilitated the origins of bird flight.

In summary, when used in conjunction with studies on live animals, musculoskeletal modeling and simulation are extremely useful tools for exploring how different anatomical features (bones, muscles, feathers) work together during locomotion. In addition, this technique allows anatomical, kinematic, and/or kinetic properties to be systematically adjusted to explicitly examine form-function relationships in ways that cannot be done empirically. Once a modeling and simulation approach has been tested using an extant analog or homolog, similar procedures can be applied to fossils to assess locomotor potential. Uncertainties in the musculoskeletal anatomy, kinematics, and kinetics of extinct animals are accounted for by using multiple models and simulations, resulting in a range of "answers" but highlighting results that are robust to modeling or simulation assumptions. Because of this, musculoskeletal modeling and simulation is one of the most rigorous tools available for assessing locomotor potential in extinct animals, including theropods with feathered forelimbs.

DISCUSSION

The methods surveyed here have all had significant impact on our understanding of early theropod flight and have been validated. This includes the example of first-principles-based modeling for the ultimate origins of theropod flight, which aligns with recent results of extremely detailed, single-species simulation approaches by a coauthor (A.M.H.) (Heers et al., 2018). Such validation is welcome and underscores the complementary nature of these two methods. For example, while musculoskeletal modeling and simulations offer a vital dynamic, three-dimensional, whole-body perspective, first-principles-based modeling is readily scalable and applicable to large, comparative datasets allowing it to identify macroevolution patterns and trends more easily (e.g., in chapter 11 by Dececchi et al.). Such a "prospect and then mine" relationship between these two methods is synergistic and should be further developed and coordinated moving forward.

Estimating flight performance requires significant time to set up, particularly musculoskeletal modeling and simulation, but their analytical products (i.e., spreadsheet equations, aerodynamics software, 3D interactive computer models) can often be reasonably easily modified if subsequent analyses involve similar subjects. In the case of mechanically informed morphospace analysis, functional morphology of structures (e.g., deltopectoral crest of the humerus) or other estimated variables (e.g., wing span and wing surface) can be compared with a large dataset of modern birds. Based on physics principles, this comparison has provided relevant information on the flight performance of a few early-diverging birds (Liu et al 2017, 2019; Serrano and Chiappe 2017; Serrano et al 2018; Chiappe et al. 2019). In addition, this approach can be complemented and validated through the construction of aerodynamic models of early birds using, for example, the software Flight v. 1.24 developed for modern birds (www.bio.bristol.ac.uk/people/pennycuick.htm; Pennycuick, 2008), which reduces the time needed to set up new analyses. The publication of several landmark studies in recent years (Dececchi et al., 2016; Heers et al., 2016; Serrano and Chiappe, 2017; Serrano et al., 2017; Heers et al., 2018; Serrano et al., 2018; Pei et al., in press) therefore promises a potentially rapid expansion in flight-performance studies in the not too distant future.

All methods of flight-performance estimation require assumptions with many needing parameters obtained from living birds because they are simply unknown in fossil taxa, e.g., the power output of flight muscle. However, with thousands of fossil birds available, it is understandable that specimens that might provide direct estimates of certain parameters may be overlooked. The leading-edge wing shape of the early-diverging paravians *Anchiornis* and *Microraptor*—as revealed by LSF (Wang et al., 2017; co-author MP & TGK, unpublished data)—are good examples of otherwise unknown information that directly affects estimations. In this case this information improves our estimation of wing area, which has since been considered in subsequent studies (Pei et al., in press), including in chapter 11 of this volume. Also in this volume, Serrano, et al. (chapter 13) use the lateral body outline of the early diverging avialan *Sapeornis*—as observed under LSF—to directly estimate the body's disc surface generating drag during flight (S_b). This surface and the body drag coefficient—which is better estimated knowing S_b—are influential parameters in modeling flight dynamics. New analytical techniques like LSF offer improved characterization of feathering, mass distribution, joint geometries, and other key modeling parameters, particularly contentious ones like feather structure as related to rigidity in flight, thereby increasing the accuracy of our understanding of early theropod flight. However, at least a portion of the missing data is probably available from existing specimens even using standard microscopy methods, such is the bounty of fossil specimens currently available. For example, some fossil taxa like *Confuciusornis* and *Anchiornis* are known from large sample sizes that are yet to be fully examined (Wang et al., 2017; Navalón et al., 2018) and the rate of new taxon discovery remains high (see Pittman et al., chapter 2). While it is easy to take this advice as a need to ramp up the number of specimens studied, past work and that by Serrano et al. (chapter 13) show that even a handful of feathered well-preserved specimens can provide accurate estimates (Liu et al., 2017; Serrano and Chiappe, 2017; Serrano et al., 2018). First-principles-based modeling remains the most readily adaptable method for studying flight performance across the breadth of Pennaraptora, but as better fossil data help to minimize potential sources of error in key parameters in particular (i.e., body mass, wing space, and lift surface), this situation could change and potentially present an opportunity for consensus results across multiple methods in the future.

ACKNOWLEDGMENTS

We would like to thank the attendees of the International Pennaraptoran Dinosaur Symposium and our reviewers for their comments and suggestions, which helped to improve the quality of this manuscript. The symposium was held at the University of Hong Kong and was supported by Kenneth HC Fung and First Initiative Foundation. This study was also supported by the Research Grant Council of Hong Kong's General Research Fund (17103315 to M.P.) and the RAE Improvement Fund of the Faculty of Science, the University of Hong Kong (to M.P. and T.G.K.). The participation of D.J.F. was also supported by UK Research and Innovation Future Leaders Fellowship MR/S032177/1.

REFERENCES

Abel, R.L., C.R. Laurini, and M. Richter. 2012. A palaeobiologist's guide to 'virtual' micro-CT preparation. Palaeontologica Electronica 15: 6T.

Ahlborn, B.K. 2000. Thermodynamic limits of body dimension of warm blooded animals. Journal of Non-Equilibrium Thermodynamics 25: 87–102.

Alexander, R.M. 2003. Principles of animal locomotion, Princeton: Princeton University Press.

Allen, V., K.T. Bates, Z.H. Li, and J.R. Hutchinson. 2013. Linking the evolution of body shape and locomotor biomechanics in bird-line archosaurs. Nature 497: 104–107.

Askew, G.N., R.L. Marsh, and C.P. Ellington. 2001. The mechanicalpower output of the flight muscles of Blue-breasted Quail (*Coturnix chinensis*) during take-off. Journal of Experimental Biology 204: 3601–3619.

Baier, D.B., S.M. Gatesy, and F.A. Jenkins. 2007. A critical ligamentous mechanism in the evolution of avian flight. Nature 445: 307–310.

Berv, J.S., and D.J. Field. 2018. Genomic Signature of an Avian Lilliput Effect across the K-Pg Extinction. Systematic Biology 67: 1–13.

Brocklehurst, N., P. Upchurch, P.D. Mannion, and J.M. O'Connor. 2012. The completeness of the fossil record of Mesozoic birds: implications for early avian evolution. PLoS One 7: e39056.

Brown, G.E., Jr., and G.A. Waychunas. 2004. X-ray absorption spectroscopy: introduction to experimental procedures. Stanford University, accessed 18/04/2018.

Brown, J.H. 1995. Macroecology, Chicago: University of Chicago Press.

Buchwald, R., and R. Dudley. 2010. Limits to vertical force and power production in bumblebees (Hymenoptera: *Bombus impatiens*). Journal of experimental Biology 213: 426–432.

Burgers, P., and L.M. Chiappe. 1999. The wing of *Archaeopteryx* as a primary thrust generator. Nature 399: 60–62.

Campione, N.E., and D.C. Evans. 2012. A universal scaling relationship between body mass and proximal limb bone dimensions in quadrupedal terrestrial tetrapods. BMC Biology 10.

Cau, A., et al. 2017. Synchrotron scanning reveals amphibious ecomorphology in a new clade of bird-like dinosaurs. Nature 552: 395–399.

Chiappe, L.M., et al. 2014. A new specimen of the Early Cretaceous bird *Hongshanornis longicresta*: insights into the aerodynamics and diet of a basal ornithuromorph. PeerJ 2: e234.

Chiappe, L.M., et al. 2019. New *Bohaiornis*-like bird from the Early Cretaceous of China: enantiornithine interrelationships and flight performance. PeerJ 7: e7846.

Close, R.A., and E.J. Rayfield. 2012. Functional morphometric analysis of the furcula in mesozoic birds. PLoS One 7(5): e36664.

Dececchi, T.A., H.C.E. Larsson, and M.B. Habib. 2016. The wings before the bird: an evaluation of flapping-based locomotory hypotheses in bird antecedents. PeerJ 4: e2159.

Delp, S.L., et al. 2007. OpenSim: open-source software to create and analyze dynamic simulations of movement. IEEE Transactions on Biomedical Engineering 54: 1940–1950.

Dial, T.R., A.M. Heers, and B.W. Tobalske. 2012. Ontogeny of aerodynamics in mallards: comparative performance and developmental implications. The Journal of Experimental Biology 215: 3693–3702.

Dyke, G., et al. 2013. Aerodynamic performance of the feathered dinosaur *Microraptor* and the evolution of feathered flight. Nature Communications 4: 2489.

Eklund, M.J., A.K. Aase, and C.J. Bell. 2018. Progressive photonics: methods and applications of sequential imaging using visible and non-visible spectra to enhance data-yield and facilitate forensic interpretation of fossils. Journal of Paleontological Techniques 20: 1–36.

Falk, A.R., T.G. Kaye, Z.H. Zhou, and D.A. Burnham. 2016. Laser fluorescence illuminates the soft tissue and life habits of the Early Cretaceous bird *Confuciusornis*. PLoS One 11: e0167284.

Feduccia, A., and H.B. Tordoff. 1979. Feathers of *Archaeopteryx*: asymmetric vanes indicate aerodynamic function. Science 203: 1021–1022.

Feo, T.J., D.J. Field, and R.O. Prum. 2015. Barb geometry of asymmetrical feathers reveals a transitional morphology in the evolution of avian flight. Proceedings of the Royal Society B 282: 20142864.

Field, D.J. 2017. Preliminary paleoecological insights from the Pliocene avifauna of Kanapoi, Kenya: implications for the ecology of *Australopithecus anamensis*. Journal of Human Evolution: in press.

Field, D.J., C. Lynner, C. Brown, and S.A. Darroch. 2013. Skeletal correlates for body mass estimation in modern and fossil flying birds. PLoS One 8: e82000.

Foth, C., H. Tischlinger, and O.W.M. Rauhut. 2014. New specimen of *Archaeopteryx* provides insights into the evolution of pennaceous feathers. Nature 511: 79–82.

Gatesy, S.M. 2001. The evolutionary history of the theropod caudal locomotor module. *In* Gauthier, J., and J.F. Gall (editors), New perspectives on the origin and early evolution of birds: 333–350. New Haven: Peabody Museum of Natural History, Yale University.

Gatesy, S.M., and K.P. Dial. 1996. From frond to fan: *Archaeopteryx* and the evolution of short-tailed birds. Evolution 50: 2037–2048.

George, J.C., and A.J. Berger. 1966. Avian myology, New York: Academic Press.

Gill, F., and D. Donsker (editors). 2017. IOC World Bird List (v 7.3).

Gillooly, J.F., J.H. Brown, G.B. West, V.M. Savage, and E.L. Charnov. 2001. Effects of size and temperature on metabolic rate. Science 293: 2248–2251.

Gillooly, J.F., E.L. Charnov, G.B. West, V.M. Savage, and J.H. Brown. 2002. Effects of size and temperature on developmental time. Nature 417: 70–73.

Greenewalt, C.H. 1975. The flight of birds: the significant dimensions, their departure from the requirements for dimensional similarity, and the effect on flight aerodynamics of that departure. Transactions of the American Philosophical Society 65: 1–67.

Guillemette, M., and J.F. Ouellet. 2005. Temporary flightlessness in pre-laying Common Eiders *Somateria mollissima*: are females constrained by excessive wing-loading or by minimal flight muscle ratio? Ibis 147: 293–300.

Hartman, F.A. 1961. Locomotor mechanisms of birds. Smithsonian Miscellaneous Collections 143: 1–91.

Heers, A.M., and R.M. Carney. 2017. Building a bird: a musculoskeletal model of the *Archaeopteryx* flight apparatus. Journal of Vertebrate Paleontology Programs and Abstracts 127.

Heers, A.M., and K.P. Dial. 2012. From extant to extinct: locomotor ontogeny and the evolution of avian flight. Trends in Ecology & Evolution 27: 296–305.

Heers, A.M., B. Tobalske, and K.P. Dial. 2011. Ontogeny of lift and drag production in ground birds. The Journal of Experimental Biology 214: 717–725.

Heers, A.M., D.B. Baier, B.E. Jackson, and K.P. Dial. 2016. Flapping before flight: high resolution, three-dimensional skeletal kinematics of wings and legs during avian development. PLoS One 11: e0153446.

Heers, A.M., J.W. Rankin, and J.R. Hutchinson. 2018. Building a bird: musculoskeletal modeling and simulation of wing-assisted incline running during avian ontogeny. Frontiers in Bioengineering and Biotechnology 6: 140.

Hone, D.W.E., H. Tischlinger, X. Xu, and F.C. Zhang. 2010. The extent of the preserved feathers on the four-winged dinosaur *Microraptor gui* under ultraviolet light. PLoS One 5: e9223.

Hutchinson, J.R. 2011. On the inference of function from structure using biomechanical modelling and simulation of extinct organisms. Biological Letters 8: rsbl.2011.0399.

Hutchinson, J.R., F.C. Anderson, S.S. Blemker, and S.L. Delp. 2005. Analysis of hindlimb muscle moment arms in *Tyrannosaurus rex* using a three-dimensional musculoskeletal computer model: implications for stance, gait, and speed. Paleobiology 31: 676–701.

Jenkins, F.A., Jr. 1993. The evolution of the avian shoulder joint. American Journal of Science 293A: 253–267.

Kaye, T.G., et al. 2015. Laser-stimulated fluorescence in paleontology. PLoS One 10: e0125923.

Kaye, T.G. et al. 2019. Detection of lost calamus challenges identity of isolated *Archaeopteryx* feather. Scientific Reports 9: 1182.

Lefèvre, U., A. Cau, D.Y. Hu, and P. Godefroit. 2020. Feather evolution in Pennaraptora. *In* C. Foth and O.W.M. Rauhut (editors), The evolution of feathers: 67-78. Cham, Switzerland: Springer.

Lentink, D., A.F. Haselsteiner, and R. Ingersoll. 2015. In vivo recording of aerodynamic force with an aerodynamic force platform: from drones to birds. Journal of the Royal Society Interface 12 (104): rsif.2014.1283.

Liu, D., et al. 2017. Flight aerodynamics in enantiornithines: information from a new Chinese Early Cretaceous bird. PLoS One 12: e0184637.

Liu, D., et al. 2019. Soft tissue preservation in two new enantiornithine specimens (Aves) from the Lower Cretaceous Huajiying Formation of Hebei Province, China. Cretaceous Research 95: 191-207.

Livezey, B.C. 1992. Flightlessness in the Galápagos cormorant (*Compsohalieus* [*Nannopterum*] *harrisi*): heterochrony, giantism and specialization. Zoological Journal of the Linnean Society 105: 155–224.

Longrich, N.R., T. Tokaryk, and D.J. Field. 2011. Mass extinction of birds at the Cretaceous–Paleogene (K–Pg) boundary. Proceedings of the National Academy of Sciences of the United States of America 108: 15253–15257.

Louchart, A., et al. 2009. Taphonomic, avian, and small-vertebrate indicators of *Ardipithecus ramidus* habitat. Science 326: 66-66e64.

Manal, K., and T.S. Buchanan. 2004. Subject-specific estimates of tendon slack length: a numerical method. Journal of Applied Biomechanics 20: 195–203.

Marden, J.H. 1987. Maximum lift production during takeoff in flying animals. Journal of Experimental Biology 130: 235–258.

Marden, J.H. 1994. From damselflies to pterosaurs: how burst and sustainable flight performance scale with size. American Journal of Physiology-Regulatory Integrative and Comparative Physiology 35: R1077–R1084.

Meseguer, J., and A. Sanz-Andres. 2007. Aerodinamica del vuelo: Aves y Aeronaves. Madrid: Aeropuertos Españoles y Navegacion Aerea.

Meunier, K. 1951. Korrelation und umkonstruktion in den grössenbeziehungen zwischen vogelflügel und vogelkörper (Correlation and restructuring in the size relationship between avian wing and avian body). Biologia Generalis 19: 403–443.

Navalón, G., J. Marugán-Lobón, L.M. Chiappe, J.L. Sanz, and Á.D. Buscalioni. 2015. Soft-tissue and dermal arrangement in the wing of an Early Cretaceous bird: Implications for the evolution of avian flight. Scientific Reports 5: 14864.

Navalón, G., et al. 2018. Diversity and evolution of Confuciusornithidae: evidence from a new 131-million-year-old specimen from the Huajiying Formation in NE China. Journal of Asian Earth Sciences 152: 12–22.

Norberg, U.M. 2002. Structure, form, and function of flight in engineering and the living world. Journal of Morphology 252: 52–81.

Nudds, R.L., and G.J. Dyke. 2010. Narrow primary feather rachises in *Confuciusornis* and *Archaeopteryx* suggest poor flight ability. Science 328: 886–889.

O'Neill, M.C., et al. 2013. A three-dimensional musculoskeletal model of the chimpanzee (*Pan troglodytes*) pelvis and hind limb. Journal of Experimental Biology 216: 3709–3723.

Otero, A., V. Allen, D. Pol, and J.R. Hutchinson. 2017. Forelimb muscle and joint actions in Archosauria: insights from *Crocodylus johnstoni* (Pseudosuchia) and *Mussaurus patagonicus* (Sauropodomorpha). PeerJ 5: e3976.

Pei, R., et al. In press. Potential for powered flight neared by most close avialan relatives but few crossed its thresholds. Current Biology.

Pennycuick, C.J. 2008. Modelling the flying bird, London: Academic Press.

Pittman, M., S.M. Gatesy, P. Upchurch, A. Goswami, and J.R. Hutchinson. 2013. Shake a tail feather: the evolution of the theropod tail into a stiff aerodynamic surface. PLoS One 8: e63115.

Pollock, C.M., and R.E. Shadwick. 1994. Relationship between body mass and biomechanical properties of limb tendons in adult mammals. American Journal of Physiology-Regulatory, Integrative and Comparative Physiology 266: R1016–R1021.

Poore, S.O., A. Ashcroft, A. Sánchez-Haiman, and G.E. Goslow. 1997a. The contractile properties of the M. supracoracoideus in the pigeon and starling: a case for long-axis rotation of the humerus. Journal of Experimental Biology 200: 2987–3002.

Poore, S.O., A. Sánchez-Haiman, and G.E. Goslow Jr. 1997b. Wing upstroke and the evolution of flapping flight. Nature 387: 799–802.

Prum, R.O., et al. 2015. A comprehensive phylogeny of birds (Aves) using targeted next-generation DNA sequencing. Nature 526: 569–573.

Rauhut, O.W.M., C. Foth, and H. Tischlinger. 2018. The oldest *Archaeopteryx* (Theropoda: Avialiae): a new specimen from the Kimmeridgian/Tithonian boundary of Schamhaupten, Bavaria. PeerJ 6: e4191.

Rayner, J.M. 1988. The evolution of vertebrate flight. Biological Journal of the Linnean Society 34: 269–287.

Rayner, J.M. 1993. On aerodynamics and the energetics of vertebrate flapping flight. Contemporary mathematics 141: 351–400.

Rosset, A., L. Spadola, and O. Ratib. 2004. OsiriX: an open-source software for navigating in multidimensional DICOM images. Journal of Digital Imaging 17: 205–216.

Rowe, T., et al. 2001. Forensic palaeontology: the *Archaeoraptor* forgery. Nature 410(6828): 539–540.

Schilling, R., B. Jastram, O. Wings, D. Schwarz-Wings, and A.S. Issever. 2014. Reviving the dinosaur: virtual reconstruction and three-dimensional printing of a dinosaur vertebra. Radiology 270: 864–871.

Schmidt-Nielsen, K. 1984. Scaling: why is animal size so important? Cambridge: Cambridge University Press.

Serrano, F.J., and L.M. Chiappe. 2017. Aerodynamic modelling of a Cretaceous bird reveals thermal soaring during avian evolution. Journal of the Royal Society Interface 14: 20170182.

Serrano, F.J., P. Palmqvist, and J.L. Sanz. 2015. Multivariate analysis of neognath skeletal measurements: implications for bodymass estimation in Mesozoic birds. Zoological Journal of the Linnean Society 173: 929–955.

Serrano, F.J., P. Palmqvist, L.M. Chiappe, and J.L. Sanz. 2017. Inferring flight parameters of Mesozoic avians through multivariate analyses of forelimb elements in their living relatives. Palaeobiology 43: 144–169.

Serrano, F.J., et al. 2018. Flight reconstruction of two European enantiornithines (Aves, Pygostylia) and the achievement of bounding flight in Early Cretaceous birds. Palaeontology 61: 359–368.

Shyy, W., Y.S. Lian, J. Tang, D. Viieru, and H. Liu. 2008. Aerodynamics of low Reynolds number flyers. Cambridge: Cambridge University Press.

Smith, N.D. 2012. Body mass and foraging ecology predict evolutionary patterns of skeletal pneumaticity in the diverse "waterbird" clade. Evolution 66: 1059–1078.

Swaddle, J.P., and R. Lockwood. 2003. Wingtip shape and flight performance in the European Starling *Sturnus vulgaris*. Ibis 145: 457–464.

Tennekes, H. 2009. The simple science of flight: from insects to jumbo jets, Cambridge: MIT Press.

Tischlinger, H., and D. Unwin. 2004. UV-Untersuchungen des Berliner Exemplars von *Archaeopteryx lithographica* H. v. Meyer 1861 und der isolierten *Archaeopteryx*-Feder. *Archaeopteryx* 22: 17–50.

Tobalske, B.W., and A.A. Biewener. 2008. Contractile properties of the pigeon supracoracoideus during different modes of flight. Journal of Experimental Biology 211: 170–179.

Tobalske, B.W., and K.P. Dial. 2007. Aerodynamics of wing-assisted incline running in birds. Journal of Experimental Biology 210: 1742–1751.

van Oorschot, K.B., H.K. Tang, and B.W. Tobalske. 2017. Phylogenetics and ecomorphology of emarginate primary feathers. Journal of Morphology 278: 936–947.

Videler, J.J. 2005. Avian flight. Oxford: Oxford University Press.

Von Mises, R. 1945. Theory of flight. *In* 672. New York: Dover Publications.

Wang, X.L., et al. 2017. Basal paravian functional anatomy illuminated by high-detail body outline. Nature Communications 8: 14576.

Wellnhofer, P. 2009. *Archaeopteryx* – the icon of evolution, München: Verlag Dr. Friedrich Pfeil.

Xu, X. 2020. Filamentous integuments in nonavialan theropods and their kin: advances and future perspectives for understanding the evolution of feathers. *In* C. Foth and O.W.M. Rauhut (editors), The evolution of feathers: 67–78. Cham, Switzerland: Springer.

Xu, X., et al. 2003. Four-winged dinosaurs from China. Nature 421: 335–340

Xu, X., et al. 2015. A bizarre Jurassic maniraptoran theropod with preserved evidence of membranous wings. Nature 521: 70–73.

Zajac, F.E. 1989. Muscle and tendon: properties, models, scaling, and application to biomechanics and motor control. Critical Reviews in Biomedical Engineering 17: 359–411.

Zheng, X.T., et al. 2014. On the absence of sternal elements in *Anchiornis* (Paraves) and *Sapeornis* (Aves) and the complex early evolution of the avian sternum. Proceedings of the National Academy of Sciences of the United States of America111: 13900–13905.

Zhou, Z.H., and F.C. Zhang. 2002. A long-tailed, seed-eating bird from the Early Cretaceous of China. Nature 418: 405–409.

Chapter 11

High Flyer or High Fashion? A Comparison of Flight Potential among Small-Bodied Paravians

T. ALEXANDER DECECCHI,[1] HANS C.E. LARSSON,[2] MICHAEL PITTMAN,[3]
AND MICHAEL B. HABIB[4]

ABSTRACT

The origin of flight in birds and its relationship to bird origins itself has achieved something of a renaissance in recent years, driven by the discovery of a suite of small-bodied taxa with large pennaceous feathers. As some of these specimens date back to the Middle Jurassic and predate the earliest known birds, understanding how these potential aerofoil surfaces were used is of great importance to answering the question: which came first, the bird or the wing? Here we seek to address this question by directly comparing key members of three of the major clades of paravians: anchiornithines, *Microraptor* and *Archaeopteryx* across their known size classes to see how they differ in terms of major flight-related parameters (wing loading; disc loading; specific lift; glide speed; takeoff potential). Using specimens with snout to vent length (SVL) ranging from around 150 mm to 400 mm and mass ranging from approximately 130 g to 2 kg, we investigated patterns of inter- and intraspecific changes in flight potential. We find that anchiornithines show much higher wing- and disc-loading values and correspondingly high required minimum glide and takeoff speeds, along with lower specific lift and flapping running outputs suggesting little to no flight capability in this clade. In contrast, we see good support for flight potential, either gliding or powered flight, for all size classes of both *Microraptor* and *Archaeopteryx*, though there are differing patterns of how this shifts ontogenetically. These findings, coupled with previous findings of a lack of wing-based locomotion in early-diverging troodontids or dromaeosaurids, suggest that flight was not a synapomorphy of Paraves. This supports the contention that flight capacity and potentially powered flight itself arose convergently in at least two distinct paravian lineages, first in birds minimally 150 million years ago, then in the microraptorines 20–30 million years later. Our work indicates that the origin of flight among paravians was likely a more complex phenomenon than previously appreciated.

---

[1] Division of Natural Sciences, Mount Marty College, Yankton, SD.

[2] Redpath Museum, McGill University, Montreal.

[3] Vertebrate Palaeontology Laboratory, Division of Earth and Planetary Science, the University of Hong Kong, Hong Kong.

[4] Dinosaur Institute, Natural History Museum of Los Angeles County, Los Angeles.

INTRODUCTION

The origin of birds and the related, but not necessarily synchronous origin of powered theropod flight is an area of intense research (Agnolín and Novas, 2013; Brusatte et al., 2014, 2015; Lee et al., 2014; Puttick et al., 2014; Xu et al., 2014; Dececchi et al., 2016; Agnolín et al., 2019), including high-resolution phylogenetic analysis to identify the interrelationships among paravian clades (Brusatte et al., 2014; Cau et al., 2017; Xu et al., 2017; Cau, 2018; Hu et al., 2018; Pei et al., in press; see also Pittman et al., chapter 2). The pathway from nonavialan theropods to birds has recently undergone a renaissance, including a greater understanding of the nonlinear nature of trait acquisition and the lack of a clear demarcation between "birds" and "nonavialan dinosaurs" (Makovicky and Zanno, 2011; Godefroit et al., 2013; Brusatte et al., 2014; Cau, 2018; Hu et al., 2018; Pei et al., in press). What was once seen as a clear path is now understood to be a complicated series of lineage-specific specializations and convergences that makes the distillation of a single well-resolved topology difficult. This goal has been further complicated by the fact that flight—one of modern birds' most quintessential and identifiable traits, long linked to their origins (Martin, 1983; Feduccia, 1996; Feduccia and Czerkas, 2015)—has recently been proposed to have more ancient beginnings (Xu et al., 2003, 2011, 2014; Han et al., 2014; Dececchi et al., 2016; Pei et al., in press). In that context, our work attempts to test whether the "four winged" bauplan seen in multiple paravian clades and linked to either powered or gliding flight (Xu et al., 2003, 2011; Zheng et al., 2013) is important in untangling a significant thread in this debate.

Recent finds document a suite of small-bodied taxa from suspected paravian lineages (Dromaeosauridae, Troodontidae, Avialae, and Anchiornithinae, the last one seen as birds by some and as troodontids or deinonychosaurians by others; see Pittman et al., chapter 2) with large pennaceous, often asymmetrical veined feathers on their fore- and hind limbs (Zheng et al., 2013; Xu et al., 2017; Hu et al., 2018). As some of these specimens date to the Middle Jurassic and predate the earliest known birds (Brusatte et al., 2015; Hu et al., 2018), understanding how they used these potential airfoil surfaces and what the limits to their flight capacity were (i.e., powered flight vs. gliding) is critical to establishing the ancestral condition for later avialans, determining the palaeoecology of the Middle Mesozoic period, and reconstructing the ecological niche space available to small nonavialan theropods across the origins of birds. Here we directly compare members of three of these lineages (Anchiornithinae, microraptorine dromaeosaurids, and the earliest well-accepted avialan, *Archaeopteryx*) to see how they differ in terms of major flight-related parameters and aerodynamic reconstructions. As feathered limbs become more widely recognized as the default of the various paravian clades and not a specialized feature, we need to move beyond the idea that "feathers make a wing" and understand how multiple parameters (wing size, feather structure, power output, input velocity, flapping angle and speed) interact to achieve volancy. Using multiple lines of evidence, we evaluate flight potential in both a strictly comparative, relative sense and against known physical benchmarks in the lineages bracketing the origin of birds. This knowledge will help us more accurately understand the evolution and ecological dynamics at play within small paravian theropods during the mid to late Mesozoic and begin to grapple with the question "What does it take to fly?"

METHODS

While there is still some uncertainty in the topology of the theropod tree nearest the origin of birds, especially placement of the anchiornithines, the scansoriopterygids, and what the sister group of Avialae is (Agnolín and Novas, 2013; Brusatte et al., 2014; Xu et al., 2014; Lefèvre et al., 2017; Xu et al., 2017; Cau, 2018; but see Pei et al., in press), there is little debate that birds emerged from a generalized, small-bodied paravian ancestor. With that in mind, we selected taxa whose phylogenetic placement

TABLE 1

Linear limb measurements for fossil paravian specimens

For individuals without published measurements of primary feather length, values were obtained in one of several ways: directly from images (BMNHC PH881, BMNHC PH804), from published wing length measurements (LVH 0026, *Archaeopteryx* specimens) or extrapolated from closely related taxa (CAGS 20-7-004, QV1002, V 12330, YFGP-T5197, YFGP-T5198, PKUP V1068). The value given in the original paper is inconsistent with other measures and other *Microraptor* specimens. As such we have included a second SVL based on our own measurements from the original images that are more consistent with relative and absolute values measured for the limb and tail regions as well as other *Microraptor* specimens. All measurements in mm. Abbreviations: **Fe**, femur; **Fore**, forelimb (H+ U+ Mc); **H**, humerus; **Hind**, hind limb (fe + Ti + Mt); **Mc**, metacarpal III; **Mt**, metatarsus; **Primary**, longest primary feather; **SVL**, snout to vent; **Ti**, tibia, **U**, ulna. LVH 0026 has two values in the SVL column. See text for details.

Taxon	Specimen number	SVL	H	U	MC	Primary	Fore	Wing	Fe	Ti	Mt	Hind
Microraptor gui	BMNHC PH881	153	47.4	44.7	31.8	140*	124	264	52.1	72.9	38.5	163.5
M. gui	IVPP V13320	215	57	53	31	186^	141	327	64	74	47	185
M. gui	IVPP V13352	297	83	70.3	45	222^	198	420	97	124.4	70.1	291.5
M. gui	QV1002	327	94.9	76.2	51.3	250#	222	472	108.9	143.6	75	327.5
M.zhaoniaus	CAGS 20-7-004	240	61.3	53.8	31.37	181#	146	327	74.8	94.2	47.76	216.8
M.zhaoniaus	IVPP V12330	145	42	37	22.3	113#	101	214	49.8	66	35.3	151.1
M.hanqingi	LVH 0026	405/360	93.5	81.9	54.9	255	230	485	111.7	137.1	75.4	324.2
Anchiornis	BMNHC PH804	185	45.7	39.8	23	50	109	159	50.9	69.1	41	161
Anchiornis	LPM-B00169	247	69	55	34	100	158	258	66.2	106.4	55.2	227.8
Anchiornis	PKUP V1068	275	72.2	59	32.1	110	163	273.3	90.5	117.7	56.4	264.6
Eosinopteryx	YFGP-T5197	166	37.9	42	21	57	101	157.8	48.5	69.5	35.5	153.5
Aurornis	YFGP-T5198	246	58	57	34	87	149	236	66.2	90.5	44	200.7
Caihong	PMoL-B00175	259	42.1	47.2	23.7	97	113	210	70.9	82.8	49	202.7
Serikornis	PMoL-AB00200	230	60.7	50.8	32	91	144	235	67.4	95.2	48.5	211.1
Xiaotingia	YFGP-T5198	295	71	65	24	107	160	267	84	-	-	-
Archaeopteryx	Eichstätt	154	41.5	36.5	17.8	-	96	191	37	52.5	30.2	119.7
Archaeopteryx	Berlin	231	63	56.2	24.8	172	144	316	52.2	68.5	37	157.7
Archaeopteryx	Solnhofen	300	83	72	34.3	-	189	375	67	92	47.5	206.5

bracket our current "best estimate" as to the origin of birds (Pei et al., in press) and that exemplify the paravian bauplan. We chose only well-represented and documented specimens, focusing on taxa with elongated pennaceous feathered limbs and with an estimated body mass less than 2 kg, using femur length (Christiansen and Farina, 2004), circumference (Campione et al., 2014), or published values based on 3-D or multivariate models (Chatterjee and Templin, 2007; Alexander et al., 2010; Dyke et al., 2013; Serrano et al., 2017). Based on these criteria, our analysis is centered on the Anchiornithinae, *Microraptor* species complex (though there is some debate as to the interrelationships of small microraptorines: O'Connor et al., 2011), and members of the Archaeopterygidae (table 1), which have all been proposed to have aerial abilities. We did not include early-diverging troodontids as previous work has shown that similar-sized troodontids had little capability for aerodynamic force production, including for nonflight-related locomotion methods such as wing-assisted incline running (WAIR)

TABLE 2

Mass estimates for fossil paravian specimens

Based on either femur length from Christiansen and Farina (2004), femoral circumference based on Campione et al. (2014) or published reconstructions (Yalden, 1984; Chatterjee and Templin, 2007; Erickson et al., 2009; Alexander et al., 2010; Dyke et al., 2013; Serrano et al., 2017). Mass in kg. Abbreviations: **Fl,** mass derived from femoral length estimate; **Fc,** mass derived from femoral circumference estimate; **3D,** mass based on published models.

Taxon	Specimen number	Mass Fl	Mass Fc	Mass 3D
Microraptor gui	BMNHC PH881	0.24	0.18	-
M. gui	IVPP V13320	0.34	0.41	-
M. gui	IVPP V13352	1.30	0.88	0.95/ 0.50
M. gui	QV1002	1.88	1.25	-
M. zhaoianus	CAGS 20-7-004	0.57	0.35	-
M. zhaoianus	IVPP V12330	0.15	0.13	-
M. hanqingi	LVH 0026	2.05	-	1.23
Anchiornis	BMNHC PH804	0.16	0.19	-
Anchiornis	LPM-B00169	0.38	0.59	-
Anchiornis	PKUP V1068	1.04	0.61	-
Eosinopteryx	YFGP-T5197	0.14	0.36	-
Aurornis	YFGP-T5198	0.38	0.52	-
Caihong	PMoL-B00175	0.47	0.3	-
Serikornis	PMoL-AB00200	0.4	0.33	-
Xiaotingia	STM 27-2	0.82	0.86	-
Archaeopteryx	Eichstätt	-	-	0.18
Archaeopteryx	Berlin	-	-	0.25/0.34
Archaeopteryx	Solnhofen	-	-	1.09/ 0.68

or flap running (Dececchi et al., 2016), and had key aerodynamic metrics that were beyond the limits seen in extant and extinct flying animals, e.g., wing loading beyond the upper limit (Pei et al., in press). Scansoriopterygids were also excluded despite *Yi* and *Ambopteryx* being proposed as volant. This is because the wings of these taxa are believed to be patagium based rather than feather based and are thus structurally and functionally different from the wing bauplan of the earliest birds (Xu et al., 2015). We have kept species-level differentiation of the genus *Microraptor* (*M. zhaoianus, M. gui* and the controversial *M. hanqingi*) as well as generic differentiation of the "Yanliao" anchiornithines in accordance with Pei et al. (in press), despite recent work questioning the validity of some of these taxa (Turner et al., 2012; Pei et al., 2017). Measurements were taken from the literature and from personal observations and communications. Element measurements not recorded in the literature or from undescribed specimens were taken from images using Inkscape software. We prioritized our own measurements when we were able to take them and found that they were within 2% of those reported in the literature. Some measurements were given through personal communications. For the details of measurement sources, see table 2.

As body size is a major determinant of behavioral ability (Dial et al., 2000), we chose to subdivide our specimens into three size classes based on snout to vent length (SVL) and reconstructed mass (table 2). For *Microraptor hanqingi*, we included a recalculated SVL based on images of the specimens as the given value (415 mm) is 125% of the length of the similar-sized QV1002 (femoral length difference of 2.5%) is inconsistent with our measurements, both of this region and other regions of the specimen and suggests a significantly higher SVL to trunk ratio than other *Microraptor* specimens. This allowed us to compare morphometric changes with allometry both intra- and interspecifically, but also to see how they differ in terms of major flight-related linear morphometric parameters and aerodynamic reconstructions. We estimated body mass using femur length (Christiansen and Farina, 2004), femoral circumference (Campione et al., 2014), or published values based on 3-D or multivariate models (Chatterjee and Templin, 2007; Alexander et al., 2010; Dyke et al., 2013; Serrano et al., 2017; see table 2). This allowed us to bracket our estimates of flight capacity across a reasonable range of values for these key specimens. Wing length was reconstructed as the length of the longest primary added to the forelimb length (humerus + ulna + major metacarpal) with wingspan taken as 2.1× the length of a single wing, following the methodology of Dececchi et al. (2016). Wing area, unless otherwise indicated, was reconstructed using a modification of the equation in Dececchi et al. (2016), which takes the chord as only 55% of the longest primary feather length as corresponding to the difference between primary and secondary feather lengths in *Microraptor* (Li et al., 2012) and produces estimates within 2% of previous published values (see Pei et al., in press, for more details).

In reconstructing our criteria for flight ability we chose to use several metrics and methodologies to produce a more complete picture of the behavioral possibilities for the taxa in question. Wing loading denotes the mass supported by the lifting surfaces of an organism and has been shown previously to be less than 245 Nm^{-2} in flying vertebrates (Meunier, 1951). This upper maximum is thought to be a strong marker: when extant birds temporally exceed this, as during egg production, there is a corresponding loss in flight capacity (Guillemette and Ouellet, 2005). Similarly, a value below this is not enough to signal flight, as prefledging birds demonstrate (Austin and Ricklefs, 1977; Wright et al., 2006; Jackson et al., 2009; Sprague and Breuner, 2010). Nonpowered gliding taxa often have significantly lower values, commonly less than 100 Nm^{-2} (Socha et al., 2015). Higher values below this upper limit are not a direct indicator of poor flight capacity per se, but they do suggest reduced performance and maneuverability as they are often associated with higher required velocities to maintain sufficient lift (Dial et al., 2000; McGuire and Dudley, 2005, 2011; Stein et al., 2008). In addition, by including the related value of wing-disc loading, calculated as the circular area swept out by the wingspan, we have another commonly used measure that has been linked to energy expenditure, flight efficiency, and drag reduction in modern birds (Pennycuick, 1975, 1989).

Specific lift is a measure of the amount of lift generated per unit of body weight by an organism, and the vertical component of specific lift must be at least 9.8 Nkg^{-1} to overcome gravity (Marden, 1987, 1994), assuming negligible contributions from drag (which we consider to be a reasonable assumption for early birds and microraptorines). To calculate specific lift requires estimates of both muscle mass and power output, which are currently unknown in the taxa examined here. We assigned a flight muscle mass value of 10% of total body mass to our specimens rather than varying it because there is little knowledge on how this varied ontogenetically and among paravian species. This value is among the lowest known for competent living flyers (Greenewalt, 1975). Our reconstruction of flight muscle mass includes all muscles contributing to flight, not just the pectoralis musculature but muscles of the wing and back that were recruited prior to the evolution of the triosseal canal and ligamentous pulley system seen in late-diverging avialans (Baier et al., 2007). This value, while lower than seen in modern birds (Marden, 1987), is at the lower end of the range reconstructed in recent 3-D modeling of *Microraptor* and *Archaeopteryx* (Allen et al., 2013; Heers et al., 2016). As such, we ran a second permutation using a higher value of 13% that more closely corresponds to the values seen in those analyses, facilitating more direct comparisons with them. For power output we adopted a range of values (225, 250, and 287 $\mathrm{WKg^{-1}}$) corresponding to those seen in extant birds during takeoff, especially in short burst fliers (Askew et al., 2001; Guillemette and Ouellet, 2005). This allows us to examine how power output requirements would have had to vary across taxa and size classes if we assume a constant ability to achieve takeoff.

Powered versus Nonpowered Flight Potential

Beyond comparisons of simple linear metrics and ratios or empirically derived maximal and minimal thresholds to determine whether a taxon was theoretically capable of powered takeoff, we set out to examine performance across the specimens examined here under both a nonpowered (gliding) and a powered flight scenario (assuming it was possible). We chose to include both scenarios as they have been regularly proposed in the literature (Feduccia, 1996; Brusatte et al., 2014, 2015; Heers et al., 2014; Xu et al., 2014; Cau, 2018) and permit the possibility of arboreal and terrestrial launch sites, given ongoing debate into the ecology of theropod flight origins (Dececchi and Larsson, 2011; Dyke et al., 2013). For gliding flight, we chose two metrics as proxies for performance: minimum glide speed and minimum turning radius (see Longrich, 2006, for a more in-depth discussion). For both of these metrics we chose coefficient of lift (CL) values of 1 and 1.5, which correspond to the upper and lower range of values seen in extant avian flight and flapping-based locomotion (Longrich, 2006; Tobalske and Dial, 2007; Usherwood, 2009; Heers et al., 2011). For turn radius we chose a constant bank of 60° following Longrich (2006). As some previous reconstructions have suggested that feathered paravian hind limbs may have had a role in gliding flight (Chatterjee and Templin, 2007; Alexander et al., 2010; Koehl et al., 2011; Dyke et al., 2013), we ran permutations with and without factoring in the hind limbs. For this we ran our specimens at an abduction angle of 45° from the vertical plane, which was probably beyond their possible range (Brougham and Brusatte, 2010; Manafzadeh and Padian, 2018). However, this mimics the "sprawled" leg position that has been previously modeled (Longrich, 2006; Alexander et al., 2010; Koehl et al., 2011; Dyke et al., 2013), permitting more direct comparisons with those studies. As there is little data on the area of the "hind wings" and as most specimens show incomplete preservation in this region we chose to model the areas based on scaling from previously published reconstructions (Longrich, 2006; Chatterjee and Templin, 2007; Dyke et al., 2013). For anchiornithines, for which there were no previous estimates, we chose to bracket our reconstructions using the forewing to hind-wing area ratio with values for *Microraptor* (around 50% of forewing area: Chatterjee and Templin, 2007; Dyke et al., 2013) as an upper bounds and *Archaeopteryx* (20% of forewing: Longrich, 2006) as the lower bound since this taxon lacks elongate feathers on the metatarsals (Foth et al., 2014). Given the length and distribution of plumage seen in the hind limbs of anchiornithines, it is more likely that their values approach the lower bounds, but we included both to be conservative. This does not mean they are not useful, as it allows us to estimate upper and lower bounds of capacity in these taxa to determine the limits of aerial behavior. We did not include the tail in our calculations as it is suspected that it functioned primarily in pitch control rather than as a high vertical force-generating surface in paravians (Han et al., 2014). However, it should be noted that this ignores any potential tail-body interactions, which could make our performance estimates more conservative, especially for taxa with more proximally located tail fans (i.e., shorter tails).

Unlike the gliding reconstructions, our flapping-based powered flight scenarios do not include lift generation from the hind limbs as they would have been held relatively vertically in these scenarios and thus would not present sufficient area to be considered active airfoils. Here we focused on reconstructing the minimal forward speed required to achieve takeoff, especially in a terrestrial setting. This required reconstructing a flap angle (70°) within the range of adduction possible for paravians based on shoulder morphology (Turner et al., 2012) and a minimal flapping speed derived from modified equations based on extant bird values, following Dececchi et al. (2016). We further examined whether these taxa could achieve takeoff using the flap running technique for thrust generation described by (Burgers and Chiappe, 1999). For this analysis we performed two major permutations of flap angle and CL to see how they would influence takeoff ability across our study group. First we ran the analysis using the CL (2) and flap angle (50°) (following Burgers and Chiappe, 1999), modifying only flapping frequency to our early equation to account for allometry. We then reduced CL to 1.5 to better approximate the value seen in living avians, and extended the flap angle to 70° to account for the greater excursion angles permitted by the paravian shoulder joint. We note that a CL of 2.0 may be generous for early avialan wings. By contrast, juvenile chukars can generate a maximum CL of nearly 1.5 just 49 days posthatching (dph), which is the stage suggested to mimic the wing development seen in *Microraptor* and *Archaeopteryx* (Heers et al., 2014), with values over 1 seen in 10 dph age class and above (Heers et al., 2011). We suggest that wing performance of these subadult galliform birds represents a more realistic model of paravian wing performance than the CL of 2 proposed by Burgers and Chiappe (1999). Interestingly, at this life stage, chukars show high wing effectiveness but low aerodynamic efficiency (i.e., high maximum CL and low lift to drag ratio (L:D)—a feature that seems to align with independent models of paravian performance (Palmer, 2014).

RESULTS

Morphometric Patterns

Examination of the linear measurements across taxa and size classes indicates several significant patterns. First, there appears to be no correlation between relative forelimb length and increasing size in either *Microraptor* or anchiornithines (slope -0.0005, p = 0.37). This does not change if we use the longer SVL for *M. hanqingi* (slope -0.0006, p = 0.07), our new estimate of SVL (slope -0.0004, p = 0.18), or if we exclude it altogether (slope -0.0005, p = 0.29). We also find that, while anchiornithines show slightly reduced forelimb lengths compared to either *Microraptor* or *Archaeopteryx* if we use SVL, they are within the range seen in both groups (table 3). We see a similar lack of decreasing relative forelimb length if we use femoral length as opposed to SVL (*Microraptor* slope = -0.003, p = 0.28; anchiornithines slope = -0.008, p = 0.23), but interestingly some members of the anchiornithines show slightly higher forelimb to femur ratios, though the difference is not significant (t test = 0.616, p = 0.55). This may be due to the relatively longer hind limbs seen in *Microraptor* compared to the other taxa examined here, something previously reported (Dececchi and Larsson, 2013) and may hint at ecological differences. Compared to both anchiornithines and *Microraptor*, *Archaeopteryx* has a notably larger forelimb to femur ratio, and one that suggests positive allometry, but this pattern is not present when we use SVL. We in fact see a slight decrease in hind-limb length with size in this taxon, which may influence the forelimb to femur value. This pattern of divergence in forelimb and hind-limb scaling is different from the other two clades, but is similar to a larger pattern observed in early birds compared to nonavialan maniraptoran theropods (Dececchi and Larsson, 2013).

While there was little differentiation between anchiornithines and *Microraptor* using forelimb length, this is not the case if we use total wing length. Here we see a distinctly larger wing length in microraptorines using

TABLE 3

Morphometrics for fossil paravian specimens

Note that we included two separate values for the SVL reconstruction of *M. hanqingi* due to the uncertainty in the original published values (see text for description). We treat these as a minimum SVL (our own reconstruction represented by [1]) and a maximum SVL ([2] per Gong et al. (2012)). We have run permutations with both extremes (see text) to determine how using either estimate affects the overall results of limb length scaling with increasing body size.

The original reconstruction of *M. hanqingi* and our own reconstruction are both included to determine how they affect the overall results with increasing body size. Abbreviations: **Fe,** femur; **FL,** forelimb; **H,** humerus; **HL,** humeral length; **SVL,** snout to vent length; **W,** wing length (forelimb + longest primary); **U,** ulna.

Taxon	Specimen number	SVL	FL/ SVL	HL/ SVL	W / SVL	FL/ Fe	W / Fe	H/ Fe
M. zhaoianus	IVPP V12330	145	0.70	1.04	1.48	2.03	4.30	0.84
M. gui	BMNHC PH881	153	0.81	1.07	1.72	2.38	5.07	0.91
Archaeopteryx	Eichstätt	153.5	0.62	0.78	1.24	2.59	5.15	1.12
Eosinopteryx	YFGP-T5197	165.8	0.61	0.93	0.95	2.08	3.25	0.78
Anchiornis	BMNHC PH804	185	0.59	0.87	0.86	2.13	3.11	0.90
M. gui	IVPP V13320	215	0.66	0.86	1.52	2.20	5.11	0.89
Serikornis	PMoL-AB00200	230	0.62	0.92	1.02	2.13	3.48	0.90
Archaeopteryx	Berlin	231	0.62	0.68	1.37	2.76	6.05	1.21
M. zhaoianus	CAGS 20-7-004	240	0.61	0.90	1.36	1.96	4.38	0.82
Aurornis	YFGP-T5198	246	0.61	0.82	0.96	2.25	3.56	0.88
Anchiornis	LPM-B00169	246.9	0.64	0.92	1.04	2.39	3.90	1.04
Caihong	PMoL-B00175	259	0.44	0.78	0.81	1.59	2.96	0.59
Anchiornis	PKUP V1068	275	0.59	0.96	0.99	1.80	3.02	0.80
Xiaotingia	STM 27-2	295	0.54	-	0.90	1.90	3.17	0.85
M. gui	IVPP V13352	297	0.67	0.98	1.42	2.04	4.33	0.86
Archaeopteryx	Solnhofen	300	0.63	0.69	1.25	2.83	5.60	1.24
M. gui	QV1002	327	0.68	1.00	1.44	2.04	4.34	0.87
M. hanqingi	LVH 0026[1]	360	0.64	0.90	1.35	2.06	4.34	0.84
M. hanqingi	LVH 0026[2]	405	0.57	0.80	1.20	2.06	4.34	0.84

either SVL (mean of 1.47× SVL compared with 0.94 for anchiornithines, t = 9.87, $p < 0.001$) or femur (mean = 4.55× femur length compared with 3.31, t = 7.04, $p < 0.001$). Notably, we do have some evidence that wing length decreases with increased SVL, though this is only significant if we use the larger measure for *M. hanqingi* (p = 0.03) and it is not seen if we use femoral length (p = 0.21). In direct comparisons across size classes we consistently see much longer wings in *Microraptor* species than in either anchiornithine or *Archaeopteryx* specimens using SVL as a measure, but not when using femoral length, again suggesting a bifurcation in the trajectory of the fore- and hind limbs in early avialans.

LOADING AND LIFT GENERATIONS

We find all wing-loading values below the maximum value of 245 Nm^{-2} seen in extant volant taxa, with the exception of *Eosinopteryx* when its body mass is estimated using femoral circumference. These values are significantly different between clades and with increasing body size, using the forewing only when fore- and hind-wing areas are combined (table 4). In a comparable size class using the same mass estimator, anchiornithines have wing-loading values 260%–680% larger than a similar-sized *Microraptor* and 230%–610% larger than a similar-sized *Archaeopteryx*. This pattern also occurs if we include hind-limb wing area. When we are reconstructing anchiornithines with hind-wing areas proportional to those seen in *Microraptor* we are likely underestimating the magnitude of this difference. The reason is that the forewing:hindwing area ratio is likely overestimated in anchiornithines relative to *Microraptor*. In the former, the tibial feathers (95%–150% of femoral length, FL) and metatarsal feathers (45%–70% of of FL) are proportionally significantly shorter than those seen in *Microraptor*, which have tibial feathers 170% of FL and metatarsal feathers 200%–210% of FL respectively. Thus the wing-loading difference between these two clades is likely only exacerbated if we include the hind wing's influence. Across size categories within *Microraptor* we see a trend of increasing wing loading in larger individuals (table 5). We do not see a clear pattern in anchiornithines, though generic level differences in wing use and behavior may be masking underlying ontogenetic trends. In *Archaeopteryx* we see the lowest loading values in intermediate sized individuals, with both smaller and larger size classes showing similar levels of loading. While this is intriguing, it requires larger sampling to confirm its validity. For disc loading we see something of an increase in loading with size, though this is most apparent between the largest individuals and not between small and medium size classes. We see a separation between anchiornithines and *Microraptor*, with the former showing values above what is expected in a gliding lineage (Sprague and Breuner, 2010), but all taxa show values within the range of extant powered fliers (Nudds and Bryant, 2000; Tobalske and Dial, 2000; Askew et al., 2001).

A similar trend is seen among specific lift numbers, though these values do appear to suggest a more restrictive subset of flight capable taxa and specimens. Using a 10% flight muscle mass fraction we find only 10 of 48 reconstructions for anchiornithines result in lift generation values sufficient to permit flight from the ground, of which 7 of them come using the femoral length mass estimation method. In contrast, 34 of a possible 51 permutations in *Microraptor* and 11 of 15 for *Archaeopteryx* show ground launch and climb-out capability. Again, we see a significant effect of increasing body size; in both *Microraptor* and *Archaeopteryx* the largest individuals in our sample require the highest levels of power output to generate sufficient lift for takeoff. One possible reason for the low number of successful launches in the latter two groups could be that a 10% flight muscle fraction is simply too low an estimate. Three-dimensional volumetric work has suggested a higher value closer to 12% or 13% in *Archaeopteryx* and *Microraptor* (Allen et al., 2013; Heers et al., 2016), which is supported by osteological evidence such as the larger sternum in *Microraptor*. Using this higher estimate, we find 43 of 48 iterations for *Microraptor* and 14 out of 15 for *Archaeopteryx* achieve the necessary lift for flight.

GLIDING FLIGHT

As glide speed is intimately linked with wing loading, we see a similar pattern of increased minimal glide speed both across the clades and with increasing size (table 6, fig. 1). While we cannot make a clear statement of a speed beyond that expected from a gliding animal, in similar environments (i.e., terrestrial tree to tree locomotion) glide speed ranges between 5 and 13 ms^{-1} across tetrapods (Emerson and Koehl, 1990;

TABLE 4

Wing loading and disc loading for fossil paravian specimens

For *Microraptor gui* IVPP V13352 two different wing area reconstructions were used to capture the range of published estimates adopted in previous aerodynamic investigations: area estimates following Chatterjee and Templin (2007) are indicated by [1] and those following Dyke et al. (2013) are indicated by [2]. There are several different mass estimates for the *Archaeopteryx* specimens studied here. Our analysis involved permutations based on these previously published values. Values accompanied by [3] correspond to those from Serrano et al. (2017), [4] for those from Yalden (1984) and [5] following Erickson et al. (2009). Abbreviations: **Fl,** mass derived from femoral length estimate; **Fc,** mass derived from femoral circumference estimate, **3D,** mass based on published models.

A. Calculated values for wing loading using the forewing area only (FW) and using forewing + hindwing area (TW)

Taxa	Specimen	FW	TW	Wing loading FW			Wing loading TW		
				Fl	Fc	3D	Fl	Fc	3D
M. gui	BMNHC PH881	0.04	0.06	55.1	41.3	-	36.7	27.6	-
	IVPP V13320	0.07	0.11	47.4	57.2	-	31.6	38.1	-
	IVPP V13352[1]	0.09	0.13	143.1	96.9	104.6	96.5	65.3	70.5
	IVPP V13352[2]	0.09	0.14	141.7	95.9	54.5	93.2	63.1	35.8
	QV1002	0.14	0.20	135.1	89.8	-	90.0	59.9	-
M. zhaoianus	CAGS 20-7-004	0.07	0.10	81.6	50.1	-	54.4	33.4	-
	IVPP V12330	0.03	0.04	52.2	45.3	-	34.8	30.2	-
M. hanqingi	LVH 0026[3]	0.14	0.28	142.5	-	85.5	70.7	-	42.4
Anchiornis	BMNHC PH804	0.01	0.01	171.3	203.4	-	114.2	135.6	-
	LPM-B00169	0.03	0.04	125.0	194.0	-	83.3	129.4	-
	PKUP V1068	0.03	0.05	293.5	172.2	-	195.7	114.8	-
Eosinopteryx	YFGP-T5197	0.01	0.02	132.5	340.6	-	88.3	227.1	-
Aurornis	YFGP-T5198	0.02	0.04	157.0	214.9	-	104.7	143.3	-
Caihong	PMoL-B00175	0.02	0.04	195.8	125.0	-	130.5	83.3	-
Serikornis	PMoL-AB00200	0.02	0.04	159.0	131.2	-	106.0	87.5	-
Xiaotingia	STM 27-2	0.03	0.05	245.1	257.1	-	163.4	171.4	-
Archaeopteryx	Eichstätt	0.02	0.03	-	-	74.3	-	-	62.0
	Berlin[4]	0.05	0.06	-	-	44.9	-	-	38.2
	Berlin[5]	0.06	0.07	-	-	55.4	-	-	46.2
	Solnhofen[4]	0.12	0.15	-	-	86.3	-	-	71.9
	Solnhofen[5]	0.12	0.15	-	-	68.1	-	-	56.7

B. Calculated values for disc loading (Nm^{-2})

Taxa	Specimen	Disc	Disc loading		
			Fl	Fc	3D
M. gui	BMNHC PH881	0.24	9.8	7.3	-
	IVPP V13320	0.37	9.0	10.8	-
	IVPP V13352[1]	0.69	14.1	20.8	13.4
	IVPP V13352[2]	0.58	14.1	20.8	8.4
	QV1002	0.77	23.9	15.9	-

TABLE 4 *continued*

Taxa	Specimen	Disc	Disc loading		
			Fl	Fc	3D
M. zhaoianus	CAGS 20-7-004	0.37	15.0	9.1	-
	IVPP V12330	0.16	9.3	8.0	-
M. hanqingi	LVH 0026	0.82	24.6	-	14.8
Anchiornis	BMNHC PH804	0.09	18.3	21.4	-
	LPM-B00169	0.23	16.1	24.9	-
	PKUP V1068	0.26	39.3	23.2	-
Eosinopteryx	YFGP-T5197	0.09			-
Aurornis	YFGP-T5198	0.19	19.3	26.6	-
Caihong	PMoL-B00175	0.15	30.3	19.5	-
Serikornis	PMoL-AB00200	0.19	20.7	16.9	-
Xiaotingia	STM 27-2	0.25	32.5	34.3	-
Archaeopteryx	Eichstätt[3]	0.13	-	-	13.7
	Berlin[4]	0.28	-	-	8.7
	Berlin[3]	0.28	-	-	12.0
	Solnhofen[3]	0.48	-	-	22.1
	Solnhofen[5]	0.48	-	-	13.9

Socha et al., 2015) with higher speeds of 10–20 ms^{-1} in soaring specialists and seabirds (Alerstam et al., 1993; Koehl et al., 2011). Using the forewings only at a CL of 1.5 we find glide speed estimates of less than 10 ms^{-1} for most of the *Microraptor* and *Archaeopteryx* reconstructed at less than 1 kg, while members of the anchiornithines show values ranging from 11.6 to 19 ms^{-1}. This places the anchiornithines at the upper range of what is seen in extant gliders. If we use a CL of 1, this range is increased to between 14.3 and 26 ms^{-1} and is comparable to speeds seen in dynamic seabirds soaring in high-wind conditions (Alerstam et al., 1993) and beyond what is seen in terrestrial taxa (Socha et al., 2015). As previously noted, our estimates of hind-wing influence are likely overstated, but we included them to mimic the "four winged" scenario that has been suggested. We find that in this scenario the minimum glide speeds are significantly reduced, though are still very high in anchiornithines compared to modern gliders ranging from 10–16.5 ms^{-1} under the *Microraptor* hindwing model and 11–18 ms^{-1} under the *Archaeopteryx* model (under a CL of 1.5 and a hip angle of 45°). Our estimates are for equilibrium gliding, for the sake of comparison with powered-flight performance characteristics. We note that in living taxa glides are often short and do not reach an equilibrium state. However, we also note that with an animal as large as *Microraptor* (~1 kg), small gaps could likely be easily cleared with leaping alone, making long distance glide performance more relevant.

We contend that minimum turning radius is a proxy of the maneuverability of an individual during gliding flight and was likely highly important in navigating forested parts of their habitats (Wang et al., 2006; Burnham, 2007; Gong et al., 2012). Given that this exact value would vary based on multiple parameters, such as the exact placement and angling of both the hind limbs and tail (Longrich, 2006), and is notoriously difficult to model accurately even in extant birds, whose characteristics often violate some of the key assumptions of this equation (Warrick et al.,

TABLE 5

Specific lift values for fossil paravian specimens

Values above 9.8 Nkg^{-1} indicate flight capability. Abbreviations: **Fl,** mass derived from femoral length estimate; **Fc,** mass derived from femoral circumference estimate; **3D,** mass based on published models.

A. Specific lift in Nkg^{-1} using a flight muscle mass estimate of 10% of total mass muscle mass for *Microraptor* and *Archaeopteryx*

Taxa	Specimen	Fl			Fc			3D		
		225	250	287	225	250	287	225	250	287
M. gui	BMNHC PH881	11.1	12.3	14.1	12.6	14.0	16.1	-	-	-
M. gui	IVPP V13320	11.4	12.7	14.5	10.5	11.7	13.4	-	-	-
M. gui	IVPP V13352	9.3	10.3	11.8	7.8	8.7	10.0	11.7/ 9.5	13.0/ 10.5	14.9/ 12.1
M. gui	QV1002	7.3	8.1	9.3	8.8	9.7	11.2	-	-	-
M. zhaoianus	CAGS 20-7-004	9.1	10.1	11.6	11.3	12.6	14.4	-	-	-
M. zhaoianus	IVPP V12330	11.4	12.7	14.6	12.2	13.5	15.5	-	-	-
M. hanqingi	LVH 0026	7.2	8.0	9.2	-	-	-	9.0	10.1	11.5
Anchiornis	BMNHC PH804	8.6	9.5	10.9	8.0	8.9	10.2	-	-	-
Anchiornis	LPM-B00169	8.9	9.9	11.3	7.3	8.2	9.4	-	-	-
Anchiornis	PKUP V1068	6.0	6.7	7.6	7.6	8.4	9.6	-	-	-
Eosinopteryx	YFGP-T5197	9.1	10.1	11.6	6.0	6.7	7.7	-	-	-
Aurornis	YFGP-T5198	8.3	9.2	10.5	7.2	7.9	9.1	-	-	-
Caihong	PMoL-B00175	6.8	7.5	8.7	8.2	9.2	10.5	-	-	-
Serikornis	PMoL-AB00200	8.0	8.9	10.2	8.8	9.7	11.2	-	-	-
Xiaotingia	STM 27-2	6.5	7.2	8.3	6.4	7.1	8.1	-	-	-
Archaeopteryx	Eichstätt	-	-	-	-	-	-	9.6	10.7	12.3
Archaeopteryx	Berlin	-	-	-	-	-	-	11.6	12.9	14.8
Archaeopteryx	Berlin	-	-	-	-	-	-	10.1	11.2	12.9
Archaeopteryx	Solnhofen	-	-	-	-	-	-	7.6	8.5	9.8
Archaeopteryx	Solnhofen	-	-	-	-	-	-	9.4	10.4	12.0

B. Specific lift in Nkg^{-1} using a flight muscle mass estimate of 13% flight muscle fraction for *Microraptor* and *Archaeopteryx*

Taxa	Specimen	Fl			Fc			3D		
		225	250	287	225	250	287	225	250	287
M. gui	BMNHC PH881	12.8	14.3	16.4	14.6	16.2	18.6	-	-	-
M. gui	IVPP V13320	13.2	14.7	16.8	12.2	13.5	15.6	-	-	-
M. gui	IVPP V13352	10.7	11.9	13.7	9.1	10.1	11.6	13.5/ 11.0	15.0/ 12.1	17.2/ 14.0
M. gui	QV1002	8.5	9.4	10.8	10.2	11.3	12.9	-	-	-
M. zhaoianus	CAGS 20-7-004	10.6	11.7	13.5	13.1	14.6	16.7	-	-	-

TABLE 5 *continued*

M. zhaoianus	IVPP V12330	13.2	14.7	16.9	14.1	15.6	18.0	-	-	-
M. hanqingi	LVH 0026	8.4	9.3	10.7	-	-	-	10.5	11.6	13.4
Archaeopteryx	Eichstätt	-	-	-	-	-	-	11.2	12.4	14.3
Archaeopteryx	Berlin	-	-	-	-	-	-	13.5	15.0	17.2
Archaeopteryx	Berlin	-	-	-	-	-	-	11.7	13.0	14.9
Archaeopteryx	Solnhofen	-	-	-	-	-	-	8.9	9.8	11.3
Archaeopteryx	Solnhofen	-	-	-	-	-	-	10.9	12.1	13.9

TABLE 6

Minimum glide speed for fossil paravians under coefficient of lift reconstructions of 1.0 and 1.5

Abbreviations: **CL,** coefficient of lift; **Fl,** mass derived from femoral length estimate; **Fc,** mass derived from femoral circumference estimate; **3D,** mass based on published models. Minimum glide speed (= stall speed) in ms^{-1}. Estimates following Chatterjee and Templin (2007) are indicated by [1] and those following Dyke et al. (2013) by [2].

Taxa	Specimen	Cl=1.5			CL=1.0		
		Fl	Fc	3D	Fl	Fc	3D
M. gui	BMNHC PH881	7.7	6.7	-	9.5	8.2	-
M. gui	IVPP V13320	7.2	7.9	-	8.8	9.6	-
M. gui	IVPP V13352	11.6	9.4	10.7[1]	14.1	11.5	13.1[1]
M. gui	IVPP V13352	11.6	9.4	7.7[2]	14.1	11.5	9.4[2]
M. gui	QV1002	12.1	9.9	-	14.9	12.1	-
M. zhaoianus	CAGS 20-7-004	9.4	7.3	-	11.5	9.0	-
M. zhaoianus	IVPP V12330	7.6	7.1	-	9.3	8.6	-
M. hanqingi	LVH 0026	12.1	-	14.9	9.9		12.1
Anchiornis	BMNHC PH804	13.8	14.9	-	16.9	18.2	-
Anchiornis	LPM-B00169	11.6	14.5	-	14.3	17.7	-
Anchiornis	PKUP V1068	17.9	13.7	-	21.9	16.8	-
Eosinopteryx	YFGP-T5197	12.0	19.2	-	14.7	23.6	-
Aurornis	YFGP-T5198	13.1	15.4	-	16.0	18.8	-
Caihong	PMoL-B00175	14.6	11.7	-	17.9	14.4	-
Serikornis	PMoL-AB00200	13.2	11.9	-	16.1	14.6	-
Xiaotingia	STM 27-2	16.3	16.7	-	20.0	20.5	-
Archaeopteryx	Eichstätt	-	-	9.0	-	-	11.0
Archaeopteryx	Berlin	-	-	7.0	-	-	8.6
Archaeopteryx	Berlin	-	-	7.8	-	-	9.6
Archaeopteryx	Solnhofen	-	-	9.7	-	-	11.9
Archaeopteryx	Solnhofen	-	-	7.7	-	-	9.4

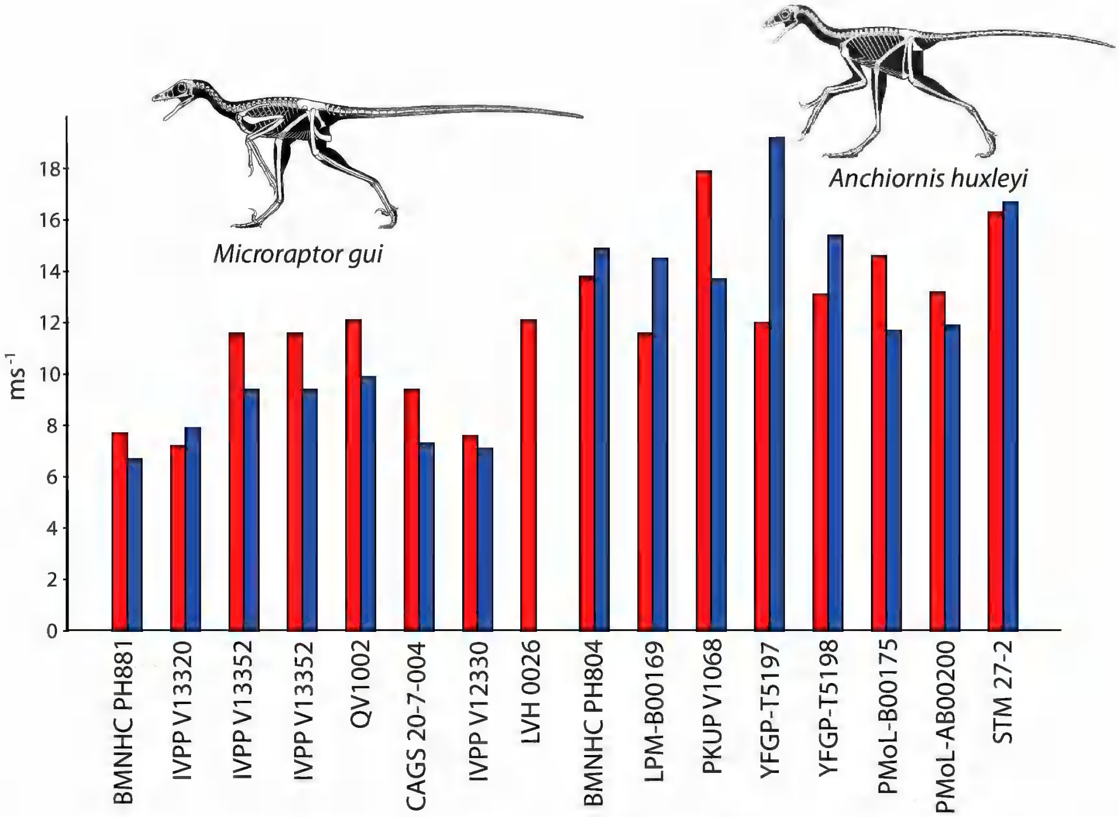

FIG. 1. Minimum glide speed (= stall speed) at CL = 1.5 for *Microraptor* specimens compared with those for anchiornithine specimens. Red bars represent masses from femoral length estimates, blue from femoral circumference. Note the higher average score, especially at comparable size classes for anchiornithines. Illustration used with the permission of Scott Hartman.

2002), we advocate using our values as relative scores rather than absolute values. Looking at the data we see that *Microraptor* specimens of similar size have a turning radius significantly smaller than anchiornithines, but similar to that of *Archaeopteryx*. For example, *Microraptor* specimen BMNHC PH881 shows a turning radius between 20% and 31% of that seen in the similar-sized *Anchiornis* specimen BMNHC PH804 and 55%–75% of that seen in the Eichstätt *Archaeopteryx* specimen (table 7). This comparatively smaller turning radius in *Microraptor* is observed even at larger size classes, e.g., the *M. gui* type specimen (IVPP V13352), as all mass estimates display values that are half those seen in the similar-sized anchiornithine *Xiaotingia* and are below those seen in any anchiornithine specimen regardless of size. This level of reduction implies significantly lower levels of maneuverability in anchiornithines than in *Microraptor* that, when coupled with their higher glide speed, would make maneuvering very difficult and inefficient.

Powered Flight and Takeoff

Unlike gliding, flapping-based takeoff methods require a significantly lower—often around 50% lower—minimal speed to achieve lift values sufficient to support the body (table 8). Again we see a pattern of increased takeoff velocity needed at larger sizes among *Microraptor* specimens, but the pattern is less clear in the other two clades. Interestingly in *Archaeopteryx* the highest required speed is found in the Eichstätt specimen, the smallest in

TABLE 7

Banking radius estimates for fossil paravians based on the criteria of Longrich (2006)

Abbreviations: **Fl,** mass derived from femoral length estimate; **Fc,** mass derived from femoral circumference estimate; **3D,** mass based on published models. Radii in °. Estimates following Chatterjee and Templin (2007) are indicated by ^{1} and those following Dyke et al. (2013) by ^{2}.

Taxa	Specimen	Fl	Fc	3D
M. gui	BMNHC PH881	7.1	5.3	-
M. gui	IVPP V13320	7.3	6.1	-
M. gui	IVPP V13352	15.5	10.5	13.4^1
M. gui	IVPP V13352	15.5	10.5	7.0^2
M. gui	QV1002	17.4	11.5	-
M. zhaoianus	CAGS 20-7-004	10.4	6.4	-
M. zhaoianus	IVPP V12330	6.8	5.9	-
M. hanqingi	LVH 0026	11.0	18.3	
Anchiornis	BMNHC PH804	22.3	26.1	-
Anchiornis	LPM-B00169	16.0	24.7	-
Anchiornis	PKUP V1068	37.6	22.2	-
Eosinopteryx	YFGP-T5197	16.9	43.6	-
Aurornis	YFGP-T5198	20.1	27.8	-
Caihong	PMoL-B00175	25.3	16.2	-
Serikornis	PMoL-AB00200	20.5	16.7	-
Xiaotingia	STM 27-2	31.3	33.0	-
Archaeopteryx	Eichstätt	-	-	9.5
Archaeopteryx	Berlin	-	-	5.8
Archaeopteryx	Berlin	-	-	7.2
Archaeopteryx	Solnhofen	-	-	11.0

our dataset, while the lowest values are in the mid-sized Berlin specimen. The subclass of small *Microraptor* specimens show the lowest minimum takeoff speed of any taxon. The similar sized Eichstätt *Archaeopteryx* has values 140%–220% higher and comparable anchiornithines have speeds 220%–450% greater than *Microraptor*. In fact, across *Microraptor* specimens we see relatively low minimal speed values, with the highest for the 2 kg reconstruction of LVH 0026 (8.3 ms^{-1}) still below the lowest value seen in any anchiornithine.

We compared these values to estimates of maximum sprint speed based on either reconstructions from Froude number (Pontzer et al., 2009) or body mass (Hirt et al., 2017) to see whether they were achievable from an unaided terrestrial run (fig. 2). We chose Froude numbers of 10 and 15 to mimic sprint speed capacity. While these numbers are high they are within the range seen in extant terrestrial birds and previously estimated for theropod dinosaurs (Hutchinson and Garcia, 2002; Sellers and Manning, 2007). These values are realistic even for small-bodied taxa such as those examined here, as modern roadrunners (*Geococcyx californianus*) have been recorded running at 5.3–6.7 ms^{-1} (Stewart, 1958), which at a hip height of around 0.16 m (Halsey, 2013) gives Froude values of 18–28. Using Froude values we find that 12 of 16 permutations of *Microraptor* achieve running speeds greater than minimum takeoff values, as do all cases using Hirt et al.'s (2017) body-mass estimates for top speed. The

TABLE 8

Minimum speed required for takeoff based under a powered flapping regime

Note that for the anchiornithines all minimum values are higher than the maximum potential sprint speed using either a Froude number (Fr) or body mass based running speed estimate. See text for description. Estimates following Chatterjee and Templin (2007) are indicated by [1] and those following Dyke et al. (2013) by [2]. Abbreviations: **Fl,** mass derived from femoral length estimate; **Fc,** mass derived from femoral circumference estimate; **3D,** mass based on published models. Speeds in ms^{-1}.

Taxa	Specimen	Flapping takeoff speed			Running speed		Speed based on Hirt et al. (2017)		
		Fl	Fc	3D	Fr=10	Fr=15	Fl	Fc	3D
M. gui	BMNHC PH881	4.1	2.8	-	4.0	4.9	4.9	4.5	-
M. gui	IVPP V13320	3.0	3.8	-	4.3	5.2	5.4	5.6	-
M. gui	IVPP V13352	7.5	5.1	6.1[1]	5.3	6.5	7.6	6.9	7.0[1]
M. gui	IVPP V13352	7.5	5.1	2.9[2]	5.3	6.5	7.6	6.9	5.9[2]
M. gui	QV1002	8.1	5.4	-	5.7	6.9	8.4	7.5	-
M. zhaoianus	CAGS 20-7-004	5.6	3.2	-	4.2	5.1	6.1	5.4	-
M. zhaoianus	IVPP V12330	4.2	3.6	-	3.9	4.7	4.3	4.2	-
M. hanqingi	LVH 0026	8.3	-	5.0	5.6	6.9	7.5	-	8.5
Anchiornis	BMNHC PH804	11.3	12.5	-	4.0	4.9	4.4	4.6	-
Anchiornis	LPM-B00169	8.4	11.5	-	4.7	5.8	5.5	6.2	-
Anchiornis	PKUP V1068	15.1	10.6	-	5.1	6.2	7.2	6.2	-
Eosinopteryx	YFGP-T5197	9.5	17.2	-	3.9	4.8	4.2	5.4	-
Aurornis	YFGP-T5198	10.1	12.6	-	4.4	5.4	5.5	6.0	-
Caihong	PMoL-B00175	12.1	8.9	-	4.5	5.5	5.8	5.2	-
Serikornis	PMoL-AB00200	10.3	8.8	-	4.6	5.6	5.6	5.3	-
Xiaotingia	STM 27-2	13.5	14.0	-	-	-	6.7	6.8	-
Archaeopteryx	Eichstätt	-	-	6.1	3.4	4.2	-	-	4.5
Archaeopteryx	Berlin	-	-	3.1	3.9	4.8	-	-	4.9
Archaeopteryx	Berlin	-	-	4.1	3.9	4.8	-	-	5.4
Archaeopteryx	Solnhofen	-	-	6.0	4.5	5.5	-	-	7.2
Archaeopteryx	Solnhofen	-	-	3.6	4.5	5.5	-	-	6.4

four reconstructions that do not all rely on body-mass reconstructions taken using femoral length produce values 40%–70% greater than the value for other metrics using the same specimen and may be considered overestimations based on known elongation of the femur in this taxon (Dececchi and Larsson, 2013). Among *Archaeopteryx* representatives, the smallest specimen (Eichstätt) fails to achieve sufficient speed through running under either scenario as does the largest specimen under its heaviest reconstruction using Froude values. No anchiornithine achieves a running speed within 2 ms^{-1} of the minimal value needed to achieve takeoff.

As running speed relies solely on thrust generated by the hind limbs, we also ran reconstructions to account for the possibility that flap-generated thrust during the run could overcome the barrier of getting airborne (Burgers and Chiappe, 1999). We find among *Microraptor* specimens that only the largest mass estimates for the largest specimens under the 50° flap angle fail to

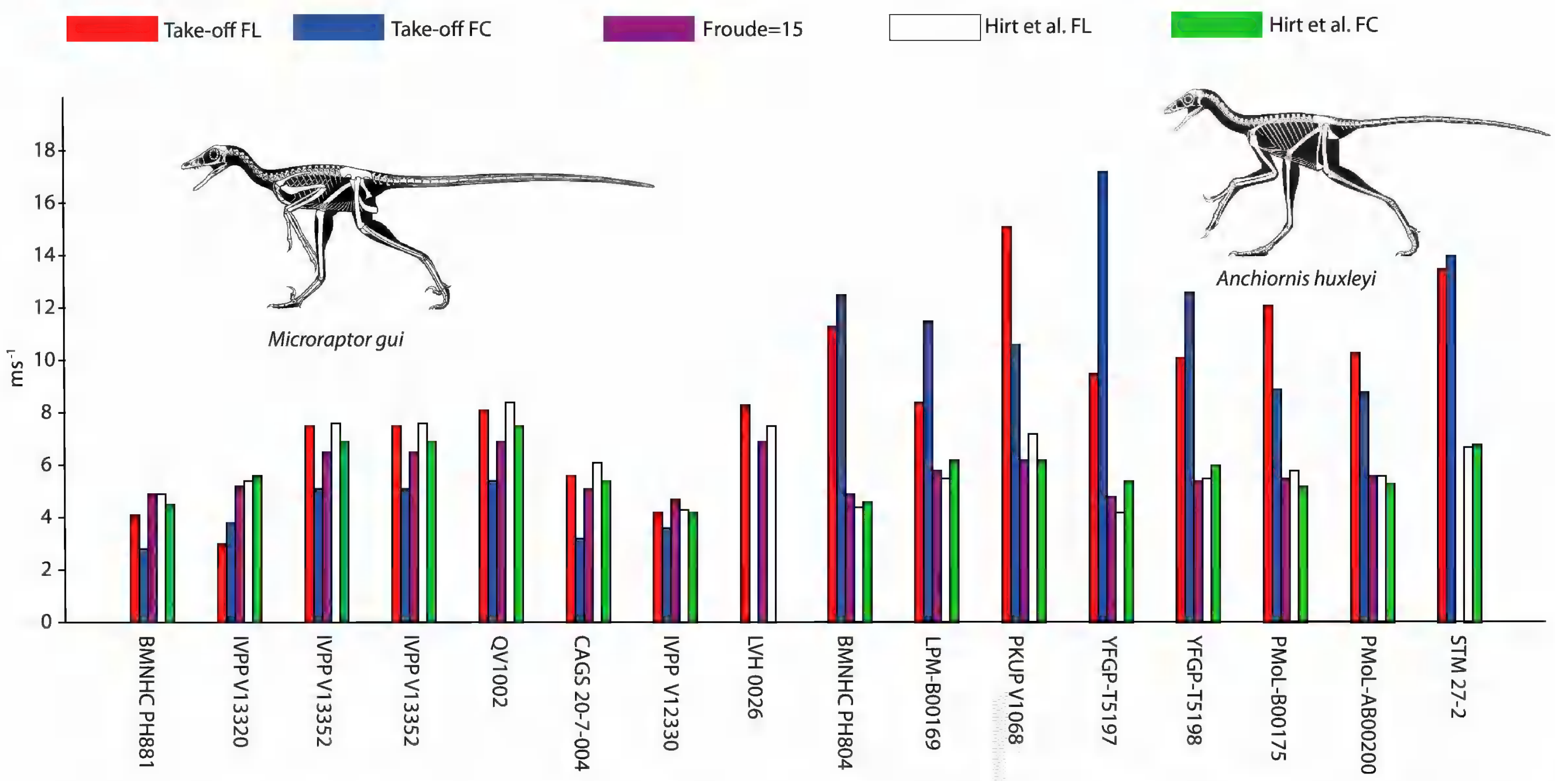

FIG. 2. Comparison of minimum flapping-based takeoff speed under mass reconstructions using femur length and circumference for *Microraptor* and anchiornithine specimens. Femoral length (FL) in red; femoral circumference (FC) in blue. These values are mapped against maximum sprint speed calculated using a Froude number of 15 (purple) or using body mass based on the equation of Hirt et al., 2017 (FL = white, FC = green). In all cases the anchiornithines show running speeds significantly too slow to allow them to achieve a ground-based takeoff. Illustration used with the permission of Scott Hartman.

TABLE 9

Takeoff potential through flap running based on the criteria of Burgers and Chiappe (1999) under several potential coefficient of lift values and flap angles

Coefficient of lift (CL) values used: 2.0 and 1.5. Flap angles (FA) used: 50° and 70°. A run was considered a success if it achieved a body weight (bw) support value of above 100% of mass in 10 seconds or less. Estimates following Chatterjee and Templin (2007) are indicated by [1] and those following Dyke et al. (2013) by [2]. Abbreviations: **Gr,** grounded, not able to achieve support of 1.0 bw or above; **TO,** achieved values above 1.0 bw; **Fl,** mass derived from femoral length estimate; **Fc,** mass derived from femoral circumference estimate; **3D,** mass based on published models.

Taxa	Specimen	CL = 2, FA = 70°			CL = 2, FA = 50°			CL = 1.5, FA = 70°			CL = 1.5, FA = 50°		
		Fl	Fc	3D	Fl	Fc	3D	Fl	Fc	3D	Fl	Fc	3D
M. gui	BMNHC PH881	TO	TO	-	TO	TO	-	TO	TO	-	TO	TO	-
M. gui	IVPP V13320	TO	TO	-	TO	TO	-	TO	TO	-	TO	TO	-
M. gui	IVPP V13352	TO	TO	TO	TO	TO	TO	TO	TO	TO	TO	TO	Gr[1]
M. gui	IVPP V13352	TO	TO	TO	TO	TO	TO	TO	TO	TO	TO	TO	TO[2]
M. gui	QV1002	TO	TO	-	Gr	TO	-	Gr	TO	-	Gr	TO	-
M. zhaoianus	CAGS 20-7-004	TO	TO	-	TO	TO	-	TO	TO	-	TO	TO	-
M. zhaoianus	IVPP V12330	TO	TO	-	TO	TO	-	TO	TO	-	TO	TO	-
M. hanqingi	LVH 0026	TO	-	TO	Gr	-	TO	Gr	-	TO	Gr	-	TO
Anchiornis	BMNHC PH804	Gr	Gr	-	Gr	Gr	-	Gr	Gr	-	Gr	Gr	-
Anchiornis	LPM-B00169	TO	Gr	-	Gr	Gr	-	Gr	Gr	-	Gr	Gr	-
Anchiornis	PKUP V1068	Gr	Gr	-	Gr	Gr	-	Gr	Gr	-	Gr	Gr	-
Eosinopteryx	YFGP-T5197	TO	Gr	-	Gr	Gr	-	Gr	Gr	-	Gr	Gr	-
Aurornis	YFGP-T5198	Gr	Gr	-	Gr	Gr	-	Gr	Gr	-	Gr	Gr	-
Caihong	PMoL-B00175	Gr	TO	-	Gr	TO	-	Gr	TO	-	Gr	TO	-
Serikornis	PMoL-AB00200	Gr	TO	-	Gr	Gr	-	Gr	Gr	-	Gr	Gr	-
Xiaotingia	STM 27-2	Gr	Gr	-	Gr	Gr	-	Gr	Gr	-	Gr	Gr	-
Archaeopteryx	Eichstätt	-	-	TO	-	-	TO	-	-	TO	-	-	TO
Archaeopteryx	Berlin	-	-	TO	-	-	TO	-	-	TO	-	-	TO
Archaeopteryx	Berlin	-	-	TO	-	-	TO	-	-	TO	-	-	Gr
Archaeopteryx	Solnhofen	-	-	TO	-	-	TO	-	-	TO	-	-	TO
Archaeopteryx	Solnhofen	-	-	TO	-	-	TO	-	-	TO	-	-	TO

takeoff (table 9), with those specimens having body weights supporting lift values well above 1 under all other permutations. Under all scenarios, the smaller specimens achieve lift off. The Solnhofen *Archaeopteryx* fails to achieve sufficient body support under the CL 1.5 and 50° flap angle reconstruction, but succeeds under all others, as do the Berlin and Eichstätt individuals in all versions. In contrast, the anchiornithines (*Eosinopteryx*, *Caihong*, *Serikiornis*, and *Anchiornis* specimen LPM-B00169) that achieve takeoff capacity do so only under the least stringent permutation (CL = 2, 70° flap angle), using the lower mass estimates with the highest body weight support value shown after 10 seconds at only 67% of that needed to achieve takeoff. No anchiornithines show this capacity with a CL of 1.5, a value that is similar to that seen in modern avians.

DISCUSSION

By looking at these three similar-sized small bodied paravians close to the origins of birds, each with a similar bauplan of elongated forelimbs and long pennaceous feathered fore- and hind limbs, we get a sense of how flight potential extends across this region of the phylogeny. Often all three have been lumped together as "four-winged" dinosaurs, under the assumption that they show similar ecological and behavioral strategies (Dyke et al., 2013; Xu et al., 2014). What is apparent from our data is that there is a distinct difference in flight capacity that may not be immediately discernable from simple linear osteological measurements alone. While any single value may be considered insufficient to draw larger conclusions on an integrated function such as flight, the combined data of these various methods of reconstruction paint a picture of significantly different aerodynamic capabilities among similar-sized paravian lineages.

We find some intriguing patterns across size classes within each of our clades. The first is there is little constant size-related change within the anchiornithines for any of our factors related to flight potential. We view this as perhaps an indication that the wings were not used for flight, as there seems to be little compensation for the rapid increase in mass that would be expected in a creature that needs to overcome gravity at larger and larger sizes. This lack of compensation is especially relevant as several of these markers such as specific lift and takeoff speed are beyond the range seen in modern volant taxa even at small sizes, where wing size may be able to overcome reduced muscle fraction for wing-assisted locomotion (Dececchi et al., 2016; Heers et al., 2018). In addition, this clade shows a combination of high wing loadings concurrent with high disc loadings. The former suggests high-speed and nonmaneuverable wings, as anchiornithines possess values that are higher than those seen in modern gliding animals (Thorington and Heaney, 1981; McGuire and Dudley, 2011; Socha et al., 2015). The latter are more in line with what we see in short-winged burst fliers (Tobalske and Dial, 2000) whose wings are energetically inefficient and require more power input to perform flight, but these insufficiencies can be overcome with larger wing muscle fractions and emarginated wing feathers (Tobalske and Dial, 2000; van Oorschot et al., 2017). Neither of those compensatory features are found in anchiornithines (Pei et al., 2017). Anchiornithines' combination of wing features, poorly designed for gliding or powered flight, is not compatible with the reconstruction of a clade that regularly used volant modes of transport: this clade had wings (including or excluding the hind limbs), but they were poorly designed for passive gliding (high glide speeds, high wing and disk loadings, and poor turn radii) and they lacked signs of strong short- or burst-flight capabilities (large muscle volumes with high power outputs) while they had symmetrical wing feathers (Hu et al., 2009; Saitta et al., 2018) that reduce aerodynamic efficiency further still (Feo et al., 2015). The combined weight of these data suggest that the "wings" of anchiornithines were not used in flight, though they could have had some aerodynamic role in other types of terrestrial behavior such as WAIR or leap assistance (Heers et al., 2014; Dececchi et al., 2016).

While we cannot rule out some gliding capability in anchiornithines, the high wing loadings, high minimum glide speeds, and larger turning radii compared to the other clades do not suggest very strong aerial mobility in this group, if it was possible. While wing-loading values are below the maximal level seen in flying animals, it should be noted that nonvolant hatchling-aged birds can also show wing-loading values below 245 Nm^{-2} (Austin and Ricklefs, 1977; Wright et al., 2006; Sprague and Breuner, 2010; Heers and Dial, 2015). Also, given that the osteological signals in this clade are inconsistent with a reconstruction of arboreality such as long distal limbs, low claw curvature, and lack of ankle or hip flexibility, one can further argue against gliding as a locomotion strategy in this group (Dececchi and Larsson, 2011; Lefèvre et al., 2017). This, coupled with the low support for any ground-based takeoff capacity, makes flight highly unlikely. We only see 21% of permutations achieve minimal specific lift levels in this clade, with no cases of running speed sufficient to achieve minimal takeoff speed and only 6% of cases, all under the most lenient conditions with a CL higher than modern bird wings, where flap running produces sufficient thrust to achieve takeoff. In no specimen, at any size class, are constant and consistent signs of flight potential shown in the clade.

We see very different patterns in the *Microraptor* and *Archaeopteryx* as both show characteristic metrics expected of animals that were aerial, though not necessarily identical patterns. Within *Microraptor* specimens we see a clear decrease in flight potential, including higher loadings, lower specific lift values, higher minimal speeds (under powered or passive gliding scenarios) and less success at flap running as we increase body size. This becomes especially apparent if we use femoral length as a proxy for size (though see Dececchi and Larsson, 2013, for evidence that this may not be an accurate proxy for this group, as under some permutations it moves the larger individuals from volant to flightless). While we understand the methods used here have limitations in their use of scaling and estimates for reconstructing wing area, thus introducing some uncertainty in the observed pattern, our results suggest that ontogeny may have a role to play in flight capacity in this clade. While none of the specimens examined here are considered to be very young juveniles, we capture 10-fold body-size changes that likely took several years to achieve (Erickson et al., 2009). Therefore, at each stage in our continuum there would be a prolonged exposure to selective pressures on wing parameters. This finding of proportionally larger and more aerodynamically effective wings in juveniles is similar to what is seen in some modern birds where there is a delay in muscle growth that is compensated for by wing area (Heers et al., 2018). The finding of juveniles outpacing adults in or even being the major exploiters of aerial locomotion would not be a completely novel finding as juvenile flight capacity that is reduced or lost in adults has previously been proposed in another paravian *Deinonychus* (Parson and Parson, 2015) and is seen in extant avians across locomotion strategy (Heers et al., 2011; Heers and Dial, 2015).

In contrast to what is seen in *Microraptor*, in *Archaeopteryx* we see an n-shaped curve with optimality at the midsize range and similar levels seen at smaller and larger sizes. This is similar to what is seen in some modern birds such as chukars, where early fledglings to subadults show lower wing loadings than either prefledglings or mature adults (Jackson et al., 2009). What is potentially different in the case of the chukar is that while adults have lower wing loadings and wing areas than fledglings and subadults, they have larger flight muscle fractions, which may overcome this difference (Dececchi et al., 2016). We have little evidence that this occured in *Archaeopteryx*, but if so it would suggest that perhaps among the earliest flying members of Avialae the pressure to gain larger wings outpaced the evolution of larger muscles. This is a pattern that is seen in the ontogeny of some modern avians (Heers et al., 2014, 2016). What is interesting is that while the pattern of proportionally larger wings appears early in the ontogeny of *Microraptor* compared with a delayed peak in *Archaeopteryx*, both seem to show this "wings first" approach, suggesting that the traditional focus on large pectoral muscles as prerequisites for flight may be incorrect. Perhaps the major consideration is gaining sufficient wing area to achieve full body weight support, with muscle mass increase becoming more important both as size increased ontogenetically and as flight became more a canalized and centralized life-history trait phylogenetically.

CONCLUSIONS

We find that despite the generalized paravian bauplan and the shared feature of elongated hind limbs giving them a "four-winged" appearance similar to proposed models of flight origins (Beebe, 1915; Xu et al., 2003, 2014), our data strongly suggest that anchiornithines were not using their wings as an aerodynamic flight surface as they lack the features required to efficiently behave as either a gliding or a powered flapping structure. Such poor aerodynamic performance cannot be explained by a lack of selection in a vacant niche space because *Anchiornis* lived in the presence of better-performing gliding mammals (Meng et al., 2006, 2017; Luo et al., 2017) and powered-flying pterosaurs. If *Anchiornis* or its sister lineages were attempting to use their feathered limbs to fly, they were too awkward to catch prey or avoid becoming prey on the wing, lacked the ability to achieve precision landing or crash avoidance, and their nonarboreal body plan would have made climbing to a sufficient height difficult, moving among branches to launch dangerous, and landing from a glide near impossible. This does not preclude them from using their wings for some aerodynamic functions such as WAIR, flap running, or leaping (Dececchi et al., 2016), but this along with hind-limb structure and proportions (Dececchi and Larsson, 2011; 2013) argues for a terrestrial, nonvolant life history for this clade.

The lack of signs of flight among the most ancient members of the paravians does not mean that their feathered limbs did not have had some functional significance. They may have facilitated ground-based behaviors such as WAIR or increased leaping distance as suggested previously (Dececchi et al., 2016). In addition, we know that they possessed striking coloration, even iridescence, and frond-shaped tails (Li et al., 2010; Hu et al., 2018), suggesting that display was a likely major life-history trait. If we restrict anchiornithines from flight capability, we see similarities in the potential for wing use primarily or in conjunction with terrestrial flapping-based locomotion strategies, for display or signaling behaviors as proposed for other feathered theropods (Pittman et al., 2013; Person et al., 2014; Xing et al., 2016; Hu et al., 2018). Combined with developmental work suggesting that hind-limb feathers may have evolved due to constraints to evolve large forelimb feathers (Domyan et al., 2016), evidence suggests the origins of the "four-winged" state lies not in the air, but on the ground.

As early-diverging avialans predating the oldest-known *Archaeopteryx* specimen (see Pittman et al., chapter 1), our anchiornithine results suggest that flight was not present in the paravian common ancestor. While this conclusion is partially dependent on the phylogenetic hypothesis used to reconstruct the ancestral state, it is reinforced by other work showing little evidence of flight capability in troodontids, some of which also had elongate hind-limb feathers (Xu et al., 2017), and in most dromaeosaurids (Dececchi et al., 2016; Hartman et al., 2019; Pei et al., in press). Thus, regardless of whether anchiornithines were early-diverging troodontids (Hu et al., 2009), sister to both troodontids and dromaeosaurids (Hu et al., 2018), or early-diverging members of the avialans (Foth and Rauhut, 2017; Cau, 2018; Rauhut et al., 2019), the conclusion remains consistent. The only possible configuration that allows for a single origin in the literature is if microraptorines are not members of the Dromaeosauridae, but a separate, later-diverging clade (Agnolín and Novas, 2013; Agnolín et al., 2019). Yet, even in this case, flight capacity is lacking in the larger, earlier-diverging members of this group such as *Tianyuraptor* and *Zhenyuanlong* (Pei et al., in press) and achieved only in the *Microraptor* species complex itself (Dececchi et al., 2016; Pei et al., in press), suggesting it is not an ancestral trait for this lineage nor plesiomorphic for Averaptora (Agnolín and Novas, 2013). The different pattern of optimization of flight-related characters also suggests different strategies to achieve volancy in *Microraptor* and *Archaeopteryx*, while their hind-limb metrics suggest perhaps different ecological roles for each (Dececchi and Larsson, 2013; Pei et al., in press).

This strongly supports the contention that flight capacity and potentially powered flight itself arose convergently in at least two distinct paravian lineages, first in birds minimally 150 million years ago, then in the microraptorines 20–30 million years later. If true, this finding leads to new avenues of investigation that look at the place of each taxon within its ecosystem, in regards to both its terrestrial and aerial interactions. It also gives us a greater glimpse into the requirements for achieving flight from a theropod body, with both the convergent and the unique solutions to the physical problems of aerial travel giving us valuable information on what it takes to fly. These findings also help reinforce the notion that the nonavialan theropod to bird transition was not a simple linear path and that the behavioral and ecological roles of players on both sides of the transition were likely diverse. We see clearly that among members of the Deinonychosauria developing flight worthiness was only one of multiple trends in niche expansion in this clade (Turner et al., 2011; Lü and Brusatte, 2015; Cau et al., 2017; Xu et al., 2017; Torices et al., 2018) and complex in a way not previously appreciated.

ACKNOWLEDGMENTS

We would like to thank M. Pittman and X. Xu for organizing the International Pennaraptoran Dinosaur Symposium where an early version of this work was presented. As well as all those in attendance and our two anonymous reviewers whose suggestions and comments greatly improved this work. Finally, we wish to thank Kenneth H.C. Fung and First Initiative Foundation for supporting the symposium and the University of Hong Kong for hosting it.

REFERENCES

Agnolín, F., and F.E. Novas. 2013. Avian ancestors: a review of the phylogenetic relationships of the theropods Unenlagiidae, Microraptoria, *Anchiornis* and Scansoriopterygidae, Berlin: Springer Netherlands.

Agnolín, F.L., M.J. Motta, F. Brissón Egli, G. Lo Coco, and F.E. Novas. 2019. Paravian phylogeny and the dinosaur-bird transition: an overview. Frontiers in Earth Science 6: 252. [doi.org/10.3389/feart.2018.00252]

Alerstam, T., G.A. Gudmundsson, and L. Bertil. 1993. Flight tracks and speeds of Antarctic and Atlantic seabirds: radar and optical measurements. Philosophical Transactions of the Royal Society B 340: 55–67.

Alexander, D.E., E. Gong, L.D. Martin, D.A. Burnham, and A.R. Falk. 2010. Model tests of gliding with different hindwing configurations in the four-winged dromaeosaurid *Microraptor gui*. Proceedings of the National Academy of Sciences of the United States of America 107: 2972–2976.

Allen, V., K.T. Bates, Z. Li, and J.R. Hutchinson. 2013. Linking the evolution of body shape and locomotor biomechanics in bird-line archosaurs. Nature 497: 104.

Askew, G.N., R.L. Marsh, and C.P. Ellington. 2001. The mechanical power output of the flight muscles of blue-breasted quail (*Coturnix chinensis*) during take-off. Journal of Experimental Biology 204: 3601–3619.

Austin, G.T., and R.E. Ricklefs. 1977. Growth and development of the rufous-winged sparrow (*Aimophila carpalis*). Condor 79: 37–50.

Baier, D.B., S.M. Gatesy, and F.A. Jenkins, Jr. 2007. A critical ligamentous mechanism in the evolution of avian flight. Nature 445: 307–310.

Beebe, W.A. 1915. Tetrapteryx stage in the evolution of birds. Zoologica 2: 39–52.

Brougham, J., and S.L. Brusatte. 2010. Distorted *Microraptor* specimen is not ideal for understanding the origin of avian flight. Proceedings of the National Academy of Sciences of the United States of America 107: E155–E156.

Brusatte, S.L., G.T. Lloyd, S.C. Wang, and M.A. Norell. 2014. Gradual assembly of avian body plan culminated in rapid rates of evolution across the dinosaur-bird transition. Current Biology 24: 2386–2392.

Brusatte, S.L., J.K. O'Connor, and E.D. Jarvis. 2015. The origin and diversification of birds. Current Biology 25: R888–R898.

Burgers, P., and L.M. Chiappe. 1999. The wing of *Archaeopteryx* as a primary thrust generator. Nature 399: 60–62.

Burnham, D.A. 2007. *Archaeopteryx* – a re-evaluation suggesting an arboreal habitat and an intermediate stage in trees down origin of flight. Neues Jahrbuch für Geologie und Paläontologie 245: 33–44.

Campione, N.E., D.C. Evans, C.M. Brown, and M.T. Carrano. 2014. Body mass estimation in non-avian bipeds using a theoretical conversion to quadruped stylopodial proportions. Methods in Ecology and Evolution 5: 913–923.

Cau, A. 2018. The assembly of the avian body plan: a 160-million-year long process. Bollettino della Società Paleontologica Italiana 57: 1–25.

Cau, A., et al. 2017. Synchrotron scanning reveals amphibious ecomorphology in a new clade of bird-like dinosaurs. Nature 552: 395.

Chatterjee, S., and R.J. Templin. 2007. Biplane wing planform and flight performance of the feathered dinosaur *Microraptor gui*. Proceedings of the National Academy of Sciences of the United States of America 104: 1576–1580

Christiansen, P., and R.A. Farina. 2004. Mass prediction in theropod dinosaurs. Historical Biology 16: 85–92.

Dececchi, T.A., and H.C. Larsson. 2011. Assessing arboreal adaptations of bird antecedents: testing the ecological setting of the origin of the avian flight stroke. PLoS One 6: e22292.

Dececchi, T.A., and H.C. Larsson. 2013. Body and limb size dissociation at the origin of birds: uncoupling allometric constraints across a macroevolutionary transition. Evolution 67: 2741–2752.

Dececchi, T.A., H.C. Larsson, and M.B. Habib. 2016. The wings before the bird: an evaluation of flapping-based locomotory hypotheses in bird antecedents. PeerJ 4: e2159.

Dial, K.P., E. Greene, and D.J. Irischick. 2000. Allometry of behaviour. Trends in Ecology and Evolution 23: 394–401.

Domyan, E.T., et al. 2016. Molecular shifts in limb identity underlie development of feathered feet in two domestic avian species. eLife 5: e12115.

Dyke, G., et al. 2013. Aerodynamic performance of the feathered dinosaur *Microraptor* and the evolution of feathered flight. Nature Communications 4: 2489.

Emerson, S.B., and M.A.R. Koehl. 1990. The interaction of behavioural and morphological change in the evolution of a novel locomotor type: "flying" frogs. Evolution 44: 1931–1946.

Erickson, G.M., et al. 2009. Was dinosaurian physiology inherited by birds? Reconciling slow growth in *Archaeopteryx*. PLoS One 4: e7390.

Feduccia, A. 1996. The origin and evolution of birds. New Haven, CT: Yale University Press.

Feduccia, A., and S. Czerkas. 2015. Testing the neoflightless hypothesis: propatagium reveals flying ancestry of oviraptorosaurs. Journal of Ornithology 156: 1067–1074.

Feo, T.J., D.J. Field, and R.O. Prum. 2015. Barb geometry of asymmetrical feathers reveals a transitional morphology in the evolution of avian flight. Proceedings of the Royal Society of London B, Biological Sciences 282(1803): 20142864.

Foth, C., and O.W.M. Rauhut. 2017. Re-evaluation of the Haarlem *Archaeopteryx* and the radiation of maniraptoran theropod dinosaurs. BMC Evolutionary Biology 17: 236.

Foth, C., H. Tischlinger, and O.W.M. Rauhut. 2014. New specimen of *Archaeopteryx* provides insights into the evolution of pennaceous feathers. Nature 511: 79.

Godefroit, P., et al. 2013. Reduced plumage and flight ability of a new Jurassic paravian theropod from China. Nature Communications 4: 1394.

Gong, E., L.D. Martin, D.A. Burnham, A.R. Falk, and L.H. Hou. 2012. A new species of *Microraptor* from the Jehol Biota of northeastern China. Palaeoworld 21: 81–91.

Greenewalt, C.H. 1975. The flight of birds: the significant dimensions, their departure from the requirements for dimensional similarity, and the effect on flight aerodynamics of that departure. Transactions of the American Philosophical Society 65: 1–67.

Guillemette, M., and J.F. Ouellet. 2005. Temporary flightlessness in pre-laying Common Eiders *Somateria mollissima*: are females constrained by excessive wing-loading or by minimal flight muscle ratio? Ibis 147: 293–300.

Halsey, L.G. 2013. The relationship between energy expenditure and speed during pedestrian locomotion in birds: a morphological basis for the elevated y-intercept? Comparative Biochemistry and Physiology Part A, Molecular and Integrative Physiology 165: 295–298.

Han, G., et al. 2014. A new raptorial dinosaur with exceptionally long feathering provides insights into dromaeosaurid flight performance. Nature Communications 5: 4382.

Hartman, S., et al. 2019. A new paravian dinosaur from the Late Jurassic of North America supports a late acquisition of avian flight. PeerJ 7: e7247.

Heers, A.M., and K.P. Dial. 2015. Wings versus legs in the avian bauplan: development and evolution of alternative locomotor strategies. Evolution 69: 305–320.

Heers, A.M., B. Tobalske, and K.P. Dial. 2011. Ontogeny of lift and drag production in ground birds. Journal of Experimental Biology 214: 717–725.

Heers, A.M., K.P. Dial, and B.W. Tobalske. 2014. From baby birds to feathered dinosaurs: incipient wings and the evolution of flight. Paleobiology 40: 459–476.

Heers, A.M., D.B. Baier, B.E. Jackson, and K.P. Dial. 2016. Flapping before flight: high resolution, three-dimensional skeletal kinematics of wings and legs during avian development. PLoS One 11: e0153446.

Heers, A.M., J.W. Rankin, and J.R. Hutchinson. 2018. Building a bird: musculoskeletal modeling and simulation of wing-assisted incline running during avian ontogeny. Frontiers in Bioengineering and Biotechnology 6: 140. [doi.org/10.3389/fbioe.2018.00140]

Hirt, M.R., W. Jetz, B.C. Rall, and U. Brose. 2017. A general scaling law reveals why the largest animals are not the fastest. Nature Ecology and Evolution 1: 1116–1122.

Hu, D., L. Hou, L. Zhang, and X. Xu. 2009. A pre-*Archaeopteryx* troodontid theropod from China with long feathers on the metatarsus. Nature 461: 640.

Hu, D., et al. 2018. A bony-crested Jurassic dinosaur with evidence of iridescent plumage highlights complexity in early paravian evolution. Nature Communications 9: 217.

Hutchinson, J.R., and M. Garcia. 2002. *Tyrannosaurus* was not a fast runner. Nature 415: 1018.

Jackson, B.E., P. Segre, and K.P. Dial. 2009. Precocial development of locomotor performance in a ground-dwelling bird (*Alectoris chukar*): negotiating a three dimensional terrestrial environment. Proceedings of the Royal Society B, Biological Sciences 276: 3457–3466.

Koehl, M.A.R., D. Evangelista, and K. Yang. 2011. Using physical models to study the gliding performance of extinct animals. Integrative and Comparative Biology 51 (6): 1002–1018.

Lee, M.S., A. Cau, D. Naish, and G.J. Dyke. 2014. Sustained miniaturization and anatomical innovation in the dinosaurian ancestors of birds. Science 345: 562–566.

Lefèvre, U., et al. 2017. A new Jurassic theropod from China documents a transitional step in the macrostructure of feathers. Science of Nature 104: 74.

Li, Q., et al. 2010. Plumage color patterns of an extinct dinosaur. Science 327: 1369–1372.

Li, Q., et al. 2012. Reconstruction of *Microraptor* and the evolution of iridescent plumage. Science 335: 1215–1219.

Longrich, N. 2006. Structure and function of hindlimb feathers in *Archaeopteryx lithographica*. Paleobiology 32(3): 417- 431.

Lü, J.C., and S.L. Brusatte. 2015. A large, short-armed, winged dromaeosaurid (Dinosauria: Theropoda) from the Early Cretaceous of China and its implications for feather evolution. Scientific Reports 5: srep11775.

Luo, Z.X., et al. 2017. New evidence for mammaliaform ear evolution and feeding adaptation in a Jurassic ecosystem. Nature 548: 326.

Makovicky, P.J., and L.E. Zanno. 2011. Theropod diversity and the refinement of avian characteristics. *In* G. Dyke and G. Kaiser (editors), Living dinosaurs: the evolutionary history of modern birds: 9–29. Wiley, Hoboken.

Manafzadeh, A.R., and K. Padian. 2018. ROM mapping of ligamentous constraints on avian hip mobility: implications for extinct ornithodirans. Proceedings of the Royal Society B, Biological Sciences 285: 20180727.

Marden, J.H. 1987. Maximum lift production during takeoff in flying animals. Journal of Experimental Biology 130: 235–258.

Marden, J.H. 1994. From damselflies to pterosaurs: how burst and sustainable flight performance scale with size. American Journal of Physiology-Regulatory, Integrative and Comparative Physiology 266: R1077–R1084.

Martin, L.D. 1983. The origins of birds and avian flight. *In* R.F. Johnston (editor), Current Ornithology 1: 105–129.

McGuire, J.A., and R. Dudley. 2005. The cost of living large: comparative gliding performance in flying lizards (Agamidae: Draco). American Naturalist 166: 93–106.

McGuire, J.A., and R. Dudley. 2011. The biology of gliding in flying lizards (Genus *Draco*) and their fossil and extant analogs. Integrative and Comparative Biology 51: 983–990.

Meng, J., Y.M. Hu, Y.Q. Wang, X.L. Wang, and C.K. Li. 2006. A Mesozoic gliding mammal from northeastern China. Nature 444: 889.

Meng, Q.J., et al. 2017. New gliding mammaliaforms from the Jurassic. Nature 548: 291.

Meunier, K. 1951. Korrelation und Umkonstruktion in den grössenbeziehungen zwischen Vogelflügel und Vogelkörper. Biologia Generalis 19: 403–443.

Nudds, R.L., and D.M. Bryant. 2000. The energetic costs of short flights in birds. Journal of Experimental Biology 203: 1561–1572.

O'Connor, J.K., Z.H. Zhou, and X. Xu. 2011. Additional specimen of *Microraptor* provides unique evidence of dinosaurs preying on birds. Proceedings of the National Academy of Sciences of the United States of America 108: 19662–19665.

Palmer, C. 2014. The aerodynamics of gliding flight and its application to the arboreal flight of the Chinese feathered dinosaur *Microraptor*. Biological Journal of the Linnean Society 113: 828–835.

Parson, W.L., and K.M. Parson. 2015. Morphological variation with the ontogeny of *Deinonychus antirrhopus* (Theropoda, Dromaeosauridae). PLoS One 10: e0121476.

Person, W.S., P. Currie, and M.A. Norell. 2014. Oviraptorosaur tail forms and functions. Acta Palaeontologica Polonica 59: 553–567.

Pei, R., Q.G. Li, Q.J. Meng, M.A. Norell, and K.Q. Gao. 2017. New specimens of *Anchiornis huxleyi* (Theropoda: Paraves) from the Late Jurassic of northeastern China. Bulletin of the American Museum of Natural History 411: 1–66.

Pei, R., et al. In press. Potential for powered flight neared by most close avialan relatives but few crossed its thresholds. Current Biology.

Pennycuick, C.J. 1975. Mechanics of flight. Avian Biology 5: 1–73.

Pennycuick, C.J. 1989. Bird flight performance: a practical calculation manual. Oxford: Oxford University Press.

Pittman, M., S.M. Gatesy, P. Upchurch, A. Goswami, and J.R. Hutchinson. 2013. Shake a tail feather: the evolution of the theropod tail into a stiff aerodynamic surface. PLoS One 8: e63115.

Pontzer, H., V. Allen, and J.R. Hutchinson. 2009. Biomechanics of running indicates endothermy in bipedal dinosaurs. PLoS One 4: e7783.

Puttick, M.N., G.H. Thomas, and M.J. Benton. 2014. High rates of evolution preceded the origin of birds. Evolution 68: 1497–1510.

Rauhut, O.W.M., H. Tischlinger, and C. Foth. 2019. A non-archaeopterygid avialan theropod from the Late Jurassic of southern Germany. eLife 8: e43789.

Saitta, E.T., R. Gelernter, and J. Vinther. 2018. Additional information on the primitive contour and wing feathering of paravian dinosaurs. Palaeontology 61: 273–288.

Sellers, W.I., and P.L. Manning. 2007. Estimating dinosaur maximum running speeds using evolutionary robotics. Proceedings of the Royal Society B, Biological Sciences 274: 2711–2716.

Serrano, F.J., P. Palmqvist, L.M. Chiappe, and J.L. Sanz. 2017. Inferring flight parameters of Mesozoic avians through multivariate analyses of forelimb elements in their living relatives. Paleobiology 43: 144–169.

Socha, J.J., F. Jafari, Y. Munk, and G. Byrnes. 2015. How animals glide: from trajectory to morphology. Canadian Journal of Zoology 93: 901–924.

Sprague, R.S., and C.W. Breuner. 2010. Timing of fledging is influenced by glucocorticoid physiology in Laysan Albatross chicks. Hormones and Behavior 58: 297–305.

Stein, K., C. Palmer, P.G. Gill, and M.J. Benton. 2008. The aerodynamics of the British late Triassic Kuehneosauridae. Palaeontology 51: 967–981.

Stewart, P.A. 1958. Locomotion of wood ducks. Wilson Bulletin 70: 184–187.

Thorington, R.W., Jr., and L.R. Heaney. 1981. Body proportions and gliding adaptations of flying squirrels (Petauristinae). Journal of Mammalogy 62: 101–114.

Tobalske, B.W., and K.P. Dial. 2000. Effects of body size on take-off flight performance in the Phasianidae (Aves). Journal of Experimental Biology 203: 3319–3332.

Tobalske, B.W., and K.P. Dial. 2007. Aerodynamics of wing-assisted incline running in birds. Journal of Experimental Biology 210: 1742–1751.

Torices, A., R. Wilkinson, V.M. Arbour, J.I. Ruiz-Omeñaca, and P.J. Currie. 2018. Puncture-and-pull biomechanics in the teeth of predatory coelurosaurian dinosaurs. Current Biology 28: 1467–1474.

Turner, A.H., D. Pol, and M.A. Norell. 2011. Anatomy of *Mahakala omnogovae* (Theropoda: Dromaeosauridae), Tögrögiin Shiree, Mongolia. American Museum Novitates 3722: 1–66.

Turner, A.H., P.J. Makovicky, and M.A. Norell. 2012. A review of dromaeosaurid systematics and paravian phylogeny. Bulletin of the American Museum of Natural History 371: 1–206.

Usherwood, J.R. 2009. The aerodynamic forces and pressure distribution of a revolving pigeon wing. Experiments in Fluids 46: 991–1003.

van Oorschot, B.K., H.K. Tang, and B.W. Tobalske. 2017. Phylogenetics and ecomorphology of emarginate primary feathers. Journal of Morphology 278: 936–947.

Wang, Y.D., X.J. Yang, W. Zhang, S.L. Zheng, and N. Tian. 2006. Biodiversity and palaeoclimate of the Middle Jurassic floras from the Tiaojishan Formation in western Liaoning, China. Progress in Natural Science 16: 13–20.

Warrick, D., M.W. Bundle, and K.P. Dial. 2002. Bird maneuvering flight: blurred bodies, clear heads. Integrative and Comparative Biology 42: 141–148.

Wright, J., S. Markman, and S.M. Denney. 2006. Facultative adjustment of pre-fledging mass loss by nestling swifts preparing for flight. Proceedings of the Royal Society B, Biological Sciences 273: 1895–1900.

Xing, L.D., et al. 2016. A feathered dinosaur tail with primitive plumage trapped in mid-Cretaceous amber. Current Biology 26: 3352–3360.

Xu, X., et al. 2003. Four-winged dinosaurs from China. Nature 421: 335–340.

Xu, X., H.L. You, K. Du, and F.L. Han. 2011. An *Archaeopteryx*-like theropod from China and the origin of Avialae. Nature 475: 465.

Xu, X., et al. 2014. An integrative approach to understanding bird origins. Science 346: 1253293.

Xu, X., et al. 2015. A bizarre Jurassic maniraptoran theropod with preserved evidence of membranous wings. Nature 521: 70–73.

Xu, X., et al. 2017. Mosaic evolution in an asymmetrically feathered troodontid dinosaur with transitional features. Nature communications 8: 14972.

Yalden, D.W. 1984. What size was *Archaeopteryx*? Zoological Journal of the Linnean Society 82: 177–188.

Zheng, X.T., et al. 2013. Hind wings in basal birds and the evolution of leg feathers. science 339: 1309–1312.

Chapter 12

Navigating Functional Landscapes: A Bird's Eye View of the Evolution of Avialan Flight

HANS C.E. LARSSON,[1] T. ALEXANDER DECECCHI,[2] MICHAEL B. HABIB[3]

ABSTRACT

One of the major challenges in attempting to parse the ecological setting for the origin of flight in Pennaraptora is determining the minimal fluid and solid biomechanical limits of gliding and powered flight present in extant forms and how these minima can be inferred from the fossil record. This is most evident when we consider the fact that the flight apparatus in extant birds is a highly integrated system with redundancies and safety factors to permit robust performance even if one or more components of their flight system are outside their optimal range. These subsystem outliers may be due to other adaptive roles, ontogenetic trajectories, or injuries that are accommodated by a robust flight system. This means that many metrics commonly used to evaluate flight ability in extant birds are likely not going to be precise in delineating flight style, ability, and usage when applied to transitional taxa. Here we build upon existing work to create a functional landscape for flight behavior based on extant observations. The functional landscape is like an evolutionary adaptive landscape in predicting where estimated biomechanically relevant values produce functional repertoires on the landscape. The landscape provides a quantitative evaluation of biomechanical optima, thus facilitating the testing of hypotheses for the origins of complex biomechanical functions. Here we develop this model to explore the functional capabilities of the earliest known avialans and their sister taxa. This mapping allows us to determine where they are placed on the landscape and how phylogenetic trends may course over the landscape. Moreover, the mapping develops a novel tool for assessing potential selection pressures and directions using the quantitative tools developed for adaptive landscapes. Combining these findings with previous work on the ontogeny of the flight stroke, especially in chukar partridges, allows us to test whether this widely used proxy is really suitable and whether we can use ontogenetic trajectories for reconstructing the evolutionary trajectory of the nonavialan theropod to bird transition.

INTRODUCTION

What does it take to fly? This simple question pervades all aspects of research into the origin of birds. For decades it was assumed that feathers were the key innovation that determined flight capability, and their presence was the direct result of an adaptation for aerial locomotion (Heilmann, 1926; Regal, 1975; Feduccia, 1996; Czerkas and Feduccia, 2014). The recent feathered dinosaur renaissance, led by findings from the Middle-Late Jurassic and Early Cretaceous of China has not only put an end to that line of reasoning, but also increased our knowledge of

---

[1] Redpath Museum, McGill University, Montreal.

[2] Division of Natural Sciences, Mount Marty College, Yankton, SD.

[3] Natural History Museum of Los Angeles County, Los Angeles.

early-diverging avialans many times over (O'Connor and Zhou, 2015), solidified the link between nonavialan theropod dinosaurs and birds (Makovicky and Zanno, 2011; Brusatte et al., 2014, 2015; Xu et al., 2014), and provided us with a trove of feathered sister lineages both predating and postdating the earliest birds (Xu et al., 2003, 2011, 2014, 2015; Zhang et al., 2008; Hu et al., 2009, 2018; Han et al., 2014).

Prior to these discoveries the phylogenetic, temporal, and morphological gap between *Archaeopteryx*, the first bird, and its closest relatives was significant, making reconstructions of potential evolutionary pathways through the transition controversial and speculative (Nopsca, 1907; Heilmann, 1926; Ostrom, 1974; Martin, 1983; Norberg, 1985; Feduccia, 1996; Dudley et al., 2007). New information, including details from the use of laser-stimulated fluorescence, or LSF (Falk et al., 2016; Kaye et al., 2015; Kaye et al., 2019a, 2019b; Wang et al., 2017; see also Serrano et al., chapter 13), and a better understanding of how skeletal, integumentary, and other soft tissues evolved across this transition are influencing biomechanical reconstructions of early flight potential and behavior. As that new information is combined with modeling work (Burgers and Chiappe, 1999; Han et al., 2014; Dececchi et al., 2016; Serrano and Chiappe, 2017; Serrano et al., 2018; see also chapter 13) and investigations of modern nonflight-related wing functions (Tobalske and Dial, 2007; Jackson et al., 2009; Fowler et al., 2011; Heers et al., 2014, 2016), we begin to understand not only what features flying organisms possess, but also what minimum values are necessary for these features to permit flight, even if it is weak and of short duration. Here we set up a novel framework for addressing how to evaluate the biomechanical gap between fliers and their antecedents.

Landscapes have played a central role in interpreting evolutionary change. Wright (1932) introduced the adaptive landscape as a tool for use with population genetics and fitness. Simpson (1944, 1953) modified it for discussions of how phenotypic variation can be mapped to fitness. Simpson also expanded this concept from its origin in population genetics to large-scale adaptive evolution across species. In their current usage, adaptive landscapes describe the relationship between mean population fitness and mean population trait values across a pool of populations (Lande, 1976, 1979; Schluter, 2000; Arnold et al., 2001) where traits are typically phenotypic in nature. The phenotypes measured between populations are required to be equivalent, thus necessitating the population samples to be either of the same or closely related species. However, because population fitness is dependent upon external factors, such as local climate and ecology, as well as internal factors, such as genetic drift, the landscape can not be static and is instead more appropriately considered a continually shifting "seascape" (Mustonen and Lassig, 2009; Steinberg and O'Stermeier, 2016). These properties make the use of adaptive landscapes difficult over long periods of time.

However, the approach of developing landscapes to interpret multidimensional data has merit. Strictly, though, adaptive landscapes may be impossible to apply to evolutionary events in deep time, simply because of the length of time involved. The fitness of populations of extinct species cannot be determined beyond their presence or absence (survival or extinction), producing a rather rarified, binary z-axis. However, adaptive landscapes offer quantitative properties that can be used to calculate a variety of variables relevant to evolutionary biology, including modeling drift, adaptation, evolutionary rates, and developmental processes underlying adaptive evolution (Rice, 2004; 2012).

We propose a novel landscape approach to examine evolutionary variation. Instead of a landscape determined by fitness or survival, we propose one calibrated on physical limitations. The axes are defined by phenotypic measures that are as orthogonal to one another as conceptually possible to maintain some semblance of independence. In combination, these axes create a space wherein functional inferences can be mapped. We call this landscape a functional landscape. Although this landscape does not directly test function, it maps where the observed, or estimated, phenotypes of taxa lie and presents a manifold by which we can draw conclusions about how particular functions map across those taxa.

To introduce this functional landscape, we present an example using powered flight and the origin of birds. Powered flight requires an aerofoil of sufficient surface area and sufficient thrust integrated over mass. Higher thrust generation at a given mass reduces the required aerofoil surface area. However, in animal-powered flight, the aerofoil itself is used to produce thrust and, in most cases, lift. Therefore, increasing aerofoil area is constrained by the requirement of increased flight muscle power. In general, increased muscle power requires increased muscle mass, which increases body mass, thereby requiring a larger aerofoil. These constraints put severe limitations on extreme biomechanical functions like powered flight, especially when considering that all other physiological functions of the animal are present as well.

Starting with first principles, we limit our functional landscape to three basic factors: body mass, wing area, and pectoral muscle mass. These essentially capture the fundamental aspects of flight: the mass to get airborne, the lifting surface size, and the power to drive the aerofoil. To limit autocorrelation, we subtract pectoral muscle mass from total body mass. These three factors are used only for the discussion of the potential of powered flight. Performance estimates and flight initiation, maneuverability, speed, efficiency, and landing cannot be deduced from these factors and require further information on wing aspect ratio, feather variation, body shape, muscle physiology, and tail shape, to name a few. However, our intent is that our simple functional landscape will result in a quantitative manifold so we can compare where different functional repertoires exist, trace evolutionary hypotheses, and plot potential routes through the landscape as hypotheses of evolutionary change.

METHODS

To obtain the largest and most diverse sample in terms of taxonomy, behavior, ecology, and morphology of extant flying birds we used published data that directly measured specimens (Heers and Dial, 2015; Wang et al., 2018). We also included measurements from metaanalyses (Greenewalt, 1975; Alerstam et al., 2007; Serrano et al., 2017; Wang et al., 2018). No flightless extant birds were used in this introductory analysis. Body masses for fossils were estimated from a combination of femoral length (Christiansen and Farina, 2004), femoral circumference (Campione et al., 2014), and 3-D reconstructions (Chatterjee and Templin, 2007; Dyke et al., 2013) to give a range of values, instead of a single value, because of the importance associated with this metric. For nonavialan theropods, primary feather length, when present, was either taken from the literature or was measured directly from images. In the latter case we verified our technique against other elements with recorded values in the literature; in all cases they differed by no more than 2%. For early-diverging birds we chose to use the dataset of Wang et al. (2018) with the addition of femoral lengths taken from several sources: Mayr et al. (2007) for *Archaeopteryx*, Chiappe et al. (2008) for *Confuciusornis*, and Benson and Choiniere (2013) supplying the rest. We chose to take our forelimb metrics from a single source to maintain a consistent measurement pattern for these taxa. Wing areas of extant birds are from Greenewalt (1975). Wing areas for fossils were estimated by following the methodology outlined in Dececchi et al. (2016) or taken directly from Wang et al. (2018) based on the multidimensional approach suggested by Serrano et al. (2017).

Pectoral muscle mass data of extant birds was taken from Greenewalt (1975). Only masses for the pectoralis major were used, in order to limit our landscape to the downstroke, which represents the most rudimentary requirement for flight. The pectoralis complex represents the majority of the flight muscle mass in extant birds, comprising 60% or more of the total forelimb mass in many birds (Hartman, 1961; Biewener, 2011). Other forelimb muscles are important for dynamic aspects of flight such as takeoff and landing (Dial, 1993). However, the pectoral muscle is the primary downstroke muscle. One major issue in comparing extant birds with earlier-diverging birds, and especially early-diverging paravian theropods, is the change of the supracoracoideus' role in the flight stroke. Due to the absence of a triosseal canal in nonavialan theropods and the earliest-diverging avialan taxa, the supracoracoideus could not act as a wing elevator. Nor was there a ligament-based stabilization system for the shoulder joint, but instead a muscle-based one in nonavialans. A ligamentous system did not evolve until well after the transition from nonavialan theropod to bird (Baier et al., 2007). In a muscle-based system, the shoulder and back muscles were likely used to elevate the wing as well as stabilize the glenoid (Baier et al., 2007). The forelimb muscles likely had a larger role in wing action, similar to what is seen in nonsteady aspects of modern bird flight (Dial, 1993). To minimize the effect of such a drastic change in the muscle proportion, as a percentage of both the flight muscle and the total body, and the shifting role of the pectoralis minor back/shoulder musculature along this transition we chose to focus only on the mass of pectoralis major as its role as the major wing depressor and its thrust generator should remain constant.

Pectoral muscle masses were estimated for all fossil taxa. Extant birds range from 6% in the Red-throated loon to 30% in the Stripe-tailed hummingbird. A value of 10% was used to estimate pectoral masses for Mesozoic birds and nonavialan paravians. This figure was chosen as it: (1) represents the lower bounds seen in competent extant flying birds (Greenewalt, 1975) and bats (Bullen and McKenzie, 2004) and (2) corresponds to the flight muscle mass estimates generated using 3-D volumetric models of the paravians *Microraptor* (Allen et al., 2013) and *Archaeopteryx* (Allen et al., 2013; Heers et al., 2016). These may be higher than what was present, given the absence of sternal keels in these taxa. Sternal keels are also absent in early-diverging birds such as *Sapeornis* and *Jeholornis* (O'Connor et al., 2015; Zhao et al., 2017) and highly reduced to absent in all but the most mature specimens of *Confuciusornis* (O'Connor et al., 2015) further implying relatively rudimentary flight capabilities of these taxa. The lower bound for extant birds is in flightless ratites. The pectoral muscles in the ostrich comprise less than 2.4% of their body mass (Dijana et al., 2010), giving a lower bound for paravians. Extant flightless neognath birds have pectoral mass percentages between 8%–15%, but using them as flightless proxies is likely confounded by their relatively recent evolution to flightlessness (McNab, 1994). In addition, relative forewing length (skeleton forelimb to hindlimb) is between 39%–45% in ostriches (Gatesy and Middleton, 1997; Middleton and Gatesy, 2000), whereas it is 68%–76% in *Microraptor* (see Dececchi et al., chapter 11) and the ability to generate aerodynamic forces (Davis, 2005) is significantly smaller in the ostrich than in these paravians, suggesting again that they possessed larger pectoral limb muscles. The pectoral muscles of extant crocodylians make up only 0.7% of their body mass (calculated from data from Allen et al., 2013), though they also have proportionally smaller pectoral limb masses than paravians, but more similar to earlier-diverging theropods (Allen et al., 2013). Therefore, for nonparavian theropods we used an estimate of 2% for pectoral masses with the exception of 1% for short-armed tyrannosaurids.

All supplemental data used is hosted at Open Science Framework (https://osf.io/26ka8/?view_only=74c334b283704479b7682871772cbb35).

RESULTS

Beginning with two variables, body mass to pectoral mass and body mass to wing area yield correlated and well distributed plots (fig. 1). In extant birds, wing area is well predicted by mass ($r^2 = 0.91$) and pectoral mass by body mass ($r^2 =$

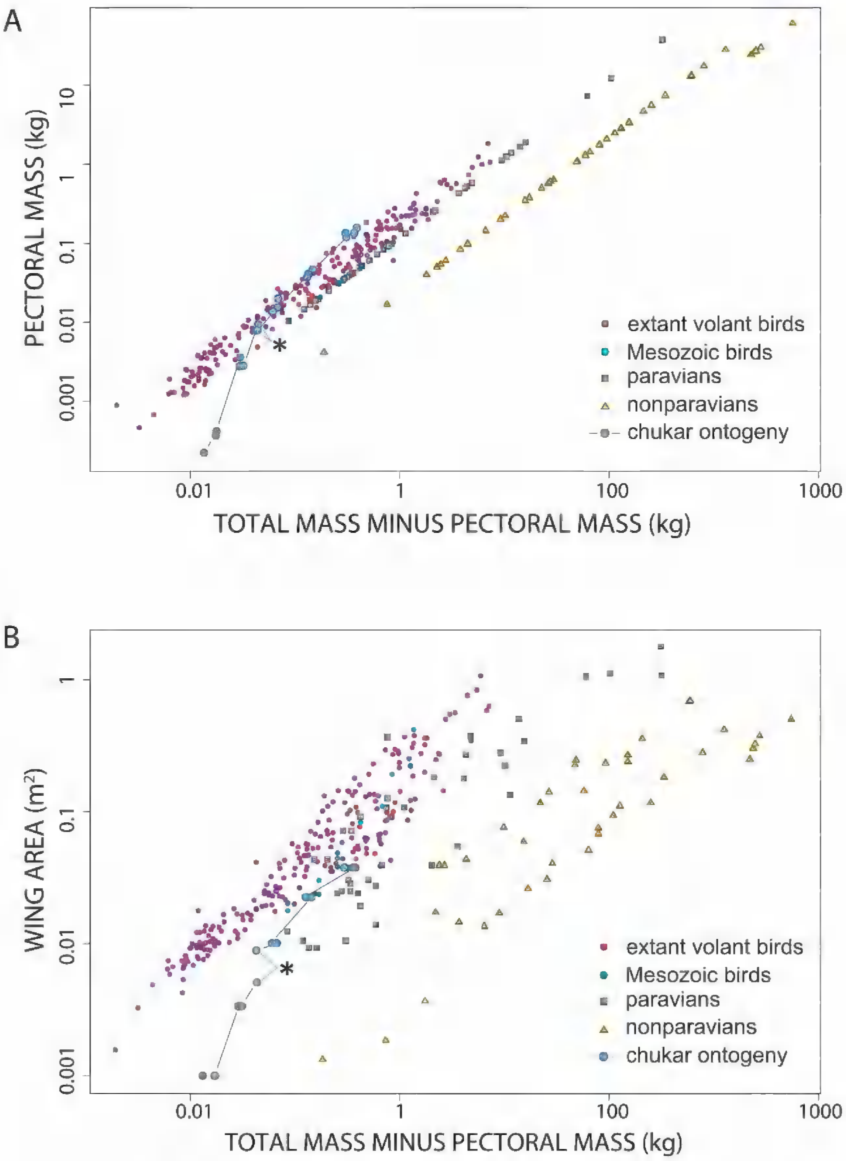

FIG 1. Log axis scatterplots of body mass, pectoral muscle mass, and wing area for extant and Mesozoic birds and nonavialan theropods. The asterisk indicates the range where chukar chicks fledge.

0.97). Pectoral mass plots linearly for the fossil taxa because of the simple estimates used. However, even with the generous 2% of body mass estimated for pectoral muscle mass for nonparavian theropods, they plot at a lower intercept than values for extant birds. The 10% pectoral estimate used for paravians and fossil birds aligns them to the lower boundary of extant birds (fig. 1A). However, wing area is more directly estimated from fossils and these taxa plot at well below the lower bounds of extant birds (fig. 1B). The one exception is *Microraptor* (IVPP V13352), with its lower mass estimate of 0.88 kg and wing area of 0.1051281 m^2.

Chukar values were used from Heers et al. (2015). These individuals represent an ontogenetic range from 3 days posthatching (dph) to 100 dph. In both graphs, chukar ontogeny plots on a relatively directed path into the range of extant birds.

When combining these three factors to construct a landscape, the data creates a surprisingly well-resolved surface (fig. 2). The spline is plotted as a smoothed regression through the entire dataset and no taxon deviates greatly from this spline. Extant birds lie along a distinct ridge on the manifold, with Mesozoic birds, paravians, and nonparavian theropods falling further downslope, respectively. As in the 2-D plots, chukar ontogeny traces a trajectory from nonparavian theropods to extant birds and lies close to the regression surface.

DISCUSSION

Unsurprisingly, the relative phylogenetic proximity of different theropod groups to birds is reflected in their mass to pectoral mass to wing areas. This relationship describes a complex manifold with extant birds occupying a sharp ridge with their antecedents, generally, at lower elevations. The lower elevations for these antecedents would be even steeper if more conservative estimates for pectoral masses were used. The ridge extant birds occupy is shaped into a ridge because of a few birds with relatively high wing areas but low pectoral masses. The sharp boundaries of where extant birds plot on the landscape implies birds may be operating within high levels of constraint to the variables of body mass, wing area, and pectoral mass. Variation in any variable has functional consequences on the other variables that in turn affect powered flight. Birds appear to be functioning in a very constricted range of these variables to maintain powered flight.

Mesozoic birds and many nonavialan paravians plot within and just downslope of extant birds. The surface extending from them to nonparavian theropods forms a smooth surface, suggesting the variables are mapping a continuum between species. By this, we mean that the variables observed in these taxa do not seem to obviously deviate from a simple landscape.

If we consider this functional landscape as a surface where evolutionary change must traverse, we can ask how particular starting points may track to end points. The shortest traverse from nonavialan to avialan realms is at small body size. In this region, nonvolant and volant taxa approach each other, implying that functionally, the step to flight may be easiest at small body sizes. This correlation has been suggested by many others, but the landscape provides a visual representation of the potential route. Larger-bodied nonparavian theropods not only have to climb further along the landscape to approach the avialan realm, but also have to climb a steeper slope. Slope and distance are used in adaptive landscape modeling to estimate evolutionary trajectories (Rice, 2004). One could use this functional landscape to estimate the evolutionary "effort" required for a large-bodied nonparavian to either track directly upslope, track along a contour, or reduce body size and then track upslope or along contours.

Very small body size evolved in the bizarre Scansoriopterygidae. This radiation of maniraptorans evolved membrane-based wings supported by elongate fingers. Adult specimens of *Yi qi* and *Ambopteryx longibrachium* have been estimated to have body masses of approximately 300 g, making them some of the smallest nonavialan theropods (Xu et al., 2015; Wang et al., 2019). This radical departure from the theropod body plan and novel wings may have been facilitated by their very small body size, making them more capable of crossing into new locomotory realms. Their ability to move with powered flight is questionable, but their foray into at least a gliding mode seems reasonable given their small body size.

An argument using an ontogenetic example of the origins of bird flight comes from juvenile chuckars. Young individuals not yet capable of flight can use their wings to assist in incline running (Dial, 2003). Interestingly, the youngest chuckar samples (3–8 dph) plot in the ranges

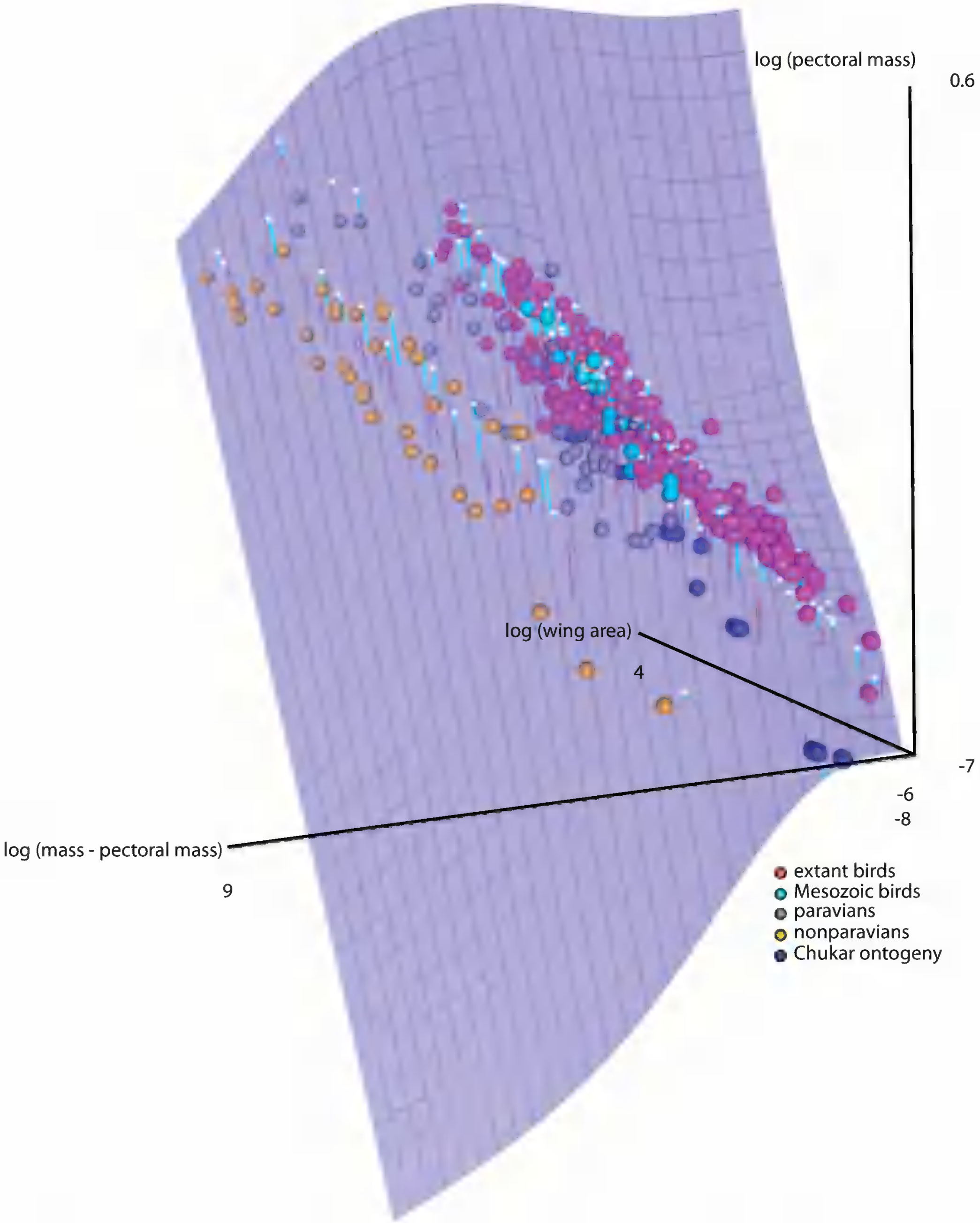

FIG. 2. Three axes scatterplot of a functional landscape of Theropoda flight capability as estimated by logged body mass, pectoral muscle mass, and wing area. The surface is a smoothed regression through all the points. The surface has a discrete ridge on which extant volant birds lie on whereas all nonavialan theropods plot on its slope.

from nonparavian theropods to paravians. Chukars of 0–5 dph are capable only of low-angle wing-assisted incline running. At this age, these birds are less than 20 g in body mass and either crawl or asymmetrically flap their wings to produce forces of approximately 6%–10% of their body weight (Jackson et al., 2009; Heers et al., 2011, 2014). They are able to ascend inclines of less than 65°, slightly greater than the level that they can ascend using their legs alone (55°–60°) (Bundle and Dial, 2003; Dial et al., 2006). However, any growth trajectory would be expected to pass this route given that birds are not born in their adult form. Chukars fledge between 14 and 18 dph, and this is the range where the chukar trajectory passes into the realm of extant birds. In spite of this extreme ontogenetic trajectory, chuckar ontogeny still plots relatively close to the functional landscape.

Further refinements are required before evolutionary models across this functional landscape can be made. In particular, more accurate estimates of body mass and pectoral mass are needed to better shape the landscape. Directly preserved body outlines would be particularly helpful in this regard with a range of obscured and otherwise invisible ones already revealed by LSF imaging (Falk et al., 2016; Wang et al., 2017; see also Serrano et al., chapter 13). Other variables, such as flapping rate, metabolic costs, wing aspect ratio, and patagium and feather properties may prove useful to differentiate between alternative hypothetical evolutionary routes. Additionally, anatomical variables, such as bone segment lengths would help construct biomechanical models at each position on the functional landscape. Furthermore, as the interrelationships among the nonavialan paravian groups and early diverging birds get more clearly resolved (see discussion of said topic in Pittman et al., chapter 2), accounting for phylogenetic signal among these variables, as well as discussions on clade-specific apomorphies that could alter flight style and ability, can and must be incorporated. Currently there is little evidence for significant differences in the material properties of the wings, distribution of muscle fiber types or metabolic rates among paravian lineages, but if discovered they could lead to an expansion or contraction of the landscape volume occupied by that group.

Although there are many caveats to estimating body mass, the major cause of concern here is our estimation of the proportion of fossil taxa pectoral muscle masses. There have been previous estimates of exceedingly low values (0.5% of body mass for *Archaeopteryx* according to Bock, 2013) that resemble those seen in flightless ratites such as the kiwi (McNab, 1994) and would, if verified, preclude any aerial locomotion in this taxa. We reject this extremely low mass estimate for flight muscle reconstruction for several reasons: (1) Recent 3-D volumetric approaches estimate the pectoral limb mass at greater than 12% total mass (Allen et al., 2013). This mass estimate does include the wing skeleton (though not feathers), but as skeletal mass averages only around 6% of total mass in extant birds (Martin-Silverstone et al., 2015) it is unlikely this is a major factor. It is also unclear if this estimate includes all the flight related musculature in the trunk region especially shoulder and back muscle, which would have a greater role in the flight stroke and wing stabilization before the origin of the ligament-based wing system of extant birds. (2) Although flight muscles in extant birds often account for a significant percentage we do know that juvenile birds often fledge with a significantly lower volume of flight muscles than adults. In chukars fledging occurs with flight muscles between one-half and two-thirds the adult percentage, with similar values for sparrows and wrens, with pectoral muscle mass making up around 10% of total body mass (Austin and Ricklefs, 1977; Heers and Dial, 2015; Heers et al., 2018). This supports recent work suggesting that it is likely wing size rather than muscle size that is a major limiting factor on the origins of flight (Heers et al., 2018). There is also evidence that suggests wing bone growth rate is the strongest influence on fledging time, suggesting that for longer-winged birds getting the wing size, not the pectoral size, right is what controls when they first take to the air (Carrier and Auriemma, 1992). For these reasons we feel that, at least for large-winged paravians near the transition, flight muscle size should not be considered an a priori reason to exclude them from the avialan realm on the functional landscape, and that it should be examined along with other variables like wing size (as estimated by wing loading) and shape when estimating flight potential, ability, and style. As an example, although *Archaeopteryx* was relatively light, at approximately 300 g for the largest specimens (Elzanowski, 2002), and surely had relatively small pectoral muscles originating on its unkeeled sternum, this taxon may still compare well with extant volant birds in terms of ability to achieve the thresholds of powered flight. Pigeons have similar body masses (300–400 g) but have pectoral muscle masses of up to 20% their total body mass. The wing areas of both taxa are similar (Dececchi et al., 2016), yet the additional surface areas from the elongate tail of *Archaeopteryx* are much larger. These additional flight surfaces likely contributed to the flight capabilities of these early birds and should be incorporated somehow into the functional landscape.

This raises the possibility that the real crux of the question "How do you make a flying bird?" may not be simply a question of what happened between nonavialan Paraves and Avialae, or even within early birds. Instead, this question may be more aptly directed toward the broader phylogenetic range between nonparavian and avialan taxa. Culminations of several overarching trends within theropods appear at Paraves: body size reduction (Carrano, 2006; Turner et al., 2012; Dececchi and Larsson, 2013; Lee et al., 2014), which is correlated with relative forelimb elongation (Benson and Choiniere, 2013; Dececchi and Larsson, 2013), pennaceous feather development and elongation (Foth et al., 2014), and changes to the pectoral girdle and enhanced range of motion (Turner et al., 2012). All these factors are prerequisites for powered flight and, as shown here, given the size range that many paravians occupy, with these fundamental aspects of the bauplan in place, bridging the gap between flightless and flighted individuals is not a huge evolutionary step. In fact, it mirrors in many ways what is seen in juvenile birds as proposed previously by Dial and colleagues (Davis, 2005; Tobalske and Dial, 2007; Jackson et al., 2009; Heers et al., 2011, 2014, 2016) with the small body size and large wing areas helping to compensate for lower relative pectoral mass, assuming they are within the range of 8%–10% of total mass.

The real question is how this extreme evolutionary change started and what were the drivers within paravians that fostered it, since it is divorced from either the selective pressures that drove the previously mentioned long-term trends within theropods. Multiple scenarios, from wing-assisted incline running (Heers et al., 2014), stability flapping during prey capture (Fowler et al., 2011), thrust production to increase running speed (Burgers and Chiappe, 1999), to increasing leaping distance and/or height for prey capture (Caple et al., 1983) have been suggested. These are all functionally and ecologically plausible and resemble behaviors seen in extant analogs. Although we do not as yet have any way to conclusively discern which of these behaviors, alone or in combination, influenced lineages within Paraves (but see Dececchi et al., 2016, for some insight into this issue), refocusing our investigations onto the multitude of small-bodied paravians may provide more insight to how dinosaurs tinkered at their functional limits before eventually conquering the air.

ACKNOWLEDGMENTS

Helpful comments and editorial suggestions were provided by Fernando Novas and Michael Pittman. Support for this project was provided by an NSERC Discovery Grant to HCEL. Special thanks go toward Michael Pittman and Xing Xu for invitation to the International Pennaraptoran Symposium held at the University of Hong Kong. The support by Kenneth H.C. Fung and First Initiative Foundation is gratefully acknowledged for supporting the symposium.

REFERENCES

Alerstam, T., M. Rosen, J. Backman, P.G.P. Ericson, and O. Hellgren. 2007. Flight speed among bird species: allometric and phylogenetic effects. PLoS Biology 5: e197.

Allen, V., K.T. Bates, Z. Li, and J.R. Hutchinson. 2013. Linking the evolution of body shape and locomotor biomechanics in bird-line archosaurs. Nature 497: 104.

Arnold, S.J., M.E. Pfrender, and A.G. Jones. 2001. The adaptive landscape as a conceptual bridge between micro- and macroevolution. Genetica 112, 9–32.

Austin, G.T., and R.E. Ricklefs. 1977. Growth and development of the rufous-winged sparrow (*Aimophila carpalis*). Condor 79: 37–50.

Baier, D.B., S.M. Gatesy, and F.A. Jenkins Jr. 2007. A critical ligamentous mechanism in the evolution of avian flight. Nature 445: 307–310.

Benson, R.B.J., and J.N. Choiniere. 2013. Rates of dinosaur limb evolution provide evidence for exceptional radiation in Mesozoic birds. Proceedings of the Royal Society B: Biological sciences 280: 20131780–20131780.

Biewener, A.A. 2011. Muscle function in avian flight: achieving power and control. Philosophical Transactions of the Royal Society of London Series B, Biological Sciences 366: 1496–1506.

Bock, W.J. 2013. The furcula and the evolution of avian flight. Paleontological Journal 47: 1236–1244.

Brusatte, S.L., G.T. Lloyd, S.C. Wang, and M.A. Norell. 2014. Gradual assembly of avian body plan culminated in rapid rates of evolution across the dinosaur-bird transition. Current Biology 24: 2386–2392.

Brusatte, S.L., J.M.K. O'Connor, and E.D. Jarvis. 2015. The origin and diversification of birds. Current Biology 25: R888–R898.

Bullen, R.D., and N.L. McKenzie. 2004. Bat flight-muscle mass: implications for foraging strategy. Australian Journal of Zoology 52: 605–622.

Bundle M.W., Dial K.P. 2003. Mechanics of wing-assisted incline running (WAIR). Journal of Experimental Biology 206: 4553–4564.

Burgers, P., and L.M. Chiappe. 1999. The wing of *Archaeopteryx* as a primary thrust generator. Nature 399: 60–62.

Campione, N.E., D.C. Evans, C.M. Brown, and M.T. Carrano. 2014. Body mass estimation in non-avian bipeds using a theoretical conversion to quadruped stylopodial proportions. Methods in Ecology and Evolution 5: 913–923.

Caple, G., R.P. Balda, and W.R. Willis. 1983. The physics of leaping animals and the evolution of preflight. American Naturalist 121: 455–476.

Carrano, M.T. 2006. Body-size evolution in the Dinosauria. *In* M.T. Carrano, T.J. Gaudin, R.W. Blob, and J.R. Wible (editors), Amniote paleobiology: perspectives on the evolution of mammals, birds, and reptiles: 225–268. Chicago: University of Chicago Press.

Carrier, D.R., and J. Auriemma. 1992. A developmental constraint on the fledging time of birds. Biological Journal of the Linnean Society 47: 61–77.

Chatterjee, S., and R.J. Templin. 2007. Biplane wing planform and flight performance of the feathered dinosaur *Microraptor gui*. Proceedings of the National Academy of Sciences of the United States of America 104: 1576–1580.

Chiappe, L.M., J. Marugán-Lobón, S.A. Ji, and Z.H. Zhou. 2008. Life history of a basal bird: morphometrics of the Early Cretaceous *Confuciusornis*. Biology Letters 4: 719–723.

Christiansen, P., and R.A. Fariña. 2004. Mass prediction in theropod dinosaurs. Historical Biology 16: 85–92.

Czerkas, S., and A. Feduccia. 2014. Jurassic archosaur is a non-dinosaurian bird. Journal of Ornithology 155: 841–851.

Davis, H.D. 2005. Negotiating a three-dimensional environment: limb kinematics of terrestrial birds during sloped ascents. Ph.D. thesis, University of Montana, Missoula.

Dececchi, T.A., and H.C.E. Larsson. 2013. Body and limb size dissociation at the origin of birds: uncoupling allometric constraints across a macroevolutionary transition. Evolution 67: 2741–2752.

Dececchi, T.A., H.C.E. Larsson, and M.B. Habib. 2016. The wings before the bird: an evaluation of flapping-based locomotory hypotheses in bird antecedents. PeerJ 4: e2159.

Dial, K.P. 1993. Avian forelimb muscles and non-steady flight: can birds fly without using the muscles in their wings? Auk 109: 874–885.

Dial K.P. 2003. Wing-assisted incline running and the evolution of flight. Science 299: 402–404.

Dial K.P., R.J. Randall, T.R. Dial. 2006. What use is half a wing in the ecology and evolution of birds? Bioscience 56: 437–445.

Dijana, N., P. Zlatko, and L. Slobodan. 2010. Evaluation of the ostrich carcass reared and slaughtered in Macedonia. Tehnologija Mesa 51: 143–148.

Dudley, R., et al. 2007. Gliding and the functional origins of flight: biomechanical novelty or necessity?

Annual Review Ecology, Evolution and Systematics 38: 179–201.

Dyke, G., et al. 2013. Aerodynamic performance of the feathered dinosaur *Microraptor* and the evolution of feathered flight. Nature Communications 4: 2489.

Elzanowski A. 2002. Archaeopterygidae. *In* L.M. Chiappe, and L.M. Witmer (editors), Mesozoic birds: above the heads of dinosaurs: 129–159. Berkeley: University of California Press.

Falk, A.R., T.G. Kaye, Z.H. Zhou, and D.A. Burnham. 2016. Laser fluorescence illuminates the soft tissue and life habits of the Early Cretaceous bird *Confuciusornis*. PLoS One 11: e0167284.

Feduccia, A. 1996. The origin and evolution of birds. New Haven, CT: Yale University Pres.

Foth, C., H. Tischlinger, and O.W. Rauhut. 2014. New specimen of archaeopteryx provides insights into the evolution of pennaceous feathers. Nature 511: 79.

Fowler, D.W., E.A. Freedman, J.B. Scannella, and R.E. Kambic. 2011. The predatory ecology of *Deinonychus* and the origin of flapping in birds. PLoS One 6: e28964.

Gatesy, S.M., and K. Middleton. 1997. Bipedalism, flight and the evolution of theropod locomotor diversity. Journal of Vertebrate Paleontology 17: 308–329.

Greenewalt, C.H. 1975. The flight of birds: the significant dimensions, their departure from the requirements for dimensional similarity, and the effect on flight aerodynamics of that departure. Transactions of the American Philosophical Society 65: 1–67.

Han, G., et al. 2014. A new raptorial dinosaur with exceptionally long feathering provides insights into dromaeosaurid flight performance. Nature Communications 5: 4382.

Hartman, F.A. 1961. Locomotor mechanisms of birds. Smithsonian Miscellaneous Collections 143: 1–91.

Heers, A.M., and K.P. Dial. 2015. Wings versus legs in the avian bauplan: development and evolution of alternative locomotor strategies. Evolution 69: 305–320.

Heers, A.M., B. Tobalske, and K.P. Dial. 2011. Ontogeny of lift and drag production in ground birds. Journal of Experimental Biology 214: 717–725.

Heers, A.M., K.P. Dial, and B.W. Tobalske. 2014. From baby birds to feathered dinosaurs: incipient wings and the evolution of flight. Paleobiology 40: 459–476.

Heers, A.M., D.B. Baier, B.E. Jackson, and K.P. Dial. 2016. Flapping before flight: High resolution, three-dimensional skeletal kinematics of wings and legs during avian development. PLoS One 11: e0153446.

Heers, A.M., J.W. Rankin, and J.R. Hutchinson. 2018. Building a bird: musculoskeletal modeling and simulation of wing-assisted incline running during avian ontogeny. Frontiers in Bioengineering and Biotechnology 6: 140.

Heilmann, G. 1926. The origins of birds. London: Witherby.

Hu, D.Y., L.H. Hou, L.J. Zhang, and X. Xu. 2009. A pre-*Archaeopteryx* troodontid theropod from China with long feathers on the metatarsus. Nature 461: 640.

Hu, D.Y., et al. 2018. A bony-crested Jurassic dinosaur with evidence of iridescent plumage highlights complexity in early paravian evolution. Nature Communications 9: 217.

Jackson, B.E., P. Segre, and K.P. Dial. 2009. Precocial development of locomotor performance in a ground-dwelling bird (*Alectoris chukar*): negotiating a three dimensional terrestrial environment. Proceedings of the Royal Society B, Biological Sciences 276: 3457–3466.

Kaye, T.G., et al. 2015. Laser-stimulated fluorescence in paleontology. PLoS One 10: e0125923.

Kaye, T.G., M. Pittman, G. Mayr, D. Schwarz and X. Xu. 2019a. Detection of lost calamus challenges identity of isolated *Archaeopteryx* feather. Scientific Reports 9: 1182.

Kaye, T.G., et al. 2019b. Fully fledged enantiornithine hatchling revealed by laser-stimulated fluorescence supports precocial nesting behavior. Scientific Reports 9: 5006.

Lande, R., 1976. Natural selection and random genetic drift in phenotypic evolution. Evolution 30: 314–334.

Lande, R., 1979. Quantitative genetic analysis of multivariate evolution, applied to brain-body size allometry. Evolution 33: 402–416.

Lee, M.S., A. Cau, D. Naish, and G.J. Dyke. 2014. Sustained miniaturization and anatomical innovation in the dinosaurian ancestors of birds. Science 345: 562–566.

Makovicky, P.J., and L.E. Zanno. 2011. Theropod diversity and the refinement of avian characteristics. *In* G. Dyke and G. Kaiser (editors), Living dinosaurs: 9–29. Hoboken, NJ: Wiley.

Martin, L.D. 1983. The origins of birds and avian flight. *In* R.F. Johnston (editor), Current Ornithology 1: 105–129.

Martin-Silverstone, E., et al. 2015. Exploring the relationship between skeletal mass and total body mass in birds. PLoS One 10: e0141794.

Mayr, G., B. Pohl, S. Hartman, and D.S. Peters. 2007. The tenth skeletal specimen of *Archaeopteryx*. Zoological Journal of the Linnean Society 149: 97–116.

McNab, B.K. 1994. Energy conservation and the evolution of flightlessness in birds. American Naturalist 144: 628–642.

Middleton, K., and S.M. Gatesy. 2000. Theropod forelimb design and evolution. Zoological Journal of the Linnean Society 128: 149–187.

Mustonen, V., and M. Lassig. 2009. From fitness landscapes to seascapes: non-equilibrium dynamics of selection and adaptation. Trends in Genetics 25: 111–119.

Nopsca, F. 1907. Ideas on the origin of flight in birds. Proceedings of the Zoological Society of London 1907: 223–236.

Norberg, U.M. 1985. Evolution of vertebrate flight: an aerodynamic model for the transition from gliding to active flight. American Naturalist 126: 303–327.

O'Connor, J.M.K., and Z.H. Zhou. 2015. Early evolution of the biological bird: perspectives from new fossil discoveries in China. Journal of Ornithology 156: 333–342.

O'Connor, J.M.K., et al. 2015. Evolution and functional significance of derived sternal ossification patterns in ornithothoracine birds. Journal of Evolutionary Biology 28: 1550–1567.

Ostrom, J.H. 1974. *Archaeopteryx* and the origin of flight. Quarterly Review of Biology 49: 27–47.

Regal, P.J. 1975. The evolutionary origin of feathers. Quarterly Review of Biology 50: 35–66.

Rice, S.H. 2004. Evolutionary theory: mathematical and conceptual foundations. Sunderland, MA: Sinauer Associates.

Rice, S.H. 2012. The place of development in mathematical evolutionary theory. Journal of Experimental Zoology B, Molecular and Developmental Evolution 318: 480–488.

Schluter, D. 2000. The ecology of adaptive radiation. Oxford: Oxford University Press.

Serrano, F.J., and L.M. Chiappe. 2017. Aerodynamic modelling of a cretaceous bird reveals thermal soaring capabilities during early avian evolution. Journal of the Royal Society Interface 14: 20170182.

Serrano, F.J., P. Palmqvist, L.M. Chiappe, and J.L. Sanz. 2017. Inferring flight parameters of Mesozoic avians through multivariate analyses of forelimb elements in their living relatives. Paleobiology 43: 144–169.

Serrano, F.J., et al. 2018. Flight reconstruction of two European enantiornithines (Aves, Pygostylia) and the achievement of bounding flight in Early Cretaceous birds. Palaeontology 61: 359–368.

Simpson, G.G. 1944. Tempo and mode in evolution. New York: Columbia University Press.

Simpson, G.G. 1953. The Major Features of Evolution. New York: Columbia University Press.

Steinberg, B., and M. O'Stermeier. 2016. Environmental changes bridge evolutionary valleys. Science Advances 2: e1500921.

Tobalske, B., and K.P. Dial. 2007. Aerodynamics of wing-assisted incline running in birds. Journal of Experimental Biology 210: 1742–1751.

Turner, A.H., P.J. Makovicky, and M.A. Norell. 2012. A review of dromaeosaurid systematics and paravian phylogeny. Bulletin of the American Museum of Natural History 371: 1–206.

Wang, M., T.A. Stidham, and Z.H. Zhou. 2018. A new clade of basal early Cretaceous pygostylian birds and developmental plasticity of the avian shoulder girdle. Proceedings of the National Academy of Sciences of the United States of America 115: 10708.

Wang, M., J.M.K. O'Connor, X. Xu, Z.H. Zhou. 2019. A new Jurassic scansoriopterygid and the loss of membranous wings in theropod dinosaurs. Nature 569: 256–259.

Wang, X.L., et al. 2017. Basal paravian functional anatomy illuminated by high-detail body outline. Nature Communications 8: 14576.

Wright, S. 1932. The roles of mutation, inbreeding, crossbreeding and selection in evolution. Proceedings of the Sixth International Congress on Genetics 1(8): 355–366.

Xu, X., et al. 2003. Four-winged dinosaurs from China. Nature 421: 335–340.

Xu, X., H.L. You, K. Du, and F.L. Han. 2011. An *Archaeopteryx*-like theropod from China and the origin of avialae. Nature 475: 465–470.

Xu, X., et al. 2014. An integrative approach to understanding bird origins. Science 346: 1253293.

Xu, X., et al. 2015. A bizarre Jurassic maniraptoran theropod with preserved evidence of membranous wings. Nature 521: 70–73.

Zhang, F.C., Z.H. Zhou, X. Xu, X.L. Wang, and C. Sullivan. 2008. A bizarre Jurassic maniraptoran from China with elongate ribbon-like feathers. Nature 455: 1105–1108.

Zhao, T., D. Liu, and Z. Li. 2017. Correlated evolution of sternal keel length and ilium length in birds. PeerJ 5: e3622.

Chapter 13

Laser-Stimulated Fluorescence Refines Flight Modeling of the Early Cretaceous Bird *Sapeornis*

FRANCISCO J. SERRANO,[1] MICHAEL PITTMAN,[2] THOMAS G. KAYE,[3] XIAOLI WANG,[4]
XIAOTING ZHENG,[4] AND LUIS M. CHIAPPE[5]

ABSTRACT

Unseen and difficult-to-see soft tissues of fossil birds revealed by laser-stimulated fluorescence (LSF) shed light on their functional morphology. Here we study a well-preserved specimen of the early pygostylian *Sapeornis chaoyangensis* under LSF and use the newly observed soft-tissue data to refine previous modeling of its aerial performance and to test its proposed thermal soaring capabilities. Under LSF, the body's lateral outline is observed, permitting direct estimates of the body's disc surface that generates drag during flight (S_b). This surface and the body drag coefficient—which is better estimated knowing S_b— are influential parameters in modeling flight dynamics. In particular, we focus on two aspects of flight dynamics: the calculation of the power margin during flapping flight (power curve), and the sinking speed during gliding (glide polar). Results from revised models using our direct soft-tissue measurements support the notion that *Sapeornis* was a thermal soarer that glided for long periods. LSF also confirms the absence of a true alula in *Sapeornis*. While the deployment of the alular digit could have enhanced control during slow flight, the position of this digit along the handwing (distal part of the wing) suggests limited maneuverability. This study demonstrates how soft-tissue preservation can be incorporated into modeling of flight dynamics in light of ever-improving palaeontological imaging techniques.

INTRODUCTION

Laser-stimulated fluorescence (LSF) uses high flux laser light to fluoresce fossil specimens at macro- and microscopic scales, improving imaging results with respect to conventional UV light (Kaye et al., 2015). LSF has revealed otherwise obscure and invisible osteological and soft-tissue details in fossil specimens facilitating the reconstruction of a range of paleobiological aspects (Kaye et al., 2015, 2019a; 2019b; Falk et al., 2016a; Mayr et al., 2016; Vinther et al., 2016; Wang et al., 2017; Yang et al., 2018). LSF has helped improve our understanding of theropod flight evolution by directly revealing soft-tissue outlines of the wings and body, providing invaluable insights into the functional morphology of the first flyers including potential candidates (e.g., the early-diverging paravian *Anchiornis* (Wang et al., 2017) and the early pygostylian *Confuciusornis* (Falk et al., 2016b).

---

[1] Real Academia de Ciencias Exactas, Físicas y Naturales, Madrid; Dinosaur Institute, Natural History Museum of Los Angeles County, Los Angeles.

[2] Vertebrate Palaeontology Laboratory, Division of Earth and Planetary Science, the University of Hong Kong, Hong Kong.

[3] Foundation for Scientific Advancement, Sierra Vista, AZ.

[4] Institute of Geology and Paleontology, Linyi University, Linyi City, Shandong, China; Shandong Tianyu Museum of Nature, Pingyi, Shandong, China.

[5] Dinosaur Institute, Natural History Museum of Los Angeles County, Los Angeles

The flight dynamics of the Early Cretaceous early pygostylian *Sapeornis chaoyangensis* have been explored through quantitative approaches (Serrano and Chiappe, 2017). Morphofunctional evidence and aerodynamic models generated for this early bird indicated that *Sapeornis* flew by gliding over long periods and using ascending air currents in continental environments for soaring (i.e., thermal soaring). Serrano and Chiappe (2017) applied information from exquisitely preserved wing feathers to reconstruct the shape and size of the wings of this bird. Nonetheless, this approach was unable to include information from the body outline due to the absence of reliable nonfeather soft-tissue evidence from the studied specimens.

The body outline provides information about the body (= parasite) drag—the aerodynamic force generated by the body against the air stream—acting on a flying bird. As the generation of aerodynamic theoretical models is limited by a few parameters that are difficult to measure in flying birds (Pennycuick, 1969; Tucker, 1973; Rayner, 1999; Pennycuick, 2008), calculations for extinct birds require assumptions about such parameters (Burgers and Chiappe, 1999; Templin, 2000; Chatterjee and Templin, 2003; Ksepka, 2014; Serrano and Chiappe, 2017; Serrano et al., 2018). Among them, the body drag is particularly controversial and yet, it is proven to have a strong influence on the results of the models (Hedenström and Rosén, 2003; Taylor et al., 2016). LSF imaging of *Sapeornis* specimen STM 15-15 (Shandong Tianyu Museum of Nature, Pingyi, China) now provides information on body shape for the first time (fig. 1). Using this new soft-tissue information, we reanalyze the flight dynamics of this early pygostylian. We also provide a novel comparative analysis for the alular digit position of this bird, as this structure is very important for controlling flight at low speeds (Meseguer et al., 2012; Lee et al., 2015). Our refined results of the flight performance of this bird—incorporating both body drag and the role of the alular digit—allow us to test existing hypotheses about the flying habits and paleoecological inferences of *Sapeornis*.

MATERIAL AND METHODS

Fossil and Estimations

Sapeornis chaoyangensis STM 15-15 (fig. 1) was examined and photographed at the Shandong Tianyu Museum of Nature (Pingyi, China). Bone measurements (table 1) were taken from photographs using ImageJ 1.51j8 (available from http://imagej.nih.gov/ij). Body width (L_b) was measured from the LSF image as the maximum length from the dorsal margin of the vertebral column to the ventral contour of the feathered body (fig. 2). Despite the well-preserved feathers revealed by LSF, the wingtip (i.e., the distance between the distal end of the second phalanx of the major digit and the tip of the wing) and the wing chord (i.e., the distance from leading to trailing edge at wrist level) are not measurable for STM 15-15. Their values were obtained assuming an isometric variation for the skeletal wing (i.e., the added length of humerus, ulna, carpometacarpus, and major digit) of specimen DNHM 3078 (Gao et al., 2012). Following Serrano and Chiappe's (2017) study of the aerodynamics of *Sapeornis*, we estimated the body mass (M_b), wingspan (B), and lift surface (S_L) of STM 15-15 using multiple regressions derived from a dataset of modern flying birds (Serrano et al., 2015; Serrano et al., 2017).

Laser-Stimulated Fluorescence (LSF)

LSF images were collected using a refined version of the original protocol of Kaye et al. (2015) (Wang et al., 2017; Kaye et al. 2019a, 2019b). *Sapeornis* specimen STM 15-15 was imaged at the Shandong Tianyu Museum of Nature with a 405 nm violet laser. An appropriate long-pass blocking filter was used in front of a Nikon D810 DLSR camera lens to prevent image saturation by the laser. The laser was dispersed into a vertical line by a Laserline Optics

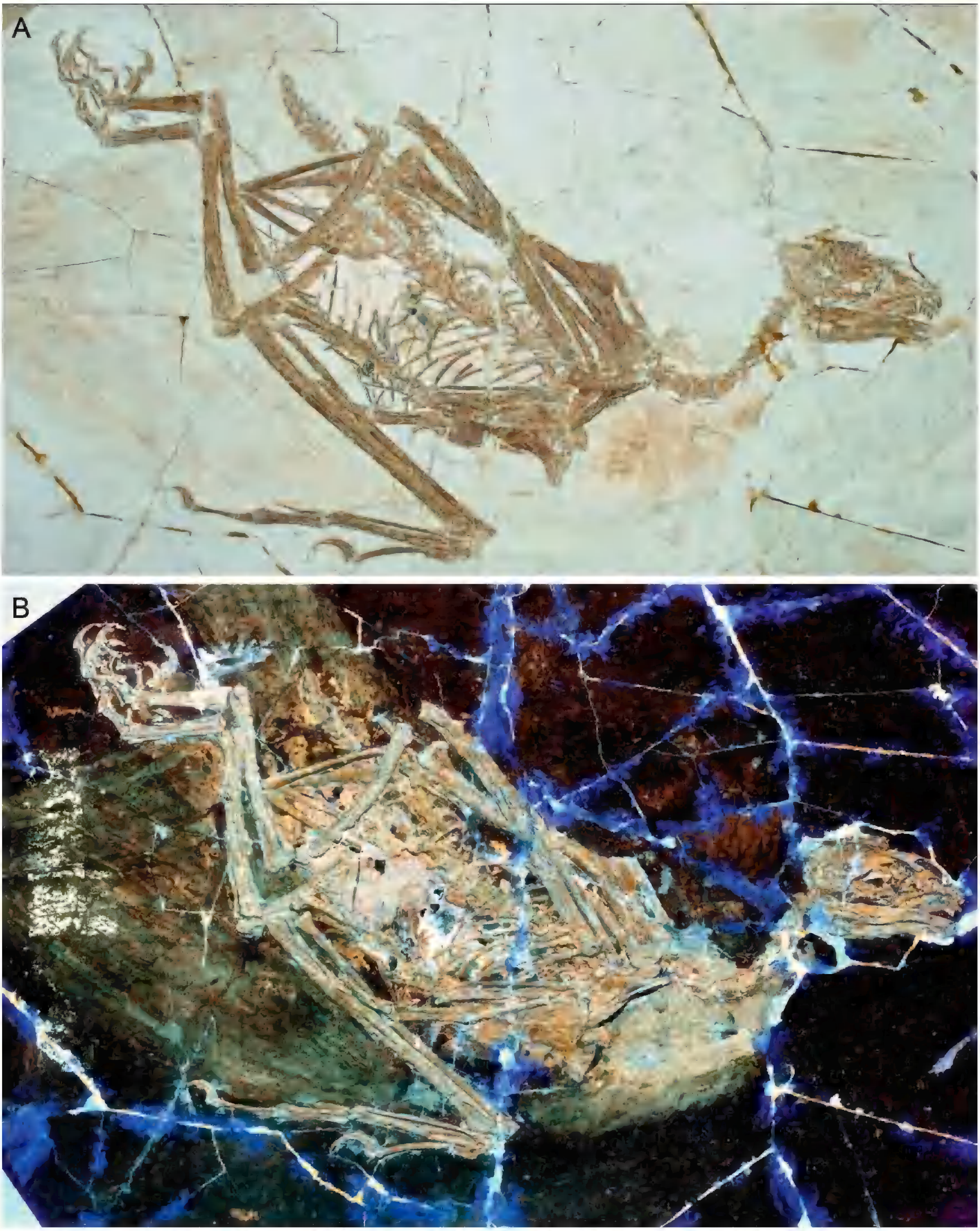

FIG. 1 Early pygostylian *Sapeornis* STM 15-15 shows faint soft-tissue details that **A,** under white light are vivid and **B,** under LSF, extensive.

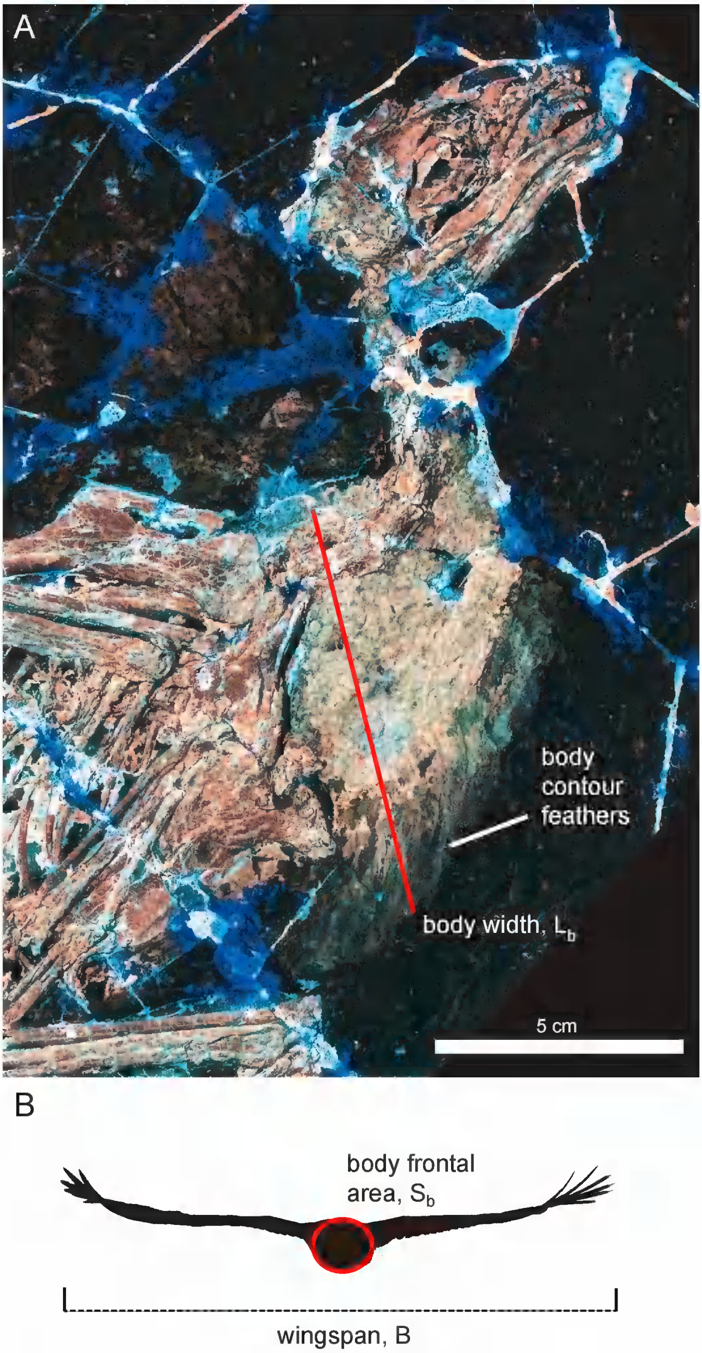
A
body contour feathers
body width, L_b
5 cm
B
body frontal area, S_b
wingspan, B

FIG. 2. **A.** The anterior region of *Sapeornis* STM 15-15 under LSF, showing contour feathers. **B.** Frontal view silhouette showing S_b and B.

Canada lens, which was mechanically swept repeatedly over the specimen during photo time exposures in the museum's dark room. The images were postprocessed in Photoshop CS6 for sharpness, color balance, and saturation. Details of the theory behind LSF imaging can be found in Wang et al. (2017).

FLIGHT DYNAMICS MODELING

In modern birds, the maximum available power output (aerobic metabolism) for attaining active flight (P_{av}) scales negatively with body size (Templin, 2000; Pennycuick, 2008). P_{av} was calculated using an oxygen consumption rate (V_{O2}, mL/s) in which 1 mL O_2/s generates 20.1 W during aerobic activity (Schmidt-Nielsen, 1997). Values of V_{O2} were estimated for *Sapeornis* using Equation 1, which was derived from birds flying at modern O_2 concentration (i.e., 20.9 mL O_2/100 mL air; Bishop and Butler, 2015):

$$(1)\ V_{O2} = 160\ M_b{}^{0.74}$$

By assuming a conversion efficiency of 0.2 from the total metabolic power input to P_{av} (Tucker, 1973; 1975; Pennycuick, 2008), and translating minutes into seconds—as Equation 1 was derived from V_{O2} measured in mL/min—the P_{av} at modern conditions was calculated using Equation 2:

$$(2)\ P_{av} = 20.1 \times 0.2\ /\ 60\ V_{O2}$$
$$P_{av} = 0.067\ V_{O2}$$

Values of P_{av} for STM 15-15 were adjusted to the O_2 atmospheric levels at 120 Myr, the estimated time of deposition for the fossil (Ward and Berner, 2011), through the percentage of variation between concentrations today and in the past (Serrano et al., 2019), calculated using Equation 3 (where AOC is atmospheric O_2 concentration):

$$(3)\ P_{av} = (0.067\ V_{O2} \cdot \%\Delta\ AOC) + 0.067\ V_{O2}$$

TABLE 1

Anatomical measurements (in mm) of *Sapeornis* STM 15-15

Asterisk indicates estimated measurements due to specimen damage or incomplete preservation.

Element	Measurement
Humerus	132.7
Humerus midshaft width	6.9
Distal humeral width	14.2
Deltopectoral crest	48
Bicipital crest	15.6
Ulna	129.5
Ulna midshaft width	7.0
Distal ulnar width	9.1
Radius	128.2
Radius midshaft width	3.5
Carpometacarpal length (semilunate to major metacarpal)	61.7
Alular digit position (semilunate to distal end of alular mc)	16.7
Proximal carpometacarpus width	11.1
Metacarpus midshaft width	6.5
Major metacarpal midshaft width	4.3
Alular digit	31.5
Major digit-1	30
Major digit-2	26.4
Wing tip*	225.8
Wing chord*	240.7
Femur	68.4
Femur midshaft width	5.9
Tibiotarsus	79.6
Metatarsal	43.6
Body width	95.7

For a given bird flying, the power curve that relates its forward speed (V_t) with its mechanical power output necessary for flapping flight (P_{mec}) is U-shaped (Pennycuick, 1969; Tucker, 1973; Rayner, 1999). This theoretical relationship is mostly supported by direct measure of the input power in modern birds flapping (Bishop and Butler, 2015). We constructed power curves for

Sapeornis STM 15-15 using the software Flight v. 1.24 (www.bio.bristol.ac.uk/people/pennycuick.htm) (Pennycuick, 2008). The values of P_{mec} for a range of velocities V_t were calculated according to Equation 4, as the summation of the induced power (P_{ind}; Equation 5, where k is the induced power factor and g is gravitational acceleration), the parasite power (P_{par}; Equation 6, where S_b is the frontal area of the body, C_{Db} is the body-drag coefficient, ρ_{air} is the density of air and B is the wingspan), and the profile power (P_{pro}; Equation 7, where V_{mp} is the minimum power speed and C_{pro} is the profile power constant).

(4) $P_{mec} = P_{ind} + P_{par} + P_{pro}$
(5) $P_{ind} = 2k\ [M_b\ g]^2\ /\ V_t\ \pi\ B^2 \rho_{air}$
(6) $P_{par} = \rho_{air}\ V_t^3\ S_b\ C_{Db}\ /\ 2$
(7) $P_{pro} = [2k\ (M_b\ g)^2\ /\ V_{mp}\ \pi\ B_2\ \rho_{air} + \rho_{air}\ V_{mp}{}^3 S_b\ C_{Db}\ /2]\ C_{pro}\ /[B_2/S_L]$

These calculations require assumptions for some components, particularly when applied to fossil taxa (Serrano et al., 2018). For example, k—a parameter that accounts for any deviations from elliptical distribution of the lift across the wingspan— was set at $k = 1.2$, a value typically observed in aircraft, while C_{pro} was fixed at 8.4 to make P_{pro} proportional to the wing area (Pennycuick, 2008). The body-drag components (i.e., S_b and C_{Db}) are highly influential parameters (Taylor et al., 2016), and they were addressed, as explained in the next section. The cruising speed or the speed with minimum cost of transport (V_{mr}), was calculated as the speed where the tangent to the power curve intersects with the origin of the speed-power plot (Rayner, 1999).

The dynamics of gliding were studied through the glide polar graph that relates the sinking speeds (V_z) to a range of forward speed (V_t). V_z calculated with Equation 8, where D is the total aerodynamic drag resulting from the addition of the induced, parasite and profile drags (Pennycuick 2008). We also assumed that wingspan decreases as a linear function of speed (i.e., linear reduction command of Flight v. 1.24) and used an induced drag factor equal to 1.0 (Taylor et al., 2016):

(8) $V_z = D\ V_t\ /\ M_b\ g$

Body-Drag Estimation

The body frontal area (S_b) of STM 15-15 was calculated directly (Equation 9) from the measurement of the body width (L_b; fig. 2). For comparison, S_b was also calculated from its allometric relationship with the body mass, M_b (Equation 10) (Pennycuick et al., 1988).

(9) $S_b = \pi * (L_b\ /\ 2)^2$
(10) $S_b = 0.00813 * M_b^{0.666}$

The body-drag coefficient (C_{Db}) is a dimensionless value that indicates the streamlined degree of the body (Pennycuick, 2008). C_{Db} value is difficult to measure in modern birds, and we used different approaches for obtaining it in *Sapeornis*.

The first approach, named model 1, was based on the Reynold's number of the body (Re_b) (Equation 11). C_{Db} was calculated from its negative allometry with Re_b (Equation 12) found in 39 modern passerines (Hedenström and Liechti, 2001).

(11) $Re_b = V_t\ L_b\ \rho_{air}\ \mu^{-1}$
(12) $C_{Db} = 0.70 - (5.8 \times 10^{-6})\ Re_b$

We took the ρ_{air} at 120 Myr (i.e., 1.209 kgm^{-3}; Serrano et al., 2019), while the dynamic viscosity of the air, μ, was assumed at modern standard conditions (i.e., 1 atm, 20° C). Under this approach C_{Db} varies with Re_b, and this Re_b is dependent on Vt. We calculated Re_b and C_{Db} at each V_t, from 7 to 24 ms^{-1} (i.e., the range for plausible flight speed of *Sapeornis* given by Serrano and Chiappe 2017). The average value of these C_{Db} was used to construct the models.

Another approach, model 2, obtained C_{Db} from S_b (Eq. 10) and the equivalent flat-plate area (A) (Equation 13). For estimating A, we followed the approach from Taylor and Thomas (2014) that assumes a body drag equivalent to the drag on a flat plate with 1% of the area of the wings (Equation 14). Rearranging equations 13 and 14, C_{Db} was estimated in Equation 15.

(13) $A = S_b \times C_{Db}$
(14) $A = 0.01\ S_L$
(15) $C_{Db} = (0.01\ S_L)\ /\ S_b$

Lastly, we generated models with minimum and maximum C_{Db} values (models 3 and 4, respectively) to obtain an uncertainty range for the curves. The minimum C_{Db} was fixed at 0.1, a value that assumes a well-streamlined body with no drag generated from the legs and feet (Pennycuick, 2008). We selected the maximum C_{Db} at 0.5 because Hedenström and Liechti (2001) suggested that C_{Db} experimentally measured above 0.4 would come from the underestimation of the maximum effort of the flying birds tested, although they found outliers above 0.5. Models 3 and 4 used S_b from Equation 10.

RESULTS

For *Sapeornis* STM 15-15 we estimated a M_b of 0.927 kg, a B of 122.3 cm and S_L of 0.235 m^2, within the range provided by Serrano and Chiappe (2017). From its M_b, STM 15-15 could generate a maximum P_{av} of 9.0 W. C_{Db} values calculated from Re_b (model 1: C_{Db} = 0.31) and from A (model 2: C_{Db} = 0.30) are within the range established between the minimum and maximum values (i.e., 0.1 and 0.5 in the models 3 and 4, respectively). The three power curves (models 1, 2, and 4) show that the P_{mec} required for sustaining flapping flight was above the value of P_{av} for the full range of V_t (fig. 3A). In model 3—the one assuming the minimum C_{Db}—the P_{mec} was slightly under P_{av} at starting values of the V_t range. At cruising speeds V_{mr}, all models show that P_{mec} was higher than the P_{av}. The four aerodynamic models thus indicate that STM 15-15 could not generate sufficient P_{mec} for sustaining a prolonged flight through wing flapping.

The glide polar graph illustrates that in STM 15-15 sinking took place at low forward speeds (fig. 3B). This gliding pattern, observed in the four analyzed models (1, 2, 3, and 4), has values within the range of modern birds that use thermal soaring. Model 1—the one using direct information from the fossil's body outline—clearly shows a glide pattern like a thermal soarer; when STM-15-15 reached its maximum lift-to-drag ratio (11.8-12.1), its gliding-forward velocity was 9.7 ms^{-1} (9.2–10.1 ms^{-1}) and its sinking speed 0.82 ms^{-1} (0.76–0.86 ms^{-1}). These values are remarkably close to those for the Red-Tailed Hawk (*Buteo jamaicensis*), as reported in Serrano and Chiappe (2017: table 2).

The position of the alular digit in STM 15-15 (fig. 4)—here based on the location of the distal end of the alular metacarpal—is farther from the wrist than that observed in similar-sized soaring birds (fig. 5). Such a distalward position resembles modern birds that are poorly competent at unsteady maneuvers, typically divers (i.e., loons, grebes, auks, diving ducks, cormorants, and storm petrels) or occasional fliers (i.e., landfowls, waterfowls, and rails). Pelicans and South American screamers, more than double the size of STM 15-15, were the only thermal soarers with a comparable distalward position of the alular digit (fig. 5).

DISCUSSION

Our study is the first to use the preserved body outline of a fossil bird—as revealed under LSF (fig. 2B)—to refine its flight modeling. Visualization of the body outline of STM 15-15 allows a direct measure of the body surface that generated drag during flight (L_b and S_b) (i.e., model 1), whereas previous aerial models of *Sapeornis* (Serrano and Chiappe, 2017) assumed a modern allometric variation for S_b (Pennycuick et al., 1988) (i.e., models 2, 3 and 4). Visualization of the body outline also allows a direct calculation of the body-drag coefficient (C_{Db}), which has proven especially controversial to calculate from theoretical approaches (Taylor et al., 2016). Our results show that C_{Db} value calculated in model 1—direct calculation through the Reynolds number of the body (Hedenström and Liechti, 2001)—was similar to the value calculated in model 2, a calculation that assumed a body-drag equivalent to the drag on a flat plate with 1% of

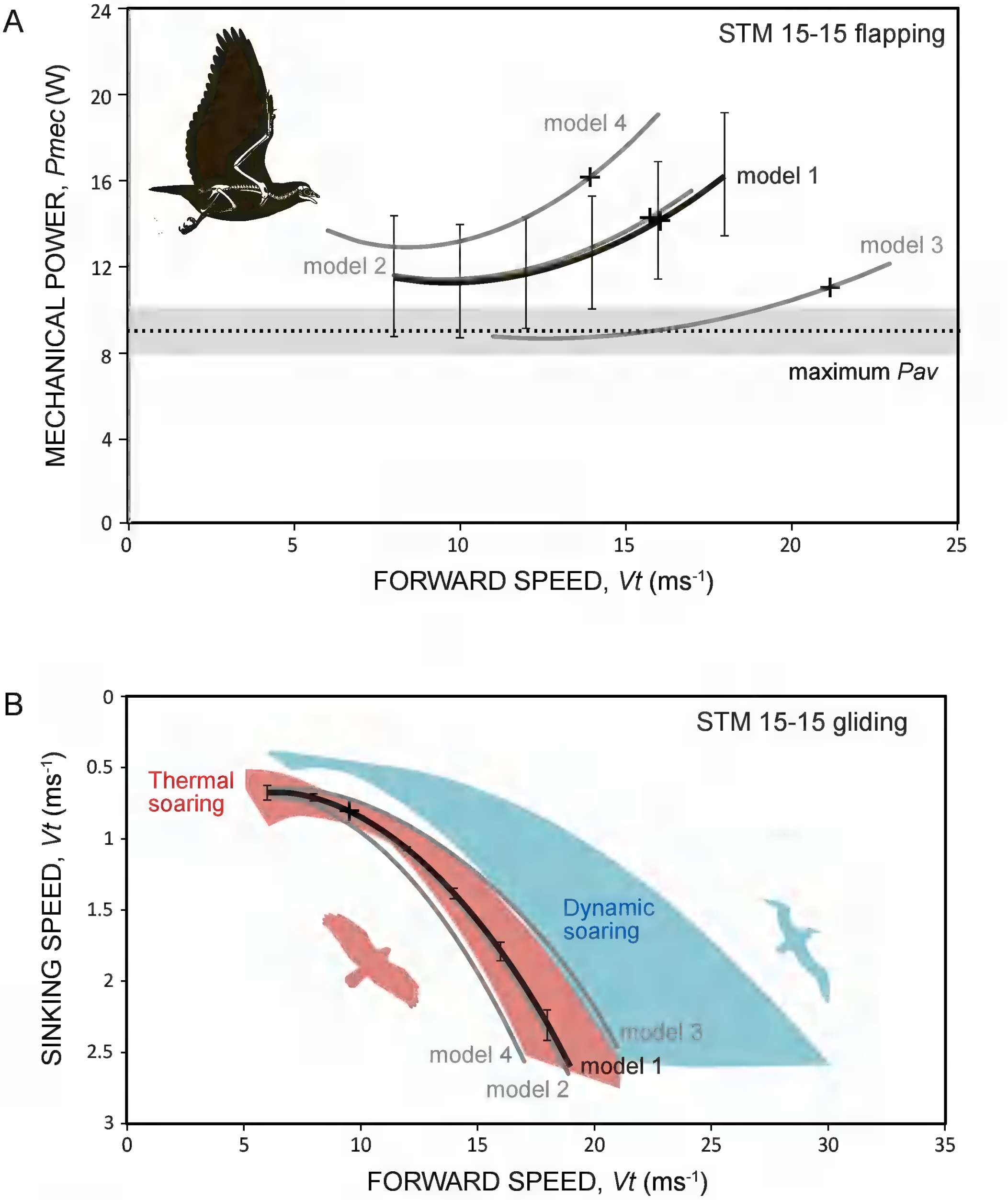

FIG. 3. **A.** Power margin in four models of *Sapeornis* STM 15-15. **B.** Glide polar graph in 4 models of STM 15-15 compared to modern soaring birds.

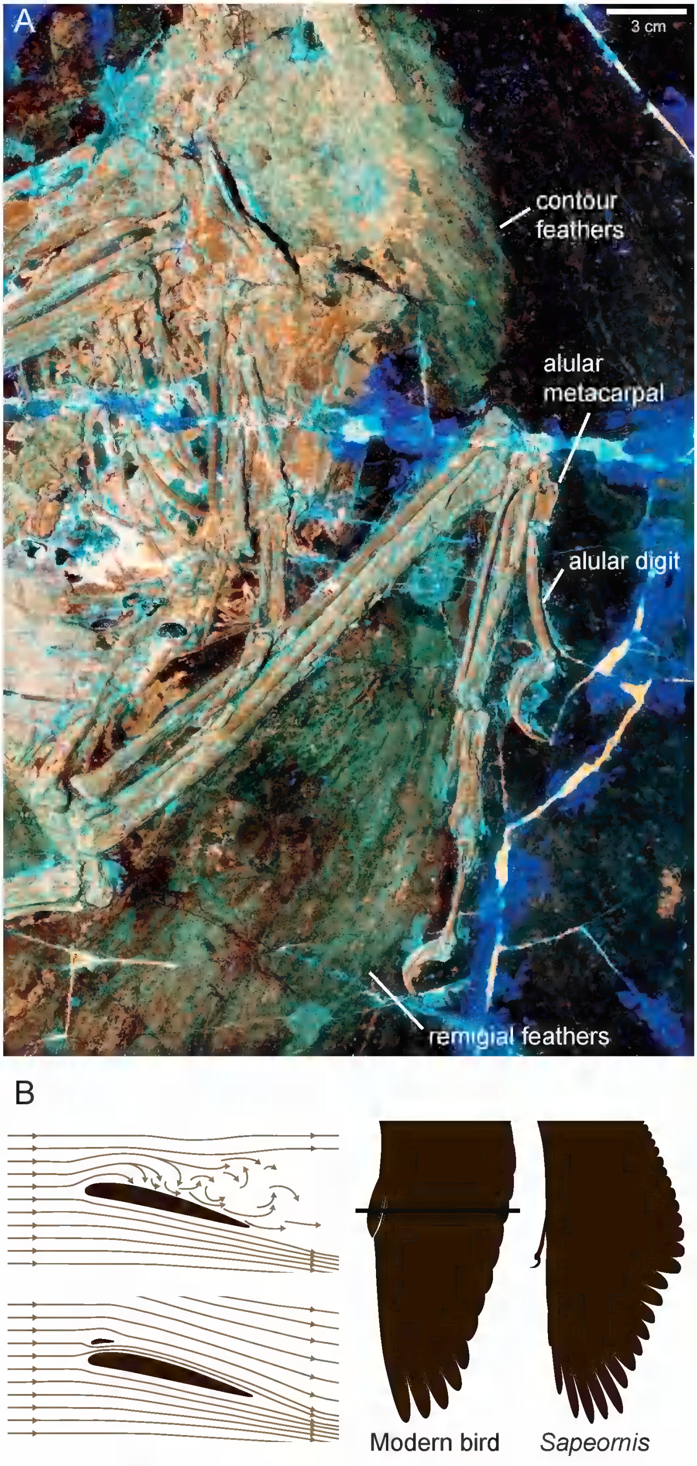
A
3 cm
contour feathers
alular metacarpal
alular digit
remigial feathers
B
Modern bird
Sapeornis

FIG. 4. **A.** LSF image of hand and feathers of STM 15-15. **B.** Effect of alula delaying stall, and wing silhouettes of an avian (crown bird) and *Sapeornis*.

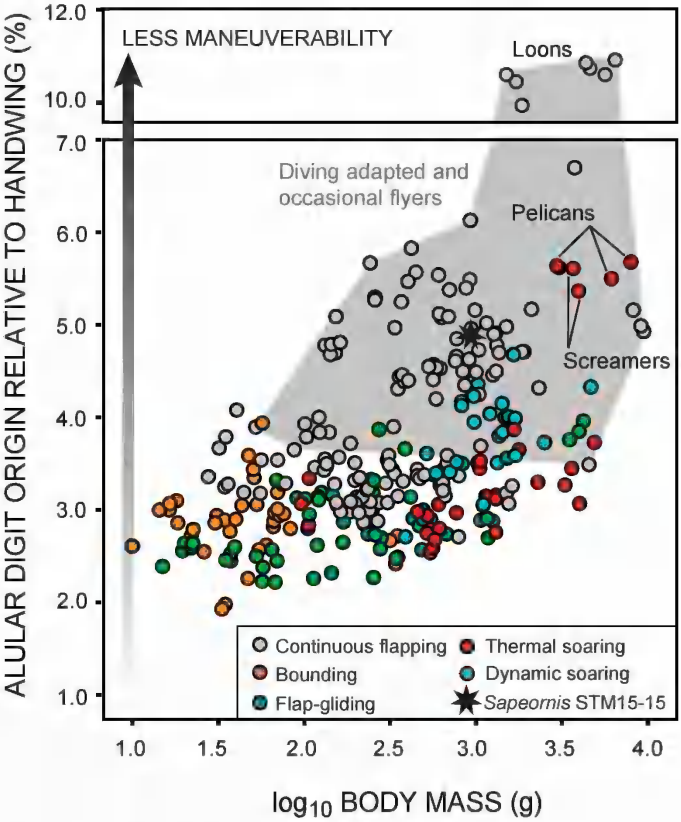

FIG. 5. Scatter graph of alular digit position against M_b, compared with modern bird morphospace.

the area of the wings (Taylor and Thomas, 2014). The congruence between the aerodynamic models 1 and 2 (fig. 3) validates the assumptions made in Serrano and Chiappe's (2017) previous assessment of the flight performance of *Sapeornis*. However, such assumptions should probably be validated on a case-by-case basis, especially given the often large morphological differences between modern and early-diverging bird species as well as the availability of direct soft-tissue data using imaging methods like LSF. In order to minimize this issue, we delimited the flight reconstruction of STM 15-15 using minimum and maximum values (models 3 and 4) based on C_{Db} observed in modern birds (Pennycuick, 2008; Hedenström and Liechti, 2001). Finally, the negative power margin during flapping flight and the gliding pattern obtained in the four models (fig. 3) corroborate the hypothesis that *Sapeornis* had thermal soaring capabilities, as proposed by Serrano and Chiappe (2017).

Furthermore, we argue that the alular digit, albeit lacking a true alula as shown by LSF (fig. 4A), was a functional precursor of the true alula (Meseguer et al., 2012), thus acting as an antistall device that increased control at low speeds (fig. 4B). Our study documents a distalward location of the alular digit of *Sapeornis* (fig. 5), which implies that a lesser portion of the proximal handwing was under the influence of this flap. Such position of the alular digit (and functional flap) suggests that the maneuverability of *Sapeornis* might have been weak when compared with that of modern soaring birds of similar size. Lastly, from a paleoecological perspective, these results indicate that if *Sapeornis* was capable of perching, as suggested by the bird's pedal anatomy (Glen and Bennett, 2007;

Chiappe and Meng, 2016), its limited capacity to maneuver would have hindered its abilities to land on a perch.

ACKNOWLEDGMENTS

We would like to thank Kenneth H.C. Fung and First Initiative Foundation for their support of the International Pennaraptoran Dinosaur Symposium, the venue where we got the idea for this study. This project was supported by the Seed Fund for Basic Research for Resubmission of GRF/ECS Proposals from the University of Hong Kong (to M.P.) and funding from the HKU MOOC course Dinosaur Ecosystems (to M.P.). F.J.S. was supported by a Juan de la Cierva – Incorporación Postdoctoral Fellowship and the Research Project CGL2016-78577-P funded by the Spanish Ministry of Economy, Industry and Competitiveness. X.L.W. was supported by the Taishan Scholars Program of Shandong Province (No. Ts20190954). We would like to dedicate this chapter to the memory of C.J. Pennycuik.

REFERENCES

Bishop, C.M., and P.J. Butler. 2015. Flight. *In* C.G. Scanes (editor), Sturkie's Avian Physiology: 919–974. London: Academic Press

Burgers, P., and L.M. Chiappe. 1999. The wing of *Archaeopteryx* as a primary thrust generator. Nature 399: 60–62.

Chatterjee, S., and R.J. Templin. 2003. The flight of *Archaeopteryx*. Naturwissenschaften 90: 27-32.

Chiappe, L.M., and Q. Meng. 2016. Birds of stone. Baltimore: Johns Hopkins University Press.

Falk, A.R., T.G. Kaye, Z.H. Zhou, and D.A. Burnham. 2016a. Laser fluorescence illuminates soft tissues and life habits of *Confuciusornis*. PLoS One: undergoing postreview corrections.

Falk, A.R., T.G. Kaye, Z.H. Zhou, and D.A. Burnham. 2016b. Laser fluorescence illuminates the soft tissue and life habits of the Early Cretaceous bird *Confuciusornis*. PLoS One 11: e0167284.

Gao, C., et al. 2012. A subadult specimen of the Early Cretaceous bird *Sapeornis chaoyangensis* and a taxonomic reassessment of sapeornithids. Journal of Vertebrate Paleontology 32: 1103–1112.

Glen, C.L., and M.B. Bennett. 2007. Foraging modes of Mesozoic birds and non-avian theropods. Current Biology 17: R911–R912.

Hedenström, A., and F. Liechti. 2001. Field estimates of body drag coefficient on the basis of dives in passerine birds. Journal of Experimental Biology 204: 1167–1175.

Hedenström, A., and M. Rosén. 2003. Body frontal area in passerine birds. Journal of Avian Biology 34: 159–162.

Kaye, T.G., et al. 2015. Laser-stimulated fluorescence in paleontology. PLoS One 10: e0125923.

Kaye, T.G., M. Pittman, G. Mayr, D. Schwarz, and X. Xu. 2019a. Detection of lost calamus challenges identity of isolated *Archaeopteryx* feather. Scientific Reports 9: 1182.

Kaye, T.G., et al. 2019b. Fully fledged enantiornithine hatchling revealed by Laser-Stimulated Fluorescence supports precocial nesting behavior. Scientific Reports 9: 5006.

Ksepka, D.T. 2014. Flight performance of the largest volant bird. Proceedings of the National Academy of Sciences of the United States of America 111: 10624–10629.

Lee, S., J. Kim, H. Park, P.G. Jabłoński, and H. Choi. 2020. The function of the alula in avian flight. Scientific Reports 5: 9914.

Mayr, G., M. Pittman, E. Saitta, T.G. Kaye, and J. Vinther. 2016. Structure and homology of *Psittacosaurus* tail bristles. Palaeontology 59: 793–802.

Meseguer, J., et al. 2012. Lift devices in the flight of *Archaeopteryx*. Spanish Journal of Paleontology 27: 125–130.

Pennycuick, C.J. 1969. The mechanics of bird migration. Ibis 111: 525–556.

Pennycuick, C.J. 2008. Modelling the flying bird. London: Academic Press.

Pennycuick, C.J., H.H. Obrecht, and M.R. Fuller. 1988. Empirical estimates of body drag of large waterfowl and raptors. Journal of Experimental Biology 135: 253–264.

Rayner, J.M. 1999. Estimating power curves of flying vertebrates. Journal of Experimental Biology 202: 3449–3461.

Schmidt-Nielsen, K. 1997. Animal physiology: adaptation and environment. Cambridge: Cambridge University Press.

Serrano, F.J., and L.M. Chiappe. 2017. Aerodynamic modelling of a Cretaceous bird reveals thermal soaring during avian evolution. Journal of the Royal Society Interface 14: 20170182.

Serrano, F.J., P. Palmqvist, and J.L. Sanz. 2015. Multivariate analysis of neognath skeletal measurements: implications for bodymass estimation in Mesozoic birds. Zoological Journal of the Linnean Society 173: 929–955.

Serrano, F.J., P. Palmqvist, L.M. Chiappe, and J.L. Sanz. 2017. Inferring flight parameters of Mesozoic avians through multivariate analyses of forelimb elements in their living relatives. Palaeobiology 43: 144–169.

Serrano, F.J., et al. 2018. Flight reconstruction of two European enantiornithines (Aves, Pygostylia) and the achievement of bounding flight in Early Cretaceous birds. Palaeontology 61: 359–368.

Serrano, F.J., et al. 2019. The effect of long-term atmospheric changes on the macroevolution of birds. Gondwana Research 65: 86–96.

Taylor, G.K., K.V. Reynolds, and A.L. Thomas. 2016. Soaring energetics and glide performance in a moving atmosphere. Philosophical Transactions of the Royal Society of London Series B Biological Sciences 371: 20150398.

Templin, R.J. 2000. The spectrum of animal flight: insects to pterosaurs. Progress in Aerospace Science 36: 393–436

Tucker, V.A. 1973. Bird metabolism during flight: evaluation of a theory. Journal of Experimental Biology 58: 689–709.

Tucker, V.A. 1975. The energetic cost of moving about: walking and running are extremely inefficient forms of locomotion. Much greater efficiency is achieved by birds, fish—and bicyclists. American Scientist 63: 413–419.

Vinther, J., et al. 2016. 3D camouflage in an ornithischian dinosaur. Current Biology 26: P2456–2462.

Wang, X.L., et al. 2017. Basal paravian functional anatomy illuminated by high-detail body outline. Nature Communications 8: 14576.

Ward, P., and R. Berner. 2011. Why were there dinosaurs? Why are there birds? *In* G. Dyke and G. Kaiser (editors), Living dinosaurs: the evolutionary history of modern birds: 30–38. Oxford: Wiley-Blackwell.

Yang, Z.X., et al. 2018. Pterosaur integumentary structures with complex feather-like branching. Nature Ecology and Evolution 3: 24–30.

Chapter 14

Pectoral Girdle Morphology in Early-Diverging Paravians and Living Ratites: Implications for the Origin of Flight

FERNANDO E. NOVAS,[1] FEDERICO L. AGNOLÍN,[2] FEDERICO BRISSON EGLI,[1]
AND GASTÓN E. LO COCO[1]

ABSTRACT

Discussions about the origin of flight almost unanimously assume that early birds positioned (and moved) their wings in the same basic manner as living flying birds, with reconstructed wings extended with the airfoil surface parallel to the ground and forelimbs moving in a dorsoventral arc. Such reconstructions of wing posture and movements for extinct avialans are based on highly specialized flying neognaths, in which the glenoid cavity is horizontally extended and laterodorsally faced, thus allowing wide humeral rotation and increased upward excursion. However, living ratites exhibit a sharply different pattern of pectoral girdle (or shoulder girdle) morphology and associated wing movements: in both *Rhea* and *Struthio* the glenoid cavity faces laterally, but its major axis is almost vertical. In consequence, wings predominantly move following an anterolateral to posteromedial abduction-adduction arc. Initial experimental results with *Rhea americana* demonstrate their inability to perform WAIR (wing-assisted incline running), suggesting a causal relationship between the inability to flap the wings vigorously and its pectoral girdle morphology (with glenoid cavity subvertically oriented, poorly developed acrocoracoid process, and m. supracoracoideus playing a protractor rather than elevator function). Early-diverging paravians (e.g., *Saurornitholestes*, *Buitreraptor*, *Microraptor*) and early-diverging birds (e.g., *Archaeopteryx*, *Anchiornis*) share a closely similar morphology of scapula and coracoid, with a glenoid cavity facing laterally and with its greater axis oriented subvertically. This condition of the glenoid resembles that of ratites, allowing one to infer that fully extended wings of early-diverging paravians (including *Archaeopteryx*) oriented their surface obliquely to the ground. Experimental results, in conjunction with anatomical observations in both flying and flightless living birds, warn about the purported generalized ability of early-diverging paravians to perform WAIR. Even if they were capable of symmetrical flapping, their wing movements were different from those of living neognaths, because the glenoid retained both a plesiomorphic morphology and orientation. Wing strokes as hypothesized here for early-diverging paravians may have generated thrust with little or no lift. WAIR behavior was present in the common ancestor of Neognathae, and also probably present in early-diverging ornithothoracines. However, WAIR performance among early-diverging paravians and early birds remains uncertain. In agreement with

---

[1] CONICET – Laboratorio de Anatomía Comparada y Evolución de los Vertebrados, Museo Argentino de Ciencias Naturales "Bernardino Rivadavia," Buenos Aires.

[2] CONICET – Laboratorio de Anatomía Comparada y Evolución de los Vertebrados, Museo Argentino de Ciencias Naturales "Bernardino Rivadavia," Buenos Aires; and Fundación de Historia Natural "Félix de Azara," Universidad Maimónides, Buenos Aires.

recent contributions, we conclude that the origin of flapping flight (and eventually WAIR) emerged in birds that diverged later than *Archaeopteryx*, with the acquisition of a horizontally placed major glenoid axis, which allowed wider dorsoventral forelimb excursions.

INTRODUCTION

Living neognaths are the main source of information used for reconstructing muscles, wing movements, and running behavior of early birds. In particular, WAIR, a form of terrestrial locomotion in steeply inclined surfaces, involving flapping and running behavior, has been considered as an evolutionary stage previous to the acquisition of flying capabilities (e.g., Dial, 2003; Bundle and Dial, 2003; Dial et al., 2008; Heers and Dial, 2012; Heers et al., 2014; Dudley et al., 2007; but see Evangelista et al., 2014). These authors used the developing wings of the ground birds (in particular, chukar partridges) as possible analogs/homologs of historical wing forms to provide empirical evaluation of aerodynamic potential in flapping theropod "protowings."

This behavior has been documented in several orders of neognathan birds (see Dial, 2003; Jackson et al., 2011), performed by both juvenile and adult individuals (Heers et al., 2018). To perform this behaviour the wings adopt a characteristic oblique posture and undergo strong anteroposterior symmetrical flapping. Notably, ratites exhibit a sharply different posture and range of movements of their wings, compared with those of neognaths. Such peculiar anatomical and behavioral features of ratites remain poorly studied and, most importantly, were virtually ignored in discussions on the origin of flight stroke, with the exception of the Ph.D. dissertation of H. Davis (2005) in which some aspects of WAIR capabilities on ratites were analyzed in detail.

Ratites have been considered as the best living analogs of extinct paravians (Feduccia, 1986). We are aware, however, that these birds are secondarily flightless, being descendants of flying avian ancestors (Faux and Field, 2017). Moreover, ratites are sharply distinguished from the remaining avians (as well as from extinct early-diverging paravians), in the absence of furcula, rectricial feathers symmetrical and with poorly cohesive vanes, acrocoracoid process (= biceps tubercle) reduced, and humerus with a pronounced exaggerated medial torsion of its distal end, thus producing the distinctive hanging of the forearms (Raikow, 1968). We will pay attention, however, to those morphological traits of ratites that, interestingly, look closer to early-diverging paravians than to flying avians.

The aim of the present paper is to explore how ratites behave when climbing slopes, and particularly how they move their wings. We will also compare the pectoral girdle anatomy of these flightless birds with that of early-diverging paravians (i.e., *Archaeopteryx, Buitreraptor*), considering the notable morphological similarities they share.

MATERIALS AND METHODS

Reconstruction of scapular position on thorax: available theropod specimens three-dimensionally or two-dimensionally preserving the pectoral (or shoulder) girdle support the view that the location of the scapula on the thorax is still a matter of discussion among of early-diverging paravians (e.g., Senter, 2006) with a high degree of uncertainty. Reconstructions presented here assume a scapular blade in an almost horizontal position, with a slight ventral inclination of the anterior extremity of the scapula, similar to that seen in living flying avians. Even assuming this derived position of the scapular blade for *Archaeopteryx* and *Buitreraptor*, the major axis of their glenoid cavities is more anteroventrally inclined than the subhorizontal major axis seen in living flying avians.

Experiments and observations carried out on living American ostriches (*Rhea americana*) were made in the Estación de Cría de Animales Silvestres (ECAS, Universidad Nacional de La Plata, Buenos Aires, Argentina) (see videos in online Supplement, at doi.org/10.5531/sd.sp.44).

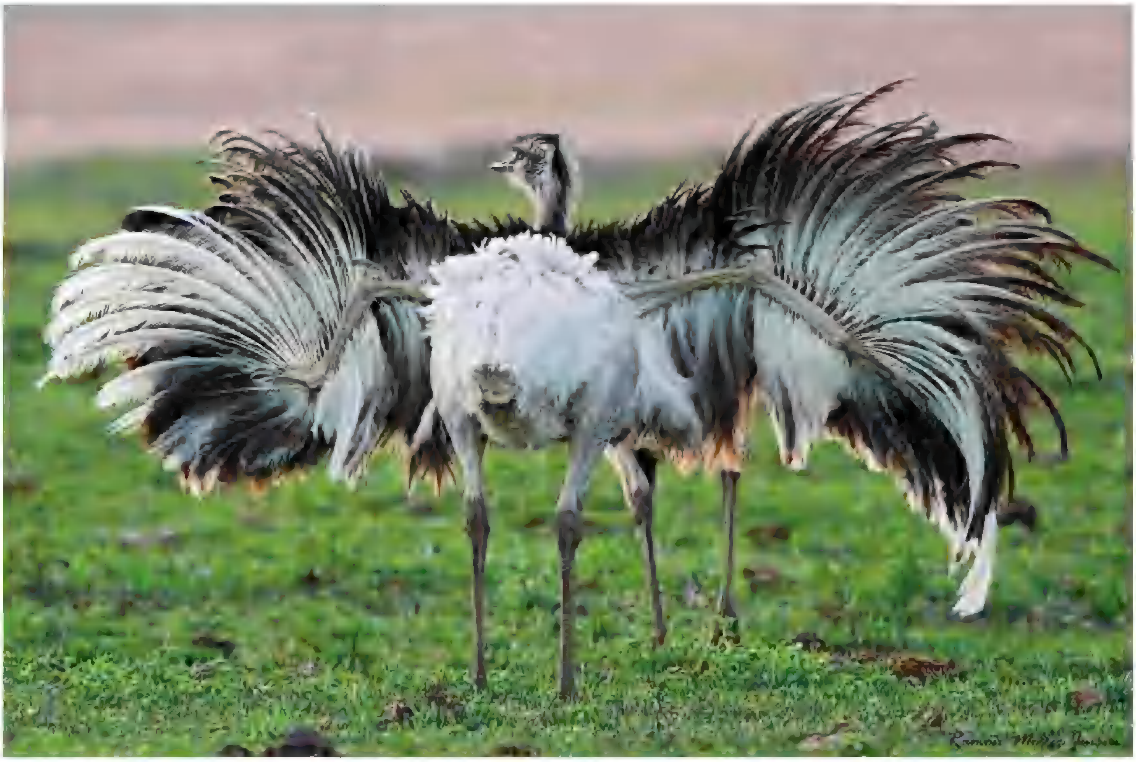

FIG. 1. Wing posture of American ostrich (*Rhea americana*) with the humerus totally abducted. Photograph taken by Ramón Moller Jensen.

We follow the phylogenetic hypothesis of Agnolín and Novas (2013) and Agnolín, et al. (2019) depicting *Anchiornis* as an early-diverging avialan (see Pittman et al., chapter 1). We use the following phylogenetic definitions: Avialae (avialans) refers to all birds including early fossil ones. Aves (avians) refers to the avian crown group only.

COMPARATIVE ANATOMY

Osteological and muscular characteristics of most living avians have been fairly well described in dozens of excellent papers (e.g., Ostrom, 1976). Thus, we will address selected features to compare ratite birds with early-diverging paravians.

Living flying avians exhibit the glenoid cavity with the long axis roughly parallel to the vertebral column. The coracoidal portion of the glenoid is horizontally extended, laterodorsally faced, with the external margin projected outward; the scapular portion of the glenoid, instead, is much smaller in size than the coracoidal portion, is vertically oriented, and faces laterally. This kind of glenoid allows wide forelimb movements, especially humeral longitudinal rotation (Poore et al., 1997). The avian humerus can adopt a position through which its flexor surface fully orientates anteriorly, thus to prepare for the downstroke, and orienting the articulation plane of both elbow and wrist perpendicular to the downstroke direction. In flying Aves the horizontal position and anterior extension of the glenoid cavity is accompanied by the anterodorsal growing of the acrocoracoidal process, which receives the attachment of m. biceps brachii (which acts to flex the forearm and to protract the humerus to a small degree) and m. coracobrachialis cranialis (one of the main protractors of the humerus), as well as different ligaments, including the ligamentun acrocoracohumerale (one of the main maintainers of the integrity of

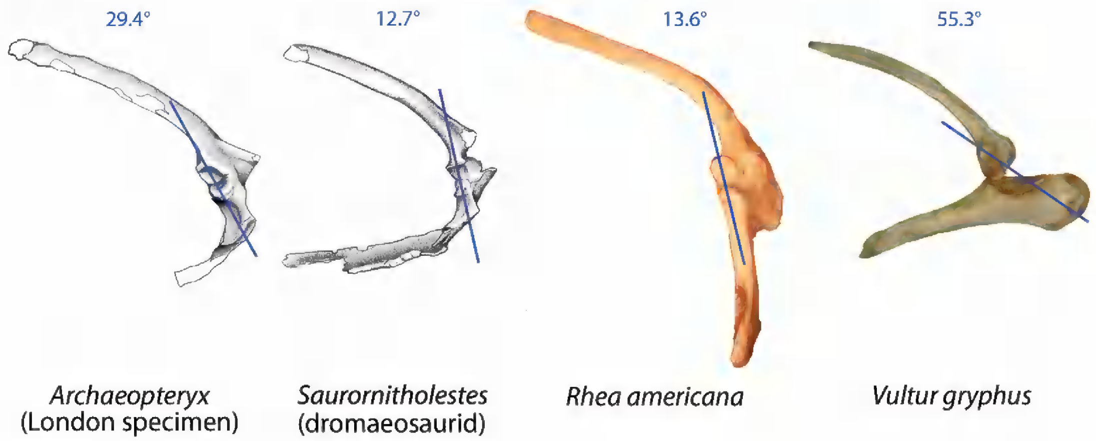
29.4°
12.7°
13.6°
55.3°
Archaeopteryx (London specimen)
Saurornitholestes (dromaeosaurid)
Rhea americana
Vultur gryphus

FIG. 2. Angle formed between the main axis of the scapulocoracoid glenoid and main vertebral column axis in selected paravians. Pectoral girdle of the London specimen of *Archaeopteryx*, *Saurornitolestes*, *Rhea americana*, and *Vultur gryphus*, in right lateral view. Not to scale.

the shoulder joint during aerial locomotion; Baier et al. 2007; 2013). The energetic and sustained wing flapping performed by living avians (mainly during takeoff and WAIR behavior) is congruent with the morphology described above for the glenoid cavity, as well as the development of m. supracoracoideus, which rotates and pulls the humerus upward (see Ostrom, 1976).

Extant flightless ratites exhibit a sharply different wing posture to that of the remaining living birds: their forearms hang ventrally when the humerus is in maximum horizontal abduction (fig. 1). Consequently, wing movements differ from those of flying living birds in that the adduction-abduction arc is predominantly anteroposterior, instead of dorsoventral. Such distinction in wing posture and movements ultimately relays in the different shape and position of the glenoid cavity, with both scapular and coracoidal portions subequal in size and occupying the same dorsoventral plane; in *Rhea* the long axis of the glenoid cavity forms an angle of approximately 13.5° with respect to the vertebral column (fig. 2).

Archaeopteryx and the remaining early-diverging paravian theropods (e.g., *Buitreraptor, Microraptor, Sinornithosaurus, Anchiornis*; Xu, 2002; Pei et al., 2017; Novas et al., 2018; Agnolín et al., 2019) share with *Rhea* a closely similar morphology of the pectoral girdle (fig. 2), with glenoids laterally oriented and with the major axis subvertical. In early-diverging birds (e.g., *Archaeopteryx*, *Anchiornis*) the glenoid facet retained the lateral orientation seen in other early-diverging paravians (e.g., *Buitreraptor*), and with both sections (scapular and coracoidal) subequal in size and aligned on the same dorsoventral plane (see Jenkins, 1993; Baier et al., 2007; Novas et al., 2018; Agnolín et al., 2019). Manipulation of bones of early-diverging paravians (e.g., *Buitreraptor*) depict movements that are predominantly anterodorsal to posteroventral, similar to those described above for *Rhea* and *Struthio*. General resemblance of pectoral girdle and humerus of early-diverging paravians (e.g., *Buitreraptor*, *Bambiraptor*, *Deinonychus*; Ostrom, 1969; Burnham, 2004) preserved three-dimensionally and early-diverging birds (e.g., *Archaeopteryx, Anchiornis*) preserved two-dimensionally on slabs suggest that the latter ones retained almost the same basic forelimb posture and range of movements as in other early-diverging paravians. Aside from glenoid orientation, early-diverging paravians (e.g., *Microraptor*, *Saurornitholestes*, *Archaeopteryx*) resemble living ratites in the presence of a nonkeeled sternum, coracoid with biceps tubercle (= acrocoracoidal process) much less developed than in neognaths, and lack of trios-

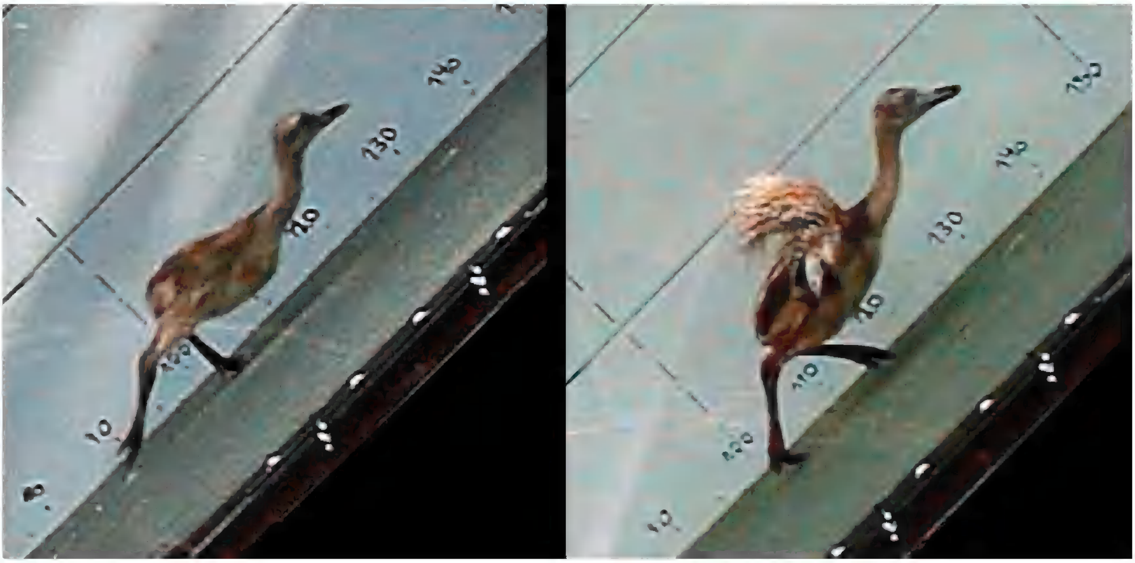

FIG. 3. *Rhea americana* siblings climbing a 45° ramp without performing WAIR. Individual on the left has its wings folded to the body, individual on the right has its wings extended.

seal canal, suggesting a feeble development of muscle mass of both m. pectoralis and m. supracoracoideus. Regarding the latter muscle, the less-developed acrocoracoidal process seen in living ratites does not modify its course. Thus, contraction of this muscle produces the forward (not upward) movement of the humerus, a function that was envisaged by Ostrom (1976) for *Archaeopteryx*.

The lack of a "twisted" glenoid (that is, without a large coracoidal surface dorsally faced) suggests that early-diverging birds (e.g., *Archaeopteryx, Anchiornis*) did not attain the amplitude of forelimb movements, nor the humeral trajectory over the glenoid, as characteristically occurs in living flying avians (Ostrom, 1976; Poore et al., 1997). But probably the most important consequence of humeral articulation over the glenoid is the wing orientation: in both early-diverging paravians (e.g., *Deinonychus, Bambiraptor*) and flying avians (e.g., *Vultur*) the longest axis of the humeral head is parallel to the major distal axis; thus, the main controller of wing-surface inclination with respect to the ground is the inclination of the major axis of the glenoid cavity.

WAIR PERFORMANCE AMONG LIVING BIRDS

Although WAIR has been hypothesized to be plesiomorphically present for paleognaths, the hypothesis was based on observations of tinamids (Dial, 2003; Dial et al., 2008; Heers et al., 2014) and experiments on their sister group (ratites) are still poorly explored (but see Davis, 2005). We offer experimental results of the running behavior of a flightless bird climbing a slope, substantiating that, among living birds, WAIR is exclusive of flying forms.

We made repeated observations on 7 juvenile specimens, 1 week old, of *Rhea americana* climbing a slope at angles of 10°, 20°, 30°, 40°, and 45°. Juveniles climbed slopes with difficulty (fig. 3; see also videos online in the Supplementary data at doi.org/10.5531/sd.sp.44), including arrests of the march, backward steps, and sometimes forward jumps. The difficulty in climbing, not surprisingly, was augmented with steeper slopes. Two types of behavior were observed: (1) climbing without extending the wings; or (2) climbing extending separately each wing to stabilize the body. In all cases, the individuals inclined their bodies forward, to avoid falling back. In sum, rhea's wings do not cooperate aerodynamically with the hind limbs to climb a slope. In conclusion, none of the studied specimens performed WAIR (videos available online at doi.org/10.5531/sd.sp.44), in agreement with previous work by Davis (2005) carried out on rheas, ostriches, and emus. Experimental results are in agreement with observations noted by early naturalists (e.g., Darwin, 1839; Muñiz, 1885), that wings of ratites do not perform symmetrical movements even when these birds are engaged in running and fighting. Recently, Schaller (2008) recorded a similar behavior for the African Ostrich, *Struthio camelus*.

DISCUSSION

The WAIR hypothesis assumes that early birds positioned (and moved) their wings in the same basic manner as in living flying birds. WAIR-based reconstructions of wing posture and movements for extinct avialans are based on the highly specialized flying neognaths, in which the glenoid cavity is laterodorsally faced and horizontally oriented, thus allowing upward and downward wing excursions.

We do not dismiss the explanatory power of the WAIR in the understanding of bird flight evolution, since this behavior might have been present in the common ancestor of Aves, and there exist anatomical reasons to suspect its presence among early-diverging ornithothoracines (Dial et al., 2008; Heers and Dial, 2012). Discussions, in fact, center on whether earlier birds (e.g., *Archaeopteryx*) already had the ability to perform WAIR. Heers and Dial (2012) claim this behavior was already present in early-diverging coelurosaurians. However, as analyzed previously, two lines of evidence weaken this WAIR interpretation: the inability of the ratites to perform WAIR (Davis, 2005, and this study), and the wing beat inferred for *Archaeopteryx* (based on general morphology of pectoral girdle, muscle pattern, and orientation and shape of the glenoid cavity).

It is remarkable that ratites, which are devoid of a derived morphology of the pectoral girdle, do not perform WAIR (both hatchlings and adults). This suggests that a causal relationship may exist between archaic pectoral girdle morphology and the inability to perform symmetrical strong flapping. In other words, their wings generate neither thrust nor lift. The weak and occasional symmetrical flapping performed by ratites may also mirror the fact that both m. supracoracoideus and m. pectoralis had postural rather than locomotor functions (Rosser and George, 1985).

As Heers, et al. (2014) pointed out, muscles of hatchling avians are less voluminous than in adults, thus lending support to the idea that early paravians were able to flap and perform WAIR, in spite of their less-developed pectoral and supracoracoidal muscle masses. Nevertheless, we concur with Dececchi, et al. (2016) in that juvenile avians already have adult pectoral attributes, including a dorsally oriented glenoid fossa and path of the tendon of m. supracoracoideus through the triosseal foramen (thus allowing the elevator action of m. supracoracoideus). These anatomical and functional characteristics described for flying avians sharply differ from ratite birds, in which the m. supracoracoideus plays a humeral protractor role, a function also inferred for early-diverging avialans (Ostrom, 1976). Wing stroke in early-diverging avialans probably lacked the upward humeral excursion and longitudinal twisting (during upstroke) of the kind occurring in living flying avians (Ostrom, 1976; Poore et al., 1997).

Even assuming that *Archaeopteryx* was able to symmetrically flap its wings in a gravitational frame as in living birds, the flapping probably did not attain the frequency and endurance as those living neognaths performing WAIR. Most recent studies on pectoral girdle anatomy and function in early-diverging paravians (Jenkins, 1993; Senter, 2006; Turner et al., 2012; Dececchi et al. 2016) agree that *Archaeopteryx* was not capable of strenuous flapping ability.

As important as frequency and endurance of flapping activity is the wing position in respect to both vertebral column and ground. Dial (2003) already interpreted the glenoid orientation of *Archaeopteryx* as an intermediate condition between early-diverging theropods and living birds (Jenkins, 1993), which allowed anteroposterior limb excursions resembling those employed by juvenile and adult ground birds during WAIR. As said before, early-diverging paravians and early birds probably had a posture of wings different from neognaths, being more similar to that of ratites, with an arc of movement anterodorsal to posteroventral, and main wing surface posteroventrally oriented in maximum abduction (Novas and Agnolín, 2014). In the same line of thought, Voeten, et al. (2018) hypothesized that *Archaeopteryx* oriented its wing surface posteroventrally (that is, oblique to the ground). Flapping wings, which moved anterodorsally to posteroventrally, may have predominantly produced thrust, but a small lift force.

This alternative reconstruction of the wing posture and movements of early-diverging avialans gives rise to the following question: could this "oblique" wing surface have generated enough lift to allow *Archaeopteryx* to become airborne? Could this kind of primitive wing have produced enough thrust to help the hind limbs in climbing pronounced slopes? The "inclined" wing surface inferred for early-diverging avialans apparently did not constitute optimal conditions to sustain gliding, but feeble development of wing muscles does not support ability for WAIR.

The oblique posture of wing surface in maximum abduction, as inferred for early-diverging paravians, invites review of aerodynamic experiments, both physically and mathematically based (e.g., Alexander et al., 2010; Evangelista et al., 2014), which assume a priori a flying avian wing posture for *Archaeopteryx* and *Microraptor*.

SUMMARY

Flying avians have been used as the best (and sole) living birds to study flight ability in early avialans. Nevertheless, living ratites constitute a source of information that cannot be neglected at this time to interpret muscle function, forelimb movements, and running-flapping behavior in early-diverging paravians. After all, the portion of the theropod phylogenetic tree comprising oviraptorosaurians, dromaeosaurids, troodontids, microraptorines, unenlagines, anchiornithines, archaeopterygids, jeholornithids, sapeornithids, and confuciusornithids saw a locomotory transition(s) from fully terrestrial to aerial animals. How to determine the ability for flight (either flapping or gliding) of some of these groups (principally microraptorines, anchiornithines, and archaeopterygids) is a matter of debate (Sullivan et al., 2016; see Pittman et al., chapter 10).

The experimental information on ratite behavior, in conjunction with the morphological resemblance among early-diverging paravians and living ratites, lends support to the interpretation that early-diverging paravians were unable to perform WAIR.

Available information suggests that the glenoid frame was still operating a "shift" among early-diverging paravians, and that it did not acquire a modern (i.e., avianlike) position and shape until much later, in the evolution of birds (e.g., probably at the level of Ornithothoraces or more likely Ornithuromorpha; Mayr, 2017). This means that early-diverging avialans must have exhibited a flight style different from that attained in ornithuromorphs. In this regard, recent studies recognize that early-diverging birds had wing-folding capacity (Sereno and Rao, 1992), remige geometry (Feo et al., 2015), feather arrangement/rachis (Nudds and Dyke, 2010; Longrich et al., 2012), and supracoracoidal muscle development (Ostrom, 1976; Mayr, 2017) that were different from ornithuromorph birds.

Moreover, the generalized presence of well-developed hind wings among early-diverging paravians and early avialans clearly shows that unusual anatomical, functional and behavioral patterns prospered during the early stages of bird evolution (Sullivan et al., 2016; Agnolín et al., 2019). The view that flying styles among early-diverging birds have no analogs among living birds is gaining ground.

ACKNOWLEDGMENTS

We thank Michael Pittman and Xing Xu for their kind invitation to contribute to this volume. We also thank Xing Xu, Angela Milner, and Carlos Muñoz for providing access to fossil paravian specimens under their care. We acknowledge S. Bogan, Y. Davies, and P. Tubaro for access to osteological collections under their care. We thank Mónica Casciaro (Dirección Flora y Fauna, Ministerio de Agroindustria), Horacio Mangudo, and the crew of the Estación de Cría de Animales Silvestres, Universidad Nacional de La Plata, for allowing access to live specimens for study. This work was supported by Agencia Nacional de Promoción Científica y Tecnológica, CONICET, and Coleman Burke. We also thank M. Motta for comments and fruitful discussions on avian forelimb function.

REFERENCES

Agnolín, F. and F.E. Novas. 2013. Avian ancestors: a review of the phylogenetic relationships of the theropods Unenlagiidae, Microraptoria, *Anchiornis* and Scansoriopterygidae. Dordrecht: Springer Science & Business Media.

Agnolín, F., M. J. Motta, F. Brissón Egli, G. Lo Coco, and F. E. Novas. 2019. Paravian phylogeny and the dinosaur-bird transition: an overview. Frontiers in Earth Science 6: 252.

Alexander, D.E., E. Gong, L.D. Martin, D.A. Burnham, and A.R. Falk. 2010. Model tests of gliding with different hindwing configurations in the four-winged dromaeosaurid *Microraptor gui*. Proceedings of the National Academy of Sciences of the United States of America 107: 2972–2976

Baier, D.B., S.M. Gatesy, and F.A. Jenkins. 2007. A critical ligamentous mechanism in the evolution of avian flight. Nature 445: 307–310.

Baier, D.B., S.M. Gatesy, and K.P. Dial. 2013. Three-dimensional, high-resolution skeletal kinematics of the avian wing and shoulder during ascending flapping flight and uphill flap-running. PLoS One 8: e63982.

Bundle, M.W. and K.P. Dial. 2003. Mechanics of wing-assisted incline running (WAIR). Journal of Experimental Biology 206: 4553–4564.

Burnham, D.A. 2004. New information on *Bambiraptor feinbergi* from the Late Cretaceous of Montana. *In* P.J. Currie, E.B. Koppelhus, M.A. Shugar, and J.L. Wright (editors), Feathered dragons: studies on the transition from dinosaurs to birds: 67–111. Indianapolis: Indiana University Press.

Darwin, C. 1839. Narrative of the surveying voyages of his majesty's ships *Adventure* and *Beagle* between the years 1826 and 1836, describing their examination of the southern shores of South America, and the *Beagle*'s circumnavigation of the globe. Journal and remarks. 1832–1836. London: Henry Colburn.

Davis, H.D. 2005. Negotiating a three-dimensional environment: limb kinematics of terrestrial birds during sloped ascents. M.S. thesis, Missoula, University of Montana.

Dececchi, T.A., H.C.E. Larsson, and M.B. Habib. 2016. The wings before the bird: an evaluation of flapping-based locomotory hypotheses in bird antecedents. Peer J. 4: e2159.

Dial, K.P. 2003. Wing-assisted incline running and the evolution of flight. Science 299: 402–404.

Dial, K.P., B. Jackson, and P. Segre. 2008. A fundamental avian wing-stroke provides new perspective on the evolution of flight. Nature 451: 1–6.

Dudley, R., et al. 2007. Gliding and the functional origins of flight: biomechanical novelty or necessity? Annual Review of Ecology, Evolution, and Systematics 38: 179–201.

Evangelista, D., S. Cam, T. Huynh, I. Krivitskiy, and R. Dudley. 2014. Ontogeny of aerial righting and wing flapping in juvenile birds. Biology Letters 10: 20140497.

Faux, C. and D.J. Field. 2017. Distinct developmental pathways underlie independent losses of flight in ratites. Biology Letters 13: 20170234.

Feo, T.J., D.J. Field, and R.O. Prum. 2015. Barb geometry of asymmetrical feathers reveals a transitional morphology in the evolution of avian flight. Proceedings of the Royal Society B, Biological Sciences 282: 20142864.

Heers, A.M., and K.P. Dial. 2012. From extant to extinct: locomotor ontogeny and the evolution of avian flight. Trends in Ecology and Evolution 27: 296–305.

Heers, A.M., K.P. Dial, and B.W. Tobalske. 2014. From baby birds to feathered dinosaurs: incipient wings and the evolution of flight. Paleobiology 40: 459–476.

Heers, A.M., J.W. Rankin, J.R. Hutchinson. 2018. Building a bird: musculoskeletal modeling and simulation of wing-assisted incline running during avian ontogeny. Frontiers in Bioengineering and Biotechnology 6:140.

Jackson, B.E., B.W. Tobalske, and K.P. Dial. 2011. The broad range of contractile behaviour of the avian pectoralis: functional and evolutionary implications. Journal of Experimental Biology 214: 2354–2361.

Jenkins, F.A. 1993. The evolution of the avian shoulder joint. American Journal of Science 293: 253–253.

Longrich, N.R., J. Vinther, Q. Meng, Q. Li, and A.P. Russell. 2012. Primitive wing feather arrangement in *Archaeopteryx lithographica* and *Anchiornis huxleyi*. Current Biology 1094: 2262–2267.

Mayr, G. 2017. Pectoral girdle morphology of Mesozoic birds and the evolution of the avian supracoracoideus muscle. Journal of Ornithology 158: 859–867.

Muñiz. F.J. 1885. Historía natural: el ñandú o avestruz pampeano. *In* D.F. Sarmiento (editor), Vida y escritos del coronel Francisco J. Muñiz: 84–90. Buenos Aires: F. Lajouane.

Novas F.E., and F.L. Agnolín. 2014. Scapular girdle morphology in paravians and implications for the origin of flight. Fourth International Palaeontological Congress, Abstract Vol. A145. September 2014. Mendoza. Argentina: CCT-CONICET.

Novas, F.E., F. Brissón Egli, F.L. Agnolín, F.A. Gianechini, and I.A. Cerda. 2018. Postcranial osteology of a new specimen of *Buitreraptor gonzalezorum* (Theropoda, Unenlagiidae). Cretaceous Research 83: 127–167.

Nudds, R.L., and G.J. Dyke. 2010. Narrow primary feather rachises in *Confuciusornis* and *Archaeopteryx* suggest poor flight ability. Science 328: 886–889.

Ostrom, J.H. 1969. Osteology of *Deinonychus antirrhopus*, an unusual theropod from the Lower Cretaceous of Montana. Peabody Museum of Natural History Bulletin 30: 1–165.

Ostrom, J.H. 1976. Some hypothetical anatomical stages in the evolution of avian flight. Smithsonian Contributions to Paleobiology: 1–21.

Pei, R., Q. Li, Q. Meng, M. Norell, and K. Gao. 2017. New specimens of *Anchiornis huxleyi* (Theropoda, Paraves) from the late Jurassic of northeastern China. Bulletin of the American Museum of Natural History 411: 1–67.

Poore, S.O., A. Sanchez-Haiman, and G.E. Goslow 1997. Wing upstroke and the evolution of flapping flight. Nature 387: 799–802

Raikow, R.J. 1968. Maintenance behavior of the Common Rhea. The Wilson Bulletin 80(3): 312–319.

Rosser, B.W.C., and J.C. George. 1985. Histochemical characterization and distribution of fiber types in the pectoralis muscle of the ostrich (*Struthio camelus*) and emu (*Dromaius novaehollandiae*). Acta Zoologicae 66: 191–198.

Schaller, N.U. 2008. Structural attributes contributing to locomotor performance in the ostrich (*Struthio camelus*). Ph.D. dissertation, University of Heidelberg, Heidelberg, Germany.

Senter, P. 2006. Scapular orientation in theropods and basal birds, and the origin of flapping flight. Acta Palaeontologica Polonica, 51: 305–313.

Sereno, P.C., and C. Rao. 1992. Early evolution of avian flight and perching: new evidence from the Lower Cretaceous of China. Science 255: 845–848.

Sullivan, C., X. Xu, J.K. O'Connor. 2016. Complexities and novelties in the early evolution of avian flight, as seen in the Mesozoic Yanliao and Jehol biotas of Northeast China. Palaeoworld 26: 212–229.

Turner, A.H., P.J. Makovicky, and M.A. Norell. 2012. A review of dromaeosaurid systematics and paravian phylogeny. Bulletin of the American Museum of Natural History 371: 1–206.

Voeten, D.F.A.E., et al. 2018. Wing bone geometry reveals active flight in *Archaeopteryx*. Nature Communications 9: 923.

Xu, X. 2002. Deinonychosaurian fossils from the Jehol Group of western Liaoning and the coelurosaurian evolution. Ph.D. dissertation, Chinese Academy of Sciences, Beijing.

SCIENTIFIC PUBLICATIONS OF THE AMERICAN MUSEUM OF NATURAL HISTORY

AMERICAN MUSEUM NOVITATES
BULLETIN OF THE AMERICAN MUSEUM OF NATURAL HISTORY
ANTHROPOLOGICAL PAPERS OF THE AMERICAN MUSEUM OF NATURAL HISTORY

PUBLICATIONS COMMITTEE
ROBERT S. VOSS, CHAIR

BOARD OF EDITORS
JIN MENG, PALEONTOLOGY
LORENZO PRENDINI, INVERTEBRATE ZOOLOGY
ROBERT S. VOSS, VERTEBRATE ZOOLOGY
PETER M. WHITELEY, ANTHROPOLOGY

MANAGING EDITOR
MARY KNIGHT

Submission procedures can be found at http://research.amnh.org/scipubs

All issues of *Novitates* and *Bulletin* are available on the web (http://digitallibrary.amnh.org/dspace). Order printed copies on the web from:
http://shop.amnh.org/a701/shop-by-category/books/scientific-publications.html

or via standard mail from:
American Museum of Natural History—Scientific Publications
Central Park West at 79th Street
New York, NY 10024

♾ This paper meets the requirements of ANSI/NISO Z39.48-1992 (permanence of paper).

ON THE COVER: PENNARAPTORAN THEROPOD DINOSAURS (LEFT TO RIGHT, TOP TO BOTTOM): *GIGANTORAPTOR ERLIANENSIS* (OVIRAPTOROSAURIA), CLARK'S NUTCRACKER, *NUCIFRAGA COLUMBIANA* (AVES), *ARCHAEOPTERYX LITHOGRAPHICA* (AVIALAE); *MICRORAPTOR* (DROMAEOSAURIDAE), *ANCHIORNIS HUXLEYI* (AVIALAE, BUT POSSIBLY TROODONTIDAE); *LATENIVENATRIX MCMASTERAE* (TROODONTIDAE), *CITIPATI OSMOLSKAE* (OVIRAPTOROSAURIA); *LINHERAPTOR EXQUISITUS* (DROMAEOSAURIDAE); *JIANIANHUALONG TENGI* (TROODONTIDAE) AND AN ENANTIORNITHINE BIRD (AVIALAE). *GIGANTORAPTOR* IS APPROXIMATELY THREE METERS TALL AT HIP HEIGHT. IMAGE CREDIT: JULIUS T. CSOTONYI.